Michael Sartor

# Synthesis and Characterization of Chiral Metal-Organic Frameworks for Stereoselective Applications

Die vorliegende Arbeit wurde im Zeitraum von April 2010 bis Juni 2015 in der Arbeitsgruppe von Prof. Dr. Michael Fröba am Institut für Anorganische und Angewandte Chemie im Fachbereich Chemie der Universität Hamburg angefertigt.

**Eidestattliche Versicherung**

Hiermit versichere ich an Eides statt, die vorliegende Dissertation selbst verfasst und keine anderen als die angegeben Hilfsmittel verwendet zu haben. Ich versichere, dass diese Dissertation nicht in einem früheren Promotionsverfahren eingereicht wurde.

# Contents

# Abbreviations

# List of Acronyms

**AmOAc** amyl acetate

**bdc** benzene-1,4-dicarboxylate

**Boc** *tert*-butyloxycarbonyl

**bipy** 4,4′-bipyridine

**bpdc** 4,4′-biphenyldicarboxylate

**BET** Brunauer-Emmet-Teller

**Bn** benzyl

**btc** benzene-1,3,5-tricarboxylate

**cam** 1,2,2-trimethylcyclopentane-1,3-dicarboxylate (camphorate)

**CUS** coordinatively unsaturated site

**Cy** cyclohexyl

**DCVC** dry column vacuum chromatography

**DMA** *N,N*-dimethylacetamide

**DMAP** 4-(dimethylamino)-pyridine

**DMF** *N,N*-dimethylformamide

**DTA** differential thermal analysis

**DUT** Dresden University of Technology

**dmsdip** (5,5′-dimethylsilanediyl)diisophthalate

**DMSO** dimethylsulfoxide

**DTA** differential thermal analysis

*ee* enantiomeric excess

**EtOAc** ethyl acetate

**GC** gas chromatography

**HKUST** Hong-Kong University of Science and Technology

**HPLC** High-Performance Liquid Chromatography

**IBU** inorganic secondary building unit

**IUPAC** International Union of Pure and Applied Chemistry

**IRMOF** Isoreticular Metal-Organic Framework

**LDA** lithium diisopropylamide

**mdip** 5,5′-methylene-di-isophthalate

**MOF** Metal-organic framework

**MOP** metal-organic polyhedron

**MS** mass spectrometry

**NaHMDS** sodium bis(trimethylsilyl)amide

**OBU** organic secondary building unit

**OMS** open metal site

**PDF** powder diffraction file

**POST** Pohang University of Science and Technology

**PTFE** polytetrafluoroethylene

**PSM** post-synthetic modification

**PXRD** powder X-ray diffraction

**RCSR** Reticular Chemistry Structural Resource

**SBU** secondary building unit

**SIM** selected ion monitoring

**SPhos** 2-dicyclohexylphosphino-2′,6′-dimethoxybiphenyl

**TFA** trifluoroacetic acid

**TG** thermogravimetric analysis

**TGMS** thermogravimetric analysis coupled with mass spectrometry

**THF** tetrahydrofuran

**TLC**  thin layer chromatography

**TTD**  TOPOS Topological Database

**UiO**  Universitetet i Oslo

# Chapter 1

# Introduction

## 1.1 Metal-Organic Frameworks

In 2013, the International Union of Pure and Applied Chemistry (IUPAC) issued recommendations for the terminology of metal-organic frameworks, providing the scientific community with a concise definition for these materials: *A metal-organic framework, abbreviated to MOF, is a coordination network with organic ligands containing potential voids.*[1]

However, the term metal-organic framework is practically self-explaining, indicating the building blocks and the resulting structures of these materials: They contain nodes from *metals* (and metal-oxygen clusters) that are interconnected by *organic* linkers. The assembly of these building blocks leads to *framework* structures. This very basic principle is depicted in Figure 1.1.
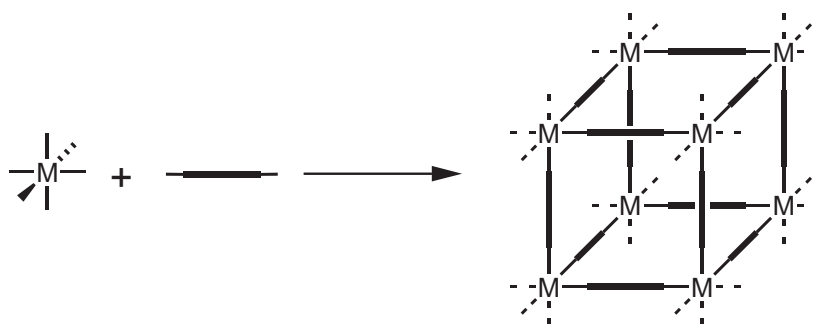


**Figure 1.1** – Assembly of octahedral metal nodes (M) with linear linkers (represented by bold bars) to a hypothetical cubic framework in which the nodes are interconnected by the linkers in all three spatial dimensions. Dashed lines on the framework indicate the infinite three-dimensional structure of the system (adapted from[2]).

As can be seen in Figure 1.1 metal ions or metal-oxygen clusters and organic linkers can assemble to form an extended network. This is for example the case in the archetypal MOF-5. Octahedral metal-oxygen clusters and linear organic linkers form a cubic framework.[3] This compound is a good starting point to understand the fundamental structure of MOFs. The crystal structure of MOF-5 (see Figure 1.2) shows an empty space. This space is originally filled by molecules of the solvent used during the synthesis of this MOF but can eventually be evacuated (see Section 1.4).

The structure of MOF-5 can be broken down into two kinds of secondary building unit (SBU): The inorganic SBU and the organic SBU (see Figure 1.3). In many publications on MOFs, the term SBU is often solely used to describe the
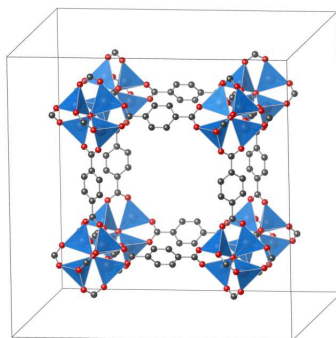
**Figure 1.2** – Crystal structure of MOF-5 that constitutes a three-dimensional framework that resembles the structure in Figure 1.1. A considerable part of the structure (74 %) is ascribed to void space[4] (blue tetrahedra represent the zinc atoms in their coordination environment, red: oxygen, grey: carbon, hydrogen atoms are omitted for clarity).

inorganic component of the MOF. To differentiate between the different building blocks of MOFs in this work, the abbreviation organic SBU will be used to describe the linker that is coordinated to a metal (cluster) and the abbreviation inorganic SBU will be used to describe the metal clusters, whose shapes are defined by their *points of extension*, which constitute the connection between the two kinds of SBU.[5] In the case of MOF-5, the inorganic SBU is formed from a tetrahedral $Zn_4O$-cluster, in which neighboring zinc atoms are bridged by six bidentate carboxylate groups that originate from six linker molecules. The $Zn_4O$-cluster and the carboxylate groups assemble into an octahedral superstructure that serves as a six-connected branching point (see Figure 1.3). The carbon atoms of the carboxylates represent the points of extension in this building block. The organic SBU of MOF-5 is derived from benzene-1,4-dicarboxylate (bdc) and serves as a linear connection between the inorganic SBUs in this structure.

If other metal ions are used to prepare a MOF, different framework structures can be expected. If for example zirconium (IV) is used together with benzenedicarboxylate in the synthesis of a MOF, a higher degree of connectivity of the inorganic SBU can be achieved (see Figure 1.4). This results in a MOF that is denser than MOF-5 and very stable due to the high number of strong zirconium-oxygen bonds.

The resulting MOF is called UiO-66 (Universitetet i Oslo) and in this structure a twelve-connected metal-oxygen cluster is formed. This cluster resembles

**(a)**                    **(b)**
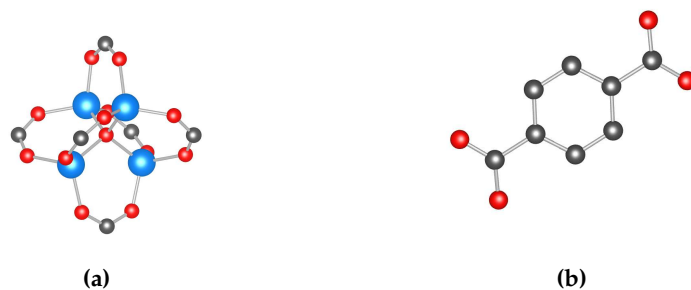
**Figure 1.3** – Individual building units within MOF-5: (a) Octahedral inorganic SBU that is formed by a tetrahedral $Zn_4O$ cluster and six carboxylate groups that each bridge two zinc atoms. The carboxylate carbon atoms constitute the points of extension of the cluster (b) linear organic SBU that is provided by bdc whose carboxylate groups also take part in the formation of the inorganic SBU (hydrogen atoms omitted for clarity).
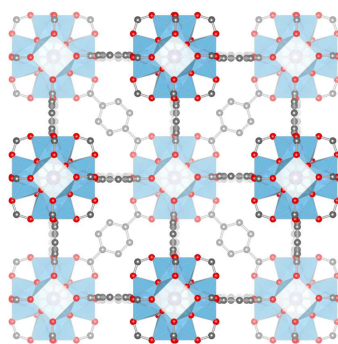


**Figure 1.4** – Crystal structure of UiO-66 which is a three-dimensional network that comprises zirconium-oxo clusters that are interconnected by bdc to form a porous framework (blue square antiprisms represent the zirconium atoms in their coordination environment, red: oxygen, grey: carbon, hydrogen atoms are omitted for clarity).

a cuboctahedron whose corners are defined by carboxylate carbon atoms that represent the points of extension within this framework. Again the organic SBU serves as a linear linker between the inorganic SBUs. The individual building units are depicted in Figure 1.5.



**(a)**                                    **(b)**
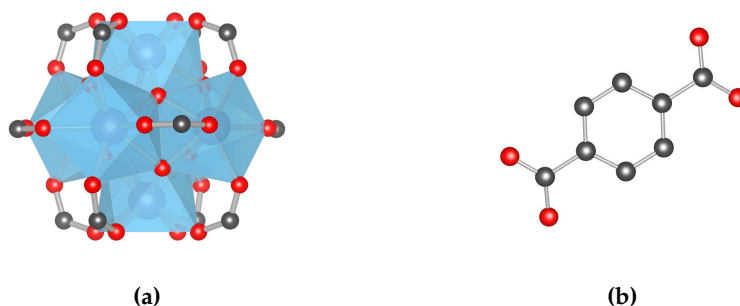
**Figure 1.5** – Individual building units within UiO-66: (a) cuboctahedral inorganic SBU that is composed of six zirconium atoms that are bridged by six oxygen atoms and twelve carboxylate groups from bdc linker molecules (b) linear organic SBU that is identical to the organic SBU of MOF-5 and serves as a two-connected linker between two inorganic SBUs (hydrogen atoms omitted for clarity).

Linkers in MOFs are of course not limited to linear dicarboxylates. The structures of MOFs are highly dependent on the geometry and the connectivity of organic linker molecules and the design of new structural motifs allows the synthesis of novel materials.[6–8] Furthermore, MOFs are not only obtained from carboxylic acids but are also available from phosphonates,[9,10] sulfonates[10] and heterocycles.[6] Examples of the connection between metal clusters and pyridinyl ligands are together with many interesting linker motifs are given in Section 1.6 page 45.

A particularly well-known example for a system from a tricarboxylic acid is HKUST-1 (Hong-Kong University of Science and Technology), which is a copper-based MOF with benzene-1,3,5-tricarboxylate (btc) serving as the organic SBU (see Figure 1.6).[11]

The inorganic SBU is composed of two copper atoms that are bridged by four carboxylates (see Figure 1.7). Due to its characteristic shape this motif is called copper paddle-wheel. The axial positions of this paddle-wheel can be occupied by coordinating solvent molecules. These solvent molecules may be removed together with the pore-filling solvent during an activation process (see 1.4.1)
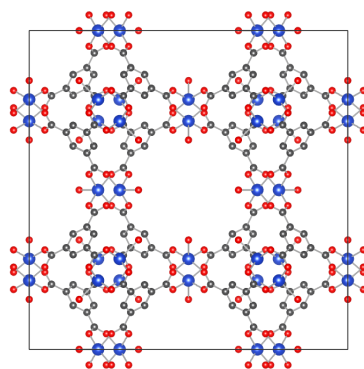
**Figure 1.6** – Crystal structure of HKUST-1, a porous three-dimensional framework formed by copper dimers and btc with the molecular formula $Cu_3(btc)_2$. Copper atoms can also be coordinated by ligands (here water) that do not take part in the formation of the framework (blue: copper, grey: carbon, red: oxygen, hydrogen atoms are omitted for clarity).

resulting in coordinatively unsaturated sites (CUS), which are also described as so-called open metal sites (OMS).

(a)             (b)

**Figure 1.7** – Building units of HKUST-1: (a) the inorganic SBU comprises a copper dimer that is bridged by four carboxylates in an arrangement that resembles the shape of a four-bladed paddle-wheel. The axial positions of the copper atoms within this structure are occupied by solvent molecules that do not contribute to the formation of a framework (b) a trigonal organic SBU that is provided by the btc linker (blue: copper, grey: carbon, red: oxygen, hydrogen atoms are omitted for clarity).

## 1.2 Network Topology

MOFs can be described by means of atomistic models that allow a precise localization of the atoms that belong to either the inorganic SBU, organic SBU or ordered guest molecules within in the pore system of the material. However, in some cases it is desirable to find other ways to represent the structure of a MOF. This is, for example, the case, when one tries to identify and classify prototypical structures.[12] If structural relationships between two frameworks structures are sought, a full description of all atomic positions does not necessarily permit a simple recognition of similarities in the assembly of the building units. A more abstract way to describe the structure of a MOF makes use of the so-called *underlying net*, meaning that three-dimensional, atomistic structures are disregarded and are deconstructed to zero-dimensional *vertices*, which are connected by *edges* in a periodic graph that can be described by mathematical formalisms.[5,13] From a mathematical point of view, the vertices of a graph can be placed arbitrarily in three-dimensional space: only the connectivity counts. Chemists may rather seek a specific representation (*embedding*) of the topology by *n*-cooordinated *nodes* and respective *links* with defined positions in three-dimensional space, which correspond to the individual SBUs. The basic principles of network topology of MOFs are explained in the following.

To obtain a representation of an underlying net, individual building units are condensed to $n$-coordinated nodes. The process of finding the underlying net is straightforward for MOF-5. The inorganic SBU of MOF-5 can be abstracted to a six-connected node. The organic SBU of MOF-5 presents a simple connection between two nodes and is itself not a node but a link. The underlying net of MOF-5 is a primitive cubic arrangement of six-coordinated vertices (see Figure 1.8). The underlying nets of MOFs are commonly named with specific codes. The IUPAC encourages the use of the three-letter codes from the Reticular Chemistry Structural Resource (RCSR).[1] However, both the EPINET database[14] and the TOPOS Topological Database (TTD)[15,16] have individual systems for the nomenclature of topologies that are commonly found in the literature.[1]. In the case of MOF-5 the underlying net is **pcu**, which hints at the primitive cubic arrangement of the nodes in the embedding with highest symmetry. However, most nets are named arbitrarily.
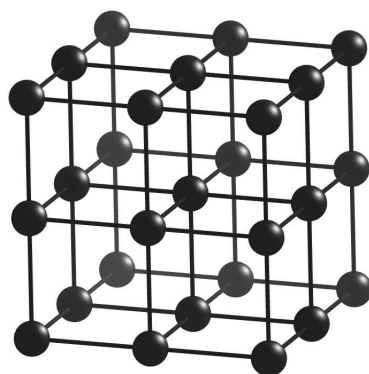


**Figure 1.8** – Part of the underlying **pcu** net of MOF-5.

The denomination of a topology with a short code allows for fast retrieval within topological databases such as the RCSR.[17] However, these descriptors hardly give any information about the connectivity in a net. To describe the underlying net more precisely the *coordination sequence and vertex symbol* of each different kind vertex of the net has to be determined (edges and vertices are of different kind, if they are not symmetry-related to each other).

The coordination sequence of a vertex simply describes the number of neighbors that are connected to the vertex via certain number of edges. This is best understood for the uninodal[2] **sql** net (see Figure 1.9). The central vertex high-

---

[1]Topological descriptors can be distinguished by their typesetting (**bold**: RCSR, *italics* TTD)
[2]Meaning that only one kind of node exists in this net

lighted in red is directly connected to four other vertices (blue) and connected to eight vertices (orange) via exactly two edges. Twelve vertices (green) are connected to the central vertex via exactly three edges and 16 vertices (grey) are exactly four edges away. This adds up to the coordination sequence of the first four degrees of topological neighbors: [3]

$$c_4 = 4, 8, 12, 16 \tag{1.1}$$
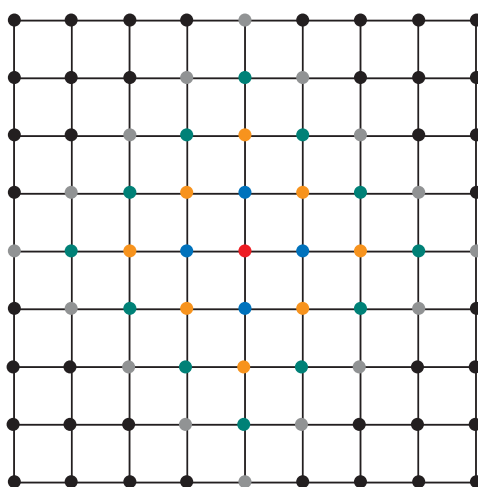


**Figure 1.9** – Part of the two-dimensional **sql** net; neighbors that are $n$ edges away from the central vertex (red) are highlighted ($n = 0$: red, $n = 1$: blue, $n = 2$: orange, $n = 3$: green, $n = 4$: grey).

The vertex symbol is a topological descriptor that gives information about *how* a vertex is connected rather then the number of topological neighbors. To obtain a vertex symbol one has to inspect all angles between the edges on a given vertex. An angle is formed by two edges joined on a vertex. For each of these angles, one has to find the shortest *ring* that includes this angle. The vertex symbol then just simply lists the sizes of the rings for each angle. An example for this procedure is given in Figure 1.10, where the **sql** net is shown again. Connected to the central vertex $v$ are four edges ($a, b, c, d$), which form four angles ($ab, bc, cd, da$). The smallest ring that includes the angle $ab$ counts four edges. This is also true for the remaining angles $bc, cd, da$. Therefore the vertex symbol for the central vertex $v$ is:

---

[3] The RCSR documents the first ten degrees of topological neighbors for each vertex.

$$\text{VS}_{v_{\text{sql}}} = 4.4.4.4 \tag{1.2}$$



**Figure 1.10** – Part of the two-dimensional **sql** net, the shortest circuit that encloses the angle $ab$ is a four-membered ring (highlighted in blue).

When determining vertex symbols, it is necessary to follow the strict definition of rings and cycles from graph theory: A path is a connection of two vertices via any number of edges. A cycle is a closed circuit path that starts and ends on the same vertex. A ring cannot be divided into *two* smaller cycles, meaning a ring must not include a short-cut to the "home vertex". A *strong ring* is defined as a ring that cannot be divided into *a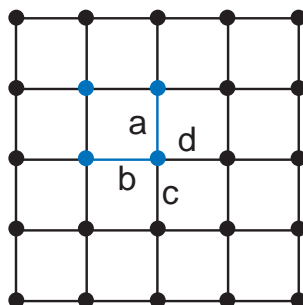ny* number of smaller cycles. A detailed, formal description of these terms has been introduced by Delgado-Friedrichs and O'Keeffe.[13] The size of a cycle or ring is defined by the number of edges (or vertices) included in this circuit.[18] In the listing of the vertex symbol only rings are included even though there may be shorter cycles present that connect the same two edges in an angle. This is for example the case in the **fxt** net which is depicted in Figure 1.11. Connected to the central vertex $v_{\text{fxt}}$ are three edges $(a, b, c)$ that form the angles $ab, bc$ and $ca$. The shortest connection between the angles $bc$ and $ca$ are a four- and six-membered ring, respectively. The shortest path between the angle $ab$ is an eight-membered cycle, which includes a short-cut to the home vertex via edge $c$. The smallest ring that includes the angle $ab$ is twelve-membered. The vertex symbol of $v_{\text{fxt}}$ is therefore:

$$\text{VS}_{v_{\text{fxt}}} = 4.6.12 \tag{1.3}$$

### 1.2.1 Tilings

A complementary way to represent the underlying nets of framework structures employs so-called *tilings*.[13] These two-dimensional polygons or three-
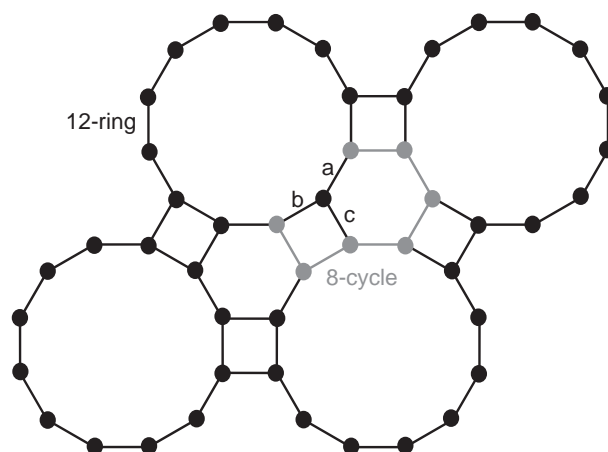
**Figure 1.11** – Part of the two-dimensional **fxt** net. The smallest ring between the edges *a* and *b* is twelve-membered and the shortest connection that involves the angle *ab* is an eight-membered cycle (grey).

dimensional polyhedra divide the space of a periodic structure. They completely fill the "empty" spaces that are generated by the net and are connected to each other via their faces. The edges of these polyhedra correspond to the edges of the net they belong to. Surfaces of these polyhedra may be curved as the rings of the net that define their faces are not always flat. The relationship of a tiling and a net can by understood by treating the tiling as the carrier of a net. An instructive and very simple example is depicted in Figure 1.12a which shows the tiling of the **pcu** net. In this case, cubes are the polyhedra that describe the divided space between the six-coordinated nodes in a primitive cubic arrangement. Another instructive tiling for is shown in 1.12b for the **dia** topology. The net resembles the crystal structure of diamond and features six-membered rings in a chair conformation which results in curved faces of the tiles shown in blue.

In principle multiple tilings are conceivable to fill the empty space of a net. An alternative tiling for the **pcu** net is shown in Figure 1.13. In this tiling the three-dimensional space is filled by double cubes. However, this tiling poorly reflects the cubic symmetry of the net **pcu** associated with it. To provide *unique* tilings a set of certain rules was developed that defines so-called natural tilings, which conserve the symmetry of the net that is carried by them.[19]

If the connectivity of organic SBUs and inorganic SBUs that forms a MOF can be represented by a net, vice versa the empty spaces in such a system can be represented as a tiling. Hence, tilings can aid the understanding of a MOF struc-

(a)                                         (b)

**Figure 1.12** – (a) View along [111] of a part of the **pcu** net together with the corresponding tiling. The six-coordinated nodes of the **pcu** net are grey. Yellow, cubic tiles comp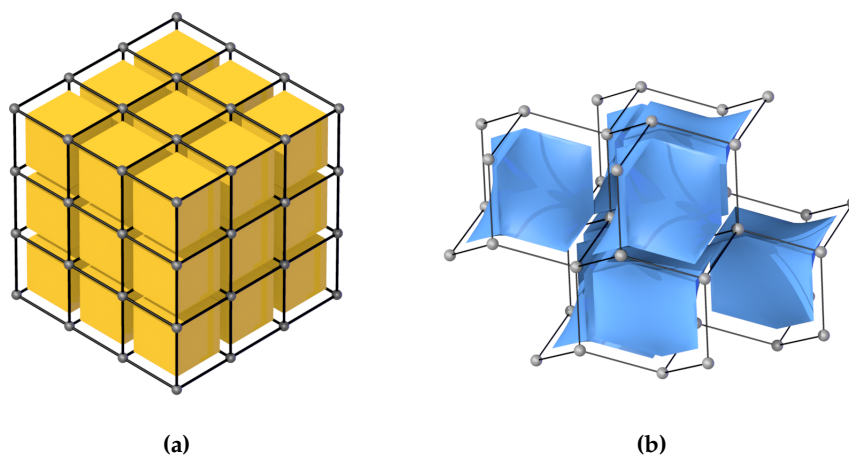letely fill the space inside the net but are slightly shrunk for clarity. (b) View along [110] of a part of the **dia** net together with the corresponding tiling. The four-coordinated nodes of the **dia** net are grey. Blue, six-faced tiles fill the space inside the net but are slightly shrunk for clarity.
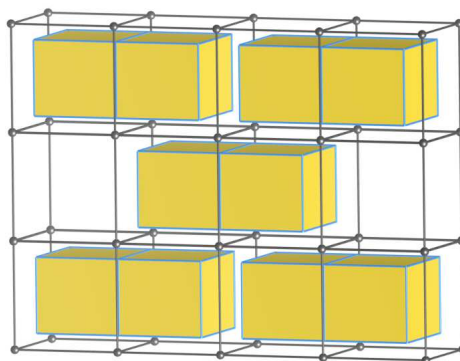
**Figure 1.13** – Part of the **pcu** net together with a non-natural tiling of the three-dimensional space. Double cubes (yellow tiles with blue edges) can be used to fill the space of the net but the tetragonal symmetry of the tiles conflicts with the cubic symmetry of the **pcu** net (grey: six-coordinated nodes, black: edges of the net, tiles are shrunk for clarity).

ture by visualizing the arrangements of the pores. This can be seen in Figure 1.14 which depicts an extended unit cell of the underlying **tbo** net of HKUST-1 together with the corresponding natural tiling. The three different types of pores are represented by three differently colored tiles (yellow, blue, and red). However, it should be noted that a tiling is merely a topological description of space and hardly gives any information about the size of different pores. Furthermore, a tiling of a MOF may not be available when the underlying net exhibits catenated rings, which prohibit a space-filling arrangement of face-sharing polyhedra.

Furthermore, tilings and the nets they carry can provide another method of classification of the topology of a structure. The *transitivity* of a net expresses how uniform a net is by assigning a four-digit number *pqrs* that specifies the number of different types of tiles ($s$), the number of different types of faces of the tiles ($r$), the number of different kinds of edges the faces have ($q$), and the number of different kinds of vertices of the faces ($p$).[13]

Nets are called vertex-transitive, if only one kind of vertex is present ($p = 1$) or edge-transitive, if the net has only one kind of edge ($r = 1$). The **dia** and **pcu** nets (see Figure 1.12) belong to the most uniform nets and have the transitivity 1111 and are vertex- and edge-transitive. As can be seen from Figure 1.14, the **tbo** net is much less uniform. The transitivity of this net is 2123. It is an edge-

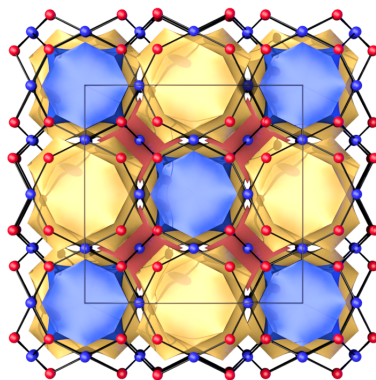**Figure 1.14** – View along the *a* axis of an extended unit cell of the **tbo** net together with the corresponding tiling. The three-coordinated, red nodes correspond to the organic SBU (btc) and the four-coordinated, blue nodes correspond to the inorganic SBU (paddle-wheels) of HKUST-1.

but not vertex-transitive net, because it has two different kinds of nodes (a three-coordinated organic SBU and a four-coordinated inorganic SBU).

## 1.3 Reticular Chemistry

In the development of new MOFs one approach has proven particularly successful and has been coined as *reticular synthesis* by Yaghi and O'Keeffe.[20] As it is shown in Figure 1.15 (see page 30) MOFs with the same net can be obtained by the elongation of the linker. The underlying net of the structures remains the same. These MOFs are called *isoreticular*.[4]

The concept of reticular chemistry builds upon the interpretation of inorganic crystal structures as nodes and spacers by Wells.[21–23] It implies that within certain restrictions, rigid building units can be designed into structures with predetermined underlying nets. The most prominent example of this approach is the so-called Isoreticular Metal-Organic Framework (IRMOF) series. Here, the geometry of the framework is determined by the octahedral carboxylate cluster. By using octahedral metal-oxygen clusters and linear dicarboxylic acids as connectors, a primitive cubic arrangement of the resulting framework can be anticipated. This kind of predetermination of the underlying net can only be achieved when the building units of the MOF can be foreseen successfully. This is difficult for simple metal ions, because they hold little directional information.[20] However, metal-oxygen-carbon clusters, that may be formed under well-defined synthetical conditions, have discrete points of extension that provide the necessary directional information to rationalize specific network structures. These clusters that can define the geometry of the resulting framework can be represented by the SBUs. Apart from the octahedral $Zn_4O$-carboxylate cluster other prominent SBUs are the square-planar copper paddle-wheel that can be found for example in HKUST-1 (see Figure 1.7a, page 21) and the twelve-connected zirconium carboxylate cluster of UiO-66, which can also be regarded as a twelve-connected SBU with a cuboctahedral shape.[24] These building units together with their abstracted polyhedral shape are depicted in Figure 1.16.

It has been proposed that a deliberate variation and combination of these building units can lead to predetermined framework structures.[20] This has been demonstrated for the paddle-wheel motif: by linking together tetrahedral and a square-planar building blocks, the **pts** topology can be obtained.[25,26] Adjoining square-planar and triangular building blocks can lead to the **tbo** net in HKUST-1 (see Figure 1.14) or the **pto**[27] topology.

For each of the SBUs depicted in Figure 1.16, the concept of reticular synthesis was successfully applied and MOFs were obtained that are isoreticular to MOF-5, HKUST-1, and UiO-66 respectively. This was achieved by employing linkers that are elongated compared to the original linker. In the first case, these MOFs constitute the archetypal IRMOF series. Conserving the underlying net of MOF-5, structural modifications were achieved using other linear carboxy-

---

[4]reticulum (Lat.), net

**(a)** IRMOF-1  **(b)** IRMOF-10  **(c)** IRMOF-16
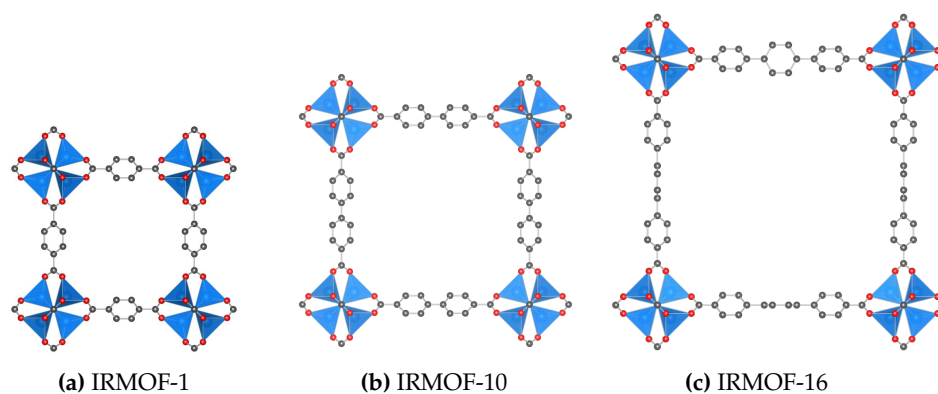
**Figure 1.15** – Three MOFs from the IRMOF series; only one face of the cubic cell is shown (blue tetrahedra: zinc atoms in their tetrahedral coordination sphere, grey: carbon, hydrogen atoms and solvent molecules are omitted, structural information obtained from CCDC number 175572 (a), 175580 (b) and 175585 (c)).
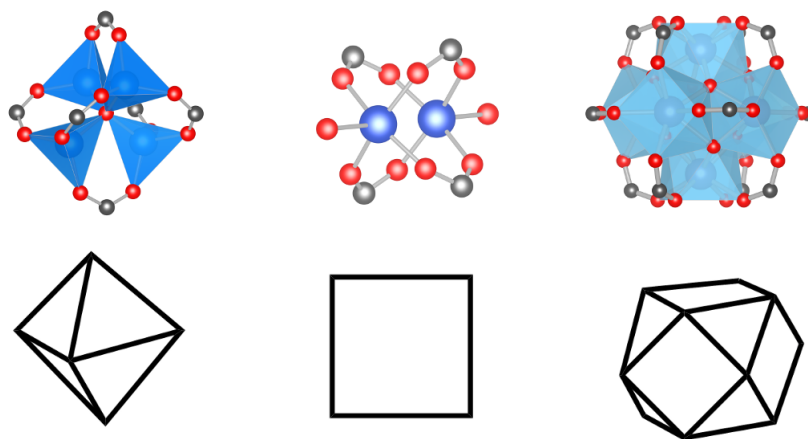


**Figure 1.16** – Inorganic SBUs of MOF-5, HKUST-1 and UiO-66 together with their abstraction to an octahedral, square-planar and cuboctahedral SBU, respectively.

lates as organic linkers.[28] By expanding the length of the linker from benzene- to biphenyl- or terphenyl dicarboxylates, pore diameters of the resulting framework were increased from 12.8 Å to 24.5 Å and 28.8 Å, respectively.

As a derivative of HKUST-1, an isoreticular MOF with enlarged pores was reported by Yaghi and co-workers.[29] For the synthesis of MOF-399, a linker was employed that is elongated by a biphenyl unit in each of the three directions of the points of extension compared to the linker used to prepare HKUST-1. This resulted in a MOF that shares the underlying **tbo** net but exhibits an outstanding low crystallographic density of $0.13\,g/cm^3$ which is ten times smaller than the density of HKUST-1. A comparison of the two unit cells of the crystal structures of these MOFs is shown in Figure 1.17.



(a)  (b)
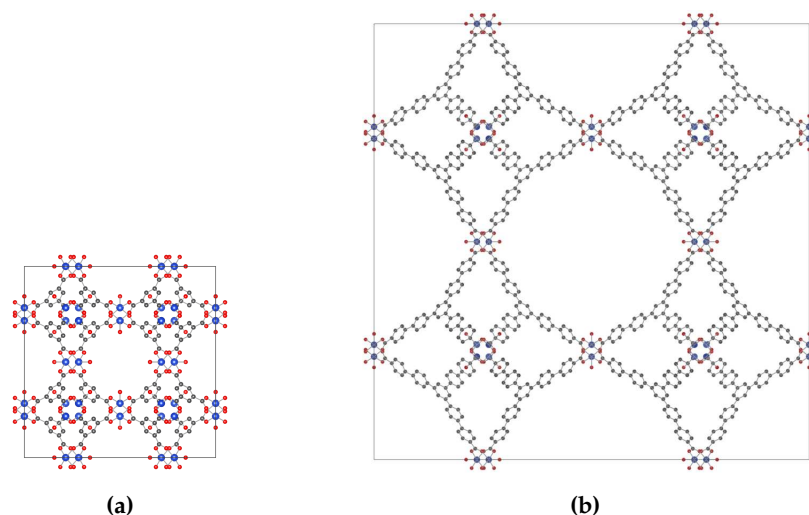
**Figure 1.17** – View along a crystallographic axis of the unit cells of two HKUST-1 (a) and MOF-399 (b) which are based on the **tbo** net (blue: copper, grey: carbon, hydrogen atoms and solvent molecules are omitted, structural information obtained from CCDC number 112954 (a) and 780452 (b), respectively).

Similar to the elongated linker in IRMOF-16, an expanded versions of UiO-66 were synthesized by the groups of Lillerud[24] and Behrens.[30,31] The latter were able to obtain single crystals for a structural analysis of Zr-tpdc-NH$_2$, in which a *para*-terphenyl dicarboxylate that bears an amino group at the central aromatic ring was used as a linker. This leads to a structure that is isoreticular to UiO-66, in which the available pore space was significantly enlarged. A representation of

the crystal structure of this MOF, which corresponds to the structure of UiO-68 is shown in Figure 1.18.



**(a)** UiO-66

**(b)** Zr-tpdc

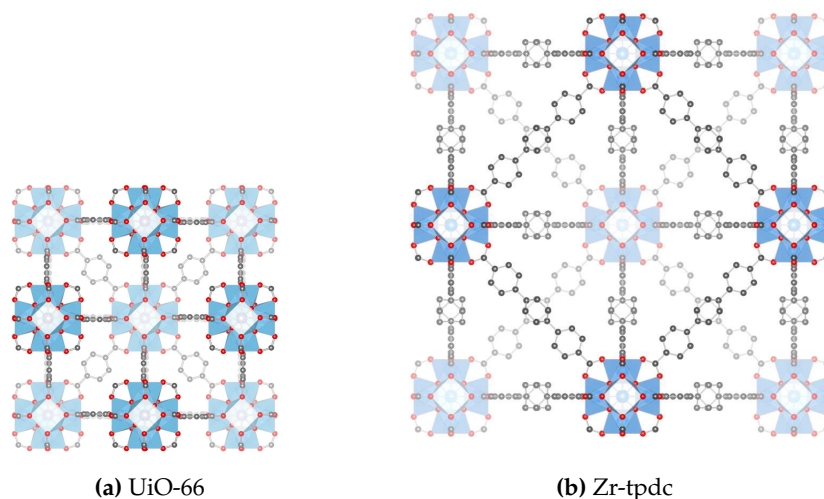**Figure 1.18** – View along a crystallographic axis on the unit cells of two isoreticular MOFs based on the **fcu** net (blue square antiprisms: zirconium, grey: carbon, red: oxygen. hydrogen atoms and solvent molecules are omitted, structural information obtained from CCDC number 7336458 (a) and 777468 (b)) Hydrogen and nitrogen atoms are omitted for clarity.

Albeit the basic principles of the concept of reticular chemistry are plausible, there are certain strengths and weaknesses of this approach: The geometry of the organic SBUs can be adjusted to a great degree by the means of organic synthesis. Also, in many cases, the geometry of the purely organic SBUs is retained during the synthesis of a MOF. However, it has been shown that a simple elongation may not necessarily lead to isoreticular networks but to new topologies.[32] This is the case because the rigidity of linker molecules inevitably decreases when the length of a linker is increased. An increased conformational freedom of elongated linker molecules allows other structures to be formed, which may be more stable than the isoreticular compounds. Therefore the nature of the organic SBU is not absolutely predictable. Unfortunately, this is also the case for inorganic SBUs as they are primarily formed during the synthesis of the MOF and thereby an exact determination of the geometry of the inorganic SBU is not always possible.

Furthermore, even if the underlying net is retained, creating greatly elongated versions of linker molecules may lead to interpenetrated frameworks. *In-*

*terpenetration* describes the phenomenon, when two or more framework structures grow intertwined with another. This effect usually increases the stability of the frameworks involved but reduces the overall porosity of the material as the frameworks occupy the pore space of each other.[33] An example for the interpenetration of two **pcu** nets is shown in Figure 1.19. This kind of interpenetration occurs for example in IRMOF-9, -11, and -13[28] and has also been observed for MOFs isoreticular to UiO-66.[31]
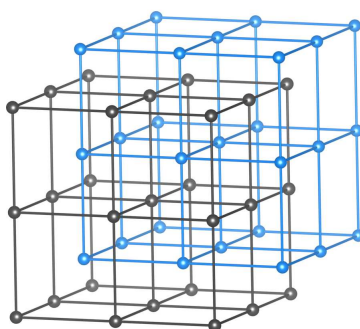


**Figure 1.19** – Schematic representation of two interpenetrated **pcu** nets. The black and the blue nets are structurally identical but the positions of the nodes are shifted by (0.5 0.5 0.5) with respect to each other.

## 1.4 Porosity

After the demonstration of permanent porosity in a MOF by the group of Yaghi in 1999, much progress has been made concerning the availability of empty space within this class of materials.[3] Recently, MOFs have been reported that exhibit extremely large surface areas, which are more than doubled compared to the surface area of MOF-5. Kaskel and co-workers have prepared DUT-32 (Dresden University of Technology) from a mixture of di- and tritopic carboxylate linkers.[34] This MOF exhibits both micro- and mesopores. The crystallographic density of this material is exceptionally low (0.27 g/cm$^3$ even compared to other MOFs such as MOF-5 with 0.61 g/cm$^3$). Furthermore, DUT-32 shows impressive nitrogen sorption properties with an apparent BET surface area of 6411 m$^2$/g. A topological representation of this MOF is shown in Figure 1.20. The structure can be divided into four distinct pore types. These pores are up to 42 Å in diameter.

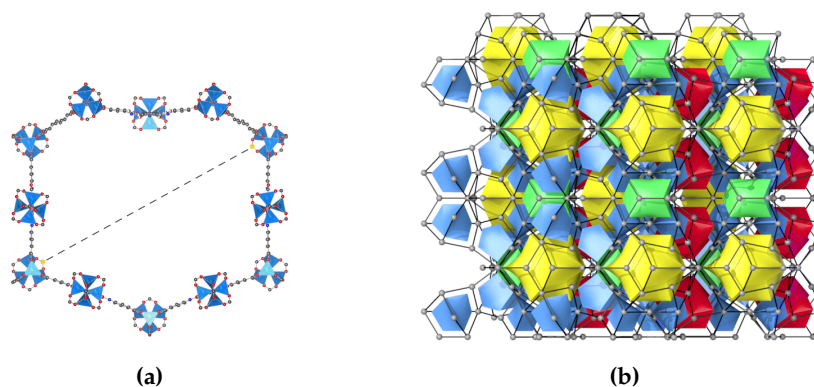**(a)**                                    **(b)**

**Figure 1.20** – Representation of DUT-32 with (a) the cross-section of the largest pore in DUT-32 (diameter 42 Å) (blue tetrahedra: zinc atoms, dark grey: carbon, red: oxygen) and (b) the underlying **umt** net together with the corresponding tiling; viewing direction along the crystallographic *b* axis of the unit cell (four distinct types of tiles represented as colored polyhedra, grey: vertices of the net, structural information obtained from CCDC number 968887).

Another MOF with a very high surface area has been synthesized in the group of Omar Yaghi.[35] MOF-210 is structurally related to DUT-32 as it is built from similar two- and three-connected organic SBUs as well as an octahedral inorganic SBU. However, the underlying **toz** net differs from the **umt** topology of DUT-32. The crystallographic density of MOF-210 of $0.25\,g/cm^3$ is slightly lower than in DUT-32 but the experimentally determined specific surface area $6240\,m^2/g$ is 2.7 % smaller. The structure of MOF-210 is shown as a topological representation in Figure 1.21. The MOF comprises three different pore types. The largest of those pores is shown as a cross-section in 1.21a and corresponds to the blue tile in the topological representation.

Among the record-holding MOFs with regard to the specific surface area is NU-110.[36] This MOF comprises relatively long hexatopic carboxylate linkers and copper paddle-wheels as the inorganic SBU. For this material, a specific surface area of $7140\,m^2/g$ has been achieved. The crystallographic density of $0.22\,g/cm^3$ is even lower than in DUT-32 and MOF-210. The underlying net of this MOF is **rht**. In structures that are based on this net the effect of interpenetration is mathematically precluded.
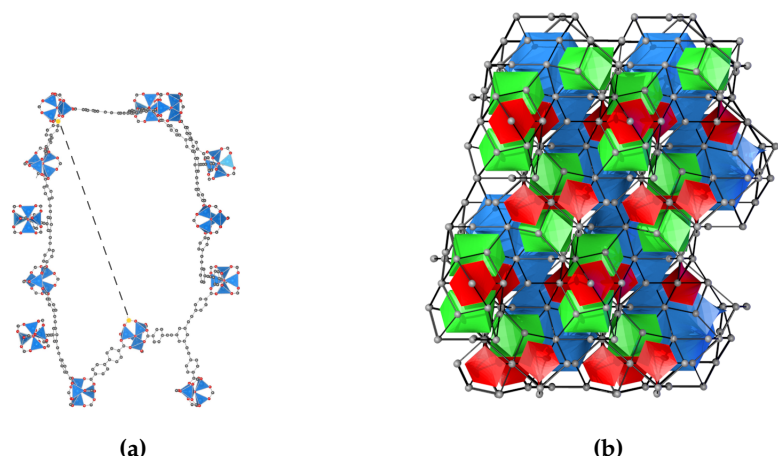
34

**(a)**                        **(b)**

**Figure 1.21** – Representation of MOF-210 with (a) the cross-section of the largest pore in this MOF (diameter 45 Å) (blue tetrahedra: zinc atoms, dark grey: carbon, red: oxygen) (b) the underlying **toz** net together with the corresponding tiling; viewing direction along the crystallographic *b* axis of the unit cell (three distinct typed of tiles represented as colored polyhedra, grey: vertices of the net, structural information obtained from CCDC number 775693).

## 1.4.1 Activation

Aristotle expressed the idea that "Nature abhors a vacuum." meaning that empty spaces are unnatural and contradict the laws of nature.[37] This idea partly holds true for MOFs. The empty space that is often depicted in MOF structures is not generated spontaneously during the preparation of the MOF. After a conventional MOF synthesis the potential void space is always filled with solvent molecules. In order to obtain permanent porosity in a framework, MOFs have to be *activated*, meaning that the solvent molecules that occupy the pores have to be removed while keeping the porous structure intact.[38] Materials with empty pores and a stable framework structure are described as exhibiting *permanent porosity*. The removal of a solvent can, in principle, be performed by evaporation. Thus, a very straight-forward approach for activation would include a simple heating of the material to force solvent molecules out of the pores into the gas phase. However, solvents used in the synthesis of MOFs such as *N*,*N*-dimethylformamide (DMF) have very high boiling points. Hence, the temperature needed for a simple thermal activation can exceed the temperature of degradation of the

MOF. Therefore, only very stable MOFs allow thermal activation. This is for example the case for UiO-66 (see Figure 1.4), a material that is stable up to 500 °C and can withstand the strong surface tensions and capillary forces that occur during the evaporation of high-boiling solvents.[24]

In many cases the high-boiling solvents that are required for the synthesis of MOFs can be replaced with low-boiling solvents after the MOF has been synthesized. The intermolecular interactions of lower boiling solvents are weaker than in a high boiling solvent, which means that surface tension and capillary forces can be minimized by such an *solvent-exchange*.[38] Even though the forces that can harm the framework of a MOF can be minimized, they do still exist for the liquid-to-gas phase transition and can impede the complete activation of a MOF. But alternative strategies can be applied to avoid these hindering forces. This can be achieved by avoiding the direct liquid-to-gas phase transition. This can be realized by sublimation of a suitable solvent or via a phase transition to a supercritical fluid. The strategies and their pathways are schematically shown in Figure 1.22.
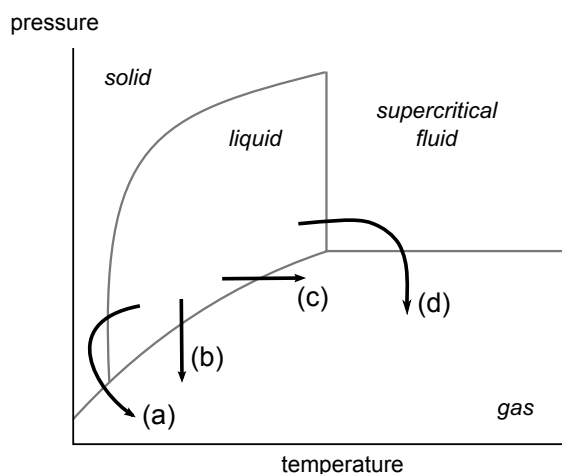


**Figure 1.22** – Schematic representation of a hypothetical phase diagram and pathways for the different strategies for the activation of porous materials. (a) Freezing and sublimation of the pore-filling solvent, (b) evaporation by reduced pressure, (c) thermal activation, (d) and conversion to a supercritical fluid followed by evaporation.

One approach to circumvent capillary forces employs a freeze-drying procedure to bypass the liquid-to-gas phase transition via the solid state of the solvent. This method has first been demonstrated by Lin and co-workers.[39] In

their reported procedure, DMF is replaced by benzene. The suspension of the MOF was cooled and the frozen organic solvent was sublimated in vacuum. An improvement of this method uses cyclohexane instead of the rather toxic benzene.[40] Both of these methods proceed via pathway (a) that is shown in Figure 1.22.

Another approach that relies on supercritical $CO_2$ has been applied to MOFs by Hupp and co-workers.[41] This procedure that corresponds to pathway (d) in Figure 1.22 has also been proven successful for the activation of other delicate porous materials such as aerogels.[42] This process usually employs a solvent exchange from the solvent of the synthesis to a solvent that is miscible with liquid $CO_2$. This solvent is then replaced with liquid $CO_2$ at elevated pressures within an appropriate chamber. Once this second solvent exchange is complete, the temperature of the chamber is raised above 31 °C to obtain $CO_2$ in the supercritical state. No capillary forces are active during the phase transition from the supercritical to the gaseous state. This makes the activation with $CO_2$ a vital method for the preparation of MOFs with ultra-high porosity such as the MOFs DUT-32 or MOF-210 which have been presented above (see 1.4, page 33).

## 1.4.2 Pore Filling

MOFs with large surface areas (such as DUT-32 or MOF-210) are prospective materials for the storage of gases such as methane.[43] Other applications use MOFs to store hydrogen[44,45] or carbon dioxide.[46,47] Apart from these sorption properties of gases, the pores of MOFs can be filled with a great variety of other substances. In the following section some instructive examples are being presented beginning with the inclusion of small organic compounds. Furthermore, examples are shown in which larger guests such as metal nanoparticles and proteins are included in the void space of the MOF.

With regard to the uptake of small organic molecules, some MOFs have been evaluated as carrier materials for drug delivery. In this context, drugs such as azidothimidine triphosphate, which is an antiretroviral drug for the treatment of HIV/AIDS (see Figure 1.23, have been deposited in the voids of MOFs that match their specific size. As the pore structure of MOFs can be tailored to a certain degree, controlled release mechanisms are possible that rely on the bio-degradation of MOFs.[48–51] Therefore MOFs that are employed in this context are preferably built from non-toxic inorganic SBUs containing only bio-compatible metal ions such as iron(III).

With growing pore sizes larger compounds can be introduced into the pore system of a MOF. Careful selection of appropriate pore sizes within a MOF allows for trapping of metal nanoparticles into mesoporous cages.[52] This can be done for example by an in situ reduction of a Pd(II) precursor in the pores of
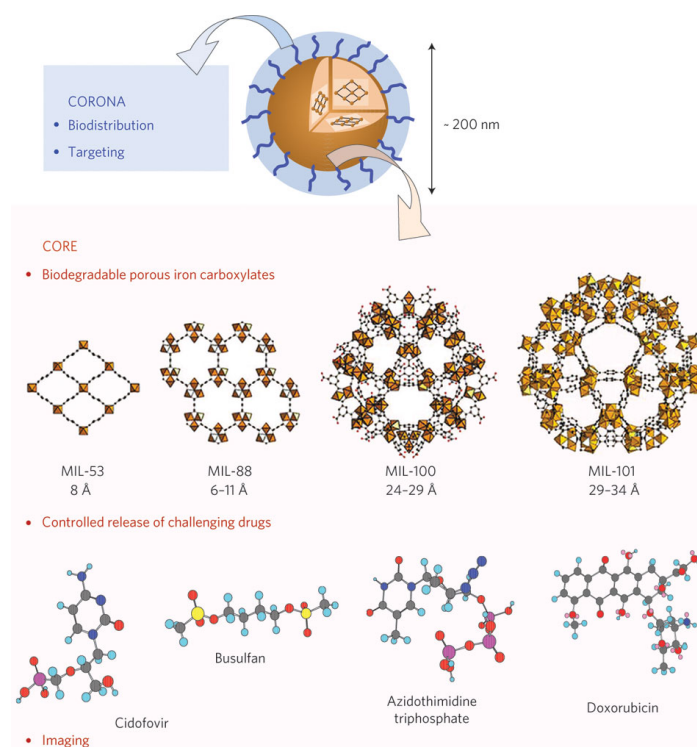
**Figure 1.23** – Overview of iron-based MOF particles used for the delivery of four different drugs that can be included in the pores. Reprinted with permission from Reference [48].

MIL-101.[53] The encapsulated palladium nanoparticles exhibit catalytic activities and benefit from the stabilizing framework, because the spatial separation inhibits the aggregation of the nanoparticles. Thereby the reusability is drastically increased. Leaching of the metal nanoparticles is minimized because the 26 Å palladium nanoparticles fit very well into the 29 Å and 34 Å pores of MIL-101. Such MOF based nanoparticles have been successfully used for example in the catalytic arylation of indoles.[54]

Recent advantages in host/guest chemistry even include proteins as pore-filling substances in MOFs. The inclusion of biomolecules requires relatively large mesopores. This has, for example, been realized with IRMOF-74XI, a MOF synthesized in the group of Yaghi.[55]

This MOF features one-dimensional channels with an extremely large diameter of 98 Å. These channels are large enough to include myoglobin, a globular protein that has the spherical dimensions $21 \times 35 \times 44$ Å, and the green fluorescent protein (GFP), which is a 45 Å long, barrel-shaped protein with a diameter of 34 Å.[56] The structure of this MOF and the GFP that can be included in the pores are shown in Figure 1.24 together with the tremendously long linker used to build this MOF.
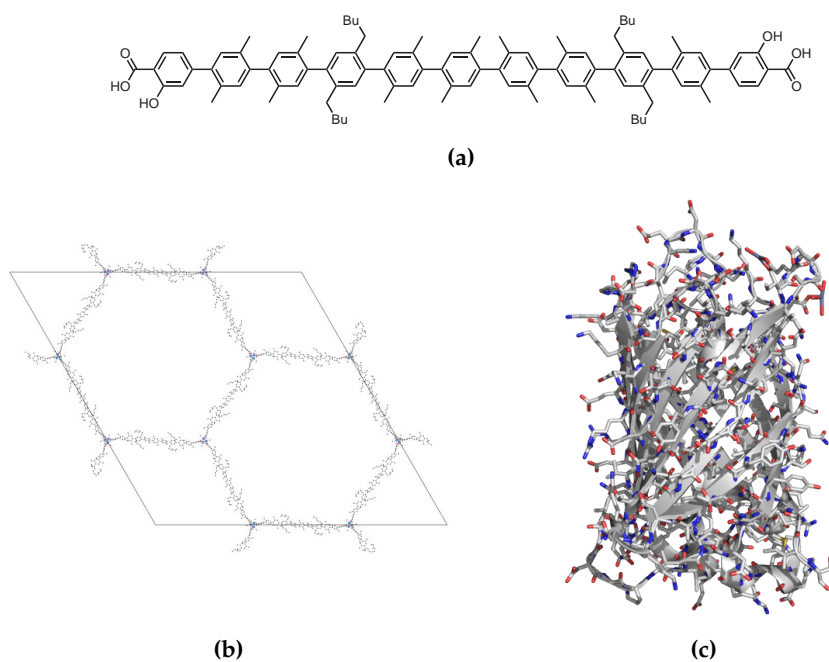
**(a)**



**(b)**



**(c)**

**Figure 1.24** – (a) The 50 Å long, linear linker used in the synthesis of MOF-74-XI. (b) Extended unit cell of the crystal structure of MOF-74-XI viewed along the crystallographic *c* axis with one-dimensional, hexagonal pores with a diameter of 98 Å (hydrogen atoms and solvent molecules are omitted, structural information obtained from CCDC number 841651). (c) Representation of the green fluorescent protein (GFP), which fits well into the pores of MOF-74-XI (ribbon drawing with side chains as sticks, red: oxygen, blue: nitrogen, structural information obtained from pdb entry 1KYS).

## 1.5  Chirality



**Scheme 1.1** – Selegiline (**1**) which is used in the treatment of Parkinson's disease and its harmful (*S*)-configurated isomer (**2**).

Objects are chiral if they are distinguishable from their mirror images. This is the case for the two molecules in Scheme 1.1 which have the same formula, an identical constitutional structure and only differ in the absolute configuration of the carbon atom that is highlighted in blue. However, for the treatment of Parkinson's disease, only the (*R*)-enantiomer (selegiline, **1**) is administered, because the metabolism of the optical isomer (**2**) would lead to harmful byproducts. Selegiline (**1**) is metabolized in the human body to D-methamphetamine.[57] Consequently the optical isomer would be metabolized to L-methamphetamine which is an infamous illicit drug known as "crystal meth" that has tremendous harmful effects.[58–60]

As can be seen from this example, the inversion of the absolute configuration of a useful pharmaceutical and its metabolites can render them useless or even harmful.[61] This has led regulatory authorities to require the production of stereochemically pure drugs, whenever possible.[62] Therefore, the preparation of enantiomerically pure compounds and the separation of racemic mixtures play important roles in the pharmaceutical industry. Solid-supported reagents that can provide so-called chiral information to substrates are highly interesting to pharmaceutical manufacturing.[63,64]

### 1.5.1  The Chiral Pool

Nature provides a vast collection of enantiopure compounds which are gathered under the term *chiral pool*. Enantiopure compounds can be found for the general classes of natural products, such as carbohydrates, alkaloids, terpenes, and amino acids. Examples for each of these classes are shown in Scheme 1.2.

The members of the chiral pool can be useful building blocks in the stereoselective synthesis of chiral compounds.[65] Strategies that exploit the chiral pool, preserve and build upon the chiral information that is provided in the starting materials. Amino acids are particularly interesting starting materials for the synthesis of MOFs for several reason: First, they are abundant and readily available.

| carbohydrates | alkaloids | terpenes | amino acids |
|:---:|:---:|:---:|:---:|
| **3** | **4** | **5** | **6** |
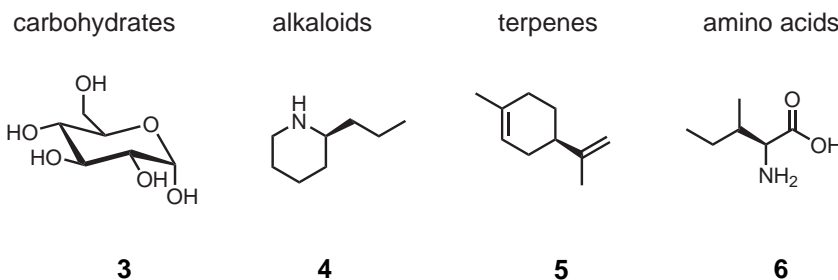
**Scheme 1.2** – An exemplary collection of members of the chiral pool: D-glucose (**3**), (*S*)-coniine (**4**), (*R*)-limonene (**5**), and L-isoleucine (**6**).

Second, the carboxylic group on these compounds constitutes an attractive target for further modification. Third, they are available with numerous different substituents on the β position, ranging from aliphatic to heterocyclic residues.

## 1.5.2   Organocatalysis

Reactions catalyzed by small organic molecules have received substantial attention in the past decade.[66–71] Organocatalysis offers several advantages compared to reactions with conventional catalysts. The absence of potentially harmful metals permits the use in environmentally friendly applications that follow the philosophy of green chemistry.[72] Additionally, organocatalysts may offer greater cost-efficiency because the catalysts are often easily obtained or synthesized from natural sources and because they are stable to air and moisture.[73] Furthermore, the application of enantiopure organic molecules allows the induction of stereochemical information on the substrates of the reaction with great success.[74]

A very popular pathway in organocatalysis involves the formation of enamines as a reactive species.[75] This is also the active intermediate in the so-called Hajos-Parrish-Eder-Sauer-Wiechert reaction, which was developed in the 1970s.[76,77] In this aldol addition, the excellent capability of proline to control the stereochemistry in an organocatalytic reaction were demonstrated for the first time. The reaction that is shown in Scheme 1.3 proceeds with quantitative yields and an excellent enantioselectivity of $ee = 93\%$[5] to give the bicyclic ketone **8** which is an important intermediate in the synthesis of steroids.

---

[5]enantiomeric excess (*ee*): $\frac{m_1 - m_2}{m_1 + m_2}$; $m_1$ : mass of enantiomer 1, $m_2$ : mass of enantiomer 2
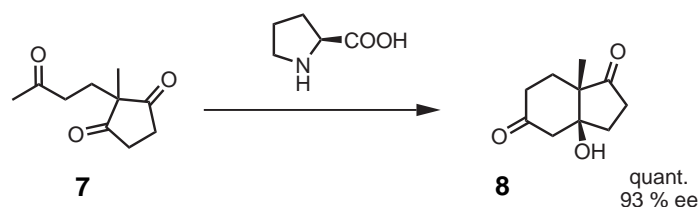
**Scheme 1.3** – Intramolecular cyclization of triketone **7** in the Hajos-Parrish-Eder-Sauer-Wiechert reaction catalyzed by L-proline yields the aldol product **8** with excellent stereochemical induction.

The mechanism of this intramolecular cyclization has been investigated thoroughly. The reaction mechanism as proposed by Clemente and Houk is depicted in Scheme 1.4.[78] In the first step of the reaction, the exocyclic carbonyl group of the substrate reacts with the secondary amine of the proline. An enamine is formed. The reaction step that defines the configuration of the newly formed stereocenters involves the formation of a six-membered Zimmermann-Traxler transition state. In this transition state a stabilizing interaction occurs between the carboxyl group of the proline and a ketone on the substrate via hydrogen bonding. As can be seen from the transition state **10** the bifunctional nature of the catalyst is decisive for the stereochemical outcome of the reaction, as both the amine and the carboxylic group participate in the stereo-defining step. Hence, a chiral amine alone cannot control the stereochemical outcome of the reaction to the same extent as proline.

The groundbreaking discoveries in the context of the Hajos-Parrish-Eder-Sauer-Wiechert reaction have sparked the interest in proline derived systems as organocatalysts not only in enamine catalysis but also *via* the formation of iminium ions.[79] Although the first examples were reported in the 1970s, the enormous potential asymmetric organocatalysis was only discovered during the last ten years when systems were established that are structurally similar to proline. An exemplary collection of these systems is shown in Scheme 1.5. The catalysts that feature the prolinol and prolinol silyl ether motif were independently developed by the groups of Jørgenson and Hayashi and have found application not only in aldol reactions but also in asymmetric α-amination, α-halogenation and conjugate additions.[80–84] Enamine catalysis with prolinol-type catalysts such as **12** is less straightforward than with the corresponding ethers (**13**), because the unprotected hydroxyl group can be involved in a parasitic intermediate during the catalytic cycle.[85] However, a rising number of reactions have been reported involving prolinol type catalysts.[86,87] Sophisticated variations of five-membered secondary amines have been developed in
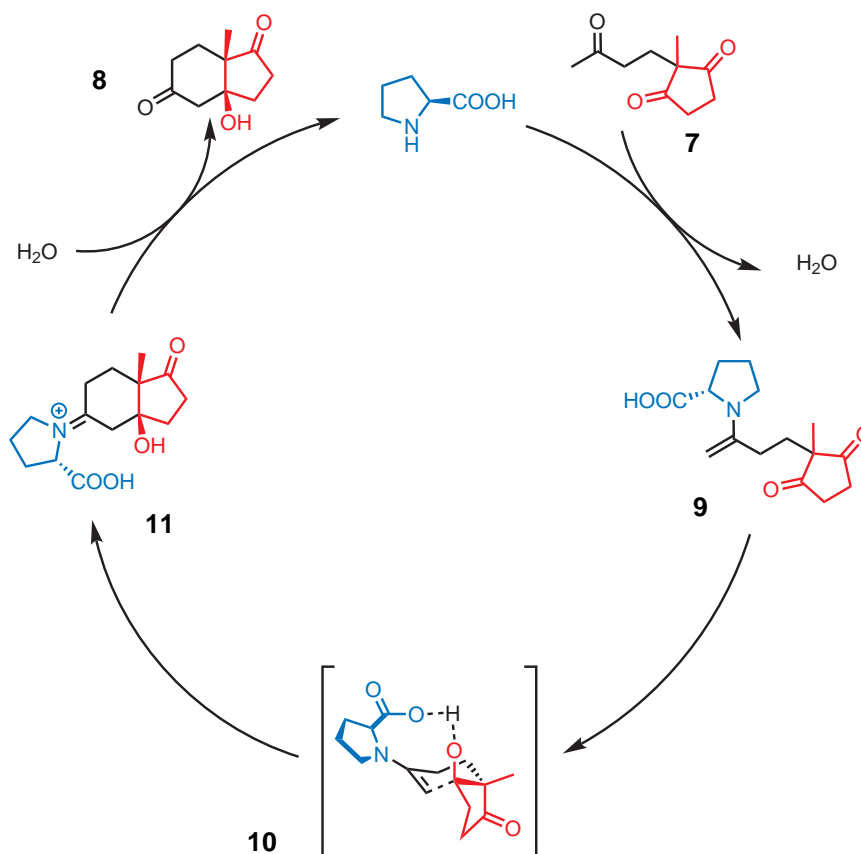
**Scheme 1.4** – Mechanism of the Hajos-Parrish-Eder-Sauer-Wiechert reaction catalyzed by L-proline: Induction of stereochemical information is achieved in a six-membered transition state and a stabilizing hydrogen bond interaction between the carboxylic group of proline and a carbonyl group on the substrate.

the group of MacMillan. Highly substituted imidazolidinone catalysts such as **14** have extended the scope of such organocatalysts to enantioselective Diels-Alder cycloadditions, Michael additions and Friedel-Crafts alkylations.[88–90]
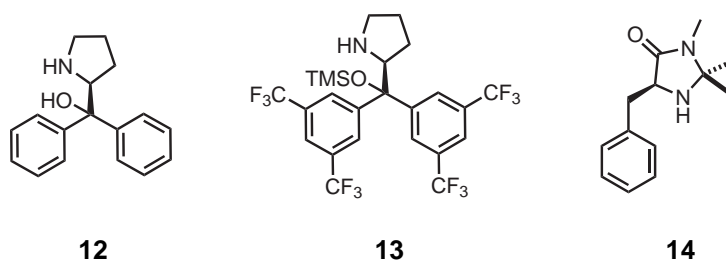


**Scheme 1.5** – Organocatalysts based on secondary amines that are part of five-membered heterocycles. The compounds **12** and **13** are directly derived from L-proline. The MacMillian catalyst (**14**) is obtained from L-phenylalanine.

## 1.6   Chirality in MOFs

Porosity and a very high density of accessible functional groups are relevant assets that make certain MOFs viable candidates for stereoselective, heterogeneous processes such as catalytic transformations or separations of stereo isomers. There are three complementary strategies available to synthesize chiral MOFs which can be divided into the following categories:

- Crystallization of achiral building blocks in a chiral space group

- Coordination of enantiopure ligands[6] to the inorganic SBU of the MOF

- Assembly of the MOF from enantiopure linker molecules

In the following sections, examples are given that illustrate these three approaches. These examples will focus primarily on the structural features of these materials and applications of the homochiral MOFs will be treated in Section 1.7.

### 1.6.1   Chiral Resolution

It is generally possible to assemble chiral materials from achiral building blocks. [91] To yield a chiral MOF these building blocks must be organized into a chiral arrangement within the three-dimensional structure of the crystal.[92,93] This

---

[6]These ligands bind to individual inorganic SBUs but to not participate in their interconnection.

behavior can indeed be observed in the formation of MOFs.[94–104] However, these forms of spontaneous resolution generally lead to racemic bulk materials with 1:1 mixture of left- and right handed crystals. Yet it has been shown that spontaneous resolution can be steered by a homochiral solvent or homochiral additives during the synthesis of the MOF.[105–108] An impressive example of the procedure has been demonstrated by the group of Duan.[109] They reported the homochiral crystallization of the two enantiomorphic MOFs Ag-1 and Ag-2 from a three-connecting pyridine imine linker and a silver salt. In these MOFs the silver atoms are tetrahedrally coordinated by two bidentate ligands from two individual linker molecules. An arrangement of two organic SBUs around a two-connected silver ion is shown in Figure 1.25.
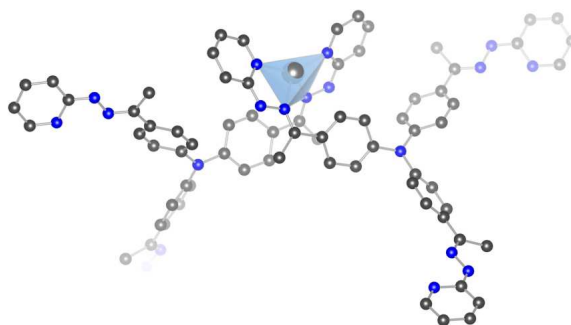


**Figure 1.25** – Representation of the distorted tetrahedral inorganic SBU of the homochiral MOF Ag-1, coordinated to two organic SBUs (blue tetrahedron to visualize the coordination figure of the silver, dark grey: carbon, blue: nitrogen, structural information obtained from CCDC number 860785).

The MOF crystallizes in the chiral space group $I2_13$. The silver atoms are located on a $2_1$ screw axis. The linkers connect three silver ions. The MOF Ag-1 is one example of a MOF where the metal ions are not topological nodes but only links. The underlying net of Ag-1 (and Ag-2 respectively) is the intrinsically chiral **srs** net. Figure 1.26 shows a representation of this net in which the red vertices of the net correspond to the three-connected linkers and the edges to the silver atoms of the MOF.

The induction of stereochemical information to the tetrahedrally coordinated silver ions was achieved by using chiral templates. The homochiral alkaloids cinchonine (**16**) and cinchonidine (**17**) were used to control the absolute stereochemistry of the MOF. These templates most likely also serve as bidentate ligands to the silver ion and are subsequently replaced by two of the linker mole-
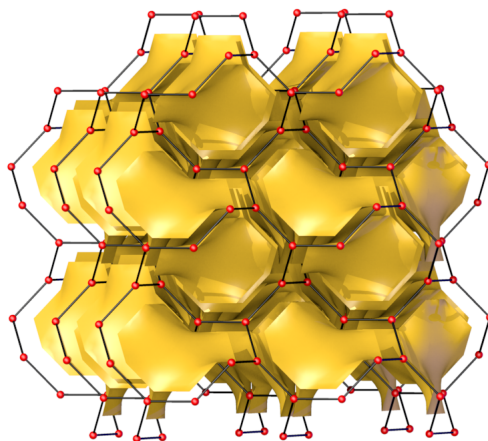
**Figure 1.26** – Topological representation of the homochiral MOF Ag-1 together with a natural tiling of the underlying **srs** net, red vertices correspond to the organic SBU, edges of the net correspond to the silver ions.

cules during the synthesis of the MOF (see Scheme 1.6).[109] The template molecules provide a chiral environment in the coordination sphere of the silver ions that is reproduced when the linker molecules coordinate to the silver. By incorporation into the framework the linker adopts a chiral conformation, which permits the transfer of the stereochemical information from one silver center to another. The two possible configurations of the coordinated silver atom is shown in Figure 1.27.

In the case of the MOFs Ag-1 and Ag-2 described above the chirality of the framework originates from a ligand that is temporarily bound to the inorganic SBU but absent in the final framework. A similar approach to chiral MOFs has been reported by the same group. They synthesized a cerium-based MOF from 5,5′-methylene-di-isophthalate (mdip) (**18**) in the presence of D- or L-*N-tert*-butoxycarboxyl-2-(imidazole)-1-pyrrolidine (see Scheme 1.6). The chiral component of this reaction system is absent in the resulting enantiomeric framework structures Ce-MDIP1 and Ce-MDIP2, respectively. These MOFs exhibit chiral channels with a cross-section of $10.5 \times 6.0\,\text{Å}^2$ as well as potential open metal sites that permit their use as heterogeneous, asymmetric catalysts (see section 1.7).
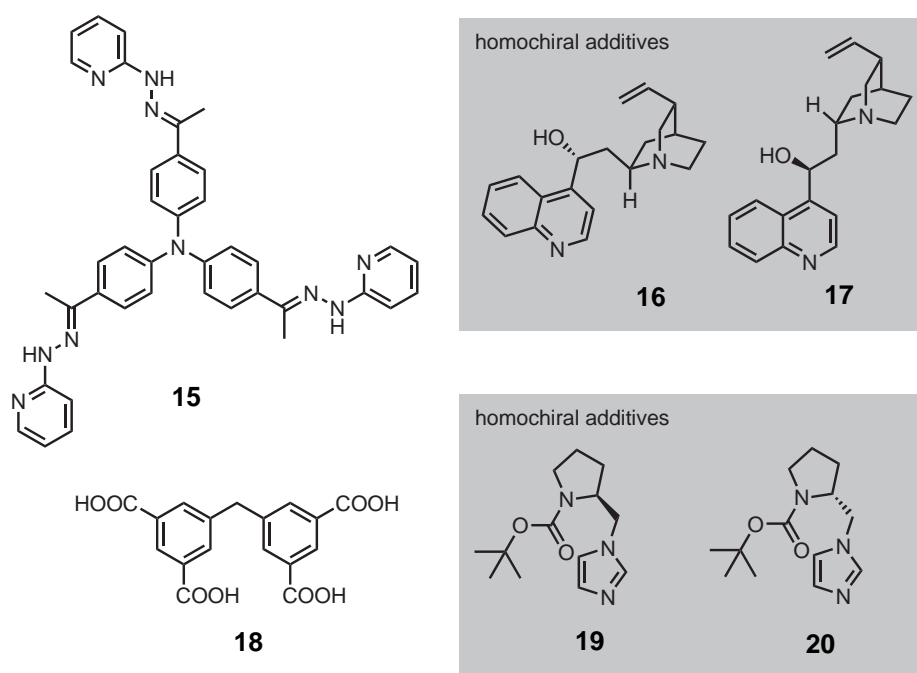
**Scheme 1.6** – Representation of achiral linkers together with chirality inducing additives used in the synthesis of homochiral MOF. Tritopic linker **15** and the homochiral additives cinchonine (**16**) or cinchonidine (**17**) are used in the synthesis of Ag-1 and Ag-2, respectively.[109] Tetracarboxylate **18** and the enantiomers of *N-tert*-butoxycarboxyl-2-(imidazole)-1-pyrrolidine are used in Ce-MDIP1 and Ce-MDIP2, respectively.[110]
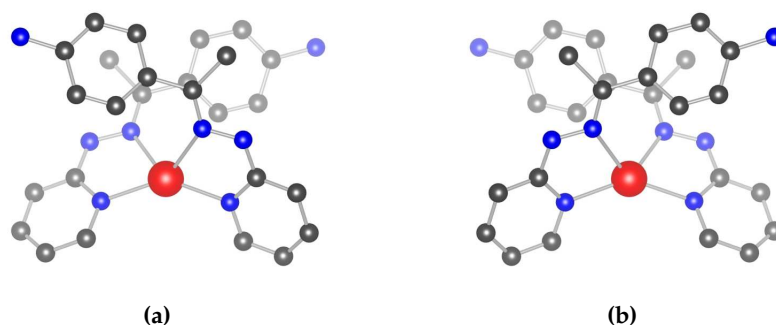
**(a)** **(b)**

**Figure 1.27** – Representation of the different stereochemical configurations in the silver based Ag-MOFs Ag-1 (a) and Ag-2 (b). (grey: carbon, blue: nitrogen, red: silver, hydrogen atoms are omitted, structural information obtained from CCDC number 860785).

## 1.6.2 Homochiral Inorganic Secondary Building Units

Other approaches to obtain chirality proceed via the modification of the inorganic SBU and employ ligands that remain present in the final structure of the MOF.[111–117] Impressive examples of this approach have been demonstrated by the group of Dybtsev.[118,119] They have synthesized homochiral MOFs by the permanent inclusion of lactic acid and mandelic acid, respectively, into the inorganic SBU of a MOF. The resulting MOFs are isoreticular. The structure of the MOF with the formula $[Zn_2(bdc)(L\text{-}lac)(dmf)]$ is shown as an example in Figure 1.29. Upon the reaction of Zn(II), bdc, and lactic acid, a microporous material is obtained. This material comprises one-dimensional, rod-shaped inorganic SBUs. In this inorganic SBU, zinc ions are bridged by the carboxylates of the bdc linker and by lactic acid molecules which are coordinated to the zinc ions via carboxylate and the hydroxyl functional groups. A segment of the one-dimensional inorganic SBU is shown in Figure 1.28.

These homochiral inorganic SBUs are interconnected via the bdc linker which results in the formation of one-dimensional channels along the crystallographic *a* axis with a diameter of 5 Å. Figure 1.29 gives a structural representation along two viewing directions of a collection of several inorganic SBUs connected by the bdc linker and the respective pore system. This pore system has been intensively investigated for the application in the separation of enantiomers as well as stereoselective reactions which are listed in Section 1.7 (page 72).

In the case of the MOFs described above, an enantiopure ligand has been introduced to the framework during the synthesis of a MOF. However, the introduction of stereochemical information may also be achieved post-synthetically.
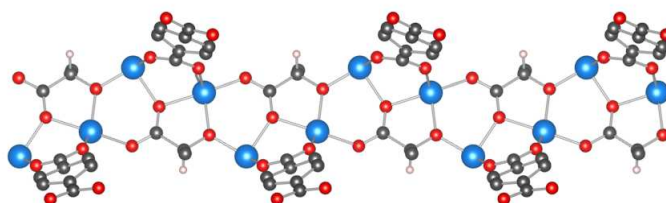
49

**Figure 1.28** – View along the *c* axis of the one-dimensional inorganic SBU of a homochiral MOF constructed from bdc and L-lactic acid (blue: zinc, grey: carbon, red: oxygen, hydrogen atoms in white are only shown for the lactic acid stereocenter, solvent molecules are omitted, structural information obtained from CCDC number 281753).

MIL-101 is is a chromium terephtalate framework that can exhibit coordinatively unsaturated site (CUS) and has relatively large pore sizes between 30 Å to 34 Å.[120] The inorganic SBU of MIL-101 is shown in Figure 1.30. It is a six-connected chromium-oxo cluster. Three positions of this cluster are originally occupied by water or other solvent molecules that can be removed upon activation.

The replacement of water from CUS with homochiral ligands was demonstrated by the group of Kim.[121] They introduced an enantiopure ligand with a coordinating pyridyl residue to MIL-101 after the actual synthesis of the MOF. This procedure is shown in Scheme 1.7. First, open metal sites are generated by heating MIL-101 for 24 hours at 150 °C in vacuum. This removes coordinated water molecules but not fluoride ions that originate from hydrofluoric acid used during the synthesis. The free coordination sites can now be occupied by (*S*)-*N*-(pyridin-4-yl)pyrrolidine-2-carboxamide which serves as a chiral ligand to the inorganic SBU. Thereby the achiral MIL-101 is switched to the chiral MOF CMIL-2. The ligand, which is derived from proline, contains a free secondary amine that can serve as an organocatalyst (see Section 1.7, page 70).

Such procedures that alter the previously synthesized framework are called post-synthetic modification (PSM) and are not only used at the inorganic SBU but more often target functional groups at the organic SBU.[122]

A similar approach to obtain two enantiomorphic, homochiral MOFs with a free homochiral secondary amine has been reported by the group of Duan.[123] However, in this case the chiral ligand that binds to the inorganic SBU has already been introduced during the synthesis of the MOF from 4,4',4''-tricarboxy-
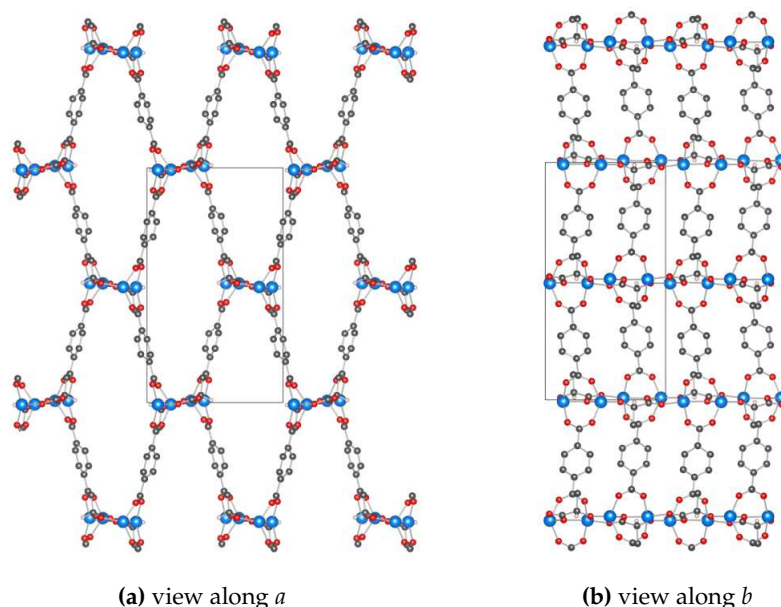
**(a)** view along *a*

**(b)** view along *b*

**Figure 1.29** – View along two crystallographic directions of an expanded unit cell of [Zn$_2$(bdc)(L-lac)(dmf)] made from lactic acid, bdc, and Zn(II) (blue: zinc, grey: carbon, red: oxygen, hydrogen atoms in white are only shown for the lactic acid stereocenter, solvent molecules are omitted).

phenylamine and Zn(II). The resulting structure is shown in Figure 1.31 and exhibits two-dimensional sheets with a honeycomb topology, in which both the organic SBU and inorganic SBU act as three-coordinated nodes. The inorganic SBUs are coordinated by one enantiomer of *N-tert*-butoxycarboxyl-2-(1-imidazolyl)-1-pyrrolidine which is the source of chirality in this MOF. [7] The two-dimensional sheets are stacked, forming one-dimensional channels with a cross-section of 12 Å × 16 Å. The chiral ligands on the inorganic SBU protrude into these pores and are in proximity of the triphenylamine moiety, allowing this MOF to be used as an asymmetric photocatalyst (see section 1.7, page 71).

Another approach to turn MIL-101 into a homochiral MOF has been demonstrated by Sels and co-workers. They synthesized a variety of MIL-101 in which a dicarboxylic acid was used that bears a sulfonic acid group.[124] The sulfonate does not participate in the formation of the framework but provides an acidic

---

[7]This compound has also been used as an additive in the stereoselective synthesis of Ce-MDIP1, see Scheme 1.6.
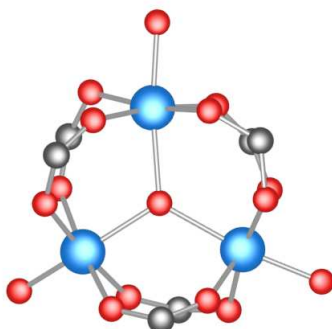
51

**Figure 1.30** – Six-connected inorganic SBU of MIL-101 that contains six car-boxylates that bridge three chromium ions, three positions are occupied by removable water molecules (grey: carbon, blue: chromium, red: oxygen, hydrogen atoms are omitted).

residue to the pore space of the MOF. Via a simple acid-base interaction it was possible to immobilize an enantiopure diamine in a MOF by a PSM. This diamine is derived from L-phenylalanine. A schematic representation of this attachment is shown in Figure 1.32

The examples above illustrate that it is possible to introduce stereochemical information to a MOF via the inorganic SBUs of a framework. This is especially interesting for a MOF like Ag-1, where the molecule that induces chirality can in principle be recycled. This permits the use of such compounds as some sort of "catalyst" in the formation of homochiral MOFs.

## 1.6.3 Homochiral Linkers

Many of the homochiral MOFs described in the literature are prepared from stoichiometrical amounts of chiral linker molecules. This approach has the advantage that the organic components can be designed with great detail and remain mostly unchanged during the preparation of a MOF, whereas the inorganic SBUs are typically formed during MOF synthesis. Thereby, the homochirality of a MOF can be controlled with greater precision by utilizing meticulously designed linkers to create homochiral MOFs.

In the following some examples for homochiral MOFs, which owe their stereochemical information to organic linkers, are given. One of the very first homochiral MOFs reported in the literature is D-POST-1 (Pohang University of Science and Technology). This MOF is obtained upon the reaction of Zn(II) with
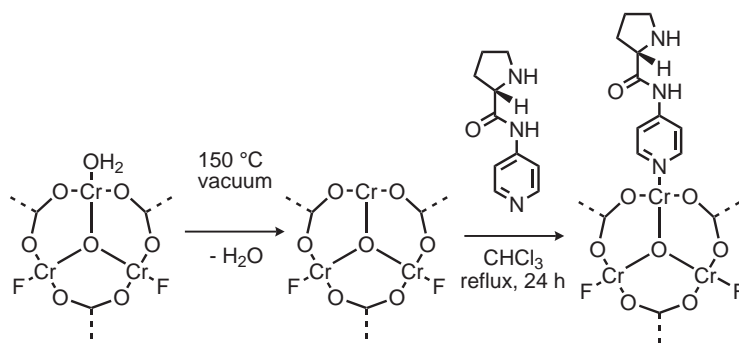
**Scheme 1.7** – Schematic representation of the PSM of an inorganic SBU of MIL-101, dashed lines indicate points of extension to the framework structure, heating in vacuum removes coordinated water molecules (but not fluoride ions), the free coordination sites can then be occupied by a chiral pyridyl ligand.
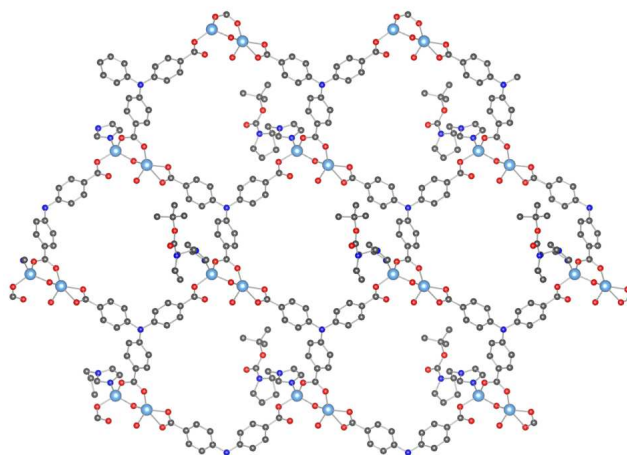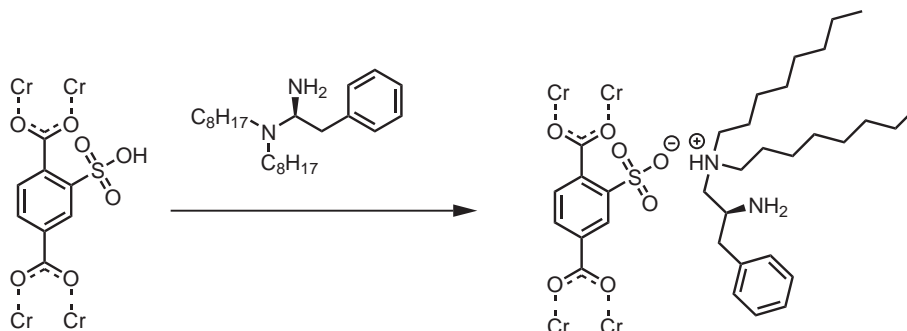


**Figure 1.31** – View along the *a* axis of the crystal structure of Zn-BCIP-1, (*S*)-*N-tert*-butoxycarboxyl-2-(1-imidazolyl)-1-pyrrolidine is coordinated to the inorganic SBU and is directed into the hexagonal pores, (structural information obtained from CCDC number 943903).

**Figure 1.32** – Schematic representation of the PSM of an organic SBU of MIL-101-SO$_3$H; dashed lines indicate points of extension to the framework structure.

an enantiopure derivative of tartaric acid.[125] This derivative is monosubstituted with a 4-amino-pyridyl substituent and the vicinal hydroxyl groups are protected as an acetal. This enables the linker to coordinate to a metal via a carboxylate group as well as a pyridyl group (see Scheme 1.8).
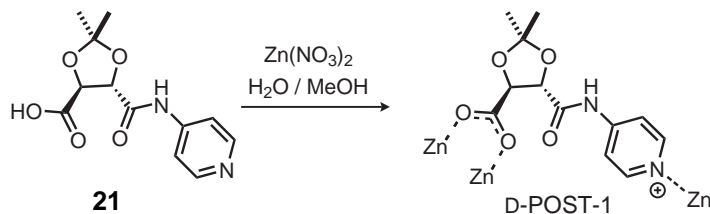


**Scheme 1.8** – Representation of the synthesis of D-POST-1 using a derivative of tartaric acid (**21**) that can connect to a metal *via* the carboxylic oxygen atoms and the nitrogen atom of the pyridyl group making this a bifunctional ditopic linker.

The inorganic SBU formed in D-POST-1 resembles the inorganic SBU of MIL-101 (see Figure 1.30) but is built from zinc ions instead of chromium ions. Two neighboring inorganic SBUs are connected via two linker molecules. In this arrangement the linkers coordinate to zinc with the bridging carboxylates and the pyridyl nitrogen atom. The coordination via nitrogen occupies the sites that correspond to the open metal sites in MIL-101. This is shown in Figure 1.33.

This connection between inorganic SBUs leads to the generation of two-dimensional infinite layers with hexagonal symmetry. These sheets stack onto
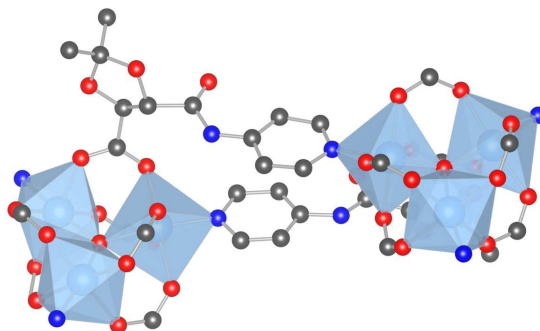
**Figure 1.33** – In D-POST-1 two neighboring inorganic SBUs are connected by two linker molecules (light blue octahedra: zinc, grey: carbon, red: oxygen, dark blue: nitrogen, hydrogen atoms are omitted, structural information obtained from CCDC number 212735).

each other along the crystallographic *c* axis and are held together by van der Waals interactions. This results in the formation of one-dimensional chiral channels with a cross-section of 13 Å. This pore system is shown in Figure 1.34.

The concept of reticular synthesis was also applied to obtain homochiral MOFs with an underlying **pcu** net.[126] An interesting example for this kind of materials is IRMOF-Pro-Boc that has been developed in the group of Telfer.[127] They employed a linker that is a derivative of amino-substituted 4,4'-biphenyl dicarboxylic acid to which proline has been connected via a peptide bond. The secondary amine of proline is protected with a Boc group. A schematic representation of the structure is given in Scheme 1.9. Only one organic SBU is drawn in detail. The rest of the structure is depicted as a cube that represents the underlying **pcu** net.

The length of linker **22** is the same as for the biphenyl linker used in the synthesis of IRMOF-10 (see Figure 1.15b). IRMOF-10 and related systems are prone to interpenetration,[28,128] which can be overcome by introducing bulky substituents to the linker such as a Boc group.[129] The Boc group in IRMOF-Pro-Boc can be cleaved thermolytically to obtain a free secondary amine (see Scheme 1.10). The liberation of the secondary amine generates a functional group in the MOF that may be used for stereoselective organocatalysis (see also Section 1.5.2, page 42).

Another MOF that has been developed using the reticular synthesis approach is DUT-32-NHProBoc.[130] This compound is isoreticular to the highly porous MOF DUT-32 that has already been depicted in Figure 1.20 (page 34). The resulting MOF is a mixed-linker system in which the two-connected dicarboxy-
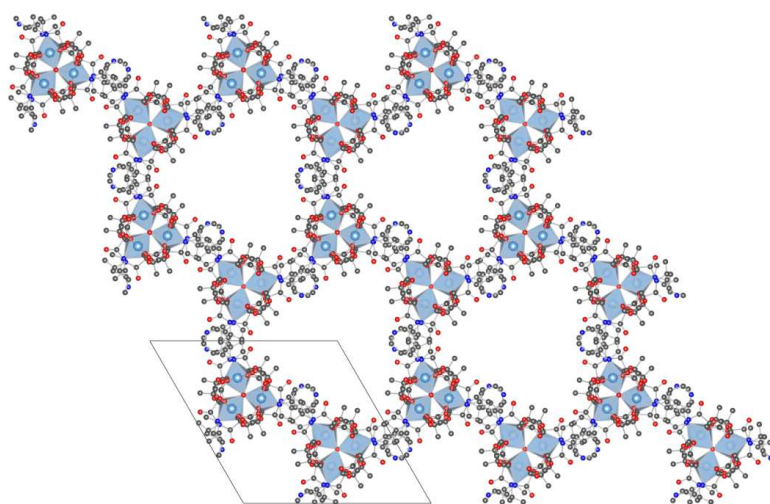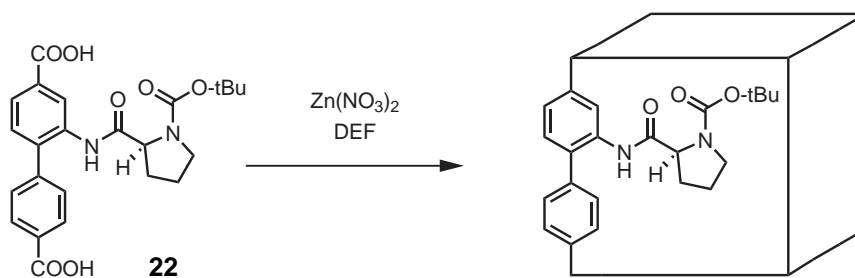
**Figure 1.34** – view along the crystallographic *c* axis of an expanded unit cell of D-POST-1; a hexagonal pore system is formed that consists of one-dimensional channels (light blue tetrahedra: zinc, grey: carbon, red: oxygen, dark blue: nitrogen, hydrogen atoms are omitted, structural information obtained from CCDC number 212735).



**Scheme 1.9** – Schematic representation of the preparation of IRMOF-Pro-Boc that is isoreticular to the IRMOF series. The underlying **pcu** net is represented as a cube, the linker employed in this synthesis carries a chiral secondary amine with an *N*-Boc protective group.
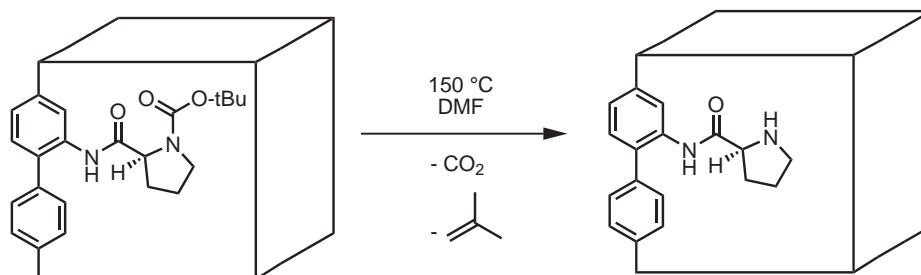
**Scheme 1.10** – Deprotection of IRMOF-Pro-Boc by thermolytic cleavage of the Boc group yields IRMOF-Pro, $CO_2$ and isobutene as volatile by-products, only one organic SBU is shown and the framework structure is simplified as a part of the underlying **pcu** net.

late was exchanged with the same *N*-Boc protected proline derivative (**22**) that has been used in the synthesis of IRMOF-Pro-Boc. In DUT-32-NHProBoc, the large mesopores known from DUT-32 are decorated with chiral amine substituents. The crystal structure is shown in Figure 1.35 together with the four distinct types of pores (I–IV) present in this MOF. In DUT-32-NHProBoc, the Boc group can be cleaved under similar conditions as shown for IRMOF-Pro-Boc in Scheme 1.10. However, this is accompanied by a loss of stereoinformation on the chiral substituent.[130] The deprotected DUT-32 derivative has also been investigated with respect to its catalytic properties (see section 1.7, page 69). By applying the principles of reticular chemistry, the same group has prepared a MOF that is isoreticular to HKUST-1 with a linker that bears three chiral 1,3-oxazolidin-2-one substituents.[131]

In the examples listed above, molecules with one or more stereogenic centers were employed as a source of stereoinformation. Linkers with axial chirality have been successfully integrated into MOFs by the groups of Lin,[132–138] Tanaka[139,140] and others[141–144] An impressive example of the use of this type of linker is the isoreticular series of CMOF-1 to CMOF-4.[145] Three of the linkers used in the synthesis of this series are shown in Scheme 1.11. The binaphtyl tetracarboxylate is incrementally elongated by an addition of ethylene or phenyl units. The adjacent hydroxyl groups on the naphtyl rings constitute the BINOL motif that is commonly found in transition metal catalysis.[146]

The crystal structure of the CMOF-1a is depicted in Figure 1.36. This MOF is constructed from **23**. The linkers serve as four-connected nodes with a distorted tetrahedral geometry. The inorganic SBUs in the CMOF series are four-connected copper paddle-wheels that act a square-planar nodes. The underly-
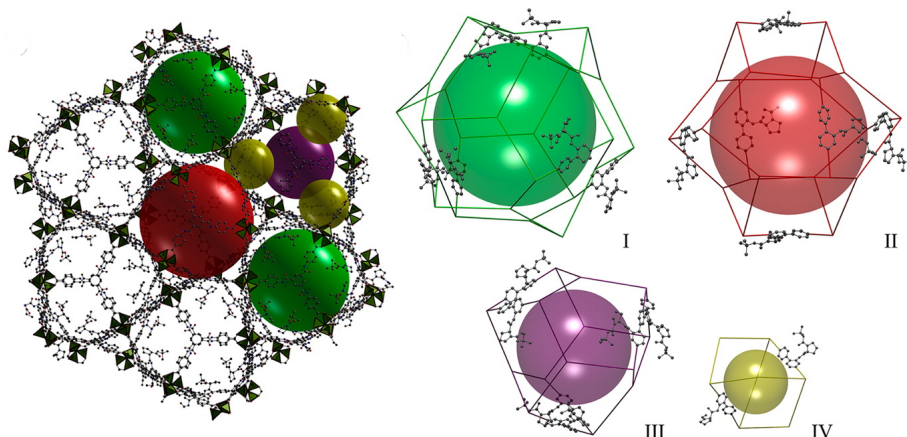
**Figure 1.35** – Crystal structure of DUT-32-NHProBoc together with parts of the underlying net that surrounds the four distinct pore types; the organic SBU bearing the chiral substituent is shown as a decoration of the underlying net (green tetrahedra: zinc, grey: carbon, red: oxygen, blue: nitrogen, hydrogen atoms are omitted). Adapted with permission from Reference[130]



**23**
CMOF-1b

**24**
CMOF-2b

**25**
CMOF-3b
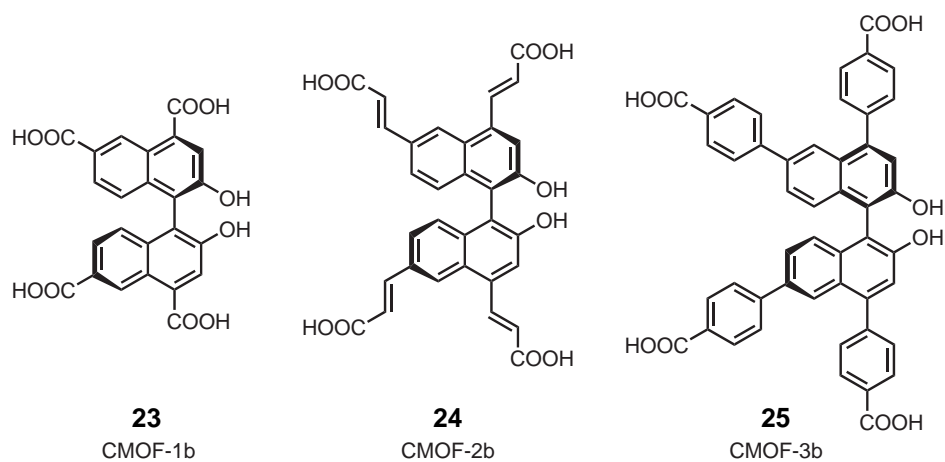
**Scheme 1.11** – Three of the linkers used in the synthesis of the isoreticular series of CMOFs.

ing net of the CMOF series is classified as **wbl** and is shown in Figure 1.36 in its augmented form, meaning that the organic nodes are represented by distorted tetrahedra and the inorganic nodes as squares. CMOF-1 exhibits interconnected channels that have a diameter of 8 Å to 13 Å.
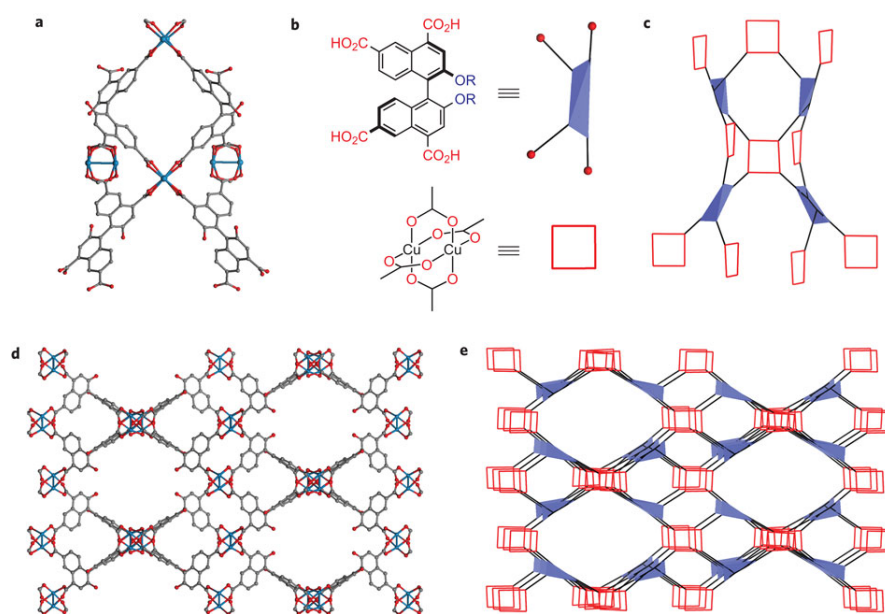


**Figure 1.36 – a)** Three-dimensional representation of the linkers and paddle-wheels in CMOF-1b. **b)** Representation of the linker as a distorted tetrahedral node (light blue polyhedron) and the copper paddle-wheel as a square-planar node (red square) **c)** augmented net representation of the arrangement of inorganic SBUs and organic SBUs from a. **d)** view along the crystallographic *a* axis showing the pore structure of CMOF-1, **e)** augmented net representation of the structure as depicted in d.(grey: carbon, blue: copper, red: oxygen, hydrogen atoms are omitted). Reprinted with permission from[145]

Because the naphtyl rings are locked in a twisted arrangement to each other, a dihydroxyl functionality, which is available for further modification, is present in a chiral environment. Consequently, the free hydroxyl groups in this framework has be modified post-synthetically with a very reactive transition metal species under an inert atmosphere.[145] By subjecting the MOF to a solution of Ti(O*i*Pr)$_4$ in dry toluene a (BINOLate)Ti(O*i*Pr)$_2$ species can be generated inside the pore system of the CMOF series. This is schematically shown in Figure 1.37.

This modification of CMOF-1b permits its use as an asymmetric heterogeneous catalyst. An application of this MOF is described in section 1.7.

Other strategies to obtain catalytically active transition metal centers in the pores of a MOF employ linker molecules that contain stable, homochiral complexes, such as metal salen compounds.[147–150]
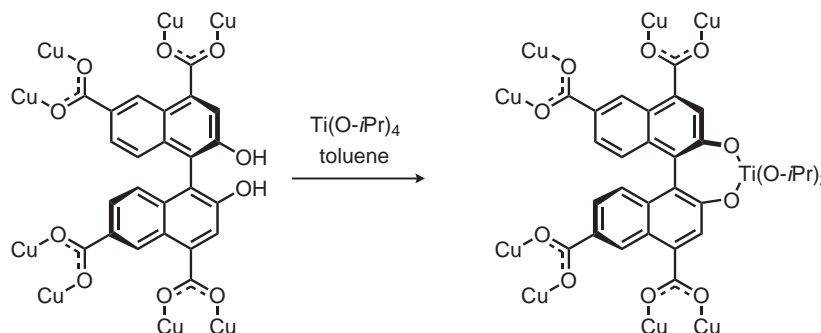


**Figure 1.37** – Post-synthetic modification of CMOF-1b to immobilize a catalytically active Ti(IV) species to the organic SBU, using a solution of Ti(O$i$Pr)$_4$ in toluene.

As described in section 1.5.1, nature provides a vast collection of enantiopure compounds that can be exploited for organic synthesis. This rich resource has been used in numerous ways to create homochiral MOFs from naturally occurring chiral molecules and their derivatives. The following examples may serve as an overview on how the principles of chiral pool synthesis are applied to the field of MOFs.

Evidently, enantiopure oligocarboxylates that can be obtained from natural sources should be ideal choices for the construction of MOFs, because they may readily provide chirality to a framework. This approach has been chosen by Bu and co-workers who synthesized a number of homochiral MOFs from different metal ion sources using D-camphoric acid (cam, **26**, see Scheme 1.12) and 4,4′-bipyridine (bipy) linkers.[151] The crystal structure of the copper-based MOF Cu$_2$(D-cam)$_2$(4,4′-bipy) is shown in Figure 1.38. Copper ions and the carboxylic groups of the camphoric acid form a paddle-wheel motif. This results in the formation of two-dimensional sheets of copper paddle-wheels and the camphorate linker in the crystallographic *bc* plane. A three-dimensional connectivity is attained by the bipy molecules that coordinate to the axial positions of the copper paddle-wheels and thereby act as spacers between the sheets. Due to the diagonal orientation of the bipy spacer, the resulting crystal structure is rather dense with a spacing of about 10 Å between the two-dimensional sheets.
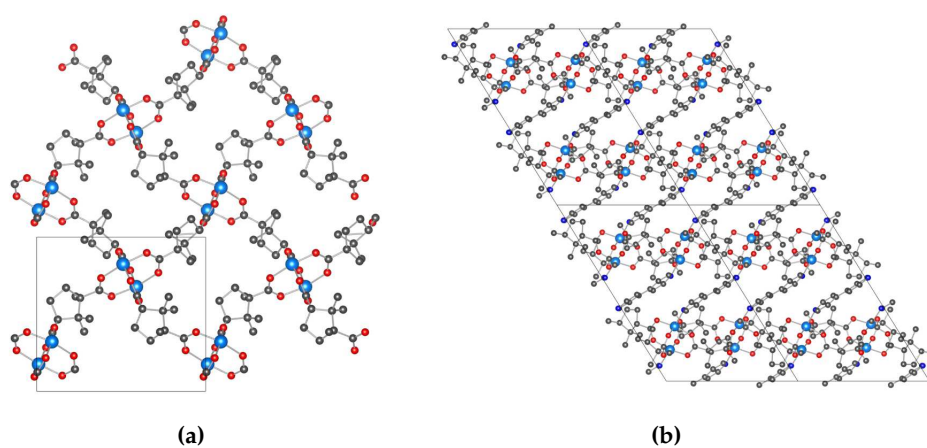
**(a)**                                    **(b)**

**Figure 1.38** – (a) view along the *a* axis onto a two-dimensional sheet formed by the carboxylate of linker **26** and copper paddle-wheels (b) view along the *b* axis of a $2 \times 2 \times 2$ supercell of $Cu_2(D\text{-cam})_2(bipy)$, two-dimensional layers of interconnected copper paddle-wheels are bridged via their axial positions (grey: carbon, light blue: copper, red: oxygen, dark blue: nitrogen, structural information obtained from CCDC number 631724).

The amino acids aspartic acid (**27**) and glutamic acid (**28**) are naturally oc-curring dicarboxylic acids that are in principle able to act as ditopic linkers in the synthesis of MOFs (see Scheme 1.12). However, these molecules are very flexible. This makes it difficult to obtain framework structure from this type of molecules.[152] Only one example of a MOF built from just an amino acid and a metal salt is documented in the literature.[153] In this example, aspartic acid is reacted with Ni(II) salt which yields one-dimensional, helical nickel-oxygen clusters that are linked by the aspartate. In order to obtain a more rigid frame-work structure, additional linkers are usually employed. This is for example the case in a material synthesized by Rosseinsky and co-workers.[154] In this struc-ture aspartic acid was indeed included in the crystal structure where it does not serve as a ditopic linker but as an auxiliary, bidentate ligand to create a homochi-ral inorganic SBU. The interconnection of the inorganic SBUs is again achieved by bipy linkers.
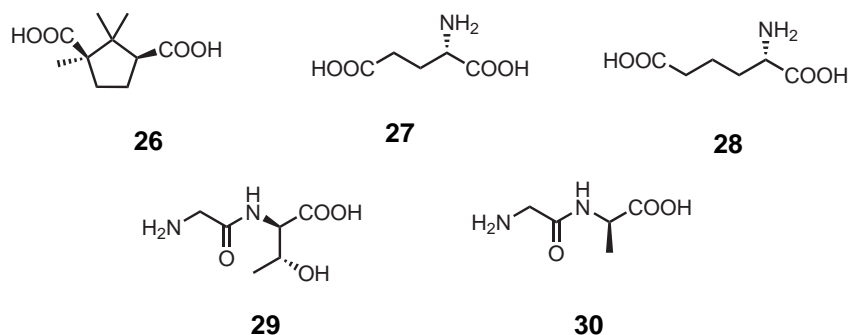


**Scheme 1.12** – Five ditopic linkers from the chiral pool that are used in the synthesis of framework structures: camphoric acid (**26**),[151,155–157] aspartic acid (**27**),[153,154,158] glutamic acid (**28**), glycylthreonine (**29**),[159] and glycy-lalanine (**30**).[160]

The intrinsic flexibility of amino acids may be overcome by the formation of peptides, which are more rigid than free amino acids due constraints im-posed by the peptide bond. This effect was exploited by Rosseinsky and co-workers.[159] They used glycylthreonine (Gly-Thr, **29**, see Scheme 1.12), which is a dipeptide with threonine on the *C* terminus and achiral glycine on the *N* ter-minus, to synthesize a zinc-based material. The crystal structure of this material is shown in Figure 1.39. In this MOF, the dipeptide Gly-Thr serves as a ditopic linker that connects two octahedral inorganic SBUs. This results in the formation of two-dimensional sheets that are stacked and thereby form one-dimensional

channels with a chiral surface due to the projection of the α-carbon of the threonine residue into the pore system. Much like in formation of secondary structures in proteins the stacking of the individual layers is stabilized by hydrogen bonds between the peptide N−H and C=O groups of adjacent layers.[159]
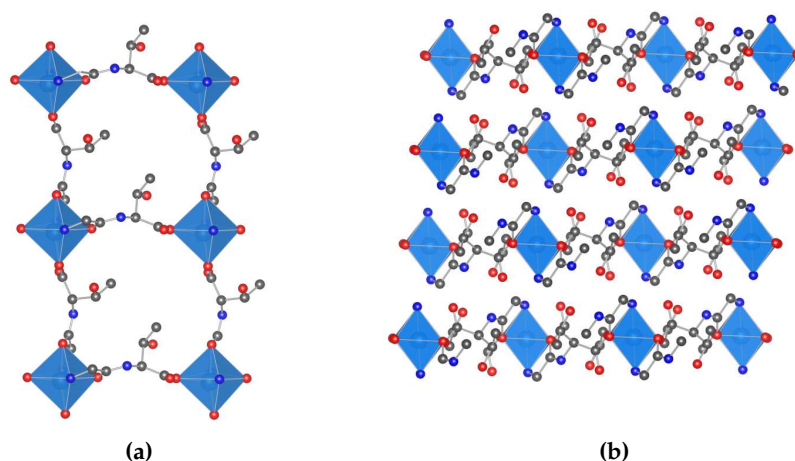


(a)                                                 (b)

**Figure 1.39** – (a) view along the [101] direction onto a two-dimensional sheet formed by the dipeptide **29** and an octahedral zinc inorganic SBU (b) view along the $b$ axis of an arrangement of stacked sheets of interconnected inorganic SBUs, (light blue octahedra: zinc, grey: carbon, red: oxygen, dark blue, nitrogen, structural information obtained from CCDC number 874400).

Because of their aforementioned flexibility, the ability to form chelates instead of connections, and the limited sites for coordination, amino acids often lead to low-dimensional framework structures.[152] Furthermore, the flexibility of amino acids contradicts the requirement of rigidity in the linker imposed by the concept of reticular chemistry.[6] This hinders the design of MOFs with adjustable pore sizes or different substituents on the framework.

To consistently synthesize three-dimensional frameworks, amino acids have been modified to improve their ability to interconnect inorganic nodes. An exemplary collection of these improved amino acid linker molecules is shown in Scheme 1.13. Modification strategies can target the amino group to form reduced imines (**31**, **32**, **33**),[161,162] imidazoles,[163] alkylated amines,[164] or they target carboxylic groups to form amides (**34**, **35**)[165–167] and heteroatoms in the side chain to form thiazolidines (**36**).[168]
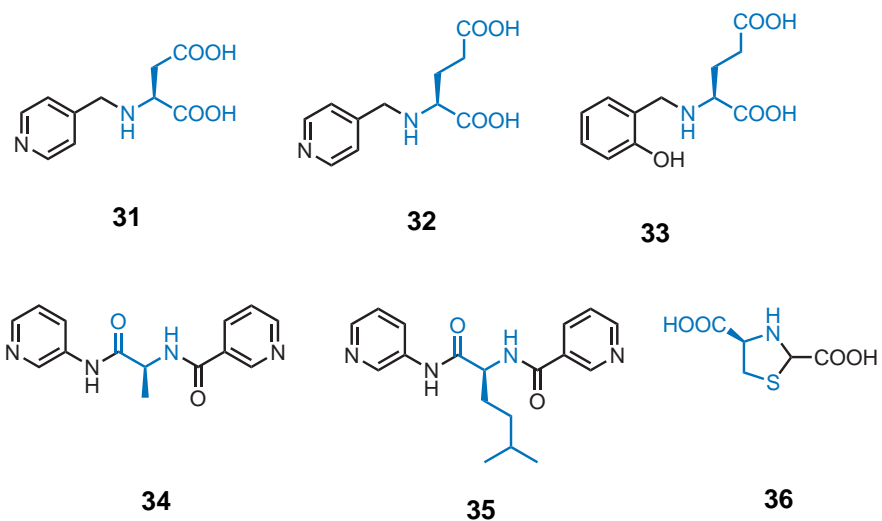
**Scheme 1.13** – Linkers synthesized from amino acid precursors. Atoms originating from the amino acids are highlighted in blue.

Amino acids and other representatives of the chiral pool are compelling structures to form homochiral MOFs. Unfortunately, the tendency of the un-functionalized small molecules to form chelates impedes the synthesis of high-dimensional structures. Nevertheless, these compounds are excellent sources of chiral information in the synthesis of rigid homochiral linkers.

## 1.7 Application of Chiral MOFs

The pores of a MOF may provide a chiral environment to discern chiral compounds. Applications of homochiral MOFs can be grouped into two main categories: asymmetric catalysis and stereoselective separation. The following section will give an overview on how MOFs are used in that regard.

The first example of an asymmetric reaction catalyzed by a MOF was reported by the group of Kim.[125] They used the MOFs D-POST-1 (see page 54) to catalyze a transesterification of 2,4-dinitrophenyl acetate with a racemic mixture of 1-phenyl-propan-2-ol (see Scheme 1.14). In this reaction, (S)-1-phenylpropan-2-yl acetate was preferably formed. However, the enantiomeric excess of 8 % in this process is only modest which can be explained by the significant distance from the stereocenters of the linker to the catalytically active pyridyl group.[169] A similar unfavorable effect has also been observed in a porous lanthanide phosphonate generated from a BINOL derivative.[132] A cyanosilylation of benzaldehyde was catalyzed by the lanthanide inorganic SBU which could not benefit from any chiral induction of the remote BINOL system. This indicates that the mere existence of chirality in a MOF does not necessarily lead to the induction of stereochemical information to guest molecules.



**Scheme 1.14** – Transesterification of 2,4-dinitrophenyl acetate with racemic 1-phenyl-propan-2-ol catalyzed by D-POST-1 results in the preferential formation of (S)-1-phenylpropan-2-yl acetate.

For certain asymmetric cycloadditions the chiral pore structure of the MOF can determine the configuration of the reaction products. This is for example the case for the Ag-1 and Ag-2 system that has been shown in Figure 1.26 on page 47.[109] Inside the chiral pores, a 1,3-dipolar cycloaddition of methyl-2-(benzylidene amino)-acetate and N-methylmaleimide was performed that is depicted in Scheme 1.15. In this reaction four new stereocenters are created. Interestingly, only the *endo*-products are formed with high enantioselectivity. The impressive *ee* of 90 % may be explained by the restricted movement of the sub-

strates in the pore system of Ag-1 when the substrates coordinate to the metal ion.
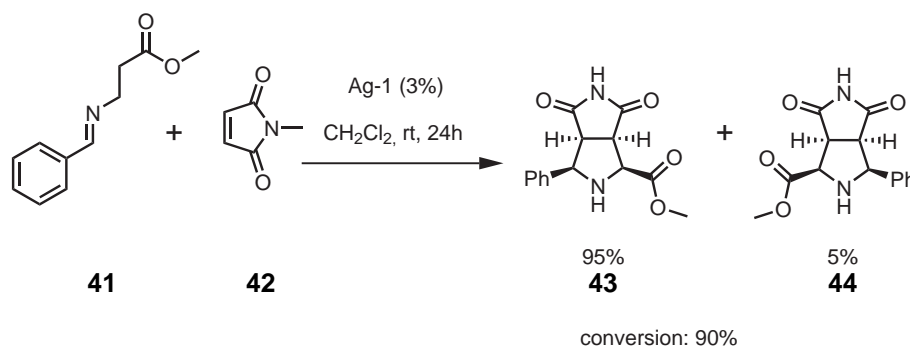


**Scheme 1.15** – 1,3-dipolar cycloaddition between $\alpha$ iminoester **41** and *N*-methylmaleimide (**42**) catalyzed by Ag-1 yielding predominantly one of the four possible stereoisomers. The *exo*-products are not observed as reaction products and are therefore omitted.

One distinguishing advantage of MOFs as heterogeneous, asymmetric catalysts over chiral polymers is their periodicity that is owed to the crystalline nature of these materials. This allows the precise description of the catalyst system and may provide insight into the processes that occur during catalysis. This has been demonstrated for the Ag-1 system. To elucidate a possible mechanism for the activation of methyl-2-(benzylidene amino)-acetate by the heterogeneous catalyst, the silver-based MOF was soaked in a solution of the $\alpha$ iminoester in CHCl$_3$. Crystals that were obtained from this procedure were suitable for single crystal diffraction experiments. The crystal structure for this adduct is shown in Figure 1.40. The crystal structure reveals an interatomic distance of 3.68 Å between the carbonyl oxygen atom and the silver center which activates the substrate towards cycloaddition reactions. Furthermore, π-π stacking between the phenyl ring of the substrate and pyridine rings of the organic SBU provides additional interaction to hold the substrate in place during the reaction.

In contrast to the aforementioned drawbacks of the catalytic BINOL-SBU system, very good stereoselectivities have been observed when the catalytically active unit is directly located on the BINOL motif.[141] An impressive example for this has been demonstrated by Lin and co-workers using metalated CMOF-3b which is described on page 58.[145] A modified MOF was used as a catalyst in alkyl- and alkynylzinc additions to aromatic aldehydes and almost complete conversions and high enantiomeric excesses were observed. Because the metrics are tunable to a certain degree within this series of isoreticular MOFs, they were
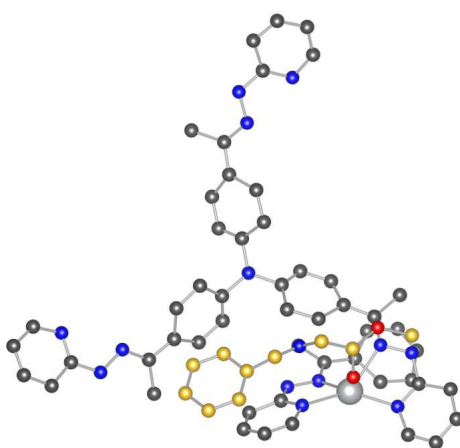
**Figure 1.40** – Positioning of methyl-2-(benzylidene amino)-acetate (**41**) within the pore system of Ag-1. The C=O group points towards the metal ion, the aromatic ring of the substrate is within proximity of the linker to benefit from π-π interaction. The substrate is highlighted in yellow (dark grey: carbon, light grey: silver, red: oxygen, blue: nitrogen, structural information obtained from CCDC number 885237).

able to impose size selectivity on the substrates used for the reactions. One example of an alkylzinc addition catalyzed by CMOF-3b is shown in Scheme 1.16.
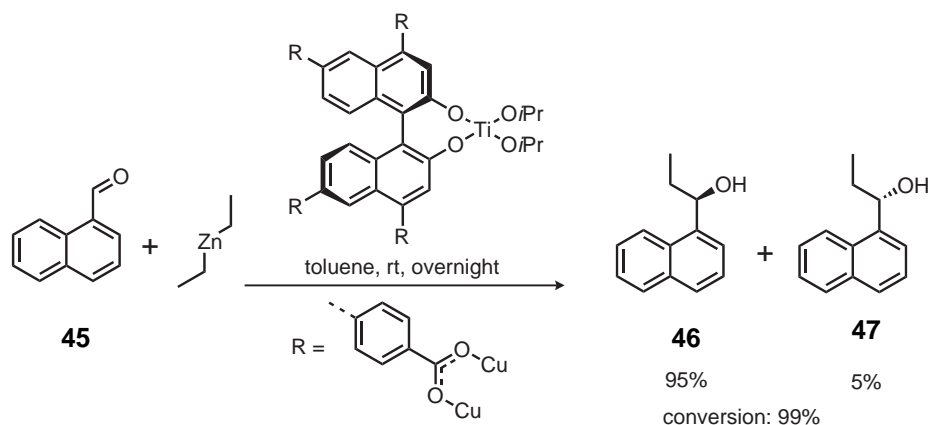


**Scheme 1.16** – Representation of an alkylzinc addition to naphtylaldehyde catalyzed by CMOF-3b to yield (*S*)-ethylnaphtyl alcohol with 91 % *ee*.

In addition to the diethyl zinc addition described above MOFs with chiral metal centers have been used in asymmetric reductions,[137] cyanations,[170] ring-openings,[150,171] and epoxidations.[147,148] Apart from catalysis mediated by chiral transition metal complexes, considerable stereoselectivity is observed in reactions were MOFs function as heterogeneous organocatalysts.[172] Proline is one of the archetypes in asymmetric organocatalysis and has been explored intensively as a structural motif in MOFs.

The structure of a proline-containing MOF that is isoreticular to the IRMOF series has already been shown in Scheme 1.10. It is obtained from a *N*-Boc protected precursor and can act as a stereoselective organocatalyst after the liberation of the secondary amine. The ability of the MOF to activate carbonyl compounds has been demonstrated by Telfer and co-workers in the asymmetric addition of cyclopentanone to 4-nitrobenzaldehyde.[127] The reaction is schematically shown in Scheme 1.17. In this reaction two new stereocenters are formed, which means that four different stereoisomeric products could be expected. It is desirable for a catalyst to exert stereoselectivity regarding both diastereomers and enantiomers. Here, a complex mixture of four stereoisomers is formed.

The diastereomeric ratio between the *syn*- and *anti*-adducts is 1:3 and the *ee* is 3 % (*syn*) and 14 % (*anti*), respectively. A comparable reaction with acetone as the enolizable carbonyl compound afforded an *ee* of 30 % in the *anti* adduct. The observed enantioselectivities for this reaction system are relatively low compared to the values that were, for example, achieved by the transition metal mediated
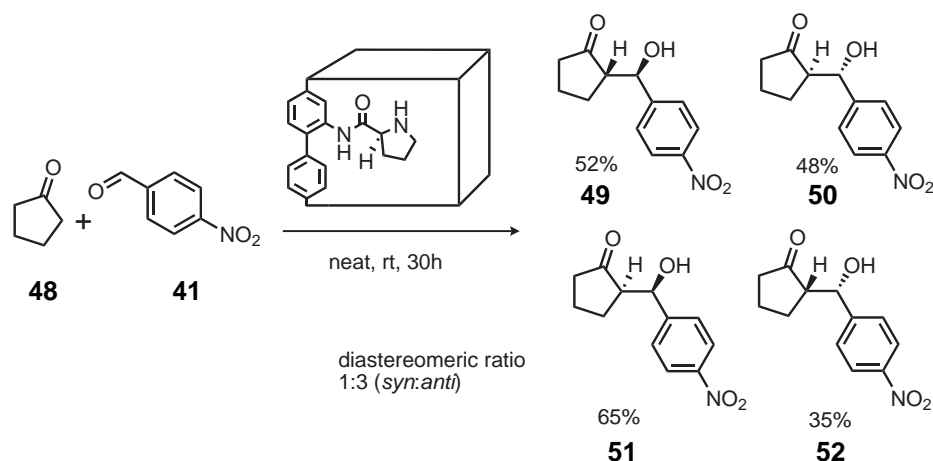
**Scheme 1.17** – Representation of an asymmetric aldol addition of cyclopentanone to 4-nitrobenzaldehyde using IRMOF-Pro as a heterogeneous organocatalyst and distribution of the resulting stereoisomers **49–52**.

catalysis of CMOF-3 (see Scheme 1.16). The authors ascribe the modest stereoselectivities to a minor degree of racemization and to a lack of organization in the reaction's transition state. This is caused by the flexibility of the proline unit with respect to the framework and by the large pore space of the MOF which allows the electrophile to approach the enamine transition state from either diastereotopic side. Furthermore, the carboxylic group of proline is attached to the framework and cannot participate in the transition state defining the stereochemistry of the products. This is unfavorable because the carboxylic group can enhance the rigidity and stability of certain transition states by hydrogen bonding to the substrate (see Scheme 1.4, page 44).[75] By obstructing the carboxylic group in an amide bond, no such hydrogen donor abilities can be expected for the carboxylic group.

A similar catalysis was reported by Kaskel and co-workers, using the proline functionalized MOF DUT-32-Pro (see Figure 1.35, page 58) in which the same chiral dicarboxylate was used as in IRMOF-Pro (see above). During the thermal deprotection a loss of stereoinformation is observed for the chiral substituent which impairs the ability of DUT-32 to act as a stereoselective catalyst. The authors performed an aldol addition of cyclohexanone to 4-nitrobenzaldehyde (similar to the reaction shown in Scheme 1.17) but were unable to observe any enantioselective formation of the products.

Asymmetric aldol additions have not only been achieved with linker-bound proline but also with proline derivatives that act as a ligand to the inorganic SBU. CMIL-1 (see Scheme 1.7, page 53) has been employed in this sense by Kim and co-workers (see Scheme 1.18).[121] They performed the stereoselective addition of several enolizable carbonyl compounds to a number of aromatic aldehydes, including the reactants of the aldol addition catalyzed by IRMOF-Pro shown in Scheme 1.17. Here, the ratio of diastereomers is shifted further towards the *anti*-product (1:4) and much higher enantioselectivites (*ee* = 66 %) are observed. The highest enantioselectivity was observed for an addition of ethylmethyl ketone to 4-nitrobenzaldehyde. Because of the asymmetric nature of the ketone, two regioisomers are observed with the preferential formation of the less substituted reaction product (ratio 9:5). The major regioisomer was obtained with *ee* = 81 % (69 % for the minor regioisomer).
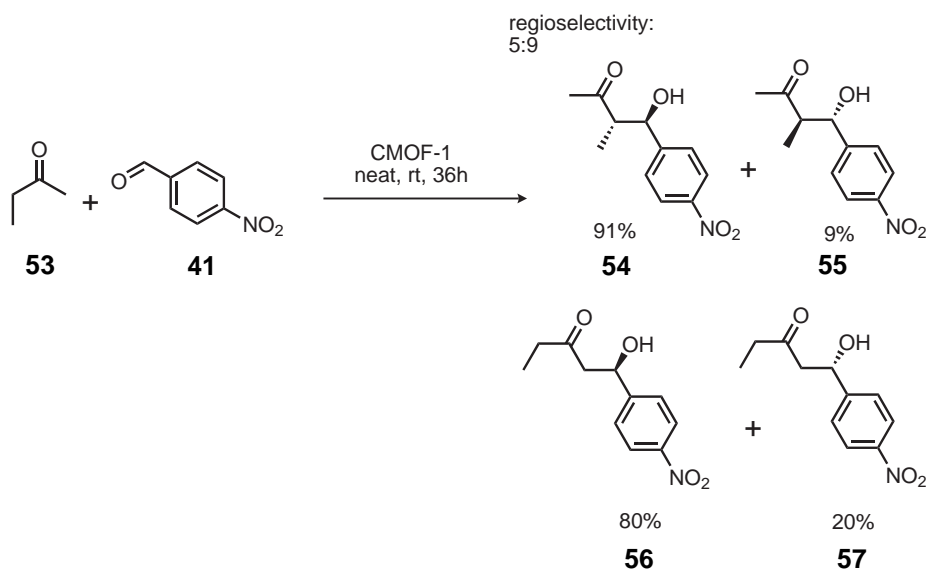


**Scheme 1.18** – Representation of an asymmetric aldol addition of ethylmethyl ketone to 4-nitrobenzaldehyde using CMIL-1 as a heterogeneous organocatalyst.

Interestingly, for the addition of acetone to 4-nitrobenzaldehyde, *ee*-values were higher with the heterogeneous CMIL-1 catalyst than in the homogeneous control reactions that use the free (*S*)-*N*-(pyridin-3-yl)pyrrolidine-2-carboxamide ligand. The authors ascribe this effect to the restricted movement of the substrates in the micropores of CMIL-1.[121]

An impressive synergistic effect between the chiral linker and the framework structure has been demonstrated by Duan and co-workers.[123] They incorporated a triphenyl amine linker into a MOF that acts as a photosensitizer in the asymmetric alkylation of aliphatic aldehydes (see Figure 1.31, page 53). To obtain a catalytically active MOF species, Zn-BCIP-1 was first liberated from the *N*-protecting Boc group in a procedure comparable to the carbamate cleavages described above (see Scheme 1.10, page 57). This deprotection yielded the MOF Zn-PYI-1 with a free secondary amine from the proline derived ligand on the inorganic SBU. This activated MOF species is shown in an abstracted form in Scheme 1.19.
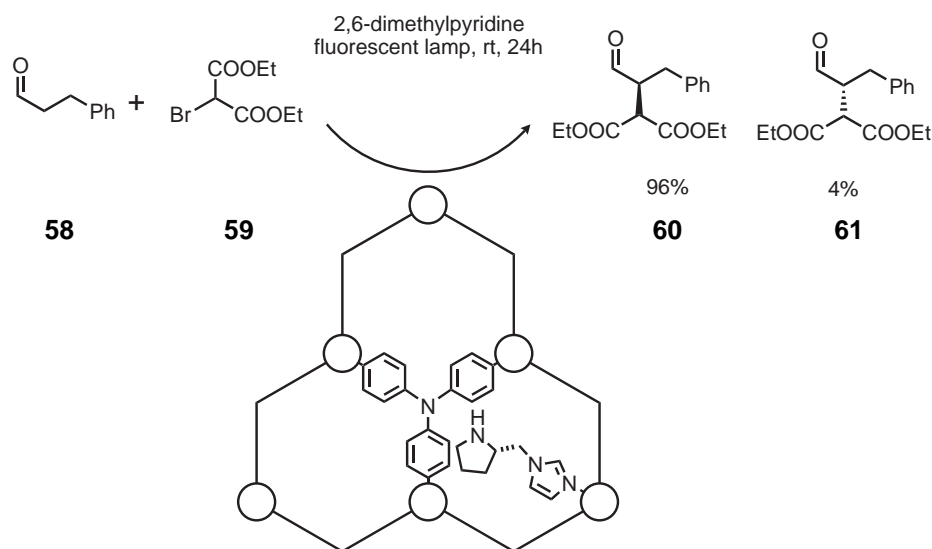


**Scheme 1.19** – Representation of an asymmetric alkylation of 3-phenyl-propanal with diethyl 2-bromomalonate together with a schematic drawing of the catalytically active Zn-PYI-1, inorganic SBUs are depicted as white spheres.

Significant differences in the solid state UV emission measurements of bare Zn-PYI-1 and the same MOF loaded with diethyl 2-bromomalonate imply a photoinduced electron transfer from an excited Zn-PYI-1 species to the substrate molecules, when irradiated with a common fluorescent lamp. Thereby, a reactive intermediate of the alkylation agent is created. This intermediate is able to react with aldehydes activated by the chiral, secondary amine bound to the inorganic SBU of the MOF. These aldehydes are immobilized in the proximity of the

alkylating agent and one enantiotopic face is effectively shielded by the chiral ligand. This synergy of photoactivation and stereoselectivity demonstrates well, how activated species can be generated in close proximity within the pores of a MOF.

Apart from the impressive applications as asymmetric catalysts where MOFs can induce chiral information to achiral substrates, MOFs may also be used to differentiate between enantiomers in stereoselective separations or in sensing.[173] Separation of enantiomers has been demonstrated for racemic mixtures of flavonoids,[174] ibuprofen,[175,176] alcohols,[167,177,178] $\beta$-hydroxyl esters,[179] amines,[138] amino acids,[176] transition metal complexes[125] sulfoxides,[180–182] terpenes,[183] and phenols.[184]

One of the very first examples of a chromatographic separation of enantiomers has been demonstrated by Fedin et al.[180] They have employed the zinc-based MOF [Zn$_2$(bdc)(L-lac)(dmf)] that owes its chirality to the inclusion of L-lactic acid into the inorganic SBU (see Figure 1.28 on page 50). They prepared a chromatographic column from 14 g of the MOF and performed conventional liquid chromatography on a semi-preparative scale with a variety of different aromatic sulfoxides (see Scheme 1.20). The racemic mixture of methylphenyl sulfoxide was completely separated using a solution of DMF in CH$_2$Cl$_2$ as the eluent. However, the separation was impeded by strong tailing effects in the resolution of sulfoxides with different substitutional patterns. This was especially pronounced for the racemate of methyl(4-bromophenyl) sulfoxide **63**, which could not be separated chromatographically, most likely because the electron withdrawing effect of the bromine atom decreases the coordinating ability of compound.



**62**  **63**  **64**  **65**
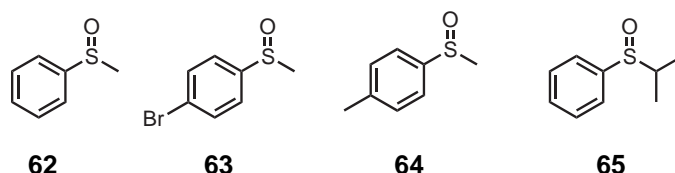
**Scheme 1.20** – Collection of the analytes in a stereoselective liquid chromatography that uses [Zn$_2$(bdc)(L-lac)(dmf)] as the stationary phase. Complete separation of enantiomers was only achieved for methylphenyl sulfoxide (**62**).

Further investigation of this MOF system includes crystallographic analysis.[185] After impregnation of [Zn$_2$(bdc)(L-lac)(dmf)] with chiral alcohols, synchrotron X-ray diffraction experiments were performed. The structural data obtained from these measurements gives insight into the relevant sorption mechanisms within

the framework and are explaining, for example, the role of coordinated solvent molecules at the zinc inorganic SBU in the separation of chiral compounds.

Further improvements in the area of stereoselective separation have been made by the group of Yuan.[184] Aiming at the application of MOFs in High-Performance Liquid Chromatography (HPLC), they have prepared a MOF with a helical pore system from Cd(II) and 4,4'-biphenyldicarboxylate (bpdc) together with L-leucine, which acted solely as an inductor of stereochemical information and was not included in the framework.[106] The structure of the helical pore system is shown in Figure 1.41.
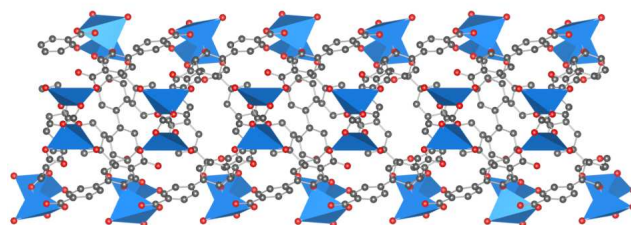


**Figure 1.41** – view along [101] on a helical channel of $[(CH_3)_2NH_2][Cd(bpdc)_1 \cdot 5]$ (blue tetrahedra: cadmium, grey: carbon, red: oxygen, structural information obtained from CCDC number 653346).

To improve the separations by the MOF, the authors removed superfluous solvent molecules from the pores by thermal activation to increase interaction between the analyte and the stationary phase. To obtain a homogeneous packing of the HPLC column, particles were ground to obtain an average size of 5 μm. Using a chromatographic column packed with this material in an HPLC system, they were able to separate a variety of different racemic alcohols, amines, and amides with considerable separation factors up to $\alpha = 4.30$.[184]

Particle shapes and sizes play a very important role in the quality of separations in HPLC applications.[186] Good separations require uniform particles with a small size distribution. HPLC applications of homochiral MOFs are still very limited, possibly due to the fact that it is difficult to obtain crystallites with a consistent size distribution.[184] Efforts are made to control both particle size and shape of MOF crystals[187–191] and to immobilize them onto support materials.[181,192–194] However, the excellent size control that can be exerted during the synthesis of silica materials is unmatched by the current methods in the synthesis of MOFs.[195]

Multiple examples where a MOF has been grown on a silica support have been reported by Yuan and co-workers. They developed a procedure to grow MOF thin films on the surface of a fused-silica open tubular capillary for gas chromatography.[183,196–199] The silica-MOF composites obtained by this method are stable up to operating temperatures of 200–220 °C of the gas chromatography system. Three out of the five examples reported by the group employ camphoric acid as a ditopic linker and result in helical channel systems. The stereoselectivities were investigated for a large number of different racemates. By constructing columns that have been coated with isolated chiral transition metal complexes, Yuan was able to prove the beneficial effects of the supramolecular structure of the MOF on the enantioseparation.[196] In the separation of certain analytes the composite materials performed even better than a commercial Chirasil-L-Val column.[200]

Another impressive example of a homochiral composite involving a MOF has been demonstrated by Liu, Sun, and co-workers.[201] They have synthesized magnetic particles whose surface is covered with a MOF prepared from Zn(II), bdc and L-lactic acid similar to the MOF reported by Fedin et al. (see Figure 1.28 on page 50). In this case however, the pore volume is slightly decreased, which is ascribed to the adaption of the conditions of synthesis that were necessary to grow the MOF on the surface of silica particles with an iron oxide core. Synthesis of the MOF in the presence of $Fe_3O_4@SiO_2$ particles yielded the $Fe_3O_4@SiO_2-[Zn_2(bdc)(L\text{-lac})]$ composite as rod-like particles (10–15 µm × 1.5 µm). Due to the ferromagnetic properties of the particles, they can be separated easily from the supernatant solution. This behavior was exploited for the separation of a racemic mixture of methylphenyl sulfoxide. The magnetic particles were suspended in a solution of the racemate in acetonitrile for several minutes. Afterwards the impregnated composite material was collected with a magnet and removed from the solution. The guest molecules were eluted from the particles and showed an impressive enantioenrichment of up to *ee* = 85.2 %. The separation procedure is schematically shown in Figure 1.42.

The well-defined crystal structures of MOFs allow the modeling of sorption processes.[202,203] Such theoretical studies have also been performed with a focus on homochiral MOFs. The ability to gain insight into these enantioselective mechanisms sparked a number of theoretical investigations.[119,204–207]

It is difficult to predict the outcome of a chiral separation on a conventional stationary phase.[208–211] However, the periodic arrangement of chiral functionalities within the pores of a MOF allows precise, theoretical investigations of the mechanisms of stereoselective separation.[204,212] This enhances the understanding of the beneficial intermolecular interactions necessary for good separation and may lead to tailored materials for the resolution of racemates. In this context, Snurr and co-workers have reported a molecular modeling study
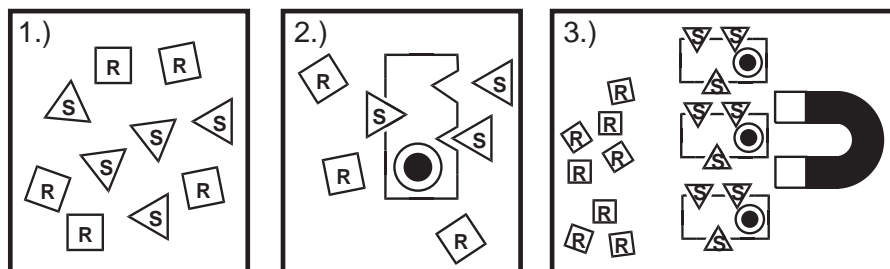
**Figure 1.42** – Schematic representation of the static chiral separation process with the $Fe_3O_4@SiO_2-[Zn_2(bdc)(L\text{-}lac)]$ composite: 1.) A racemic mixture of enantiomers (depicted by squares and triangles) 2.) a composite material is introduced, which selectively absorbs the (*S*) enantiomer (chiral pores are simplified as triangular notches on the rectangular particle, $Fe_3O_4@SiO_2$ is represented as black and white circles) 3.) particles impregnated with the (*S*) enantiomer are collected by the application of a magnetic field.

of the sorption of different chiral alcohols in a MOFs built from D-saccharate as a chiral linker, and a MOF with a homochiral pore structure that was induced by (−)-cinchonine, respectively. For the second system, they were able to identify how a small compositional perturbation of the analyte leads to a change in the preferred adsorption site resulting in a change of enantioselectivity in the separation of alkan-2-ols with increasing chain length. They found that as the chain length of the analyte is increased, different preferred adsorption sites in the chiral pore of the MOF are occupied. The authors ascribe this effect to a corrugated surface of the chiral pore and suggest that even chiral pores lead to more consistent enantioselectivites.

## 1.8 Motivation

As described in the previous sections, MOFs can be useful tools in the preparation of enantiopure compounds, which are vital for the preparation of valuable and safe pharmaceuticals.

The aim of this work was the development of a novel family of chiral MOFs, which can contribute to this field. The chosen approach to obtain homochiral MOFs uses molecules from the chiral pool as starting materials and transforms them into carboxylic acid linkers. Amino acids were chosen for three reasons. First, they provide a carboxylic carbon atom that can serve as an electrophilic target for nucleophilic substitution. Second, numerous amino acids that differ

in the substituent on the β-carbon, are readily available in nature or can be easily synthesized.[65] Last, the nitrogen atom, inherent to amino acids, enables these compounds and their derivatives to act as stereoselective organocatalysts by providing a functional group that can bind substrates via enamine or imine bonds and thereby tethering the substrate in a chiral environment.[213,214] This is for example the case in reactions catalyzed by the $\alpha,\alpha$-bisarylprolinol-system described in Section 1.5.2. Although derivatives of L-proline have been used as MOF-based heterogenous organocatalysts (see Section 1.7), MOFs that bear an $\alpha,\alpha$-bisarylprolinol moiety have not been reported so far. In this work, a strategy should be devised to include this and other useful structural motifs in a linker molecules. This strategy should result in starting materials for MOFs with accessible functional groups that can be employed in heterogenous, stereoselective processes.

Furthermore, the MOFs should be characterized with regard to their structure in relation to previously synthesized materials. Their porosity and thermochemical behavior is to be studied. The integrated functionality should be examined with regard to the usability of the functional groups. Finally, the organocatalysis should be performed with the synthesized MOFs to evaluate their potential with regard to heterogenous, stereoselective catalysis. Scheme 1.21 summarizes the concept of this work in a flow diagram.
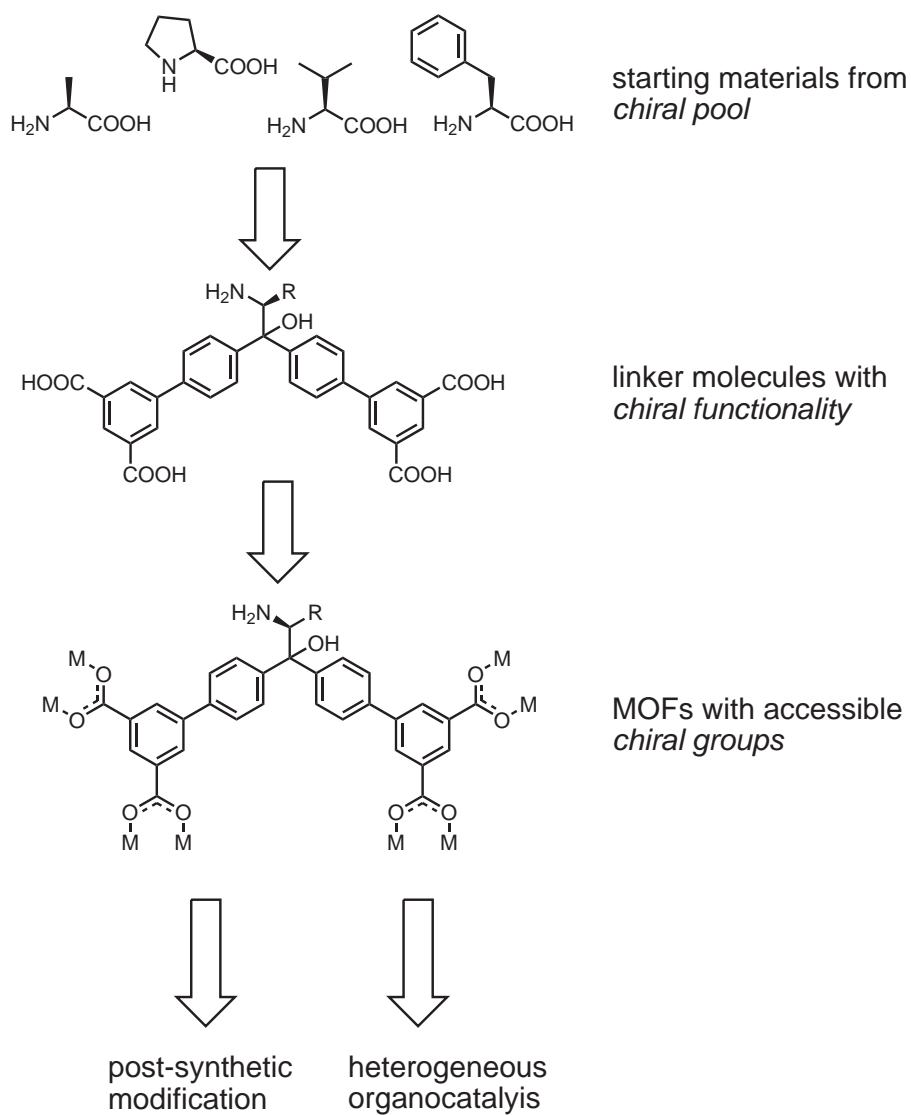
**Scheme 1.21** – Flow diagram to represent the concept of this work.

# Chapter 2

# Methods

## 2.1 Polarimetry

Enantiopure compounds are called optically active because they can cause rotation of the plane of polariziation of light that passes through them. This effect can be ascribed to birefringence:[215] linearly polarized light can be described as the sum of left- and right-circularly polarized light. These polarizations differ in their velocity of propagation when passing a chiral medium, because they experience different refractive indices. This is the case, for example, for solutions of chiral compounds and leads to an phase difference ($\Delta\theta$) of the two inversely polarized electromagnetic waves that is dependent on the difference of the refractive indices ($\Delta n$):

$$\Delta\theta = \frac{\Delta n l \pi}{\lambda} \tag{2.1}$$

where $\lambda$ is the wavelength of the polarized light, and $l$ is the path length of the beam of light through the chiral medium. As a result of this phase difference, the direction of the plane of polarization of the combined waves is rotated.

The magnitude of this effect is determined as follows. Light passes through a polarizer to produce a plane polarized beam. This beam passes first through a sample in which the plane of polarization is rotated and afterwards through a second, rotatable polarizer. If two polarizers are oriented parallel to each other, light emerging from the first polarizer will pass the second polarizer (analyzer) without a loss of intensity. If the analyzer is turned by 90°, no light will pass through it. Therefore, the rotation angle and direction of the analyzer in which the maximum intensity of light is measured, specifies the observed rotation of the plane of polarization. To discern between very large and very small rotations of opposite directions, such as +10° and −350°, variation of the concentration of the chiral medium or the path length of the beam of light through the chiral medium allows the determination of the true value. A schematic representation of an apparatus to determine the optical rotation is shown in Figure 2.1.

The optical rotation of a compound is substance-specific and typically measured from a solution of the enantiopure compound in an appropriate solvent. The magnitude of the observed optical rotation is dependent on the wave length ($\lambda$)[1], temperature ($T$), concentration ($c$), length of the sample ($l$), and the solvent. These parameters are typically given together with the specific rotation value that is calculated from the observed rotation as follows:

$$[\alpha]_\lambda^T = \frac{\alpha}{lc} \tag{2.2}$$

The observed rotation $\alpha$ is measured in degrees, the path length is given in decimeters (dm) and the concentration is given in g/100 mL.

---

[1]In many cases the wavelength used for polarimetry is 589 nm, which corresponds to the D line of sodium and is commonly abbreviated as D.
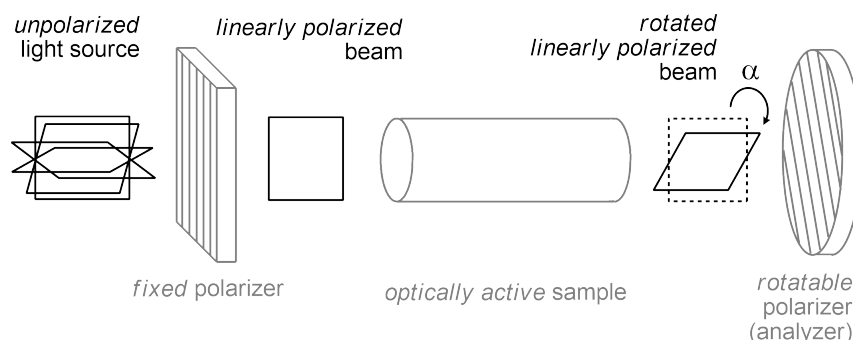
**Figure 2.1** – Schematic representation of the measurement of optical activity; unpolarized light passes a polarizer, the resulting polarized beam passes an optically active sample; the emitted beam exhibits a rotated orientation of the polarization, whose magnitude is determined by a second, rotatable polarizer.

The effect of optical activity has been employed for a long time to discern enantiomers and has been utilized by Pasteur to deduce an asymmetric structure of tartaric acid.[216–218] He observed that the value of optical rotation by two enantiomeric compounds was equal, but the directions were inverse to each other. As the sign of the optical rotation is a characteristic to differentiate two enantiomers it is commonly given as a prefix to the name of a compound. However, the denominators $(+)$ and $(-)$ give no information about the absolute configuration $(R)$ or $(S)$ of a stereocenter.

## 2.2 Thermal Analysis

A full analysis of the properties of newly synthesized compounds includes the observation of the behavior at different temperatures in a certain atmosphere. This comprises, for example, the temperatures at which phase changes may occur in organic materials, such as melting or boiling points. To investigate the thermal and decomposition properties of MOFs, more advanced methods such as thermogravimetric analysis (TG) are applied. This method records the mass of a substance upon heating in a controlled atmosphere.[219,220] In most cases a weight loss is observed that can be ascribed to various modes of decomposition or expulsion of solvent molecules. However, weight gains are principally possible, for example, if samples are oxidized. To investigate the interaction of

the sample with the gas phase, TG can be performed in the presence of reactive gases such as oxygen or hydrogen.[221]

In addition to TG, a simultaneous differential thermal analysis (DTA) can be performed. This thermoanalytic technique allows the determination of exo- or endothermic processes that occur in a sample. The examination of the enthalpies of a sample can give insight to enthalpic processes that occur during the temperature program. DTA monitors a reference crucible that is heated with the same temperature program as the actual sample but analyzed by a separate thermocouple.

During TG of MOFs, the analyte may decompose to volatile products or solvent may be evaporated from the pores. The composition of the evolved gas can be monitored by IR spectroscopy and mass spectrometry. A schematic representation of such a coupled setup is depicted in Figure 2.2.
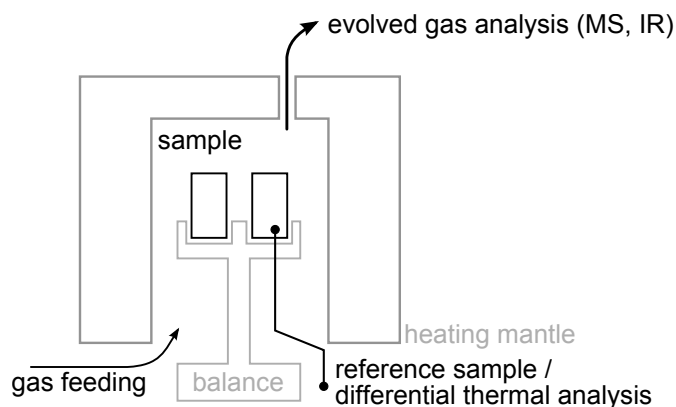


**Figure 2.2** – Illustration of a TG system; the sample is placed in an oven and heated in a controlled atmosphere; weight changes are recorded simultaneously with DTA and MS or IR, respectively.

This coupling of analytic methods allows the assignment of a weight loss to a certain event, for example, the cleavage of certain functional groups or the expulsion of a solvent. This technique is very useful for the analysis of MOFs, because the completeness of a solvent exchange can be indicated by the absence of the corresponding signal of a replaced solvent in the mass spectrum.

In a typical TG procedure, MOFs are heated from room temperature to 800 °C in an argon-oxygen atmosphere (80:20), which leads to combustion of organic material and oxidation of the inorganic components. The results of the analysis are plotted against the temperature. The combined diagrams in this work (see Chapter 4) contain the weight loss (given as percentages) and DTA of the sample

together with the traces of selected ions from mass spectrometry. These ions are characteristic for the pore-filling solvents (DMF or tetrahydrofuran (THF)) and decomposition products (water, carbon dioxide).

## 2.3 Physisorption

The controlled adsorption of gases is one the most-established methods for the characterization of porous materials. Physisorption measurements can provide information about the surface area and the pore volume of a material. In a physisorption experiment, an absorptive such as nitrogen experiences attractive van-der-Waals forces to a potentially porous solid (for example a MOF), which serves as an adsorbent, and an adsorbate is formed on the solid surface. This reversible process mainly involves London and Van-der-Waals forces. The adsorption enthalpies lie in the range of $4\,kJ/mol$ to $40\,kJ/mol$.[222]

The progression of adsorption processes at constant temperatures can be represented by sorption isotherms in which the adsorbed volume is plotted against the relative pressure $p/p_0$ where $p$ is the vapor pressure and $p_0$ is the saturation pressure of the absorptive. The progression of the isotherms in adsorption and desorption processes are characteristic of the type of porosity observed in the material. Isotherms are grouped in six different types according to the IUPAC. These isotherms are denoted with Roman numerals and are depicted in Figure 2.3.[223]
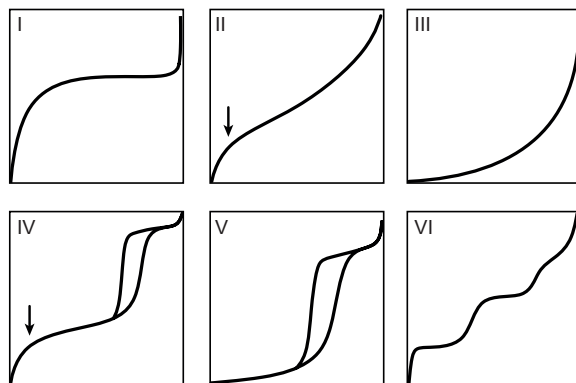


**Figure 2.3** – Six different sorption isotherms according to IUPAC recommendations in which the adsorbed volume is plotted against the relative pressure $p/p_0$; arrows indicate the pressure points where the adsorption in a monolayer is completed.[223]

The two most commonly observed adsorption isotherms are of type I and IV and constitute the most relevant isotherms with regard to MOFs. Microporous solids exhibit a type I adsorption isotherms. In these materials, the adsorption potential is strong due to the narrow pores. This leads to an overlap of adsorption potentials of the walls and the adsorption enthalpy is increased significantly. Therefore, type I adsorption is dominated by the primary filling of micropores by fluid-wall interactions. This behavior is commonly observed for MOFs, which often exhibit, but are not limited to, pores with a diameter of less than 2 nm.

Materials that have pores in the range of 2 nm to 50 nm show type IV adsorption isotherms. This is the case, for example, for the MOFs with ultra-high surfaces areas described in Section 1.4 (see page 33). Here, a hysteresis may be observed in the isotherm as a result of differences between the adsorption and desorption process: Due to the formation of metastable films during adsorption, capillary-condensation occurs in partially filled pores and leads to a delay of the vapor-liquid transition. Such metastabilities do not occur during desorption, because the liquid-vapor interface is already present.[222]

The type II adsorption isotherm is typically observed for non- or macroporous solids. The progress of this isotherm exhibits a shoulder which indicates the beginning of multilayer generation. The type III adsorption is considered a special case of the type II adsorption in which an increase in the interaction between the molecules of the adsorbate is observed. Another special case is the type V adsorption that can be derived from a type IV isotherm in which the interaction between adsorbent and adsorbtive is weak. A step-wise adsorption leads to the type VI isotherm, in which each step corresponds to a complete monolayer adsorption.

As can be seen from the type IV and type V isotherms, a hysteresis may occur between the adsorption and the desorption process. This behavior is usually observed for mesoporous materials.[222] After the formation of a multilayer with a critical thickness, the prevalent role of fluid-fluid interaction leads to capillary condensation. Hystereses have been grouped by the IUPAC into four different types and are shown in Figure 2.4. The shape of a hysteresis loop generally correlates with the pore geometry in a material. For cylindrical pores with a narrow pore size distribution, hysteresis H1 is commonly observed. More complex pore structures that involve network effects, such as pore blocking or percolation, are typically associated with hysteresis H2. Hysteresis H3 and H4 are commonly observed if slit-shaped pores are present, whereas for H3 theses pores are formed by an interparticular arrangement.
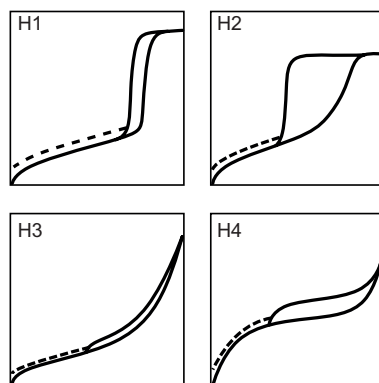
**Figure 2.4** – Four different types of hysteresis according to IUPAC recommendations in which the a dashed line indicates a possible hysteresis at low pressures.[223]

### 2.3.1 Determination of the Specific Surface Area

The mathematic description of adsorption processes allows the calculation of the specific surface area of an adsorbent. These calculations are based on empirical models, such as the Brunauer-Emmet-Teller (BET) theory.[224] This approach is an extension to the Langmuir theory and takes the formation of multilayers into account. It is commonly used to describe the adsorption of gases by micro- and mesoporous materials. It is expressed by the following equation.

$$\frac{p/p_0}{n(1 - p/p_0)} = \frac{1}{n_m C} + \frac{C - 1}{n_m C} \cdot p/p_0 \tag{2.3}$$

where $n_m$ is the monolayer capacity, $n$ is the amount of adsorbate, and $C$ is an empirical constant.[222] Knowledge of the monolayer capacity allows the calculation of the specific surface area if $n_m$ is divided by the molecular cross-sectional area of the adsorbate. To solve equation 2.3, a physisorption isotherm is transformed into a BET graph in which the left term of equation 2.3 is plotted against $p/p_0$. The slope and the y-intercept of this linear graph are used to calculate the $C$ constant. This permits the determination of $n_m$ from which the specific surface area can be calculated by

$$S_{BET} = n_m \cdot N_A \cdot \sigma \tag{2.4}$$

where $N_A$ is the Avogadro number and $\sigma$ is the cross-sectional area of a molecule of the adsorbate within a monolayer. For nitrogen, it is assumed that $\sigma = 0.162\,\text{nm}^2$. The BET equation is generally applicable in the relative pressure range of $p/p_0$

from 0.05 to 0.3 for non-porous and mesoporous adsorbents. In a strict sense the BET method is not applicable for microporous adsorbents.[225,226] However, the determination of the surface area by nitrogen physisorption is generally accepted in the literature as an adequate expression for the surface area if certain quality criteria are applied.[227,228]

1. The empirical constant $C$ must be positive.

2. The term $n \cdot (p/p_0)$ must increase monotonically in the chosen range of $p/p_0$.

3. The endpoint of monolayer formation $(p/p_0)_{nm} = \frac{1}{\sqrt{C}+1}$ must lie within the chosen range of $p/p_0$.

BET plots of adsorptions isotherms of nitrogen physisorption may exhibit linearity in more than one range of $p/p_0$. The application of these quality criteria provides reproducibility by excluding certain pressure ranges.

## 2.4 Crystal Structure Determination of Metal-Organic Frameworks

Due to the crystalline nature of MOFs, their structure can principally be determined by X-ray diffraction experiments. These methods are well-established for the structural investigation of so-called small molecules. However, the elucidation of crystal structures of porous materials is challenging for several reasons that will be discussed in the following.

The void space is filled with a large number of disordered solvent molecules. This disorder contributes significantly to the R-factor which describes the discrepancy between the experimental diffraction data and the crystallographic model. This effect can be overcome with the so-called SQUEEZE procedure.[229,230] This method assumes that the total electron density can be divided into two parts: one part contains the structural model that can be described by fractional coordinates, occupancy factors and anisotropic displacement parameters. The other part contains, for example, heavily disordered solvent molecules which cannot be described satisfactorily in a chemical sense. In terms of a MOF, a distinction is made between the actual structure of the framework and a solvent accessible region. The solvent accessible region is used as a mask to disregard the contribution of disordered molecules in the diffraction experiment. This provides a modified reflection file that is used in further refinements of the structural model.

An additional limitation to the crystal structure determination of MOFs is imposed by the difficulty to obtain crystals that are suitable for single crystal diffraction experiments. Crystals that are too small may not provide enough lattice planes for satisfactory diffraction and a broadening of the reflections is observed because destructive inteference is incomplete close to the Bragg angles. Crystals from small molecules can be recrystallized until the conditions are determined that yield appropriate single crystals. This process is not applicable to MOFs, where crystal growths occurs simultaneously to the irreversible generation of an extended framework structure, which is insoluble. Furthermore, the modification of the synthetical conditions can result in the formation of polymorphs.[231–240] Therefore, these conditions have to be optimized to obtain the desired phase and to control the size and quality of the crystals. Additionally, the size of the crystals can be enlarged by so-called modulators that compete with linkers at the coordination sites and thereby decelerate crystal growth, which can yield high quality crystals.[30,241,242]

The minimum size of a crystal in a diffraction experiment depends on the scattering power of its components as well as intensity of the X-ray beam. If very powerful beam is needed to measure small crystals, diffraction experiments may be performed with synchrotron radiation at specialized facilities.[234] For the analysis of MOFs on a laboratory scale, copper anodes are commonly chosen over molybdenum anodes as radiation sources, because of the greater diffraction power of the copper $K\alpha$ X-ray beam. Another advantage of copper anodes over molybdenum anodes is an increase in the separation of diffraction spots. MOFs are often associated with large unit cells that exhibit cell dimensions greater than 30 Å. This leads to d spacings of the lattice planes at which constructive diffraction occurs. According to Bragg's law the diffraction angles for the corresponding peaks are relatively small and they may overlap. When using copper $K\alpha$ radiation this effect is less pronounced compared to molybdenum $K\alpha$ radiation because of the difference in wavelengths ($\lambda_{Cu\,K\alpha}$ = 1.5406 Å, $\lambda_{Mo\,K\alpha}$ = 0.7107 Å), which directly influence the diffraction angles according to Bragg's law. An illustration of this relationship is depicted in Figure 2.5. However, with longer wavelengths less reflections are available for structure refinement because of an reduction of the observable reciprocal space. Furthermore, the application of molybdenum $K\alpha$ radiation allows the measurement of samples that show strong X-ray absorption.

Another method to analyze even very small crystals is electron crystallography. In these methods, X-ray beams are replaced by electron beams, which interact more strongly with the analyte and exhibit significantly smaller wavelenghts compared to, for example, copper $K\alpha$ radiation.[243] Kolb and co-workers have applied electron crystallography to determine the structure of MOF crystals ranging from 200 nm to 300 nm in length.[244]

short wavelength          long wavelength
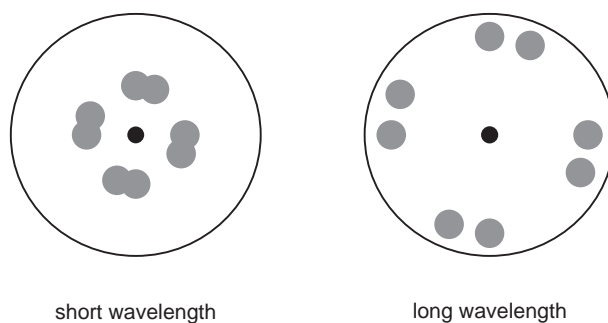
**Figure 2.5** – Illustration of two hypothetical X-ray diffraction patterns of a compound with a large unit cell; short wavelengths lead to small diffraction angles that cause overlap of diffraction peaks; long wavelengths lead to separation of diffraction peaks.

In many cases, suitable single crystals for diffraction experiments are inaccessible. However, structural information can also be acquired from powder X-ray diffraction (PXRD). This procedure is not trivial because initial solutions are hard to find due to the difficulties in recovering the phase information from PXRD data. A successful *ab initio* approach has been demonstrated, for example, in the elucidation of the crystal structure of UiO-66 by applying direct methods to powder diffraction data obtained from a synchrotron source.[24] These methods have been implemented in the EXPO software.[245]

Another approach to solve crystal structures from PXRD data is based on the identification of regions with high and low electron density. In the case of a MOF an obvious distinction can be made between the framework structure and the void space. Brenner and co-workers reported a procedure that defines a surface between high and low electron density areas as a structure envelope.[246,247] This allows the reduction of space where atoms that belong to the framework can be located. These restrictions can be used to improve charge-flipping calculations to solve the crystallographic phase problem. An adaption of the structural envelope method to MOFs has been reported by Zhou and co-workers on the basis of HKUST-1 as a model structure.[248] A representation of a structural envelope that has been determined for HKUST-1 is shown in Figure 2.6

In some cases, certain structural information about the crystal is already known. This is the case, for example, for certain rigid linkers that are employed in the synthesis of MOFs. This allows the application of so-called direct space methods, which are based on the localization of the linkers in the unit cell by using systematic or random moves of these building blocks and comparision
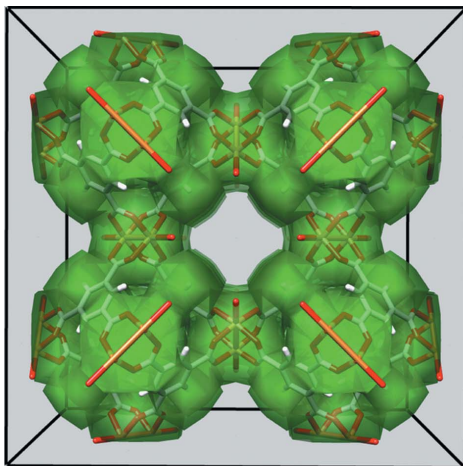
**Figure 2.6** – Three-dimensional representation of the unit cell of HKUST-1 overlapped with a structural envelope determined from PXRD data; the volume with a high electron density lies within the boundaries of the green surface and corresponds to the framework structure (green surface: structural envelope, grey: carbon, red: oxygen, brown: copper, white: hydrogen, reprinted from reference [248]).

of the calculated and observed diffraction pattern.[249] This approach has been demonstrated for a pyrazolyl-based MOF by Bordiga and co-workers..[250]

In contrast to structure determination of small molecules, preconceived assumptions about the framework topology are possible for MOFs, which may help in finding structural solutions. In principle, it is possible to limit the number of possible networks from which crystal structures can be derived by such a *homology modeling*. This means it is possible to create structural models that are related to existing compounds with known crystal structures. One of the earliest homology modeling of a MOF structure has been reported by Ferey and co-workers.[251] Furthermore, this technique has been applied to determine the structure of the series of MOF-74-I to MOF-74-XI on the basis of MOF-74 (see 1.24c on page 40 for a representative).[55] To obtain crystal structures, models were constructed by adding phenylene units with aliphatic substituents to the organic SBU under the retention of the inorganic SBU of MOF-74. The structural models were then subjected to a Rietveld refinement against the powder diffraction data. This procedure is generally applicable for MOFs that exhibit an isoreticular relationship to each other.

# Chapter 3

# Results and Discussion

## 3.1 Synthesis of the Linker Molecules

For the preparation of homochiral MOFs, a linker motif was targeted that offers a high degree of variability. Starting point and source of stereoinformation for this endeavor were natural amino acids from the chiral pool. Amino acids exist as a multitude of differently substituted compounds that differ in their substituent on the β-carbon atom. The carboxylic group of these compounds constitutes a good possibility to functionalize these small, homochiral molecules to rigid linker molecules. The strategy for the synthesis of chiral linker molecules can be grouped as follows: First, a homochiral precursor motif was prepared that is initially inapt to form framework structures. Second, this precursor molecule was further modified by cross-coupling reactions to introduce substituents that have the ability to form metal-oxygen clusters. This strategy of synthesis permits flexibility with regard to the choice of coordinating functional groups and allows – in principle – not only the implementation of the chiral precursors in MOFs but also in other network structures such as organosilica materials.
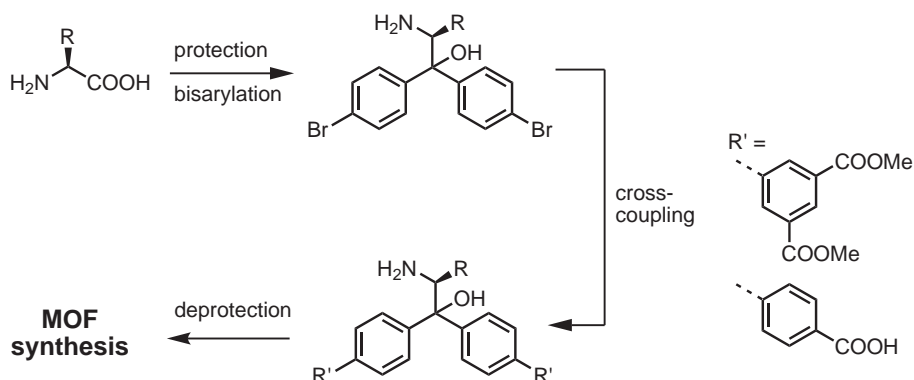


**Scheme 3.1** – Brief overview of the strategy to synthesize chiral linkers from amino acids.

### 3.1.1 Synthesis of the Homochiral Precursor

The reaction sequence to construct homochiral precursors for the synthesis of linker molecules started with natural amino acids in their L-configuraration which are members of the so-called chiral pool and are readily available.

To successfully employ amino acids as building blocks of linker molecules, protection or derivatization was necessary for the amino and the carboxylic

groups, respectively. In the case of the acidic group, the formation of a carboxylic ester was targeted which is a straightforward process. Esterifications of amino acids are commonly achieved by a Fischer esterification, which was also performed in this work. An anhydrous solution of hydrogen chloride was generated *in situ* in methanol which serves as the solvent and as the reaction partner to the amino acid. Acetyl chloride was used in this reaction, which reacts with methanol to form methyl acetate and hydrogen chloride. This very rigorous reaction was cooled in an icebath and the mixture brought to room temperature after thirty minutes. To ensure complete conversions, the reaction solutions were stirred overnight. Due to the excess of hydrogen chloride in the reaction mixture, methyl esters of the amino acids are obtained as hydrochloride salts. The general reaction of amino acids in an acid catalyzed esterification is shown in Scheme 3.2.
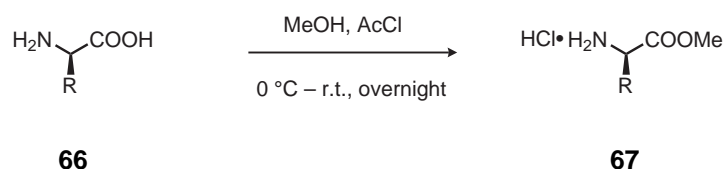


**Scheme 3.2** – Esterification of an amino acid with methanol which is catalyzed by hydrogen chloride generated from acetyl chloride to obtain the hydrochloride of the amino acid methyl ester.

After removal of excess solvent and hydrogen chloride under reduced pressure, the carboxy-protected amino **67** acid was subjected to a protection of the amino group. Amino groups can be protected by many different functional groups that differ in their stabilities at different reaction conditions. For the preparation of a homochiral linker, a protective group is necessary that is stable under the alkaline conditions that occur during substitution reactions at the carboxylic carbon atom which are necessary to obtain a useful structural motif. Here, the *tert*-butyloxycarbonyl (Boc) protective group was chosen as it is stable against most nucleophiles and bases and offers other useful synthetic pathways (see Scheme 3.11, page 101).

A reaction scheme of the *N*-Boc protection reaction of an amino acid is shown in Scheme 3.3. The Boc group can be placed upon the amine by reaction with di-*tert*-butyl dicarbonate, resulting in the reaction product as well as carbon dioxide and isobutene as volatile side products. Because the reaction product of the previous step was used without further purification, an excess of triethylamine was added to the reaction mixture to convert the hydrochlorides of the the respective *N*-protected amino acid into the free amines.
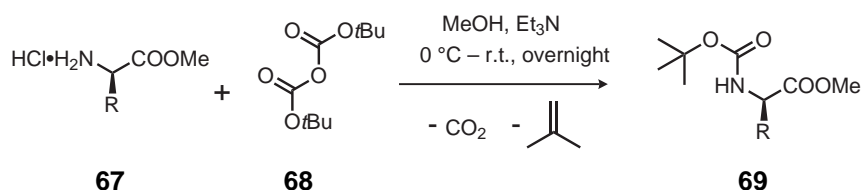
**Scheme 3.3** – *N*-Boc protection of an amino acid methyl ester with di-*tert*-butyl dicarbonate in methanol using triethylamine as an auxiliary base.

The reaction described above was performed with sub-stoichiometrical amounts of the protecting agent. With respect to the amount of the amino acid employed in the esterification procedure, 0.9 equivalents of di-*tert*-butyl dicarbonate were used for the protection of the amino acid. The chosen ratio of starting materials reduces the theoretical yield of the reaction with regard to the amino acid. However, this allowed a workup procedure that is applicable on a large scale up up to 40 g of the reaction product. By ensuring that all di-*tert*-butyl dicarbonate is consumed in the reaction, the desired product can be isolated from unreacted polar byproducts (amino acids with free carboxy or amino groups) by simple extraction with diethyl ether from aqueous acids or bases.

The protection procedure described above was successfully applied to alanine, valine, leucine, phenylalanine and proline. The protected amino acid derivatives were obtained in similar yields ranging from 84 %–88 % determined with respect to the amino acid over two steps. The results of the subsequent esterification and *N*-protection are shown in Scheme 3.4.

After the amino acids have been protected, a bis-arylation was performed at the carboxylic carbon atom. The methyl esters of the modified amino acids can be attacked by carbon nucleophiles to yield a ketone via substitution of methanolate. If an excess of a strong nucleophile is provided, a second attack of a nucleophile yields an alcohol by an addition to the carbonyl group. To obtain a structure that provides the necessary rigidity to form MOFs, a reaction with an aryl system was chosen in the synthetic route. This aryl system provides a position that allows the connection of further substituents via cross-coupling reactions.

Most cross-coupling reactions require halides or pseudo-halides on the electrophilic cross-coupling partner and a metalated carbon atom or a boronic acid on the nucleophilic reaction partner. In order to avoid an additional functionalization of the substrate, the reaction with the amino acid derivatives should be performed with a reactant that already bears a halogen atom on a suitable position of the aromatic system. This is the case, for example, in 4-bromophenyllithium (**77**). This reagent was obtained from 1,4-dibromobenzene (**75**) with
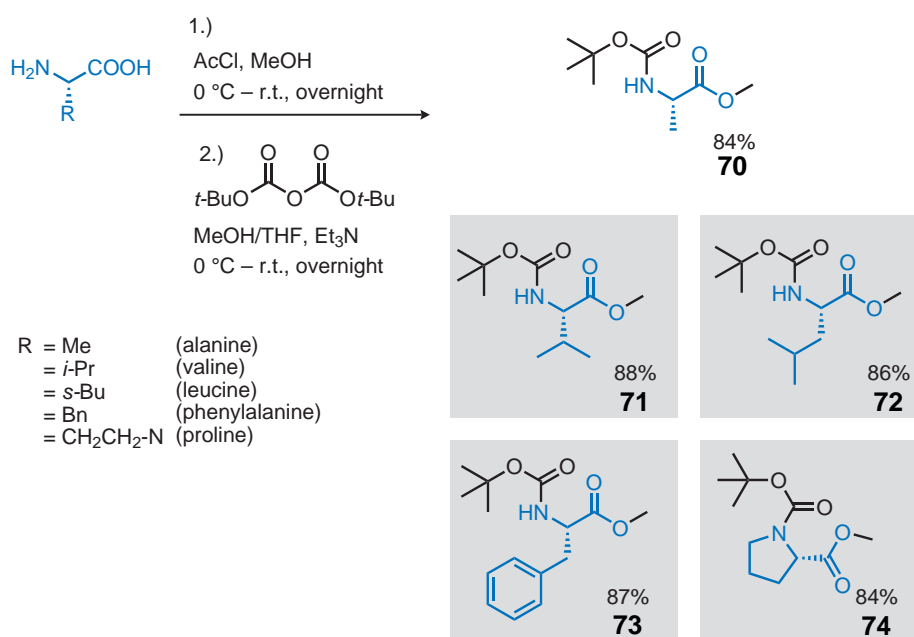
**Scheme 3.4** – Schematic representation of the two subsequent reactions to protect the *C*- and *N*-termini of the amino acids used for the construction of the linker molecules.

equimolar quantities of *n*-butyllithium (**76**). Only monolithiated product is obtained if the reagent was added dropwise to 1,4-dibromobenzene at −78 °C and the reaction mixture was stirred under argon atmosphere for one hour at the temperature given. This reaction is shown in Scheme 3.5.



**75**          **76**                    **77**          **78**
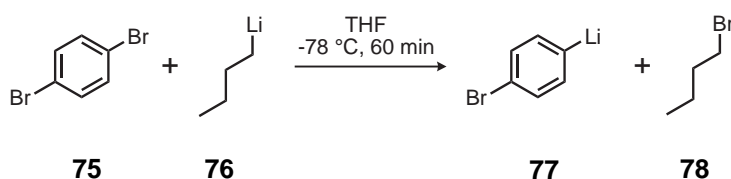
**Scheme 3.5** – Schematic representation of the monolithiation of 1,4-dibromobenzene with *n*-butyllithium that yields 4-bromophenyllithium and 1-bromobutane.

The organometal reagent **77** is unstable at room temperature and must therefore be generated in situ in the reaction with the corresponding amino acid derivatives. The mechanism of the substitution and addition process is shown in Scheme 3.6. In the first step of the reaction the NH group of the carbamate is deprotonated by one equivalent of the phenyllithium species. This anion is stabilized by delocalization over the carbonyl of the Boc group and protects the substrate against further deprotonation that may result in racemization of the stereocenter.[252] In the next step, a substitution of methanolate by the 4-bromophenyl anion occurs at the carbonyl group of the amino acid. This leads to the formation of ketone **82**, which reacts with a third equivalent of (4-bromophenyl)lithium in a nucleophilic addition to yield the alkoxide **83**. After quenching of the anion with aqueous acid, a tertiary *N*-Boc protected amino alcohol is obtained.

The arylation reactions of the modified amino acids are shown in Scheme 3.7. They were performed with three equivalents of the phenyllithium species to account for the loss of one equivalent to the deprotonation step of the reaction. After the generation of the monolithiated aryl species, the respective amino acid methyl esters were added to the cooled reaction mixture as solutions in THF under an argon atmosphere. The reactions were slowly warmed to room temperature and were monitored by thin layer chromatography (TLC). Reactions were quenched with an aqueous solution of ammonium chloride upon the complete consumption of the methyl esters to avoid intramolecular cyclization (see Scheme 3.11, page 101). Tertiary *N*-protected amino alcohols were obtained for the derivatives of alanine, valine, leucine, and phenylalanine in very good yields.
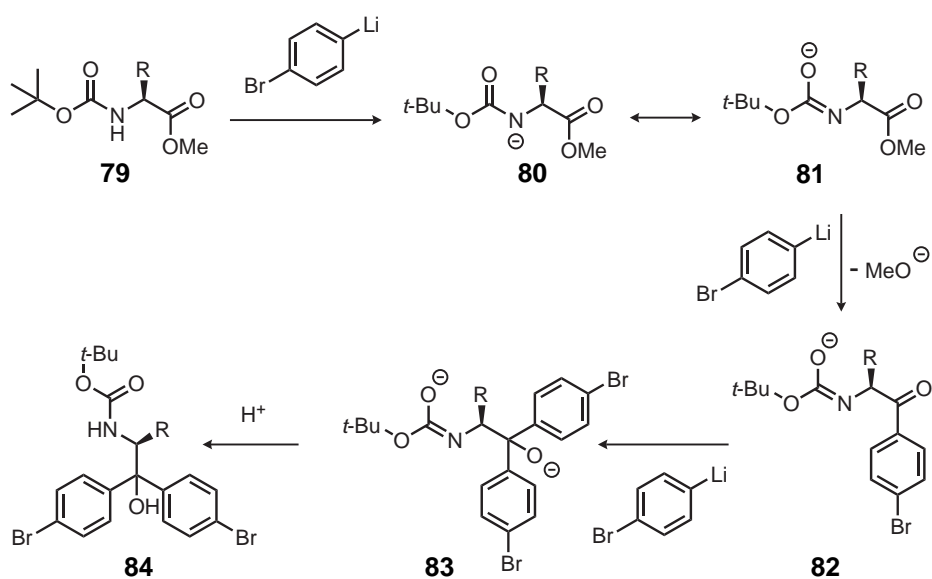
**Scheme 3.6** – Schematic representation of the synthesis of a di(4-bromophenyl) substituted amino acid derivative. The first step of the reaction is a deprotonation of the carbamate that yields an anion which is stabilized by the carbonyl group. In the second step, methanolate is expelled in a substitution reaction with (4-bromophenyl)lithium. The subsequent addition to the ketone yields an alcoholate that is quenched before workup.

**70**   R = Me
**71**   R = *i*-Pr
**72**   R = *s*-Bu
**73**   R = Bn
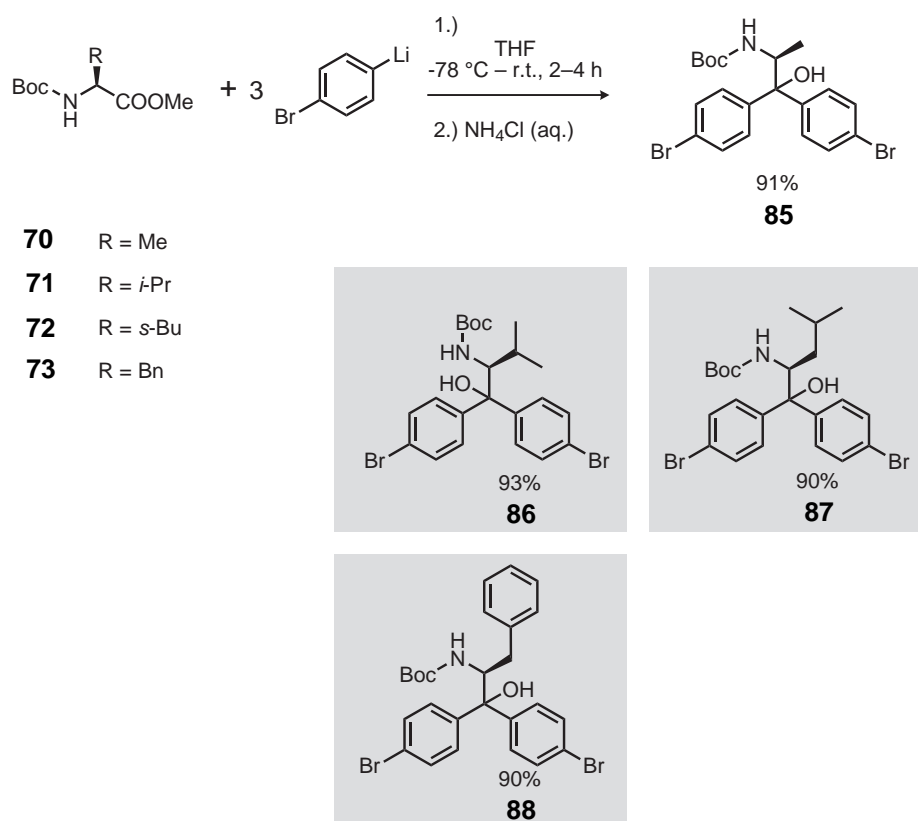
**Scheme 3.7** – Formation of the chiral tertiary *N*-Boc protected amino alcohols from the *N*-Boc protected amino acid methyl esters and (4-bromophenyl)lithium.

Unfortunately, the bisarylation procedure described above proved to be unsuccessful for the modification of *N*-Boc-proline methyl ester. Even after prolonged reaction times, only the monosubstituted ketone was obtained (compare Scheme 3.8). The impeded reaction may be explained by the absence of a stabilized anion on the carbamate that protects the substrate from an irreversible deprotonation at the stereogenic center. The enolate resulting from a deprotonation cannot be attacked by another equivalent of organolithium reagent and leads to the formation of the racemic ketone **89** upon reprotonation.
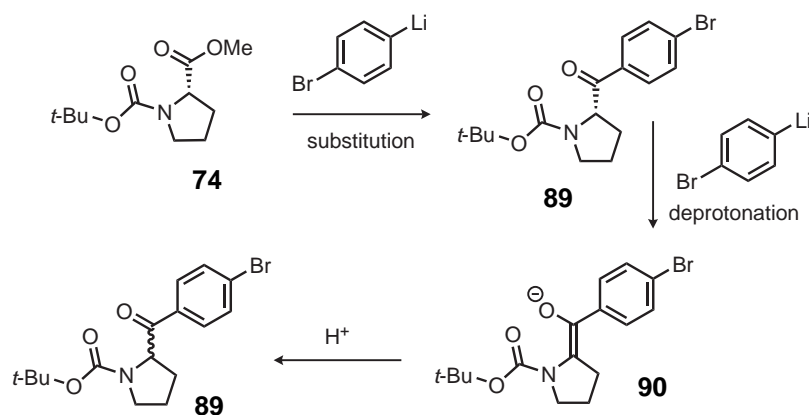


**Scheme 3.8** – Formation of the racemic *N*-Boc protected ketone from *N*-Boc proline methyl ester and (4-bromophenyl)lithium that first acts in a substitution reaction, then as a strong base to deprotonate the proline derivative at the stereogenic center, which results in loss of stereoinformation.

The formation of the unwanted ketone led to an adaption of the protection strategy for the formation of a proline based linker. Instead with a Boc group, the secondary amine of the proline system was protected with a benzyl group. The protection procedure of the carboxylic group remained unchanged. After the esterification, the hydrochloride of the proline methyl ester was reacted with benzyl bromide according to a literature procedure by Manyem and co-workers.[253] Again, an excess of triethylamine was provided to obtain the free amine that can react with benzyl bromide in a nucleophilic substitution (see Scheme 3.9). Compared to the carbamates obtained in the protection strategy described above, the purification of the tertiary amine synthesized by reaction with benzyl bromide requires more effort, because it cannot be separated from the starting materials by an extraction process. Therefore, the product was purified chromatographically. This furnished the pure *N*-benzyl proline methyl esters in a good yield of 78 %.
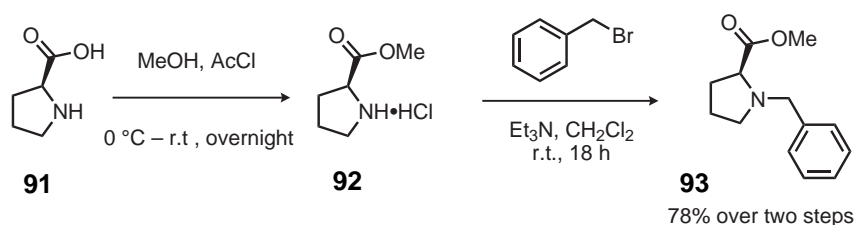
**Scheme 3.9** – Adapted protection procedure for proline. After formation of the ester in an acid catalyzed reaction, the amino group was protected as a tertiary benzylic amine.

The protected proline methyl ester was then successfully employed in a reaction with (4-bromophenyl)lithium in a procedure comparable to the reaction shown in Scheme 3.6. However, for the reaction with the proline derivative only two equivalents of the organo lithium species were employed in the reaction, because no deprotonation occurs that consumes the carbon nucleophile **77**. The substitution-addition sequence gave the desired tertiary amino alcohol in a very good yield of 94 % (see Scheme 3.10). The unwanted ketone that was the main product in the reaction with the *N*-Boc derivative, was not observed in this reaction.
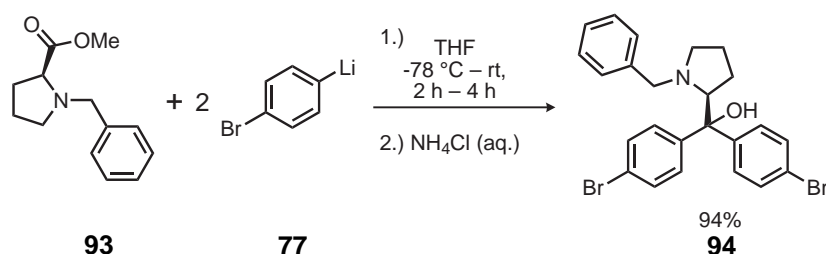


**Scheme 3.10** – Formation of the *N*-benzyl protected prolinol **94** from *N*-benzylproline methyl ester (**93**) and (4-bromophenyl)lithium, that was generated *in situ* from 1,4-dibromobenzene.

The four different compounds obtained through arylation of the amino acid methyl esters are versatile precursors and offer many reaction paths that may lead to a large variety of linker molecules. They can not only be used as precursors to linkers in MOFs but also for the synthesis of porous organosilicas.[254]

The *N*-Boc protected amino alcohol offers an interesting possibility for further modification. The hydroxyl group of the tertiary alcohol can be deproto-

nated with strong bases. The resulting alkoxide can then attack the carbonyl group of the carbamate that protects the amino group. This expels *tert*-butanolate from the molecule, by an addition-elimination mechanism. A general mechanism for this reaction is shown in Scheme 3.11. The intramolecular cyclization results in a five-membered heterocycle. This 1,3-oxazolidin-2-one group is a well-known motif in stereoselective organic synthesis known as the so-called Evans-auxiliary.[255,256] The 1,3-oxazolidin-2-ones obtained here differ from the classical Evans-auxiliaries by the two aryl substituents at the 5-position of the heterocycle. However, similar compounds that are 5,5-diphenyl substituted were reported as *super Quat* auxiliaries which show improved stereoselectivities over the classical Evans-auxiliary.[252,257]
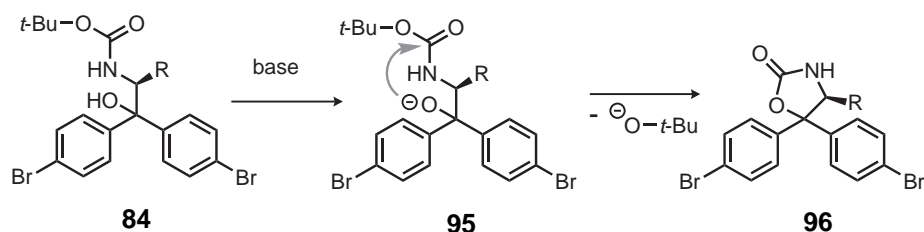


**Scheme 3.11** – General mechanism for the reaction of tertiary *N*-Boc protected amino alcohols with strong bases that can convert the alcohol **84** to an alkoxide **95** which can perform an intramolecular nucleophilic substitution that yields a 1,3-oxazolidin-2-one (**96**).

Intramolecular cyclizations according to the scheme above were performed with the bisarylated derivatives of valine (**86**) and phenylalanine (**88**). A solution of the respective amino alcohol was combined with a solution of potassium *tert*-butanolate, which is also eliminated from the carbamate upon cyclization. The conversion from alcohol to 1,3-oxazolidin-2-one was monitored by TLC over the course of several hours and proceeded with excellent yields (see Scheme 3.12).

R = *i*-Pr **86**      R = *i*-Pr **97** quant.

R = Bn **88**      R = Bn **98** 96%
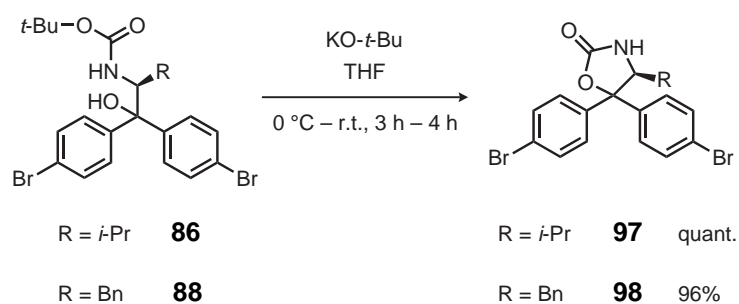
**Scheme 3.12** – Cyclization of the tertiary amino alcohols derived from valine (**86**) and phenylalanine (**88**) to the corresponding oxazolidinones (**97**, **98**) mediated by potassium *tert*-butanolate.

### 3.1.2 Cross-Coupling Reactions with the Chiral Precursor

In the previous section, the synthesis of a chiral bifunctional precursor molecules was described. These precursors need further modification with coordinating functional groups to act as linkers in the synthesis of MOFs.

In a very straightforward approach, bisarylated precursors may be extended to dicarboxylic acids in a cross-coupling reaction. Simple boronic acids such as 4-carboxyphenylboronic acid are commercially available. They can be coupled to the bisarylated precursor in a Suzuki reaction (see Scheme 3.13). This palladium-catalyzed reaction works under mild conditions. The reaction was performed in a solvent mixture of DMF and water to ensure the solubility of the reaction partners. The reactants formed the desired product upon heating to reflux for three to four hours. After the reaction of the bisarylated amino acid precursors with the boronic acid, the resulting dicarboxylic acids were precipitated directly from the reaction and used without further purification because a conventional chromatographic workup is difficult due to the high polarity of the carboxylic groups.



| R = Me | **85** | | R = Me | **99** | 69% |
| R = *i*-Pr | **86** | | R = *i*-Pr | **100** | 63% |
| R = Bn | **88** | | R = Bn | **101** | 70% |
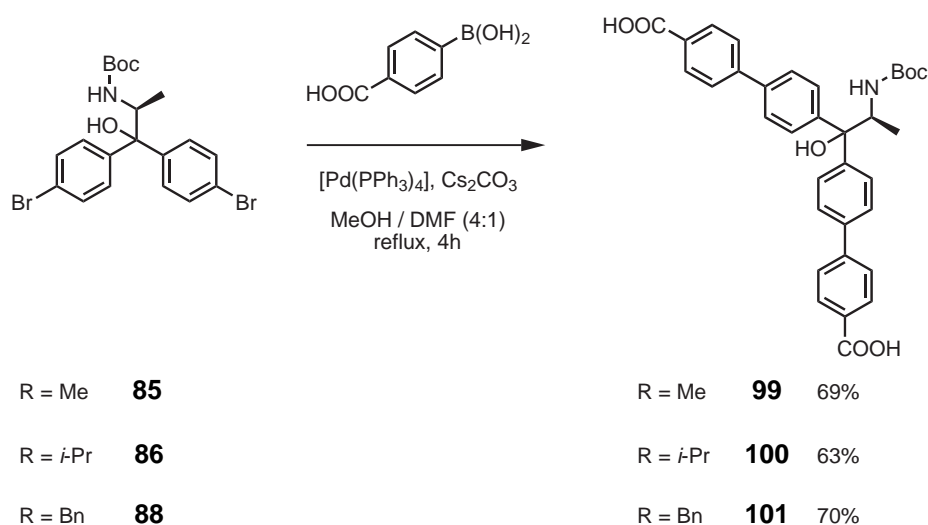
**Scheme 3.13** – Suzuki cross-coupling reaction between 4-carboxyphenyl boronic aicd and the bisarylated precursors derived from alanine (**85**), valine (**86**) and phenylalanine (**88**) to synthesize the corresponding dicarboxylic acids **99**, **100**, and **101**.

The catalytic cycle of the first coupling between one equivalent of the boronic acid and the bisarylated compound is shown is Scheme 3.14. The second catalytic cycle that yields the dicarboxylic acid proceeds analogous to the first.

To obtain tetracarboxylic acids, a suitable building block is needed, that can be coupled to the bisarylated amino acid precursors in a cross-coupling reaction. This is the case, for example, for an isophthalic acid derivative that bears a boronic acid, which can be exploited in a Suzuki cross-coupling reaction. Such a building block was obtained from dimethyl 5-aminoisophthalate **107** in a two-step reaction sequence. In the first step of the sequence, a Sandmeyer-type radicalic substitution was performed at the aromatic amine which is transformed into the corresponding diazonium salt.[258] This activated aromatic species is then converted to *O,O*-dimethyl-5-iodoisophthalate **109**. In contrast to typical Sandmeyer conditions, the reaction depicted in Scheme 3.15 is copper-free and the catalytic cycle comprises different radical iodine species.[259,260]

In the next reaction, the iodide **109** is converted to a boronic acid. This is achieved by the attack of a carbon nucleophile to trimethylborate and subsequent hydrolysis. The carbon nucleophile was obtained in a halogen-metal exchange of the iodide **109** with the so-called TurboGrignard reagent isopropyl-magnesium chloride lithium chloride complex (*i*PrMgCl · LiCl).[261] This reagent excels in the halogen-magnesium exchange and can be used to synthesize metalated aryl species. In contrast to the direct metalation with elemental magnesium or with organolithium compounds, a large number of functional groups are tolerated – including carboxylic esters, because the exchange reactions can be performed at temperatures below $-20\,^\circ$C.[262] In the TurboGrignard reagent, lithium chloride introduces a negative charge on the magnesium center. This increases the nucleophilicity of the isopropyl group on a magnesiate-type dimetal intermediate which enhances the rate of the halogen-magnesium exchange.[263] To synthesize the boronic acid, the iodide **109** was reacted with the TurboGrignard reagent at $-20\,^\circ$C to obtain the isophthalate Grignard species **110** (see Scheme 3.16). This metalated intermediate was reacted with a large excess of trimethyl borate to prevent the di- and trisubstitution at the boron atom. The methyl boronate ester was then hydrolyzed under mild acidic conditions to retain the ester functionality of the isophthalate residue. Precipitation from an aqueous solution gave the desired product with 88 % yield.

The boronic acid that was obtained in the procedure described above was applied to the synthesis of tetracarboxylic acids. The bisarylated amino acid precursors were reacted under similar conditions as described for the dicarboxylic acids in Scheme 3.13. However, the reactions to synthesize the dicarboxylic linkers were carried out in a solution of DMF and methanol and 2-dicyclohexylphosphino-2′,6′-dimethoxybiphenyl (SPhos) was added to the reaction mixture. This organophosphorous compound increases the activity of the
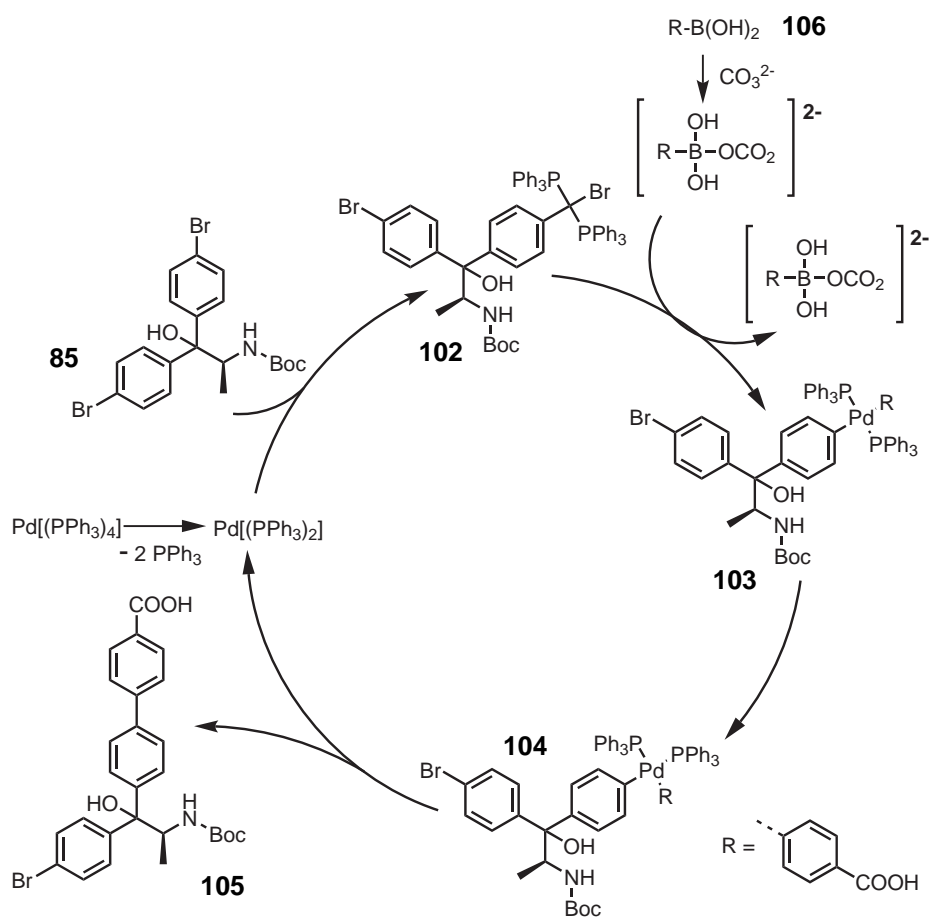
**Scheme 3.14** – Mechanism of the Suzuki cross-coupling reaction; after the loss of two PPh$_3$ ligands, the Pd(0) species inserts into the C$-$R bond in an oxidative addition. The boronate generated from **106** and an appropriate base reacts in a transmetalation with the Pd$-$Br complex and the aryl group is transferred onto the substrate **103**, followed by rearrangement to **104** in which both aryl groups are oriented *cis* to each other. Reductive elimination restores the catalytically active Pd(0) species and provides the monoarylated compound **105**.

105
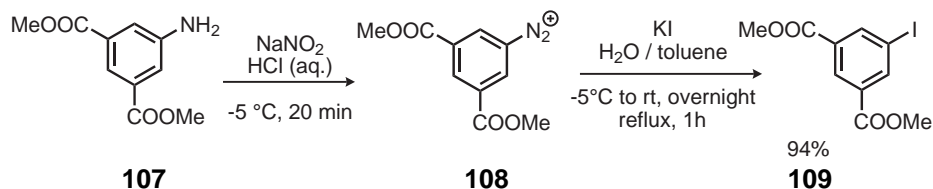
**Scheme 3.15** – Sandmeyer-type reaction of *O,O*-dimethyl-5-amino isoph-thalate to the iodo-substituted dimethylisophthalate (**109**) via the diazo-nium salt **108** in a radical reaction.
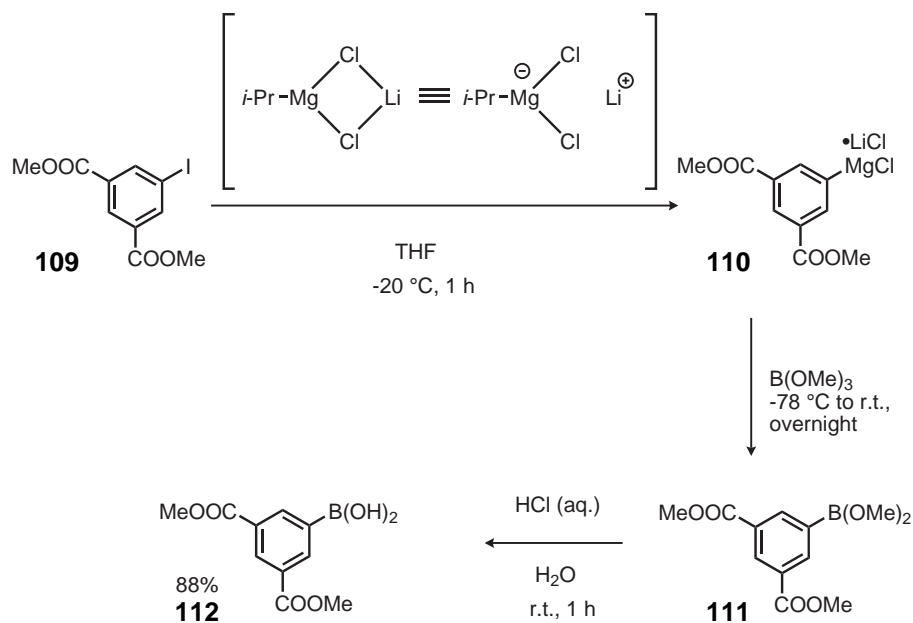


**Scheme 3.16** – Synthesis of dimethyl 5-boronoisophthalic acid **112** from *O,O*-dimethyl-5-iodoisophthalate. A Grignard intermediate (**110**) is ob-tained through a halogen-metal exchange with the TurboGrignard reagent that benefits from coordination of lithium chloride to induce an extra nega-tive charge on the magnesium atom. The aryl magnesium species **110** reacts with trimethyl borate to the boronate ester **111** which is hydrolyzed selec-tively to the boronic acid **112**.

106

palladium complex that catalyzes the Suzuki reaction due to the electrondonating capacity of the phosphorus atom in the ligand.[264,265] Scheme 3.17 shows the cross-coupling reactions of the *N*-Boc protected amino alcohols that were successfully performed for the derivatives of alanine, valine, leucine and phenylalanine with yields between 50 % to 64 %. Because the carboxylic groups are protected as methyl esters, the polarity of the molecules is lower than the free dicarboxylic acids described in Scheme 3.13. Therefore, the tetracarboxylate esters were purified using a chromatographic procedure.



| R = Me | **85** | | R = Me | **113** | 56% |
| R = *i*-Pr | **86** | | R = *i*-Pr | **114** | 64% |
| R = *s*-Bu | **87** | | R = *s*-Bu | **115** | 50% |
| R = Bn | **88** | | R = Bn | **116** | 59% |
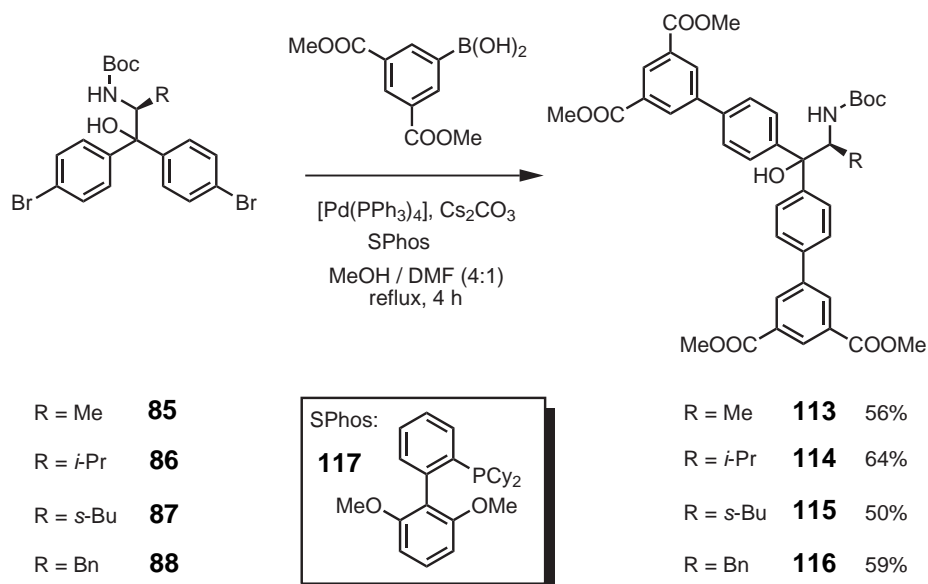
**Scheme 3.17** – Synthesis of the tetracarboxylic methyl esters from the bisarylated derivatives of alanine (**85**), valine (**86**), leucine (**87**), and phenylalanine (**88**) in a palladium catalyzed cross-coupling with two equivalents of the isophthalateboronic acid **112**. The SPhos ligand (**117**, Cy: cyclohexyl) is added to obtain a highly active Pd(0) species.

Cross coupling reactions were carried out using freshly prepared tetrakis-(triphenylphosphine)palladium(0) (Pd[(PPh$_3$)$_4$]) and degassed solvents to prevent the oxidation of the catalyst. The reactions of the bisarylated Evans auxiliaries and the *N*-benzyl protected proline derivative proceed analogous to the procedure described above and are depicted in Scheme 3.18 and Scheme 3.19,

respectively.[1] The yields of the reactions are comparable to those of the *N*-Boc protected amino alcohols.



R = *i*-Pr    **97**

R = Bn    **98**

R = *i*-Pr    **118**   75%

R = Bn    **119**   56%

**Scheme 3.18** – Synthesis of the tetracarboxylic methyl esters from the bis-arylated 1,3-oxazolidinones derived from valine (**97**) and phenylalanine (**98**) in a palladium-catalyzed cross-coupling with two equivalents of the isophthalateboronic acid **112**. The SPhos ligand was only applied in the cross-coupling with **97**.

The Suzuki couplings presented above, provided tetramethyl ester that need to be converted into the corresponding free acids to be applicable as linkers in the synthesis of MOFs. The hydrolysis of carboxylic esters is a straightforward process if they are reacted with aqueous bases. However, due to the extended aromatic system of the compounds, the tetramethyl esters are insoluble in water. Therefore, the reaction was performed in a biphasic system of THF and an aqueous solution of potassium hydroxide. Upon complete consumption of the starting materials, the organic solvent was removed in vacuum. The reaction products were then obtained in good yields by precipitation if the alkaline aqueous solution was acidified with concentrated hydrochloric acid. The results of the hydrolysis of the *N*-Boc protected tetracarboxylic methyl esters are shown in Scheme 3.20.

In an analogous procedure, the Evans-type linkers were obtained with better yields than those for *N*-Boc protected amines. The results of these deprotection reactions are shown in Scheme 3.21.

---

[1]The reaction of the benzyl substituted 1,3-oxazolidin-2-one **98** is an exception because it was performed in absence of SPhos.

**Scheme 3.19** – Synthesis of the tetracarboxylic methyl ester from the bis-arylated derivative of proline (**94**), in a palladium-catalyzed cross-coupling with two equivalents of the isophthalateboronic acid **112**.
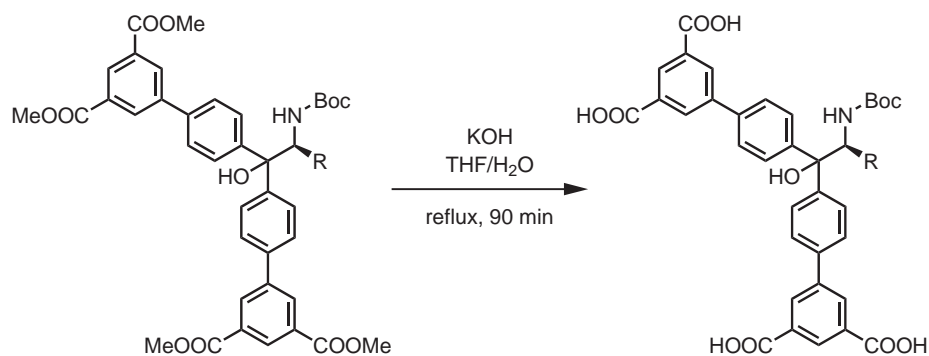


| | | | | | |
|---|---|---|---|---|---|
| R = Me | **113** | | R = Me | **121** | 85% |
| R = *i*-Pr | **114** | | R = *i*-Pr | **122** | 80% |
| R = *s*-Bu | **115** | | R = *s*-Bu | **123** | 82% |
| R = Bn | **116** | | R = Bn | **124** | 82% |

**Scheme 3.20** – Hydrolysis of the *N*-Boc protected tetracarboxylic methyl esters derived from alanine (**113**), valine (**114**), leucine (**115**), and phenylalanine (**116**), in a biphasic mixture of THF and aqueous potassium hydroxyide providing the free carboxylic acids after acidic workup.

R = *i*-Pr **118**

R = Bn **119**

R = *i*-Pr **125** 85%

R = Bn **126** quant.
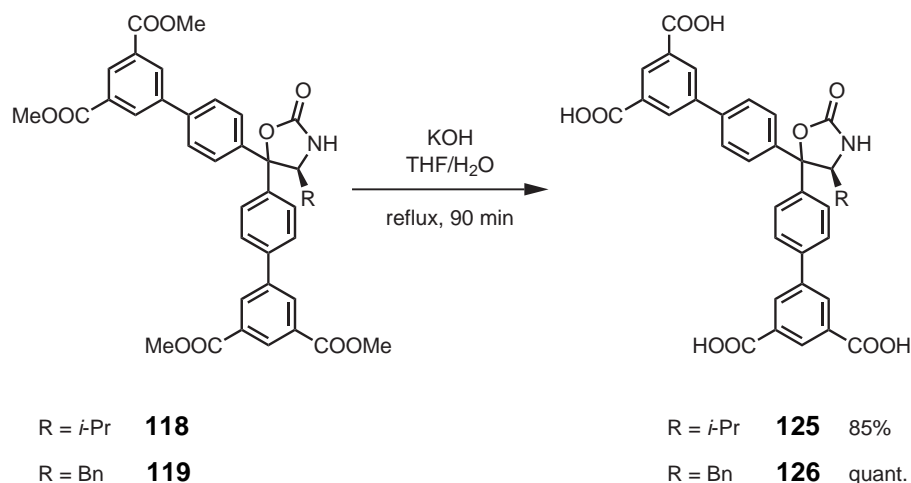
**Scheme 3.21** – Hydrolysis of the methyl esters bearing a 1,3-oxazolidin-2-one derived from valine (**118**) and phenylalanine (**119**), in a biphasic mixture of THF and aqueous potassium hydroxide providing the free carboxylic acids after acidic workup.

The removal of the *N*-benzyl protective group is usually performed under a hydrogen atmosphere together with palladium/charcoal as a heterogeneous catalyst. This reaction system requires a good solubility of the protected substrate. Therefore, the deprotection of the *N*-benzyl group was performed with the tetramethyl ester instead of the carboxylic acid. An attempted reaction in methanol using a hydrogen-filled balloon to provide a hydrogen atmosphere together with a palladium catalyst (10 wt% on charcoal) gave only unsatisfactory results. After several days, no conversion of the *N*-benzyl protected amine was observed. The reaction was repeated in an autoclave heated to 40 °C under a hydrogen pressure of 50 bar. Here, a deprotection was observed but the reaction was very slow. This is possibly the case, because the deprotected amine can coordinate to the palladium and inhibit further reactions. To overcome this effect, the reaction was carried out again with the addition of sulfuric acid at 40°C and 50 bar. After evaporation of most of the solvent, the reaction product was obtained as the sulfuric acid adduct of the amine and was used directly in the next step. The deprotection reaction of the secondary amine is depicted in Scheme 3.22.

The residue with the hydrosulfate **127** that was obtained in the previous step was directly utilized in the deprotection of tetracarboxylic methyl esters. The remaining sulfuric acid was neutralized by the large excess of potassium hy-
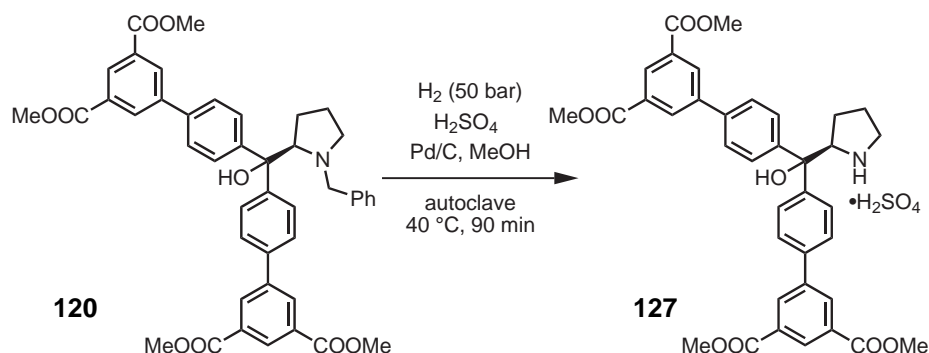
**Scheme 3.22** – Hydrogenolysis of the *N*-benzyl protective group on the tetramethyl esters bearing the proline derivative **120** using palladium on charcoal as a heterogeneous catalyst provides the unprotected amine as a hydrosulfate salt (**127**).

droxide that was used as a reagent to cleave the ester groups. After heating the mixture to reflux for two to three hours, the organic solvent was removed in vacuum and an aqueous solution was obtained. The addition of hydrochloric acid to the alkaline solution of the carboxylate led to the precipitation of the reaction product. The product was obtained with 71 % yield over two steps as a hydrochloride salt (see Scheme 3.23). The deprotected tetracarboxylic acid was used without further purification in the synthesis of MOFs.
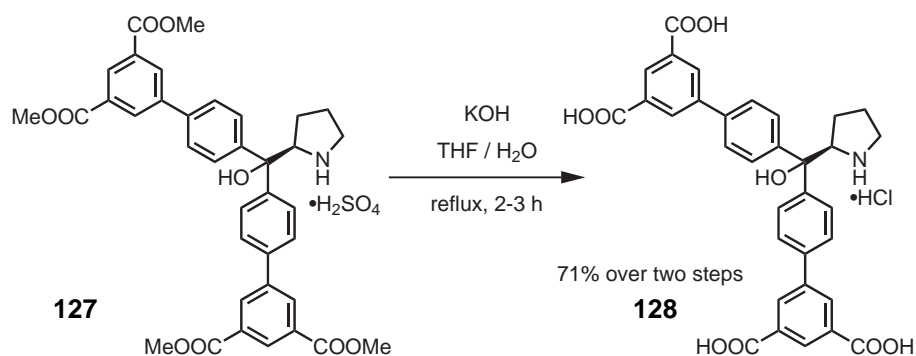


**Scheme 3.23** – Hydrolysis of the methyl esters on the deprotected derivative of proline (**127**) in a biphasic mixture of THF and aqueous potassium hydroxide provides the free carboxylic acids after acidic workup.

111

Deprotection of the *N*-Boc functionalized amines group can be achieved using acidic catalysis.[266] After protonation of the C=O group of the carbamate, a rearrangement reaction is induced. This cleaves the Boc group from the amine and produces carbon dioxide and isobutene. The reaction was performed in a solution of trifluoroacetic acid (TFA) and dichloromethane and is depicted in Scheme 3.24. The deprotected amines were obtained in good yields as TFA salts, upon precipitation after the addition of diethyl ether as a non-polar antisolvent.
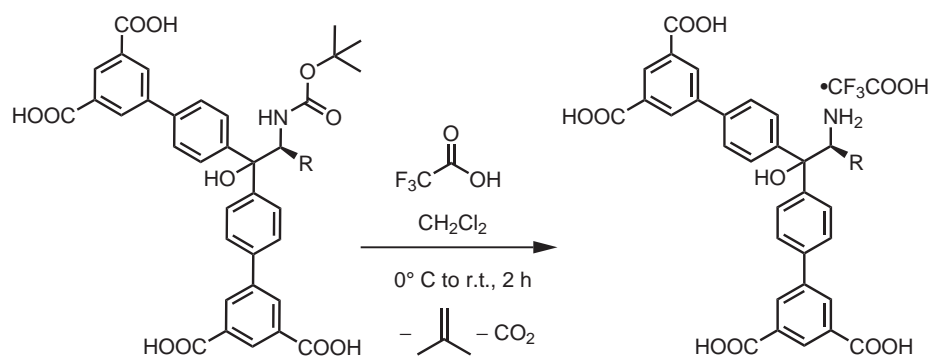


| | | |
|---|---|---|
| R = Me | **121** | |
| R = *i*-Pr | **122** | |
| R = *s*-Bu | **123** | |
| R = Bn | **124** | |

| | | |
|---|---|---|
| R = Me | **129** | 74% |
| R = *i*-Pr | **130** | 72% |
| R = *s*-Bu | **131** | 80% |
| R = Bn | **132** | 75% |

**Scheme 3.24** – Cleavage of the *N*-Boc protective group from the tetracarboxylic acids derived from the different amino acids using TFA in $CH_2Cl_2$.

### 3.1.3 Synthesis of a Benzophenone Tetracarboxylate

In attempts to obtain a homochiral linker that resembles the linker used in the synthesis of UHM-3,[267] a structure was targeted that has a geometry similar to (5,5'-dimethylsilanediyl)diisophthalate (dmsdip) but exhibits a carbonyl carbon atom, that may be functionalized with chiral substituents. In the first step of this reaction sequence, a Grignard reaction was performed on ethyl formiate (see Scheme 3.25). The Grignard reagent was obtained from 1-bromo-3,5-dimethylbenzene (**133**) in a reaction with magnesium in THF. This organomagnesium compound was reacted with the ethyl ester of formic acid in a addition-elimination reaction followed by a nucleophilic addition to the resulting ketone. After quenching of the reaction solution, a secondary alcohol was obtained with 88 % yield after recrystallization from diethyl ether.
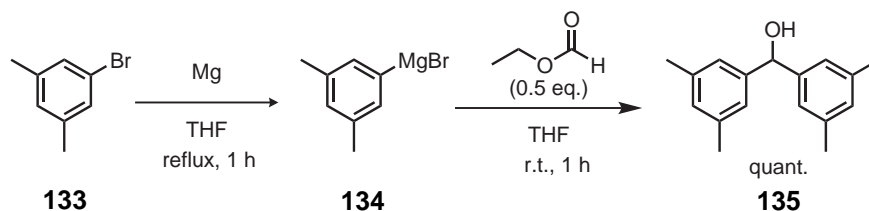


**Scheme 3.25** – Formation of a Grignard reagent from 1-bromo-3,5-dimethyl benzene (**133**) and the subsequent reaction with 0.5 equivalents of ethyl formiate which results in the formation of the secondary alcohol **135**.

In the next step, the secondary alcohol was oxidized. The oxidation was performed under relatively harsh conditions: In a steel autoclave lined with polytetrafluoroethylene (PTFE), a suspension of the alcohol **135** in nitric acid (20 %) was heated to 140 °C for 14 hours. This afforded the material as pale, plate-like crystals with a yield of 53 %. This procedure oxidized both the methyl groups to carboxylic acids and the secondary alcohol to the desired ketone.

Attempts of further modification of the tetracarboxylic acid or its tetramethyl ester derivative with chiral diols into acetals were unsuccessful. However, the tetracarboxylate was used in experiments to create new MOF structures (see Section 3.4.1, page 156). Furthermore, this linker motif was used in another work: In her experiments with this tetracarboxylic linker, Peikert developed a modification strategy using a condensation with alkyl amines followed by a reduction of the resulting imines. This led to tetracarboxylic alkyl amines that were successfully applied in the synthesis of achiral MOFs.[268]

113
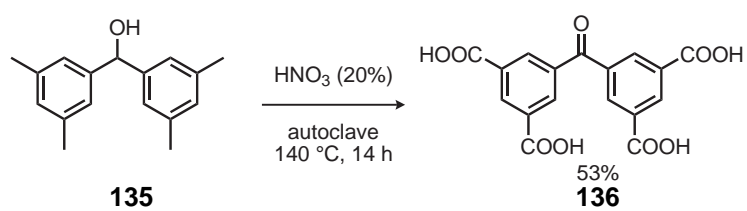
**Scheme 3.26** – Oxidation of the secondary alcohol **135** in hot nitric acid converts the alcohol to a ketone and the methyl groups to carboxylic acids in 3,3′,5,5′-tetracarboxylbenzophenone.

## 3.2 Synthesis and Characterization of UHM-24

In an effort to obtain homochiral MOFs from the V-shaped ditopic linker system, the dicarboxylic acids were subjected to a solvothermal syntheses with a Zn(II) species in DMF. The reactions to synthesize a framework material were performed in small reaction vessels with a volume of circa 8 mL that were tightly sealed by crimping. After heating the reaction mixture to 80 °C for 24 hours, crystalline material was obtained from the reaction with the linkers derived from alanine, valine and phenylalanine (see Scheme 3.27).



R = Me    **99**                R = Me    **137**

R = *i*-Pr    **100**           R = *i*-Pr    **138**

R = Bn    **101**               R = Bn    **139**
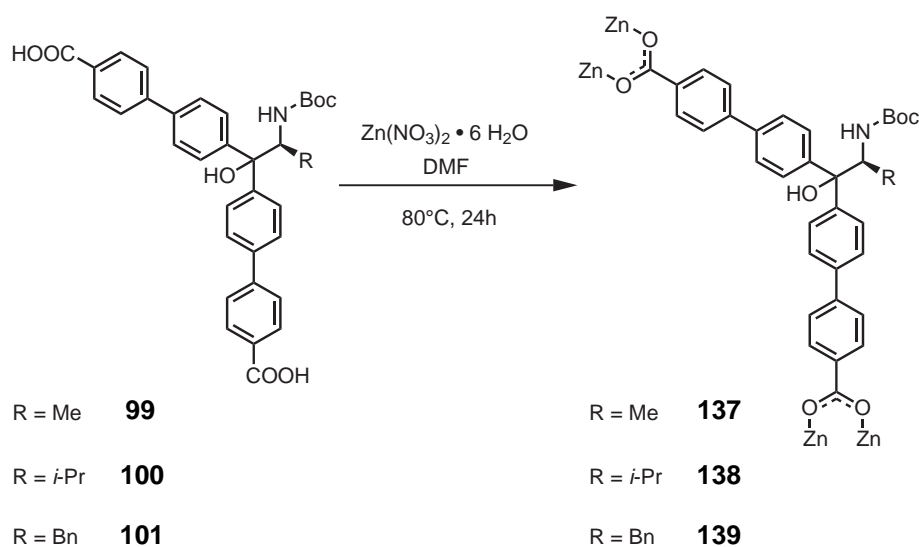
**Scheme 3.27** – Schematic representation of the reaction of the dicarboxylic linkers derived from alanine, valine and phenylalanine with a Zn(II) source that yields a fine, crystalline material (bonds to zinc atoms are added to indicate the participation in a framework structure).

In a reaction of the dicarboxylic linker **99** with a solution of $Zn(NO_3)_2 \cdot 6\,H_2O$ in DMF, very fine needles were obtained. A single crystal of this material was analyzed by X-ray diffraction methods. Because of the very small size of the crystal only a limited amount of structural information could be deduced. However, on the basis of this information a structural model was deduced by homology modeling that was refined against the PXRD data of microcrystalline UHM-24 (see Figure 3.5). The simulated and the experimental PXRD patterns are in good agreement.

115

UHM-24-Ala-Boc crystallizes in the orthorhombic space group *I*222 with the unit cell parameters $a = 5.9940$ $b = 20.4794$ $c = 38.3283$ Å. The inorganic SBU of this material comprises zinc atoms that are bridged by oxo- and carboxylate groups. This results in the formation of infinite, one-dimensional zinc-oxygen chains. The chains resemble the inorganic SBU that can be found in MOF-69 series.[269,270] In these chains, two type of zinc atoms are stacked along the crystallographic *a* axis and are distributed in a ratio of 2:1 in alternating arrangement. The first kind of zinc atom is coordinated by four oxygen atoms in a distorted tetrahedral arrangement that shares an edge with another tetrahedral zinc-oxygen cluster. These tetrahedral zinc atoms can be transformed into each other by a $C_2$-rotation along the crystallographic *a* axis. The other type of zinc atoms is octahedrally coordinated by six oxygen atoms. Each octahedral zinc-oxygen cluster is connected to the corners of four tetrahedral zinc-oxygen clusters via $\mu_3$ oxygen atoms and to four bridging carboxylic groups of the linkers. The two tetrahedrally coordinated zinc atoms and the octahedrally coordinated zinc atom are connected to each other via two $\mu_3$ oxygen atoms. The coordinating carboxylate groups of the linker are bound to both an octahedral and a tetrahedral zinc atom in a bi-monodentate fashion. The different types of zinc-oxygen clusters are stacked regularly in an alternating arrangement of tetrahedral and octahedral clusters. A part of the infinite SBU is shown in Figure 3.1.
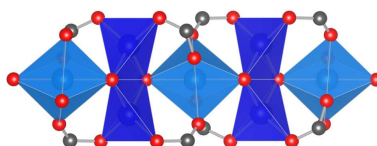


**Figure 3.1** – View along the *b* direction on a part of the infinite, one-dimensional inorganic SBU in UHM-24. Tetrahedral and octahedral zinc-oxygen clusters are stacked along the *c* direction, clusters are bridged via $\mu_3$ oxygen atoms and the carboxylic groups of the linkers (grey: carbon, red: oxygen, light blue polyhedra: octahedral zinc, dark blue polyhedra: tetrahedral zinc).

Two-dimensional tertiary structures that resemble pleated sheets are formed by the interconnection of neighboring inorganic SBUs via the V-shaped organic SBUs. These sheet-like structure comprise infinite rhombic channels and are depicted in 3.2b.

The sheets are tightly stacked along the *c* axis (see Figure 3.3). In this arrangement, the chiral substituents of the linkers are pointing into a cavity formed

**(a)**



**(b)**
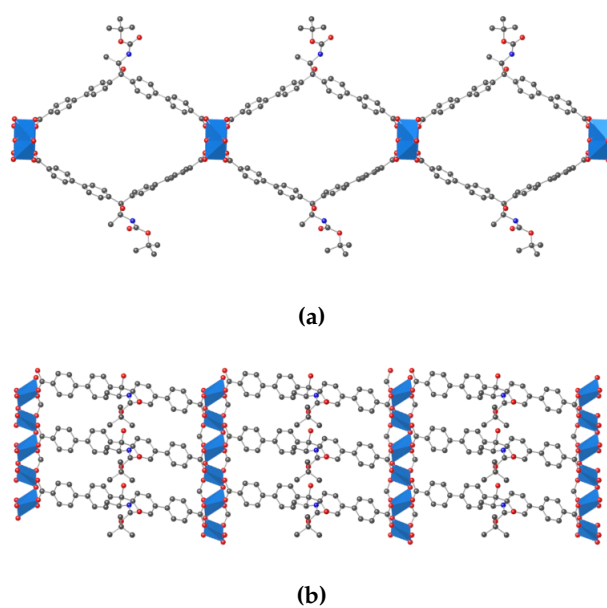
**Figure 3.2** – (a) view along the crystallographic *a* axis of a two-dimensional superstructure formed in UHM-24-Ala (b) view along the *c* direction of the same superstructure; one-dimensional inorganic SBUs are connected by V-shaped dicarboxylates resuling in rhombic channels (grey: carbon, red: oxygen, blue octahedra: zinc, blue tetrahedra: zinc).

by the inorganic SBU and two organic SBUs of a neighboring two-dimensional sheet. This is a very unfavorable position of the chiral residues with regard to the usability of the substituent as it is most likely shielded in this cavities.
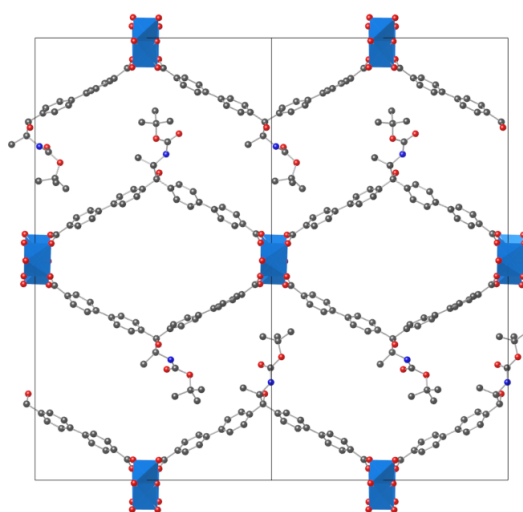


**Figure 3.3** – View along the *a* direction of a 2 × 2 × 2 super cell of UHM-24-Ala. Stacked sheets are formed in which the chiral residues are pointing into a cavity spanned by two halves of a linker molecule bound to the inorganic SBU (grey: carbon, red: oxygen, blue octahedra: zinc, blue tetrahedra: zinc).

The occurrence of such two-dimensional sheets may be explained by the preferred conformation of the linker in the organic building unit. Similar systems have been reported, where such V-shaped linkers led to either one-dimensional chains or two-dimensional sheets.[271,272] O'Keeffe, Yaghi and co-workers postulated that such low-dimensional system can be expected from ditopic linkers in which the carboxylic groups are arranged with an "folded" orientation.[18] This orientation can be viewed as a linear linker in which the carboxylic groups were originally coplanar that has been folded into a 120°angle. If zero-dimensional inorganic SBU, such as paddle wheels, are connected by such linkers, one-dimensional chains are formed. Correspondingly, two-dimensional sheets are observed, if the linkers connect one-dimensional inorganic SBUs, which is the case in UHM-24. A schematic representation of this concept is shown in Figure 3.4.

Unfortunately, in the reactions with the linkers derived from valine (**100**) and phenylalanine (**101**), only microcrystalline material was obtained, that did not

**(a)**

**(b)**
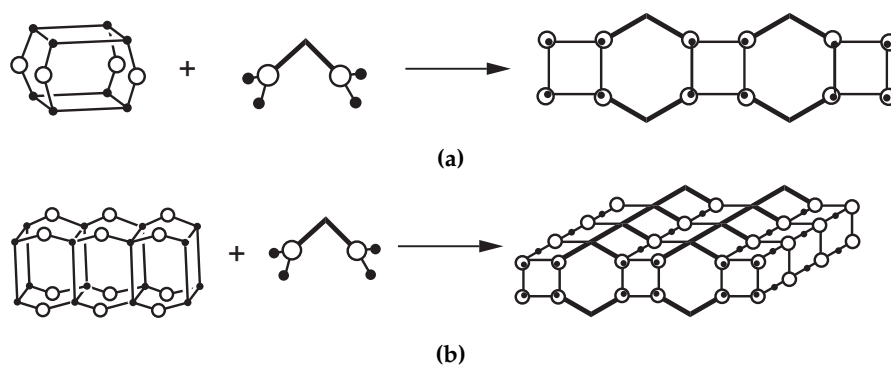
**Figure 3.4** – Schematic representation of (a) the preferred formation of a one-dimensional chain from square-planar and V-shaped building units and (b) the formation of two-dimensional sheets from hypothetical rod-like and V-shaped building units (white circles: carbon, black dots: oxygen).

allow any single crystal diffraction experiments. However, in each case the X-ray powder diffraction pattern indicates an isostructural relationship between the materials obtained from these linkers and the material from the linker derived from phenylalanine (**101**). Powder diffraction data for the three isoreticular compounds are shown in Figure 3.5. The crystallinity of UHM-24-Ala is less pronounced than for the isoreticular compounds UHM-24-Val and UHM-24-Phe.

MOFs of the UHM-24 series showed no porosity in nitrogen physisorption measurements after thermal activation. This can be attributed to the dense crystal structure of the materials. Because of their crystal structure in which the chiral residues are blocked, UHM-24 has low prospects in stereoselective applications. Therefore, no further evaluation of these materials was carried out.
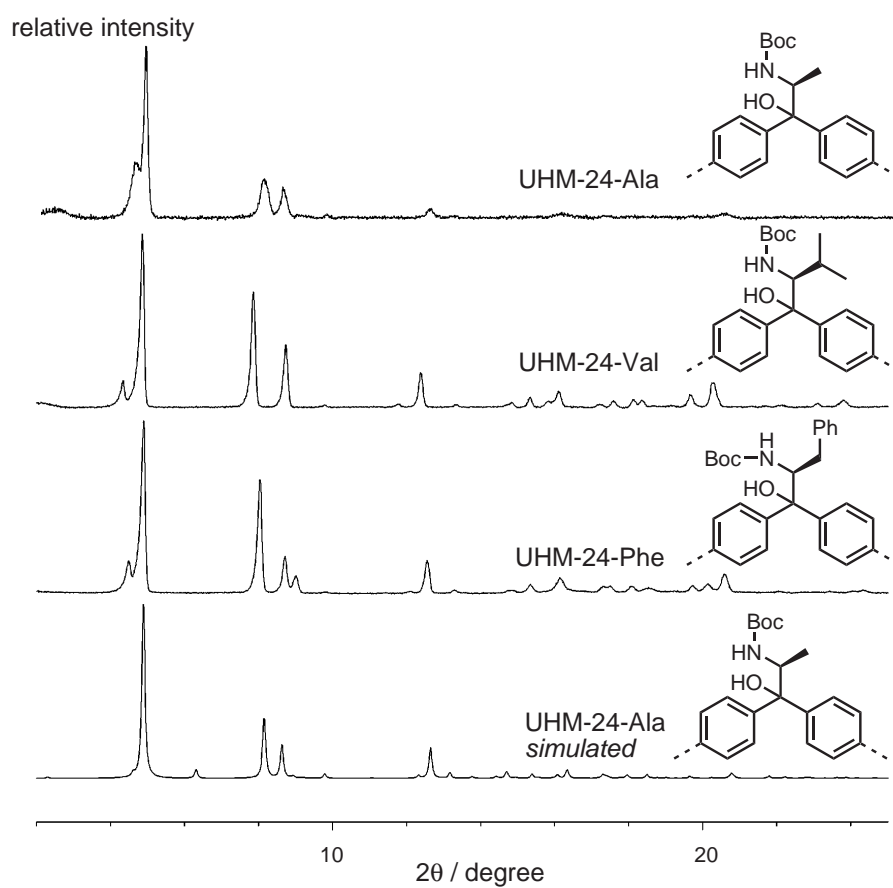
**Figure 3.5** – PXRD data for the materials of the UHM-24 series; similar diffraction patterns are observed for all materials of the isoreticular UHM-24 series and show good agreement with the simulated PXRD pattern of UHM-24-Ala (bottom).

## 3.3 Synthesis and characterization of UHM-25

To increase the dimensionality of the frameworks formed by the oligocarboxylic derivatives of amino acids, further studies were performed using tetracarboxylic instead of a dicarboxylic linkers. The tetracarboxylic acids were employed in solvothermal syntheses that were performed in screw-capped flasks. After heating to 40 °C for three days, crystalline materials were obtained from the reaction of a Cu(II) salt with the *N*-Boc protected linkers derived from alanine, valine, leucine and phenylalanine (see Scheme 3.28). This reaction is shown in Scheme 3.28. In the synthesis of the MOFs, copper nitrate and the linker were used in a molar ratio of 10 : 6. The reaction was performed in a mixture of DMF and water. Furthermore, twelve equivalents of nitric acid was added to reaction mixture as a modulator. The materials, which are obtained as light blue crystals, were isolated by filtration from the mother liquor, washed with DMF and stored under solvent (DMF or THF).

In a small-scale reaction of the tetracarboxylic linker **121** with a solution of $Cu(NO_3)_2 \cdot 3 H_2O$ in DMF/water/$HNO_3$, blue, block-shaped crystals were obtained.[2] A single crystal of this material was analyzed by X-ray diffraction and the crystal structure of the MOF was determined as follows.

UHM-25-Ala-Boc crystallizes in the cubic space group *P*432 with the unit cell parameters $a = b = c = 28.9431$ Å. The tetracarboxylate linker serves as a four-connected organic SBU. Copper paddle wheel motifs constitute four-connected inorganic SBU. Due to the angle of 120° between the carboxylic groups on the isophthalate moieties, cuboctahedral metal-organic polyhedra (MOPs) are formed as subunits in this MOF. These MOPs are well-known structural motifs on their own[273–277] or in extended frameworks.[278–280] The arrangement of 24 isophthalic residues and twelve copper paddle wheels that form the MOP is shown in Figure 3.6. The resulting subunit can be represented as a cuboctahedron in which the inorganic SBUs constitute the corners and the isophthalate residues occupy the edges of the polyhedron. The interatomic distance of two opposing copper atoms that lie on the corner of the cuboctahedron is 15.7 Å; taking into account the van-der-Waals radii of the atoms the pore diameter for the cuboctahedral pore amounts to 12 Å.

The cuboctahedral MOPs form a primitive cubic arrangement in the three dimensions of the crystal structure. Each MOP is connected to a neighboring MOP via the organic SBUs that carry the isophthalate residues. A representation of an extended unit cell is shown in Figure 3.7. In this structure, four V-shaped linker molecules connect four MOPs that lie on the corners of the unit cell. To increase clarity, any disorder of the organic SBU has been omitted. The disorder arises

---

[2]Single crystals of MOFs were also obtained from linkers **122-124** but but showed poor X-ray diffraction.

| R = Me | **121** | | R = Me | **140** | UHM-25-Ala-Boc |
|---|---|---|---|---|---|
| R = *i*-Pr | **122** | | R = *i*-Pr | **141** | UHM-25-Val-Boc |
| R = *s*-Bu | **123** | | R = *s*-Bu | **142** | UHM-25-Leu-Boc |
| R = Bn | **124** | | R = Bn | **143** | UHM-25-Phe-Boc |
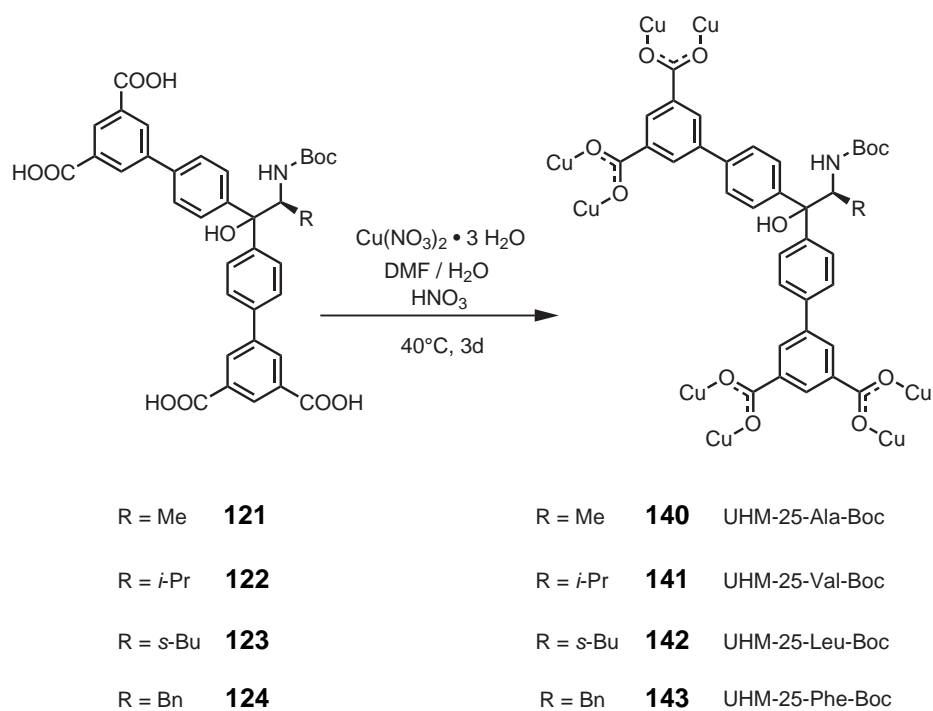
**Scheme 3.28** – Schematic representation of the reactions of the tetracarb-oxylic linkers derived from alanine (**121**), valine (**122**), leucine (**123**), and phenylalanine (**124**) with a Cu(II) source that yield a blue crystalline material for each of the materials.
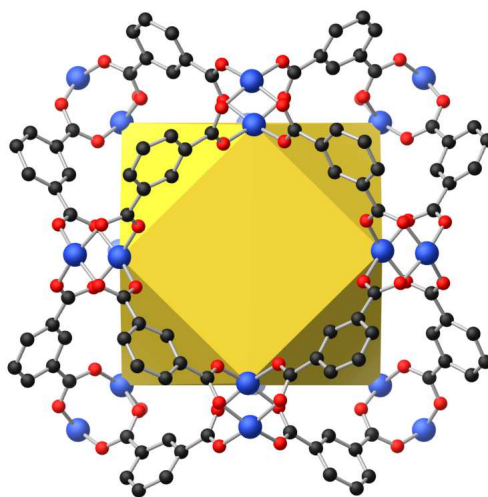
**Figure 3.6** – Metal-organic polyhedron formed by 24 isophthalic groups of the organic SBU and twelve inorganic SBUs. The resulting shape is a cuboctahedron whose corners are occupied by the copper paddle wheels. Only the isophthalates that bridge the copper paddle wheels of the cuboctahedron are shown and the rest of the linker molecules are omitted for clarity (grey: carbon, red: oxygen, blue: copper, omitted: hydrogen atoms as well as oxygen atoms occupying the axial positions of the inorganic SBU).

from pseudo $C_2$-symmetry of the tetracarboxylate with regard to the isophthalate groups, which results in two possible orientations of the chiral residue that is located at the center of the linker.
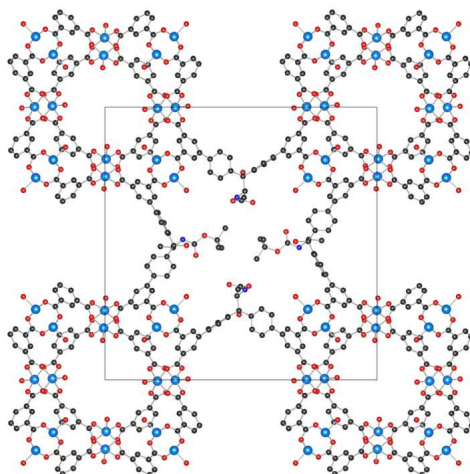


**Figure 3.7** – View along the *a* axis on an extended unit cell of UHM-25-Ala. MOPs are connected via the V-shaped organic SBU along all three crystallographic directions. No disordering and only four complete linker molecules are shown to increase clarity (grey: carbon, red: oxygen, light blue: nitrogen, dark blue: copper, omitted: hydrogen).

To evaluate the phase purity of the bulk phase of UHM-25-Ala, PXRD data was collected and compared with a simulated PXRD pattern. The simulated pattern was calculated for a hypothetical structure in which the chiral residue was specifically excluded so that the crystal structure contains only the backbone of the linker. After this simplification of the structure, the patterns of the bulk phase and the simulated pattern are in reasonable agreement (see Figure 3.8). However, this is not the case for the simulated PXRD pattern of the structural model with the chiral residues in place. This can be explained by the high degree of disorder of these groups that cannot be sufficiently reproduced from the diffraction data. Therefore the chiral substituent in UHM-25 has been modeled as a chemically reasonable substituent without any disorder which leads to a discrepancy between simulated and experimental PXRD pattern.

To investigate and prove the stability of the chiral linker after the MOF synthesis, the reaction product UHM-25-Ala-Boc was digested in diluted HCl. This allowed the reisolation of the linker which could then be examined by spec-
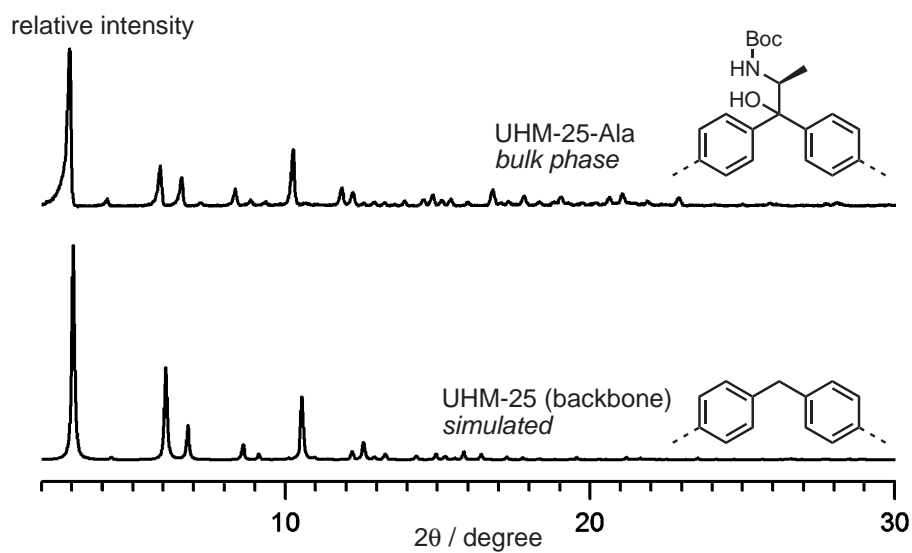
**Figure 3.8** – Experimental PXRD for UHM-25-Ala as-synthesized (top) and a calculated PXRD pattern for the UHM-25 backbone bearing no substituents on the sp$_3$-hybridized carbon of the organic SBU (bottom).

troscopic methods. The integrity of the linker was independently verified by
$^1$H-NMR spectroscopy and mass spectrometry (see Section 4.42). The retention
of chirality in the linker was confirmed by polarimetry measurements of the
reisolated material, which showed only a slight decrease of optical activity. An
overview of the optical rotation of the *N*-Boc protected linker molecules before
MOF synthesis and after resisolation is given in Table Table 3.1 on page 140.

### 3.3.1 Topological Considerations

In order to determine an underlying net for UHM-25-Ala, the building units
that serve as nodes have to be identified. The first node of the framework is
the copper paddle wheel, which constitutes a four-coordinated square-planar
node. In some cases, di-isophthalate organic SBUs have been described as four-
coordinated nodes.[281–283] However, this interpretation leads to a misassign-
ment of the underlying topology.[5] In UHM-25, treatment of the tetracarboxy-
late system as a four-coordinated node would lead to the assignment of the
**rhr** net. This uninodal net is vertex and edge transitive. The embedding of this
net with the highest symmetry belongs to the body centered cubic space group
*Im3̄m*, which contradicts with the primitive cubic structure found in UHM-25-
Ala.

The topological analysis of the underlying net is more precise when the
branching points of the organic SBU are explicitly included. Therefore, the or-
ganic SBU was treated as a combination of two triangular, three-coordinating
nodes. These nodes correspond to the individual isophthalates of the organic
SBU. Topological analysis was carried out treating the UHM-25 structure as a
binodal net. A representation of the abstracted form of the organic SBU is shown
in Figure 3.9.



(a)                                    (b)

**Figure 3.9** – (a) Three-dimensional representation of the linker used to syn-
thesize UHM-25-Ala-Boc and (b) the same linker deconstructed into two
three-coordinated nodes shown in the augmented form.

Topological analysis and the determination of a natural tiling was performed
using the TOPOSPro[284] and Systre[285] software. The topology of the underly-

ing net was determined as **ucp** by both of these programs. The embedding with the highest symmetry of the **ucp** net belongs to the space group $Pm\bar{3}m$. This is compatible with the space group of UHM-25-Ala, because $Pm\bar{3}m$ is the proper supergroup of $P432$. The transitivity of the **ucp** net is $pqrs = 2244$. It is a binodal net with two kind of vertices and edges and four distinct kinds of tiles and faces. The **ucp** topology has been described as one of at least three possibilities to connect cuboctahedral MOPs by O'Keeffe and Yaghi, but has not been found in a MOF so far.[5]



| (a) | (b) |
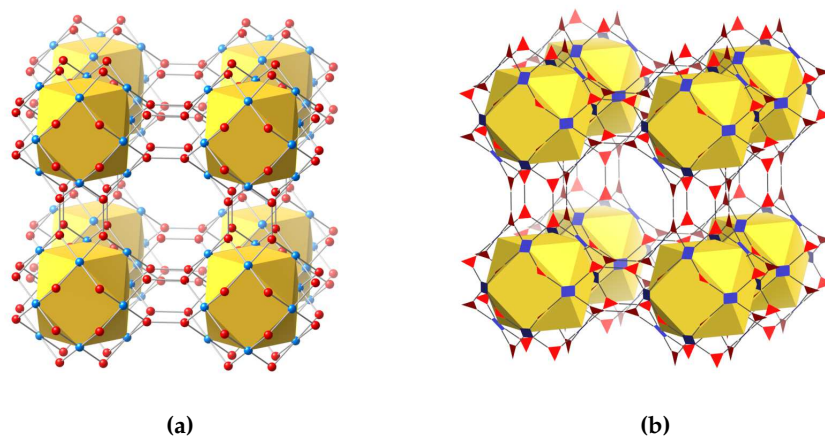
**Figure 3.10** – (a) representation of **ucp** net (b) representation of the augmented net **ucp-a** that represents the nodes as polygons, red: three-coordinated nodes derived from the organic SBU, blue: four-coordinated node derived from the inorganic SBU, yellow polyhedra derived from the MOPs are added as a guide to the eye.

The topology of interconnected MOPs from isophthalates and copper paddle wheels has been described by treating the MOPs either as cuboctahedra[279] or as rhombic cuboctahedra.[280,286,287] However, the treatment of the MOPs as rhombic cuboctahedra neglects the role of the copper paddle wheel as a node because only the organic branching points are considered as vertices. This leads to the description of an underlying 5-c net (**pcu-i**), whereas neither the linker nor the paddle wheel show this connectivity. Hence, Yaghi and O'Keeffe have proposed to treat such systems as interconnected cuboctahedra.[5] There are at least three ways to connect two neighboring cuboctahedra:

**(a)** In an arrangement where two faces of an octahedron are directed at each other.

**(b)** In an arrangement where the corners of the cuboctahedra are directed at each other.

**(c)** In an arrangement where a corner of one cuboctahedron is directed at the face of the neighboring cuboctahedron.

Three nets that represent interconnected cuboctahedra have been documented by Yaghi and O'Keeffe: **zmj**, **zhc** and **ucp**.[5] In the **zmj** net, the arrangements (a) and (b) can be observed, meaning that the cuboctahedral MOPs are connected via their corners or their faces. This is shown in Figure 3.11. Along the crystallographic $c$ axis neighboring polyhedra are oriented face-to-face to each other. In the crystallographic $ab$ plane the cuboctahedra are oriented corner-to-corner to each other.



**(a)** view along the $a$ axis.  **(b)** view along the $c$ axis.
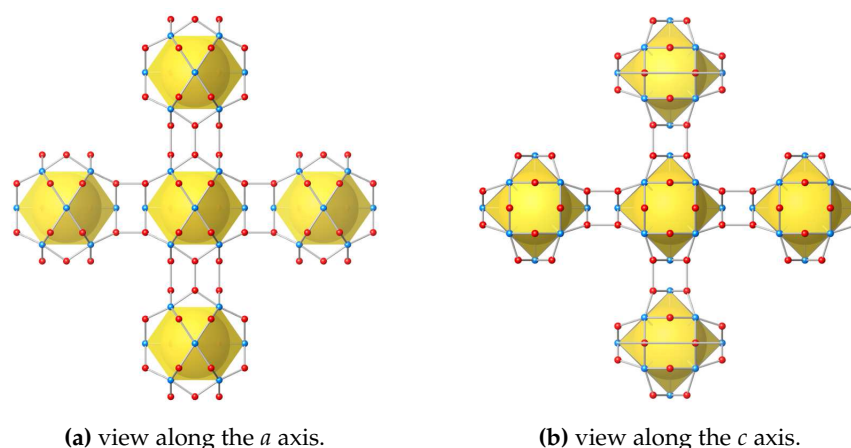
**Figure 3.11** – Representation of the **zmj** net, red: three-coordinated nodes derived from the organic SBU, blue: four-coordinated node derived from the inorganic SBU, yellow polyhedra derived from the MOPs.

In the **zhc** net the arrangements (a) and (c) are observed, meaning that the MOPs are connected via their faces and via face-corner connections. This is shown in Figure 3.12. As in the **zmj** net, the cuboctahedra are oriented face-to-face along the $c$ axis. In the $ab$ plane neighboring cuboctahedra are oriented corner-to-face.

The **ucp** topology of UHM-25 constitutes the simplest of the three nets as there is only the arrangement of type (a) present, meaning that all cuboctahedra are connected so that their faces are directed at each other along all crystallographic directions. This is shown in Figure 3.13.

**(a)** view along [110].  **(b)** view along the *c* axis.
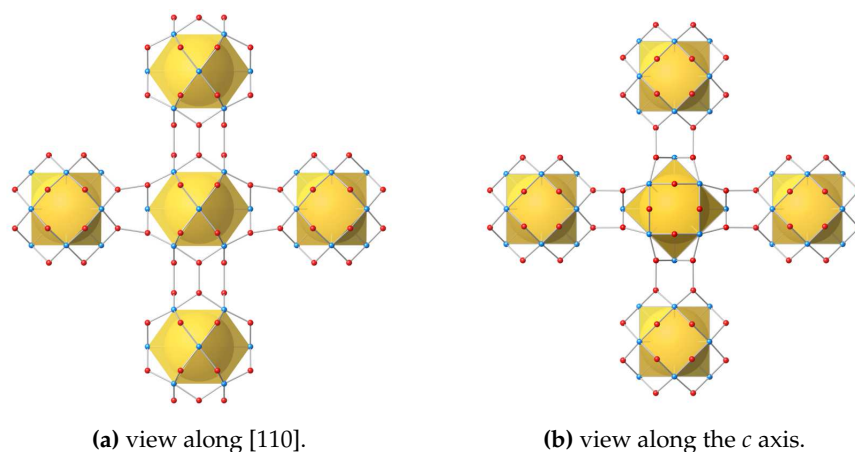
**Figure 3.12** – Representation of the **zhc** net viewed along two different orientations, along the *c* direction MOPs are oriented face-to-face and in the *ab* plane MOPs are oriented corner-to-face (red: three-coordinated nodes derived from the organic SBU, blue: four-coordinated node derived from the inorganic SBU, yellow polyhedra derived from the MOPs.

The topologies **zmj**, **zhc** and **ucp** are only observed if V-shaped tetracarboxylates are used to build MOFs. A collection of linkers that resulted in the formation of interconnected cuboctahedral MOPs is presented in Scheme 3.29.

Apart from different conditions of synthesis (solvent, temperature), the structural properties of the linker are particularly decisive for the formation of certain topologies. The formation of the three different types of connection between the cuboctahedra requires the linkers to adopt certain conformations, which will be discussed in the following.

To connect two cuboctahedra in in the manner (a), where two faces are directed at each other, the linker needs to adopt a conformation in which the isophthalates are oriented non-coplanar. In the UHM-25 structure, the isophthalates adopt a conformation that can be described by a torsion angles of 89.83° and 90.29°, respectively. A representation of the conformation of the organic SBU is depicted in Figure 3.14.

To achieve a connection of type (b) in which the corners of two cuboctahedra are directed at each other, the linker needs to adopt a conformation in which the isophthalates are coplanar. In the case of UHM-6, which is depicted in Figure 3.15, the isophthalates essentially lie in the same plane and have a low torsion angles of 10.00° and 7.94°, respectively.[288]

**(a)** view along the *a* axis.　　　　**(b)** view along the *c* axis.
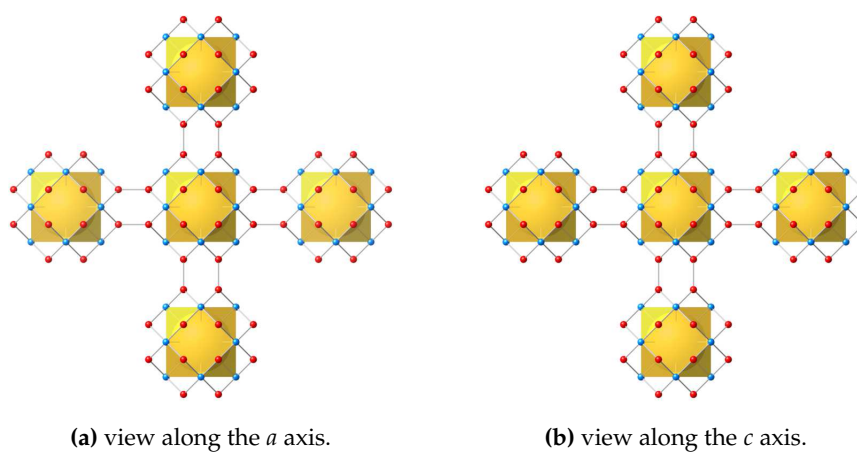
**Figure 3.13** – Representation of the **ucp** net, neighboring MOPs are connected-via face-to-face connection in all three crystallographic directions (red: three-coordinated nodes derived from the organic SBU, blue: four-coordinated node derived from the inorganic SBU, yellow polyhedra derived from the MOPs. All cuboctahedra are connected to their neighbors via their faces).
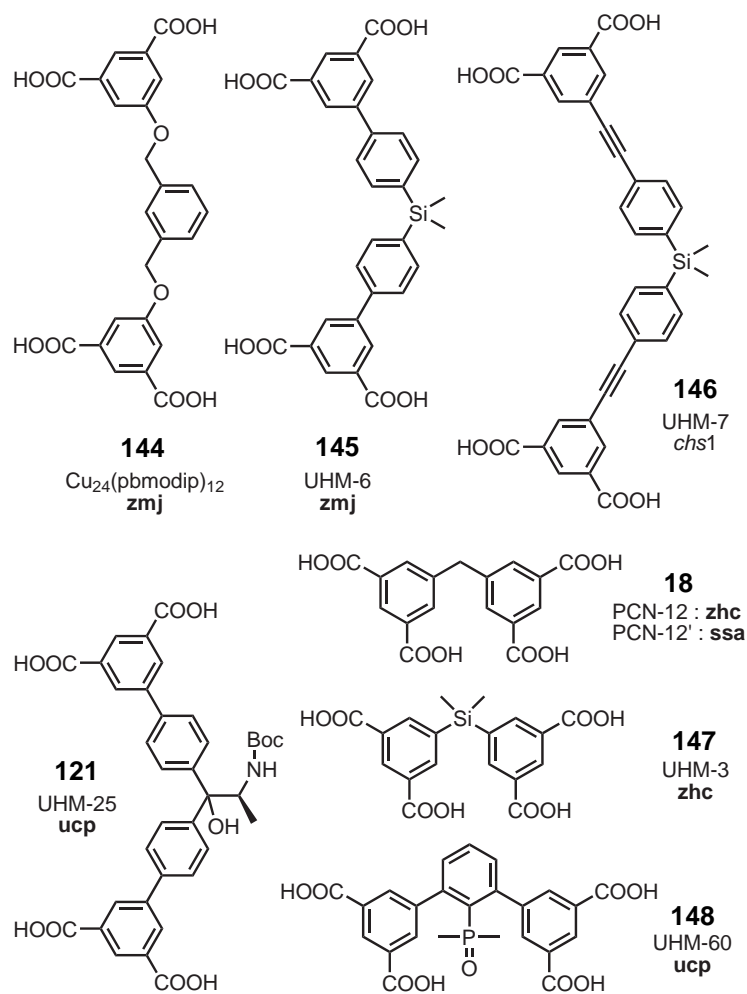
**Scheme 3.29** – Tetracarboxylate linkers that yield structures with inter-connected cuboctahedral MOPs (**144**,[286] **145**,[288] **146**,[289] **18**,[287] **147**,[267] **148**[290]).

131

**(a)**

**(b)**

**(c)**
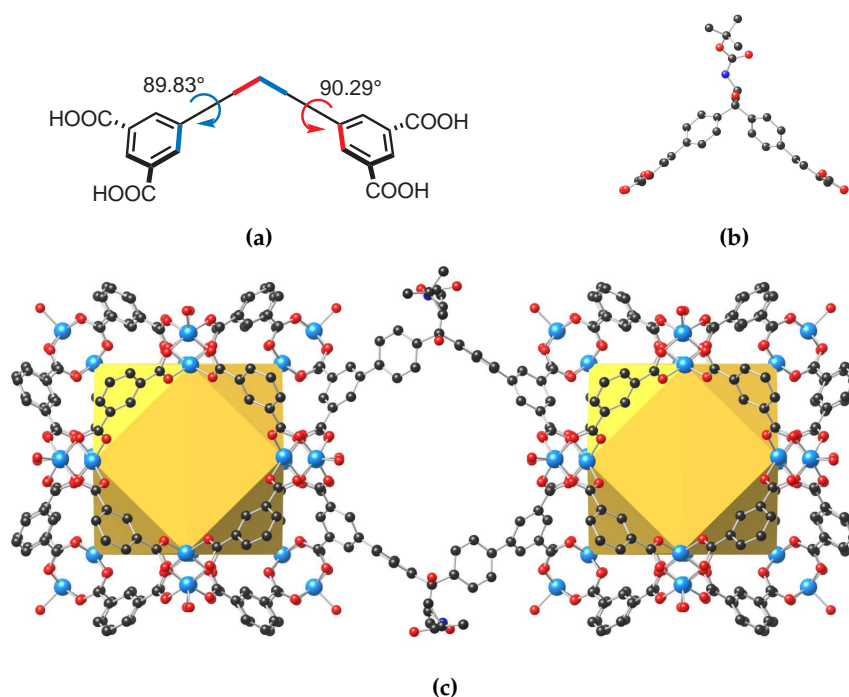
**Figure 3.14** – (a) Schematic representation of the torsion angles of the isophthalates in a linker as seen in a face-to-face connection of two neighboring cuboctahedra in UHM-25 (torsion is defined by the dihedral angle of the bonds highlighted in red or blue, respectively). (b) Three-dimensional model of the alanine based tetracarboxylate (**121**) that forms a face-to-face connection of two MOPs. (c) View along the *c* axis on two neighboring cuboctahedra from the crystal structure of UHM-25-Ala-Boc that has the underlying **ucp** net. (grey: carbon, red: oxygen, light blue: copper, hydrogen atoms are omitted, yellow polyhedra are added to illustrate the relative orientation of the MOPs).

**(a)**



**(b)**



**(c)** view along the *c* axis.
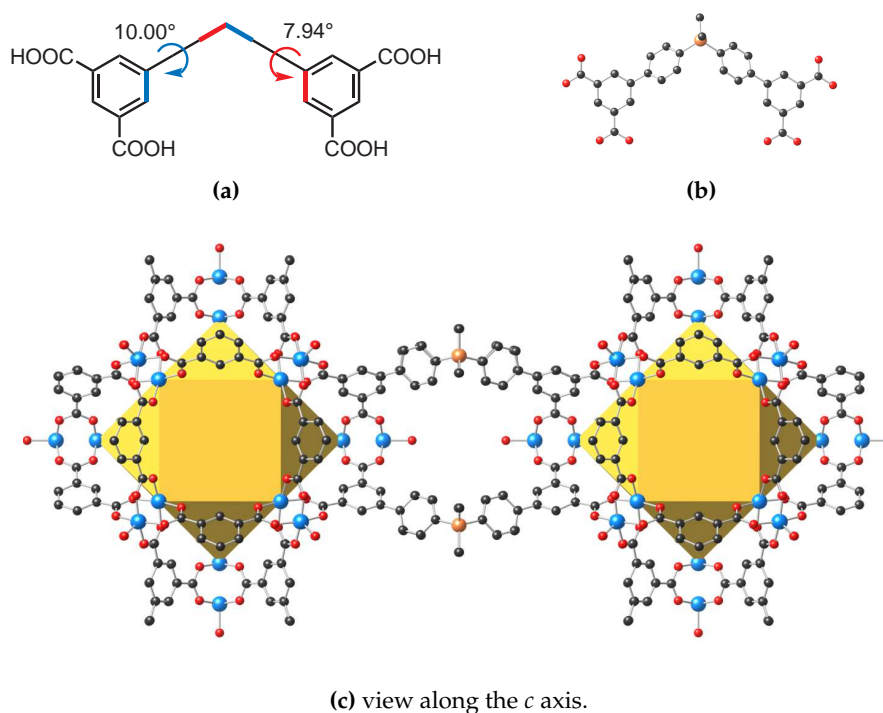
**Figure 3.15** – (a) Schematic representation of the torsion angles of the isoph-thalates in a linker as seen in a corner-to-corner connection of two neigh-boring cuboctahedra in UHM-6 (torsion is defined by the dihedral angle of the bonds highlighted in red or blue, respectively). (b) Three-dimensional model of the tetracarboxylate of linker **145** that forms a corner-to-corner connection of two MOPs in UHM-6. (c) Two neighboring cuboctahedra from the crystal structure of UHM-6 that has the underlying **zmj** net (grey: carbon, red: oxygen, orange: silicon, light blue: copper, hydrogen atoms are omitted, yellow polyhedra to illustrate the relative orientation of the MOPs).

To achieve a connection of type (c) in which one corner of a cuboctahedron is connected to the face of the next cuboctahedron, a non-coplanar conformation of the linker is required again. Such a conformation is observed in PCN-12.[287] The isophthalates of an organic SBU in PCN-12 are twisted by 96.64° and 19.56°, respectively. A part of the crystal structure of PCN-12 is shown in Figure 3.16 as an example for this type of connection of cuboctahedra in the **zhc** net.

The different conformations that the tetracarboxylate linkers adopt can explain the preferential formation of certain topologies. In order to obtain the **zmj** topology the linker needs to adopt a coplanar arrangement of the isophthalates to connect the cuboctahedra via their corners. Such a conformation is impeded in the mdip linker system (**18**) by steric hindrance that arises from the *ortho*-hydrogen atoms on the isophthalate residues. By increasing the distance between these hydrogen atoms – for example through phenyl rings that act as spacers – this conformation is no longer energetically disfavored and corner-to-corner connections may be formed. This has been realized in the synthesis of UHM-6, in which the elongated tetracarboxylate **145** was employed as a linker.[288] Interestingly, further elongation of linker **145** by two ethinylene units to obtain linker **146** gives rise to the more complex topology *chs*1 in UHM-7. The occurrence of this topology has been partly explained by the increased flexibility of the linker that can span distances from 18 Å to 22 Å between two cuboctahedral MOPs.[289]

The formation of the **ucp** topology in the UHM-25 series may be explained by an energetically favored conformation with "folded" isophthalates as shown in Figure 3.14. If no other conformations are adopted by this type of linker, then the **ucp** topology must result as the only possible arrangement of interconnected MOPs. The fact that the geometrically related linker **145** has been observed in the "folded" conformation but has not been observed in a **ucp** net, suggests that the substituents on the central carbon of the chiral linker **121** play an important role and may inhibit the formation of a coplanar arrangement of the isophthalates in compound **121** and its derivatives.

However, the preferred topology of a MOF cannot be solely explained by a preferential conformation of the linker. Identical building blocks can lead to the formation of different framework structures, which has been demonstrated, for example, for mdip (**18**): By the alteration of the synthetical conditions (temperature, solvent) PCN-12′ was obtained with the **ssa** topology, in which cuboctahedral MOPs are absent.[287] Extensive assessments of the thermodynamic and kinetic aspects that contribute to the certain topologies are very complex and difficult to determine.

**(a)**

**(b)**



**(c)** view along the *c* axis.
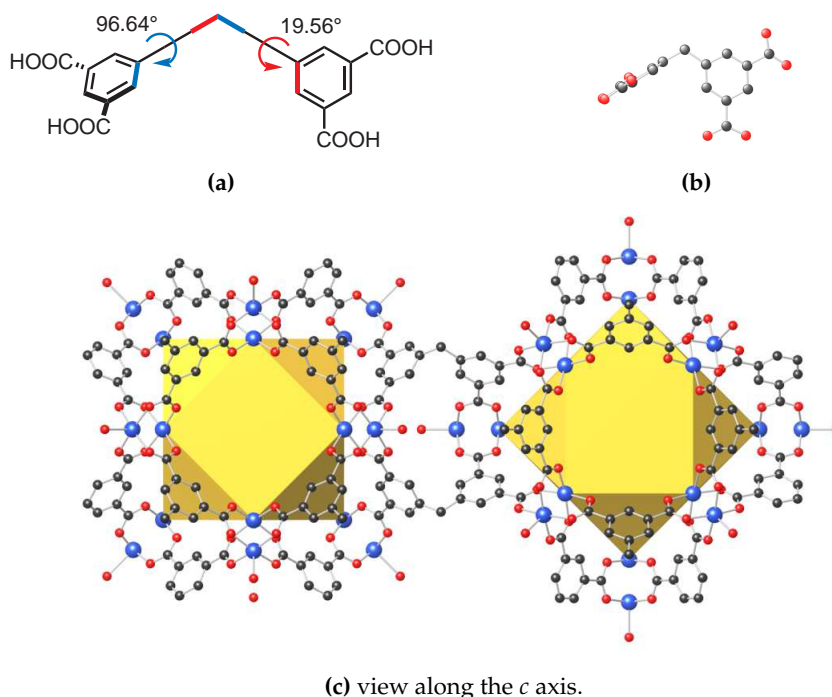
**Figure 3.16** – (a) Schematic representation of the torsion angles of the isophthalates in a linker as seen in a corner-to-face connection of two neighboring cuboctahedra in PCN-12 (torsion is defined by the dihedral angle of the bonds highlighted in red or blue, respectively). (b) Three-dimensional model of the tetracarboxylate of mdip (**18**) that forms a corner-to-face connection of two MOPs in PCN-12. (c) Two neighboring cuboctahedra with a corner-to-face connection from the crystal structure of PCN-12 that has the underlying **zhc** net. (grey: carbon, red: oxygen, light blue: copper, hydrogen atoms are omitted, yellow polyhedra to illustrate the relative orientation of the MOPs, structural information obtained from CCDC number 662918).

### 3.3.2 Tiling and Pore Structure

The representation of the UHM-25 structure by a tiling may help in the understanding of the pore system in the MOF. A natural tiling was determined for the **ucp** topology by a calculation with the TOPOSPro Suite.[291] This tiling is described in the following section. The tiling comprises four different kinds of tiles with four different faces. A graphical representation of the tiling is shown Figure 3.17



**(a)**                                                    **(b)**
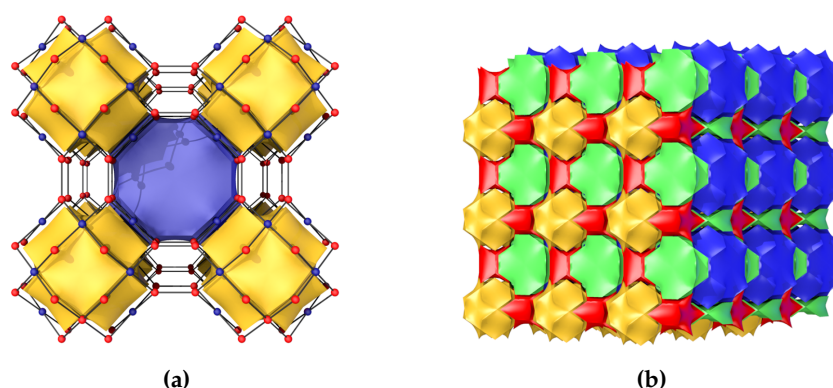
**Figure 3.17** – (a) Segment of the natural tiling for the **ucp** topology together with the net carried by the tiling; only two of the four distinct types of tiles are shown for clarity, the yellow tiles correspond to the space inside the MOP and the blue tile corresponds to the space in the center of the unit cell (red: three-coordinated nodes derived from the organic SBU, blue: four-coordinated node derived from the inorganic SBU) (b) a $3 \times 3 \times 3$ super cell of the same tiling including the other two types of tiles (green and red) that connect the blue and yellow tiles in a primitive cubic fashion.

Based on the separation of three-dimensional space provided by the tiling, four different types of pores can be described for UHM-25-Ala. The yellow tile corresponds to the MOP and already has been discussed on page 123. The red tiles can be described as the connection between the yellow tiles. The red tiles lie on the edges of the unit cell and correspond to the void that is depicted in Figure 3.18. The framework that surrounds this space comprises eight inorganic SBUs and four distinct organic SBUs. The pore resembles a capped square bipyramid which is highlighted in Figure 3.18 in red. The interatomic distance of two central $sp^3$-hybridized carbons of the backbone of the linker that oppose each other is 20.7 Å; taking into account the van-der-Waals radii of the atoms, the pore diameter for this pore amounts to 15 Å.
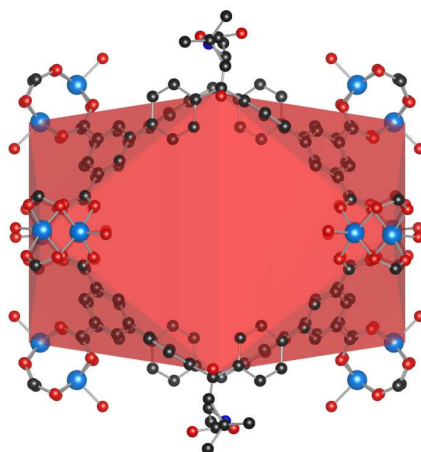
**Figure 3.18** – View along the *a* axis of the pore space that corresponds to the red tile in the natural tiling of **ucp**. A capped square bipyramid colored in red indicates the shape of this pore (grey: carbon, red: oxygen, dark blue: nitrogen, light blue: copper, omitted: hydrogen).

The blue tile in Figure 3.17 corresponds to the pore space in the center of the unit cell. The shape of this pore is defined by convex sides of the V-shaped linkers and the chiral residues of the linker that protrude into this space. The framework that surrounds this pore comprises twelve organic SBUs and 24 inorganic SBUs and is depicted in Figure 3.19. The interatomic distance of two central, $sp^3$-hybridized carbons of the backbone of the linker that oppose each other is 20.2 Å. Due to the high degree of flexibility, the amino alcohol side chains are highly disordered and difficult to localize which impedes an exact measurement of the pore diameter.

The green tile comprises the pore space that is located on the faces of the unit cell. The shape of this pore is defined by convex sides of the V-shaped linkers. The framework that surrounds this pore consists of twelve organic SBUs and 24 inorganic SBUs and is depicted in Figure 3.20. The pore that corresponds to the green tile connects the pores with the chiral residues (represented by the blue tiles) with each other to create a three-dimensional pore system. The interatomic distance of two central, $sp^3$-hybridized carbons that oppose each other is 20.4 Å. Taking into account the van-der-Waals radii of the atoms, the pore diameter amounts to 15 Å.
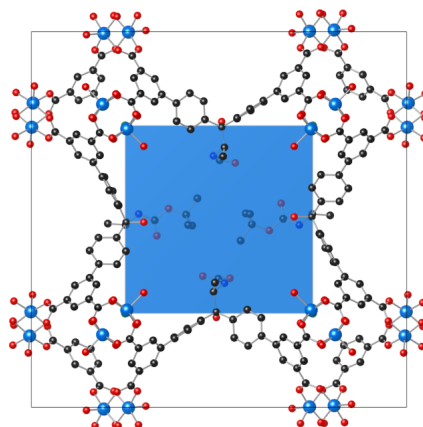
**Figure 3.19** – View along the *a* axis on the pore space that corresponds to the blue tile in the natural tiling of **ucp**. The pore is located at the center of the unit cell and is indicated as a blue square. The chiral residues of the organic SBUs protrude into the space of the pore. The organic SBUs are shown only one of the possible conformations for clarity (grey: carbon, red: oxygen, dark blue: nitrogen, light blue: copper, omitted: hydrogen).
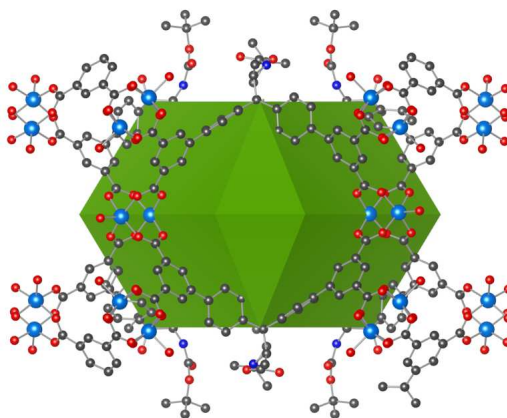


**Figure 3.20** – View along the *a* axis on the pore space that corresponds to the green tile in the natural tiling of **ucp**. A green polyhedron is placed at the center of the structure as a guide to the eye. The organic SBUs are shown for only one of their possible conformations for clarity (grey: carbon, red: oxygen, dark blue: nitrogen, light blue: copper, omitted: hydrogen).

### 3.3.3 Powder X-Ray Diffraction and Optical Rotation

Unfortunately, for the reactions with the tetracarboxylic linkers derived from valine (**122**) and leucine (**123**) and phenylalanine (**124**) no crystals were obtained that allowed successful single crystal diffraction experiments. However, in each case the PXRD pattern of the microcrystalline phases indicates an isostructural relationship between the materials obtained from these linkers and the material from the linker derived from the *N*-Boc protected alanine derivative **121**. Powder diffraction data for the four isoreticular compounds are shown in Figure 3.21. Although there is some slight variation observed between the different diffractograms, the positions of the major reflections are the same. Judging by relatively low signal to noise ratio, the crystallinity in UHM-25-Leu-Boc is not as pronounced as in the other MOFs of this series.
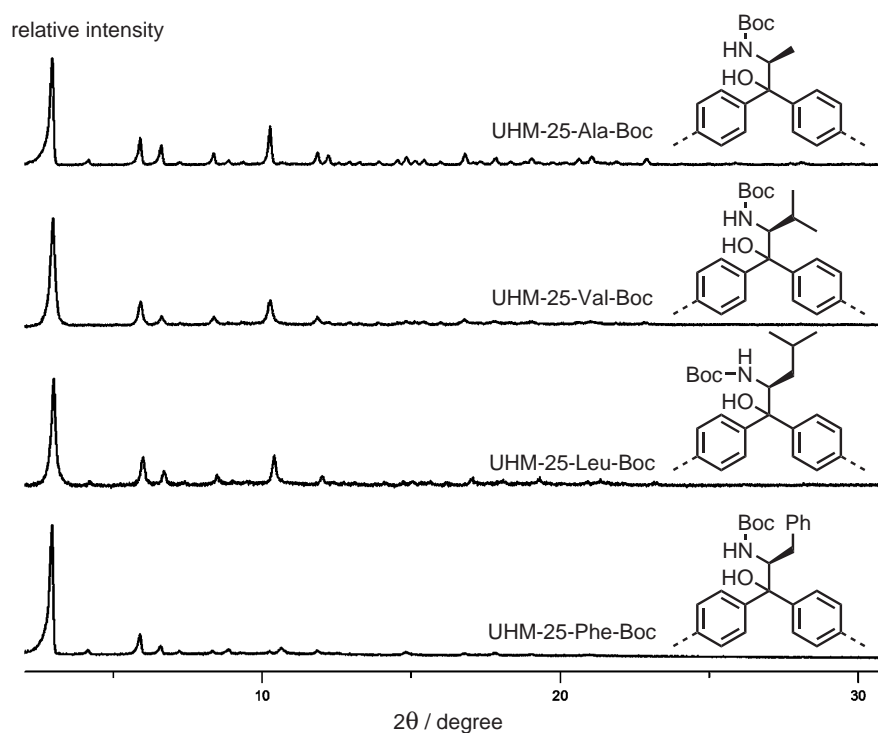


**Figure 3.21** – Powder X-ray diffraction data for the materials of the UHM-25 series that carry a Boc protecting group, a similar diffraction pattern is observed for all materials of the isoreticular UHM-25 series.

To investigate and prove the stability of the chiral linkers after the MOF syntheses, the reisolated linkers were examined by spectroscopic methods (compare Section 3.3 on page Figure 3.8). The integrity of the linker was independently verified by $^1$H-NMR spectroscopy and mass spectrometry (see Chapter 4 for details). The retention of chirality in the linker was confirmed by polarimetry measurements of the reisolated material. An overview of the optical rotation of the N-Boc protected linker molecules before MOF synthesis and after resisolation is given in Table Table 3.1.

**Table 3.1** – Optical rotation of the linker before and after synthesis of the unprotected UHM-25 MOFs (all samples measured as solutions in methanol).

| | | before | | | reisolated | | |
|---|---|---|---|---|---|---|---|
| | | opt. rot. degree | | c g/100 ml | opt. rot. degree | | c g/100 ml |
| UHM-25-Ala-Boc | **140** | $[\alpha]_D^{25}$ | -21.7 | 0.24 | $[\alpha]_D^{25}$ | -18.7 | 0.33 |
| UHM-25-Val-Boc | **141** | $[\alpha]_D^{25}$ | -12.7 | 0.22 | $[\alpha]_D^{25}$ | -12.3 | 0.30 |
| UHM-25-Leu-Boc | **142** | $[\alpha]_D^{26}$ | +13.6 | 0.44 | $[\alpha]_D^{26}$ | +12.4 | 0.56 |
| UHM-25-Phe-Boc | **143** | $[\alpha]_D^{25}$ | +21.8 | 0.44 | $[\alpha]_D^{25}$ | +22.9 | 0.28 |

Five more MOFs were obtained from linkers with a free amino group. Telfer and co-workers reported that the presence of deprotected amino groups on the linker inhibited the formation of MOFs.[129] However, no specific reasons were stated for this behavior. This kind of inhibition was not observed for the deprotected linkers in the UHM-25 series. Crystalline materials were obtained under the same conditions that were used to synthesize the N-Boc protected derivatives (see Scheme 3.28). A schematic representation of the synthesis of UHM-25 MOFs from unprotected amino alcohols derived from alanine, valine, leucine, phenylalanine and proline is shown in Scheme 3.30; the synthesis was performed using the linkers as they were obtained from the deprotection reaction as ammonium salts of either trifluoroacetic acid or hydrogen chloride.

The light blue crystals that were obtained from the unprotected amino alcohol linkers were examined using PXRD (see Figure 3.22). Powder X-ray diffractograms of the unprotected UHM-25 MOFs match the data obtained for their N-Boc protected counterparts. This implies an isoreticular relationship between the five amino alcohol MOFs UHM-25-Ala, UHM-25-Val, UHM-25-Leu, UHM-25-Phe and UHM-25-Pro and the N-Boc protected materials described above.

The diffractograms of the MOFs UHM-25-Val and UHM-25-Leu show significant broadening of the reflections and a low signal to noise ratio, indicating

| X = CF$_3$COO | R = Me | **129** |
| X = CF$_3$COO | R = $i$-Pr | **130** |
| X = CF$_3$COO | R = $s$-Bu | **131** |
| X = CF$_3$COO | R = Bn | **132** |
| X = Cl | R = C$_2$H$_4$-N (cyclic) | **128** |

| R = Me | **149** | UHM-25-Ala |
| R = $i$-Pr | **150** | UHM-25-Val |
| R = $s$-Bu | **151** | UHM-25-Leu |
| R = Bn | **152** | UHM-25-Phe |
| R = C$_2$H$_4$-N (cyclic) | **153** | UHM-25-Pro |

**Scheme 3.30** – Schematic representation of the reaction of the tetracarboxylic linkers derived from alanine (**129**), valine (**130**), leucine (**131**), phenylalanine (**132**) and proline (**128**, for proline R is a pyrrodinyl system that includes the amino group as a secondary amine) with a Cu(II) source that yields a blue, crystalline material.

141
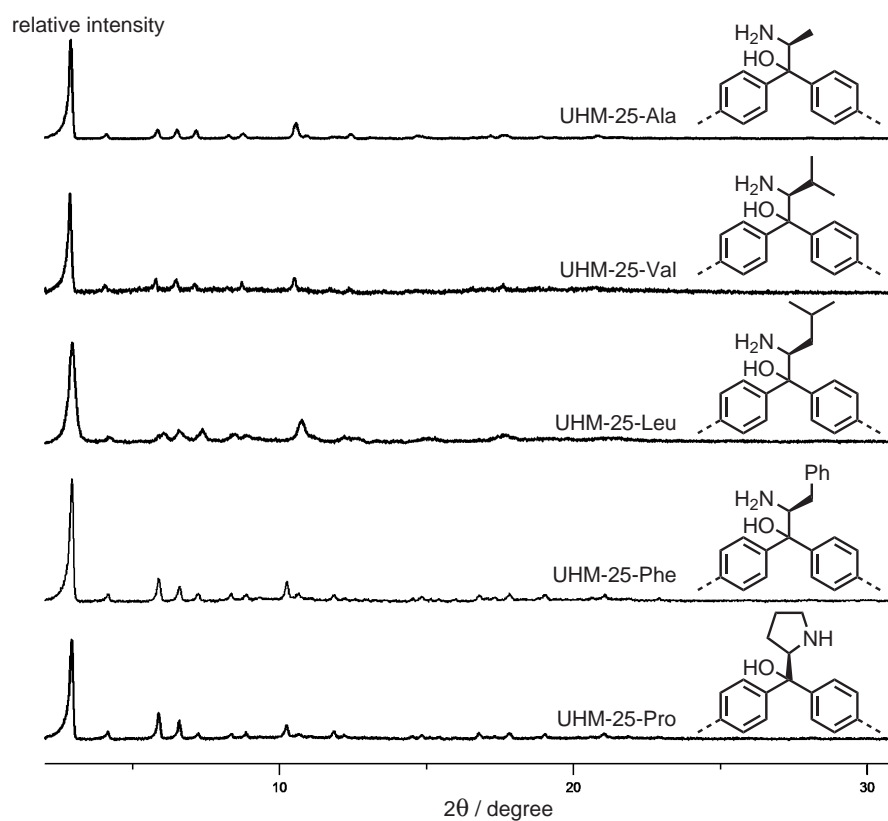
**Figure 3.22** – PXRD data for the materials of the UHM-25 series that are obtained from the deprotected amino alcohol linkers, a similar diffraction pattern is observed for all materials of the isoreticular UHM-25 series.

142

that this material is not as crystalline as the other MOFs observed in this series. Single crystals suitable for structural analysis could only be obtained for the MOF synthesized from the secondary amine linker that is derived from proline. The material crystallizes in the *P*432 space with the unit cell parameters $a = b = c = 29.0261$ Å. This corresponds well with the metrics of the unit cell of UHM-25-Ala-Boc (see Figure 3.7). The crystal structure of UHM-25-Pro is isoreticular to UHM-25-Ala-Boc and shows the same disorder of the pseudo $C_2$-symmetric linker that is also observed for the *N*-Boc protected MOF, which inhibits the exact localization of the chiral pyrrolidine substituent even though this substituent is more rigid than an acyclic protected amine. A representation of the crystal structure of UHM-25-Pro is shown in Figure 3.23.
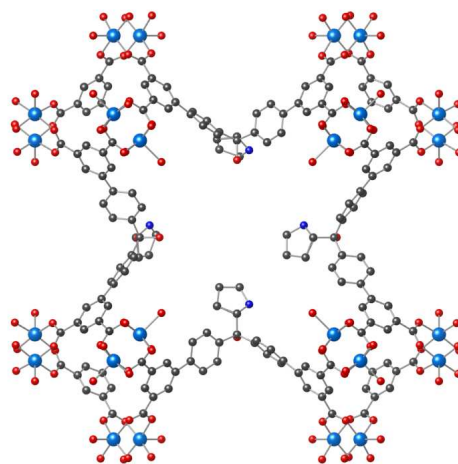


**Figure 3.23** – Crystal structure of UHM-25-Pro; view along the *a* axis on the pore space that corresponds to the blue tile in the natural tiling of **ucp**. The chiral residues of the organic SBUs protrude into the space of the pore. The organic SBUs are shown only one of the possible conformations for clarity (grey: carbon, red: oxygen, dark blue: nitrogen, light blue: copper, omitted: hydrogen).

The reisolated linkers were examined by spectroscopic methods (see Chapter 4 for details). The retention of chirality in the linker was confirmed by polarimetry measurements of the reisolated material. An overview of the optical rotation of the linker molecules with a free amino alcohol is given in Table 3.1.

**Table 3.2** – Optical rotation of the linker before and after synthesis of the un-protected UHM-25 MOFs (all samples measured as solutions in methanol).

| | | | before | | reisolated | |
| | | opt. rot. degree | | c g/100 ml | opt. rot. degree | | c g/100 ml |
|---|---|---|---|---|---|---|---|
| UHM-25-Ala | **149** | $[\alpha]_D^{26}$ | -17.5 | 0.40 | $[\alpha]_D^{26}$ | -17.9 | 0.32 |
| UHM-25-Val | **150** | $[\alpha]_D^{25}$ | -19.2 | 0.26 | $[\alpha]_D^{25}$ | -18.8 | 0.34 |
| UHM-25-Leu | **151** | $[\alpha]_D^{26}$ | +15.0 | 0.60 | $[\alpha]_D^{26}$ | +15.6 | 0.51 |
| UHM-25-Phe | **152** | $[\alpha]_D^{25}$ | +21.2 | 0.52 | $[\alpha]_D^{25}$ | +20.2 | 0.50 |
| UHM-25-Pro | **153** | $[\alpha]_D^{26}$ | +41.3 | 0.30 | $[\alpha]_D^{26}$ | +41.0 | 0.35 |

In addition to the protected and unprotected amine linker systems, chiral MOFs were also obtained for the linkers that bear the chiral oxazolidinone substituent that resembles the Evans auxiliary. The conditions that were successfully employed in the MOFs described above were also applied to the synthesis from the Evans-type linkers. Solvothermal reaction of the linkers in a mixture of DMF and water with copper nitrate for three days at 40 °C afforded light blue crystals that were washed with DMF and stored under solvent (DMF or THF).

PXRD data for these MOFs is shown in Figure 3.24. The results obtained for the MOFs correspond well to the diffraction patterns observed for the MOFs that carry the chiral amino alcohol substituents (see Figure 3.21). The results of the polarimetry measurements of the reisolated linker molecules are given in Table 3.3.

**Table 3.3** – Optical rotation of the linker before and after synthesis of the Evans-type UHM-25 MOFs (all samples measured as solutions in methanol).

| | | | before | | reisolated | |
| | | opt. rot. degree | | c g/100 ml | opt. rot. degree | | c g/100 ml |
|---|---|---|---|---|---|---|---|
| UHM-25-Val-Evans | **154** | $[\alpha]_D^{27}$ | -82.7 | 0.73 | $[\alpha]_D^{27}$ | -81.5 | 0.38 |
| UHM-25-Phe-Evans | **155** | $[\alpha]_D^{27}$ | -45.0 | 0.20 | $[\alpha]_D^{27}$ | -43.8 | 0.27 |

In total, eleven different MOFs were obtained that carry a large variety of functional groups. All MOFs of the UHM-25 series are isoreticular to each other.
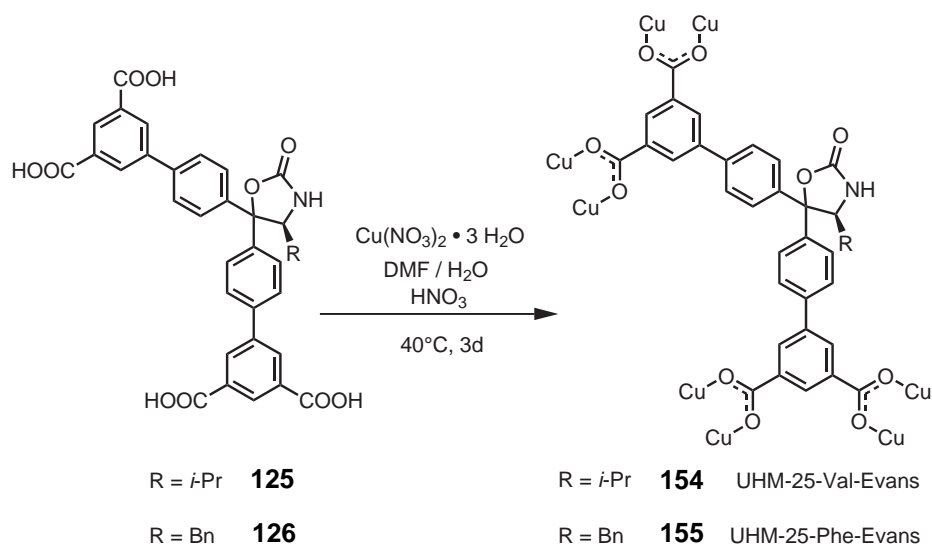
**Scheme 3.31** – Schematic representation of the reaction of the tetracarboxylic linkers that bear an Evans-type auxiliary on the central carbon with a Cu(II) source that yields a blue, crystalline material.
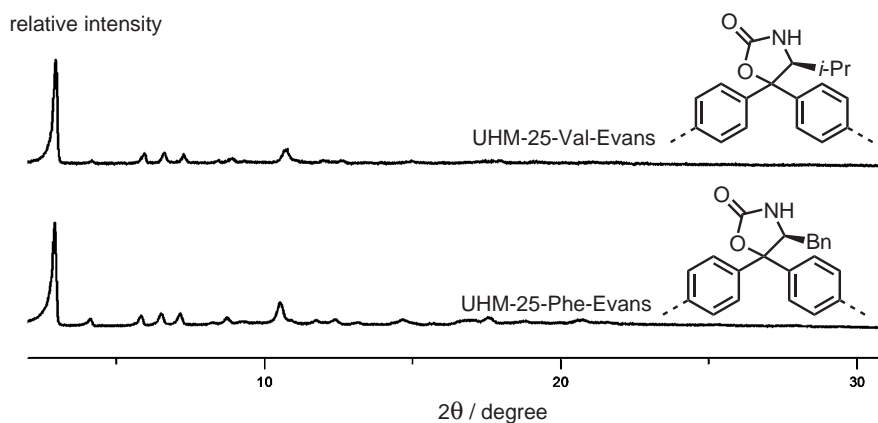


**Figure 3.24** – PXRD data for the materials of the UHM-25 series that are obtained from the tetracarboxylic linkers derived from bisarylated Evans-auxiliary; the diffraction patterns that are observed correspond with the data of the MOFs with protected and unprotected amino alcohols.

In the next sections, the results of the characterization of the materials with regard to their physicochemical properties are presented. Furthermore, selected MOFs are evaluated as catalysts and as substrates for PSM (see Section 3.6.1).

### 3.3.4   Thermogravimetric Analysis

Thermogravimetric analysis coupled with mass spectrometry (TG/MS) was performed with MOFs of the UHM-25 series. In this section the thermochemical properties of UHM-25-Val-Boc, UHM-25-Val and UHM-25-Val-Evans are presented. They are exemplary for the MOFs of the UHM-25 series. For the thermogravimetric data of each individual MOF of the UHM-25 series see Chapter 4.

UHM-25-Val-Boc that underwent solvent exchange with THF was heated at a rate of $1\,\mathrm{K/s}$ from room temperature to $800\,^{\circ}\mathrm{C}$ in a stream of $\mathrm{Ar/O_2}$ (80 : 20). Weight loss, DTA and selected MS traces are shown in Figure 3.25



| $\Delta T$ | $\Delta m$ | fragments |
|---|---|---|
| $^{\circ}\mathrm{C}$ | % | m/z |
| 25–150 | 11 | 18, 42 |
| 150–240 | 19 | 44, 56 |
| 240–338 | 23 | 18, 42, 44 |
| 338–443 | 29 | 18, 44 |
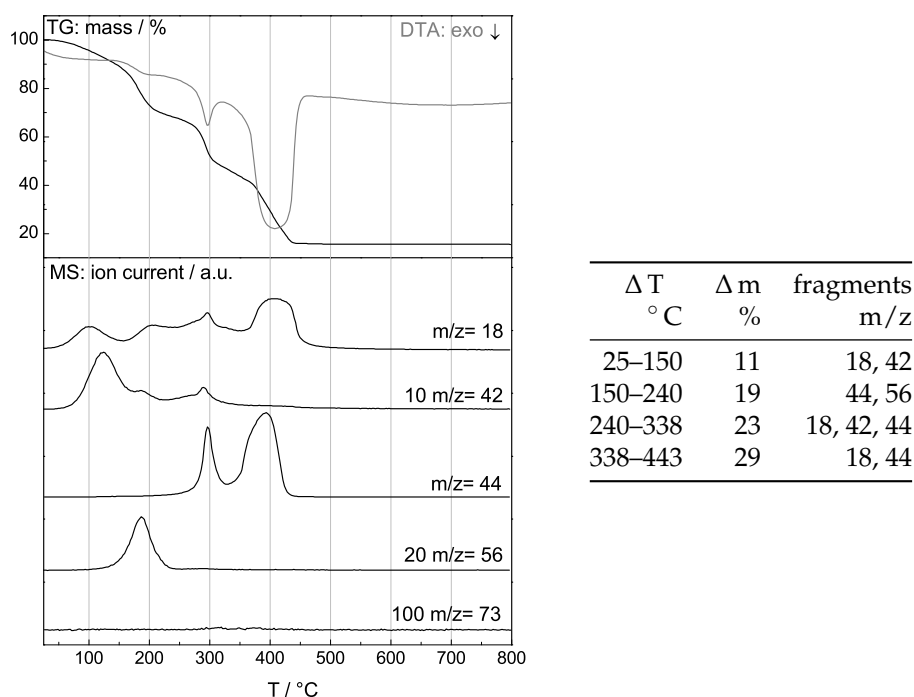
**Figure 3.25** – TG/MS analysis of UHM-25-Val-Boc (**141**), weight loss (black) and DTA (grey) are plotted in the upper part and in the lower part of the diagram the characteristic single ion currents are shown for $\frac{m}{z}$ = 18 ($H_2O$), 42 (THF), 44 ($CO_2$), 56 (isobutene), and 73 (DMF).

The first weight loss of the sample corresponds to 11 % of its weight and occurs between room temperature and $150\,^{\circ}\mathrm{C}$. This weight loss is ascribed to evap-

147

oration of solvent (THF, residual water) from the pore volume. A second weight loss occurs between 150 °C–240 °C. In this range, selected ion monitoring (SIM) of the temperature-resolved MS detects ions at $m/z = 44$ and $m/z = 56$. These signals correspond to the molecular masses of carbon dioxide and isobutene, which are the cleavage products of the $N$-Boc group, which can be cleaved thermolytically. Two final weight losses are observed between 240 and 338 °C and 338 and 443 °C, respectively. They amount to 23 and 29 % of the sample weight and can be assigned to a decomposition of the organic building units of the MOF. These losses are accompanied by SIM signals at $m/z = 18$ and $m/z = 56$ that correspond to water and carbon dioxide. After the heating to 800 °C, a solid residue remained that corresponds to 15 % of the sample weight and was identified as copper(II) oxide by PXRD (see Figure 3.26). The efficiency of the solvent exchange is indicated by the absence of the characteristic signals of DMF ($m/z = 73$) in the mass spectra recorded during the analysis. Instead, THF ($m/z = 42$) can be detected as the pore-filling solvent.
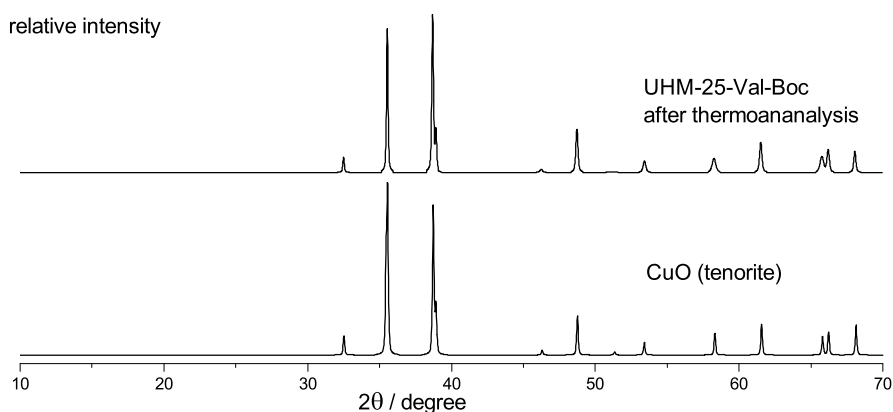


**Figure 3.26** – PXRD data of the residue obtained after heating UHM-25-Val-Boc (**141**) to 800 °C under an atmosphere of Ar/$O_2$ (80 : 20), together with a diffractogram of tenurite (CuO, PDF No. 00-005-0661) for comparison.

The gap between the temperatures, where cleavage of the $N$-Boc group and decomposition of the organic building units occurs, suggests that the $N$-Boc protecting group can cleaved from the MOF post-synthetically. This strategy may be chosen, if it is impossible to obtain a MOF from the non-protected amines.[127,129,130] However, this procedure is unsuitable for the MOFs of the UHM-25 series. Heating the $N$-Boc-protected MOFs to 160 °C resulted in brown and amorphous materials that were inferior to those, which were directly synthesized from the ammonium salts of the linker bearing the unprotected amino alcohols.

The results of the thermogravimetric analysis for UHM-25-Val are shown in Figure 3.27. The THF exchanged MOF was heated at a rate of 1 K/s from room temperature to 800 °C in a stream of $Ar/O_2$ (80 : 20).



| $\Delta T$ | $\Delta m$ | fragments |
|:---:|:---:|:---:|
| °C | % | m/z |
| 25–142 | 7 | 18 |
| 142–266 | 13 | 18, 42 |
| 266–336 | 24 | 18, 42, 44 |
| 336–450 | 37 | 18, 44 |
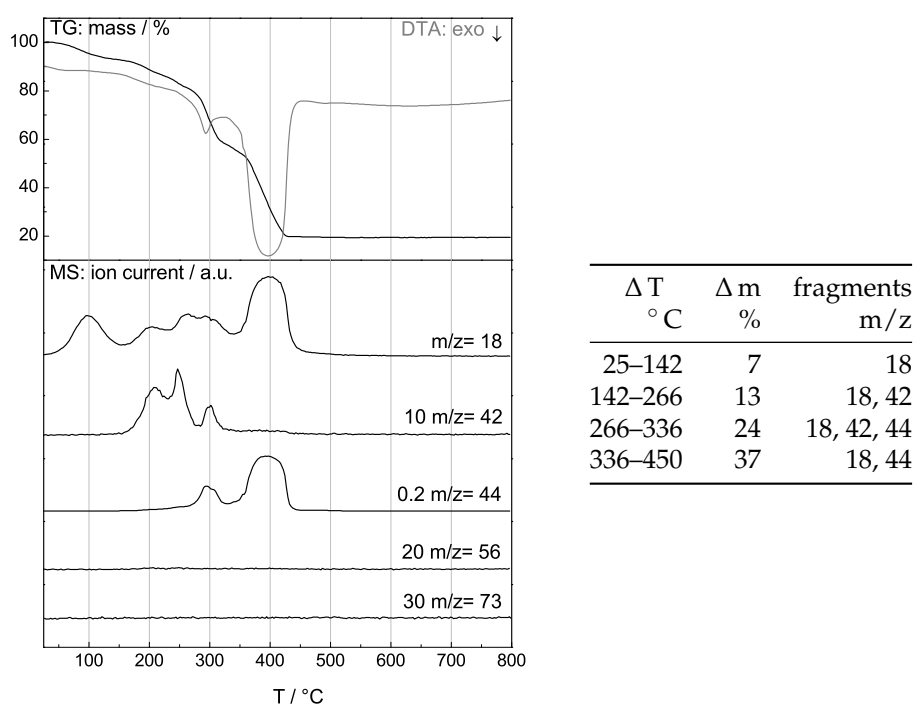
**Figure 3.27** – TG/MS analysis of UHM-25-Val (**150**), weight loss (black) and DTA (grey) are plotted in the upper part and in the lower part of the diagram the characteristic single ion currents are shown for $\frac{m}{z}$ = 18 ($H_2O$), 42 (THF), 44 ($CO_2$), 56 (isobutene), and 73 (DMF).

From room temperature to 142 °C only 7 % weight loss is observed. Judging from the recorded mass spectra, this weight loss can by solely ascribed to the loss of water from the sample. A second weight loss occurs between 142 °C and 266 °C and amounts to 13 % of the sample weight. It is observed simultaneously to the expulsion of solvent from the framework that can be detected as a fragment with $m/z = 42$ in the SIM trace. Framework decomposition occurs in a two-step process: Between 266 °C and 336 °C a weight loss of 24 % is observed and another 37 % are lost between 336 °C and 450 °C. In both cases, water and carbon dioxide can be observed as the combustion products of the

organic SBU in the respective SIM traces ($m/z = 18, 44$). After heating to 800 °C a black solid residue was obtained that corresponds to 19 % of the original sample weight. This residue has been identified by PXRD as CuO. In comparison with the TG/MS of the $N$-Boc protected MOF **141** (15 %, see Figure 3.25), less organic material is present in UHM-25-Val, which can be ascribed to the lower molecular mass of the linker. No signal was detected for $m/z = 56$ because the amino groups of the linker used for the synthesis of UHM-25-Val was already deprotected beforehand (see Scheme 3.24). Furthermore, no signals were detected that correspond to DMF. This indicates that the solvent exchange from DMF to THF proceeded quantitatively.

As an example for the Evans-type MOFs, the results of the thermoanalysis of UHM-25-Val-Evans are shown below. The linker used in the synthesis of this MOF is derived from valine and therefore bears the same isopropyl substituent as in the other two MOFs. The THF exchanged Evans-auxiliary MOF was heated at a rate of 1 K/s from room temperature to 800 °C in a stream of $Ar/O_2$ (80 : 20).

The first weight loss of the sample corresponds to 15 % of its weight and occurs between room temperature and 170 °C. This weight loss is ascribed to evaporation of solvent (THF, residual water) from the pore volume. In a second step, more of the pore filling solvent is expelled and between 170 °C and 262 °C another 17 % of the sample weight are lost. Combustion of the MOF occurs in two steps. In the first step between 262 °C and 337 °C a weight loss of 20 % is observed. The data from SIM show not only the combustion products of this process ($H_2O$ and $CO_2$) but also a peak in the signal of $m/z = 42$, which corresponds to THF that is liberated upon the decomposition of the UHM-25-Val-Evans. In the second step of combustion 31 % of the sample weight are lost between 337 °C and 456 °C. After this step, the sample weight remains constant. The resulting solid residue of this process amounts to 16 % of the original sample weight and has been identified as CuO by powder X-ray diffraction just like in the two examples above.

The resemblance of the crystal structures of the UHM-25 MOFs leads to similar observations in the respective TG/MS measurements: The decomposition of the MOFs proceeds in a two-step process in similar temperature ranges. In each case, a comparable residual mass of 15-19 % is obtained after heating to 800 °C. Furthermore, DMF was absent in all of the samples after solvent exchange. A noticable difference between the three sample is the observation of the cleavage products of the protective group together with a distinct loss of mass around 180 °C in UHM-25-Val-Boc (**141**).

| $\Delta$ T | $\Delta$ m | fragments |
|---|---|---|
| ° C | % | m/z |
| 25–170 | 15 | 18, 42 |
| 170–262 | 17 | 18, 42 |
| 262–337 | 20 | 18, 42, 44 |
| 337–456 | 31 | 18, 44 |
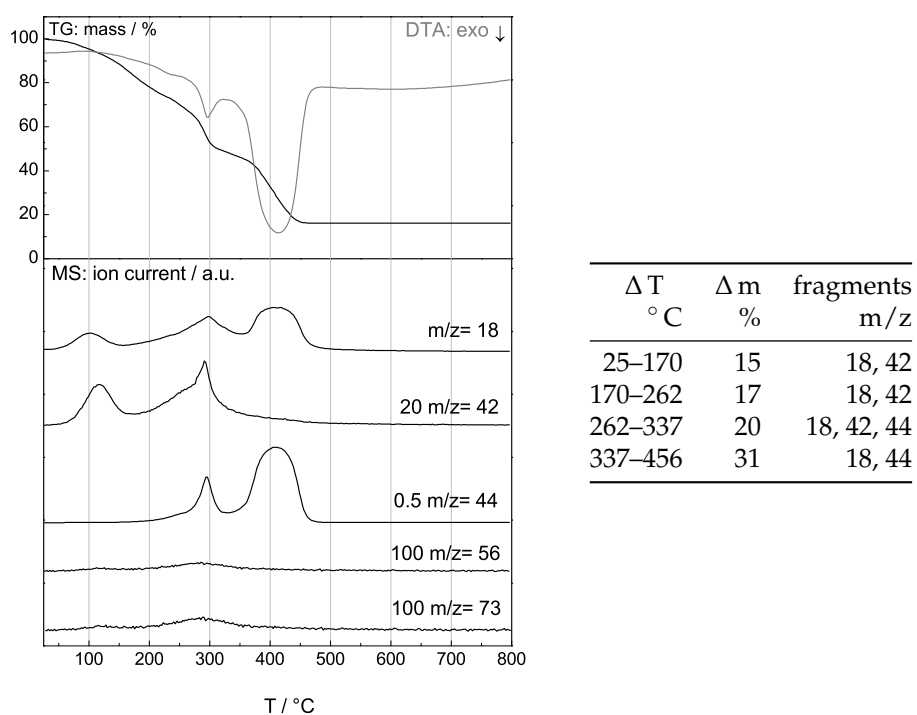
**Figure 3.28** – TG/MS analysis of UHM-25-Val-Evans (**154**), weight loss (black) and DTA (grey) are plotted in the upper part and in the lower part of the diagram the characteristic single ion currents are shown for $\frac{m}{z}$ = 18 ($H_2O$), 42 (THF), 44 ($CO_2$), 56 (isobutene), and 73 (DMF).

### 3.3.5 Porosity

In order to evaluate the porosity of the UHM-25 MOF series nitrogen physisorption measurements were carried out. Activation of the MOFs involved a twofold solvent exchange (first with a fresh portion of the synthesis solvent DMF followed by THF). The second solvent exchange resulted in a color change of the MOF from light blue to dark blue, possibly due to a exchange of the axially coordinated ligands at the copper paddle-wheels. The MOFs were evacuated at room temperature for one hour. Unfortunately, any thermal treatment at higher temperatures resulted in all cases in completely non-porous samples. Even if these mild activation conditions were applied not in all cases appreciable values for the specific surface area could be inferred, indicating a limited robustness of the framework with respect to complete solvent removal. Figure 3.29 shows a nitrogen physisorption measurement at 77 K of UHM-25-Val-Evans that has been subjected to a solvent exchange.
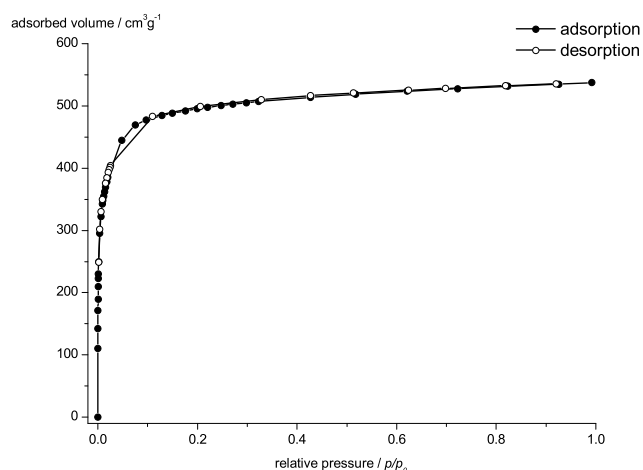


**Figure 3.29** – Nitrogen physisorption isotherm of UHM-25-Val-Evans after solvent exchange and activation at 40 °C and vacuum measured at 77 K.

In the sorption experiment, a type-I-isotherm is observed for UHM-25-Val-Evans, which is typical for microporous materials. The specific surface area was determined as $S_{BET} = 1978 \, m^2/g$ which was calculated from the adsorption branch and in the relative pressure interval from 0.012 to 0.075 $p/p_0$. The micropore volume is $V_{pore} = 0.76 \, cm^3/g$ (calculated at $p/p_0 = 0.20$). The theoretical surface area of the material is $S_{theor.} = 2200 \, m^2/g$ in a completely activated state

evaluated with the Atom Surface and Volume tool of the Accelrys Materials Studio suite.[292]

The individual sorption isotherms for the UHM-25 series can be found in the Experimental section (see Chapter 4). Table 3.7 lists the results for the specific surface areas and micropore volumes for the activated MOFs of the UHM-25 series.

**Table 3.7** – Specific surface areas and micropore volumes of the UHM-25 MOFs calculated from the adsorption branch of the physisorption isotherms with their respective values for $p/p_0$ determined after solvent exchange with THF and thermal activation at $40\,°C$ and vacuum for one hour.

| | $S_{BET}$ | | $V_{pore}$ | |
| | $m^2g^{-1}$ | $p/p_0$ | $cm^3g^{-1}$ | $p/p_0$ |
|---|---|---|---|---|
| UHM-25-Ala-Boc | 151.9 | 0.155-0.300 | 0.06 | 0.17 |
| UHM-25-Val-Boc | 1134 | 0.013-0.050 | 0.46 | 0.20 |
| UHM-25-Leu-Boc | 979.9 | 0.015-0.076 | 0.41 | 0.20 |
| UHM-25-Phe-Boc | 578.8 | 0.017-0.074 | 0.24 | 0.20 |
| UHM-25-Ala | 99.5 | 0.123-0.278 | 0.04 | 0.17 |
| UHM-25-Val | 536.3 | 0.013-0.050 | 0.21 | 0.18 |
| UHM-25-Leu | 224.7 | 0.128-0.275 | 0.07 | 0.18 |
| UHM-25-Phe | | non-porous | | |
| UHM-25-Pro | | non-porous | | |
| UHM-25-Val-Evans | 1978 | 0.012-0.075 | 0.76 | 0.20 |
| UHM-25-Phe-Evans | 574.8 | 0.019-0.075 | 0.23 | 0.20 |

As a general trend, it can be observed, that the MOFs bearing an *N*-Boc group show higher surface areas, than their non-protected counterparts. Furthermore, the MOFs with the smallest amino acid residues UHM-25-Ala-Boc and UHM-25-Ala show only very small specific surface areas. This indicates that the stability of the framework structures may benefit from sterically demanding residues on the organic SBU.

Unfortunately, not all MOFs of the UHM-25 series could be activated by the procedure described above. The experimental specific surface areas for UHM-25-Ala-Boc, UHM-25-Ala, and UHM-25-Leu are very low. For UHM-25-Phe and UHM-25-Pro the activation procedure yielded non-porous materials. As an alternative strategy for activation, solvent exchange with supercritical carbon diox-

ide was evaluated as a procedure that avoids capillary forces during the removal of the pore-filling solvent (see Section 1.4.1).

In a typical activation procedure, the supernatant of the reaction was replaced with DMF (three times) and then with THF (three times). This resulted in a color change of the MOF from light blue to dark blue. Afterwards, THF was replaced with amyl acetate (AmOAc) (three times). Samples were placed in a steel autoclave, which was sealed and filled with liquid carbon dioxide at 10 °C and 45 bar. Over the course of ten days, the supernatant that was saturated with AmOAc was replaced with fresh carbon dioxide once a day. The liquid carbon dioxide was heated to 35 °C to reach the supercritical state. The chamber was at vented at this temperature and the activated sample was stored under argon atmosphere. The experimentally determined specific surface areas and pore volumes of the UHM-25 series for this activation procedure are listed in Table 3.8.

**Table 3.8** – Specific surface areas and micropore volumes of the UHM-25 MOFs calculated from the adsorption branch of the physisorption isotherms with their respective values for $p/p_0$ determined after activation with supercritical $CO_2$.

| | $S_{BET}$ | | $V_{pore}$ | |
| --- | --- | --- | --- | --- |
| | $m^2g^{-1}$ | $p/p_0$ | $cm^3g^{-1}$ | $p/p_0$ |
| UHM-25-Ala-Boc | 1474 | 0.016-0.100 | 0.58 | 0.20 |
| UHM-25-Val-Boc | 1922 | 0.009-0.020 | 1.00 | 0.20 |
| UHM-25-Leu-Boc | 1738 | 0.016-0.074 | 0.68 | 0.20 |
| UHM-25-Phe-Boc | 623.2 | 0.007-0.024 | 0.25 | 0.20 |
| UHM-25-Ala | 975.7 | 0.010-0.048 | 0.39 | 0.20 |
| UHM-25-Val | 1286.3 | 0.011-0.049 | 0.51 | 0.20 |
| UHM-25-Leu | 1351 | 0.010-0.049 | 0.53 | 0.20 |
| UHM-25-Phe | 469.6 | 0.014-0.075 | 0.19 | 0.20 |
| UHM-25-Pro | 371.5 | 0.010-0.048 | 0.15 | 0.20 |
| UHM-25-Val-Evans | 1454 | 0.014-0.075 | 0.56 | 0.20 |
| UHM-25-Phe-Evans | 728.9 | 0.022-0.104 | 0.31 | 0.21 |

.

The experimentally determined specific surface areas of the UHM-25 MOFs are significantly higher after activation with supercritical carbon dioxide compared to the surface areas of the materials obtained from solvent exchange with THF. Interestingly, the observed surface areas of the *N*-Boc protected MOFs are higher than their non-protected counterparts, which may be explained by a greater stability of the *N*-Boc protected MOFs during the activation proce-

dure. Unfortunately, the theoretical surface area of about $S_{\text{theor.}} = 2200 \, \text{m}^2/\text{g}$ is still not reached by this method of activation. Nevertheless, these measurements prove the presence of micropores in the UHM-25 MOFs. Furthermore, the disability to achieve the full theoretical permanent porosity should not impede the application of the UHM-25 series in stereoselective reactions.

## 3.4 Further Topological Studies

### 3.4.1 Synthesis and Structure of UHM-20

In an attempt to synthesize a MOF with a chiral inorganic SBU, an interesting structure was obtained. The reaction to synthesize the material is shown in Scheme 3.32. In a solvothermal synthesis, 3,3′,5,5′-tetracarboxy-benzophenone (**136**) was reacted with zinc nitrate in *N,N*-dimethylacetamide (DMA). *N*-Boc-valinol was added as a chiral additive, attempting an inclusion in the inorganic SBUs of a MOF. A crystalline material was obtained after heating the reaction mixture at 80 °C for 18 hours in a sealed vessel, which was filtered and washed with DMA. Unfortunately, no phase purity could be achieved in the bulk material. Therefore, further investigations of the physicochemical properties such as nitrogen physisorption experiments were disregarded. However, the observed structure of UHM-20 is highly interesting from a topological point of view.
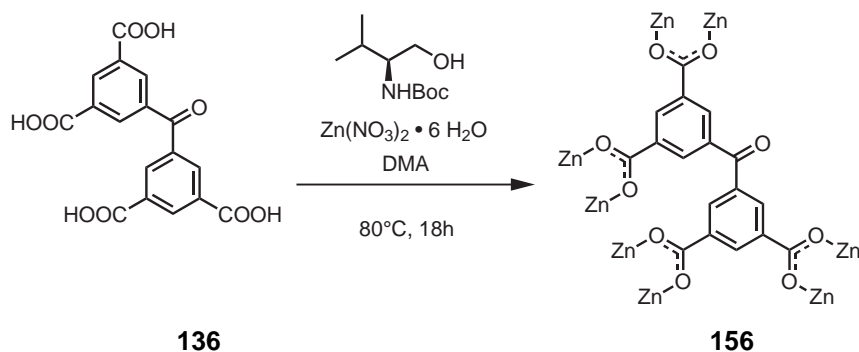


**Scheme 3.32** – Schematic representation of the reaction of 3,3′,5,5′-tetracarboxy benzophenone with a Zn(II) source in the presence of *N*-Boc-valinol that yields a crystalline material.

The material that was obtained from the reaction contained crystals that were suitable for single crystal X-ray diffraction experiments. Unfortunately, the inclusion of the chiral additive into the framework was not observed. UHM-20 $(Zn_5(C_{13}H_6O_9)_5)$ crystallizes in the tetragonal space group $I4/m$ with the unit cell parameters $a = b = 26.7514$ Å and $c = 35.7016$ Å. The tetracarboxylate of **136** is included in the framework as a four-connected organic SBU.

Although the benzophenone linker **136** has a similiar geometry to linker **147** (see Scheme 3.29, 131) that leads to the **zhc** topology in UHM-3, no isoreticular relationship is observed between this UHM-3 and UHM-20. Interestingly, there are two different kinds of inorganic SBU present in the MOF that are struc-

turally related. The carboxylates from the linker and zinc dimers form paddle wheel structures that are either three- or four connecting. The axial positions of the paddle wheels are coordinated by solvent molecules. In the case of the three-bladed paddle wheel an additional solvent molecule is coordinated to the inorganic SBU. The two different kinds of inorganic SBU are shown in Figure 3.30. There is a 4:3 distribution of three- and four connecting inorganic SBUs.
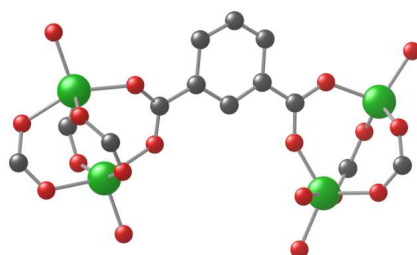


**Figure 3.30** – Two different kinds of zinc paddle wheel inorganic SBUs connected by an isophthalate residue of the organic SBU in UHM-20: a four-connected inorganic SBU built from a zinc dimer and four carboxylates and a three-connected inorganic SBU built from a zinc dimer and three carboxylates. In addition to the axially bound solvent molecules, there is another solvent molecule bound on the three-bladed-paddle wheel. (for the solvent molecules only the coordinating oxygen atoms are shown, green: zinc, grey: carbon, red: oxygen, hydrogen atoms omitted for clarity).

MOPs are formed from the isophthalate moieties of the linkers and two different paddle-wheel motifs as subunits in this MOF. These MOPs, depicted in Figure 3.31, contain eight three-connected inorganic SBUs and six four-connected inorganic SBUs. The inorganic SBUs are connected to each other via 24 of the isophthalate residues that belong the organic SBU. This arrangement can be described as a rhombic dodecahedron whose corners are occupied by the zinc dimers. The interatomic distance of two opposing zinc atoms is 16.5 Å taking into account the van-der-Waals radii of the atoms the pore diameter for the cuboctahedral pore amounts to 12.0 Å.

The MOPs of UHM-20 are arranged on a tetragonal, body-centered lattice. In this arrangement, each of the MOPs is connected to twelve neighboring MOPs via bridging by two individual organic SBUs to each of the neighbors. An arrangement of six distinct, interconnected MOPs is shown in Figure 3.32. The space that is surrounded by six of the MOPs constitutes a second type of pore in UHM-20. These pores have a diameter of 8 Å and are highlighted in Figure 3.32 as a green sphere. A third type of pore is shown in Figure 3.32 as a red sphere.
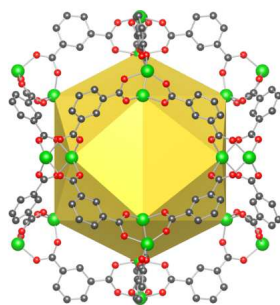
**Figure 3.31** – MOP from 24 isophthalic groups of the organic SBU, eight three-connected inorganic SBUs and six four-connected inorganic SBUs. The resulting shape is a rhombic dodecahedron whose corners are occupied by the zinc paddle wheels. Only the isophthalates that bridge the paddle wheels and lie on the edges of the rhombic dodecahedron are shown. The rest of the linker molecules and coordinated solvent molecules are omitted for clarity (grey: carbon, red: oxygen, green: zinc, omitted: hydrogen atoms as well as oxygen atoms occupying the axial positions of the inorganic SBU)

It is surrounded by four MOPs with a tetrahedral geometry and has a diameter of 4 Å.

The crystal structure of UHM-20 may be described as a packing of MOPs. In contrast to the cubic primitive arrangement of MOPs in the UHM-25 series, the MOPs of UHM-20 are in a tetragonal body centered arrangement. This results in the formation of tetrahedral and octahedral voids between the MOPs.

In order to determine the underlying net for UHM-20, the building units that serve as nodes have to be identified. The first set of nodes are the two kinds of paddle wheels that constitute the inorganic SBUs of the MOF. In the case of UHM-20, they constitute three-coordinated trigonal-planar and four-coordinated square-planar nodes, respectively. As discussed in section 3.3.1, the branching points of the organic SBU are explicitly included in the topological analysis as a combination of two triangular, three-coordinated nodes. The topological analysis of UHM-20 and the determination of a natural tiling was performed using the TOPOSPro[284] and Systre[285] software. The underlying topology of the framework structure has not been reported so far. It has been registered at the TOPOSPro personal database with the name *fhs*1.[293] It is a (3,3,3,3,4,4)-c net with the following vertex symbols and coordination sequences:

**(a)**          **(b)**

**(c)**          **(d)**
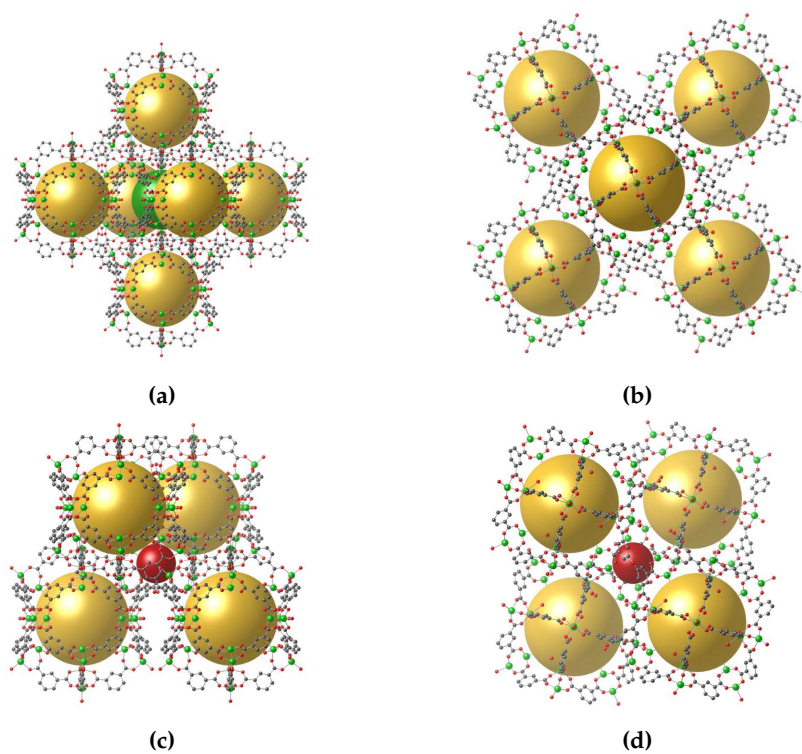
**Figure 3.32** – (a) view along the (210) direction of an arrangement of six interconnected MOPs (yellow spheres) in UHM-20, the green sphere is located in the pore space that is surrounded by six MOPs in a distorted octahedral arrangement (b) view along the $c$ axis of the same arrangement of six MOPs (c) view along the (210) direction of an arrangement of four interconnected MOPs, red sphere is located in the pore space that is surrounded by four MOPs is a distorted tetrahedral arrangement (green: zinc, grey: carbon, red: oxygen, solvent molecules and hydrogen atoms are omitted for clarity).

| vertex | vertex symbol $VS_n$ |
|---|---|
| 1 (3-c) | $6.8.8$ |
| 2 (3-c) | $6.8_2.9_2$ |
| 2 (3-c) | $6.8_2.9$ |
| 3 (3-c) | $6.8_2.9$ |
| 4 (3-c) | $8.8.8.8.12_3.12_3$ |
| 5 (4-c) | $6.8.8.8.12_3.12_3$ |
| 6 (4-c) | $3.3.3.6.6.6.20_{252}.*.*.*$ |

| vertex | coordination sequence $c_n$ | | | | | | | | | |
|---|---|---|---|---|---|---|---|---|---|---|
| | 1 | 2 | 3 | 4 | 5 | 6 | 7 | 8 | 9 | 10 |
| 1 (3-c) | 3 | 6 | 14 | 26 | 43 | 66 | 83 | 115 | 148 | 181 |
| 2 (3-c) | 3 | 7 | 14 | 27 | 44 | 61 | 88 | 110 | 147 | 177 |
| 3 (3-c) | 3 | 7 | 14 | 26 | 43 | 61 | 87 | 115 | 150 | 179 |
| 4 (3-c) | 3 | 7 | 14 | 26 | 43 | 60 | 87 | 114 | 145 | 180 |
| 5 (4-c) | 4 | 8 | 16 | 28 | 44 | 69 | 84 | 117 | 140 | 172 |
| 6 (4-c) | 4 | 8 | 15 | 26 | 42 | 61 | 87 | 115 | 148 | 174 |

The embedding with the highest symmetry of the underlying net of UHM-20 belongs to the space group $I4/m$. This is in accordance with the space group for the actual crystal structure of this MOF. The transitivity of the net is $pqrs = 6853$. A representation of the underlying topology is shown in Figure 3.33.

Interestingly, the underlying net is by far more complex than the topologies observed for the interconnected MOPs of UHM-25 described in Section 3.3.1 (page 126). In principle, the arrangement of rhombic dodecahedral MOPs could occur similar to the arrangements described for the cuboctahedral MOPs. In fact, a primitive cubic arrangement of rhombic dodecahedral MOPs has been reported recently by Lah and co-workers for a zinc based MOF that exhibits the same inorganic SBUs as in UHM-20.[294] However, they have employed elongated di-isophthalic acid linkers. This resulted in a connection of neighboring MOPs by four individual organic SBUs via the corners of the rhombic dodecahedron that has been classified as **zjz**. The augmented version of this net is depicted in Figure 3.34.

Such a simple connectivity of the MOPs is not observed for the *fhs*1 topology. The natural tiling of the *fhs*1 net is depicted in Figure 3.35. There are three different tiles that correspond to the individual pore spaces of the MOF. The yellow tiles are assigned to the void inside the MOP. The red and green tiles correspond to the tetrahedral and octahedral voids, respectively.
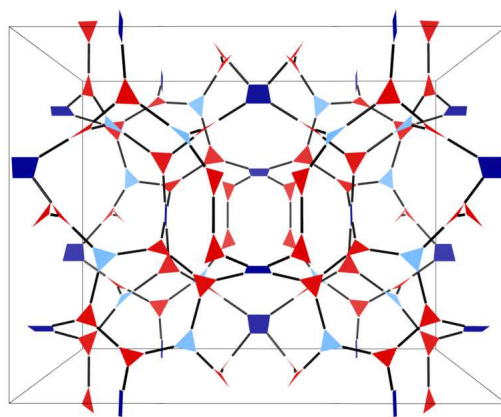
**Figure 3.33** – Perspective drawing of the underlying *fhs*1 topology of UHM-20 as an augmented net. The light blue triangles and dark blue squares correspond to the three- and four-coordinating nodes formed by the zinc paddle wheels. The red triangles correspond to the three connecting nodes formed by the isophthalate substituents of the organic SBU.

The MOPs are connected to each other via two adjacent edges. This is in contrast to the connectivity observed for other interconnected MOPs in which the neighbors were connected via the faces or corners of the polyhedra, such as those in the **zhc**, **zmj** or **ucp** topologies. A representation of the connectivity of the MOPs is shown in Figure 3.36. It demonstrates the connectivity of the MOPs.
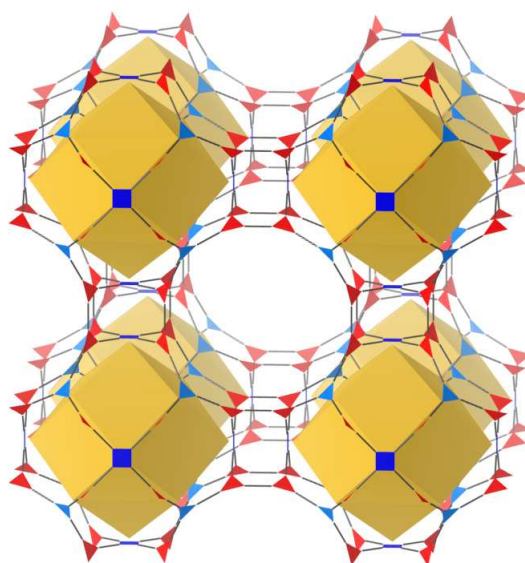
**Figure 3.34** – Representation of the **zjz** topology as an augmented net. The light blue triangles and dark blue squares correspond to the three- and four-coordinating nodes formed by the zinc paddle wheels. The red triangles correspond to the three connecting nodes formed by the isophthalate substituents of the organic SBU; yellow polyhedra derived from the MOPs are added as a guide to the eye.
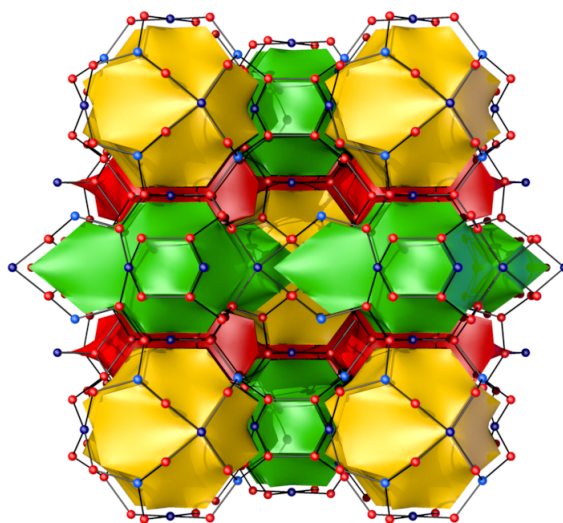
**Figure 3.35** – (a) Segment of the tiling and *fhs*1 net carried by the tiling, the yellow tiles correspond to the space inside the MOPs and the green tile corresponds to the space that is octahedrally surrounded by the MOPs. The space that is represented by the red tiles is surrounded by the MOPs in a tetrahedral arrangement. The corresponding net is represented as a collection of colored nodes (red: three-coordinated nodes derived from the branching points of the four connecting organic SBU, light blue: three-coordinated node derived from the three-connected inorganic SBU, dark blue: four-coordinated node derived from the four-connected inorganic SBU).
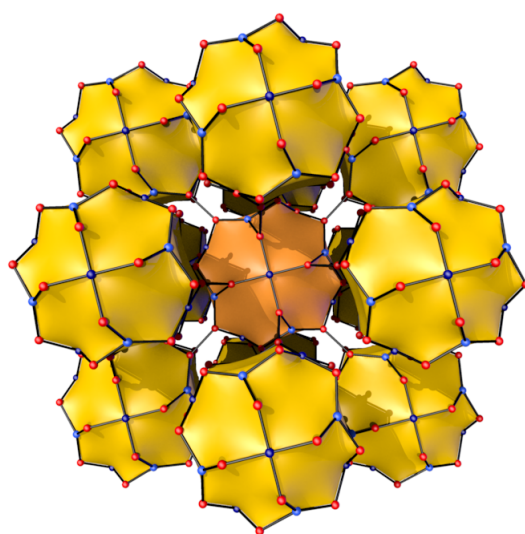
**Figure 3.36** – Section of the tiling of UHM-20 and *fhs*1 net carried by the tiling; only the tiles that correspond to the space inside the MOPs are shown. The central, orange tile is connected to each of the twelve neighboring yellow tiles via two edges of the *fhs*1 net which is represented as a collection of colored nodes (red: three-coordinated nodes derived from the branching points of the four connecting organic SBU, light blue: three-coordinated node derived from the three-connected inorganic SBU, dark blue: four-coordinated node derived from the four-connected inorganic SBU).

### 3.4.2   Synthesis and Structure of UHM-26

The tetracarboxylate linker **136** has also been used in the synthesis of a MOF with a Cu(II) salt. In this synthesis, conditions were applied that are similar to those of the preparation of the UHM-25 series (see Section 3.3). The reaction is shown in Scheme 3.33. The tetracarboxylic acid was subjected to solvothermal synthesis in screw-capped flask at 40 °C for three days. This yielded the MOF UHM-26 as a light blue, crystalline material. However, phase purity could not be achieved in the bulk material and further investigations of the physicochemical properties were disregarded. But the topology of the network and the role of the organic SBU in this MOF are interesting from a structural point of view, which are discussed in the following.
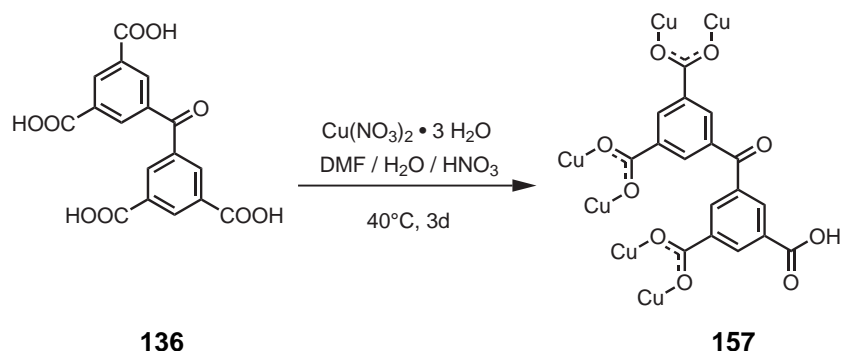


**Scheme 3.33** – Schematic representation of the reaction of 3,3′,5,5′-tetracarboxy benzophenone with a Cu(II) source in a mixture of DMF and water in the presence of diluted $HNO_3$. Copper atoms indicate the incorporation of three out of four carboxylic groups into the framework structure.

The synthesis described above yielded single crystals that were suitable for X-ray diffraction experiments that allowed the determination of a crystal structure. The structure found for this material shows an interesting connectivity of the organic SBU and can be described as follows.

UHM-26 crystallizes in the monoclinic space group $C2/c$ with the unit cell parameters $a = 32.0220$ Å, $b = 21.4733$ Å, $c = 9.4652$ Å, and $\beta = 101.090°$. Although the linker used in the synthesis of UHM-26 is principally tetratopic, one carboxylic group of the linker remains uncoordinated. Therefore, the linker serves as a three-connected organic SBU in the framework. Each organic SBU is connected to two distinct kinds of inorganic building units. First, one carboxylate group from each of the isophthalate groups of the linker is bound to a copper paddle wheel each. Second, a carboxylic group of one of the isophthalates is

165

additionally connected to a one-dimensional rod-like SBU. This connectivity is depicted in Figure 3.37.



<center>(a)    (b)</center>
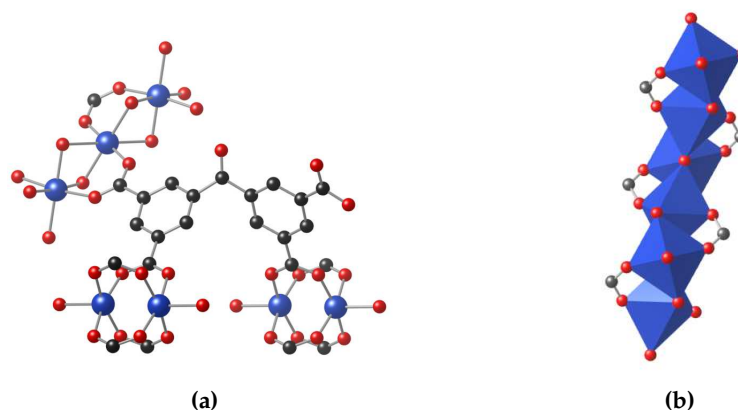
**Figure 3.37** – (a) Three-dimensional structure of the organic SBU together with two four-connected copper-paddlewheels and a segment of a one-dimensional rod-like SBU. (b) View along the crystallographic *b* axis of a segment of the infinite, rod-like inorganic SBU in UHM-26 that consists of edge-sharing octahedra bridged by carboxylate groups in an alternating arrangement (blue octahedra: copper in the rod-like SBU, blue: copper, red: oxygen, grey: carbon, hydrogen atoms and disordered solvent molecules are omitted for clarity).

The one-dimensional inorganic SBUs run along the crystallographic *c* axis and lie at the centers of four faces of the unit cell. Neighboring rod-like SBUs are connected via two isophthalate groups of the organic SBU that are bridged by a copper paddle wheel. A representation of an expanded unit cell of UHM-26 that demonstrates this connectivity is depicted in Figure 3.38. The formation of one-dimensional SBUs is often associated with the formation of a channel-like pore system. This is also the case for UHM-26. Here, rectangular, one-dimensional pores run parallel to the infinite SBUs. These pores are decorated with the un-coordinated carboxylic groups of the organic SBU. The interatomic distance of two carboxylic carbon atoms that oppose each other is 10.05(5) Å and the distance of two oxygen atoms that oppose each other on different rod-like SBUs is 15.45(5) Å.

For MOFs with infinite SBUs this process is not as straightforward as for MOFs with discrete metal clusters.[5] In the case of UHM-26 the rod-like SBU is abstracted to a collection of four-coordinated nodes. The paddle wheel structure

<center>166</center>

**(a)**  **(b)**
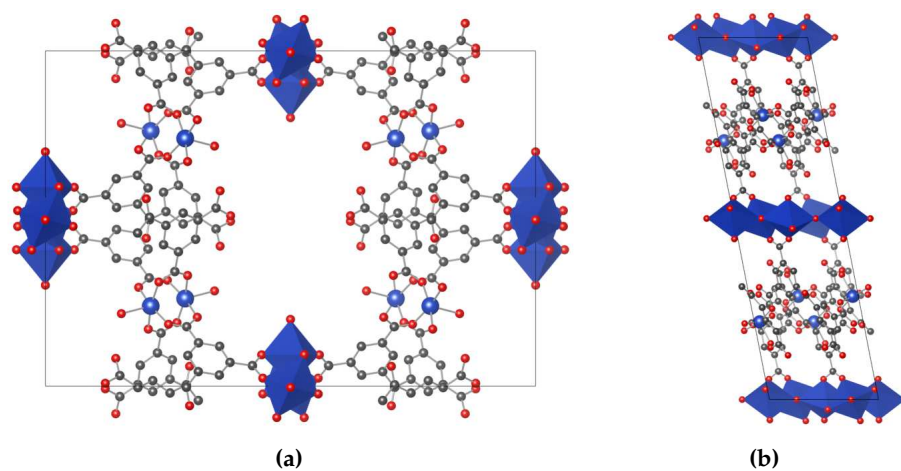
**Figure 3.38** – (a) View along the crystallographic *c* axis of an expanded unit cell of UHM-26 in which rod-like inorganic SBUs run along the viewing direction, the rectangular one-dimensional pore in the center of the unit cell is lined with uncoordinated carboxylic groups; (b) view along the crystallographic *c* axis of the same cell (blue octahedra: copper in the rod-like SBU, blue: copper, red: oxygen, grey: carbon, hydrogen atoms and disordered solvent molecules are omitted for clarity).

167

of the other inorganic SBU is treated as a four-coordinated node with square-planar geometry. The organic SBU that is derived from the tetracarboxylate linker is treated as a three-coordinated node with a trigonal-planar geometry. The abstracted building units of UHM-26 are shown in Figure 3.39 in their augmented forms.



|  (a)  |  (b)  |

**Figure 3.39** – (a) The infinite inorganic SBU of UHM-26 can be abstracted as a ladder-type arrangement of 4-c nodes, shown here in the augmented form (b) the abstracted 4-c paddle wheel motif (blue square) and 3-c organic SBU (red triangle) in their augmented form.

Using the abstraction of the SBUs as described above, a topological analysis of UHM-26 was performed using the TOPOSPro.[291] The underlying topology of the framework structure has not been reported so far. It is a (3,4,4)-c net with the following vertex symbols and coordination sequences:

| vertex | vertex symbol $VS_n$ |
|---|---|
| 1 (3-c) | $4.6.6$ |
| 2 (4-c) | $4.4.6.6.8_2.8_2$ |
| 3 (4-c) | $4.4.6.6.22_{1680}.22_{1680}$ |

The net that represents the topology of UHM-26 is shown in Figure 3.40. The ideal space group for embedding of this net has been determined with Systre[285] as *Cccm* which is the proper supergroup of the space group *C2/c* of the crystal

168

| | coordination sequence $c_n$ | | | | | | | | | |
|---|---|---|---|---|---|---|---|---|---|---|
| | 1 | 2 | 3 | 4 | 5 | 6 | 7 | 8 | 9 | 10 |
| 1 (3-c) | 3 | 8 | 12 | 22 | 33 | 42 | 60 | 81 | 113 | 153 |
| 2 (4-c) | 4 | 6 | 14 | 22 | 32 | 44 | 52 | 80 | 120 | 154 |
| 3 (4-c) | 4 | 9 | 16 | 23 | 32 | 49 | 715 | 93 | 114 | 114 |

structure of this MOF. To obtain this high symmetry embedding, the net that was simplified with TOPOSPro[284] was further idealized by a repositioning of the three-coordinanted vertex with the Accelrys Materials Studio suite[292] to obtain a trigonal-planar geometry.



**(a)**          **(b)**
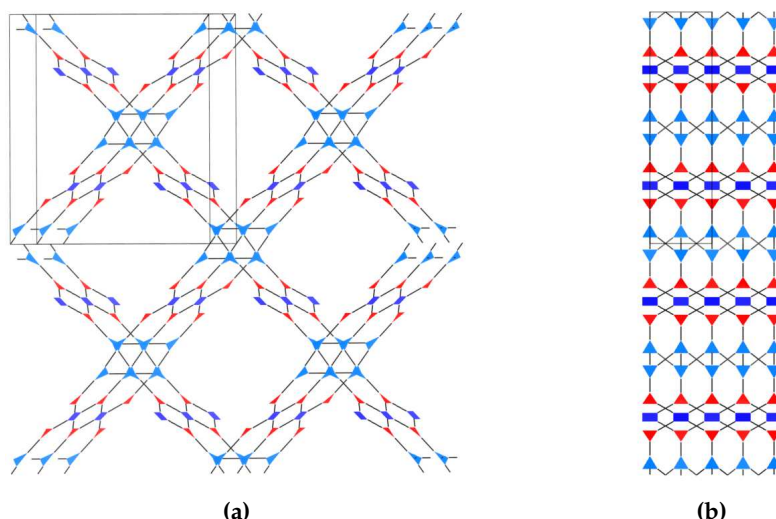
**Figure 3.40** – (a) View along the (011) direction of a perspective drawing of a 2 × 2 × 2 super cell of the underlying net of UHM-26 in its augmented form; the nodes that correspond to the rod-like inorganic SBU run across the *ac* and the *bc* face of the unit cell. (b) View along the crystallographic *b* axis on the same super cell. (light blue distorted tetrahedra correspond to the 4-c nodes of the rod-like inorganic SBU, dark blue squares correspond to copper paddle-wheels, and red triangles correspond the the organic SBU).

The transitivity of the net is *pqrs* = 3442. The natural tiling of the underlying topology of UHM-26 is depicted in Figure 3.41. There are two different tiles that correspond to the one-dimensional pore space of the MOF. The tiles are stacked along the *c* direction in an alternating arrangement.
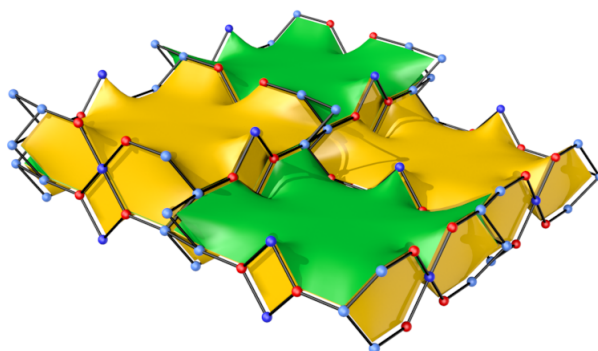
**Figure 3.41** – (a) Segment of the tiling derived from the crystal structure of UHM-26 and the net carried by the tiling, the yellow and green tiles correspond to the space inside the one-dimensional pore system. The tiles are stacked along the *c* direction in an alternating arrangement. The corresponding net is represented as a collection of colored nodes (red: three-coordinated nodes derived from the organic SBUs, dark blue: four-coordinated nodes derived from the copper paddle-wheels, light blue: four-coordinated nodes derived from the one-dimensional inorganic SBUs).

The benzophenone tetracarboxylate **136** is structurally related to the linker molecules (see Scheme 3.29 page 131) that yielded interconnected cuboctahedral MOPs under the same general synthetical conditions. It is remarkable that the benzophenone linker (**136**) formed a framework structure that bears no resemblence to the systems described in Section 3.3.1. The reason for this behavior may be the lack of conformational flexibility of the benzophenone motif which may impede its ability to adopt the conformations that are necessary for the interconnection of cuboctahedral MOP.

170

## 3.5   Catalysis

Among the substituents on the organic SBUs from MOFs of the UHM-25 series are functional groups that makes them feasible candidates for heterogeneous, asymmetric catalysis. Because reactions mediated by a pyrrodinyl system have been studied intensively (see Section 1.5.2), UHM-25-Pro has been identified as the most promising candidate from the UHM-25 series for such applications. UHM-25-Pro bears a free secondary amine inside a five-membered heterocycle, enabling it to form reactive enamine species that can attack carbonyl compounds. A well-studied example for this type of reaction is the self-directed aldol addition of acetaldehyde. Hayashi and co-workers have reported a series of diaryl prolinol systems that have been successfully applied in the synthesis of 3-hydroxybutanal.[295] Chiral β-hydroxyaldehydes are synthetically versatile intermediates. Methods to obtain this building block often proceed via indirect pathways.[296,297] However, direct methods from acetaldehyde are straightforward since they employ a very simple building block to obtain a useful chiral carbonyl compound.[298] A proposed mechanism for this reaction shown in Scheme 3.34.

Attempts to synthesize 3-hydroxybutanal with UHM-25-Pro as a catalyst were performed in $CH_2Cl_2$. This solvent was chosen because it allows a direct monitoring of the reaction by gas chromatography. Therefore, to prepare UHM-25-Pro for the assessment of enantioselectivity, the solvent exchanged material that was obtained after the synthesis was treated repeatedly with $CH_2Cl_2$. This procedure replaced THF from the pores which was used in the final wash procedure in the preparation of the UHM-25 MOFs. UHM-25-Pro that was exchanged with $CH_2Cl_2$ was weighed and suspended in $CH_2Cl_2$. This suspension was degassed to remove oxygen that might oxidize the reactants. Acetaldehyde was added to the suspension of the MOF in $CH_2Cl_2$ to yield a 10 % solution by volume. After five days at room temperature, the formation of the desired product was observed by GC-MS measurements. However, not only the desired product was present. Because an excess of acetaldehyde in the reaction mixture is present, a cyclic acetal can be formed from the hydrated acetal **163**. This reversible process is shown in Scheme 3.35.

To overcome the formation of this byproduct, the reaction was modified according to a literature procedure in which the aldehyde **163** was protected as an acetal.[295] The reaction to form 3-hydroxybutanal (**163**) by catalysis with UHM-25-Pro was prepared and performed as described above. After stirring for five days at room temperature, the MOF was filtered off. The filtrate was treated with methanol and Amberlyst® 15, which serves as a resin-bound sulfonyl catalyst. This heterogeneous acid catalyst converted the 3-hydroxybutanal (**163**) to the corresponding dimethyl acetal **165**. Furthermore, this subsequent protection
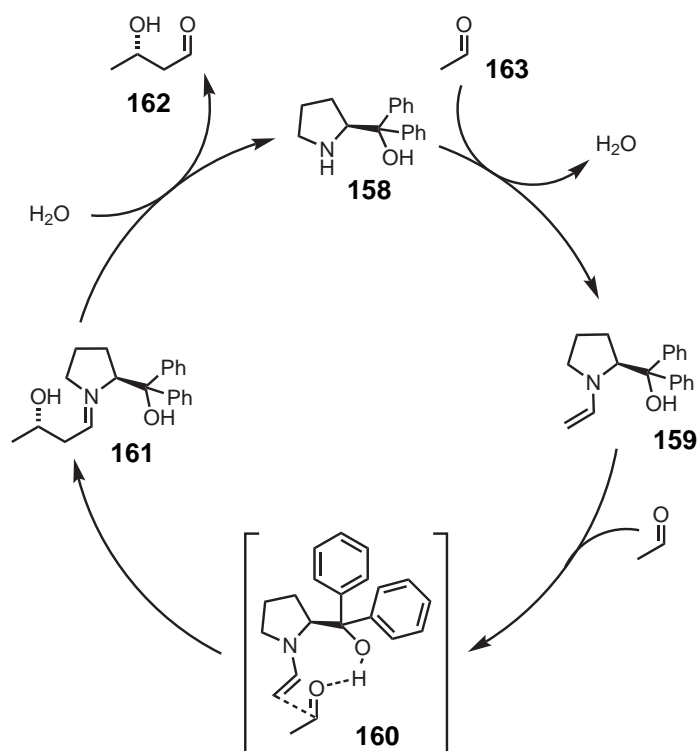
**Scheme 3.34** – Schematic representation of the catalytic cycle of the self-directed aldol addition of acetalydehyde catalyzed by α,α-diphenyl prolinol. In the first step, acetaldehyde reacts with the secondary amine of the amino alcohol **158** to form an enamine. The addition of the enamine to another molecule of acetaldehyde proceeds via a transition state in which the aldehyde is tethered to the tertiary alcohol by a hydrogen bond (**160**). Through this interaction, the nucleophilic addition to the electrophile takes place on the *si*-face of the enamine. In the last step, 3-hydroxybutanal is liberated from the diaryl species by hydrolysis.
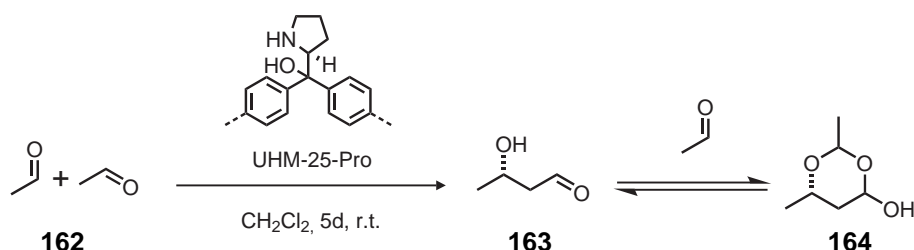
**Scheme 3.35** – Schematic representation of the self-directed aldol addition of acetalydehyde catalyzed by UHM-25-Pro. In the first step of the reaction sequence, acetaldehyde reacts with another molecule of acetaldehyde (**162**), catalyzed by UHM-25-Pro. Hydration of 3-hydroxybutanal (**163**) leads to the reaction with a third equivalent of acetaldehyde. The cyclic trimer **164** is formed which is in equilibrium with the acyclic aldol product.

of the aldehyde facilitated the isolation and analysis of the reaction product. The reaction sequence for this procedure is shown in Scheme 3.36.

After the conversion of the aldehyde to the acetal, the reaction mixture was filtered and the solution was concentrated in vacuum. The dimethylacetal was obtained as a clear liquid with a yield of 45 %. Compared to a literature procedure[295] that uses a structurally similar but homogeneous prolinol derivative that gives the reaction product with 48 % yield, similar to the homogeneous version of this reaction.

In the self-directed aldol addition of acetaldehyde catalyzed by UHM-25-Pro, one new stereocenter is formed at the carbonyl group that serves as the electrophile (compare Scheme 3.34). To evaluate the stereoselectivity of this reaction, a relative quantification of the individual enantiomers is necessary. This analysis was performed using enantioselective gas chromatography (GC). Hydrogen was used as a carrier gas and the enantioseparation was performed on a stationary silica phase modified with heptakis-(2,3-di-*O*-methyl-6-*O*-*tert*-butyldimethylsilyl)-β-cyclodextrin. A complete separation of the enantiomers on the GC column was achieved using a temperature gradient of $1\,°C/\text{min}$ after keeping the column heated to $70\,°C$ for five minutes after injection of the sample. A chromatogram of the separation of the reaction product is shown in Figure 3.42.

The chromatogram displays a shift in the baseline after six minutes that can be ascribed to the change in temperature after an isothermic phase during the temperature program. Between the retention times of eight to eleven minutes small, overlapping peaks are detected. These signals were identified by comparison of the recorded mass spectra with a reference database as the two enan-
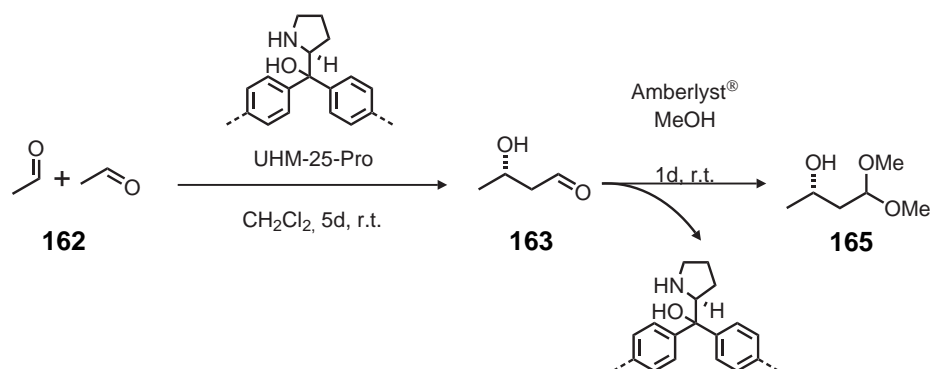
**Scheme 3.36** – Schematic representation of the self-directed aldol addition of acetalydehyde catalyzed by UHM-25-Pro. In the first step of the reaction sequence, acetaldehyde reacts with another molecule of acetaldehyde, catalyzed by UHM-25-Pro. To protect the 3-hydroxyaldehyde, UHM-25-Pro is removed and the solution is treated with methanol and a resin-bound sulfonyl catalyst (Amberlyst®) to form the corresponding dimethylacetal (**165**).
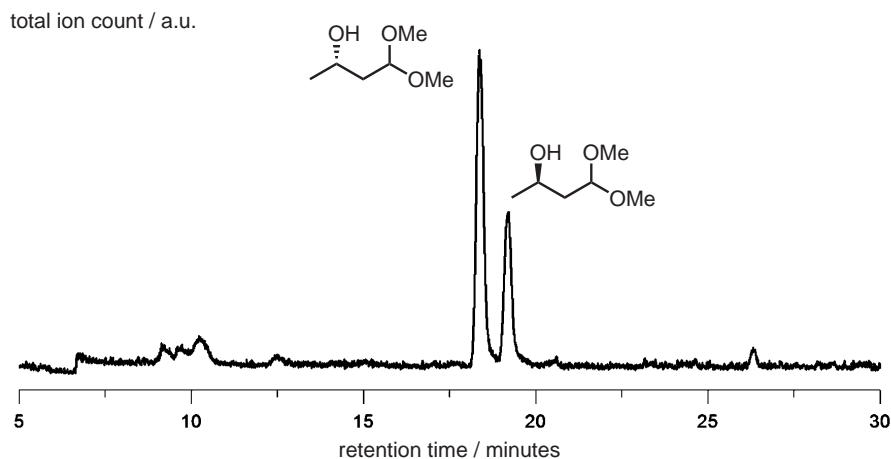


**Figure 3.42** – Total ion count of the enantioselective gas chromatographic separation of the reaction product (**165**) from the self-directed aldol addition of acetaldehyde catalyzed by UHM-25-Pro. Baseline separation was achieved for the major products on a β-cyclodextrin column with a temperature gradient program.

tiomers of the deprotected aldehyde (**163**). The presence of the free carbonyl compound may be explained by a partial decomposition of the dimethyl acetal **165** on the hot injector block of the GC system. At the retention times of 18.4 min and 19.2 min two isolated peaks can be observed. Mass spectra recorded for the individual peaks show identical fragmentation, indicating that these peaks can be ascribed to a set of enantiomeric compounds. The mass spectra for the individual peaks are shown in Figure 3.43 and can be assigned to the 1,1-dimethoxy-3-hydroxy-butane (**165**) via the fragmentation pattern in the mass spectra. Due to the high tendency of acetals to dissociate during mass spectrometry, the ion with the highest mass ($m/z = 103$) does not correspond to the molecular ion but to one of its fragments. The most intensive signals of the spectrum at $m/z = 75$ and $m/z = 59$ can be assigned to the fragments that result from an $\alpha$-cleavage next to the acetal.
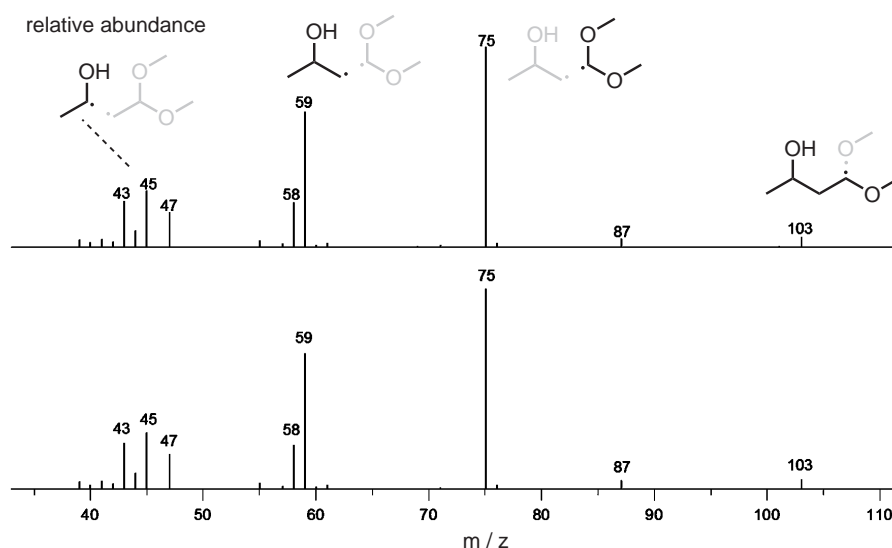


**Figure 3.43** – Mass spectra for the peaks at retention time 18.4 (top) and 19.2 minutes (bottom). The fragmentation patterns of the separated compounds are identical because they are caused by the enantiomers of the same compound; fragments of the molecular ions are highlighted in black.

As it is clearly visible from the chromatogram in Figure 3.42, one enantiomer is preferentially formed in the aldol addition. The exact ratio of the enantiomers that are formed in the reaction can be determined by the integration of the total ion count of the individual peaks of the chromatogram. This integration reveals

175

an enantiomeric ratio of 70:30 between the two enantiomers. This corresponds to an *ee* of 40 %.

The assignment of the absolute configuration of the reaction products was achieved on the basis of a control experiment: a homogeneous catalysis was performed using the same reaction conditions for the aldol addition of acetaldehyde. Here, α,α-diphenyl prolinol was used as a soluble catalyst instead of solid UHM-25-Pro. Hayashi and co-workers reported the (*S*)-configurated aldehyde as the main product of the reaction aldol addition with this proline derivative.[295] ³ Comparison of the chromatograms of the heterogeneous and homogeneous reaction shows that the same enantiomer is formed as the major reaction product. An enantiomeric ratio of 74:26 was observed for the homogeneous control reaction, which is slightly higher than the heterogeneous reaction catalyzed be UHM-25-Pro.

Although secondary amino alcohols are the prevalent species in enantioselective organocatalysis, enamine catalysis may also proceed through reaction with primary amino alcohols.[301] Therefore, the MOFs of the UHM-25 series that feature unprotected primary amino alcohols were also assessed as stereoselective organocatalysts using the same reaction parameters as described for the catalysis with UHM-25-Pro. An overview of these reactions with the respective UHM-25 MOFs is given in Scheme 3.37

Workup and analysis for the individual reactions were performed analogous to the procedure described for UHM-25-Pro. However, the use of the primary amino alcohols as catalysts led to a significant decrease in the yield of the reaction. None of the reactions shown in Scheme 3.37 provided the crude reaction product **165** with a yield of more than 5 %. Nevertheless, enantioselective gas chromatography was performed with the reaction products that were obtained. A collection of the chromatograms is shown in Figure 3.44. In addition to the dimethyl acetal **165**, a number of unknown byproducts was observed. To determine the *ee* of the reactions signals were integrated that are characteristic for the reaction product ($m/z = 75$). Unfortunately no stereochemical induction could be observed for the reactions catalyzed by UHM-25-Val and UHM-25-Leu. In the aldol addition catalyzed by UHM-25-Phe and the subsequent formation of the acetal, (*R*)-1,1-dimethoxy-3-hydroxy-butane was preferentially formed with an enantiomeric ratio of 44 : 56. Although the stereochemical induction is very low, this is interesting because it is in contrast to the reaction catalyzed by the proline derivatives, where the (*S*) product is formed preferably.

---

³ Hayashi and co-workers assigned the absolute configuration of the stereocenter by a reduction of **163** to (*S*)-1,3-dihydroxybutane, which is a derivative of (*S*)-malic acid and whose optical rotation and absolute configuration are documented in the literature.[299,300]
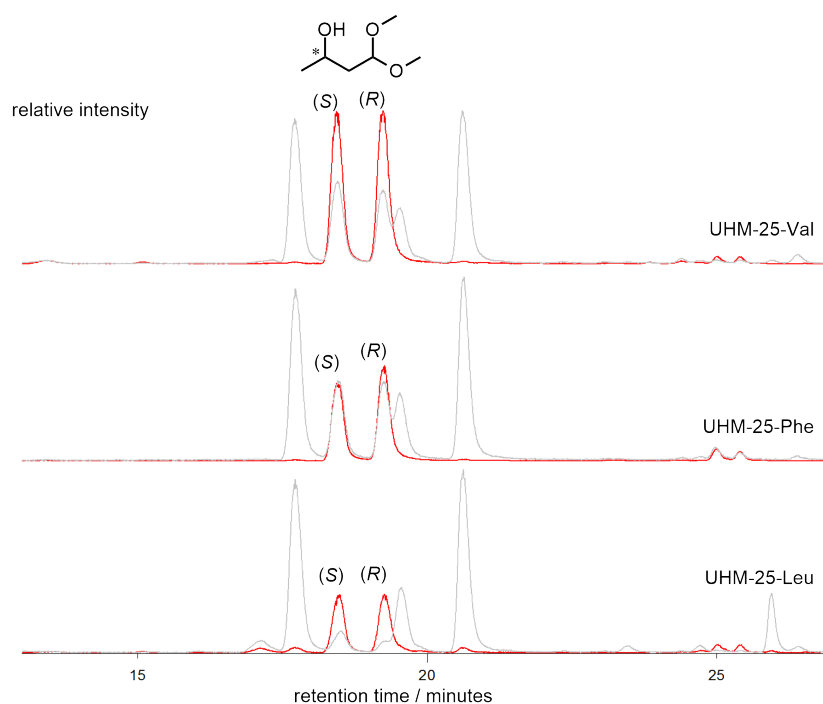
**Figure 3.44** – Comparision of the chromatograms of reaction product of the self-directed aldol additions of acetaldehyde catalyzed by UHM-25-Val, UHM-25-Phe, and UHM-25-Leu. Each chromatogram shows the total ion count (grey) and the ion count of $m/z = 75$ (red), which is a characteristic fragment for the reaction product (**165**).
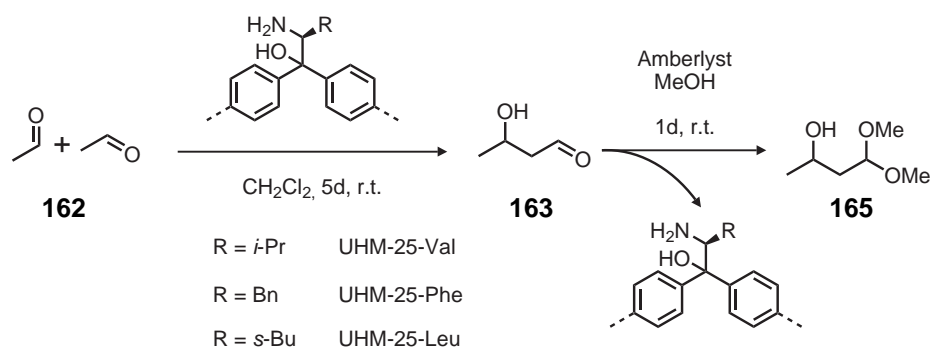
**Scheme 3.37** – Schematic representation of the self-directed aldol addition of acetalydehyde catalyzed by UHM-25 MOFs with different substituents on the amino alcohol substituent. The reaction yields γ-hydroxy aldehyde that is protected as the corresponding dimethyl acetal in a reaction with methanol catalyzed by an ion exchange resin after the removal of the MOF by filtration.

## 3.6  Post-Synthetic Modification

Due to the large amount of available functional groups, the UHM-25 MOFs may be applicable not only for catalytic processes but also for reaction in which these groups serve as solid support that provides a homochiral environment for subsequent reactions. A three step procedure was envisioned to employ the UHM-25-Evans MOFs in stereoselective applications. In such processes the nitrogen atom of the 1,3-oxazolidin-2-one may be acylated with an achiral carboxylic acid. Due to the defined stereocenter on the MOF-bound heterocycle one enantiotopic face of the resulting amide **166** may be effectively shielded during the formation of an enolate that can react with electrophiles in an aldol addition. In the hypothetical reaction shown in Scheme 3.38, two new stereocenters are formed on the substrate. This type of reaction requires stoichiometrical amounts of the MOF. However, the immobilization of the auxiliary in a solid material should allow a convenient recovery of the reagent after the elimination of the reaction product.

### 3.6.1  Post-synthetic modification (PSM) of UHM-25-Val-Evans

To evaluate the potential of the UHM-25 MOFs as chiral, solid auxiliaries they were subjected to post-synthetic modification. In the first step of this reaction procedure, an acylation of the MOF-bound oxazolidinone was attempted. A
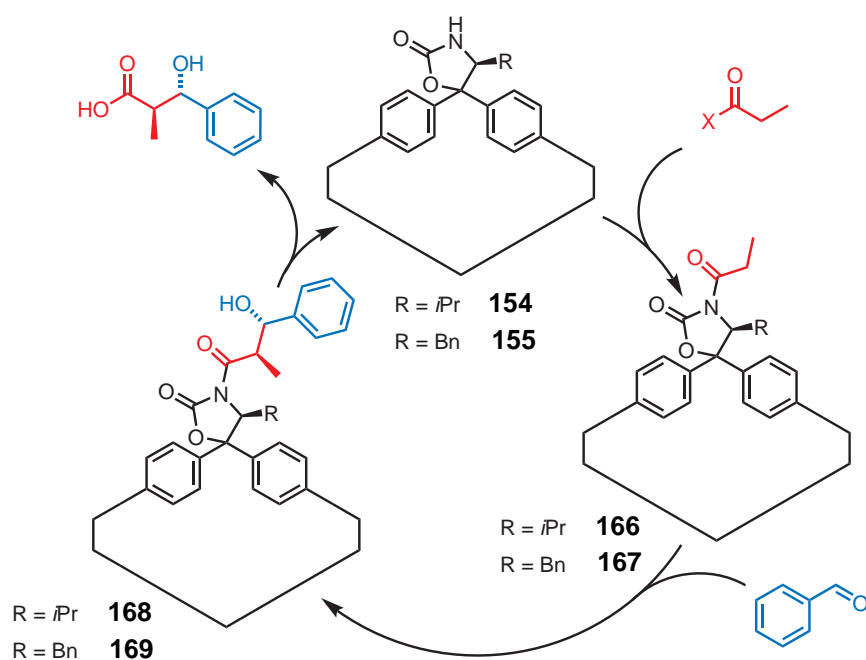
**Scheme 3.38** – Schematic representation of a hypothetic aldol reaction mediated by a solid state Evans-auxiliary provided by a UHM-25-Evans MOF (R = *i*Pr or Bn). After an acylation of the free oxazolidinone (**154**/**155**) with an activated carboxylic acid (highlighted in red), a stereoselective addition can occur with a carbonyl compound to yield a MOF-bound aldol product (**168**/**169**). Hydrolysis of the amidic bond can liberate the chiral carboxylic acid and the unsubstituted oxazolidinone (**154**/**155**).

very widespread method to achieve the acylation of a 1,3-oxazolidin-2-one employs *n*-butyllithium (*n*-BuLi) and an acylchloride or anhydride.[302] In this reaction, the organolithium reagent serves a very strong base to deprotonate the NH-group of the auxiliary. The resulting oxazolidinide can then react with an activated carboxylic acid to form the acylated auxiliary. This procedure was applied to UHM-25-Val and is shown in Scheme 3.39 Because the organolithium reagent decomposes in the presence of water, the MOF was exchanged repeatedly with dry THF before use and was kept under a protective atmosphere. To deprotonate the auxiliary, *n*-BuLi was added to a suspension of UHM-25-Val-Evans in THF at $-78\,°C$ and was stirred at the same temperature. After the deprotonation step, the supernatant was replaced with a solution of propionic anhydride and the reaction mixture was slowly warmed to room temperature.
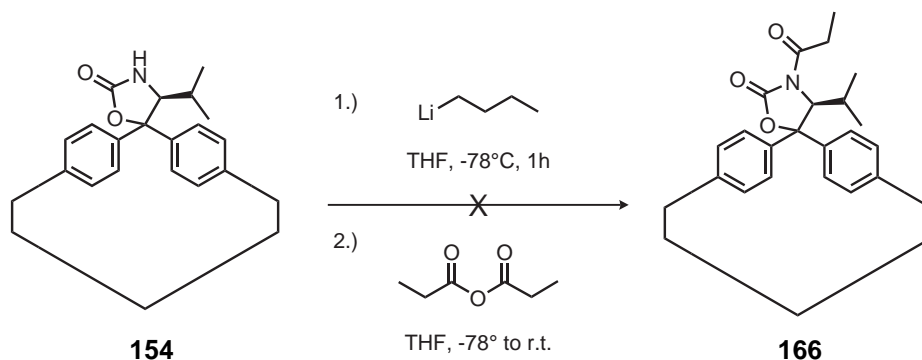


**Scheme 3.39** – Failed attempt to acylate **154** in a two-step procedure in which the oxazolidinone moiety of UHM-25-Val-Evans should have been deprotonated by *n*-butyllithium followed by a reaction with propionic anhydride.

To investigate the success of this modification, UHM-25-Val was washed with repeatedly with THF, dried in vacuum and was then digested in hydrochloric acid. Unfortunately no conversion to the desired *N*-acylated product was observed. This is probably the case, because of the tendency of *n*-BuLi to form tetrameric aggregates.[303] It is possible that the size of these aggregates prevents these species from entering the pore system of UHM-25-Val. This is in agreement with a report by Rood who attempted a lithiation of an MOF-bound amino group with methyl lithium which was also unsuccessful.[304]

An alternative pathway for the acylation of oxazolidinones can be initiated by lithium chloride. Proposed mechanisms for such an activation include the chelation of the lithium ion by the anhydride, which increases its reactivity by a coordination of the lithium to the amide which results in an increased acid-

ity of the NH proton.[305] The attempted reaction employing LiCl is shown in Scheme 3.40. UHM-25-Val was suspended in THF and triethylamine, propionic anhydride were added to the reaction mixture. Upon the addition of LiCl the supernatant of the reaction immediately turned green. The reaction was stirred for 18 hours.



**154**                                                    **166**
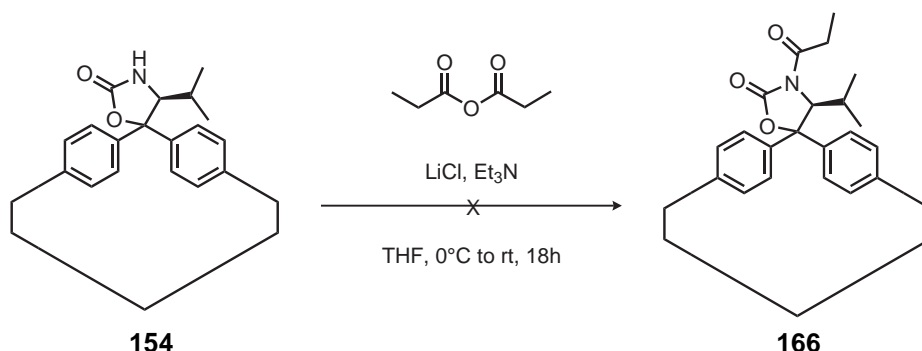
**Scheme 3.40** – Attempt to acylate **154** in a procedure in which the oxazolidinone moiety of UHM-25-Val-Evans should have been activated by lithium chloride followed by a reaction with propionic anhydride.

After filtration and digestion of the MOF, a molecule with the same molecular weight as the desired *N*-acylated product was observed in the mass spectrum of the reisolated linker. However, after the addition of the lithium salt a considerable amount of the MOF was dissolved. This can be explained by the formation of dilithium tetrachlorocuprate which is soluble in THF. This process removes copper from the framework structure and thereby destroys the MOF. Therefore, a homogeneous reaction in which the free linker was acylated cannot be ruled out.

To obtain the *N*-acylated derivative of UHM-25-Val-Evans without the destruction of the framework structure, a third acylation procedure was investigated. This method uses 4-(dimethylamino)-pyridine (DMAP) as a catalyst to acylate the carbamates. The pyridine derivative first reacts with the propionic anhydride. The resulting *N*-acylated pyridinium salt then acts as acyl donor to the oxazolidinone and transfers the propionyl group to the nitrogen atom.[306,307]

The acylation as performed on UHM-25-Val-Evans is shown in Scheme 3.41. The MOF was suspended in THF together with triethylamine. A solution of DMAP in THF and propionic anhydride were added to the suspension. After one to three days, the MOF was isolated from a light green supernatant, washed with THF and dried in vacuum.
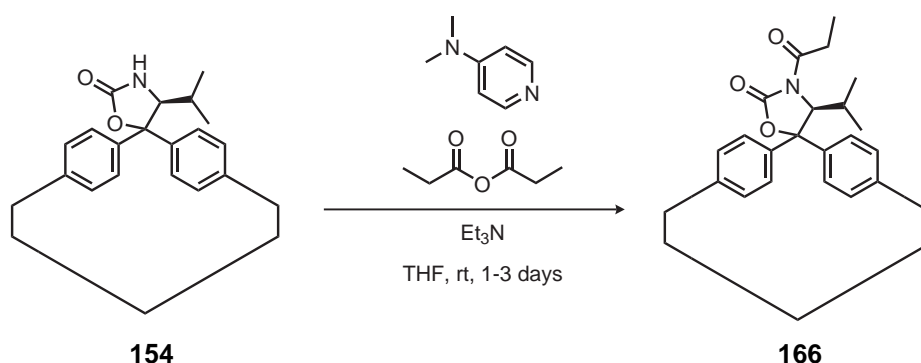
**Scheme 3.41** – *N*-Acylation of the chiral 1,3-oxazolidin-2-one of UHM-25-Val-Evans (**154**) using propionic anhydride in conjunction with catalytic amounts of DMAP; Et$_3$N is added as a base to capture propionic acid byproduct.

To evaluate the performance of the reaction, the MOF was digested in diluted hydrochloric acid (1 M) in an ultrasonic bath. The reisolated linker was dried and then analyzed by ESI-HRMS and $^1$H-NMR measurements. The acylation reactions were performed with varying durations and concentrations of the reactants. The results for these experiments are listed in Table 3.9. The reactions were performed with a large excess of the reagents with respect to the free NH groups on the UHM-25 MOF. The molecular mass of UHM-25-Val was estimated[4] as 996 g/mol judging from the results of the thermogravimetric analysis (shown in Figure 3.28), assuming that the combustion of the UHM-25-Val-Evans proceeds quantitatively to CuO. The calculation of the conversion was determined from an integration of characteristic signals in the $^1$H-NMR spectra of the reisolated linker after digestion of the MOF. The desired product was obtained for all entries in the following table which was confirmed by the spectroscopic data of the reaction products.

The results in Table 3.9 show that a duration of the reaction of 24 hours gives only a modest conversion of 37 % (entry 1). Therefore, the duration of the reaction was increased to 72 hours. With this increase in time the conversion rate was raised to 85 % to 90 % (entries 2-5). To further improve the conversion rate, the amount of reagents was increased to a 26-fold excess and the reaction was performed at elevated temperatures of 40 °C. This resulted in acylation of up to 96 % of the 1,3-oxazolidin-2-one groups of UHM-25-Val-Evans (entry 6). How-

---

[4]A molecular mass of the *solvent-free* MOF can be calculated as 732.6 g/mol according to the UHM-25 crystal structure.

**Table 3.9** – *N*-Acylation of the 1,3-oxozolidinone of UHM-25-Val-Evans using propionic anhydride in conjunction with triethylamine and catalytic amounts of DMAP; reactions were performed in THF.

| entry | $n_{MOF}$ µmol | reaction conditions time hours | temperature °C | reagents eq. | yield | conversion |
|---|---|---|---|---|---|---|
| 1 | 90 | 24 | rt | 13 | n.d. | 37 % |
| 2 | 90 | 24 | rt | 13 | 76 % | 30 % |
| 3 | 90 | 72 | rt | 13 | 79 % | 85 % |
| 4 | 90 | 72 | rt | 13 | 74 % | 90 % |
| 5 | 90 | 72 | rt | 13 | 71 % | 89 % |
| 6 | 90 | 72 | 40 | 26 | 61 % | 96 % |
| 7 | 90 | 72 | 40 | 26 | 64 % | n.d. |
| 8 | 185 | 72 | rt | 20 | 67 % | n.d. |

ever, the yield of the reaction decreased from 71 %–79 % (entries 2-5) to 61 %–67 % (entries 6-8). Furthermore, the reaction solutions turned green after some time, which indicates a leaching of Cu(II) from the MOF. This effect was more pronounced for the reactions with increased equivalents of the reagents. This leads to the assumption that one of the components or a product of the reaction induces a partial dissolution of the MOF. It is conceivable that a propionate can coordinate to the copper paddle wheels and can thereby replace carboxylic groups of the organic SBU as a ligand from the copper dimer.

The as-synthesized material that was obtained from the modification of UHM-25-Val-Evans with propionic anhydride, DMAP and triethylamine turned out to be essentially X-ray amorphous. However, the crystallinity of the material was reinstated by a solvent exchange with DMF. In Figure 3.45 diffractograms of acylated UHM-25-Val-Evans are shown that were obtained before and after a solvent exchange. The as-synthesized sample of the acylated UHM-25-Val-Evans shows only a very broad reflection at 3.5 °2θ and a broad signal between 10-12 °2θ. After restoring DMF as the pore-filling solvent, the original diffraction pattern of UHM-25-Val-Evans can be observed. The mechanism for this behavior is unknown. However, the shift of the first reflection indicates a fundamental change in the dimensions of the unit cell that may be explained by a contraction of the organic SBU.

The introduction of the propionyl group to UHM-25-Val-Evans provides a carbonyl group to the material that can be identified by a characteristic absorption frequency in the IR spectrum of the material. A juxtaposition of the IR spec-
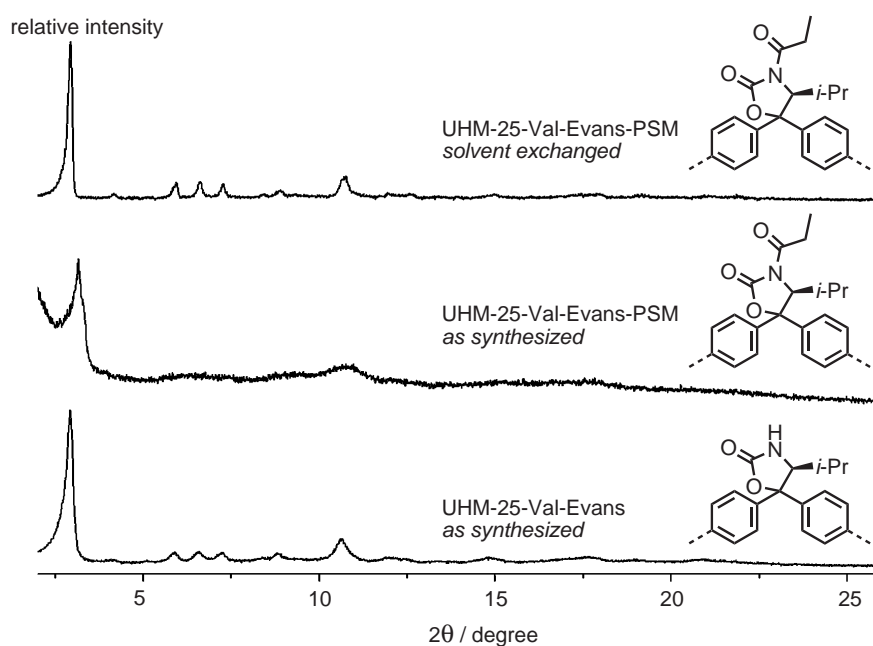
**Figure 3.45** – Comparision of the PXRD data of UHM-25-Val-Evans before and after the post-synthetic modification and solvent exchange, respectively. The diffraction pattern of UHM-25-Val-Evans (bottom) was not observed after the post-synthetic modification with propionic anhydride (center) and the first reflection is shifted about 0.3 °2θ towards higher diffraction angles. The original crystal diffraction pattern is reinstated after a solvent exchange with DMF (top).

184

tra of UHM-25-Val-Evans and the acylated derivative is shown in Figure 3.46. For the unmodified MOF, the peak at $1755\,\text{cm}^{-1}$ can be attributed to the carbonyl group of the 1,3-oxazolidin-2-one. The absorption band of this carbonyl group is shifted to $1786\,\text{cm}^{-1}$ in the acylated reaction product. As can be seen from the IR-spectrum of the MOF after the post-synthetic modification, a new absorption band appears at $1711\,\text{cm}^{-1}$ that can be ascribed to the carbonyl group of the propionyl imide. The observed absorption bands are in accordance with the reported spectroscopic data for the "classical" Evans auxiliary 5-isopropyl-1,3-oxazolidin-2-one and the $N$-acylated derivative.[308]
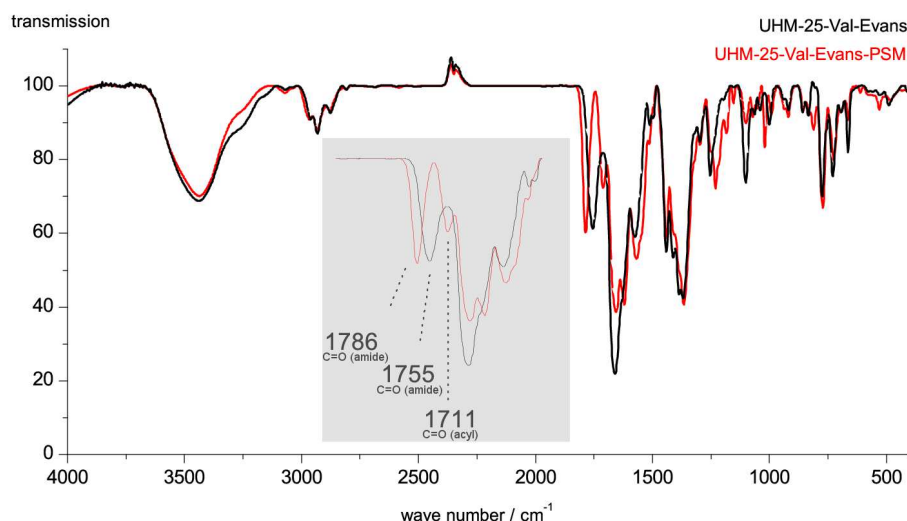


**Figure 3.46** – Comparision of the IR-spectra recorded for UHM-25-Val-Evans before (black lines) and after the post-synthetic modification (red lines). The area between $2000\text{-}1500\,\text{cm}^{-1}$ is enlarged (grey background). The absorption band of the carboxyl group in the oxazolidinone ($1755\,\text{cm}^{-1}$) is shifted towards higher wavenumbers in the $N$-acylated derivative ($1786\,\text{cm}^{-1}$) and an additional absorption band appears at $1711\,\text{cm}^{-1}$ that originates from the acyl residue.

To unambiguously identify the reaction product, further analysis was performed with the reisolated linker from UHM-25-Val-Evans-PSM. The ESI-HRMS spectrum of the linker after PSM is shown in Figure 3.47 and shows the match of the calculated isotope pattern of a molecule with the same molecular formula as the $N$-acylated linker ($C_{37}H_{31}NO_{11}$)

185

relative intensity

666.1971
22.22%

667.1990
8.56%

668.2000
2.31%

672.1687
1.09%

665   666   667   668   669   670   671   672   673   674   675   676
m/z / Da

| observed | | calculated | |
|---|---|---|---|
| $m/z$ | rel. int. | $m/z$ | rel. int. |
| 666.1971 | 22 % | 666.1970 | 100 % |
| 667.1990 | 8.6 % | 667.2004 | 40 % |
| 668.2000 | 2.3 % | 668.2037 | 7.8 % |
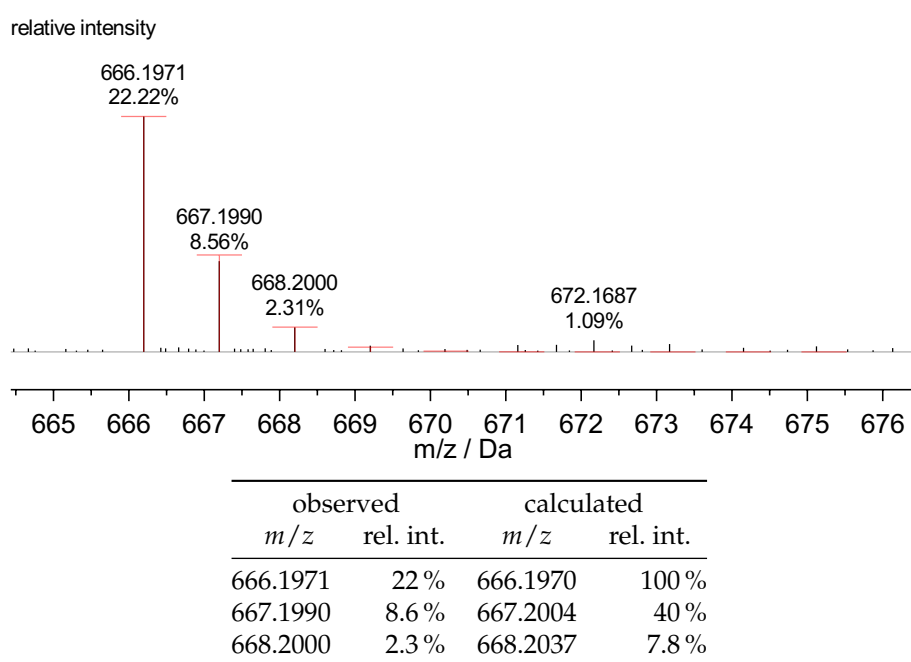
**Figure 3.47** – High resolution mass spectrum (ESI+) of the linker that was reisolated after the post-synthetic modification of UHM-25-Val-Evans. The recorded isotope pattern (black lines) can be match well with the calculated pattern (red lines) of the *N*-acylated derivative of the linker (calculated $m/z$ for $[C_{37}H_{31}NO_{11} + H]^+$).

186

Furthermore, the reisolated linker was characterized by ^{1}H-NMR spectroscopy. A segment of the spectrum is shown in Figure 3.48. Two baseline separated signals (mulitplicity dq) that can be ascribed to the $CH_2$ group are visible as a pair of diastereotopic protons, because they are in the vicinity of the isopropyl group of the auxiliary which provides a chiral environment to these hydrogen atoms. Markedly shifts towards higher field occur for the signals of the protons of the isopropyl substituent. These protons are in direct environment of the acylated position and the obvious change in the chemical environment of these protons confirms the modification of the linker. Furthermore the signal of the NH proton at 8.42 ppm of the 1,3-oxazolidin-2-one disappears almost completely from the spectrum upon the PSM of UHM-25-Val-Evans
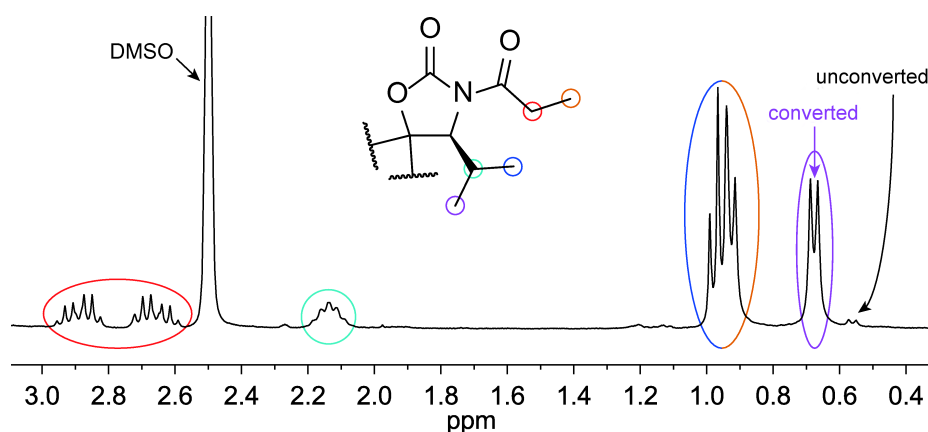


| shift / ppm | multiplicity | integral | assignment |
|:---:|:---:|:---:|:---|
| 2.89 | dq | 1 H | $CH_2CH_3$ |
| 2.68 | dq | 1 H | $CH_2CH_3$ |
| 2.15 | m | 1 H | $CH(CH_3)_2$ |
| 0.95 | m | 6 H | $CH(CH_3)_2$, $CH_2CH_3$ |
| 0.68 | d | 3 H | $CH(CH_3)_2$ |

**Figure 3.48** – Segment of the ^{1}H-NMR spectrum of the linker that was reisolated after the post-synthetic modification of UHM-25-Val-Evans with a conversion rate of 96 % (Table 3.9, entry 6). Signals of the *N*-acylated product and the corresponding protons are identified by color coding. Signals of the unreacted starting material can be observed as a traces only.

187

To quantify the conversion of the Evans-auxiliary to the acylated product, the integrals of characteristic signals in the ^{1}H-NMR spectrum were compared. The signals of one of the $CH_3$ group is best suited for this calculation, because it is observed as an isolated doublet that is significantly shifted towards higher fields in the reaction product. Therefore, no overlap occurs between the signals. The results of the conversion by the PSM are listed in Table 3.9.

To eliminate the necessity of a solvent exchange after the reaction in order to reinstate the crystallinity the MOF that is lost if the MOF is reacted as a suspension in THF, the acylation reaction was investigated in amyl acetate and DMF, respectively. The PXRD patterns of the materials after the acylation are shown in Figure 3.49.
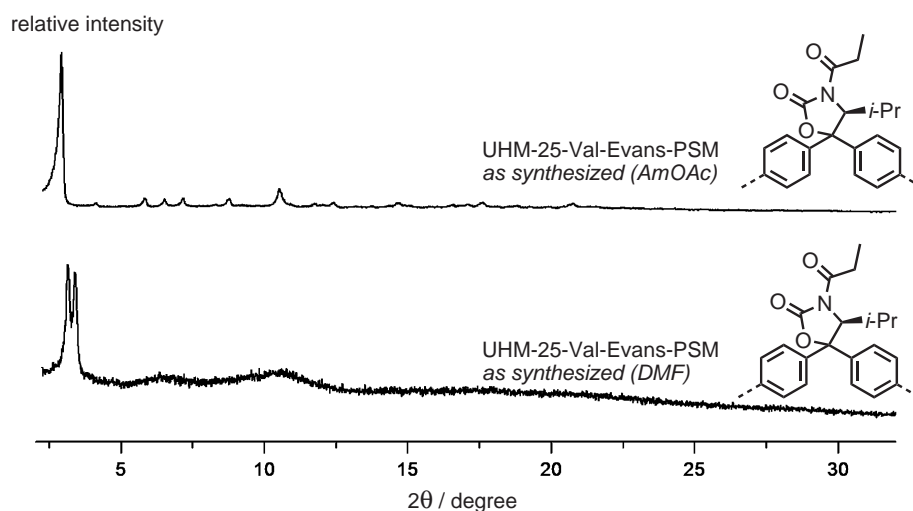


**Figure 3.49** – Comparison of the PXRD data of UHM-25-Val-Evans after the post-synthetic modification in AmOAc and DMF, respectively. The diffraction pattern of UHM-25-Val-Evans is not observed after the PSM in DMF (bottom) and retained after PSM in AmOAc (top).

The PXRD pattern is retained when amyl acetate is employed as the reaction medium, while the reaction in DMF shows a similar diffraction pattern as for the synthesis in THF. Table 3.10 lists the reaction parameters of the reactions in DMF and amyl acetate, respectively. The reaction was performed for 24 hours, which led to a conversion rate of 37 % when performed in THF (see Table 3.9). The acylation in amyl acetate gives a lower conversion of only 21 %. Interestingly the conversion in DMF is considerably more efficient than in amyl acetate or THF.

188

After the same period of time a conversion of 86 % is achieved, possibly due to a better stabilization of the reaction intermediates in the more polar solvent.

**Table 3.10** – *N*-Acylation of the 1,3-oxozolidinone of UHM-25-Val-Evans using propionic anhydride in conjunction with triethylamine and catalytic amounts of DMAP in three different solvents.

| entry (solvent) | $n_{MOF}$ μmol | reaction conditions time hours | temperature °C | reagents eq. | yield | conversion |
|---|---|---|---|---|---|---|
| 1 (amyl acetate) | 45 | 24 | rt | 13 | n.d. | 21 % |
| 2 (DMF) | 45 | 24 | rt | 13 | n.d. | 86 % |
| 3 (THF) | 90 | 24 | rt | 13 | n.d. | 37 % |

### 3.6.2 Post-Synthetic Modification (PSM) of UHM-25-Phe-Evans

Based on the findings for the valine-based MOF **154** (see section 3.6.1), the procedure for the *N*-acylation of the NH group using DMAP as a catalyst was applied the phenylalanine-based system UHM-25-Phe-Evans. The reaction of this MOF with propionic anhydride is schematically shown in Scheme 3.42



**155**                                                                  **167**
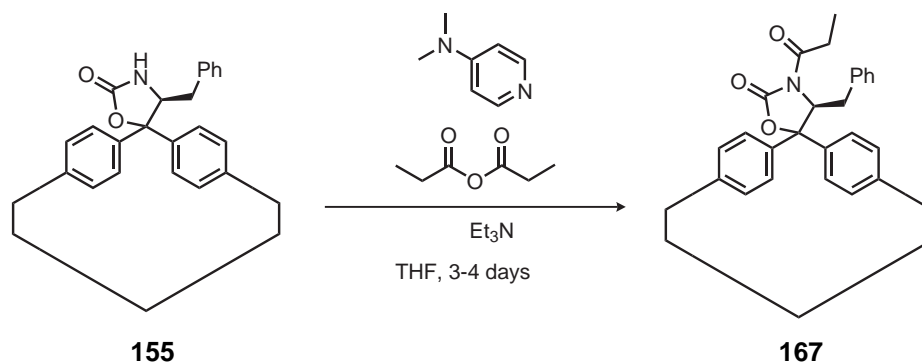
**Scheme 3.42** – *N*-Acylation of the chiral 1,3-oxazolidin-2-one moiety of UHM-25-Phe-Evans (**155**) using propionic anhydride in conjunction with catalytic amounts of DMAP; Et$_3$N is added as a base to capture the byproduct propionic acid.

Two reactions were performed at different temperatures. At room temperature and at 40 °C excellent conversion rates of up to 100 % were obtained after three to four days. The conversion rates for *N*-acylation of UHM-25-Phe are higher than for UHM-25-Val if using 13 equivalents of the reagents. The reaction parameters for the post-synthetic modification of UHM-25-Phe-Evans are listed in Table 3.11.

As can be seen in Figure 3.50, the modified material no longer shows the characteristic powder diffraction pattern of the UHM-25 series. However, the crystallinity of the sample was reinstated by a solvent exchange with DMF.

Analogous to the change in the IR-spectra of unmodified and acylated UHM-25-Val-Evans, characteristic spectra of the UHM-25-Phe-Evans system were obtained which are shown in Figure 3.51. The unreacted UHM-25-Phe-Evans MOF (black line) shows an absorption band at 1757 cm$^{-1}$ that can be ascribed to the carbonyl group of the free 1,3-oxazolidin-2-one. In the *N*-acylated material (red line), this band is shifted to 1786 cm$^{-1}$. Furthermore, a new absorption band that corresponds to the carbonyl of the exocyclic imide is visible at 1709 cm$^{-1}$. The values are in good accordance with the bands observed in UHM-25-Val-Evans (see Figure 3.46).

**Table 3.11** – Reaction conditions of the *N*-Acylation of the 1,3-oxozolidin-2-one of UHM-25-Phe-Evans using propionic anhydride in conjunction with triethylamine and catalytic amounts of DMAP; reactions were performed in THF.

| | | | reaction conditions | | | |
|---|---|---|---|---|---|---|
| entry | $n_{MOF}$ μmol | time hours | temperature °C | reagents eq. | yield | conversion |
| 1 | 89 | 72 | 40 | 26 | 51 % | 98 % |
| 2 | 71 | 96 | rt | 13 | 69 % | 100 % |
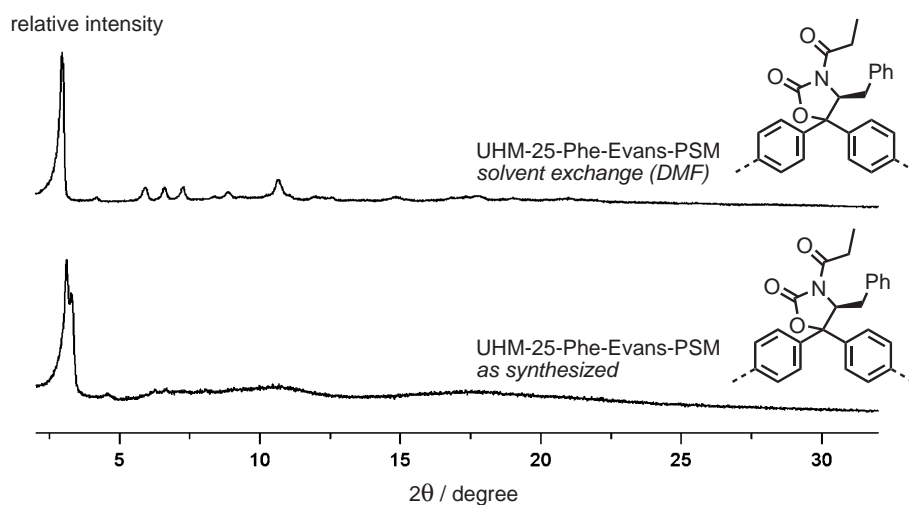


**Figure 3.50** – Comparision of the PXRD data of UHM-25-Phe-Evans after the PSM and solvent exchange with DMF. The diffraction pattern of UHM-25-Phe-Evans is not observed after the reaction with propionic anhydride (bottom) and the first reflection is shifted about 0.3 °2θ towards higher diffraction angles. The diffraction pattern is reinstated after a solvent exchange with DMF (top).

191
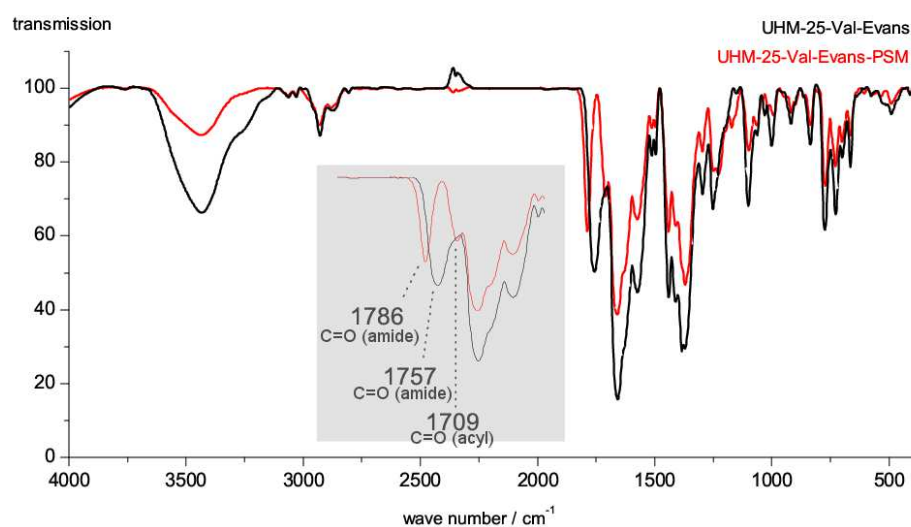
**Figure 3.51** – Comparision of the IR-spectra recorded for UHM-25-Phe-Evans before (black lines) and after the post-synthetic modification (red lines). The area between 2000-1500 cm$^{-1}$ is enlarged (grey background). The absorption band of the carbonyl group in the oxazolidinone (1757 cm$^{-1}$) is shifted towards higher wavenumbers in the *N*-acylated derivative (1786 cm$^{-1}$) and an additional absorption band appears at 1709 cm$^{-1}$ that originates from the acyl residue.

To unambiguously identify the reaction product, the modified linker of UHM-25-Phe-Evans was reisolated after digestion of reaction product in diluted hydrochloric acid. To determine the molecular formula of the modified linker an ESI-HRMS spectrum was recorded. This mass spectrum is depicted in Figure 3.52 and shows the match of the calculated isotope pattern of a molecule with the same molecular formula as the N-acylated linker derived from phenylalanine ($C_{37}H_{31}NO_{11}$).

relative intensity

714.1944
24.47%

715.1978
11.13%

716.2016
3.01%

713  714  715  716  717  718  719  720  721  722  723  724  725
m/z / Da

| observed | | calculated | |
| --- | --- | --- | --- |
| $m/z$ | rel. int. | $m/z$ | rel. int. |
| 714.1944 | 24 % | 714.1970 | 100 % |
| 715.1978 | 11 % | 715.2004 | 40 % |
| 716.2016 | 3.0 % | 716.2037 | 7.8 % |
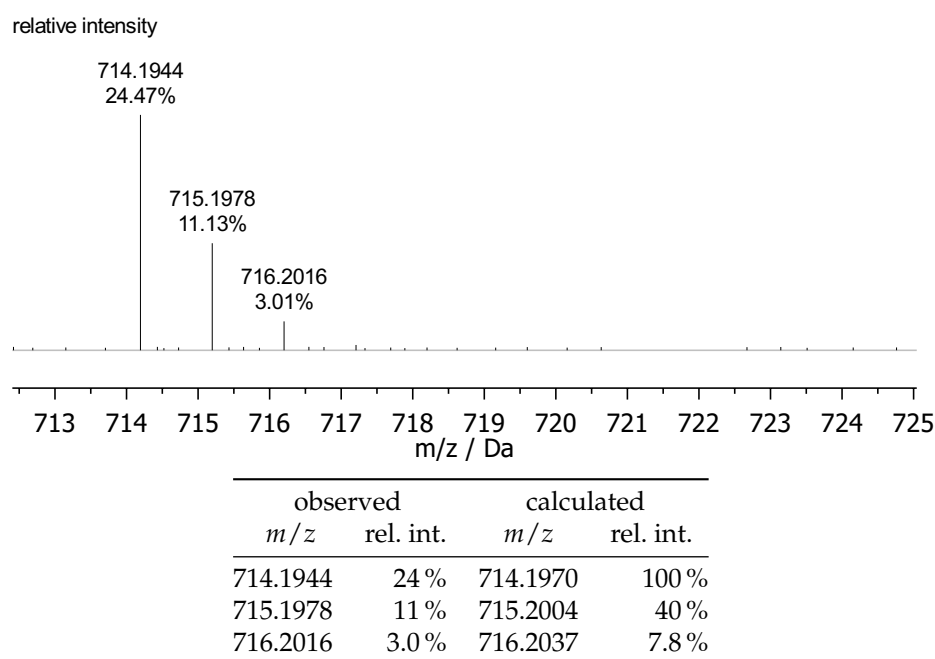
**Figure 3.52** – High resolution mass spectrum (ESI+) of the linker that was reisolated after the post-synthetic modification of UHM-25-Phe-Evans. The recorded isotope pattern (black lines) can be match well with the calculated pattern (red lines) of the N-acylated derivative of the linker (calculated $m/z$ for $[C_{41}H_{31}NO_{10} + H]^+$).

The isolated linker of the reaction product was characterized by $^1$H-NMR spectroscopy. A segment of the spectrum of the reisolated linker is shown in Figure 3.53. Two characteristic signal are observed that can be ascribed to the propionyl substituent on the oxazolidin-2-one: a triplet at 0.94 ppm that corresponds to the $CH_3$ group and a multiplet between 2.96-2.53 ppm that corresponds the

193

CH$_2$ group which overlaps with the signal of the benzylic protons. Due to the high conversion rate of the *N*-acylation the signal of the NH group of the unmodified linker is not observed in the spectrum. The signal of the proton on the stereocenter of the heterocycle is shifted about 1 ppm towards higher fields and shows a coupling to an amidic proton. To quantify the conversion of the Evans-auxiliary the integrals of characteristic signals in the ^{1}H-NMR spectrum were compared. This was done using the signal of the proton on the stereocenter because it shifts significantly after the acylation and does not overlap with other signals.



| shift / ppm | multiplicity | integral | assignment |
|:---:|:---:|:---:|:---:|
| 2.96-2.53 | m | 4 H | C*H*$_2$PhC*H*$_2$CH$_3$ |
| 0.94 | t | 3H | CH$_2$C*H*$_3$ |
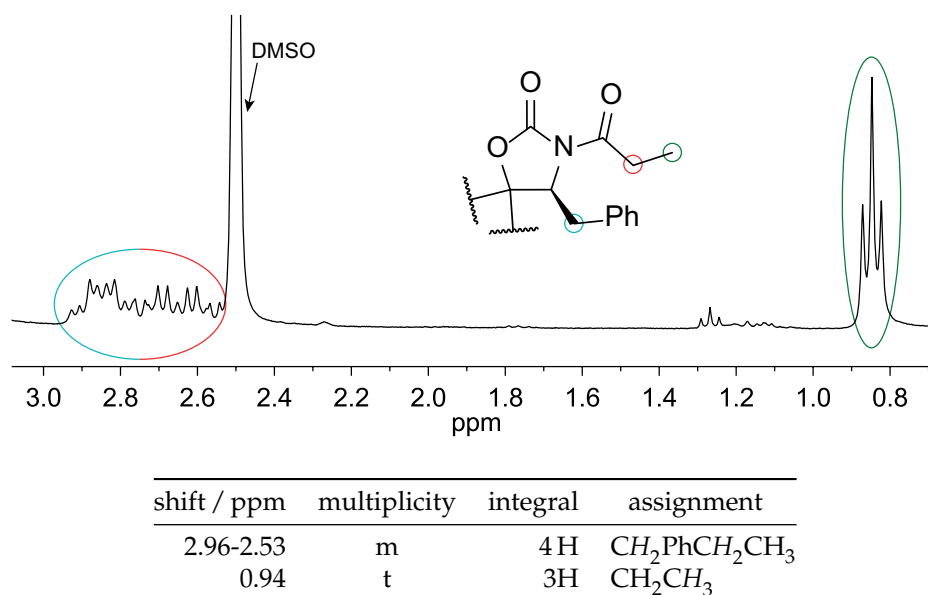
**Figure 3.53** – Segment of the ^{1}H-NMR spectrum of the linker that was reisolated after the post-synthetic modification of UHM-25-Phe-Evans with a conversion rate of 100 % (Table 3.9, entry 2). Signals of the *N*-acylated product and the corresponding protons are identified by color coding. Signals of the unreacted starting are not observed.

### 3.6.3 Aldol Addition with UHM-25-Val-Evans-PSM

After the promising results for the post-synthetic modification of UHM-25-Val-Evans and UHM-25-Phe-Evans, the second reaction step in the preparation of chiral substrates on UHM-25-Val-Evans was investigated. To obtain a nucleophilic species on the MOF, the formation of an enol equivalent was necessary. As this is the stereodefining step in the reaction procedures, it has been investigated thoroughly in the literature and different strategies have been developed to ensure high enantioselectivies.[256,309,310] These methods mostly rely on the formation of a rigid enolate in which one diastereotopic side is shielded by the substituent on the 1,3-oxazolidine-2-one. This may be achieved, for example, through the reaction with dibutylboryl triflate.[311]

The formation of a boron enolate was attempted using a suspension of UHM-25-Val-Evans-PSM in $CH_2Cl_2$ with triethylamine (see Scheme 3.43). This was cooled to 0 °C and a solution dibutyl borontriflate was added. After the addition of benzaldehyde the reaction was stirred at the same temperature for several hours. Afterwards the MOF was filtered, washed and digested in diluted hydrogen chloride to reisolate the linker. Unfortunately neither $^1$H-NMR spectroscopy nor mass spectrometry showed the formation of the desired product. Possibly, because the bulky boron derivative is unable to enter the pore system of the MOF an enolate cannot be formed.
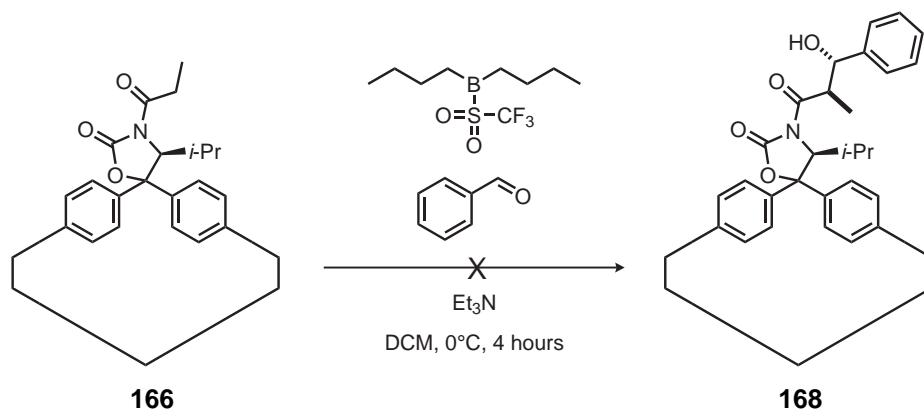


**Scheme 3.43** – Failed attempt of an aldol addition on UHM-25-Val-Evans-PSM using dibutyl borontriflate in conjunction with $Et_3N$ to synthesize an enolate that can react with benzaldehyde to form the chiral aldol product **168**.

Enolates may also be formed by deprotonation with lithium diisopropyl-amide (LDA). Because this strong base is sensitive to water, the reaction was performed under a protective argon atmosphere on a MOF that has been exchanged with dry THF. The attempted reaction is depicted in Scheme 3.44. The suspension of UHM-25-Val-Evans-PSM was cooled to $-78\,^{\circ}C$, a solution of LDA was added and the reaction mixture was stirred for four hours. The supernatant was carefully removed and the MOF was washed twice with THF before a solution of the benzaldehyde in THF was added. The reaction mixture was stirred overnight and slowly warmed to room temperature. Unfortunately none of the desired product was observed in mass spectrometry after digestion of the MOF. However, the reaction mixture turned black overnight, which is probably caused by a redox reaction of benzaldehyde and Cu(II).
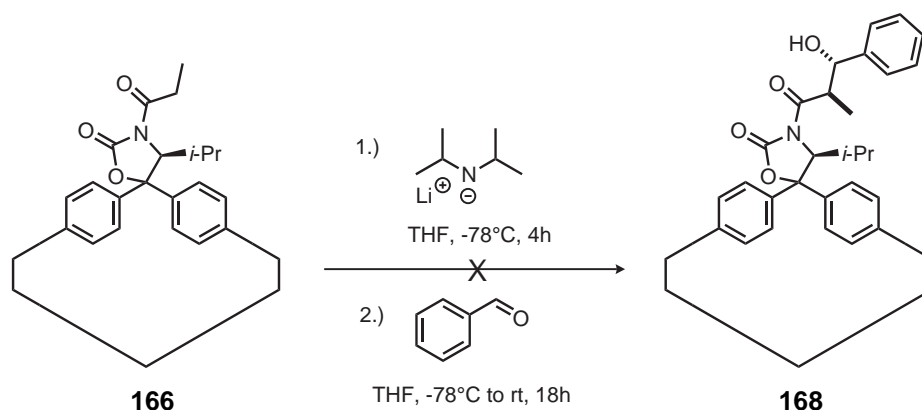


**Scheme 3.44** – Failed attempt of an aldol addition on UHM-25-Val-Evans-PSM using lithium di-isopropyl amide in the first step to synthesize an enolate that can react in the second step with benzaldehyde to form the chiral aldol product **168**.

To eliminate the interfering side reaction that leads to reduction of Cu(II), the benzaldehyde was replaced with benzylbromide. Furthermore, another base was tested for the formation of an enolate. Sodium hexamethyldisilazide is a strong base that has be used to generate enolate derivatives.[312,313] It has therefore been applied to a suspension of UHM-25-Val-Evans-PSM in dry THF as represented in Scheme 3.45. After stirring a room temperature for one hour, the supernatant was carefully removed and MOF was washed with THF. Then a solution of benzyl bromide in THF was added and the reaction was stirred at room temperature overnight. Afterwards the MOF was filtered, washed with

THF and digested in diluted hydrochloric acid. The reisolated linker was then used to investigate the conversion rate.
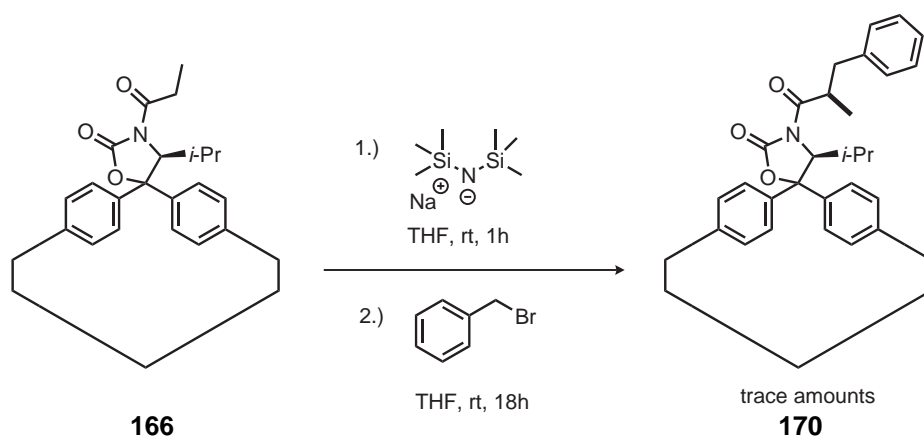


**Scheme 3.45** – Attempt of an aldol addition on UHM-25-Val-Evans-PSM using sodium hexamethyldisilazide in the first step to synthesize an enolate in that can react in the second step with benzaldehyde to form the chiral aldol product **170** in trace amounts.

The mass spectrum of the reaction showed a peak with an isotope pattern that matches the molecular formula of the desired $\alpha$-alkylated reaction product. However, the intensity of this peak is very small. Another peak that can be ascribed to the reaction of the unmodified oxazolidin-2-one with benzyl bromide was observed with much greater intensity . Residual 1,3-oxazolidin-2-one can be deprotonated with sodium bis(trimethylsilyl)amide (NaHMDS) to form a nucleophilic amide. This species can then react with the benzyl bromide in a nucleophilic substitution. This reaction pathway is presented in Scheme 3.46. It seems that the formation of an enolate is proceeding very slowly compared to the reaction of NaHMDS with the free NH group of the 1,3-oxazolidin-2-one.

None of the experiments described above delivered the desired product. Possibly, because the formation of the enolate is difficult to be realized in the restricted pore space of the MOF. The formation of a reactive species requires the participation of multiple reaction partner in a sterically demanding transition state, which could not be realized with the reagents used in this work.
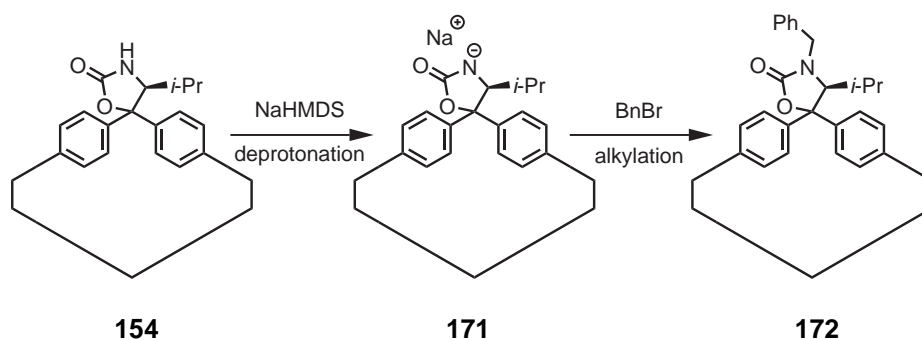
**Scheme 3.46** – Possible side reaction that occurs on the free NH groups of the 1,3-oxazolidin-2-one of UHM-25-Val-Evans. After deprotonation of **154**, the oxazolidinonide **171** can undergo an alkylation with benzyl bromide to form **172**.

### 3.6.4   Diels Alder Reaction on UHM-25-Val-Evans

The quantitative formation of enol equivalents in the pore space of UHM-25-Val-Evans could not be realized. However, the Evans auxiliary has not only been used in aldol additions and similar functionalizations of the $\alpha$-carbon atoms of an acyl group. Another application for chiral 1,3-oxazolidin-2-ones include, for example, cycloadditions such as the Diels-Alder reaction.[314] In these 4+2 cycloadditions, up to four new stereocenters are formed. By shielding one side of the dieneophile, stereocontrol may be realized for these processes. In contrast to the large structures that occur in aldol reaction, the stereodefining transition state only comprises the two unsaturated reaction partners. Due to this smaller size of the transition state, these reactions may be more suitable for the UHM-25 pore system.

In order to perform a cycloaddition on a UHM-25 substrate, an appropriate dienophile, such as an unsaturated anhydride, needs to be bound the 1,3-oxazolidin-2-one inside the pores. Since the conversion rates were almost quantitatively when using DMAP for the acylation with saturated anhydrides, the same reaction conditions were also applied for acylation with unsaturated anhydrides. The attempted reaction of UHM-25-Val-Evans is shown in Scheme 3.47. The MOF was suspended in THF and a solution of DMAP and triethylamine was added. After the addition of crotonic anhydride, the reaction mixture turned dark red after a couple of minutes. After three days, the MOF was isolated from a dark red supernatant washed with THF and dried in vacuum.

The isolated MOF was digested in diluted hydrochloric acid and the linker was reisolated. Unfortunately the desired reaction product was not observed in
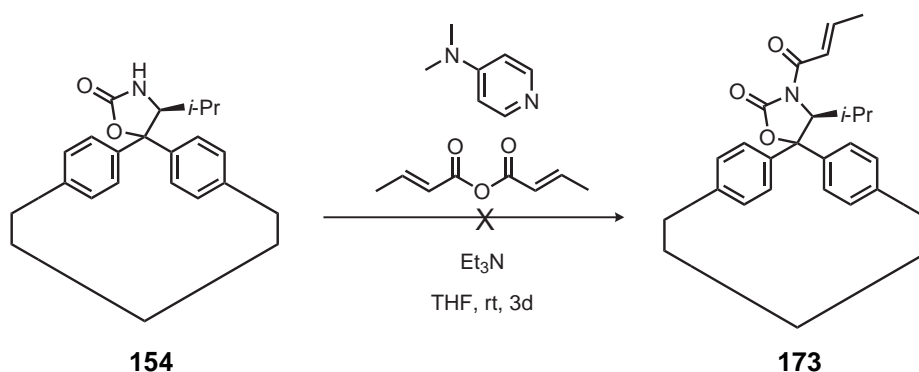
**Scheme 3.47** – Failed attempt of *N*-Acylation of the chiral 1,3-oxazolidin-2-one (**154**) on UHM-25-Val-Evans using crotonic anhydride in conjunction with catalytic amounts of DMAP; Et₃N is added as a base to capture the carboxylic acid byproduct.

the mass spectrum of the linker. This is surprising because the acylation with the saturated anhydride of similar size proceeded well on the same MOF (see section 3.6.1). The failure of the acylation with unsaturated acid anhydride is probably caused by a side reaction that consumes the anhydride before a reaction with the MOF can take place. Such a side reaction was not observed in the acylation of UHM-25-Val-Evans or UHM-25-Phe-Evans with propionic anhydride because of the low reactivity of the triethylamine as a nucleophile. However, unsaturated anhydrides are more reactive and a reaction has been reported for a similar system that comprises triethylamine and maleic anhydride that react to a charge transfer complex.[315] The immediate color change in the reaction mixture in the PSM of UHM-25-Val indicates that a similar reaction takes place in the attempted modification of the MOF. A possible pathway of the consumption of the crotonic acid anhydride is shown in Scheme 3.48. It proceeds via the formation of a π- and a σ-complex to yield a charge transfer complex.

As an alternative path to obtain an acylate the MOF with an unsaturated anhydride, the reaction was performed in the absence of DMAP and triethylamine but with NaHMDS as a base. This bulky base is capable to abstract a proton of the oxazolidinone to generate a reactive anion. Additionally, NaHMDS is sterically congested and does not undergo any reactions with the crotonic anhydride. The PSM of UHM-25-Val-Evans is shown in Scheme 3.49. To prepare UHM-25-Val-Evans for a reaction with the strong base the MOF was suspended with dry THF before use. A solution of the NaHMDS was then added to a suspension of the MOF in THF. The anhydride was added and the reaction was
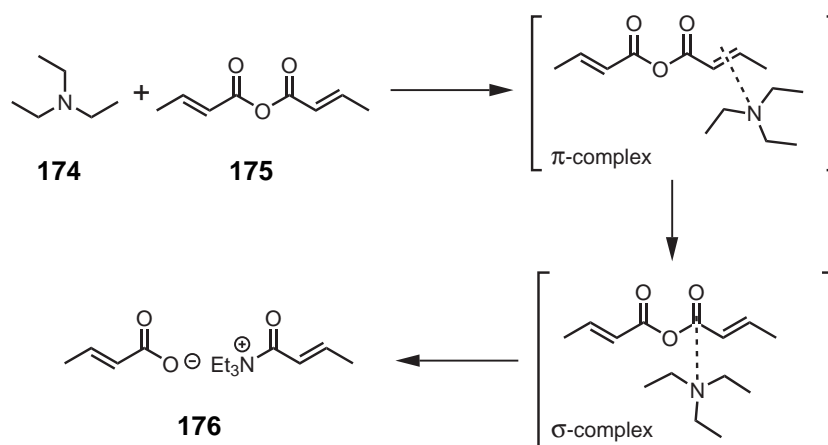
**Scheme 3.48** – Consumption of the crotonic anhydride in a reaction with triethylamine to the charge transfer complex **176** via the formation of a π- and a σ-complex.

stirred for 18 hours at room temperature and 60 °C, respectively. The MOF was filtered, washed and dried. After digestion of the MOF, the linker was reisolated.

After the reaction at room temperature, no conversion of the MOF was observed. However, the mass spectrum of the linker isolated from the PSM performed at 60 °C showed the signal for a molecule with the formula of the desired reaction product.

Furthermore, the ^{1}H-NMR spectrum of the isolated linker shows characteristic signals of a pair of protons on a double bond. Like in the spectrum of the linker acylated with the saturated anhydride, one of the $CH_3$ groups of the isopropyl substituents is significantly shifted towards higher fields. The integration of the signals of the unmodified and *N*-acylated linker allows the determination of the conversion rate. Unfortunately the reaction is incomplete, as only 50 % of the chiral substituents could be acylated. However, the free oxazolidinone groups should not impede the Diels-Alder reaction that may be performed on the *N*-acylated material.

In the next step, the modified MOF was employed in an attempted Diels-Alder Reaction. The MOF was suspended in THF and a freshly distilled cyclopentadiene was added to the suspension. The reaction was stirred for four days at room temperature. Afterwards the MOF was washed, dried and the linker was reisolated by a digestion with hydrochloric acid. The attempted Diels-Alder reaction of *N*-acylated UHM-25-Val-Evans is shown in Scheme 3.50.

**154** → **173**
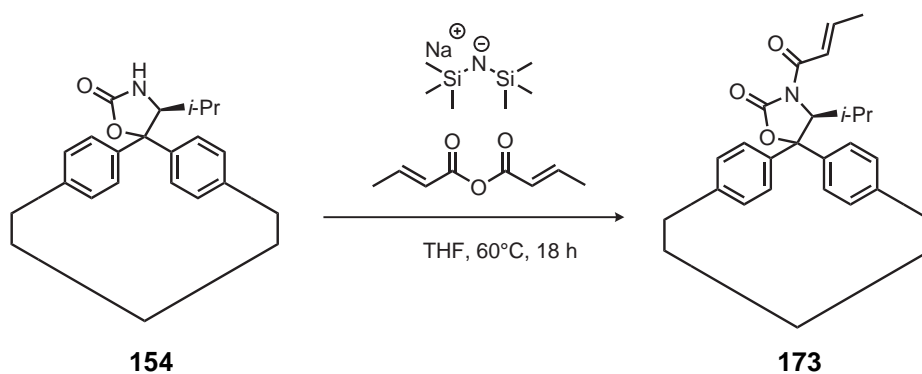
**Scheme 3.49** – *N*-Acylation of the chiral 1,3-oxazolidin-2-one (**154**) on UHM-25-Val-Evans using crotonic anhydride and NaHMDS as a strong base to deprotonate the NH group of the auxiliary.



**173** → **177**

traces
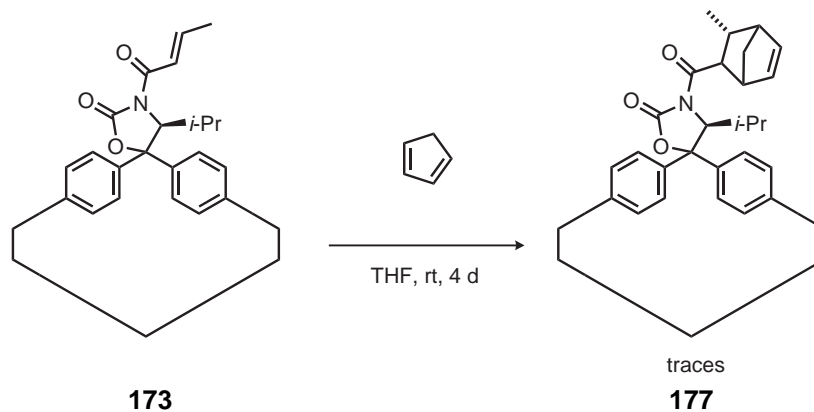
**Scheme 3.50** – Attempted Diels-Alder reaction on UHM-25-Val-Evans that has been acylated with propionic anhydride. Cyclopentadiene has been used as the diene in this reaction in an attempt for form a chiral bicyclic residue on the oxazolidinone.

201

| observed | | calculated | |
| --- | --- | --- | --- |
| $m/z$ | rel. int. | $m/z$ | rel. int. |
| 678.1982 | 5.1 % | 678.1975 | 100 % |
| 679.2002 | 2.2 % | 679.2009 | 41 % |
| 680.2065 | 0.7 % | 680.2042 | 8.2 % |
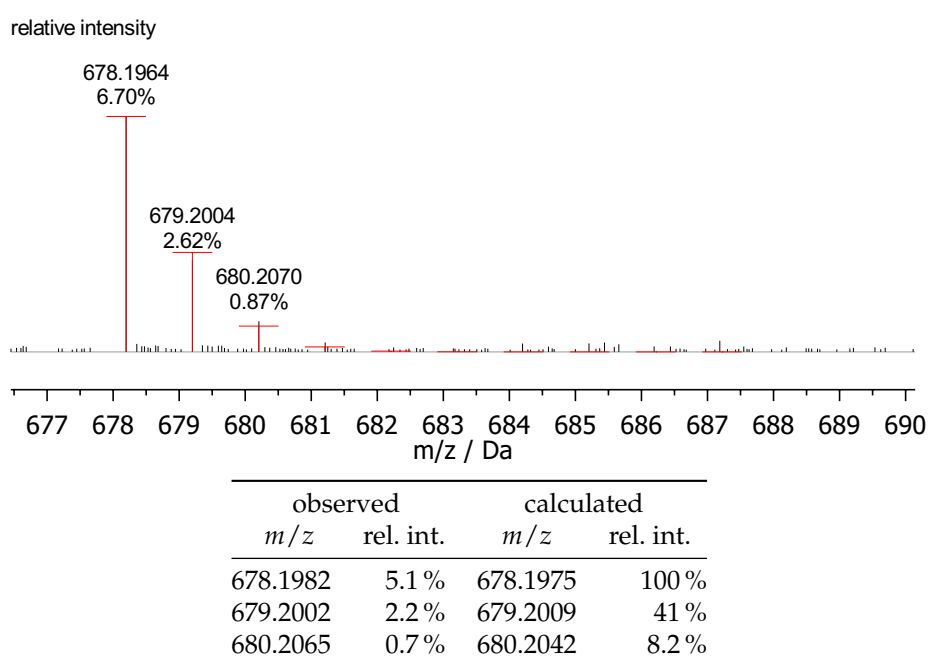
**Figure 3.54** – High resolution mass spectrum (ESI+) of the linker that was reisolated after the post-synthetic modification of UHM-25-Val-Evans. The recorded isotope pattern (black lines) can be match well with the calculated pattern (red lines) of the unsaturated, *N*-acylated derivative of the linker (calculated $m/z$ for $[C_{81}H_{31}NO_{11} + H]^+$).
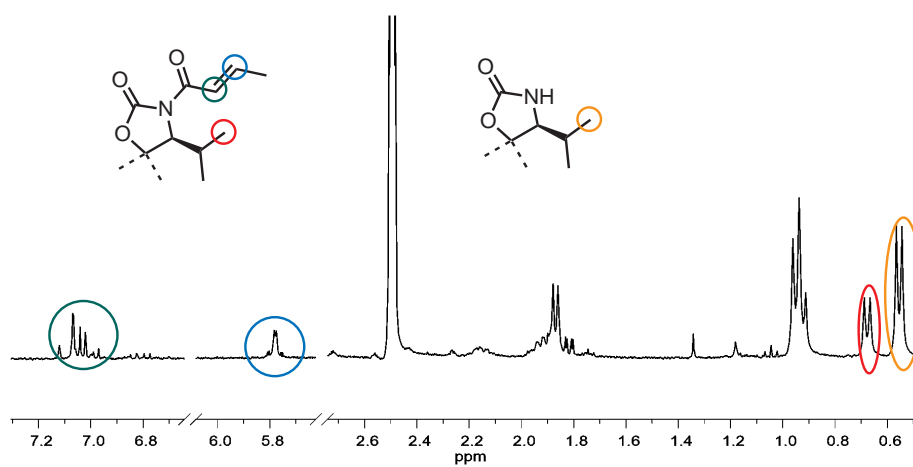
| shift / ppm | multiplicity | integral | assignment |
|---|---|---|---|
| 7.10-7.00 | m | 1 H | $CH{=}CH$ |
| 5.77 | m | 1 H | $CH{=}CH$ |
| 0.65 | d | 3 H | $CH(CH_3)_2$ |
| 0.55 | d | 3 H | $CH(CH_3)_2$ |

**Figure 3.55** – Segments of the ^{1}H-NMR spectrum of the linker that was reisolated after the post-synthetic modification of UHM-25-Val-Evans with crotonic acid and NaHMDS at 60 °C with conversion rate of 50 %. Characteristic signals of the *N*-acylated product and the starting material and the corresponding protons are identified by color coding.

Unfortunately, no conversion of the dieneophile was observed in the $^1$H-NMR of the isolated linker. However, the mass spectrum showed a signal that corresponds to the molecular formula of the cycloaddition product. In an attempt to increase the yield of this conversion, the reaction was repeated with the addition of a solution of AlCl$_3$ which is a common catalyst in Diels-Alder reaction and has also been used in cycloadditions with Evans-auxiliaries.[314] Unfortunately, this additive acted as a Lewis-acid and resulted in the decomposition of the MOF.

Overall, the experiments that targeted the PSM of the MOFs UHM-25-Val-Evans and UHM-25-Phe-Evans were only partially successful. This can be explained by the restrictions that are associated with heterogeneous reactions of porous solids. First, the reagents need to reach the functional groups that are targeted for modification. If these reagents are too large to enter the pores of the material, PSM can only occur on the outermost surface of the crystals. This inhibited, for example, the deprotonation of UHM-25-Val-Evans with (*n*-BuLi). Second, the reaction conditions that were developed for the homogeneous equivalents of a PSM may not be applicable to a MOF, because it can lead to decomposition of the framework structure. This was observed in the reaction of UHM-25-Val-Evans with LiCl, which led to the formation of a soluble cuprate species. However, when the right reaction parameters and reagents are chosen, excellent conversion rates can be achieved. This was demonstrated in the acylation of UHM-25-Val-Evans and UHM-25-Phe-Evans mediated by DMAP as a relatively small reagent for activation. These acylations are the first examples of a PSM of an Evans-auxiliary that is bound to a MOF. Unfortunately the remaining steps to achieve an auxiliary-controlled reactions on a MOF could not be taken. The reagents tried in the PSM of acylated UHM-25-Val-Evans led to unwanted side reactions or were either too large to enter the pore space of the material. To further explore the possibility of a MOF-based chiral auxiliary for stereoselective applications, an adaption of the underlying structure of the MOF may be necessary to achieve mesoporosity, which would allow large reagents to enter the pores and react with the chiral moieties. This could be achieved for example by the employment of other inorganic SBUs or by MOF synthesis with a mixed linker system of the chiral tetracarboxylic acids and another oligocarboxylic acid.

## 3.7   Summary

The aim of this work was the synthesis of new homochiral MOFs and their characterization with respect to their potential in heterogeneous stereoselective applications. To realize this objective, several new chiral linker molecules were synthesized. They can be grouped into di- and tetracarboxylic acids. An overview of these linkers, the corresponding MOFs, and their respective names is given in Table 3.13 on page 210. The tetracarboxylic acids carry either an *N*-protected amino alcohol, a free amino alcohol or a 1,3-oxazolidin-2-one (the so-called Evans-auxiliary) as chiral substituents. The dicarboxylic acids have been synthesized exclusively with different *N*-Boc protected amino alcohols as substituents. To synthesize the different linker molecules the same general synthetic route was chosen, which is described in the following.

Syntheses were performed with the natural amino acids: L-alanine, L-valine, L-leucine, L-phenylalanine and L-proline, which constitute members of the so-called chiral pool. These starting materials were converted to chiral linker molecules in four to five steps. First, the amino acids were protected at the carboxy group as methyl esters and the nitrogen atom as either carbamates or benzyl amines (L-proline). Bisarylated intermediates were obtained from these protected amino acid derivatives by nucleophilic reactions at the carboxylic carbon atom. These $\alpha,\alpha$-biaryl amino alcohols were employed as substrates in Suzuki reactions. These cross coupling reactions were performed with mono- and dicarboxy aryl boronic acids with good yields. This afforded either free dicarboxylic acids or methyl esters of tetracarboxylic acids, which were deprotected via saponification. A general overview of the reactions involved in the preparation of the linkers is shown in Scheme 3.51.

In reactions of dicarboxylic acids that carry an *N*-Boc protected amino alcohol moiety, and are derived from L-alanine, L-valine or L-phenylalanine, with a zinc(II) source the MOFs UHM-24-Ala-Boc, UHM-24-Val-Boc and UHM-24-Phe-Boc were obtained as crystalline material. The structure of this material was determined by a combination of single crystal X-ray diffraction and homology modeling of the PXRD pattern. This revealed that the obtained framework structures exhibit an isoreticular relationship. Unfortunately, in the UHM-24 series only a two-dimensional connectivity was achieved in the MOFs, which comprise one-dimensional, rod-like inorganic secondary building unit (SBU)s that are connected by the organic SBUs in a parallel arrangement. This can be explained by the two-connecting, V-shaped structure of the linker molecules. Furthermore, the structural model of the UHM-24 series shows an insufficient accessibility to the chiral residues of the linker molecules due to the packing of the two-dimensional structural units. This detrimental position of the chiral moi-
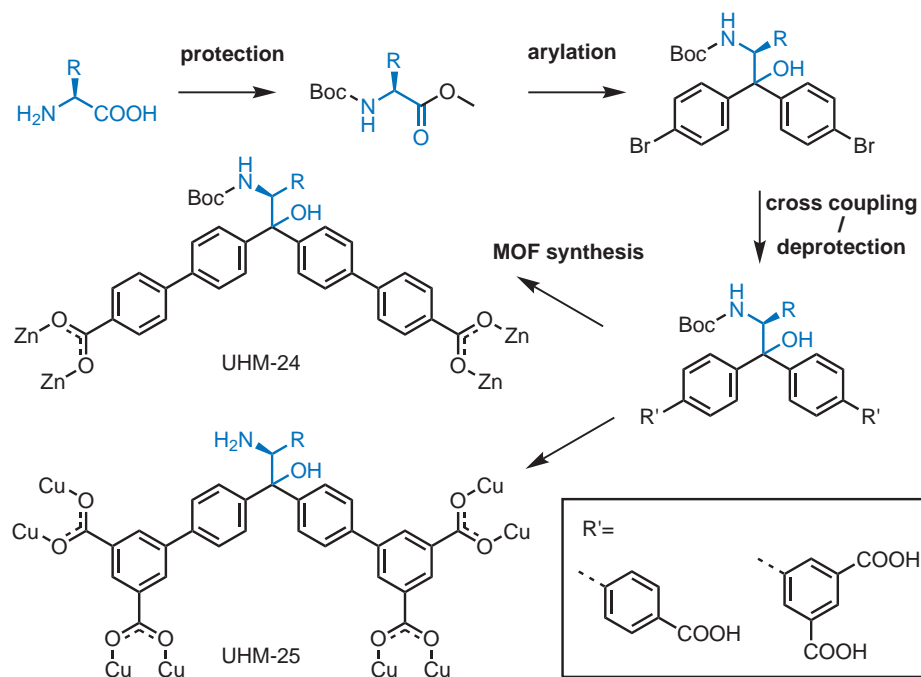
**Scheme 3.51** – Brief overview of the efforts to synthesize chiral MOFs from amino acids (atoms belonging to the amino acid starting material are highlighted in blue).

eties impairs the use of the UHM-24 series for enantioselective applications in separation or catalysis.

A three-dimensional connection of the framework was realized by performing solvothermal syntheses with a copper(II) source and tetracarboxylic acids (see Table 3.13). A protocol was developed to synthesize pure phases of MOFs of the UHM-25 series. Single crystals that were suitable for X-ray diffraction experiments were obtained for UHM-25-Ala-Boc and UHM-25-Pro. These experiments revealed that all MOFs of the UHM-25 series share the same novel structure based on the **ucp** topology which is discussed below.

However, even though the general structure of the MOFs is the same throughout the UHM-25 series the physico-chemical properties of the materials exhibit diversity, for example, with regard to the crystallinity. Furthermore, the permanent porosity differs considerably among the UHM-25 MOFs: Although specific surface areas of up to $1900\,\mathrm{m^2/g}$ were observed for some MOFs

of the UHM-25 series, not all samples could be activated to the same extent, even though a complete replacement of the solvent of synthesis with THF was successful in every case.[5] The activation procedure by a solvent-exchange with THF and subsequent evacuation revealed that certain UHM-25 MOFs are sensitive to the removal of the pore-filling solvent. Particularly, the MOFs with the non-protected amino alcohols "collapsed" during attempts to activate them. This behavior may be explained by strong capillary forces that occur during this process, which are not withstood by the MOFs with the free amino alcohol moieties, probably because they lack a stabilizing effect of the protective group.

This disadvantage was overcome by the application of an activation protocol that proceeds via the release of supercritical carbon dioxide from the pores of the MOFs. This afforded materials with permanent porosity from each of the constituents of the UHM-25 series. However, specific surface areas were significantly lower for the MOFs that bear unprotected amino alcohol moieties, which is consistent with the results of the conventional activation in vacuum. The specific surface areas that were determined for the UHM-25 MOFs after activation with supercritical carbon dioxide are given in Table 3.12.

**Table 3.12** – Specific surface areas and micropore volumes of the UHM-25 MOFs calculated from the adsorption branch of the physisorption isotherms with their respective values for $p/p_0$ determined after activation with supercritical carbon dioxide.

| | $S_{\mathrm{BET}}$ | | $V_{\mathrm{pore}}$ | |
|---|---|---|---|---|
| | $\mathrm{m^2 g^{-1}}$ | $p/p_0$ | $\mathrm{cm^3 g^{-1}}$ | $p/p_0$ |
| UHM-25-Ala-Boc | 1474 | 0.016-0.100 | 0.58 | 0.20 |
| UHM-25-Val-Boc | 1922 | 0.009-0.020 | 1.00 | 0.20 |
| UHM-25-Leu-Boc | 1738 | 0.016-0.074 | 0.68 | 0.20 |
| UHM-25-Phe-Boc | 623.2 | 0.007-0.024 | 0.25 | 0.20 |
| UHM-25-Ala | 975.7 | 0.010-0.048 | 0.39 | 0.20 |
| UHM-25-Val | 1286.3 | 0.011-0.049 | 0.51 | 0.20 |
| UHM-25-Leu | 1351 | 0.010-0.049 | 0.53 | 0.20 |
| UHM-25-Phe | 469.6 | 0.014-0.075 | 0.19 | 0.20 |
| UHM-25-Pro | 371.5 | 0.010-0.048 | 0.15 | 0.20 |
| UHM-25-Val-Evans | 1454 | 0.014-0.075 | 0.56 | 0.20 |
| UHM-25-Phe-Evans | 728.9 | 0.022-0.104 | 0.31 | 0.21 |

---

[5]The completeness of the solvent exchange was indicated by the absence of the characteristic signal of DMF in TG/MS measurements.

It should be noted that – unlike for gas storage applications – the achievement of permanent porosity with respect to gas sorption is beneficial but not a necessity for a successful application of these materials in heterogeneous stereoselective synthesis, which may include but is not limited to catalysis. Here, it is important to replace the solvent of the synthesis and that the functional, chiral groups within the pores of the MOFs are accessible. This has been investigated by performing a post-synthetic modification (PSM) of UHM-25-Val-Evans and UHM-25-Phe-Evans in which an acylation mediated by 4-(dimethylamino)-pyridine (DMAP) was carried out with excellent conversion rates. This shows that the individual functional groups of the material are accessible to the reagents. However, other procedures, which are commonly applied to acylate the Evans-auxiliary, failed in PSMs of the MOFs possibly due to the size of the deprotonating reagents or due to incompatibilities between certain metal salts and the inorganic SBUs that led to a decomposition of the MOF as was ascertained for UHM-25-Val-Evans. This shows that well-established functional groups are not necessarily compatible with the procedures that were developed for the corresponding homogeneous reactions and that other routes have to be tried to achieve similar results in MOF-based reactions. This was also the case during attempts of a further modification following the first PSM of UHM-25-Val-Evans. Here, an asymmetric auxiliary-controlled reaction was tested that did not show any satisfying conversion. Although the restricted space in the pore system of UHM-25 series permitted the first PSM with relatively small reagents, it seems that not enough space can be provided for the second PSM to further modify the chiral groups on the organic SBU. Nevertheless, UHM-25-Val-Evans and UHM-25-Phe-Evans constitute the first MOFs in which the Evans-auxiliary can be chemically modified at the carbamate nitrogen atom, although this auxiliary has been included in MOFs before.[177]

UHM-25-Pro is the first MOF that bears an $\alpha,\alpha$-diaryl prolinol functionality, which is a well-known motif in stereoselective organocatalysis. This MOF has been used to evaluate the applicability of the UHM-25 series in heterogeneous catalysis. Specifically, a self-directed asymmetric aldol addition of acetaldehyde was carried out. This resulted in the formation of chiral 3-hydroxybutanal which was protected *in situ* as a dimethyl acetal. The induction of stereoinformation was quantified by gas chromatography coupled with mass spectrometry. The ratio of the (*R*)- and (*S*)-enantiomer was determined as 70:30. The selective formation of the (*R*)-enantiomer proved the ability of UHM-25-Pro to act as a heterogeneous, stereoselective catalyst. The observed stereoselectivity of the heterogeneous reaction is lower than for certain homologous equivalents of this reaction system.[295] However, these reactions are highly dependent on the nature of the aromatic substituents on the diaryl prolinol catalyst as well as solvent effects. Bulky, electron-withdrawing aryl rings may stabilize impor-

tant reaction intermediates.[85] Therefore, there is room for improvement for the heterogeneous catalyst system of UHM-25-Pro, by introducing substituents that significantly reduce the electron density on the geminal aromatic rings.
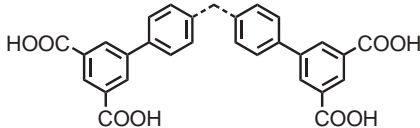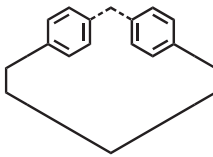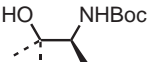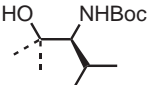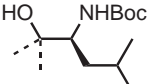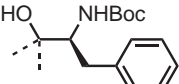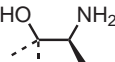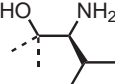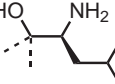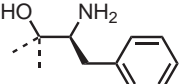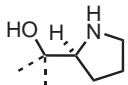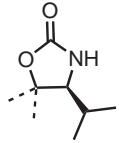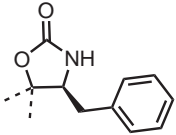
Regardless of the type of chiral substituent included in the structures, all MOFs of the UHM-25 series are isoreticular to each other, which has been examined by PXRD. This shows that the variability that is present in amino acids as a subgroup of the chiral pool can be reproduced in a MOF, while the underlying topology is primarily defined by the geometry of the points of extension on the organic SBU. This serves as a proof of the principles of the *isoreticular chemistry* approach to the synthesis of novel MOFs.
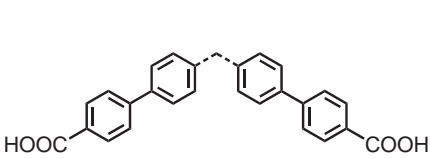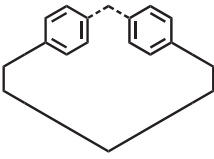
In addition to the physico-chemical properties of the MOFs, the connectivity of the framework was examined. Topological analysis of the UHM-25 structure revealed an underlying (3,4)-c binodal net. This underlying net has been classified as the **ucp** topology. In the embedding of the highest symmetry, the **ucp** net can be described as an arrangement of interconnected cuboctahedra which reflects the structural motif of the MOPs that constitute characteristic building blocks of UHM-25. The **ucp** net has been described as one of several possibilities to arrange interconnected cuboctahedral MOPs.[5] However, it was only theoretically described and was observed in a MOF for the first time in the UHM-25 series. This is interesting because there were only three possibilities documented by Yaghi and O'Keeffe to arrange this kind of MOP into a MOF (**ucp**, **zmj** and **zhc**) nevertheless the most simple of these arrangements has remained undiscovered the longest.
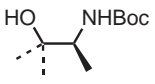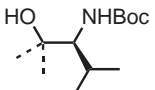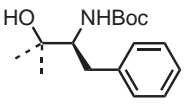
In further topological studies two topologies were determined that were previously unknown. The corresponding MOFs comprise either zinc or copper paddle-wheel motifs, respectively, and 3,3',5,5'-benzophenonetetracarboxylate, which has been obtained as an intermediate in attempts to synthesize another chiral linker molecule. The embedding with the highest symmetry of one of these hitherto unknown topologies describes the interconnection of rhombic dodecahedra in a body-centered arrangement, which reflects the MOPs as structural motifs of the corresponding MOF. This net has been registered at the Topos Tological Database (TTD) as *fhs*1.

**Table 3.13** – Overview of the different types of linkers used in the UHM MOFs. Linkers and MOFs are named with the three-letter code of the respective amino acid used for the preparation of the linker, ta stands for tetracarboxylic acid. Boc appendix indicates the presence of the *N*-Boc protecting group (dashed lines mark the connection points to the framework host).

| Linker | | Name | No. | MOF |
|---|---|---|---|---|
| | | Ala-Boc-ta | **121** | UHM-25-Ala-Boc |
| | | Val-Boc-ta | **122** | UHM-25-Val-Boc |
| | | Leu-Boc-ta | **123** | UHM-25-Leu-Boc |
| | | Phe-Boc-ta | **124** | UHM-25-Phe-Boc |
| | | Ala-ta | **129** | UHM-25-Ala |
| | | Val-ta | **130** | UHM-25-Val |
| | | Leu-ta | **131** | UHM-25-Leu |
| | | Phe-ta | **132** | UHM-25-Phe |

| | | | |
|---|---|---|---|
|  | Pro-ta | **128** | UHM-25-Pro |
|  | Val-Evans-ta | **178** | UHM-25-Val |
|  | Phe-Evans-ta | **179** | UHM-25-Phe |



| | | | |
|---|---|---|---|
|  | Ala-Boc-da | **99** | UHM-24-Ala-Boc |
|  | Val-Boc-da | **100** | UHM-24-Val-Boc |
|  | Phe-Boc-da | **101** | UHM-24-Phe-Boc |

## 3.8   Zusammenfassung

Das Ziel dieser Arbeit war die Synthese einer Reihe neuartiger, homochiraler MOFs. Diese sollten auf im Hinblick auf ihr Potential in heterogenen, stereoselektiven Anwendungen untersucht werden. Um diese Aufgabenstellung zu verwirklichen, wurden chirale Linkermoleküle synthetisiert, die in Di- und Tetracarbonsäuren eingeteilt werden können. Ein Überblick über diese Linker, die zugehörigen MOFs und die jeweiligen Namen ist in Tabelle 3.15 auf Seite 218 dar-

gestellt. Die Tetracarbonsäuren tragen entweder einen N-geschützten Amino-
alkohol, einen freien Aminoalkohol oder ein 1,3-Oxazolidin-2-on (das sogenann-
te Evans-Auxiliar) as chiralen Substituenten. Die Dicarbonsäuren wurden aus-
sschließlich mit N-geschützten Aminoalkoholen als chirale Reste synthetisiert.
Die Synthese der unterschiedlichen Linker folgt der gleichen, generellen Syn-
theseroute, die im Folgenden beschrieben ist.

Die Synthesen wurden mit den Aminosäuren L-Alanin, L-Valin, L-Leucin,
L-Phenylalanin und L-Prolin durchgeführt, die als natürlich vorkommende A-
minosäuren Mitglieder des *chiral pools* darstellen. Aus diesen einfachen, leicht
verfügbaren Edukten wurden in vier bis fünf synthetischen Schritten chirale
Linkermoleküle erhalten. Zunächst wurden hierfür die Aminosäuren an der
Carboxyfunktion als Methylester und an der Aminofunktion als Carbamat be-
ziehungsweise als Benzylamin (L-Prolin) geschützt. Aus den geschützten Ami-
nosäurederivaten wurden durch nucleophile Reaktionen am Carboxyl-Kohlen-
stoffatom bisarylierte Intermediate in sehr guten Ausbeuten erhalten. Diese ge-
schützten $\alpha,\alpha$-Aminoalkohole wurden in Suzuki-Reaktionen eingesetzt. Die-
se Kreuzkupplungsreaktionen wurden mit Mono- und Dicarboxyl-boronsäuren
mit guten Ausbeuten durchgeführt. Hieraus wurden entweder freie Dicarbon-
säuren oder die Methylester von Tetracarbonsäuren erhalten, die in Verseifungs-
reaktionen entschützt wurden. Eine Übersichtsdarstellung der gewählten Syn-
theseroute ist in Schema 3.52 gezeigt.

Die aus L-Alanin, L-Valin und L-Phenylalanin hergestellten Dicarbonsäure-
linker wurden in Solvothermalsynthesen von MOFs als *N*-geschützte Amino-
alkohole eingesetzt. In Reaktionen mit einer Zink(II)-Quelle konnten kristalline
Materialien isoliert werden, welche in einer Kombination aus Einkristall-Rönt-
genstrukturanalyse und Homologie-Modeling anhand von Röntgenpulverdif-
fraktogrammen strukturell beschrieben werden konnten. Dabei wurde festge-
stellt, dass die erhaltenen netzwerkartigen Verbindungen eine isoretikuläre Be-
ziehung zueinander besitzen. Allerdings konnte in den MOFs der UHM-24-
Reihe nur eine zweidimensionale Konnektivität eines Netzwerkes erreicht wer-
den, in dem eindimensionale, stabförmige, anorganische SBUs in paralleler An-
ordnung über die organischen SBUs verknüpft sind. Dies wurde auf die zwei-
fach verknüpfende, V-förmige Struktur der eingesetzten Dicarbonsäuren zu-
rückgeführt. Das ermittelte Strukturmodell für die UHM-24-Klasse zeigt zudem
eine schlechte Zugänglichkeit der chiralen Reste der eingesetzten Linkermole-
küle durch die dichte Packung der benachbarten zweidimensionalen Struktu-
reinheiten. Diese ungünstige Position der chiralen Reste beeinträchtigt die Eig-
nung von MOFs der UHM-24-Reihe für enantioselektive Anwendungen in der
Stofftrennung oder Katalyse.

Eine dreidimensionale Verknüpfung in einem Netzwerk wurde durch Sol-
vothermalsynthesen mit einer Kupfer(II)-Quelle und verschiedenen Tetracarb-
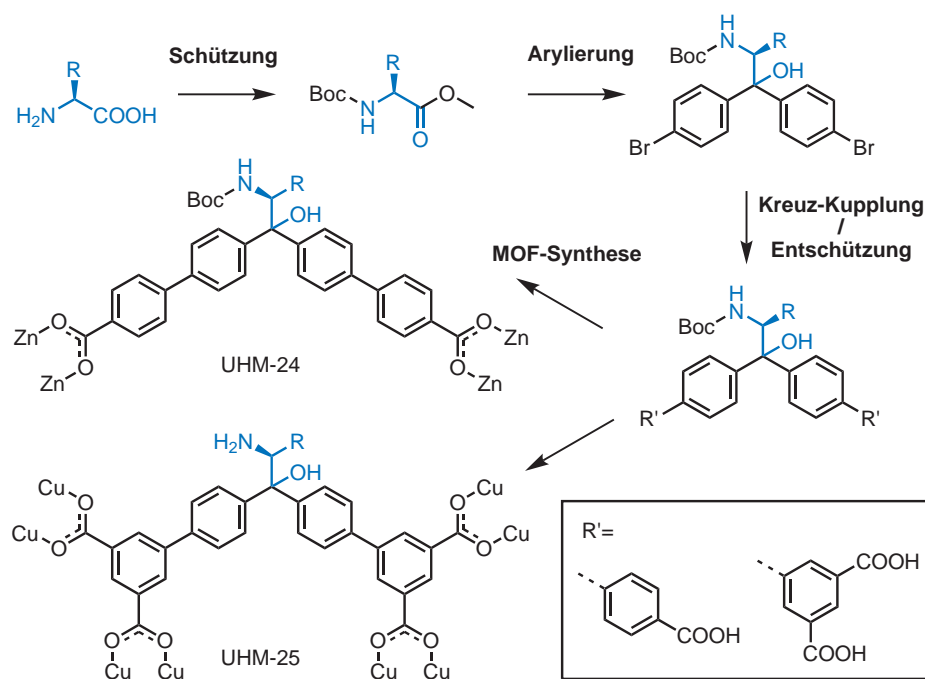
**Schema 3.52** – Übersicht zur Synthesestrategie von chiralen MOFs ausgehend von natürlichen Aminosäuren (Atome, die der eingesetzten Aminosäure zugehörig sind, sind in blau hervorgehoben).

onsäuren erreicht (siehe Table 3.13, Seite 210). Hierdurch konnte phasenreines, kristallines Material von MOFs der UHM-25-Reihe synthetisiert werden. Außerdem konnten für UHM-25-Ala-Boc und UHM-25-Pro Einkristalle erhalten werden, die sich für Röntgenbeugungsexperimente eigneten. Diese Experimente zeigten, dass die MOFs der UHM-25-Reihe die gleiche, neuartige Struktur besitzen, die durch die **ucp** Topologie beschrieben werden kann (siehe unten).

Obwohl die grundlegende Struktur innerhalb der UHM-25-Reihe identisch ist, unterscheiden sich die einzelnen MOFs in ihren physiko-chemischen Eigenschaften, was zum Beispiel durch die Unterschiede in der Kristallinität deutlich wird. Zudem unterscheidet sich die ermittelte permanente Porosität erheblich innerhalb der UHM-25-Reihe. Obwohl spezifische Oberflächen von $1900\,\mathrm{m^2/g}$ für einige MOFs beobachtet wurden, konnten nicht alle Vertreter dieser Reihe im selben Maß aktiviert werden, obwohl ein vollständiger Austausch des Synthe-

selösungsmittels DMF gegen THF in allen Fällen erfolgreich war.[6] Das Verfahren zur Aktivierung durch einen Lösungsmittelaustausch mit anschließender thermischer Aktivierung bei 40 °C zeigte, dass bestimmte MOFs der UHM-25-Reihe empfindlich gegenüber dem Entfernen des Lösungsmittels in den Poren sind. Besonders die MOFs mit nicht-geschützten Aminoalkoholen kollabierten bei Versuchen zur Aktivierung. Dieses Verhalten wird zurückgeführt auf starke Kapillarkräfte, die während dieses Prozesses auf das Material wirken. Möglicherweise können die MOFs, die über eine freie Aminoalkohol-Funktionalität verfügen, diesen Kräften nicht standhalten, weil die stabilisierende Wirkung der Carbamat-Schutzgruppe fehlt.

Diese Einschränkung wurde durch die Anwendung eines Aktivierungsverfahrens, bei dem die Poren mit überkritischem Kohlenstoffdioxid gefüllt werden, umgangen. Durch diese Vorgehensweise wurde für jeden Vertreter der UHM-25-Reihe eine gewisse permanente Porosität erreicht. Jedoch sind auch mit diesem Verfahren die Oberflächen jener MOFs kleiner, die über ungeschützte Aminoalkohol-Funktionen verfügen. Dies korreliert mit den Ergebnissen nach konventioneller Aktivierung im Vakuum. Die spezifischen Oberflächen der UHM-25-MOFs nach der Aktivierung mit überkritischem Kohlenstoffdioxid sind an Tabelle 3.14 angegeben.

Es ist jedoch anzumerken, dass – im Gegensatz zu Gasspeicherungsanwendungen – das Erreichen von vollständiger, permanenter Porosität für heterogene, stereoselektive Anwendungen, wie zum Beispiel enantioselektive Katalyse, zuträglich, aber nicht notwendig ist. Hierbei ist es vielmehr wichtig, dass ein Lösungsmittelaustausch stattfinden kann und die funktionellen, chiralen Gruppen im Porensystem der MOFs zugänglich sind. Diese Eigenschaft wurde anhand von post-synthetischen Modifizierungen von UHM-25-Val-Evans und UHM-25-Phe-Evans untersucht. Hierbei wurde eine Acylierung durchgeführt, die mit 4,4′-Dimethylaminopyridin (DMAP) vermittelt wurde, und bei der hervorragende Umsätze erzielt wurden. Jedoch führten andere Protokolle, die häufig für die Acylierung des Evans-Auxiliars in homogener Phase angewandt wurden, nicht zu den erwünschten Ergebnissen. Dies ist vermutlich auf den sterischen Anspruch der Deprotonierungsreagenzien beziehungsweise auf Inkompabilitäten zwischen bestimmten Metallsalzen und den anorganischen SBUs zurückzuführen, die zu einer Zersetzung der MOFs führten, was bei UHM-25-Ala-Evans beobachtet wurde. Diese Erkenntnisse zeigen, dass gut etablierte funktionelle Gruppen aus der stereoselektiven Synthese nicht unbedingt mit den Verfahren modifiziert werden können, die für die entsprechenden Reaktionen in homogener Phase entwickelt wurden. Dies macht eine Anpassung von Reaktionsbedingungen beziehungsweise die Erprobung neuer synthetischer Rou-

---

[6]Die Vollständigkeit des Lösungsmittelaustausches wurde mit TG/MS-Messungen durch die Abwesenheit des charakteristischen Signals von DMF belegt.

**Tabelle 3.14** – Spezifische Oberflächen und Mikroporenvolumina der UHM-25-MOFs, die aus dem Adsorptionsast der Physisorptionsisotherme berechnet wurde, zusammen mit den jeweiligen Werten für $p/p_0$. Die Bestimmung erfolgte nach der Aktivierung mit überkritischem Kohlenstoffdioxid.

| | $S_{BET}$ | | $V_{pore}$ | |
|---|---|---|---|---|
| | $\mathrm{m^2g^{-1}}$ | $p/p_0$ | $\mathrm{cm^3g^{-1}}$ | $p/p_0$ |
| UHM-25-Ala-Boc | 1474 | 0.016-0.100 | 0.58 | 0.20 |
| UHM-25-Val-Boc | 1922 | 0.009-0.020 | 1.00 | 0.20 |
| UHM-25-Leu-Boc | 1738 | 0.016-0.074 | 0.68 | 0.20 |
| UHM-25-Phe-Boc | 623.2 | 0.007-0.024 | 0.25 | 0.20 |
| UHM-25-Ala | 975.7 | 0.010-0.048 | 0.39 | 0.20 |
| UHM-25-Val | 1286.3 | 0.011-0.049 | 0.51 | 0.20 |
| UHM-25-Leu | 1351 | 0.010-0.049 | 0.53 | 0.20 |
| UHM-25-Phe | 469.6 | 0.014-0.075 | 0.19 | 0.20 |
| UHM-25-Pro | 371.5 | 0.010-0.048 | 0.15 | 0.20 |
| UHM-25-Val-Evans | 1454 | 0.014-0.075 | 0.56 | 0.20 |
| UHM-25-Phe-Evans | 728.9 | 0.022-0.104 | 0.31 | 0.21 |

ten notwendig, um vergleichbare Resultate bei MOF-basierten Reaktionen zu erreichen. Dies zeigte sich auch in Versuchen zur weiteren Modifikation im Anschluss an die erste PSM von UHM-25-Val-Evans. Hier wurde unter anderem eine asymmetrische, auxiliar-kontrollierte Reaktion erprobt, die keine zufriedenstellenden Umsätze zeigte. Obwohl der begrenzte Platz im Porensystem von UHM-25 die erste PSM mit relativ kleinen Reagenzien erlaubte, steht offenbar nicht genug Raum zur Verfügung für eine zweite PSM, um den chiralen Rest der organischen SBU weiter zu funktionalisieren. Gleichwohl stellen die Vertreter der UHM-25-Reihe die ersten MOFs dar, bei denen das Evans-Auxiliar am Carbamat-Stickstoffatom chemisch modifiziert werden kann, obwohl dieses Auxiliar bereits in anderen MOFs integriert wurde.[177]

UHM-25-Pro ist der erste MOF, der eine $\alpha,\alpha$-Diarylprolinol-Funktionalität trägt, welche ein hinreichend bekanntes Motiv in der stereoselektiven Organokatalyse darstellt. Dieser MOF wurde eingesetzt, um das Anwendungspotential von MOFs der UHM-25-Serie als heterogene Katalysatoren zu beurteilen. Hierfür wurde eine selbstgerichtete asymmetrische Aldoladdition von Acetaldehyd durchgeführt. Dabei wurde zunächst das chirale 3-Hydroxybutanal erhalten, welches *in situ* zum Dimethylacetal umgesetzt wurde. Die Induktion von stereo-

chemischer Information wurde durch enantioselektive Gas-Chromatographie mit gekoppelter Massenspektrometrie quantifiziert. Das Verhältnis des (*R*)- und des (*S*)-Enantiomers beträgt 70:30. Die bevorzugte Bildung des (*R*)-Enantiomers belegt die grundsätzliche Eignung von UHM-25-Pro als heterogener, stereoselektiver Katalysator. Allerdings ist die beobachtete Stereoselektivität in der heterogenen Katalyse geringer als für bestimme homogene Systeme, die dieser Reaktion entsprechen.[295] Diese Prolin-vermittelten Reaktionen sind stark abhängig von der Art der aromatischen Substituenten am Diarylprolinolsystem sowie von Lösungsmitteleffekten.[85] Dementsprechend ist eine Verbesserung der Stereoselektivität durch eine Modifikation der Substituenten oder durch den Einsatz von anderen Lösungsmitteln denkbar.

Unabhängig von den chiralen Substituenten, die sich bei den einzelnen MOFs unterscheiden, weisen alle MOFs der UHM-25-Reihe eine isoretikuläre Beziehung zueinander auf, was durch PXRD-Messungen belegt wurde. Dies zeigt, dass die Variabilität, die in der Klasse der natürlichen Aminosäuren beobachtet wird, in einem MOF reproduziert werden kann, wobei die zugrundeliegende Topologie im Wesentlichen durch die Geometrie der Verknüpfungspunkte in Form der organischen SBU definiert wird. Dies stellt einen Beleg der Prinzipien der *isoretikulären Chemie* zur Synthese von neuartigen MOFs dar.

Zusätzlich zu den physiko-chemischen Eigenschaften der UHM-25-MOFs, wurde die Konnektivität des zugehörigen Netzwerkes untersucht. Durch eine softwaregestüze Analyse der UHM-25-Struktur wurde ein binodales (3,4)-c-Netz als zugrundeliegende Topologie ermittelt, welche als **ucp** klassifiziert wurde. In der Einbettung mit höchstmöglicher Symmetrie kann das **ucp** Netz als eine Anordnung von miteinander verknüpften Kuboktaedern beschrieben werden. Diese spiegeln das strukturelle Motiv der MOPs wider, welche charakteristische Baueinheiten der UHM-25-Struktur darstellen. Das **ucp** Netz wurde beschrieben als eine Variante der Verknüpfung von kuboktaedrischen MOPs.[5] Jedoch wurde dieses Netz bisher nur theoretisch beschrieben und wurde nun das erste Mal bei den MOFs der UHM-25-Reihe beobachtet. Dies ist interessant, weil von den drei von Yaghi und O'Keffe publizierten Varianten für die Anordnung von kuboktaedrischen MOPs (**ucp**, **zhc** und **zmj**) die einfachste der drei Anordnungen am längsten unentdeckt blieb.
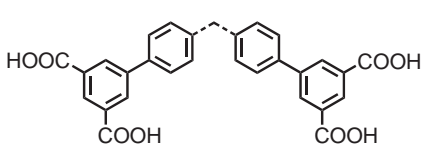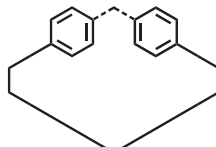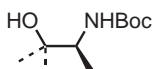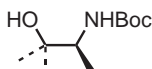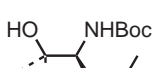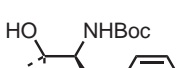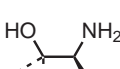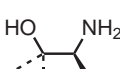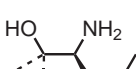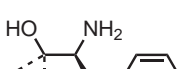
In weiteren topologischen Analysen wurden zwei Topologien bestimmt, die bisher unbekannt waren. Die zugehörigen MOFs setzen sich aus Zink- beziehungsweise Kupfer-Schaufelrad-Motiven und 3,3',5,5'-Benzophenontetracarboxylat zusammen.[7] Eines dieser bisher unbekannten Netze beschreibt in der Einbettung mit höchstmöglicher Symmetrie die Verknüpfung von rhombischen Dodekaedern in einer innenzentrierten Anordnung, welche den MOP-Struktur-

---

[7] 3,3',5,5'-Benzophenontetracarboxylat wurde als Intermediat bei Versuchen zur Synthese eines weiteren chiralen Linkers erhalten.
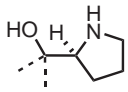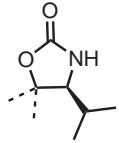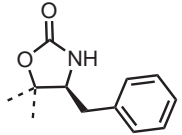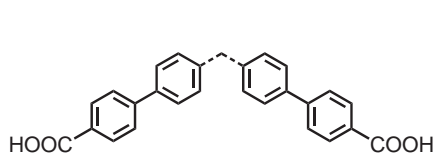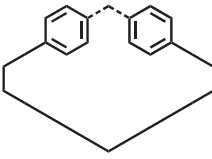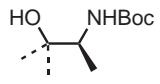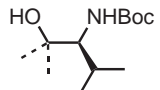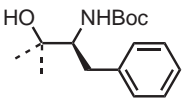
motiven im zugehörigen MOF entspricht. Dieses Netz wurde bei der Topos To-logical Database (TTD) als *fhs*1 registriert.

**Tabelle 3.15** – Übersicht der unterschiedlichen Linker, die für die Synthese der UHM-MOFs eingestzt wurden. Die Linker und MOFs sind mit den Drei-Buchstaben-Codes der jeweiligen Aminosäure benannt, die für die Synthese des Linkers eingesetzt wurde; ta steht für tetracarboxylic acid (Tetracarbonsäure). Die Endung Boc zeigt die Anwesenheit der *N*-Boc-Schutzgruppe an. Die gestrichelten Linien markieren die Verknüpfung zum Netzwerk des MOF.



| | | | |
|---|---|---|---|
| | Ala-Boc-ta | **121** | UHM-25-Ala-Boc |
| | Val-Boc-ta | **122** | UHM-25-Val-Boc |
| | Leu-Boc-ta | **123** | UHM-25-Leu-Boc |
| | Phe-Boc-ta | **124** | UHM-25-Phe-Boc |
| | Ala-ta | **129** | UHM-25-Ala |
| | Val-ta | **130** | UHM-25-Val |
| | Leu-ta | **131** | UHM-25-Leu |
| | Phe-ta | **132** | UHM-25-Phe |

218

 Pro-ta **128** UHM-25-Pro

 Val-Evans-ta **178** UHM-25-Val

 Phe-Evans-ta **179** UHM-25-Phe



 Ala-Boc-da **99** UHM-24-Ala-Boc

 Val-Boc-da **100** UHM-24-Val-Boc

 Phe-Boc-da **101** UHM-24-Phe-Boc

# Chapter 4

# Experimental

## 4.1 General Remarks

To investigate and prove the stability of the chiral linker after the MOF synthesis, the UHM-25 MOFs were digested in diluted hydrochloric acid. This allowed the reisolation of the linker which could then be examined by spectroscopic methods. The integrity of the linker was independently verified by ^{1}H-NMR spectroscopy, mass spectrometry and optical rotation.

Representations of crystal structures were created with VESTA.[316]

### 4.1.1 Powder X-Ray Diffraction

PXRD measurements of the MOFs were performed with the as synthesized material before exchanging solvents, dried in air. Powder X-ray diffractograms were recorded on a STOE Stadi P by STOE & Cie GmbH in a Debye/Scherrer procedure in the range of $2\theta = 0° - 70°$.

### 4.1.2 Thermal Analysis

TG/DTA/MS experiments were performed with a thermobalance STA 449 F3 *Jupiter* coupled with a Netzsch quadrupol mass spectrometer QMS 40 C Aëolos. All measurements were performed in a stream of an argon/oxygen mixture (80:20) with a flow rate of 20 ml/min. Circa 20 mg sample were heated in an aluminium oxide crucible from room temperature to 800 °C with a heating rate of 5 °C/min.

### 4.1.3 Physisorption

Physisorption measurements were performed with a QUADRASORB SI-MP by Quantachrome GmbH & Co KG with nitrogen at 77 K. The determination of the specific surface area was performed on the basis of the micropore assistent provided in the Quantachrome ASiQwin software. MOFs were activated for one hour at 40 °C or after exchange with super critical carbon dioxide for one hour at room temperature.

The exchange with super critical carbon dioxide was carried out as follows: About 30 mg of the material was subjected to a solvent exchange with amyl acetate, which was replaced two times with fresh solvent after 24 hours. After another 24 hours the solvent was decanted and the dark blue crystals were placed in a porous container. A solvent exchange was performed with liquid carbon dioxide 10 °C and 55 bar in a steel autoclave. The liquid carbon dioxide was replaced ten times in intervals of 6-18 hours. After the last exchange the autoclave was sealed and slowly heated to 35 °C to reach the supercritical state

of carbon dioxide. The autoclave was then slowly vented and the samples were kept under argon before nitrogen physisorption was measured.

### 4.1.4  Characterization of Organic Reaction Products

MS experiments were performed with a 6224 Accurate-Mass TOF-MS by Agilent Technologies. TLC was carried out on ALUGRAM Xtra SIL G/UV$_{254}$. NMR measurements were performed at room temperature with a Fourier 300 from Bruker BioSpin GmbH. Spectra were referenced to the known chemical shifts of the deuterated solvents.[317] In addition to one-dimensional $^1$H and proton decoupled $^{13}$C spectra, correlation spectroscopy (COSY), heteronuclear single quantum coherence (HSQC) and heteronuclear multiple bond correlation experiments were performed when necessary for an precise assignment of the NMR signals. IR spectroscopy was performed with potassium bromide disks or by attenuated total reflection (ATR) with a VERTEX 70 by Bruker. Elementary analysis was performed with a vario EL III by Elementar Analysensysteme GmbH and EuroEA Elemental Analyzer by HEKAtech GmbH.

## 4.2 *N-tert*-butoxycarbonyl alanine methyl ester (70)
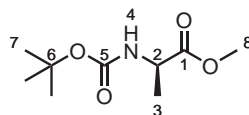


A suspension of alanine (20.0 g, 224 mmol, 1 eq.) in methanol (400 mL) was cooled to 0 °C. Acetyl chloride (40.0 mL, 463 mmol, 2.07 eq.) was added over five minutes via syringe. The reaction was allowed to warm to room temperature and was stirred overnight. The solvent was removed by rotary evaporation. The obtained white solid was used without purification in the next step.

Alanine methyl ester hydrochloride was dissolved in a 1:1 mixture of THF and MeOH (400 mL) . Triethylamine (93.3 mL, 673 mmol, 3 eq.) was added and the mixture was cooled to 0 °C. A solution of di-tert-butyl dicarbonate (44.0 g, 202 mmol, 0.90 eq.) in THF (100 mL) was added via transfer cannula. The reaction was allowed to warm to room temperature and was stirred overnight. Diethylether was added, resulting in precipitation of triethylammonium hydrochloride. Water was added to dissolve the precipitate. The phases were separated and the organic phase was washed with aqueous solutions of HCl (1 M), $NaHCO_3$ (sat.) and NaCl (sat.). The organic layer was separated and dried over $Na_2SO_4$. After removal of solvent via rotary evaporation a clear oil was obtained that crystallized upon cooling.

Yield: 38.2 g (188 mmol, 83%); colorless crystals; **M:** [$C_9H_{17}NO_4$] 203.1 $\frac{g}{mol}$;
**TLC:** $R_f = 0.36$ (heptane/EtOAc, 4:1); **opt. rot.:** $[\alpha]_D^{27} = -38.0$ (c = 1.0, MeOH);
**HRMS (ESI+):** $\frac{m}{z} = 226.1065$ (calc. for MNa$^+$: 226.1055). **elem. anal.:** % = calc.
for $C_9H_{17}NO_4$: C (53.19), H (8.43), N (6.89), O (31.49).
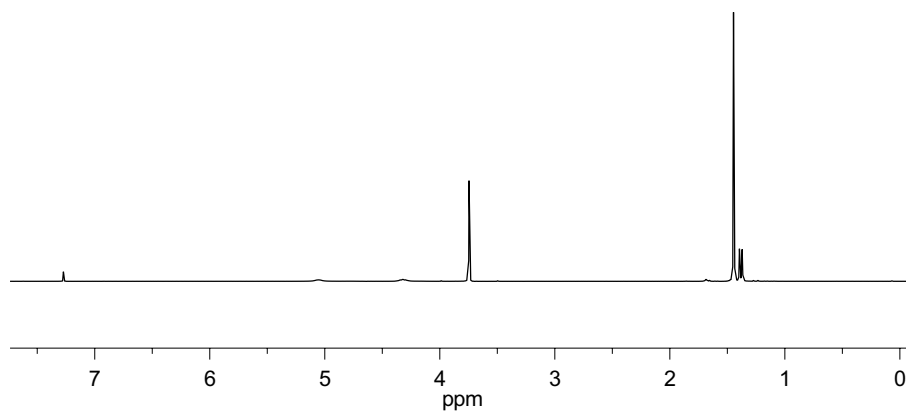
**$^1$H-NMR (300 MHz, CDCl$_3$):** $\delta$ [ppm] = 5.05 (s, 1H, H4), 4.32 (t, 1H, $^3J_{\text{H-H}}$ = 7.7 Hz H2), 3.75 (s, 3H, H8), 1.45 (s, 9H, H7), 1.38 (d, 3H, $^3J_{\text{H-H}}$ = 7.7 Hz H3).
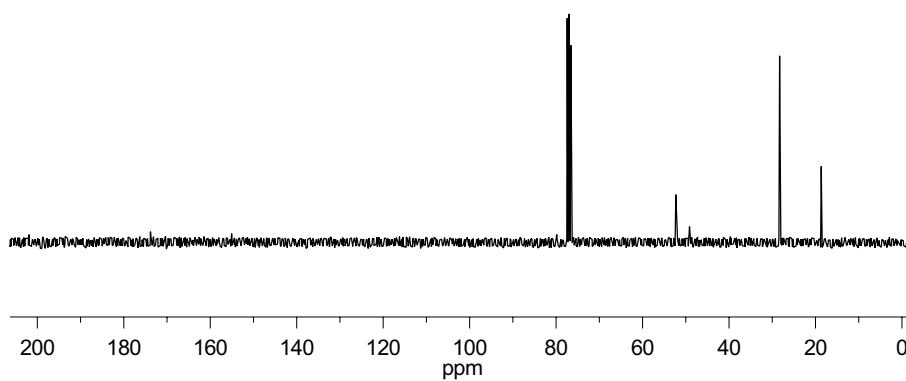


**$^{13}$C-NMR (75 MHz, CDCl$_3$):** $\delta$ [ppm] = 173.8 (1C, C1), 155.0 (1C, C5), 79.8 (1C, C6), 52.3 (1C, C8), 49.1 (1C, C2), 28.3 (3C, C7), 18.7 (1C, C3).
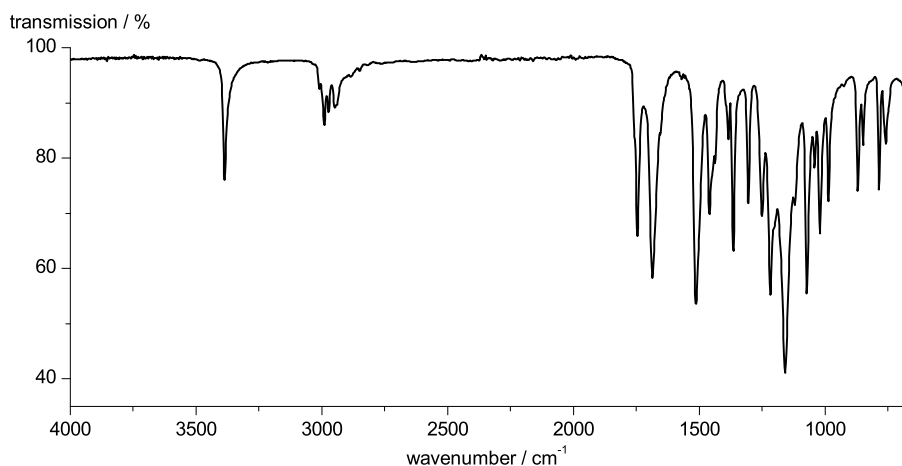
**IR (ATR):** $\widetilde{\nu}$ = 3388 (m), 3008 (w), 2989 (w), 2989 (w), 2973 (w), 2948 (w), 1747 (m), 1685 (s), 1513 (s), 1459 (m), 1363 (m), 1251 (m), 1215 (m), 1215 (m), 1161 (s), 1072 (s), 985 (m), 867 (m), 784 (m).

## 4.3   N-*tert*-butoxycarbonyl valine methyl ester (71)
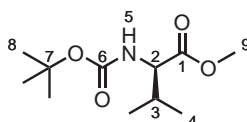


A suspension of valine (20.0 g, 171 mmol, 1 eq.) in methanol (400 mL) was cooled to °C. Acetyl chloride (40.0 mL, 463 mmol, 2.70 eq.) was added over five minutes via syringe. The reaction was allowed to warm to room temperature and was stirred overnight. The solvent was removed by rotary evaporation. The obtained white solid was used without purification in the next step.

Valine methyl ester hydrochloride was dissolved in a 1:1 mixture of THF and MeOH (400 mL). Triethylamine (71.0 mL, 512 mmol, 3 eq.) was added and the mixture was cooled to 0 °C. A solution of di-tert-butyl dicarbonate (33.7 g, 154 mmol, 0.90 eq) in THF (100 mL) was added via transfer cannula. The reaction was allowed to warm to room temperature and was stirred overnight. Diethylether was added, resulting in precipitation of triethylammonium hydrochloride.

Water was added to dissolve the precipitate. The phases were separated and the organic phase was washed with aqueous solutions of HCl (1 M), NaHCO$_3$ (sat.) and NaCl (sat.). The organic layer was separated and dried over Na$_2$SO$_4$. After removal of solvent via rotary evaporation a clear oil was obtained.

Yield: 34.8 g (151 mmol, 88%); clear oil; **M:** [C$_{11}$H$_{21}$NO$_4$] 231.3 $\frac{g}{mol}$; **TLC:** $R_f$ = 0.42 (heptane/EtOAc, 4:1); **opt. rot.:** $[\alpha]_D^{27}$ = −21.6 (c = 1.0, MeOH); **HRMS (ESI+):** $\frac{m}{z}$ = 254.1370 (calc. for MNa$^+$: 254.1368).
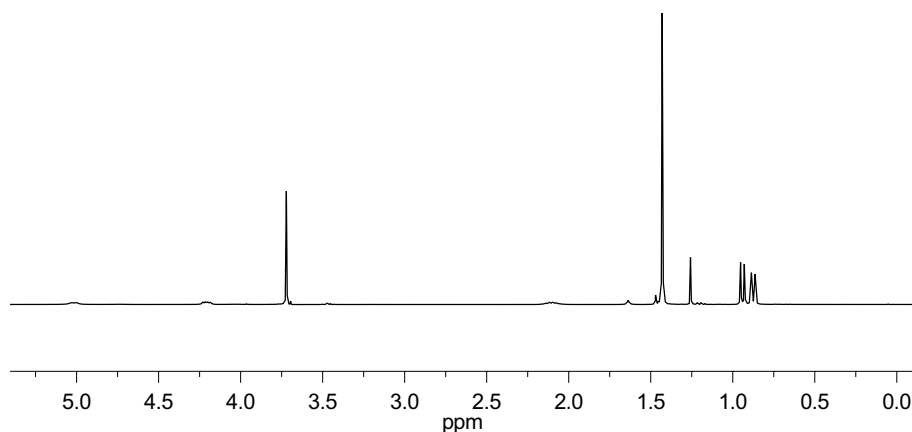


**$^1$H-NMR (300 MHz, CDCl$_3$):** $\delta$ [ppm] = 5.02 (d, 1H, $^3J_{\text{H-H}}$ = 9.2 Hz, H5), 4.21 (dd, 1H; $^3J_{\text{H-H}}$ = 9.2, 4.2 Hz, H2), 3.72 (s, 3H, H-5), 2.19-2.00 (m, 1H; H3), 1.43 (s, 9H, H8), 0.94 (d, 2H; $^3J_{\text{H-H}}$ = 6.9 Hz Hz H4A), 0.87 (d, 2H; $^3J_{\text{H-H}}$ = 6.9 Hz Hz H4B).
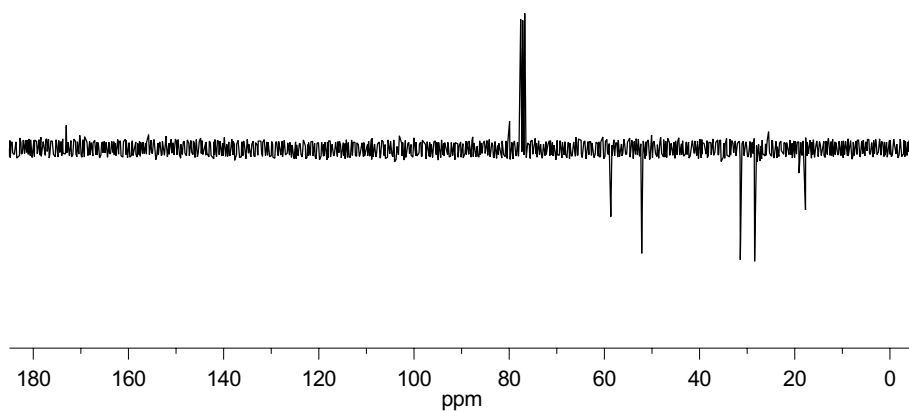
**$^{13}$C-NMR (75 MHz, CDCl$_3$):** $\delta$ [ppm] = 173.1 (1C, C1), 155.8 (1C, C6), 79.9 (1C, C7), 58.7 (1C, C2), 52.2 (1C, C9), 31.4 (1C, C3), 28.4 (3C, C8), 19.1 (1C, C4A), 17.7 (1C, C4B).
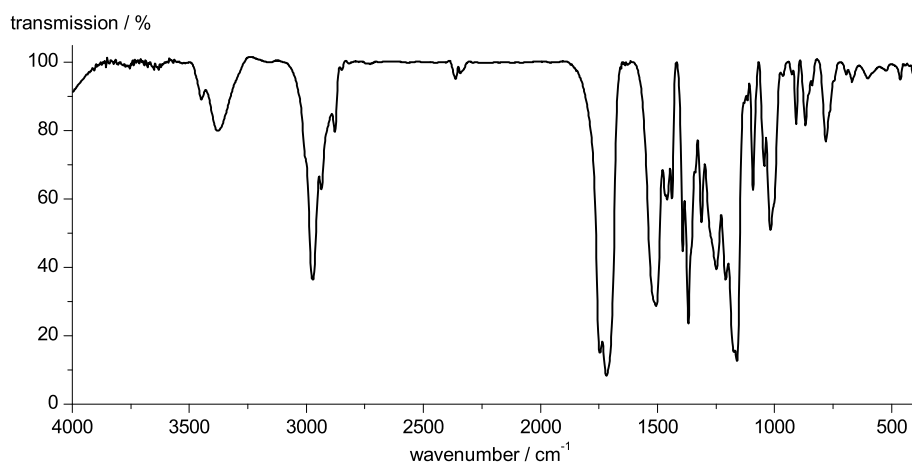


**IR (KBr):** $\widetilde{\nu}$ [cm$^{-1}$] = 3377 (m), 2972 (s), 2936 (m), 2878 (m), 1746 (s), 1719 (s), 1506 (s), 1466 (m), 1458 (m), 1439 (m), 1393 (s), 1367 (s), 1339 (m), 1312 (m), 1248 (s), 1209 (s), 1175 (s), 1161 (s), 1092 (m), 1043 (m), 1016 (m), 908 (w), 868 (w), 781 (m).

228

## 4.4  *N-tert*-butoxycarbonyl leucine methyl ester (72)
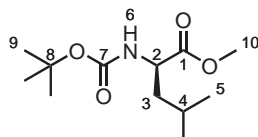


A suspension of leucine (20.0 g, 152 mmol, 1 eq.) in methanol (400 mL) was cooled to 0 °C. Acetyl chloride (40.0 mL, 463 mmol, 3.04 eq) was added over five minutes via syringe. The reaction was allowed to warm to room temperature and was stirred overnight. The solvent was removed by rotary evaporation. The obtained white solid was used without purification in the next step.

Valine methyl ester hydrochloride was dissolved in a 1:1 mixture of THF and MeOH (400 mL) . Triethylamine (63.4 mL, 457 mmol, 3 eq.) was added and the mixture was cooled to 0 °C. A solution of di-tert-butyl dicarbonate (30.2 g, 137 mmol, 0.90 eq.) in THF (100 mL) was added via transfer cannula. The reaction was allowed to warm to room temperature and was stirred overnight. Diethylether was added, resulting in precipitation of triethylammonium hydrochloride. Water was added to dissolve the precipitate. The phases were separated and the organic phase was washed with aqueous solutions of HCl (1 M), NaHCO$_3$ (sat.) and NaCl (sat.). The organic layer was separated and dried over Na$_2$SO$_4$. After removal of solvent via rotary evaporation a clear oil was obtained.

Yield: 32.0 g (130 mmol, 85%); clear oil; **M:** [C$_{12}$H$_{23}$NO$_4$] 245.1 $\frac{g}{mol}$; **TLC:** $R_f = 0.46$ (heptane/EtOAc, 4:1); **opt. rot.:** $[\alpha]_D^{26} = -4.2$ (c = 1.0, CH$_3$Cl); **HRMS (ESI+):** $\frac{m}{z} = 268.1520$ (calc. for MNa$^+$: 268.1525).
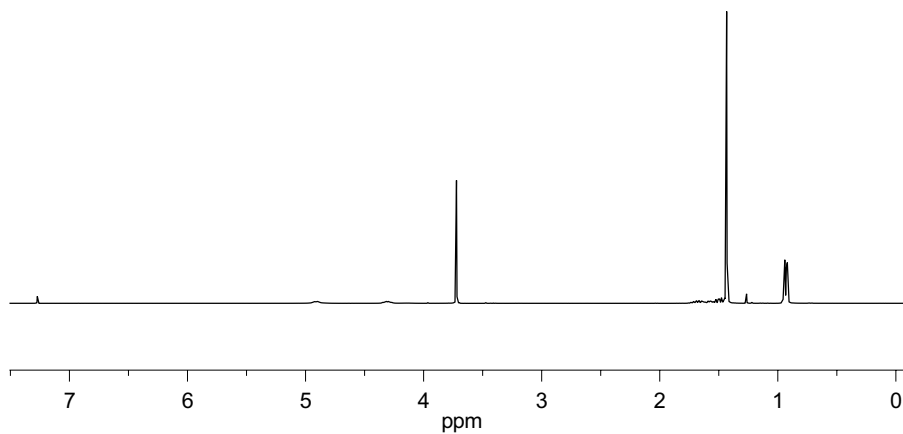
**¹H-NMR (300 MHz, CDCl₃):** $\delta$ [ppm] = 4.90 (d,$^3J_{\text{H-H}}$ = 9.0 Hz, H6), 4.39-4.21 (m, 1H, H2), 3.71 (s, 3H, H9), 1.78-1.60 (m, 1H, H4), 1.56 (dd, $^3J_{\text{H-H}}$ = 8.0, 5.4 Hz, H3A), 1.53-1.44 (m, 1H, H3B), 1.42 (s, 9H, H9), 0.93 (d, 3H, $^3J_{\text{H-H}}$ = 2.4 Hz, H5B), 0.91 (d, 3H, $^3J_{\text{H-H}}$ = 2.5 Hz, H5B).
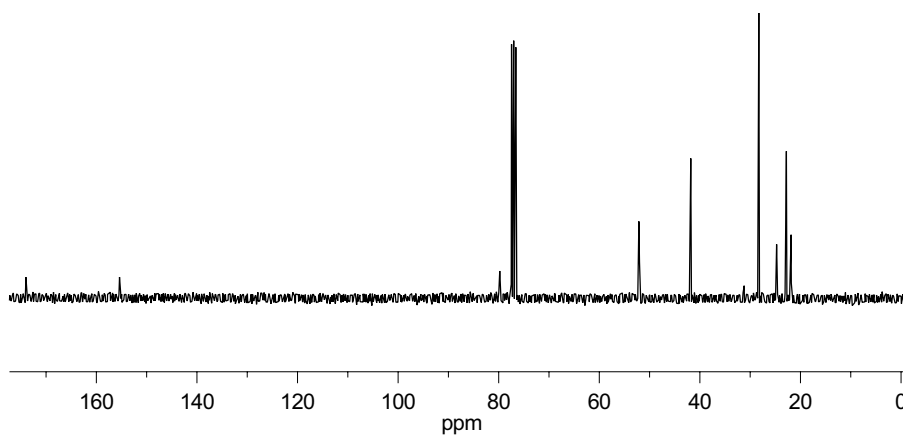


**¹³C-NMR (75 MHz, CDCl₃):** $\delta$ [ppm] = 174.0 (C1, C1), 155.4 (C1, C7), 79.8 (C1, C8), 52.1 (1C, C2), 52.0 (1C, C10), 41.8 (1C, C3), 28.3 (3C, C9), 24.8 (1C, C5A), 22.8 (1C, C4), 21.9 (1C, C5B).
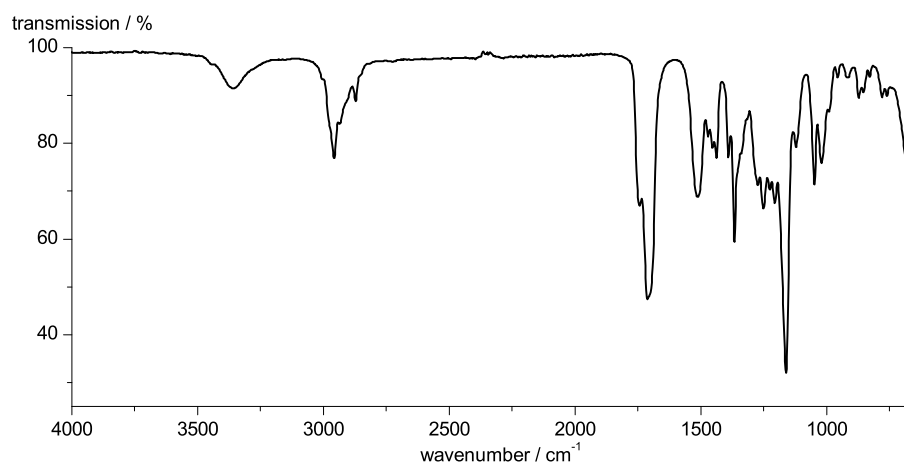
**IR (ATR):** $\tilde{\nu}$ = 3359 (m), 2958 (w), 2933 (w), 2871 (w), 1743 (m), 1710 (s), 1512 (m), 1471 (m), 1454 (m), 1436 (m), 1390 (m), 1365 (m), 1274 (m), 1249 (m), 1203 (m), 1161 (s), 1047 (m), 1018 (m), 667 (m).

## 4.5 *N-tert*-butoxycarbonyl phenylalanine methyl ester (73)
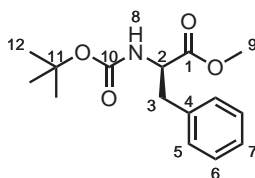


A suspension of phenylalanine (20.0 g, 152 mmol, 1 eq.) in methanol (400 mL) was cooled to 0 °C. Acetyl chloride (40.0 mL, 463 mmol, 3.04 eq) was added over five minutes via syringe. The reaction was allowed to warm to room temperature and was stirred overnight. The solvent was removed by rotary evaporation. The obtained white solid was used without purification in the next step.

Valine methyl ester hydrochloride was dissolved in a 1:1 mixture of THF and MeOH (400 mL) . Triethylamine (50.4 mL, 363 mmol, 3 eq.) was added and the mixture was cooled to 0 °C. A solution of di-tert-butyl dicarbonate (24.0 g,

109 mmol, 0.90 eq.) in THF (100 mL) was added via transfer cannula. The reaction was allowed to warm to room temperature and was stirred overnight. Diethylether was added, resulting in precipitation of triethylammonium hydrochloride. Water was added to dissolve the precipitate. The phases were separated and the organic phase was washed with aqueous solutions of HCl (1 M), NaHCO$_3$ (sat.) and NaCl (sat.). The organic layer was separated and dried over Na$_2$SO$_4$. After removal of solvent via rotary evaporation a clear oil was obtained.

Yield: 28.5 g (102 mmol, 84%); colorless oil that crystallized upon cooling; **M:** [C$_{15}$H$_{21}$NO$_4$] 279.3 $\frac{g}{mol}$; **m.p.:** 42 °C; **TLC:** $R_f = 0.38$ (heptane/EtoAc, 4:1); **opt. rot.:** $[\alpha]_D^{27} = -3.0$ (c = 1.0, MeOH); **HRMS (ESI+):** $\frac{m}{z} = 302.1377$ (calc. for MNa$^+$: 302.1368). **elem. anal.:** % = C (64.32), H (7.53), N (4.93), O (22.95) calc. for C$_{15}$H$_{21}$NO$_4$: C (64.50), H (7.58), N (5.01), O (22.91).
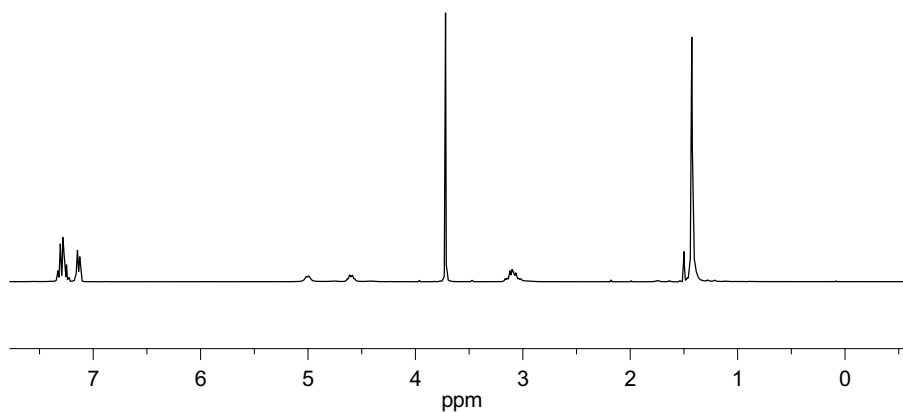


**$^1$H-NMR (300 MHz, DMSO$-$d$_6$):** $\delta$ [ppm] = 7.35-7.22 (m, 3H, H5, H7), 7.17-7.10 (m, 2H, H6), 5.00 (d, 1H, $^3J_{\text{H-H}} = 7.5$ Hz, H8), 4.68-4.53 (m, 1H, H2), 3.72 (s, 3H, H9), 3.20-3.00 (m, 2H, H3), 1.43 (s, 9H, H12).

**13C-NMR** (75 MHz, **CDCl₃):** $\delta$ [ppm] = 174.5 (1C, C1), 136.1 (1C, C4), 129.4 (2C, C5), 128.6 (2C, C6), 127.1 (1C, C7), 80.0 (1C, C11), 54.5 (1C, C2), 52.2 (1C, C9), 38.5 (1C, C3), 28.4 (3C, C12).
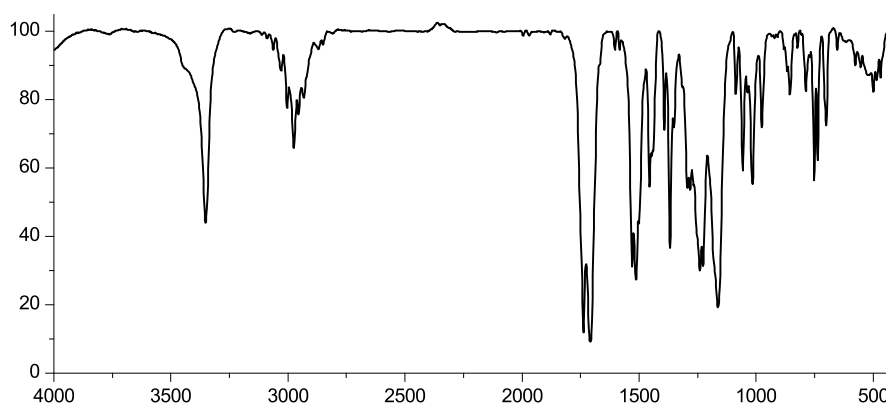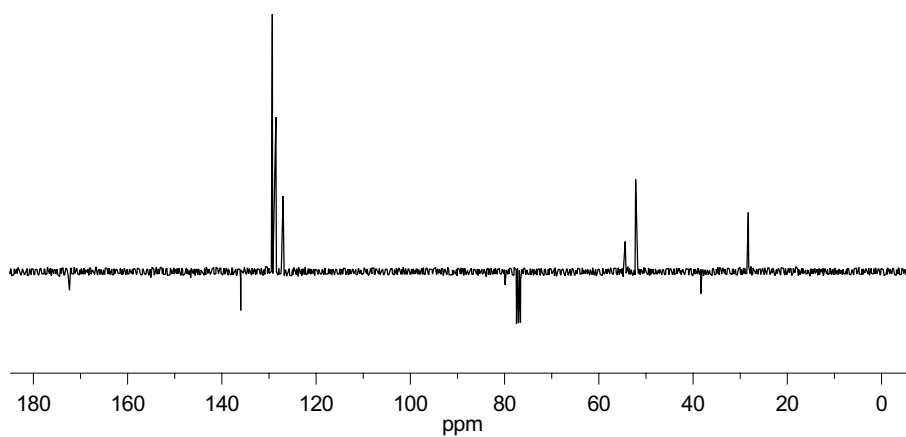


**IR (KBr):** $\widetilde{\nu}$ = 3352 (m), 3003 (w), 2974 (w), 2955 (w), 2932 (w), 1738 (s), 1709 (s), 1530 (s), 1514 (s), 1501 (m), 1456 (m), 1447 (m), 1439 (m), 1393 (w), 1367 (s), 1350 (w), 1315 (w), 1294 (m), 1283 (m), 1240 (s), 1227 (s), 1163 (s), 1088 (w), 1057 (m), 1038 (w), 1015 (m), 976 (w), 856 (w), 787 (w), 752 (m), 737 (m), 700 (w), 500 (w).

## 4.6   1,1-Di(4-bromophenyl)*N*-*tert*-butoxycarbonyl alani-nol (85)
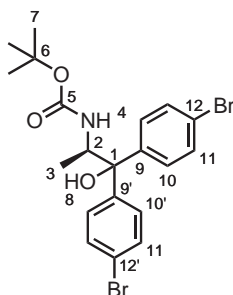


The reactions were performed oven-dried glassware under argon. A solution of 1,4-dibromobenzene (60.8 g, 258 mmol, 3.6 eq) in THF (375 mL) was cooled to -78 °C. A solution of *n*-butyl lithium in hexanes (2.5 M, 100 mL, 258 mmol, 3.6 eq) was added over thirty minutes. The reaction was allowed was stirred for another sixty minutes at -78°C. To the resulting colorless suspension of 4-bromophenyl lithium a solution of the *N*-protected amino acid methylester **70** (14.5 g, 71.4 mmol, 1 eq.) in THF (15.0 mL) was added dropwise. The reaction was stirred for another 60 minutes and was slowly warmed to room temperature. The reaction was monitored by TLC. Upon consumption of compound **70**, the reaction was quenched by the addition of a saturated solution of $NH_4Cl$ in water (500 mL). The reaction mixture extracted with EE (750 mL). Phases were seperated and the aqueous phase was extracted with EtOAc again (2× 150 mL). The combined organic phases were washed with aqueous HCl (1 M, 2× 250 mL), a saturated solution of $NaHCO_3$ (2× 250 mL) and brine (2× 250 mL). The organic phase was dried over $Na_2SO_4$ and the solvent was evaporated under reduced pressure. The crude reaction product was purified by dry column vacuum chromatography (DCVC).[318]

Yield: 31.4 g (65.0 mmol, 91%); colorless crystals; **M:** $[C_{20}H_{23}Br_2NO_3]$ 484.0 $\frac{g}{mol}$; **TLC:** $R_f = 0.45$ (heptane/EtOAc, 4:1); **opt. rot.:** $[\alpha]_D^{27} = -30.6$ (c = 0.58, MeOH); **HRMS (ESI+):** $\frac{m}{z}$ = 505.9956 (calc. for MNa$^+$: 505.9942). **elem. anal.:** % = C (49.82), H (4.83), Br (n.d.), N (2.54) O (9.99) calc. for $C_{20}H_{23}Br_2NO_3$: C (49.51), H (4.78), Br (32.94), N (2.89), O (9.89).
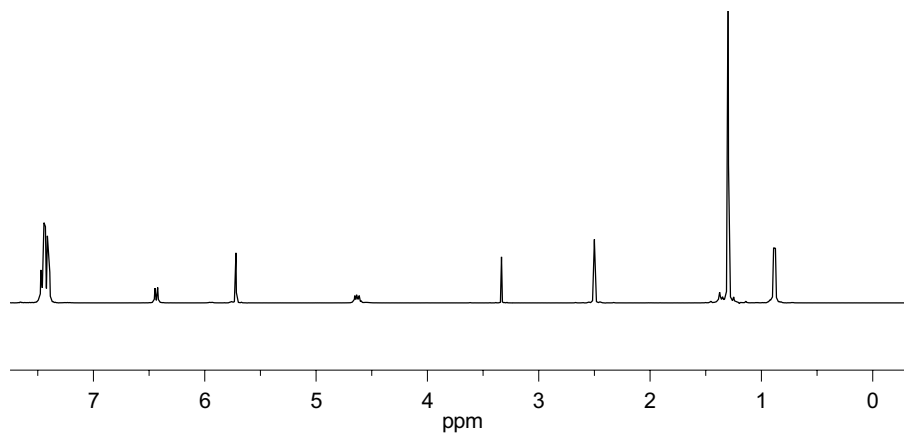
**¹H-NMR (300 MHz, DMSO−d₆):** $\delta$ [ppm] = 7.48-7.39 (m, 8H, H10, H11) 6.44 (d, 1H, $^3J_{H\text{-}H}$ = 9.5 Hz, H4), 5.72 (s, 1H, H8), 4.63 (dq, 1H, $^3J_{H\text{-}H}$ = 9.5, 6.5 Hz, H2), 1.30 (s, 9H, H7), 0.88 (d, 3H, $^3J_{H\text{-}H}$ = 6.5 Hz H3).
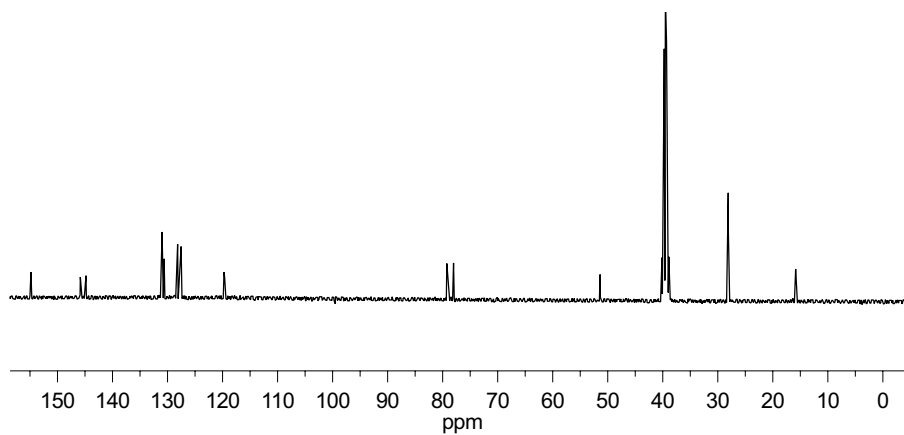


**¹³C-NMR (75 MHz, DMSO−d₆):** $\delta$ [ppm] = 154.8 (1C, C5), 145.6, 144.8 (2C, C12), 131.0, 130.6, 128.2, 127.5 (4C, C10, C11), 119.7, 119.6 (2C, C9), 79.2 (1C, C1), 78.0 (1C, C6), 51.4 (1C, C2), 28.1 (3C, C7), 15.6 (1C, C3).
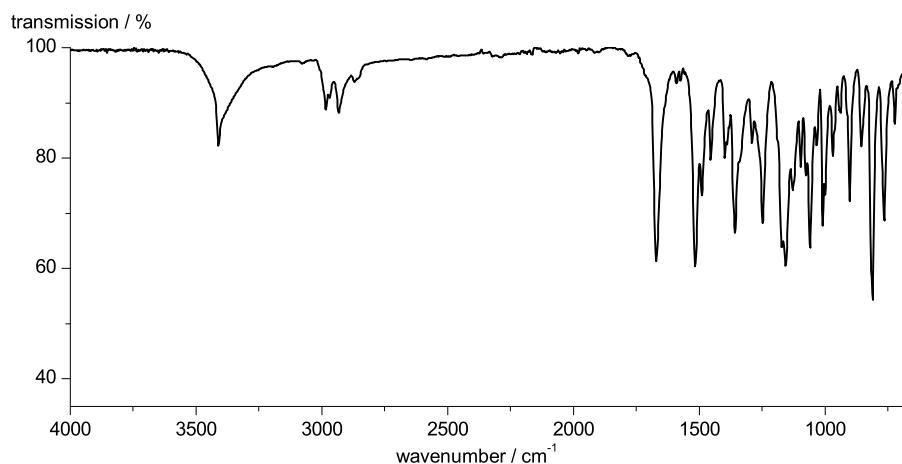
**IR (ATR):** $\widetilde{\nu}$ = 3411 (m), 3083 (w), 2968 (w), 2933 (w), 2869 (w), 2850 (w), 1672 (s), 1515 (s), 1490 (m), 1454 (m), 1398 (m), 1357 (s), 1247 (m), 1172 (s), 1157 (s), 1074 (m), 1060 (s), 1008 (s), 900 (m), 811 (s), 765 (s).

## 4.7 1,1-Di(4-bromophenyl)*N*-*tert*-butoxycarbonyl valinol (86)
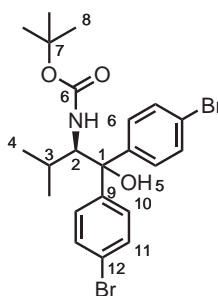


The reactions were performed oven-dried glassware under argon.

A solution of 1,4-dibromobenzene (60.8 g, 258 mmol, 3.6 eq.) in THF (375 mL) was cooled to −78 °C. A solution of *n*-butyl lithium in hexanes (2.5 $\frac{mol}{L}$, 100 mL, 258 mmol, 3.6 eq.) was added over thirty minutes. The reaction was allowed

was stirred for another sixty minutes at −78 °C. To the resulting colorless suspension of 4-bromophenyl lithium a solution of the *N*-protected amino acid methylester **71** (16.5 g, 71.4 mmol, 1 eq.) in THF (15.0 mL) was added dropwise. The reaction was stirred for another 60 minutes and was slowly warmed to room temperature. The reaction was monitored by TLC. Upon consumption of compound **71**, the reaction was quenched by the addition of a saturated solution of $NH_4Cl$ in water (500 mL). The reaction mixture extracted with EtOAc (750 mL). Phases were seperated and the aqueous phase was extracted with EtOAc again (2× 150 mL). The combined organic phases were washed with aqueous HCl (1 $\frac{mol}{L}$, 2× 250 mL), a saturated solution of $NaHCO_3$ (2× 250 mL) and brine (2× 250 mL). The organic phase was dried over $Na_2SO_4$ and the solvent was evaporated under reduced pressure. The crude reaction product was purified by DCVC.[318]

Yield: 20.3 g (34.1 mmol, 93%); colorless crystals; **M:** [$C_{22}H_{27}Br_2NO_3$] 513.3 $\frac{g}{mol}$; **TLC:** $R_f$ = 0.49 (heptane/ EtOAc, 4:1); **m.p.:** 214 °C; **opt. rot.:** $[\alpha]_D^{27}$ = −36.4 (c = 0.85, MeOH); **HRMS (ESI+):** $\frac{m}{z}$ = 534.0255 (calc. for MNa$^+$: 534.0258). **elem. anal.:** % = C (51.70), H (5.36), Br (n.d.), N (2.48), O (9.69), calc. for $C_{10}H_{11}BO_6$: C (51.48), H (5.30), Br (n.d.), N (2.73), O (9.35).
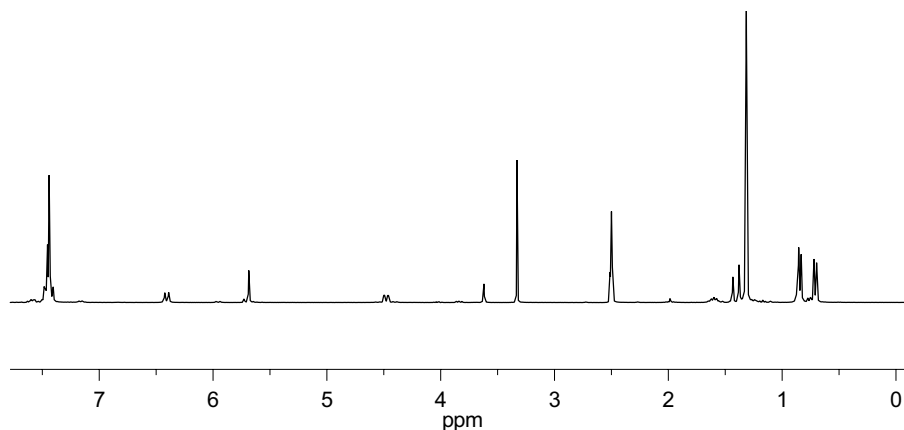


**$^1$H-NMR (300 MHz, CDCl$_3$):** $\delta$ [ppm] = 7.54-7.37 (m, 8H; H11, H11', H12, H12'), 5.96 (d, 1H, $^3J_{H-H}$ = 10.4 Hz, H6), 5.69 (s, 1H, H5), 4.48 (dd, 1H, $^3J_{H-H}$ = 10.4, 2.3 Hz, H2), 1.60 (m, 1H, H3), 1.31 (s, 9H; H9), 0.84 (d, 3H, $^3J_{H-H}$ = 6.6 Hz, H4A), 0.71 (d, 3H, $^3J_{H-H}$ = 6.9 Hz, H4B).
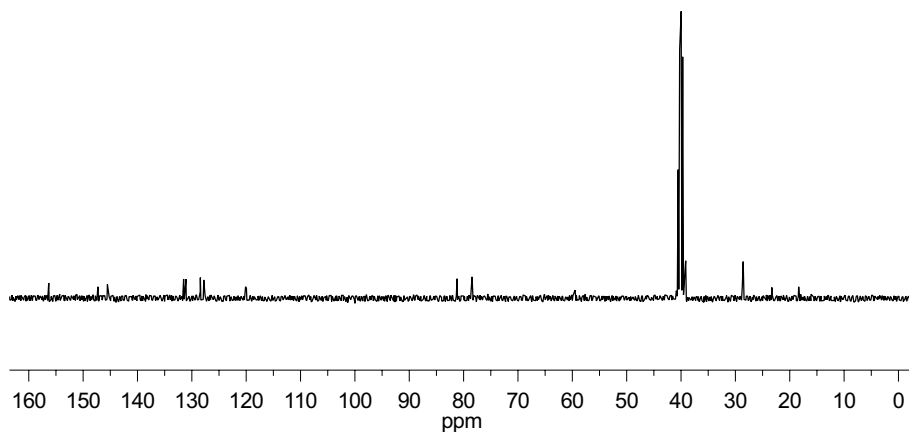
**¹³C-NMR (75 MHz, DMSO−d₆):** $\delta$ [ppm] = 156.3 (1C, C7), 147.3, 145.5 (2C, C13, C13′), 131.5, 131.1, 128.4, 127.8 (4C; C11, C11′, C12, C12′), 120.1, 120.0 (2C; C10, C10′), 81.2 (1C, C1), 78.5 (1C, C8), 59.5 (1C, C2), 28.7 (1C, C3), 28.6 (3C, C9), 23.3, 18.4 (2C, C4A, C4B).
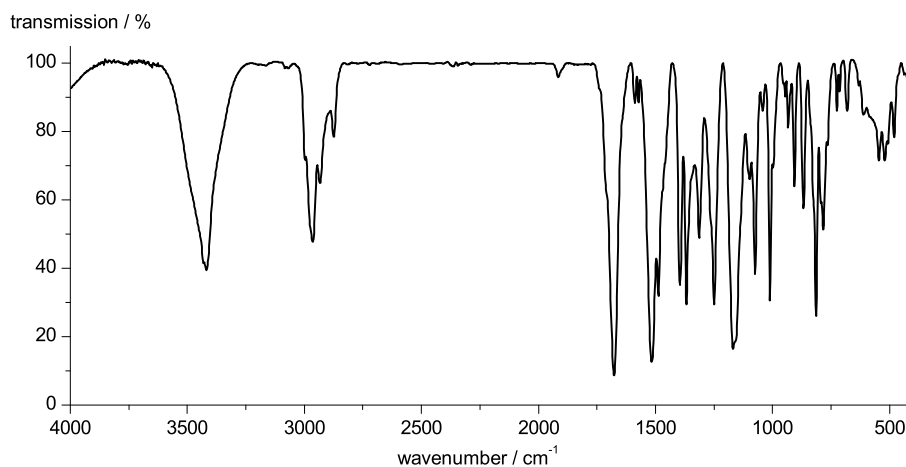


**IR (KBr):** $\widetilde{\nu}$ [cm⁻¹] = 3431 (m), 3420 (m), 2997 (m), 2964 (m), 2934 (m), 2874 (m), 1676 (s), 1516 (s), 1487 (s), 1396 (m), 1367 (s), 1313 (m), 1250 (s), 1169 (s), 1097 (m), 1074 (m), 1042 (w), 1011 (s), 997 (m), 934 (w), 907 (m), 868 (m), 814 (m), 783 (m), 766 (m), 725 (w), 681 (w), 613 (w), 546 (m), 521 (m), 507 (m), 480 (m).

## 4.8 1,1-Di(4-bromophenyl)*N-tert*-butoxycarbonyl leucinol 87
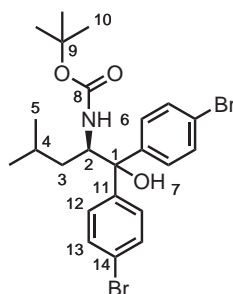


The reactions were performed oven-dried glassware under argon.

A solution of 1,4-dibromobenzene (36.4 g, 154 mmol, 3.6 eq.) in THF (225 mL) was cooled to $-78\,°C$. A solution of *n*-butyl lithium in hexanes (2.5 $\frac{mol}{L}$, 60 mL, 154 mmol, 3.6 eq.) was added over thirty minutes. The reaction was allowed was stirred for another sixty minutes at $-78\,°C$. To the resulting colorless suspension of 4-bromophenyl lithium a solution of the *N*-protected amino acid methylester **72** (10.5 g, 42.9 mmol, 1 eq.) in THF (10.0 mL) was added dropwise. The reaction was stirred for another 60 minutes and was slowly warmed to room temperature. The reaction was monitored by TLC. Upon consumption of compound **72**, the reaction was quenched by the addition of a saturated solution of NH$_4$Cl in water (300 mL). The reaction mixture extracted with EtOAc (400 mL). Phases were seperated and the aqueous phase was extracted with EtOAc again (2× 100 mL). The combined organic phases were washed with aqueous HCl (1 $\frac{mol}{L}$, 2× 100 mL), a saturated solution of NaHCO$_3$ (2× 100 mL) and brine (2× 100 mL). The organic phase was dried over Na$_2$SO$_4$ and the solvent was evaporated under reduced pressure. The crude reaction product was purified by DCVC.[318]

Yield: 20.3 g (38.7 mmol, 90%); colorless crystals; **M:** [C$_{23}$H$_{29}$Br$_2$NO$_3$] 527.3 $\frac{g}{mol}$; **TLC:** $R_f$ = 0.47 (heptane/EtOAc, 4:1); **opt. rot.:** $[\alpha]_D^{27}$ = −6.4 (c = 0.78, MeOH); **HRMS (ESI+):** $\frac{m}{z}$ = 548.0406 (calc. for MNa$^+$: 548.0412). **elem. anal.:** % = C (53.02), H (5.86), Br (n.d.), N (2.62), O (10.04) calc. for C$_{23}$H$_{29}$Br$_2$NO$_3$: C (52.39), H (5.54), Br (30.31), N (2.66), O (9.10).
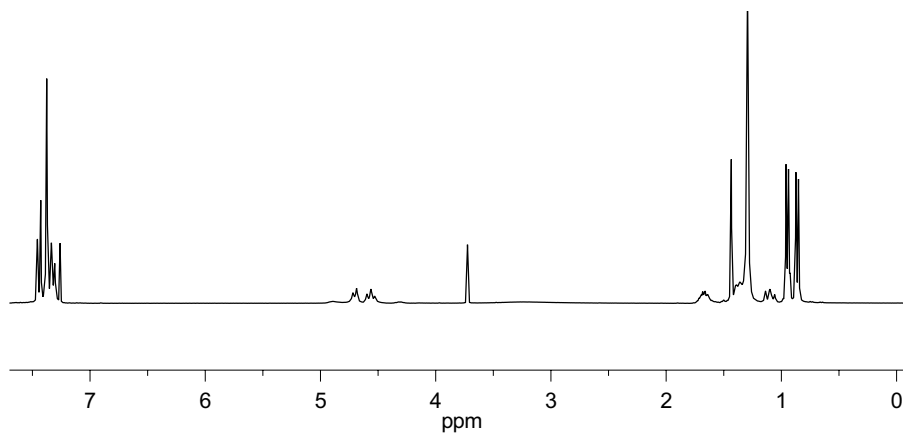
**¹H-NMR (300 MHz, CDCl₃):** $\delta$ [ppm] = 7.48-7.29 (m, 8H, H12, H13, H12′, H13′) 4.70 (d, 1H, $^3J_{H\text{-}H}$ = 9.7 Hz, H6), 5.72 (s, 1H, H8), 4.56 (t, 1H, $^3J_{H\text{-}H}$ = 10.4 Hz, H2), 3.72 (s, H7), 1.75-1.58 (m, 1H, H4), 1.37 (dd, 1H, $^3J_{H\text{-}H}$ = 10.9, 3.0 Hz, H3A), 1.29 (s, 9H, H10), 1.18-1.03 (m, 1H, H3B), 0.95 (d, 3H, $^3J_{H\text{-}H}$ = 6.5 Hz, H5A) 0.86 (d, 3H, $^3J_{H\text{-}H}$ = 6.7 Hz, H5B).
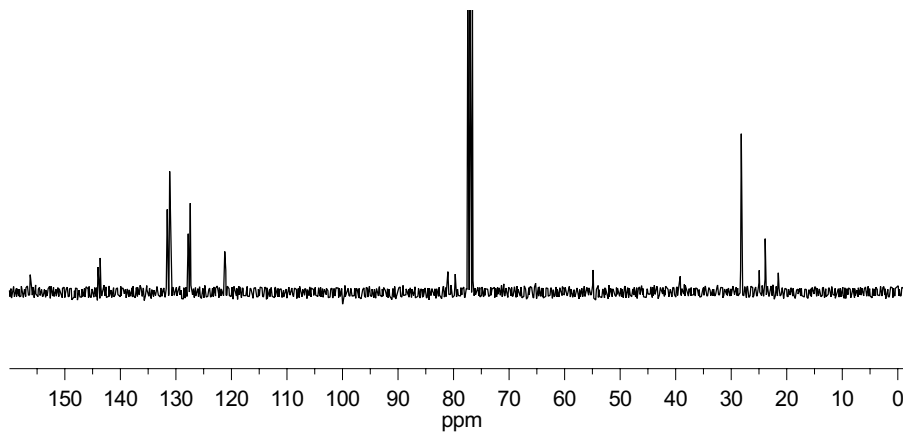


**¹³C-NMR (75 MHz, DMSO−d₆):** $\delta$ [ppm] = 156.2 (1C, C8), 144.0, 143.6 (2C, C14, C14′), 131.6, 131.1, 127.8, 127.4 (4C, C12, C12′, C13, C13′), 121.2, 121.0 (2C, C11, C11′), 81.1 (1C, C1), 79.7 (1C, C9), 54.9 (1C, C2), 39.2 (1C, C3), 28.2 (3C, C10), 25.2 (1C, C4), 23.9, 21.5 (2C, C5A, C5B).
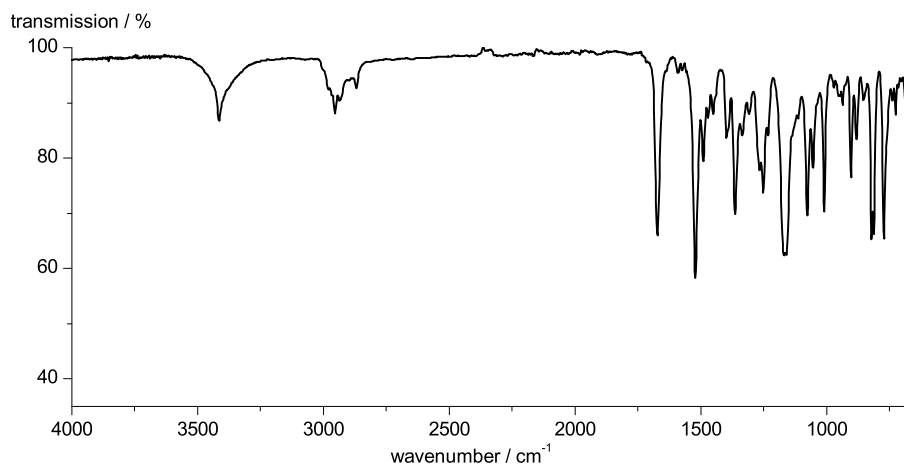
**IR (ATR):** $\tilde{\nu}$ = 3415 (m), 2979 (w), 2954 (w), 2869 (w), 1672 (s), 1521 (s), 1488 (m), 1450 (m), 1363 (m), 1267 (m), 1170 (m), 1159 (m), 1076 (m), 1008 (m), 902 (m), 819 (m), 811 (m), 771 (m).

## 4.9  *N*-Benzyl proline methyl ester (88)
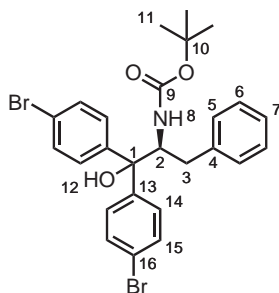


A solution of 1,4-dibromobenzene (36.4 g, 154 mmol, 3.6 eq.) in THF (225 mL) was cooled to −78 °C. A solution of *n*-butyl lithium in hexanes (2.5 $\frac{mol}{L}$, 60 mL, 154 mmol, 3.6 eq.) was added over thirty minutes. The reaction was allowed was stirred for another sixty minutes at −78 °C. To the resulting colorless suspension of 4-bromophenyl lithium a solution of the *N*-protected amino acid methylester **73** (12.0 g, 42.9 mmol, 1 eq.) in THF (10.0 mL) was added dropwise.

The reaction was stirred for another 60 minutes and was slowly warmed to room temperature. The reaction was monitored by TLC. Upon consumption of compound **73**, the reaction was quenched by the addition of a saturated solution of $NH_4Cl$ in water (300 mL). The reaction mixture extracted with EtOAc (400 mL). Phases were seperated and the aqueous phase was extracted with EtOAc again (2× 100 mL). The combined organic phases were washed with aqueous HCl (1 $\frac{mol}{L}$, 2× 100 mL), a saturated solution of $NaHCO_3$ (2× 100 mL) and brine (2× 100 mL). The organic phase was dried over $Na_2SO_4$ and the solvent was evaporated under reduced pressure. The crude reaction product was purified by DCVC.[318]

Yield: 22.6 g (40.2 mmol, 94%); colorless crystals; **M:** $[C_{26}H_{27}Br_2NO_3]$ 561.3 $\frac{g}{mol}$; **TLC:** $R_f = 0.31$ (heptane/ EtOAc, 4:1); **m.p.:** 131 °C; **opt. rot.:** $[\alpha]_D^{27} = -30.6$ (c = 0.53, MeOH); **HRMS (ESI+):** $\frac{m}{z}$ = 582.0255 (calc. for $MNa^+$: 582.0248). **elem. anal.:** % = C (55.60), H (4.81), Br (n.d.), N (2.31), O (8.76), calc. for $C_{26}H_{27}Br_2NO_3$: C (55.63), H (4.85), Br (28.47), N (2.50), O (8.55).
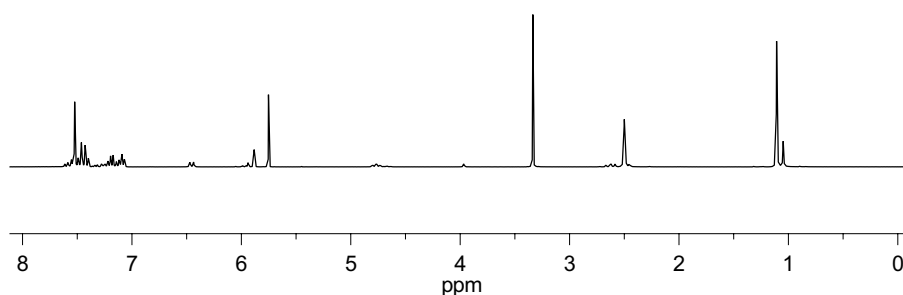


**$^1$H-NMR (300 MHz, DMSO−d$_6$):** $\delta$ [ppm] = 7.57-7.50 (m, 4H, H14A, H15A), 7.47-7.41 (m, 4H, H14B, H15B), 7.20-7.05 (m, 5H, H5, H6, H7), 5.97 (d, 1H, $^3J_{H\text{-}H} = 10.5$ Hz, H8), 5.88 (s, 1H, H12), 4.78 (td, 1H, $^3J_{H\text{-}H} = 10.5, 2.8$ Hz, H2), 2.63 (dd, 1H, $^2J_{H\text{-}H} = 14.1$ Hz, $^3J_{H\text{-}H} = 10.7$ Hz, H3A), 2.48 (dd, 1H, $^2J_{H\text{-}H} = 14.1$ Hz, $^3J_{H\text{-}H} = 2.8$ Hz, H3B), 1.11 (s, 9H, H12).

**¹³C-NMR (75 MHz, CDCl₃):** $\delta$ [ppm] = 155.4 (1C, C9), 146.3, 145.4 (2C, C16), 139.4 (1C, C4), 131.6, 130.9 (2C, C15), 129.5 (2C, C5), 128.6 (2C, C14A), 128.3 (2C, C6), 128.1 (2C, C15B), 126.2 (1C, C7), 120.2, 120.1 (2C, C13), 80.4 (1C, C1), 78.2 (1C, C10), 58.0 (1C, C2), 28.4 (3C, C11), 28.0 (1C, C3).



**IR (KBr):** $\widetilde{\nu}$ [cm⁻¹] = 3404 (s), 3028 (m), 3003 (w), 2978 (w), 2932 (m), 1747 (w), 1672 (s), 1524 (s), 1489 (s), 1454 (m), 1398 (s), 1366 (s), 1250 (s), 1167 (s), 1076 (s), 1049 (m), 1028 (m), 1009 (s), 962 (w), 907 (m), 891 (w), 816 (s), 773 (m), 756 (m), 725 (m), 700 (s), 681 (w), 579 (w), 554 (m), 528 (m), 501 (m).
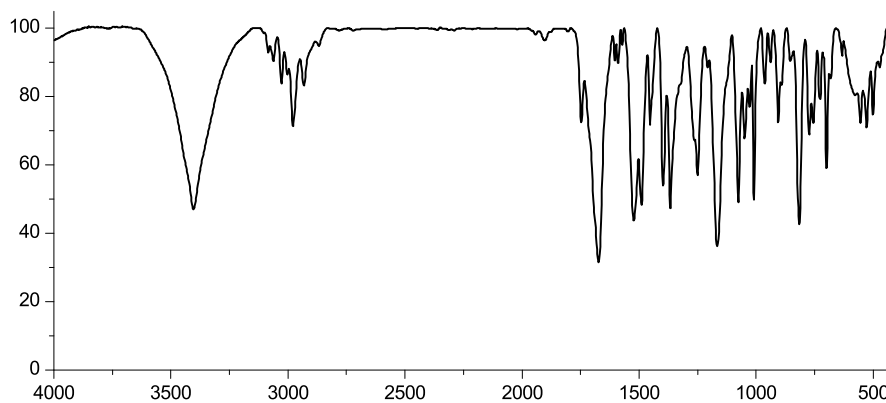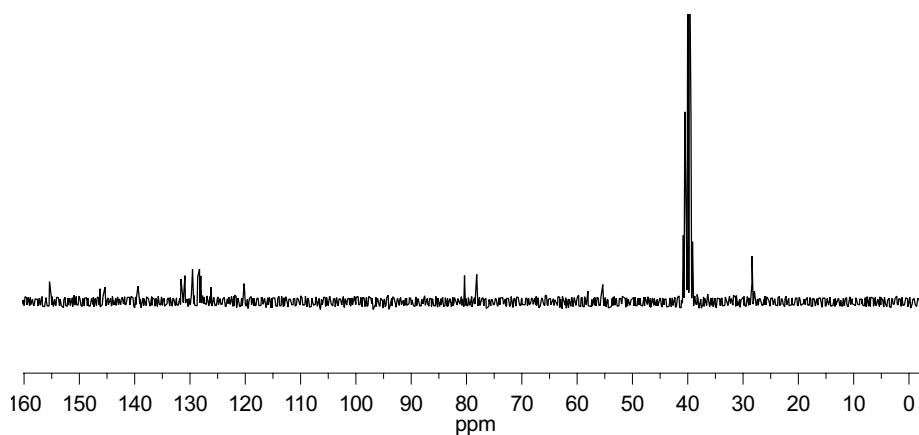
## 4.10   *N*-Benzyl proline methyl ester 93
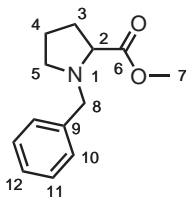


A suspension of proline (20.0 g, 174 mmol, 1 eq.) in methanol (400 mL) was cooled to 0 °C. Acetyl chloride (40.0 mL, 463 mmol, 2.7 eq.) was added over five minutes via syringe. The reaction was allowed to warm to room temperature and was stirred overnight. The solvent was removed by rotary evaporation. The obtained clear oil was used without purification in the next step.

The hydrochloride of the proline methyl ester was suspended in $CH_2Cl_2$ (250 mL) To this suspension $Et_3N$ (57.8 mL, 417 mmol, 2.4 eq.) was added. The resulting precipitate was filtered off and discarded. Benzyl bromide (24.8 mL, 209 mmol, 1.2 eq.) was added to the filtrate and stirred overnight at room temperature. EE (24.8 mL) was added to the reaction mixture, which was then washed wird water (24.8 mL) and brine (24.8 mL). The organic phase was dried over $Na_2SO_4$ and the solvent was evaporated under reduced pressure. The crude reaction product was purified with DCVC.

Yield: 29.8 g (136 mmol, 78%); **M:** $[C_{13}H_{17}NO_2]$ 219.3 $\frac{g}{mol}$; **TLC:** $R_f = 0.31$ (heptane/EtOAc, 4:1); **opt. rot.:** $[\alpha]_D^{26} = 65.6$ (c = 1.0, MeOH); **HRMS (ESI+):** $\frac{m}{z}$ = 220.1397 (calc. for $MH^+$: 220.1338) .
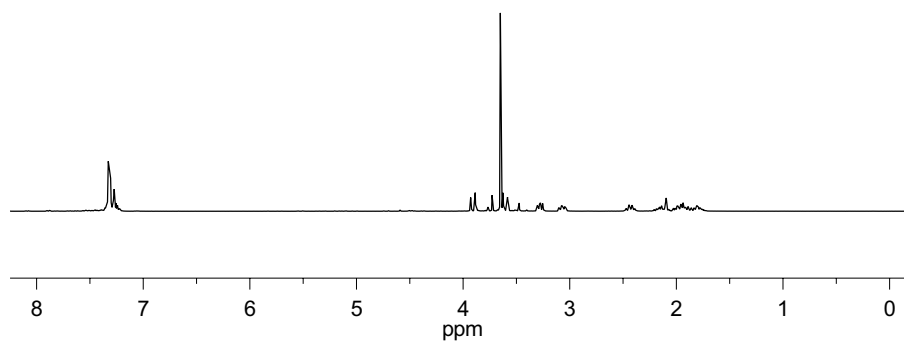
**$^1$H-NMR (300 MHz, CDCl$_3$):** $\delta$ [ppm] = 7.36-7.20 (m, 5H, H10, H11, H12), 3.90 (d, 1H, $^2J_{\text{H-H}}$ = 12.7 Hz, H8A), 3.64 (s, 3H, H7), 3.59 (d, 1H, $^2J_{\text{H-H}}$ = 12.7 Hz H8B), 3.27 (dd, 1H $^3J_{\text{H-H}}$ = 8.8, 6.0 Hz, H2), 3.10-3.01 (m, 1H, H5A), 2.42 (m, 1H, 1H, H5B), 2.22-2.04 (m, 1H, H4A), 2.02-1.71 (m, 3H, H4B, H5).
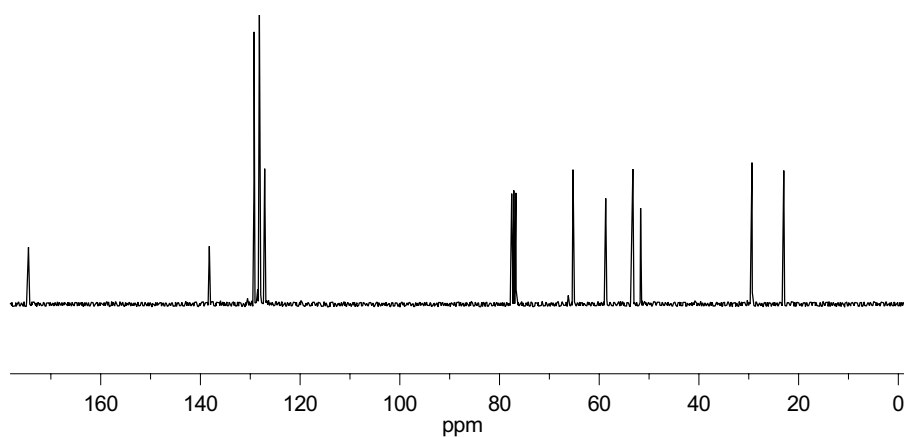


**$^{13}$C-NMR (75 MHz, CDCl$_3$):** $\delta$ [ppm] = 174.49 (1C, C6), 138.21 (1C, C9), 129.24, 128.17 (5C, C10, C11, C12), 127.11 (1C, C12), 65.25 (1C, C7), 58.70 (1C, C8), 53.25 (1C C2), 51.69 (1C, C5), 29.35 (1C, C3), 22.98 (1C, C4).

transmission / %
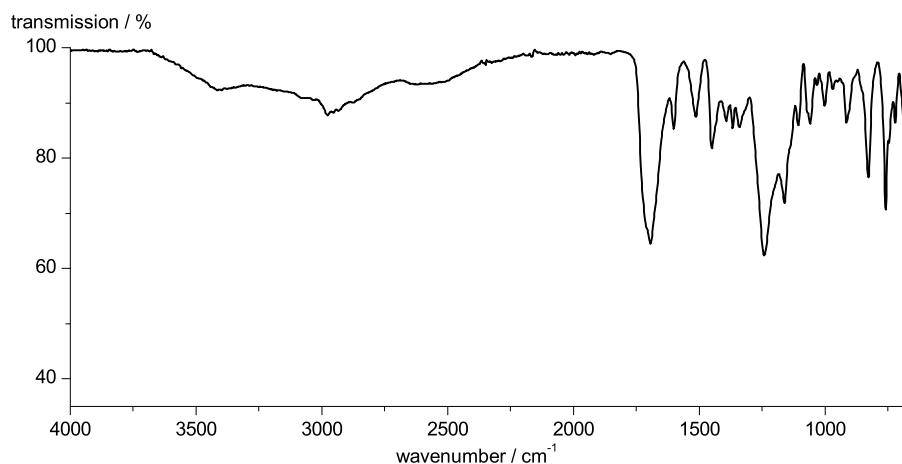


**IR (KBr):** $\widetilde{\nu}$ [cm$^{-1}$] = 3417 (w), 2979 (w), 2952 (w), 1695 (s) 1602 (m), 1510 (m), 1448 (m), 1392 (m), 1369 (m), 1338 (m), 1240 (s), 1161 (m), 1107 (m), 1056 (m), 1000 (m), 914 (m), 821 (m), 757 (s), 671 (m).

## 4.11 1,1-Di(4-bromophenyl)*N*-benzyl prolinol (94)

The reactions were performed oven-dried glassware under argon.

A solution of 1,4-dibromobenzene (36.2 g, 154 mmol, 2.2 eq.) in THF (220 mL) was cooled to −78 °C. A solution of *n*-butyl lithium in hexanes (2.5 $\frac{mol}{L}$, 60 mL, 154 mmol, 2.2 eq.) was added over thirty minutes. The reaction was allowed was stirred for another sixty minutes at −78 °C. To the resulting colorless suspension of 4-bromophenyl lithium a solution of the *N*-protected amino acid methylester **93** (15.7 g, 71.4 mmol, 1 eq.) in THF (15.0 mL) was added dropwise. The reaction was stirred for another 60 minutes and was slowly warmed to room temperature. The reaction was monitored by TLC. Upon consumption of compound **71**, the reaction was quenched by the addition of a saturated solution of NH$_4$Cl in water (500 mL). The reaction mixture extracted with EtOAc (600 mL). Phases were seperated and the aqueous phase was extracted with EtOAc again (2× 150 mL). The combined organic phases were washed with aqueous HCl (1 $\frac{mol}{L}$, 2× 250 mL), a saturated solution of NaHCO$_3$ (2× 250 mL) and brine (2× 250 mL). The organic phase was dried over Na$_2$SO$_4$ and the solvent was evaporated under reduced pressure. The crude reaction product was purified by DCVC.[318]

Yield: 20.3 g (33.8 mmol, 94%); yellow oil; **M:** [$C_{24}H_{23}Br_2NO$] 499.0 $\frac{g}{mol}$; **TLC:** $R_f = 0.49$ (heptane/EtOAc, 4:1); **opt. rot.:** $[\alpha]_D^{27} = 66.6$ (c = 0.74, MeOH);
**HRMS (ESI+):** $\frac{m}{z}$ = 500.0258 (calc. for MH$^+$: 500.0219)
**elem. anal.:** % = C (57.81), H (4.79), Br (n.d.), N (2.61), O (3.61), calc. for $C_{24}H_{23}Br_2NO$: C (57.51), H (4.62), Br (31.88), N (2.79), O (3.19).
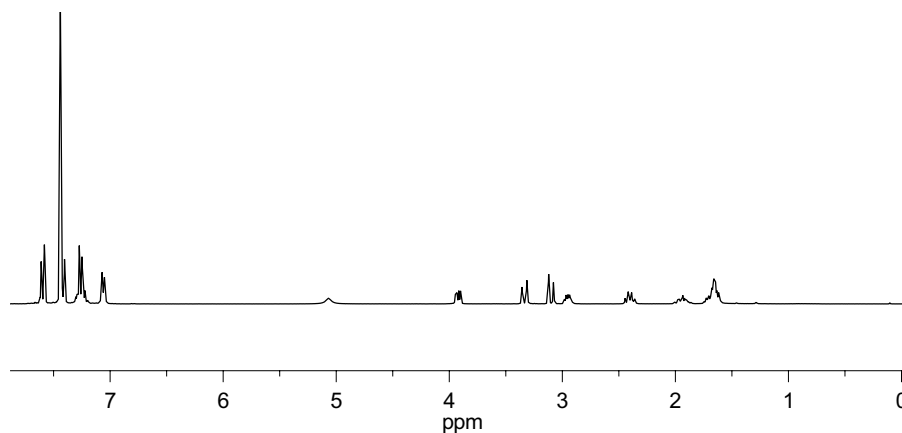


**$^1$H-NMR (300 MHz, CDCl$_3$):** $\delta$ [ppm] = 7.64-7.56 (m, 2H, H14), 7.48-7.38 (m, 6H, H14', H15, H15'), 7.35-7.18 (m, 3H, H10, H12), 7.10-7.02 (m, 2H, H11), 5.07 (s, 1H, H7), 3.92 (dd, 1H, $^3J_{H-H}$ = 9.2, 4.3 Hz, H2), 3.33 (d, 1H, $^2J_{H-H}$ = 12.7 Hz, H8A), 3.10 (d, 1H, $^2J_{H-H}$ = 12.7 Hz, H8B), 2.95 (ddd, 1H $^2J_{H-H}$ = 8.1 Hz, $^3J_{H-H}$ = 4.9, 3.3 Hz H5A), 2.40 (dt, 1H, 1H $^2J_{H-H}$ = 8.1 Hz $^3J_{H-H}$ = 9.5 Hz Hz, H5B), 2.03-1.84 (m, 1H, H3A), 1.77-1.57 (m, 3H, H3B, H4).
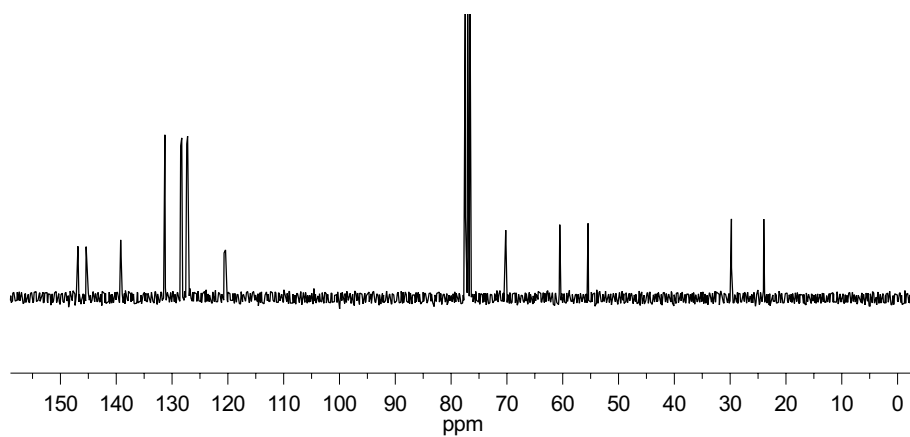
**$^{13}$C-NMR (75 MHz, DMSO$-$d$_6$):** $\delta$ [ppm] = 146.9, 145.4 (2C, C16, C16′), 139.2 (1C, C9), 131.4, 131.3 (2C, C15, C15′), 128.5,128.3 (4C, C10, C11), 127.4, 127.2 (2C, C14, C14′), 127.1 (1C, C12), 120.7, 120.4 (2C, C13, C13′), 70.2 (1C, C2), 60.5 (1C, C8), 55.5 (1C, C5), 29.8 (1C, C3), 24.0 (1C, C4).
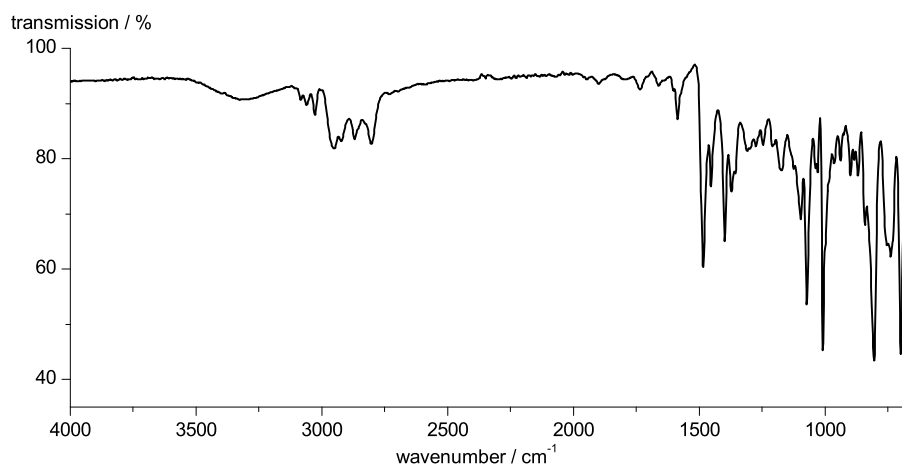


**IR (KBr):** $\widetilde{\nu}$ [cm$^{-1}$] = 3313 (br), 3083 (w), 3062 (w), 3029, (w), 2952 (w), 2921 (w), 2869 (w), 2802 (w), 1587 (w), 1485 (s), 1452 (m), 1398 (m), 1373 (m), 1243 (m), 1178 (m), 1097 (m), 1072 (s), 1008 (s), 840 (m), 804 (s), 698 (s).

## 4.12 4,4-Di(4-bromophenyl)5-isopropyl-oxazolidin-2-one (97)
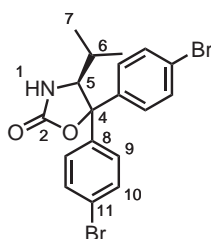


A solution of the *N*-Boc-protected amino alcohol **86** (4.50 g, 8.77 mmol, 1 eq.) in THF (90 mL) was cooled to 0 °C. Potassium *tert*-butoxide (1.18 g, 10.5 mmol, 1.2 eq.) was added. The reaction was allowed allowed to warm to room temperature and was stirred for another three hours. The reaction was monitored by TLC. Upon consumption of compound **86**, the reaction mixture was diluted with EE (250 mL) and extracted with a saturated solution of $NH_4Cl$ in water (100 mL). Phases were seperated and the aqueous phase was extracted with EtOAc again (2× 100 mL) The combined organic phases were washed with brine (2× 100 mL), dried over $Na_2SO_4$ and the solvent was evaporated under reduced pressure.

Yield: 3.81 g (8.73 mmol, quant.); colorless oil (crystallized upon cooling); **M:** [$C_{18}H_{17}Br_2NO_2$] 439.1 $\frac{g}{mol}$; **m.p.:** 119 °C; **TLC:** $R_f = 0.56$ (heptane/EtoAC, 1:1); **opt. rot.:** $[\alpha]_D^{27} = -137.0$ (c = 0.70, MeOH); **HRMS (ESI+):** $\frac{m}{z} = 459.9524$ (calc. for MNa$^+$: 459.9513); **elem. anal.:** % = C (50.31), H (4.22), Br (n.d.), N (2.80), O (9.07) calc. for $C_{18}H_{17}Br_2NO_2$: C (49.23), H (3.90), Br (36.39), O (7.29).
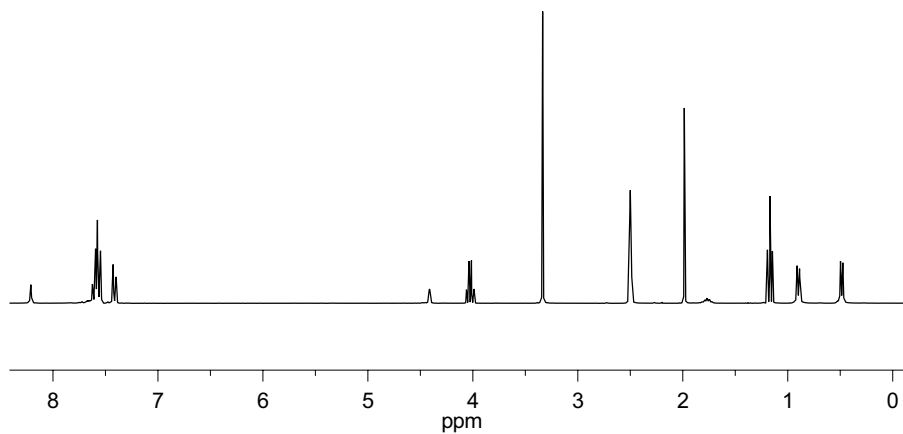
**$^{1}$H-NMR (300 MHz, CDCl$_3$):** $\delta$ [ppm] = 8.21 (s, 1H, H1), 7.68-7.38 (m, 8H, H9, H9', H10, H10'), 4.41 (dd, 1H, $^{3}J_{\text{H-H}}$ = 2.2, 1.0 Hz, H5), 1.83-1.70 (m, 1H, H6), 0.90 (d, 3H, $^{3}J_{\text{H-H}}$ = 6.9 Hz, H6A), 0.49 (d, 3H; $^{3}J_{\text{H-H}}$ = 6.6 Hz, H6B).
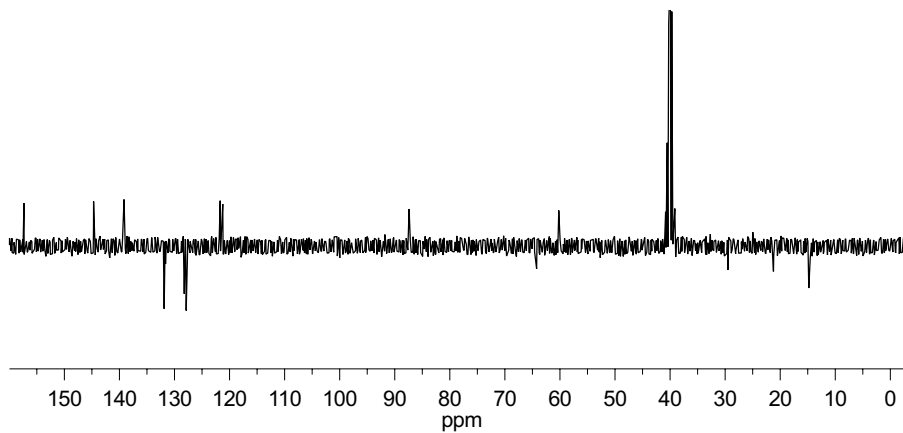


**$^{13}$C-NMR (75 MHz, CDCl$_3$):** $\delta$ [ppm] = 157.3 (1C, C2), 144.7, 139.2 (2C; C11, C11'), 131.9, 131.6 (4C, C10, C10'), 128.9, 128.2 (4C, C9, C9'), 121.7, 121.2 (2C, C8, C8'), 87.4 (1C, C4), 60.2 (1C; C5), 29.5 (1C, C6), 21.2 (1C, C6A ), 14.8 (1C, C6B ).
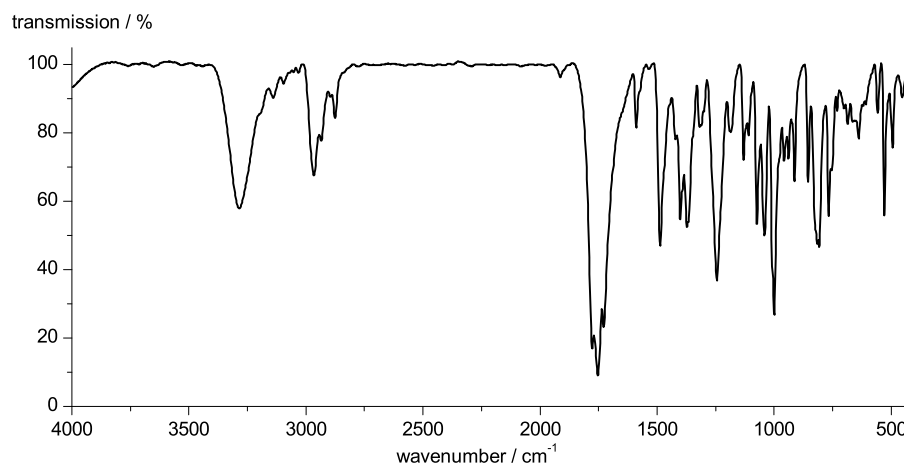
**IR (KBr):** $\widetilde{\nu}$ [cm$^{-1}$] = 2955 (m), 1767 (s), 1726 (s), 1601 (m), 1514 (w), 1448 (m), 1435 (m), 1396 (m), 1379 (m), 1344 (m), 1246 (s), 1196 (m), 1132 (m), 1109 (w), 1090 (w), 1072 (m), 1059 (w), 1026 (w), 999 (m), 962 (m), 930 (w), 910 (w), 833 (m), 756 (s), 733 (m), 719 (m), 704 (m), 683 (m), 646 (w), 635 (w), 606 (w), 523 (w).

## 4.13   4,4-Di(4-bromophenyl)5-benzyl-oxazolidin-2-one (98)
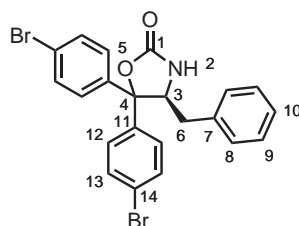


A solution of the *N*-Boc-protected amino alcohol **88** (4.34 g, 7.73 mmol, 1 eq.) in THF (80 mL) was cooled to 0 °C. Potassium *tert*-butoxide (1.06 g, 9.41 mmol, 1.2 eq.) was added. The reaction was allowed allowed to warm to room temperature and was stirred for another three hours. The reaction was monitored by TLC. Upon consumption of compound **88**, the reaction mixture was diluted with EE (250 mL) and extracted with a saturated solution of NH$_4$Cl in water (100 mL).

Phases were separated and the aqueous phase was extracted with EtOAc again ($2\times 100\,\text{mL}$) The combined organic phases were washed with brine ($2\times 100\,\text{mL}$), dried over $Na_2SO_4$ and the solvent was evaporated under reduced pressure.

Yield: 3.61 g (7.41 mmol, 96 %); colorless solid; **M:** $[C_{22}H_{17}Br_2NO_2]$ 487.2 $\frac{\text{g}}{\text{mol}}$; **m.p.:** 244 °C; **TLC:** $R_f = 0.39$ (heptane/EtOAC, 4:1); **opt. rot.:** $[\alpha]_D^{27} = -127.5$ (c = 0.50, MeOH); **HRMS (ESI+):** $\frac{m}{z}$ = 507.9512 (calc. for MNa$^+$: 507.9524); **elem. anal.:** % = C (55.50), H (3.60), Br (n.d.), N (2.88), O (6.75) calc. for $C_{22}H_{17}Br_2NO_2$: C (54.24), H (3.52), Br (24.05), O (6.57).
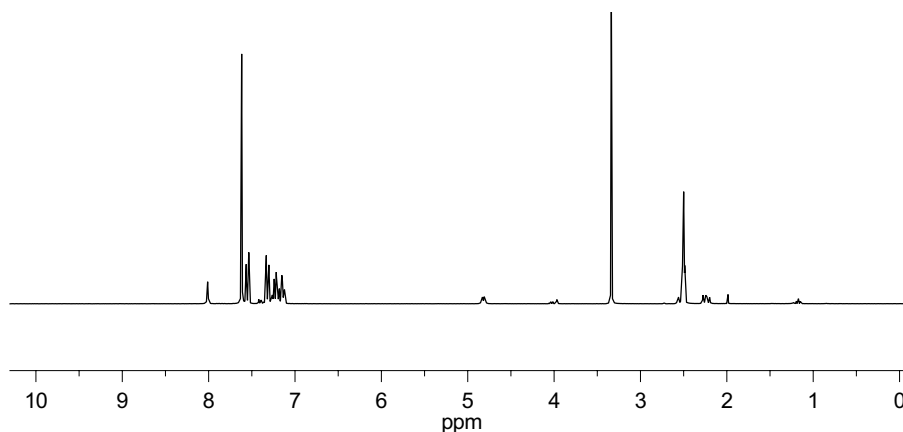


**$^1$H-NMR (300 MHz, DMSO$-$d$_6$):** $\delta$ [ppm] = 8.01 (s, 1H, H4), 7.65-7.10 (m, 13H, H7, H8, H9, H11, H12), 4.82, (ddd, 1H, $^3J_{\text{H-H}} = 9.8, 4.2, 1.3$ Hz, H3), 2.54 (dd, 1H, $^2J_{\text{H-H}} = 13.5$ Hz, $^3J_{\text{H-H}} = 4.1$ Hz, H6A), 2.24 (dd, 1H, $^2J_{\text{H-H}} = 13.7$ Hz, $^3J_{\text{H-H}} = 9.8$ Hz, H6B).

**¹³C-NMR (75 MHz, DMSO−d₆):** $\delta$ [ppm] =
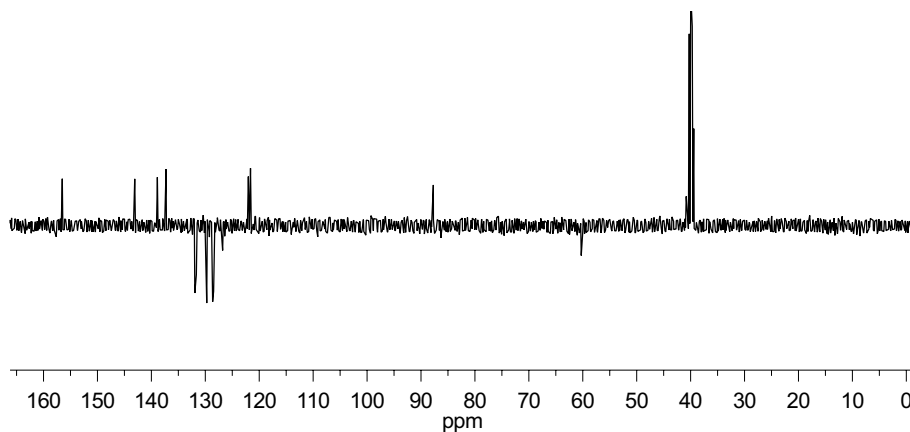
156.5 (1C, C1), 143.1 (1C, C15A), 138.9 (1C, C14B), 137.3 (1C, C7), 131.9 (2C, C13A), 131.7 (2C, C13B), 129.7 (2C, C8), 128.6 (2C, C12A), 128.6 (2C, C9), 128.5 (2C, C12B), 126.8 (1C, C10), 122.0 (1C, C11A), 121.6 (1C, C11B), 87.7 (1C, C4), 60.3 (1C, C3), 39.2 (1C, C6).
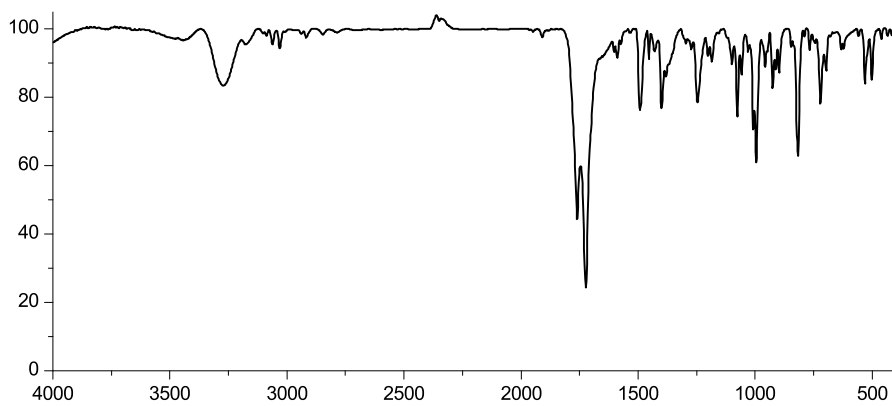


**IR (KBr):** $\widetilde{\nu}$ = 3271 (m), 1761 (m), 1722 (s), 1651 (w), 1589 (w), 1493 (s), 1454 (w), 1400 (s), 1381 (m), 1367 (m), 1246 (s), 1202 (w), 1184 (w), 1099 (m), 1076 (s), 1057 (m), 1009 (s), 995 (s), 957 (m), 926 (m), 912 (m), 897 (m), 816 (s), 721 (s), 696 (m), 530 (m), 501 (m).

253

## 4.14   1,1-Di-(4'-carboxybiphenyl)*N-tert*-butyloxycarbonyl-alaninol (99)
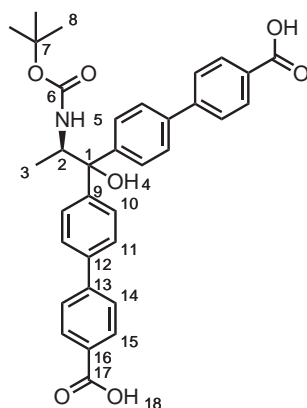


The reaction was performed in oven-dried glassware under argon. Solvents were degassed by three freeze-pump-thaw cycles prior to use. To a suspension of the bis-arylated amino acid derivative **85** (1.00 g, 2.07 mmol, 1 eq.), 4-carboxyphenyl boronic acid **180** (1.07 g, 12.0 mmol, 3.1 eq.) and sodium carbonate (Na$_2$CO$_3$, 1.77 g, 5.38 mmol, 2.6 eq.) in water (50 mL) and DMF (50 mL) was added tetrakis(triphenylphosphine)palladium ([Pd(PPh$_3$)$_4$], 161 mg, 0.103 mmol, 0.05 eq.). The reaction was heated to reflux for four hours and was monitored by TLC. Upon consumption of compound **86**, the reaction mixture was allowed to cool to room temperature. The reaction mixture was filtered over celite. The filtrate was diluted with water (200 mL) and concentrated hydrochloric acid was added until pH 5 was reached. This resulted in the precipitation of the dicarboxylic acid as a white solid. The reaction product was filtered, washed with water and dried in vacuum.

Yield: 0.81 g (1.43 mmol, 62 %); white powder; **TLC:** $R_f = 0.00$
(heptane/EtOAc, 1:1); **HRMS (ESI+):** $\frac{m}{z}$ = 590.2153 (calc. for MNa$^+$: 590.2155).

254
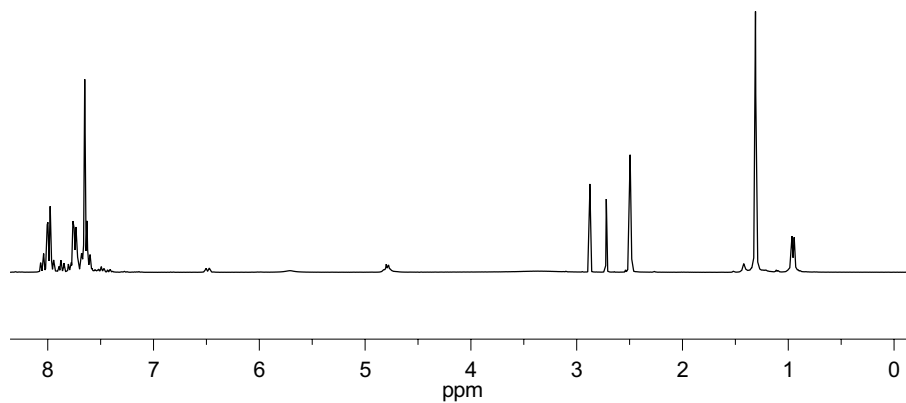
**$^1$H-NMR (300 MHz, DMSO−d$_6$):** $\delta$ [ppm] = 8.03-7.95 (m, 4H, H15), 7.77-7.71 (m, 4H, H14), 7.69-7.59 (m, 8H, H10, H11), 6.49 (d, 1H, $^3J_{\text{H-H}}$ = 9.5 Hz, H5), 4.88-4.73 (m, 1H, H2), 1.31 (s, 9H, H8), 0.95 (d, 3H, $^3J_{\text{H-H}}$ = 6.4 Hz, H3).
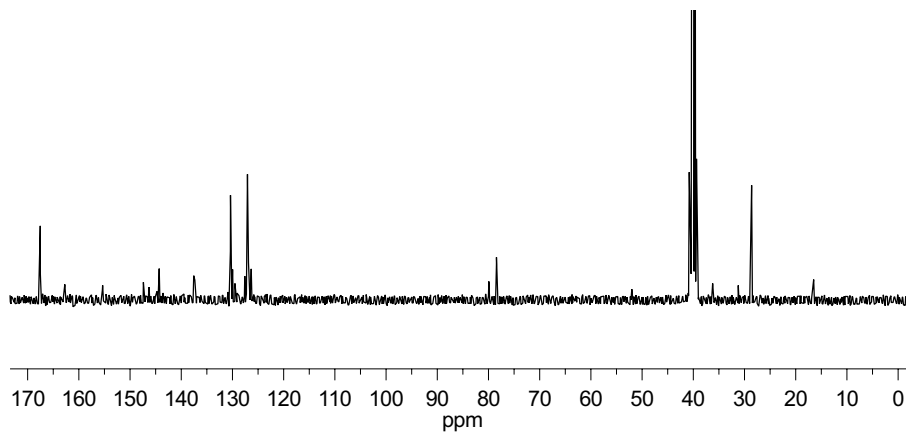


**$^{13}$C-NMR (75 MHz, DMSO−d$_6$):** $\delta$ [ppm] = 167.4 (2C, C17), 155.5 (1C, C6), 147.4, 146.4, 144.3, 144.2 (4C, C9, C12), 143.5 (1C, C4), 137.5, 137.4 (2C, C13), 132.0, 131.9 (2C, C16), 130.5, 130.4 (8C, C14, C15), 129.6, 129.5, 128.3 (3C, C5, C7), 127.6, 127.1, 127.0, 126.4 (8C, C10, C11), 126.1 (2C, C6), 80.7 (1C, C1), 78.1 (1C, C7), 58.4 (1C, C2), 29.8 (1C, C3), 28.4 (3C, C8).
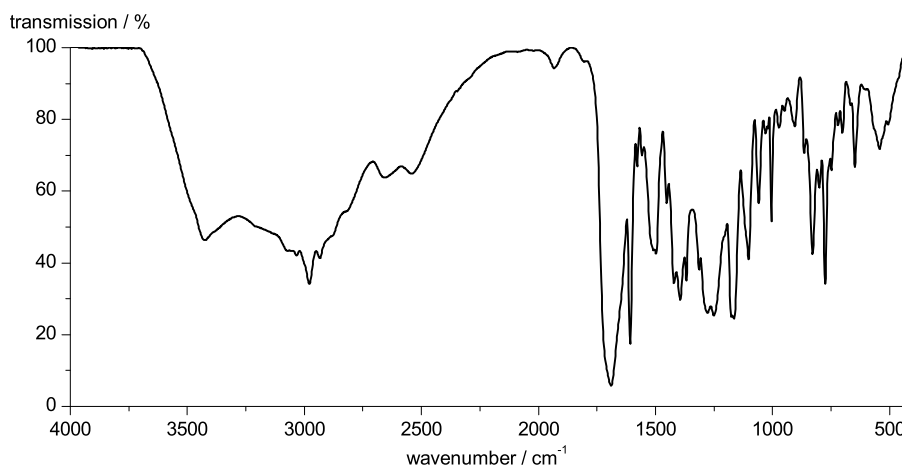
**IR (KBr):** $\tilde{\nu}$ = 3424 (m), 3033 (m), 2978 (m), 2934 (m), 2656 (w), 1689 (s), 1608 (s), 1497 (m), 1452 (m), 1421 (m), 1394 (m), 1368 (m), 1250 (m), 1164 (m), 1102 (m) 1059 (w), 829 (m), 775 (m).

## 4.15 1,1-Di-(4'-carboxybiphenyl)*N-tert*-butyloxycarbonyl-valinol (100)
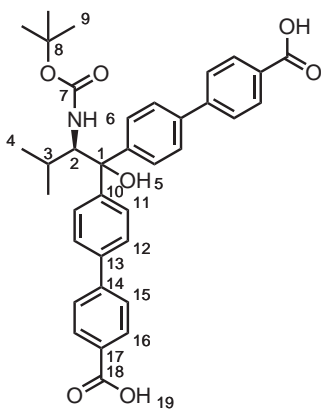
The reaction was performed oven-dried glassware under argon. Solvents were degassed by three freeze-pump-thaw cycles prior to use. To a suspension of the bis-arylated amino acid derivative **86** (2.00 g, 3.61 mmol, 1 eq.), 4-carboxyphenyl boronic acid **180** (1.85 g, 11.211 mmol, 3.1 eq.) and sodium carbonate ($Na_2CO_3$, 1.18 g, 9.40 mmol, 2.6 eq.) in water (100 mL) and DMF (100 mL) was added tetrakis(triphenylphosphine)palladium ([Pd(PPh$_3$)$_4$], 303 mg, 0.179 mmol, 0.05 eq.).

The reaction was heated to reflux for four hours and was monitored by TLC. Upon consumption of compound **86**, the reaction mixture was allowed to cool to room temperature. The reaction mixture was filtered over celite. The filtrate was diluted with water (100 mL) and concentrated hydrochloric acid was added until pH 5 was reached. This resulted in the precipitation of the dicarboxylic acid as a white solid. The reaction product was filtered, washed with water and dried in vacuum.

Yield: 1.50 g (2.46 mmol, 63 %); white powder; **M:** [$C_{36}H_{37}NO_7$] 595.7 $\frac{g}{mol}$; **TLC:** $R_f = 0.00$ (heptane/EtOAc, 1:1); **HRMS (ESI+):** $\frac{m}{z} = 618.2474$ (calc. for MNa$^+$: 618.2468);
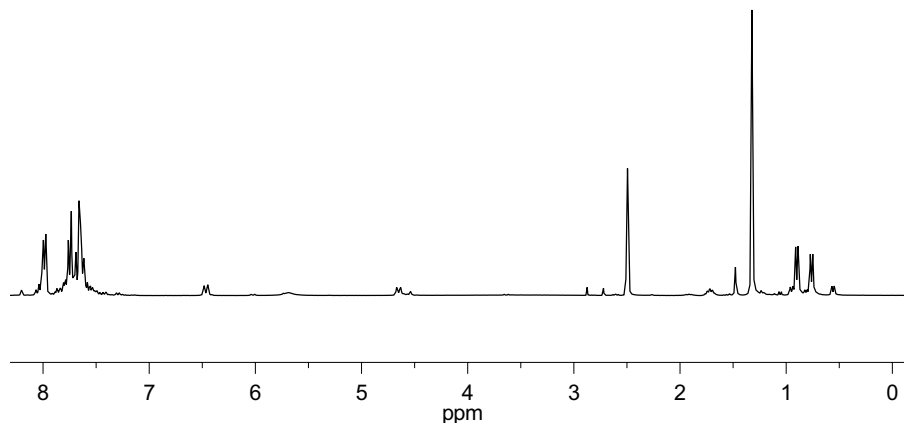


**$^1$H-NMR (300 MHz, DMSO$-$d$_6$):** $\delta$ [ppm] = 8.02-7.95 (m, 4H. H16), 7.78-7.74 (m, 4H, H15), 7.72-7.60 (m, 8H, H11, H12), 6.47 (d, 1H, $^3J_{H\text{-}H} = 10.1$ Hz, H6), 4.65 (dd, 1H, $^3J_{H\text{-}H} = 10.1, 2.2$ Hz, H2), 1.77-1.66 (m, 1H, H3), 1.32 (s, 9H, H9), 0.90 (d, 3H, $^3J_{H\text{-}H} = 6.7$ Hz, H4A), 0.76 (d, 3H, $^3J_{H\text{-}H} = 6.9$ Hz, H4B).
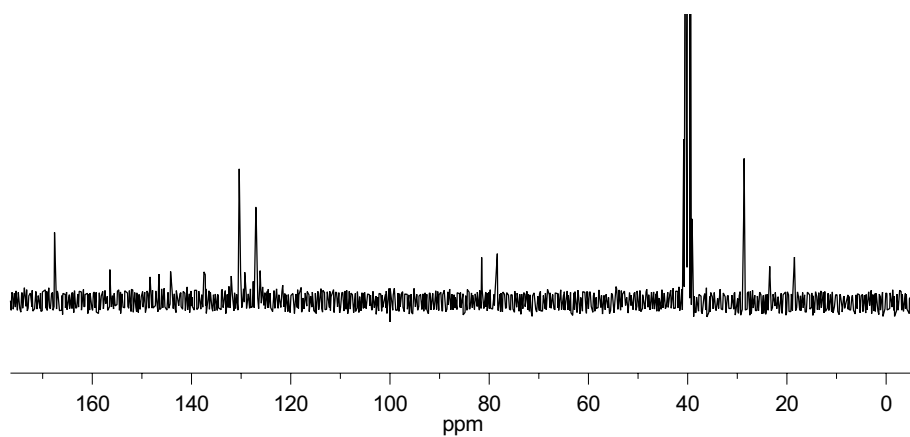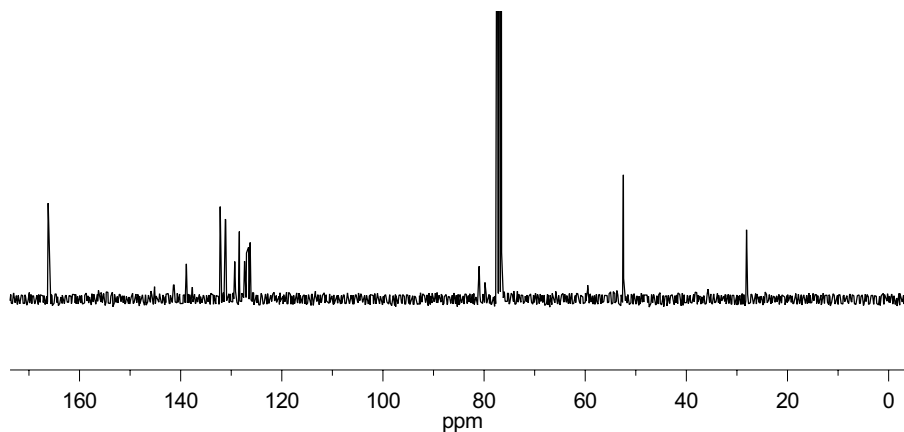
**$^{13}$C-NMR (75 MHz, DMSO$-$d$_6$):** $\delta$ [ppm] = 167.6 (2C, C18), 156.4 (1C, C7), 148.4, 146.6, 144.3, 144.2 (4C, C10, C13), 137.5, 137.2 (2C, C14), 132.0, 131.9 (2C, C17), 130.4, 130.3 (8C, C15, C16), 127.1, 127.0, 126.9, 126.8 (8C, C11, C12); 81.5 (1C, C8), 78.4 (1C, C1), 57.9 (1C, C2), 28.8 (1C, C3), 28.6 (3C, C9), 23.46, 18.48 (2C, C4).
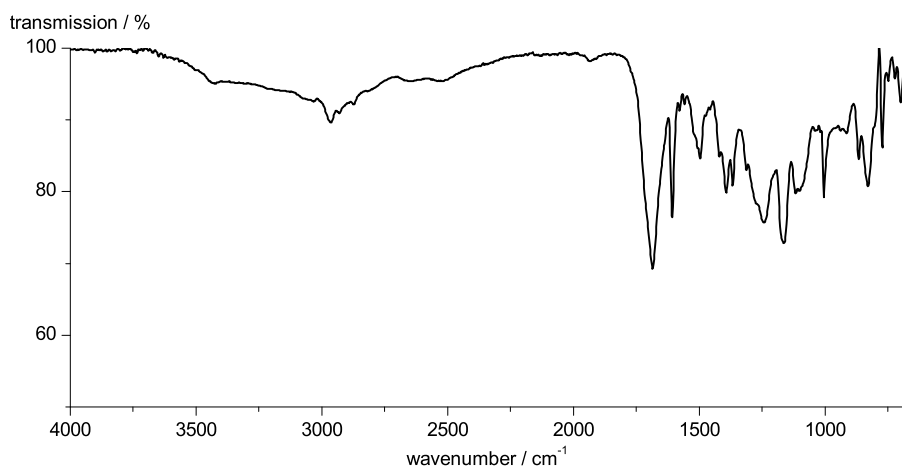


**IR (ATR):** $\widetilde{\nu}$ = 2964 (w), 2931 (w) 2874 (w), 1685 (s), 1607 (s), 1577 (m), 1558 (m), 1495 (m), 1419 (m), 1392 (m), 1366 (m), 1243 (s), 1163 (s), 1004 (s), 865 (m), 829 (m), 747 (m), 697 (m).

## 4.16   1,1-Di-(4'-carboxybiphenyl)*N-tert*-butyloxycarb-onyl-phenylalaninol (99)
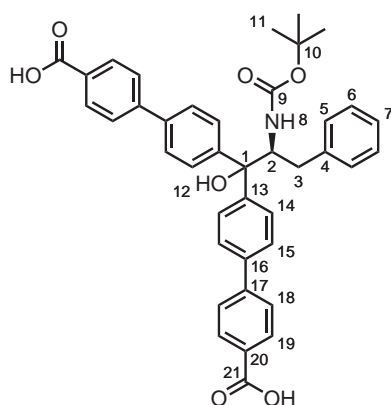


The reaction was performed in oven-dried glassware under argon. Solvents were degassed by three freeze-pump-thaw cycles prior to use. To a suspension of the bis-arylated amino acid derivative **88** (1.00 g, 1.78 mmol, 1 eq.), 4-carboxyphenyl boronic acid **180** (0.92 g, 5.52 mmol, 3.1 eq.) and sodium carbonate ($Na_2CO_3$, 1.53 g, 4.63 mmol, 2.6 eq.) in water (50 mL) and DMF (50 mL) was added tetrakis(triphenylphosphine)palladium ([$Pd(PPh_3)_4$], 138 mg, 0.089 mmol, 0.05 eq.).

The reaction was heated to reflux for four hours and was monitored by TLC. Upon consumption of compound **86**, the reaction mixture was allowed to cool to room temperature. The reaction mixture was filtered over celite. The filtrate was diluted with water (200 mL) and concentrated hydrochloric acid was added until pH 5 was reached. This resulted in the precipitation of the dicarboxylic acid as a white solid. The reaction product was filtered, washed with water and dried in vacuum.

Yield: 0.80 g (1.43 mmol, 70 %); white powder; **TLC:** $R_f = 0.00$ (heptane/EtOAc, 1:1); **HRMS (ESI+):** $\frac{m}{z} = 666.2448$ (calc. for MNa$^+$: 666.2468);
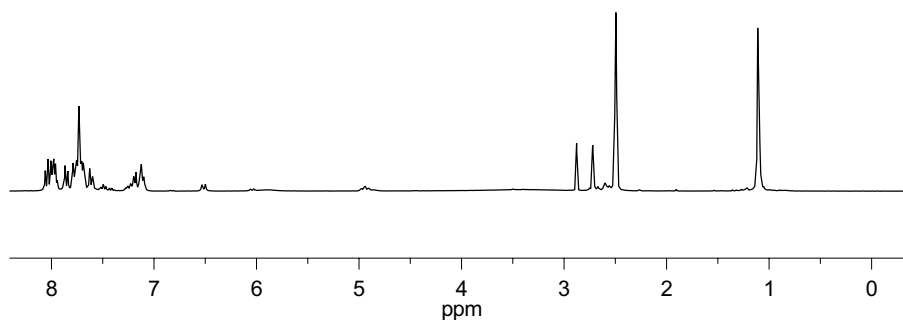
**¹H-NMR (300 MHz, DMSO−d₆):** $\delta$ [ppm] =1H NMR 8.11-7.83 (m, 8H, H18, H19), 7.82 âĂŞ 7.58 (m, 8H, H14, H15), 7.30 âĂŞ 7.04 (m, 5H; H5, H6, H7), 6.52 (d, $^3J_{H-H}$ = 10.2 Hz, H8), 5.00-4.88 (m, 1H, H2), 2.68 âĂŞ 2.53 (m, 2H, H3), 1.11 (s, 9H, H11).
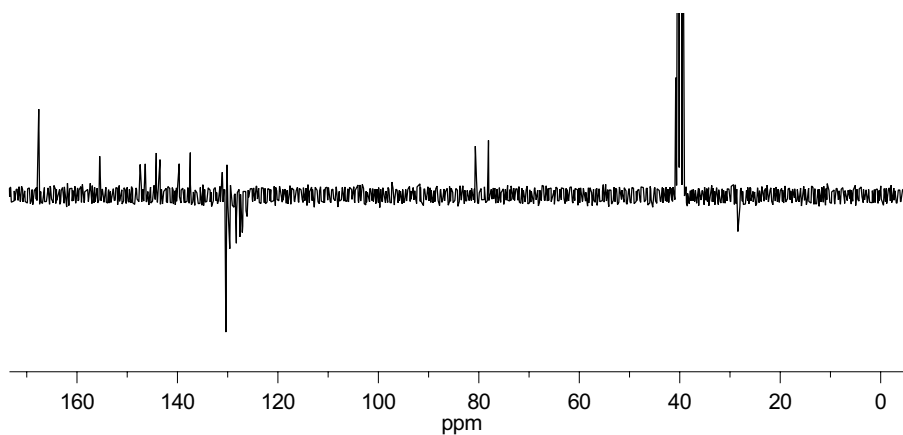


**¹³C-NMR (75 MHz, DMSO−d₆):** $\delta$ [ppm] = 167.5 (2C, C21), 155.4 (1C, C9), 147.4, 146.3, 144.4, 144.3 (4C, C13, C16), 137.5, 137.4 (2C, C17), 132.0, 131.9 (2C, C20), 130.4, 130.3 (8C, C18, C19), 127.2, 127.1, 127.0, 126.9 (8C, C14, C15), 79.9 (1C, C1), 78.4 (1C, C9), 52.0 (1C, C2), 28.6 (3C, C10).
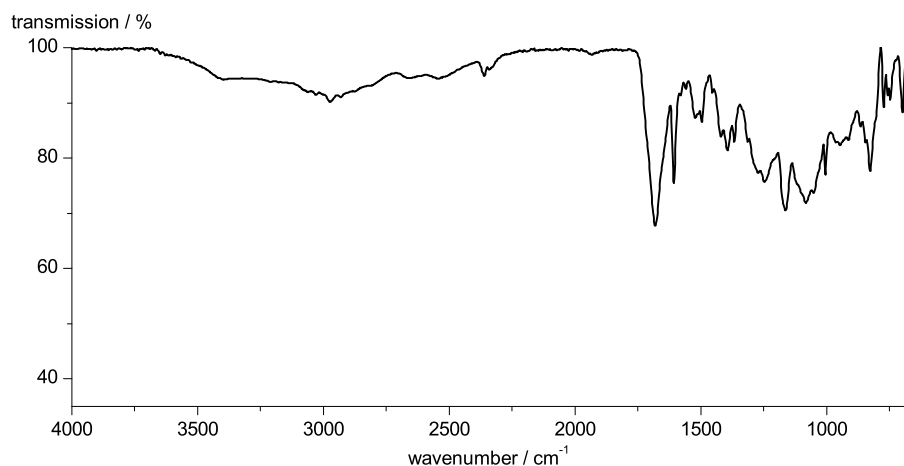
**IR (ATR):** $\widetilde{\nu}$ = 3029 (w), 1974 (w), 1930 (w), 2544 (w), 2360 (w), 2342 (w), 1681 (s), 1607 (m), 1579 (w), 1521 (m), 1495 (m), 1163 (m), 865 (w), 845 (w), 826 (m), 697 (m).

## 4.17   *O,O*-dimethyl-3',5'-dicarboxy-1-iodo-benzene (109)
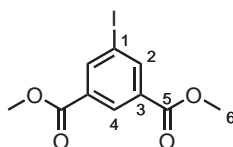


The reaction described here is an upscaled version of a procedure developed by König and Mazik.[319] A suspension of 1-amino-*O,O*-dimethyl-3',5'-dicarb-oxybenzene (**181**, 40.0 g, 95.6 mmol, 1 eq.) in hydrochloric acid (6.2 $\frac{mol}{L}$, 120 mL) was cooled to $-5\,°C$. Solutions of $NaNO_2$ (13.20 g, 191.4 mmol, 1 eq.) in water (400 mL) and KI (128.1 g, 772 mmol, 4 eq.) in water (300 mL) were prepared and cooled to $4\,°C$. The solution of $NaNO_2$ was added dropwise over the course of 20 minutes maintaining the reaction temperature. Then ice-cold toluene (400 mL) was added in one portion, before the solution of KI was added dropwise. he reaction mixture was stirred for 18 hours and was allowed to warm to room temperature and was then heated to reflux for one hour. Phases were separated

and the aqueous phase was extracted with toluene (2× 100 mL). The combined organic phases were dried over $Na_2SO_4$ and the solvent was evaporated in vacuum. The reaction product was recrystallized three times from methanol.

Yield: 33.6 g (105 mmol, 55%); light-yellow solid; **M:** [$C_{10}H_9IO$] 238.0 $\frac{g}{mol}$; **TLC:** $R_f = 0.49$ (heptane/EtOAc, 4:1); **m.p.:** 108 °C; **HRMS (ESI+):** $\frac{m}{z}$ = 320.9624 (calc. for MH$^+$: 320.9624); **elem. anal.:** % = C (39.31), H (3.08), I (n.d.), O (n.d.) calc. for $C_{10}H_{11}BO_6$: C (37.52), H (2.8), I (39.65), O (19.99).
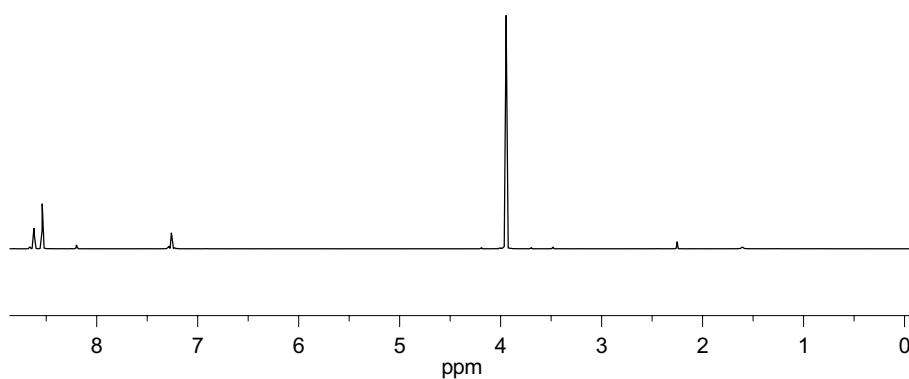


**$^1$H-NMR (300 MHz, DMSO−d$_6$):** $\delta$ [ppm] = 8.62 (d, 2H, $^4J_{H-H}$ = 1.6 Hz, H2), 8.54 (d, 1H; $^4J_{H-H}$ = 1.5 Hz, H4), 3.94 (s, 6H; H6)
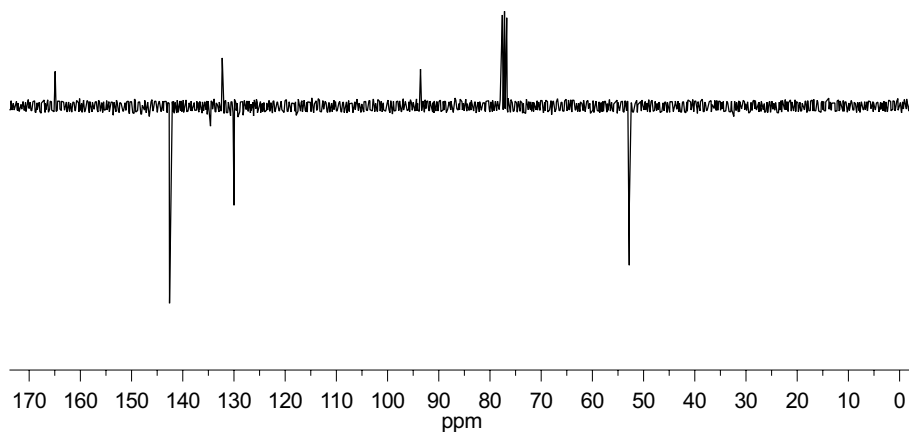
**$^{13}$C-NMR (75 MHz, CDCl$_3$):** $\delta$ [ppm] = 164.9 (2C, C5), 142.6 (2C, C2), 132.3 (2C, C3), 130.0 (1C, C4), 93.6 (1C, C1), 52.8 (2C, C6).
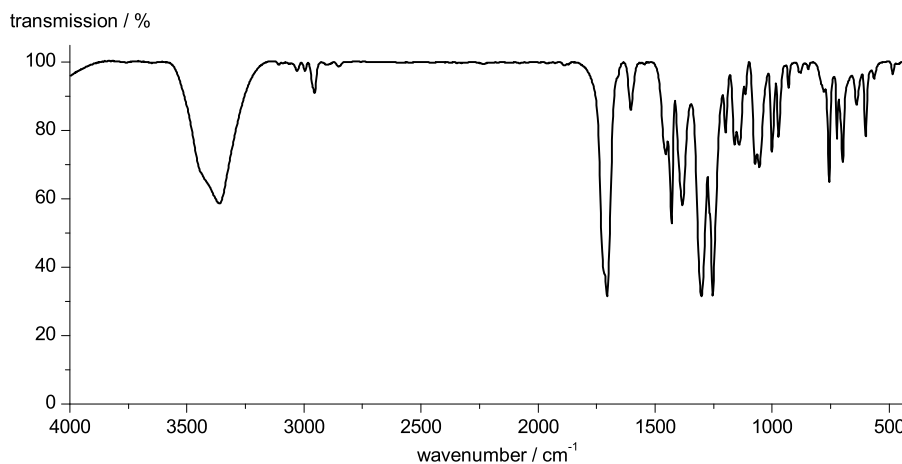


**IR (KBr):** $\widetilde{\nu}$ [cm$^{-1}$] = 3418 (w), 3084 (w), 3061 (w), 3005 (w), 2951 (m), 1854 (w), 1817 (w), 1717 (s), 1601 (w), 1570 (m), 1530 (w), 1439 (s), 1427 (m), 1421 (m), 1294 (s), 1246 (s), 1192 (m), 1136 (m), 1101 (m), 995 (m), 964 (m), 930 (w), 895 (w), 870 (w), 824 (w), 746 (s), 716 (m), 660 (w), 486 (w), 467 (w).

## 4.18 (*O,O*-dimethyl-3′,5′-dicarboxyphenyl) boronic acid (112)
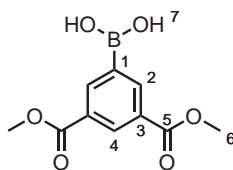


The reaction was performed oven-dried glassware under argon. A solution of the iodide **109** (8.3 g, 26 mmol, 1 eq.) in THF (80 mL) was cooled to $-20\,^\circ$C. To this solution was added the lithium chloride adduct of isopropyl magnesium chloride in THF ($i-$PrMgCl $\cdot$ LiCl, 1.3 $\frac{\text{mol}}{\text{L}}$, 30 mL, 39 mmol, 1.5 eq.). The organo

magnesium reagent was added dropwise over the course of 15 minutes. The reaction was stirred for another 60 minutes at $-20\,°C$ and was then cooled to $-78\,°C$. Trimethyl borate (16.0 mL, 144 mmol, 5.5 eq.) was added over the course of ten minutes at the same temperature, resulting in an orange precipitate which required vigorous stirring. The reaction mixture was stirred for 18 hours and was allowed to warm to room temperature. Hydrochloric acid (5 $\frac{mol}{L}$) was added until the precipitate was dissolved. The reaction mixture was concentrated in vacuum. Hydrochloric acid (1 $\frac{mol}{L}$, 100 mL) was added to the residue, the suspension was stirred at room temperature for 60 minutes and then filtered. The solid residue was washed with water ($3\times$ 20 mL), $CH_2Cl_2$ ($3\times$ 20 mL) and dried in vacuum.

Yield: 5.5 g (23 mmol, 88%); colorless solid; **M:** $[C_{10}H_{11}BO_6]$ 238.0 $\frac{g}{mol}$; **m.p.:** 322 °C; **HRMS (ESI+):** $\frac{m}{z}$ = 239.0727 (calc. for $MH^+$: 239.0731); **elem. anal.:** % = C (50.57), H (4.73), B (n.d.), O (36.21) calc. for $C_{10}H_{11}BO_6$: C (50.46), H (4.66), B (4.54), O (40.33).
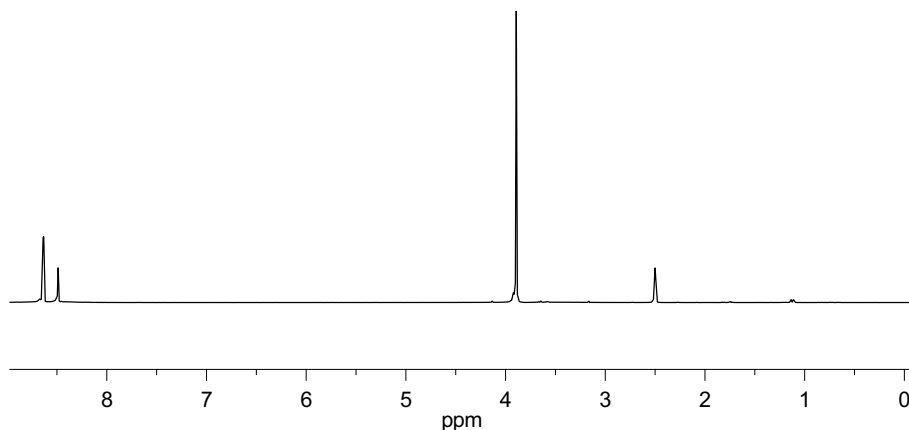


**$^1$H-NMR (300 MHz, DMSO$-$d$_6$):** $\delta$ [ppm] = 8.64 (d, 2H, $^4J_{\text{H-H}}$ = 1.8 Hz, H2), 8.49 (d, 1H; $^4J_{\text{H-H}}$ = 1.8 Hz, H4), 3.89 (s, 6H; H6)
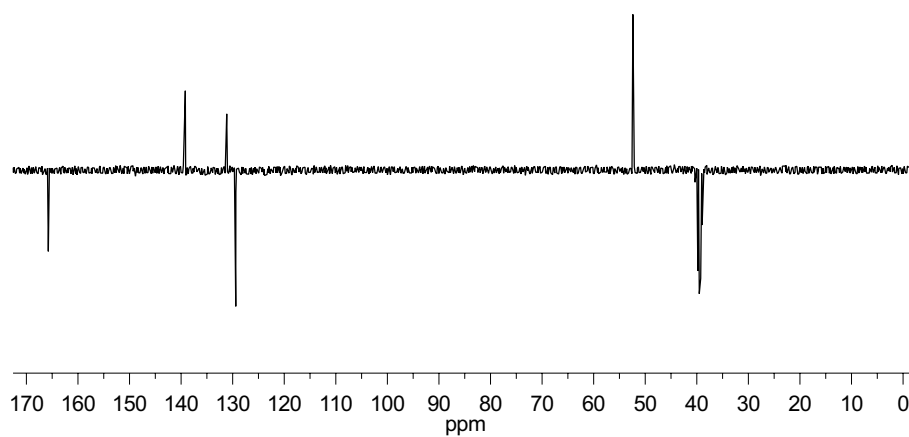
**$^{13}$C-NMR (75 MHz, CDCl$_3$):** $\delta$ [ppm] = 165.7 (2C, C5), 139.2 (2C, C2), 131.2 (1C, C4), 129.4 (2C, C3), 52.4 (2C, C6).
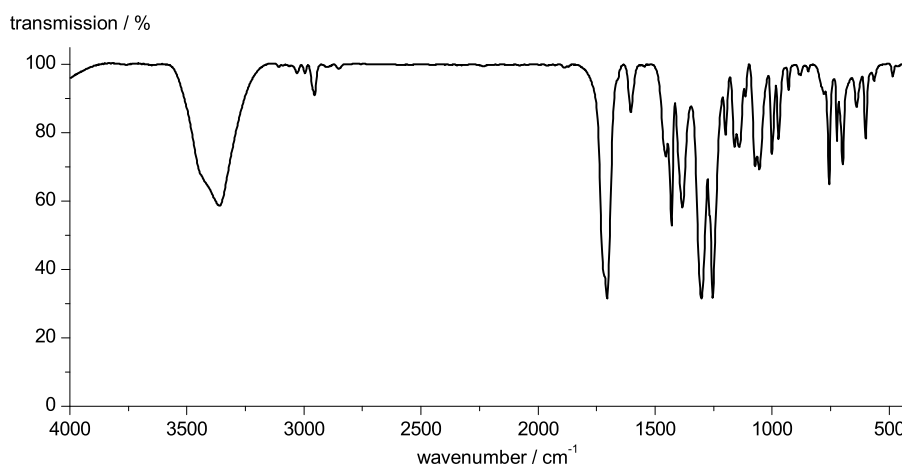


**IR (KBr):** $\widetilde{\nu}$ [cm$^{-1}$] = 3362 (m), 2955 (w), 1705 (s), 1603 (w), 1454 (w), 1429 (m), 1383 (m), 1302 (s), 1254 (s), 1200 (w), 1161 (m), 1142 (m), 1115 (w), 1072 (m), 1055 (m), 1001 (m), 972 (m), 930 (w), 777 (w), 756 (m), 723 (m), 698 (m), 638 (w), 600 (m).

## 4.19 Di-(O,O-dimethyl-3′,5′-dicarboxybiphenyl)-*N*-*tert*-butyloxycarbonyl-alaninol (113)
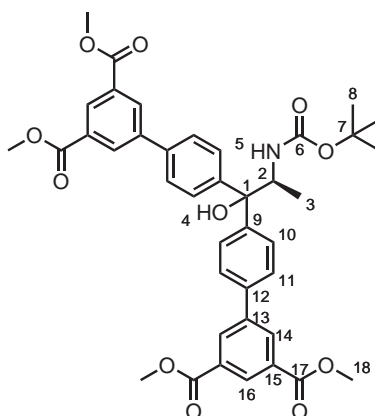


The reaction was performed oven-dried glassware under argon. Solvents were degassed by three freeze-pump-thaw cycles prior to use. To a suspension of the bis-arylated amino acid derivative **85** (3.00 g, 6.21 mmol, 1 eq.), *O,O′*-dimethyl-isopthalic boronic acid **112** (4.44 g, 18.6 mmol, 3.0 eq.) and cesium carbonate (Cs$_2$CO$_3$, 6.06 g, 18.6 mmol, 3.0 eq.) in MeOH (100 mL) and DMF (25 mL) were added tetrakis(triphenylphosphine)palladium ([Pd(PPh$_3$)$_4$], 483 mg, 0.31 mmol, 0.05 eq.) and SPhos (127 mg, 0.31 mmol, 0.05 eq.). The reaction was heated to reflux for four hours and was monitored by TLC. Upon consumption of compound **85**, the reaction mixture was allowed to cool to room temperature. The reaction mixture was concentrated in vaccum to remove most of the MeOH and DMF. The residue was diluted in a mixture of EtOAc (400 mL) and water (200 mL). The organic phase was separated and washed with a saturated solution of NaHCO$_3$ (2× 100 mL) and brine (2× 100 mL). The organic phase was dried over Na$_2$SO$_4$ and the solvent was evaporated under reduced pressure. The crude reaction product was purified by DCVC.[318]

Yield: 2.50 g (3.51 mmol, 56%); yellow foam; **M:** [C$_{40}$H$_{41}$NO$_{11}$] 711.8 $\frac{g}{mol}$; **TLC:** $R_f = 0.19$ (heptane/EtOAc, 2:1); **opt. rot.:** $[\alpha]_D^{27} = -9.4$ (c = 0.68, MeOH); **HRMS (ESI+):** $\frac{m}{z} = 734.2614$ (calc. for MNa$^+$: 734.2577) **elem. anal.:** % = C (67.62), H (6.30), N (1.59), O (23.48), calc. for C$_{40}$H$_{41}$NO$_{11}$: C (67.50), H (5.81), N (1.97), O (24.73) .
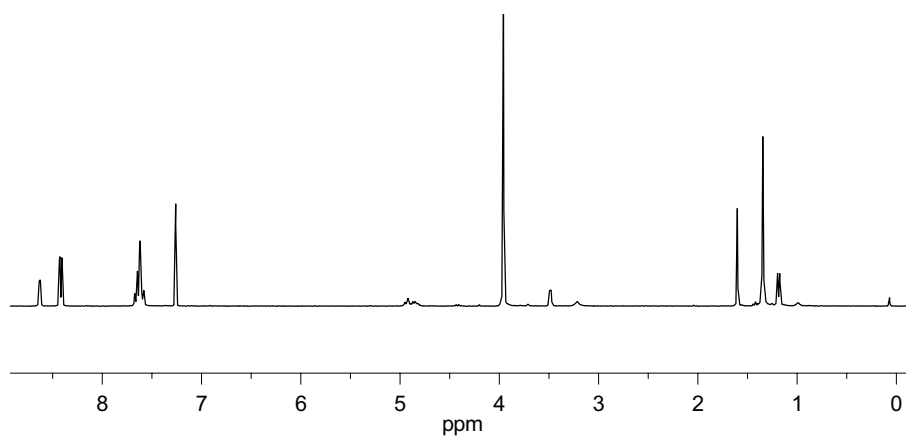
**¹H-NMR (300 MHz, CDCl₃):** $\delta$ [ppm] = 8.63 (m, 2H, H16), 8.43 (d, 2H $^4J_{H\text{-}H}$ = 1.6 Hz, H14A), 8.41 (d, 2H $^4J_{H\text{-}H}$ = 1.6 Hz, H14B), 7.70-7.56 (m, 8H, H10, H11), 4.94 (d, $^3J_{H\text{-}H}$ = 9.5 Hz, H5), 4.88-4.81 (m, 1H, H2), 3.96 (s, 12H, H18), 3.21 (s, 1H, H4), 1.35 (s, 9H, H8), 1.19 (d, 3H, $^2J_{H\text{-}H}$ = 6.3 Hz, H3).
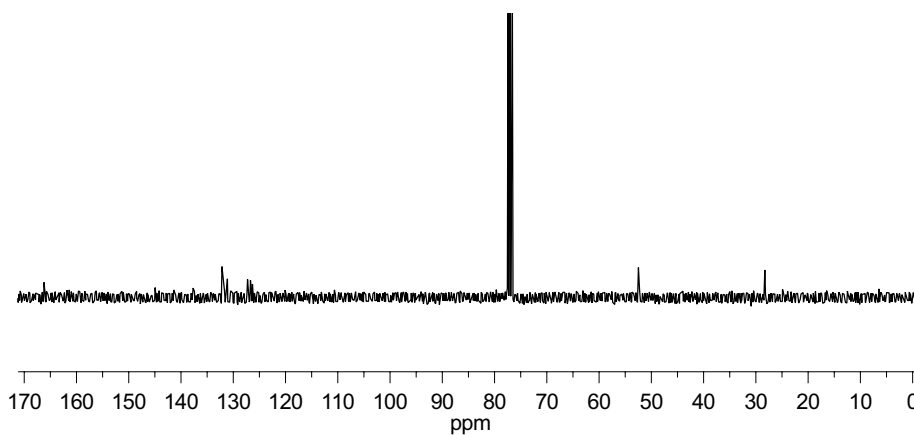


**¹³C-NMR (75 MHz, CDCl₃):** $\delta$ [ppm] = 166.21, 166.18 (4C, C17), 132.17(br) (4C, C14), 131.16, 131.12 (2C, C13), 127.3, 127.0, 126.7, 126.3 (8C, C10, C11), 80.8 (1C, C1), 79.7 (1C, C7), 52.5(br) (4C, C18), 28.3 (3C, C8), 24.90 (1C, C3).
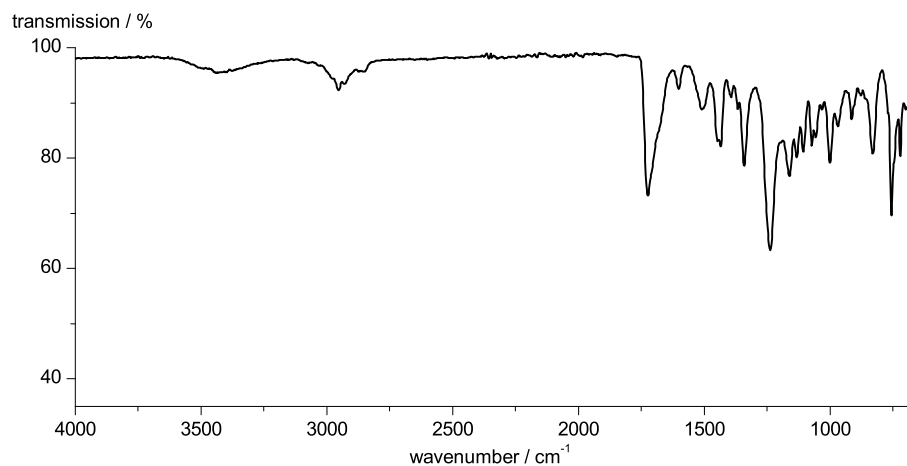
**IR (ATR):** $\widetilde{\nu}$ = 3425 (br), 2979 (w), 2954 (w), 2929 (w), 1722 (s), 1679 (m), 1602 (w), 1512 (m), 1448 (m), 1432 (m), 1363 (m), 1340 (m), 1238 (s), 1161 (m), 1132 (m), 1105 (m), 1074 (m), 1054 (m), 999 (m), 964 (m), 914 (w), 829 (m), 754 (s), 721 (m).

## 4.20 Di-(*O*,*O*-dimethyl-3′,5′-dicarboxybiphenyl)-*N*-*tert*-butyloxycarbonyl-valinol (114)
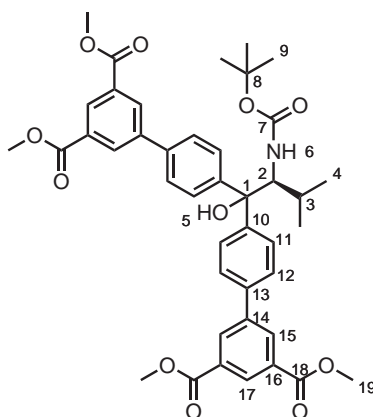
The reaction was performed oven-dried glassware under argon. Solvents were degassed by three freeze-pump-thaw cycles prior to use. To a suspension of the bis-arylated amino acid derivative **86** (4.60 g, 8.96 mmol, 1 eq.), *O,O'*-dimethylisopthalic boronic acid **112** (6.37 g, 26.9 mmol, 3.0 eq.) and cesium carbonate ($Cs_2CO_3$, 8.84 g, 26.9 mmol, 3.0 eq.) in MeOH (125 mL) and DMF (30 mL) were added tetrakis(triphenylphosphine)palladium ([Pd(PPh$_3$)$_4$], 663 mg, 0.42 mmol, 0.05 eq.) and SPhos (176 mg, 0.42 mmol, 0.05 eq.). The reaction was heated to reflux for four hours and was monitored by TLC. Upon consumption of compound **86**, the reaction mixture was allowed to cool to room temperature. The reaction mixture was concentrated in vaccuum to remove most of the MeOH and DMF. The residue was diluted in a mixture of EtOAc (500 mL) and water (250 mL). The organic phase was separated and washed with a saturated solution of $NaHCO_3$ (2× 125 mL) and brine (2× 125 mL). The organic phase was dried over $Na_2SO_4$ and the solvent was evaporated under reduced pressure. The crude reaction product was purified by DCVC.[318]

Yield: 4.22 g (5.70 mmol, 64%); yellow foam; **M:** [$C_{42}H_{45}NO_{11}$] 739.8 $\frac{g}{mol}$; **TLC:** $R_f = 0.25$ (heptane/EtOAc, 2:1); **opt. rot.:** $[\alpha]_D^{27} = -12.8$ (c = 0.51, MeOH); **HRMS (ESI+):** $\frac{m}{z}$ = 762.2894 (calc. for NaM$^+$: 762.2890), **elem. anal.:** % = C (67.67), H (6.34), N (1.50), O (22.39), calc. for $C_{42}H_{45}NO_{11}$: C (68.19), H (6.13), N (1.89), O (23.79) .
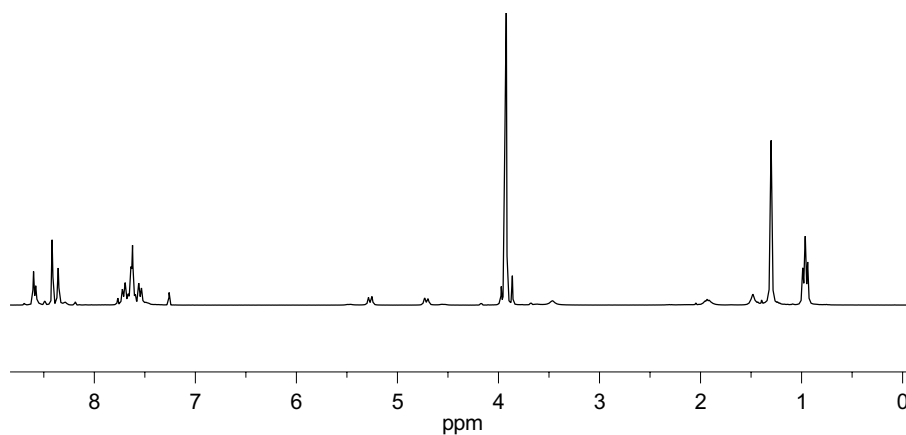


**¹H-NMR (300 MHz, CDCl$_3$):** $\delta$ [ppm] = 8.60 (t, 2H, $^4J_{H-H} = 1.6$ Hz, H17), 8.59-8.57 (m, 4H, H15), 7.74-7.68 (m, 2H, H11 or H12), 7.76-7.59 (m, 4H, H11 or H12), 7.58-7.52 (m, 2H, H11 or H12), 5.27 (d, 1H, $^3J_{H-H} = 10.3$ Hz, H6), 4.77-4.65

(m, 1H, H2), 3.93 (s, 6H, H19A), 3.92 (s, 6H, H19B), 2.00-1.86 (m, 1H, H3), 1.30 (s, 9H, C9), 0.98 (t, 3H, $^3J_{\text{H-H}}$ = 6.6 Hz, H4A), 0.95 (t, 3H, $^3J_{\text{H-H}}$ = 6.9 Hz, H4B).
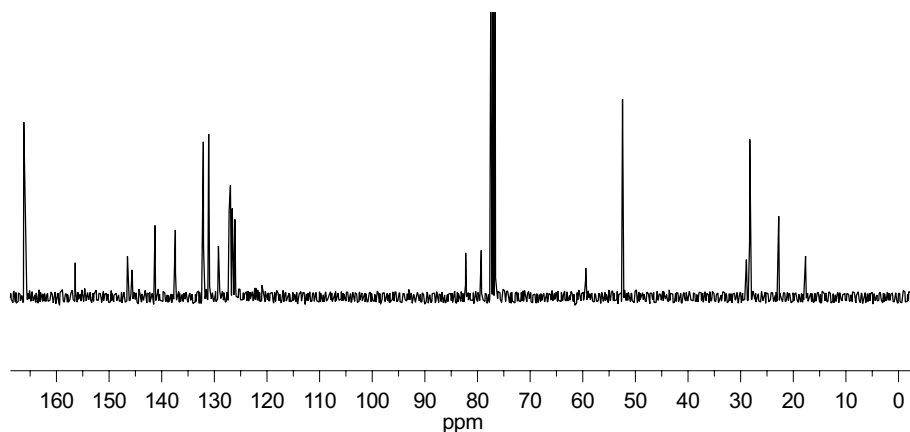


**$^{13}$C-NMR (75 MHz, CDCl$_3$):** $\delta$ [ppm] = 166.2 (4C, C18) 156.4 (1C, C7), 146.5, 145.6 (4C, C16), 141.4, 141.3, 137.4(br) (4C, C10, C13), 132.14, 132.09 (4C, C15), 131.08, 131.05 (2C, C14), 129.31, 129.22 (2C, C17), 127.19, 126.94, 126.59, 126.10 (8C, C11, C12), 82.3 (1C, C1), 79.3 (1C, C8), 59.4 (1C, C2), 52.45, 52.42 (4C, C19), 28.9 (1C, C2), 28.3 (3C, C9), 22.8, 17.7 (2C, C4).
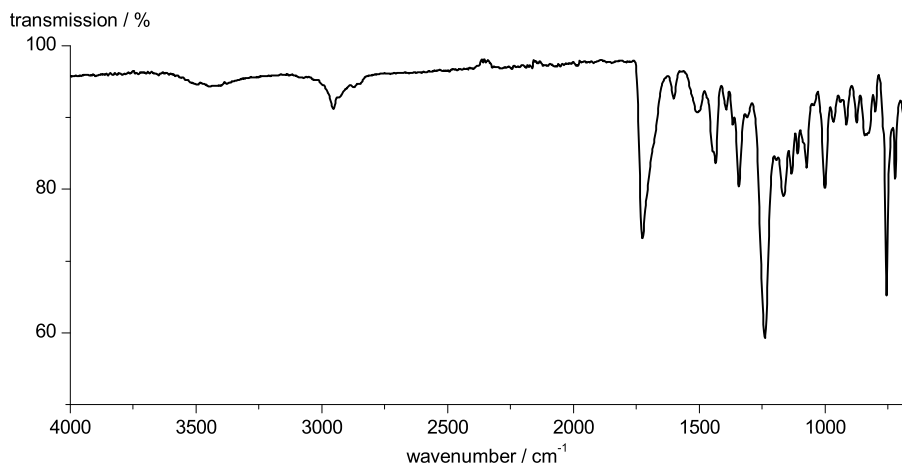
**IR (KBr):** $\widetilde{\nu}$ [cm$^{-1}$] = 2954 (w), 2873 (w), 2848 (w), 1726 (s), 1596 (w), 1434 (m), 1367 (w), 1342 (m), 1236 (s), 1164 (m), 1132 (m), 1000 (m), 914 (m), 873 (m), 798 (m), 754 (m), 719 (m).

## 4.21  Di-(O,O-dimethyl-3′,5′-dicarboxybiphenyl)-*N*-*tert*-butyloxycarbonyl-leucinol (115)
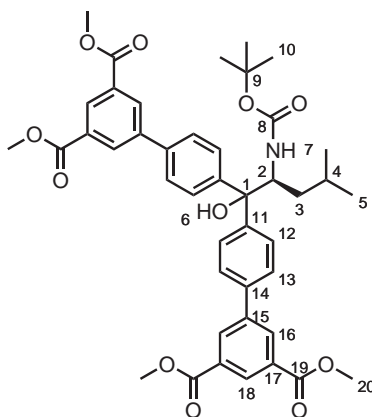


The reaction was performed oven-dried glassware under argon. Solvents were degassed by three freeze-pump-thaw cycles prior to use. To a suspension of the bis-arylated amino acid derivative **87** (4.50 g, 8.57 mmol, 1 eq.), *O,O′*-dimethyl-isopthalic boronic acid **112** (6.12 g, 25.7 mmol, 3.0 eq.) and cesium carbonate (Cs$_2$CO$_3$, 8.45 g, 25.7 mmol, 3.0 eq.) in MeOH (125 mL) and DMF (30 mL) were added were added tetrakis(triphenylphosphine)palladium ([Pd(PPh$_3$)$_4$], 663 mg, 0.42 mmol, 0.05 eq.) and SPhos (176 mg, 0.42 mmol, 0.05 eq.). The reaction was heated to reflux for four hours and was monitored by TLC. Upon consumption of compound **87**, the reaction mixture was allowed to cool to room temperature. The reaction mixture was concentrated in vaccum to remove most of the MeOH and DMF. The residue was diluted in a mixture of EtOAc (500 mL) and water (250 mL). The organic phase was separated and washed with a saturated solution of NaHCO$_3$ (2× 125 mL) and brine (2× 125 mL). The organic phase was dried over Na$_2$SO$_4$ and the solvent was evaporated under reduced pressure. The crude reaction product was purified by DCVC.[318]

Yield: 3.77 g (5.00 mmol, 50%); orange foam; **M:** [C$_{43}$H$_{47}$NO$_{11}$] 753.8 $\frac{g}{mol}$; **TLC:** $R_f$ = 0.22 (heptane/EtOAc, 2:1); **opt. rot.:** $[\alpha]_D^{27}$ = +8.0 (c = 0.80, MeOH);

**HRMS (ESI+):** $\frac{m}{z}$ = 776.3050 (calc. for NaH$^+$: 776.3047); **elem. anal.:** % = C (69.94), H (6.56), N (1.45), O (22.85), calc. for $C_{43}H_{47}NO_{11}$: C (68.51), H (6.28), N (1.86), O (23.35) .
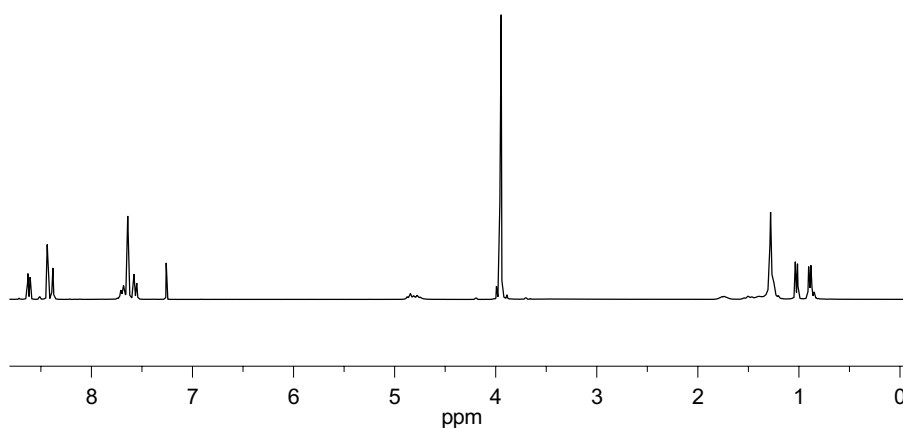


**$^1$H-NMR (300 MHz, CDCl$_3$):** $\delta$ [ppm] = 8.63 (t, 1H, $^4J_{H-H}$ = 1.6 Hz, H18A), 8.61 (t, 1H, $^4J_{H-H}$ = 1.6 Hz, H18B), 8.43 (d, 1H, $^4J_{H-H}$ = 1.6 Hz, H16A), 8.38 (d, 1H, $^4J_{H-H}$ = 1.6 Hz, H16B), 7.74-7.53 (m, 8H, H12, H13), 4.86 (d, 1H, J = 9.8 Hz, H7), 4.83-4.71 (m, 1H, H2), 3.96 (s, 6H, H20A), 3.95 (s, 6H, H20B), 1.88-1.65 (m, 1H, H4), 1.60-1.40 (m, 1H, H3A), 1.28 (s, 9H, H10), 1.27-1.23 (m, 1H, H3B), 1.02 (d, 3H, $^3J_{H-H}$ = 6.5 Hz, H5A), 0.89 (d, 3H, $^3J_{H-H}$ = 6.7 Hz, H5B).
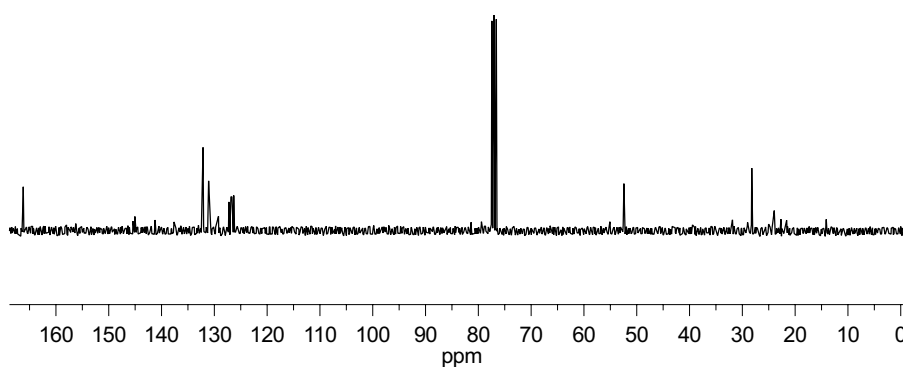
**$^{13}$C-NMR (75 MHz, CDCl$_3$):** $\delta$ [ppm] = 166.21, 166.19 (4C, C19), 156.25 (1C, C8), 145.42, 145.05 (4C, C17), 141.52, 141.22, 137.64, 137.47 (4C, C11, C14), 132.1, (4C, C16) 131.1, 131.1 (2C, C15), 129.37, 129.22 (2C, C18), 127.2, 126.9, 126.7, 126.3 (8C, C12, C13), 81.37 (1C, C1), 79.41 (1C, C9), 55.08 (1C, C2), 52.46, 52.43 (4C, C20), 39.44 (1C, C3), 28.22 (3C, C10), 25.03 (1C, C4), 23.95, 22.68 (2C, C5). .
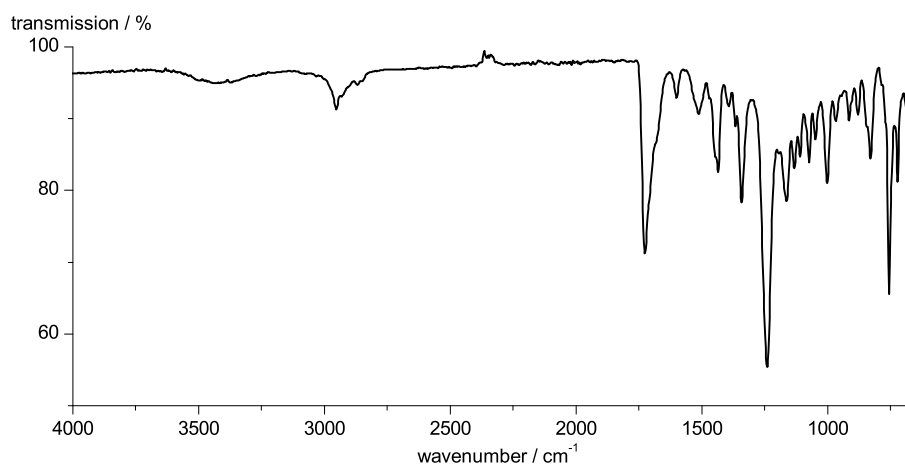


**IR (ATR):** $\widetilde{\nu}$ = 2952 (w), 2929 (w), 2867 (w), 1726 (s), 1598 (w), 1432 (m), 1342 (m), 1240 (s), 1161 (m), 1072 (m), 1000 (m), 829 (m), 754 (s), 721 (m).

## 4.22 Di-(*O*,*O*-dimethyl-3′,5′-dicarboxybiphenyl)-*N*-*tert*-butyloxycarbonyl-valinol (116)
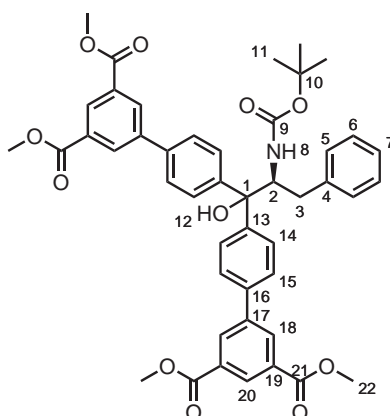


The reaction was performed oven-dried glassware under argon. Solvents were degassed by three freeze-pump-thaw cycles prior to use. To a suspension of the bis-arylated amino acid derivative **88** (4.10 g, 7.31 mmol, 1 eq.), *O*,*O*′-dimethyl-isopthalic boronic acid **112** (5.15 g, 21.9 mmol, 3.0 eq.) and cesium carbonate ($Cs_2CO_3$, 7.21 g, 21.6 mmol, 3.0 eq.) in MeOH (125 mL) and DMF (30 mL) were added tetrakis(triphenylphosphine)palladium ([$Pd(PPh_3)_4$], 568 mg, 0.37 mmol, 0.05 eq.) and SPhos (150 mg, 0.37 mmol, 0.05 eq.). The reaction was heated to reflux for four hours and was monitored by TLC. Upon consumption of compound **116**, the reaction mixture was allowed to cool to room temperature. The reaction mixture was concentrated in vaccuum to remove most of the MeOH and DMF. The residue was diluted in a mixture of EtOAc (500 mL) and water (250 mL). The organic phase was separated and washed with a saturated solution of $NaHCO_3$ (2× 125 mL) and brine (2× 125 mL). The organic phase was dried over $Na_2SO_4$ and the solvent was evaporated under reduced pressure. The crude reaction product was purified by DCVC.[318]

Yield: 3.40 g (4.32 mmol, 59%); orange foam; **M:** [$CC_{46}H_{45}NO_{11}$] 787.3 $\frac{g}{mol}$; **TLC:** $R_f = 0.19$ (heptane/EtOAc, 2:1); **opt. rot.:** $[\alpha]_D^{26} = +22.6$ (c = 0.68, MeOH); **HRMS (ESI+):** $\frac{m}{z} = 810.2840$ (calc. for $NaM^+$: 810.2890).
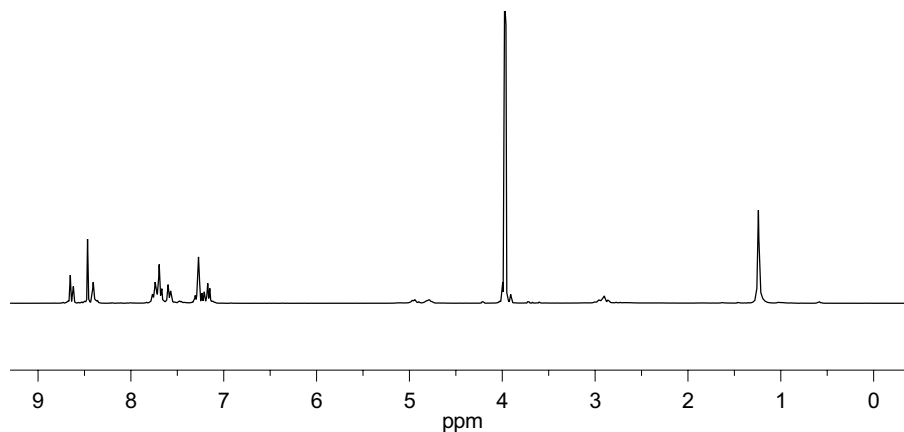
**¹H-NMR (300 MHz, CDCl₃):** $\delta$ [ppm] = 8.65 (t, 1H, $^4J_{\text{H-H}}$ = 1.6 Hz, H20A), 8.62 (t, 1H, $^4J_{\text{H-H}}$ = 1.6 Hz, H20B), 8.46 (d, 1H, $^4J_{\text{H-H}}$ = 1.6 Hz, H18A), 8.43-8.39 (m, 2H, H18B), 7.79-7.64 (m, 6H, H14A, H15), 7.63-7.54 (m, 2H, H14B), 7.32-7.22 (m, 3H, H5, H7), 7.20-7.14 (m, 2H, H6), 4.96 (d, 1H, $^3J_{\text{H-H}}$ = 9.0 Hz, H8), 4.85-4.73 (m, 1H, H2), 3.98 (s, 6H, H22A), 3.96 (s, 6H, H22B), 2.99-2.83 (m, 2H, H3), 1.24 (s, 9H, H11).



**¹³C-NMR (75 MHz, DMSO−d₆):** $\delta$ [ppm] = 166.2 (4C, C21), 156.2 (1C, C9) 145.8, 145.1 (4C, C19), 141.4, 141.3, 138.9(br) (4C, C13, C16), 137.9 (1C, C4), 132.2, 132.1 (4C, C18) 131.2, 131.10 (2C, C17), 129.3 (2C, C5), 128.4 (2C, C6), 127.4, 127.0, 126.6 (6C, C14A, C15), 126.3 (1C, C7), 126.3 (2C C14B), 81.0 (1C, C1), 79.8 (1C, C10), 59.5 (1C, C2), 52.5 (1C, C22A), 52.4 (1C, C22B), 28.1 (4C, C3, C11).

275
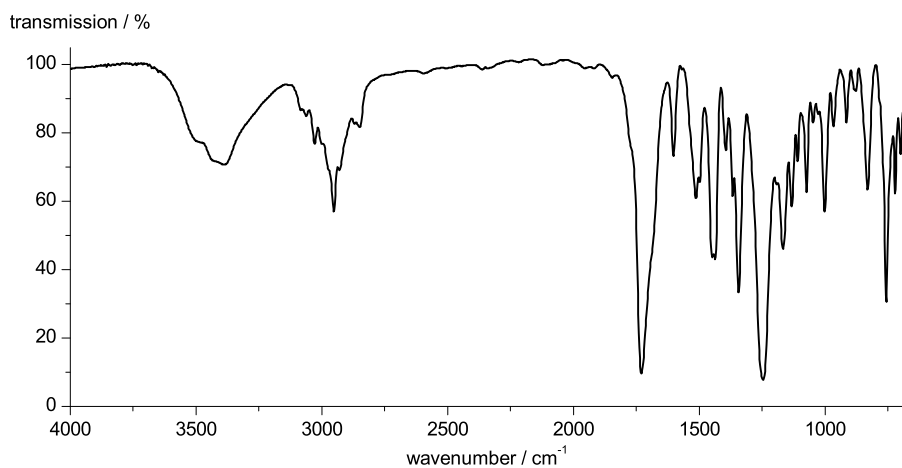
**IR (KBr):** $\widetilde{v}$ = 3494 (w), 3396 (w), 3083 (s), 3062 (s), 3031 (m), 2952 (m), 2929 (m), 2848 (m), 1728 (s), 1602 (m), 1513 (m), 1448 (s), 1436 (s), 1342 (s), 1243 (s), 1166 (m), 1072 (m), 1000 (m), 831 (m), 756 (m).

## 4.23    4,4-Di-(O,O-dimethyl-3′,5′-dicarboxybiphenyl)-5-isopropyl-oxazolidin-2-one (118)
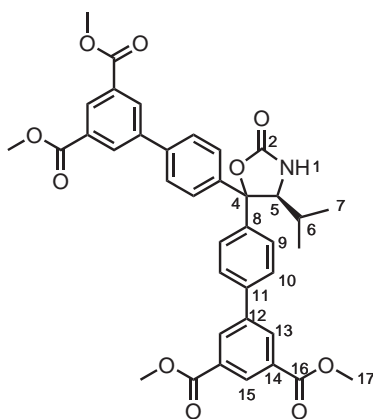


276

The reaction was performed oven-dried glassware under argon. Solvents were degassed by three freeze-pump-thaw cycles prior to use. To a suspension of the bis-arylated amino acid derivative **97** (4.30 g, 9.86 mmol, 1 eq.), $O,O'$-dimethyl-isopthalic boronic acid **112** (6.95 g, 29.6 mmol, 3.0 eq.) and cesium carbonate ($Cs_2CO_3$, 9.73 g, 29.6 mmol, 3.0 eq.) in MeOH (160 mL) and DMF (40 mL) were added tetrakis(triphenylphosphine)palladium ([Pd(PPh$_3$)$_4$], 767 mg, 0.49 mmol, 0.05 eq.) and SPhos (202 mg, 0.49 mmol, 0.05 eq.). The reaction was heated to reflux for four hours and was monitored by TLC. Upon consumption of compound **97**, the reaction mixture was allowed to cool to room temperature. The reaction mixture was concentrated in vaccuum to remove most of the MeOH and DMF. The residue was diluted in a mixture of EtOAc (500 mL) and water (250 mL). The organic phase was separated and washed with a saturated solution of $NaHCO_3$ (2× 150 mL) and brine (2× 150 mL). The organic phase was dried over $Na_2SO_4$ and the solvent was evaporated under reduced pressure. The crude reaction product was purified by DCVC.[318]

Yield: 4.90 g (7.37 mmol, 75%); yellow foam; **M:** [$C_{38}H_{35}NO_{10}$] 665.7 $\frac{g}{mol}$; **TLC:** $R_f$ = 0.22 (heptane/EtOAc, 1:1); **m.p.:** 118 °C; **opt. rot.:** $[\alpha]_D^{27}$ = −71.3 (c = 0.38, MeOH); **HRMS (ESI+):** $\frac{m}{z}$ = 666.2333 (calc. for MH$^+$: 666.2333); **elem. anal.:** % = C (64.09), H (5.42), N (1.23), O (26.03) calc. for $C_{38}H_{35}NO_{10}$: C (68.56), H (5.30), N (2.10), O (24.03).
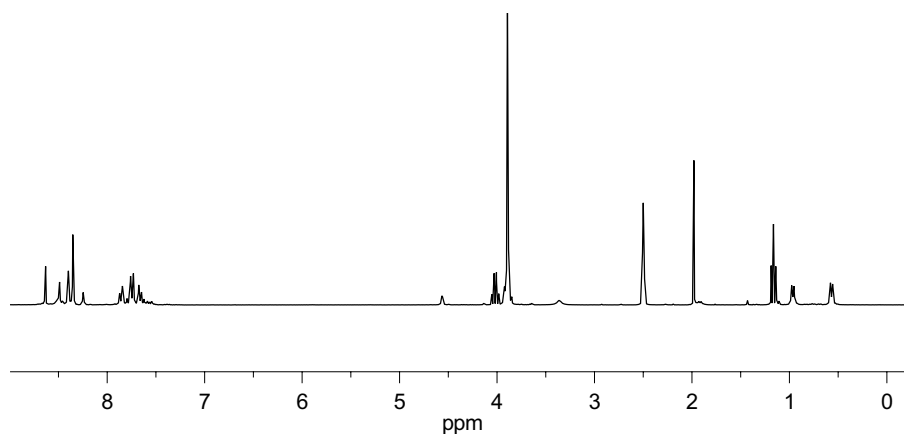


**$^1$H-NMR (300 MHz, DMSO−d$_6$):** $\delta$ [ppm] = 8.39-8.36 (m, 2H, H15), 8.33-8.28 (m, 4H, H13), 8.25 (s, 1H, H1), 7.90-7.81 (m, 2H, H9A), 7.80-7.49 (m, 6H, H9B, H10), 4.61-4.53 (m, 1H, H5), 3.87 (s, 12H, H17), 1.97-1.84 (m, 1H, H6), 0.97 (d, $^3J_{\text{H-H}}$ = 6.8 Hz, H7A), 0.57 (d, $^3J_{\text{H-H}}$ = 6.5 Hz, H7B).
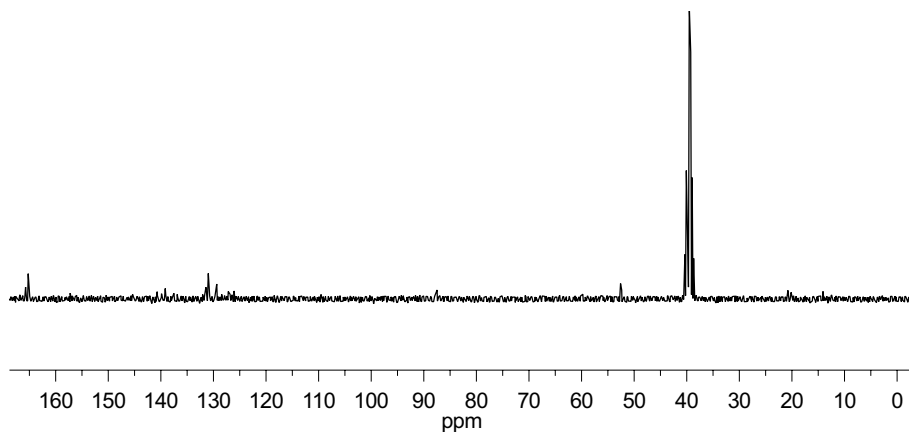
**$^{13}$C-NMR (75 MHz, DMSO$-$d$_6$):** $\delta$ [ppm] = 165.2 (4C, C16), 157.3 (1C, C2), 145.1, 145.4 (2C, C14), 139.9(br), 137.5, 136.9 (4C, C8, C11), 131.43, 131.38 (4C, C13), 128.8, 128.7 (2C, C14), 128.4 (2C, C12), 127.1, 126.8, 126.5, 126.1 (8C, C9, C10), 87.5 (1C, C4), 64.2 (1C, C5), 52.5 (4C, C17), 29.2 (1C, C6), 20.2, 14.6 (2C, C7).
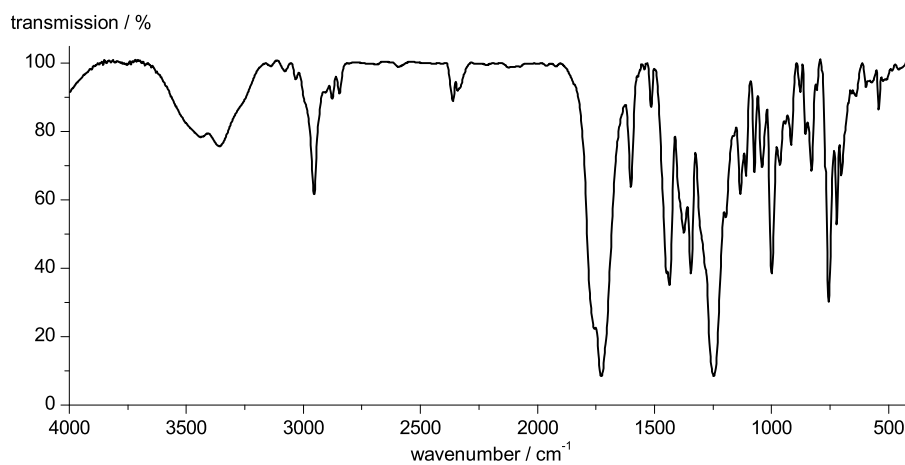


**IR (KBr):** $\tilde{\nu}$ [cm$^{-1}$] = 3441 (m), 3360 (m), 2955 (m), 2878 (w), 2361 (w), 1757 (s), 1728 (s), 1601 (m), 1514 (w), 1448 (s), 1437 (s), 1375 (m), 1344 (s), 1246 (s), 1196 (m), 1134 (m), 1109 (m), 1072 (m), 1042 (m), 999 (s), 964 (m), 941 (w), 916 (m), 854 (m), 829 (m), 756 (s), 721 (m), 702 (m), 640 (w), 542 (w).

## 4.24   4,4-Di-(O,O-dimethyl-3′,5′-dicarboxybiphenyl)-5-benyzl-oxazolidin-2-one (119)
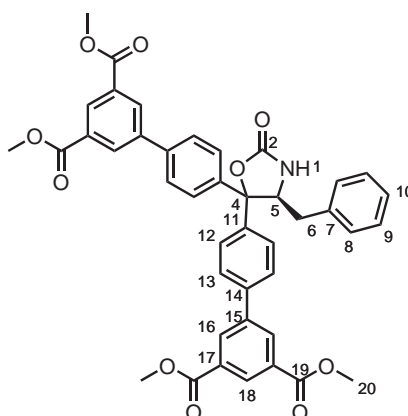


The reaction was performed oven-dried glassware under argon. Solvents were degassed by three freeze-pump-thaw cycles prior to use. To a suspension of the bis-arylated amino acid derivative **98** (3.50 g, 7.19 mmol, 1 eq.), *O,O′*-dimethyl-isopthalic boronic acid **112** (5.07 g, 21.6 mmol, 3.0 eq.) and cesium carbonate (Cs$_2$CO$_3$, 7.09 g, 21.6 mmol, 3.0 eq.) in MeOH (160 mL) and DMF (40 mL) was added tetrakis(triphenylphosphine)palladium ([Pd(PPh$_3$)$_4$], 559 mg, 0.36 mmol, 0.05 eq.).

The reaction was heated to reflux for four hours and was monitored by TLC. Upon consumption of compound **98**, the reaction mixture was allowed to cool to room temperature. The reaction mixture was concentrated in vaccuum to remove most of the MeOH and DMF. The residue was diluted in a mixture of EtOAc (500 mL) and water (250 mL). The organic phase was separated and washed with a saturated solution of NaHCO$_3$ (2× 150 mL) and brine (2× 150 mL). The organic phase was dried over Na$_2$SO$_4$ and the solvent was evaporated under reduced pressure. The crude reaction product was purified by DCVC.[318]

Yield: 2.88 g (4.04 mmol, 56%); yellow foam; **M:** [C$_{42}$H$_{35}$NO$_{10}$] 713.7 $\frac{g}{mol}$; **TLC:** $R_f$ = 0.30 (heptane/EtOAc, 1:1); **m.p.:** 171.5 °C; **opt. rot.:** $[\alpha]_D^{26}$ = −42.0 (c = 0.10, MeOH); **HRMS (ESI+):** $\frac{m}{z}$ = 714.2344 (calc. for MH$^+$: 714.2334); **elem. anal.:** % = C (66.60), H (4.93), N (1.48), O (23.69) calc. for C$_{42}$H$_{35}$NO$_{10}$: C (70.68), H (4.94), N (1.96), O (22.42).
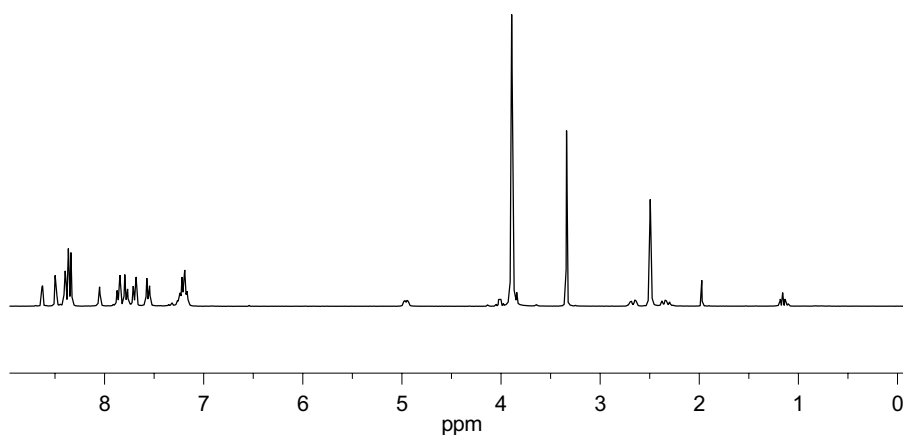
**¹H-NMR (300 MHz, DMSO−d₆):** $\delta$ [ppm] = 8.39-8.36 (m, 2H, H18), 8.34 (d, 2H, $^4J_{\text{H-H}}$ = 1.6 Hz, H16A), 8.31 (d, 2H, $^4J_{\text{H-H}}$ = 1.6 Hz, H16B), 8.06 (s, 1H, H1), 7.88-7.83 (m, 2H, H12A), 7.81-7.71 (m, 2H, H13A), 7.71-7.64 (m, 2H, H13B), 7.59-7.53 (m, 2H, H12B), 7.31-7.13 m, 5H, H8, H9, H10), 4.96 (dd, 1H, $^3J_{\text{H-H}}$ = 9.7, 4.3 Hz, H5), 3.89 (s, 12H, H20), 2.67 (dd, 1H, $^2J_{\text{H-H}}$ = 13.7 Hz, $^3J_{\text{H-H}}$ = 4.3 Hz, H6A), 2.35 (dd, 1H, $^2J_{\text{H-H}}$ = 13.7 Hz, $^3J_{\text{H-H}}$ = 9.7 Hz, H6B).
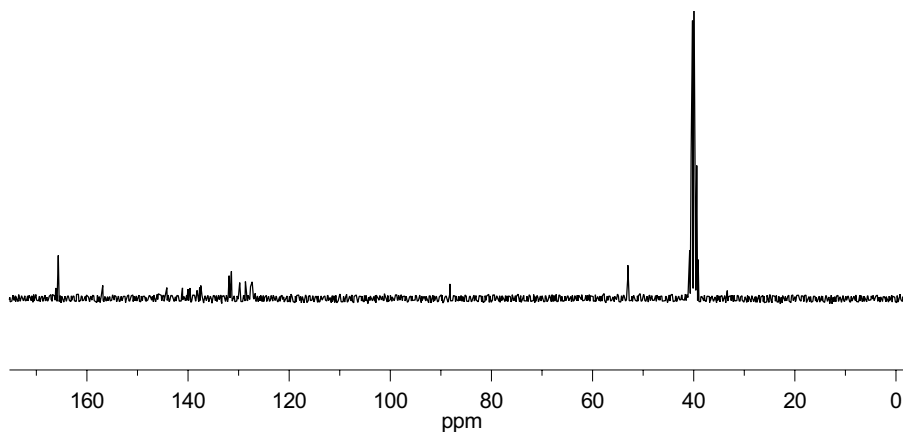


**¹³C-NMR (75 MHz, DMSO−d₆):** $\delta$ [ppm] = 165.2 (4C, C19), 156.4 (1C, C2), 143.7, 139.6 (1C, C14), 137.8 (1C, C11), 137.2 (1C, C7), 137.0 (1C, C11), 131.4 (2C, C16A), 130.9 (6C, C16B, C17), 129.3 (2C, C8), 128.5, 128.4 (1C, C18A) 128.2 (4C, C15, C9), 127.2 (2C, C13A), 126.8 (4C, 13B, C12A), 126.7 (2C, C12B), 126.3 (1C, C10), 87.8 (1C, C3), 60.2 (1C, C4), 52.6 (4C, C20), 38.6 (1C, C6).
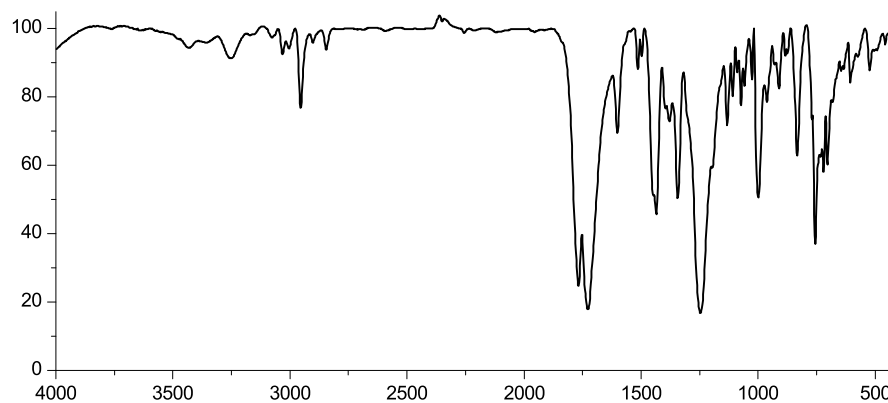
**IR (KBr):** $\widetilde{\nu}$ [cm$^{-1}$] = 2955 (m), 1767 (s), 1726 (s), 1601 (m), 1514 (w), 1448 (s), 1435 (s), 1396 (m), 1379 (m), 1344 (s), 1246 (s), 1196 (s), 1132 (m), 1109 (w), 1090 (w), 1072 (m), 1059 (w), 1026 (w), 999 (s), 962 (m), 930 (w), 910 (w), 833 (m), 756 (s), 733 (m), 719 (s), 704 (m), 683 (m), 646 (w), 635 (w), 606 (w), 523 (w).

## 4.25 Di-(O,O-dimethyl-3′,5′-dicarboxybiphenyl)-*N*-benzyl-prolinol (120)
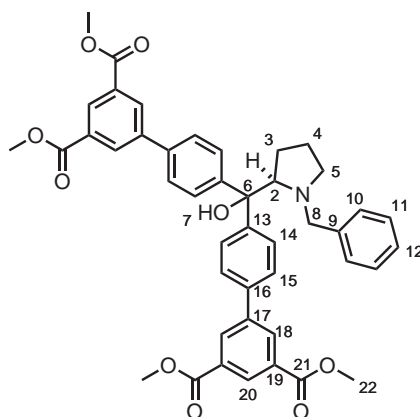
The reaction was performed oven-dried glassware under argon. Solvents were degassed by three freeze-pump-thaw cycles prior to use. To a suspension of the bis-arylated amino acid derivative **94** (4.60 g, 8.96 mmol, 1 eq.), *O,O'*-dimethyl-isopthalic boronic acid **112** (6.12 g, 25.7 mmol, 3.0 eq.) and cesium carbonate ($Cs_2CO_3$, 8.45 g, 25.7 mmol, 3.0 eq.) in MeOH (125 mL) and DMF (30 mL) were added tetrakis(triphenylphosphine)palladium ([Pd(PPh$_3$)$_4$], 697 mg, 0.45 mmol, 0.05 eq.) and SPhos (184 mg, 0.45 mmol, 0.05 eq.). The reaction was heated to reflux for four hours and was monitored by TLC. Upon consumption of compound **94**, the reaction mixture was allowed to cool to room temperature. The reaction mixture was concentrated in vaccuum to remove most of the MeOH and DMF. The residue was diluted in a mixture of EtOAc (500 mL) and water (250 mL). The organic phase was separated and washed with a saturated solution of NaHCO$_3$ (2× 125 mL) and brine (2× 125 mL). The organic phase was dried over Na$_2$SO$_4$ and the solvent was evaporated under reduced pressure. The crude reaction product was purified by DCVC.[318]

Yield: 4.03 g (5.54 mmol, 59%); yellow foam; **M:** [$C_{44}H_{41}NO_9$] 727.8 $\frac{g}{mol}$; **TLC:** $R_f = 0.67$ (heptane/EtOAc, 2:1); **opt. rot.:** $[\alpha]_D^{26} = +54.0$ (c = 0.80, MeOH); **HRMS (ESI+):** $\frac{m}{z} = 728.2913$ (calc. for MH$^+$: 728.2854).
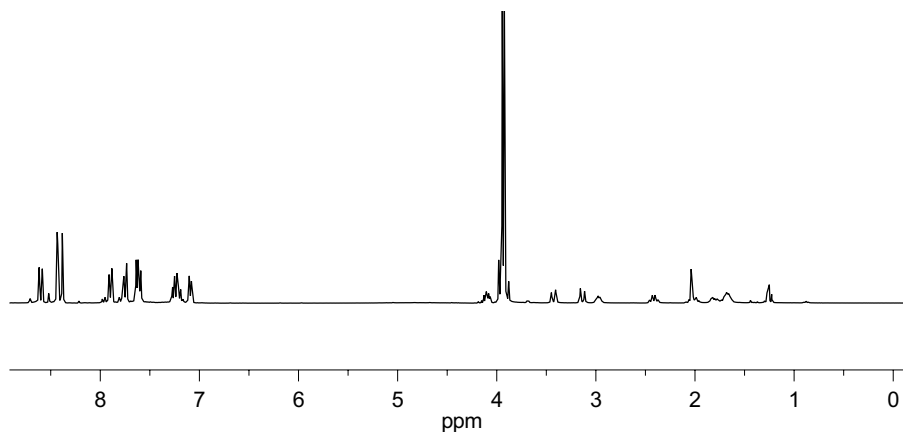


**$^1$H-NMR (300 MHz, CDCl$_3$):** $\delta$ [ppm] = 8.62 (t, 1H, $^4J_{H-H}$ = 1.6 Hz, H20A), 8.59 (t, 1H, $^4J_{H-H}$ = 1.6 Hz, H20B), 8.43 (d, 2H, $^4J_{H-H}$ = 1.6 Hz, H18A), 8.38 (d, 2H, $^4J_{H-H}$ = 1.6 Hz, H18B), 7.92-7.85 (m, 2H, H14A or H15A), 7.76-7.70 (m, 2H, H14B or H15B), 7.66-7.57 (m, 4H, H14 or H15), 7.29-7.18 (m, 3, H10, H12), 7.12-7.05 (m, 2H, H13), 4.10 (dd, 1H, $^3J_{H-H}$ = 9.4, 4.7 Hz, H2) 3.96 (s, 6H, C22A),

3.94 (s, 6H, C22B), 3.41 (d, 1H, $^2J_{\text{H-H}}$ = 12.6 Hz, C8A), 3.13 (d, 1H, $^2J_{\text{H-H}}$ = 12.6 Hz, C8B), 2.98 (dd, 1H, $^3J_{\text{H-H}}$ = 9.7, 5.1 Hz, H5A), 2.50-2.36 (m, 1H, H5B), 2.03 (dd, $^2J_{\text{H-H}}$ = 12.6 Hz, $^3J_{\text{H-H}}$ = 9.0 Hz, H3A), 1.88-1.74 (m, 1H, H3B), 1.74-1.55 (m, 2H, H4).
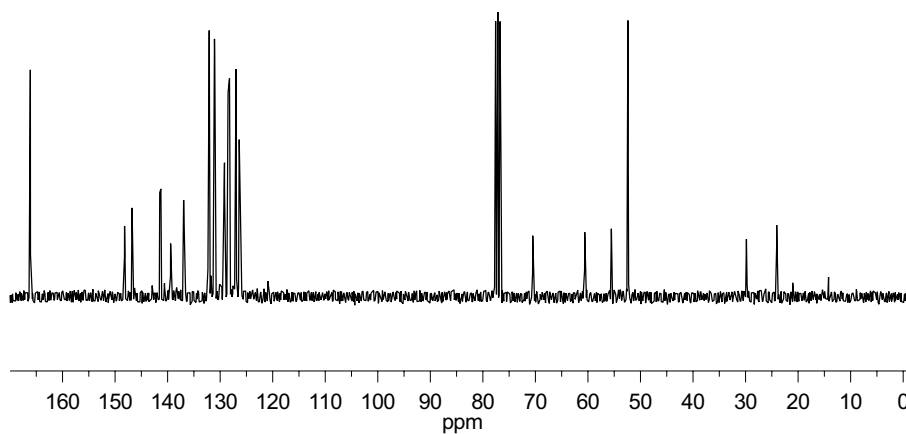


**$^{13}$C-NMR (75 MHz, CDCl$_3$):** $\delta$ [ppm] = 166.24, 166.20 (4C, C22), 148.16, 146.72 (4C, C19), 141.56, 141.33 (2C, C13 or C16), 139.44 (1C, C9), 137.13, 137.03 (4C, C13 or C16) 132.16, 132.13 (4C, C18), 131.08, 131.03 (2C, C17), 129.20(br)(2C, C20), 128.51, 128.22 (4C, C10, C11), 127.10, 127.03 (4C, C14 or C15), 126.97 (1C, C12) 126.32, 126.16 (4C, C14 or C15);
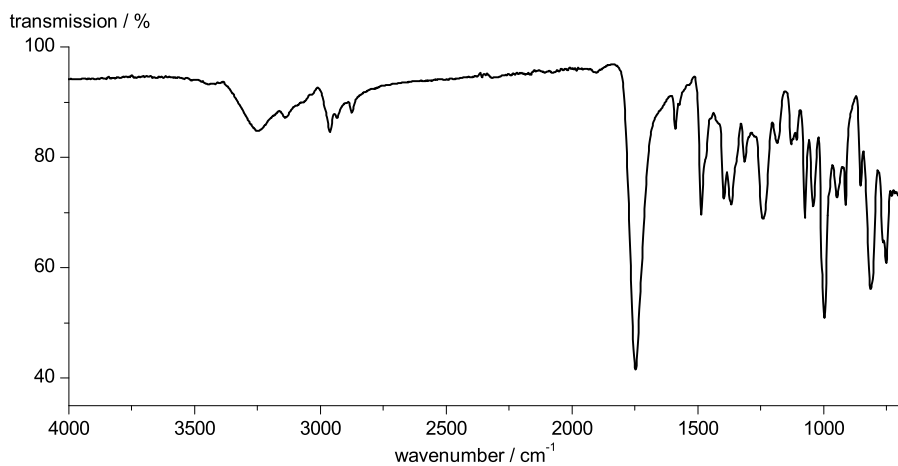
**IR (KBr):** $\widetilde{\nu}$ [cm$^{-1}$] = 3251 (br), 3135 (w), 2962 (w), 2933 (w), 2873 (w), 1747 (s), 1587 (w), 1485 (m), 1398 (m), 1365 (m), 1313 (m), 1240 (m), 1074 (m), 1041 (m), 995 (m), 945 (m), 912 (m), 810 (m).

## 4.26  1,1-Di-(3',5'-dicarboxybiphenyl)N-tert-butyloxy-carbonyl-alaninol (121)
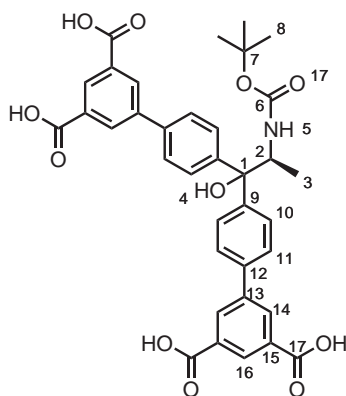


To a solution of the tetramethyl ester **113** (2.00 g, 2.81 mmol, 1 eq.) in tetrahydrofuran (100 mL) was added water (100 mL) and a solution of potassium hydroxide (KOH, 2 $\frac{\text{mol}}{\text{L}}$, 9.8 mL, 20 mmol, 7 eq.). The reaction was heated to reflux for 2-3 hours and was monitored by TLC. Upon consumption of compound **113**, the reaction mixture was allowed to cool to room temperature. The reaction mixture was concentrated in vaccuum to remove most of the THF. The residue was diluted with water (200 mL) and concentrated hydrochloric acid was added dropwise until pH $2 - 5$ was reached. This resulted in the precipitation of the tetracarboxylic acid. The suspension was centrifuged and the liquid phase was discarded. The precipitate was washed with water and then dried in vacuum.

Yield: 1.57 g (2.40 mmol, 85%); white powder; **M:** [C$_{36}$H$_{33}$NO$_{11}$] 655.6 $\frac{\text{g}}{\text{mol}}$; **opt. rot.:** $[\alpha]_D^{27} = -21.7$ (c = 0.24, MeOH); **HRMS (ESI+):** $\frac{m}{z}$ = 678.1960 (calc. for MNa$^+$: 655.1951), **elem. anal.:** % = C (59.47), H (5.54), N (1.63), O (26.29), calc. for C$_{36}$H$_{33}$NO$_{11}$: C (65.95), H (5.07), N (2.14), O (26.84) .

**¹H-NMR (300 MHz, CD₃OD):** $\delta$ [ppm] = 8.60-8.58 (m, 2H, H16), 8.37 (d, 2H $^4J_{\text{H-H}}$ = 1.7 Hz, H14A), 8.36 (d, 2H, $^4J_{\text{H-H}}$ = 1.6 Hz, H14B), 7.70-7.54 (m, 8H, H10, H11), 4.84 (q, 1H $^3J_{\text{H-H}}$ = 6.5 Hz, H2), 1.30 (s, 9H, H8), 1.12 (d, 3H, $^3J_{\text{H-H}}$ = 6.5 Hz, H3).



**¹³C-NMR (75 MHz, CD₃OD):** $\delta$ [ppm] = 168.84(br) (4C, C14), 157.67 (1C, C6), 147.63, 146.93 (2C, C9 or C12), 142.69, 142.51 (2C, C9 or C12), 138.60 (2C, C13), 133.10(br) (4C, C14), 132.89(br) (4C, C17), 130.48, 130.44 (2C, C16), 128.05, 127.81, 127.65, 127.58 (8C, C10, C11), 81.38 (1C, C1), 80.18 (1C, C7), 53.42 (1C, C2), 28.68 (3C, C8), 26.44 (1C, C3);
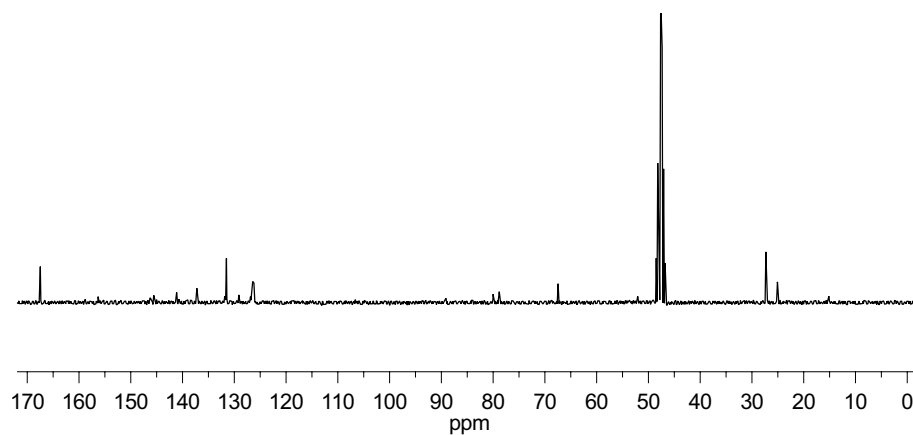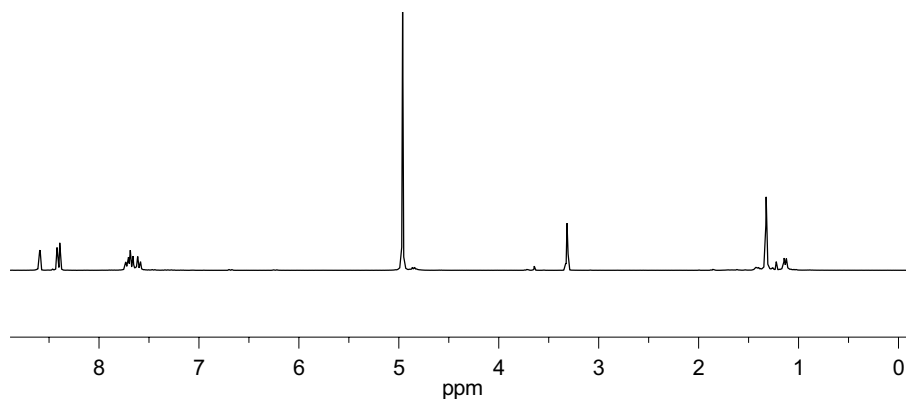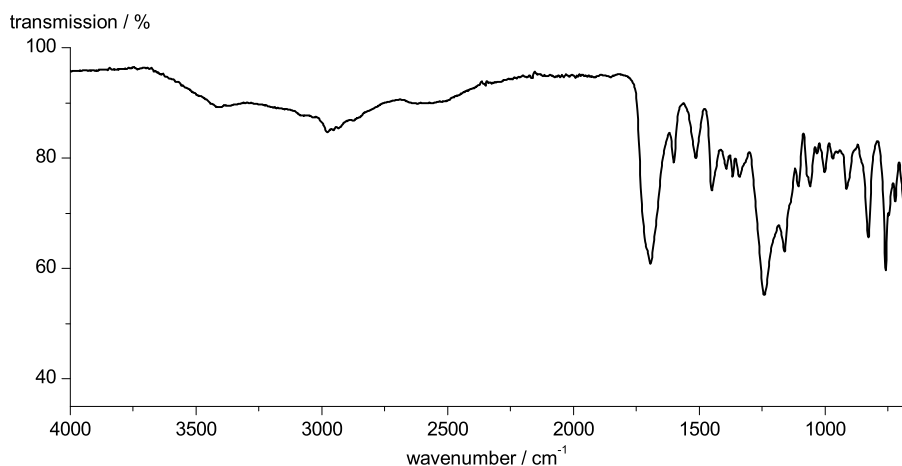
**IR (ATR):** $\widetilde{\nu}$ = 3425 (br), 2977 (w), 2952 (w), 2931 (w), 2561 (br), 1712 (s), 1695 (s), 1600 (m), 1513 (m), 1446 (m), 1392 (m), 1365 (m), 1338 (m), 1240 (br), 1162 (s), 1107 (m), 1056 (m), 1000 (w), 916 (m), 829 (m), 757 (s), 719 (m), 671 (m).

## 4.27 1,1-Di-(3′,5′-dicarboxybiphenyl)N-tert-butyloxy-carbonyl-valinol (122)
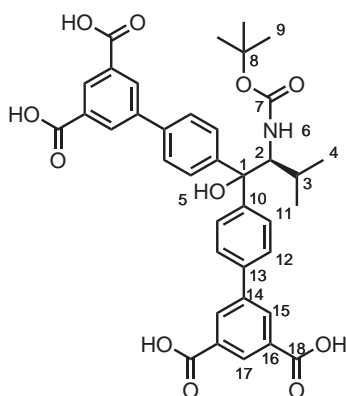


To a solution of the tetramethyl ester **114** (2.00 g, 2.70 mmol, 1 eq.) in tetrahydro-furan (100 mL) was added water (100 mL) and a solution of potassium hydrox-

ide (KOH, 2 $\frac{mol}{L}$, 9.5 mL, 19 mmol, 7 eq.). The reaction was heated to reflux for 2-3 hours and was monitored by TLC. Upon consumption of compound **115**, the reaction mixture was allowed to cool to room temperature. The reaction mixture was concentrated in vaccuum to remove most of the THF. The residue was diluted with water (200 mL) and concentrated hydrochloric acid was added dropwise until pH $2-5$ was reached. This resulted in the precipitation of the tetracarboxylic acid. The suspension was centrifuged and the liquid phase was discarded. The precipitate was washed with water and then dried in vacuum.

Yield: 1.47 g (2.15 mmol, 80%); **M:** $[C_{38}H_{37}NO_{11}]$ 683.2 $\frac{g}{mol}$; **opt. rot.:** $[\alpha]_D^{27} = -12.7$ (c $= 0.22$, MeOH); **HRMS (ESI+):** $\frac{m}{z} = 706.2183$ (calc. for NaM$^+$: 706.2264) **elem. anal.:** % = C (61.06), H (5.31), N (1.68), O (24.84), calc. for $C_{39}H_{39}NO_{11}$: C (66.76), H (5.45), N (2.05), O (25.74) .
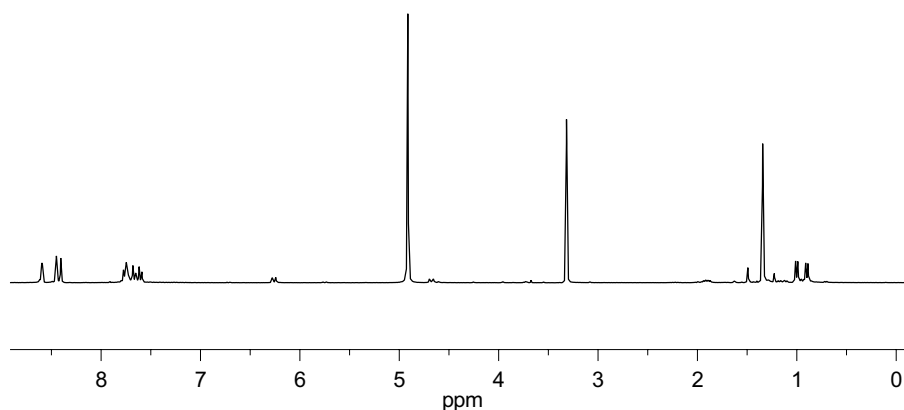


**$^1$H-NMR (300 MHz, CD$_3$OD):** $\delta$ [ppm] = 8.63-8.58 (m, 2H, H17), 8.45 (d, 2H, $^3J_{H-H} = 1.6$ Hz H15A), 8.40 (d, $^3J_{H-H} = 1.6$ Hz H15B), 7.79-7.57 (m, 8H, H11, H12), 6.26 (d, 1H, $^3J_{H-H} = 10.5$ Hz, H6), 4.68 (dd, 1H, $^3J_{H-H} = 10.5, 2.2$ Hz, H2), 1.98-1.82 (m, 1H, H3), 1.34 (s, 9H, H9, 1.00 (d, 3H, $^3J_{H-H} = 6.7$ Hz, H4A), 0.90 (d, 3H, $^3J_{H-H} = 6.7$ Hz, H4B).

287
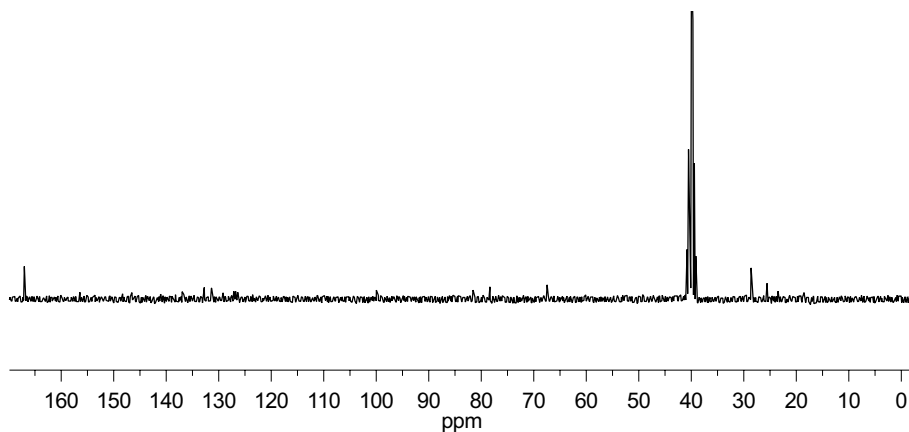
**¹³C-NMR (75 MHz, DMSO−d₆):** $\delta$ [ppm] = 167.0 (4C, C18), 156.4 (1C, C7), 148.3, 146.5 (2C, C10 or C13), 141.06, 140.95 (2C, C10 or C13), 137.0 (2C, C14), 132.8, 132.7 (4C, C16), 131.41, 131.35 (4C, C15), 129.16 (2C, C17), 127.14, 127.07, 126.8, 126.4 (8C, C11, C12), 81.6 (1C, C1), 78.4 (1C, C8), 60.1 (1C, C2) 28.9 (1C, C3) 28.6 (3C, C9), 23.5 (1C, C4A), 18.5 (1C, C4B).
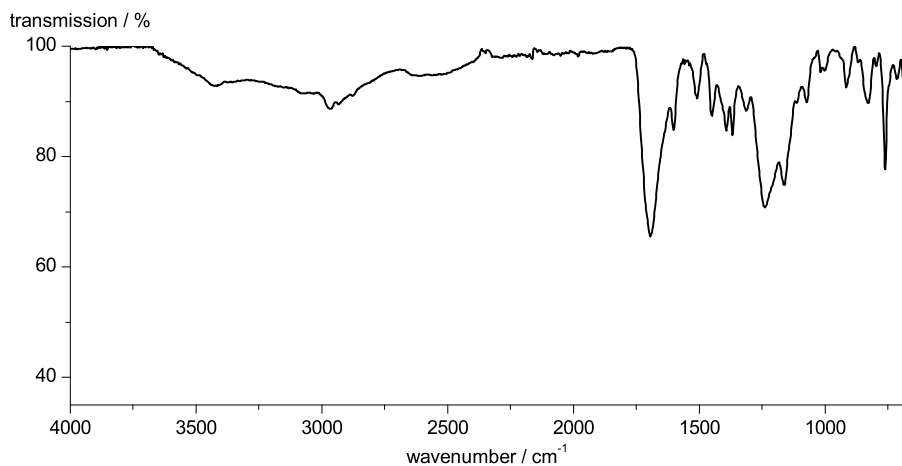


**IR (ATR):** $\widetilde{\nu}$ = 3415 (br), 2970, (w), 2931 (w), 2873 (w), 2514 (br), 1693 (s), 1600 (m), 1508 (m), 1448 (m), 1394 (m), 1367 (m), 1238 (s), 1161 (m), 914 (m), 827 (m), 759 (m), 663 (m).

## 4.28 1,1-Di-(3′,5′-dicarboxybiphenyl)N-tert-butyloxy-carbonyl-leucinol (123)
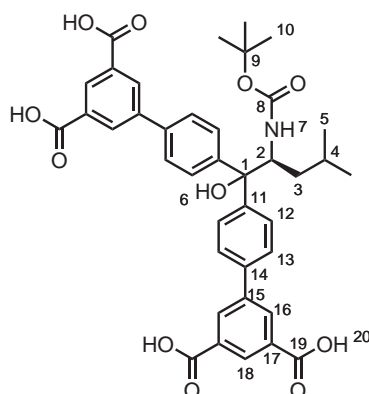


To a solution of the tetramethyl ester **115** (1.50 g, 1.99 mmol, 1 eq.) in tetrahydro-furan (70 mL) was added water (70 mL) and a solution of potassium hydroxide (KOH, 2 $\frac{mol}{L}$, 7.0 mL, 14 mmol, 7 eq.). The reaction was heated to reflux for 2-3 hours and was monitored by TLC. Upon consumption of compound **115**, the reaction mixture was allowed to cool to room temperature. The reaction mixture was concentrated in vaccuum to remove most of the THF. The residue was diluted with water (150 mL) and concentrated hydrochloric acid was added dropwise until pH $2 - 5$ was reached. This resulted in the precipitation of the tetracarboxylic acid. The suspension was centrifuged and the liquid phase was discarded. The precipitate was washed with water and then dried in vacuum.

Yield: 1.12 g (1.64 mmol, 82%); **opt. rot.:** $[\alpha]_D^{26} = +13.6$ (c = 0.44, MeOH); **HRMS (ESI+):** $\frac{m}{z}$ = 720.2431 (calc. for NaM$^+$: 720.2421) **elem. anal.:** % = C (54.52), H (5.06), N (1.42), O (24.51), calc. for $C_{39}H_{39}NO_{11}$: C (67.13), H (5.63), N (2.01), O (25.22) .
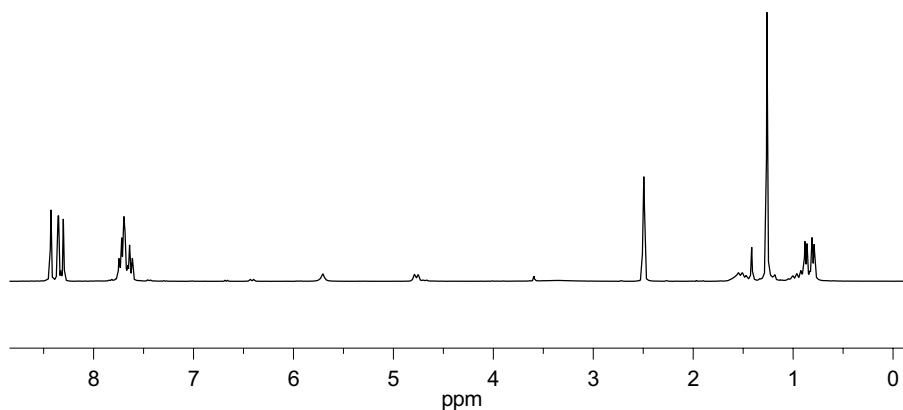
**¹H-NMR (300 MHz, DMSO−d₆):** $\delta$ [ppm] = 13.38 (s, 4H, H20), 8.43 (t, 2H, $^4J_{\text{H-H}}$ = 1.5 Hz, H18), 8.36 (d, 2H, $^3J_{\text{H-H}}$ = 1.5 Hz, H16A), 8.30 (d, 2H, $^3J_{\text{H-H}}$ = 1.5 Hz, H16B), 7.76-7.60 (m, 8H, H12, H13), 6.43 (d, 1H, $^3J_{\text{H-H}}$ = 10.0 Hz, H7), 5.71 (s, 1H, H6), 4.78 (t, 1H, $^3J_{\text{H-H}}$ = 10.6 Hz, H2), 1.63-1.44 (m, 2H, H3), 1.27 (s, 9H, H10), 1.01-0.90 (m, 1H, H4), 0.88 (d, 3H, $^3J_{\text{H-H}}$ = 6.4 Hz, H5A), 0.80 (d, 3H, $^3J_{\text{H-H}}$ = 6.4 Hz, H5B).
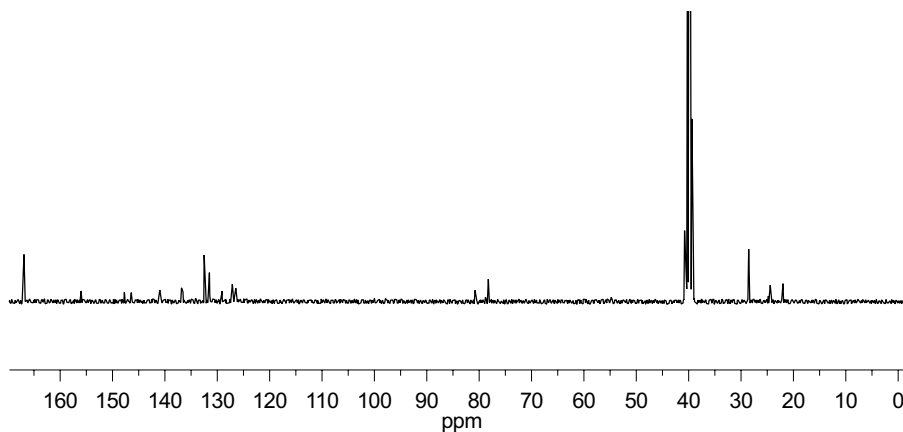


**¹³C-NMR (75 MHz, DMSO−d₆):** $\delta$ [ppm] = 166.5 (4C, C19), 155.7 (1C, C8), 147.3, 146.0 (2C, C11 or C14), 140.9, 140.6 (2C, C11 or C14), 136.4, 136.1,(2C, C15) 132.1 (4C, C17), 131.1(br) (4C, C16), 128.7(br) (2C, C18), 126.7 (br), 126.29, 126.04 (8C, C12, C13), 80.4 (1C, C1), 77.8 (1C, C9), 54.4 (1C, C2), 39.8 (1C, C3, determined from HMBC) 28.1 (3C, C10), 24.0 (1C, C5A), 21.4 (1C, C4), 21.5 (1C, C5B).
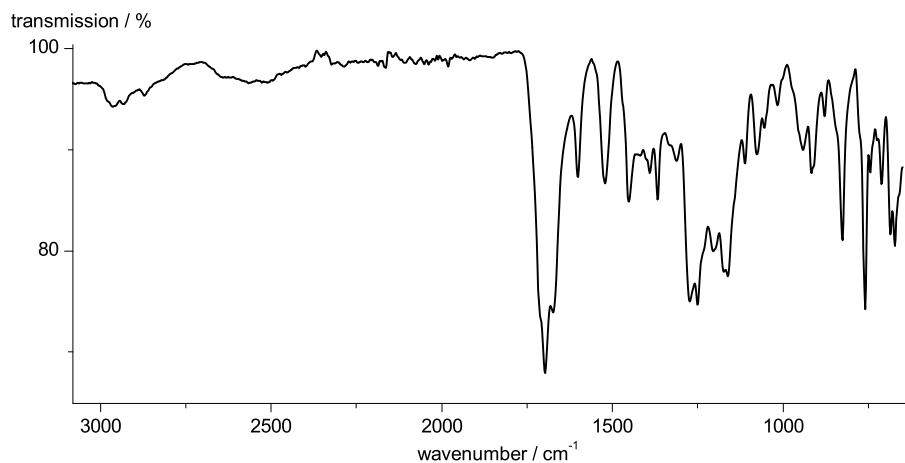
**IR (ATR):** $\widetilde{\nu}$ = 3415 (w), 2966 (w), 2865 (w), 2528 (br), 1967 (s), 1670 (s), 1602 (m), 1521 (m), 1450 (m), 1365 (m), 1272 (m), 1249 (m), 1201 (m), 1172 (m), 916 (m), 825 (m), 759 (m), 684 (m), 669 (m).

## 4.29   1,1-Di-(3′,5′-dicarboxybiphenyl)*N*-tert-butyloxy-carbonyl-phenylalaninol (124)
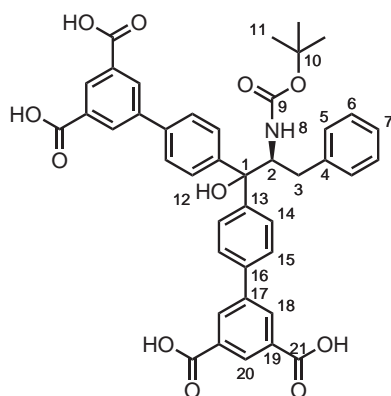


To a solution of the tetramethyl ester **116** (2.00 g, 2.54 mmol, 1 eq.) in tetrahydrofuran (100 mL) was added water (100 mL) and a solution of potassium hydrox-

291

ide (KOH, 2 $\frac{mol}{L}$, 8.9 mL, 18 mmol, 7 eq.). The reaction was heated to reflux for 2-3 hours and was monitored by TLC. Upon consumption of compound **116**, the reaction mixture was allowed to cool to room temperature. The reaction mixture was concentrated in vaccuum to remove most of the THF. The residue was diluted with water (200 mL) and concentrated hydrochloric acid was added dropwise until pH $2-5$ was reached. This resulted in the precipitation of the tetracarboxylic acid. The suspension was centrifuged and the liquid phase was discarded. The precipitate was washed with water and then dried in vacuum.

Yield: 1.52 g (2.08 mmol, 82%); white powder; **M:** $[C_{42}H_{37}NO_{11}]$ 731.2 $\frac{g}{mol}$; **opt. rot.:** $[\alpha]_D^{25} = +21.8$ (c = 0.44, MeOH); **HRMS (ESI+):** $\frac{m}{z}$ = 754.2211 (calc. for $NaM^+$: 754.2262).
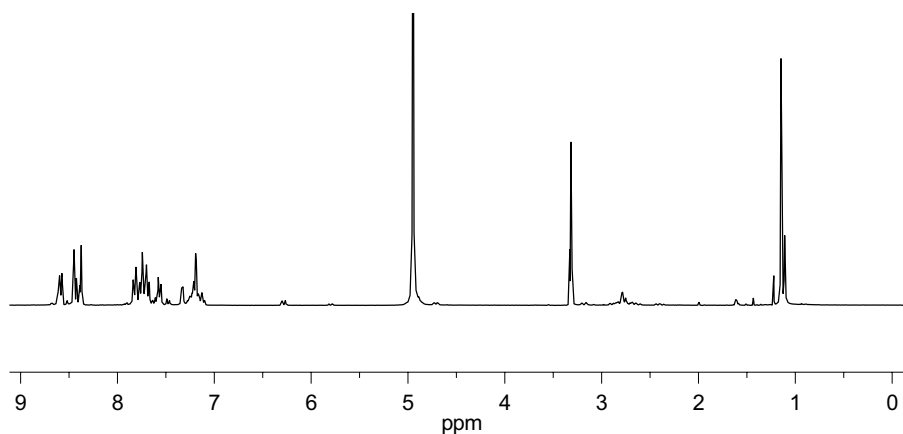


**¹H-NMR (300 MHz, DMSO$-$d$_6$):** $\delta$ [ppm] = 8.64-8.56 (m, 2H, H20), 8.45 (d, 2H, $^4J_{H-H}$ = 1.6 Hz, H18A), 8.38 (d, 2H, $^4J_{H-H}$ = 1.6 Hz, H18B), 7.87-7.65 (m, 6H, H14A, H15), 7.60-7.53 (m, 2H, H14B), 7.37-7.08 (m, 5H, H5, H6, H7), 6.28 (d, 1H, $^3J_{H-H}$ = 10.1 Hz, H8), 4.74-4.68 (m, 1H, H2), 2.96-2.56 (m, 2H, H3), 1.15 (s, 9H, H11).
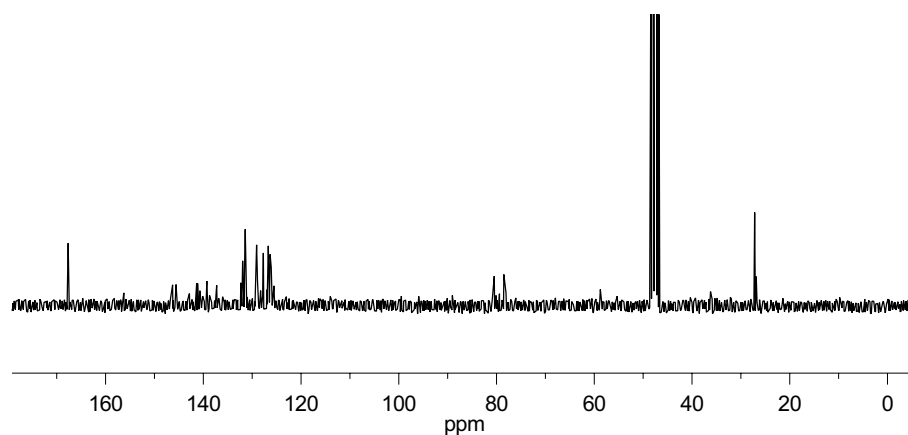
**¹³C-NMR (75 MHz, DMSO−d₆):** $\delta$ [ppm] = 167.7 (4C, C21), 156.3 (1C, C9) 146.3, 145.6 (4C, C19), 142.8, 142.7, 139.3. 139.2 (4C, C13, C16), 137.5 (1C, C4), 132.0, 131.9 (4C, C18) 131.5, 131.4 (2C, C17), 129.1 (2C, C5), 128.4 (2C, C6), 127.7, 126.7, 126.7 (6C, C14A, C15), 126.3 (1C, C7), 126.1 (2C C14B), 80.5 (1C, C1), 78.5 (1C, C10), 58.8 (1C, C2), 27.2 (3C, C11), 26.9 (1C, C3).
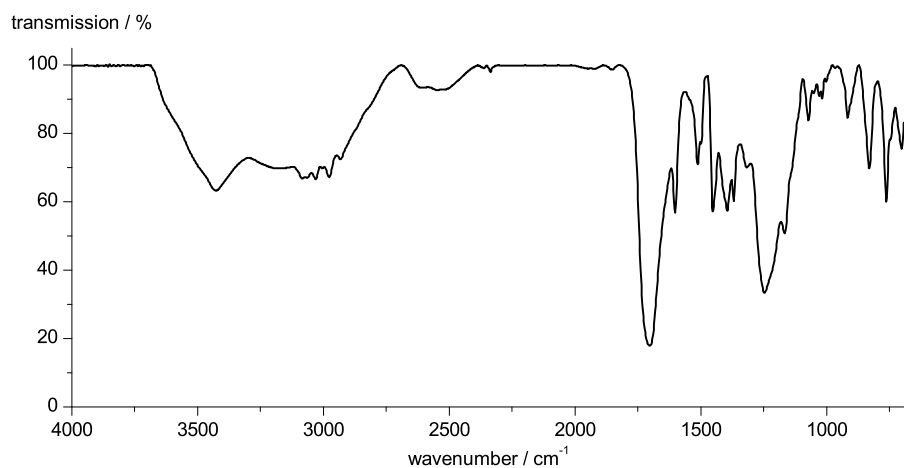


**IR (KBr):** $\widetilde{\nu}$ = 3432 (br), 3186, (w), 3083 (s), 3029 (s), 2975 (s), 2929 (s), 2605 (s), 1708 (s), 1604 (m), 1510 (m), 1452 (m), 1394 (m), 1367 (m), 1247 (s), 1164 (m), 1072 (s), 912 (m), 831 (m), 762 (m), 669 (m).

## 4.30  4,4-Di-(3′,5′-dicarboxybiphenyl)-5-isopropyl-oxa-zolidin-2-one (125)
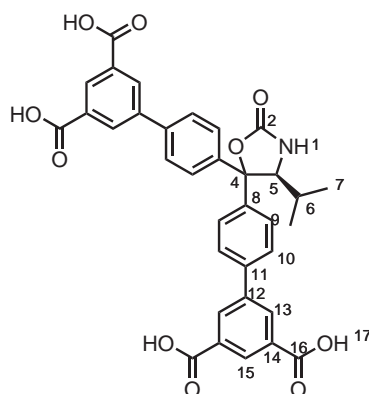


To a solution of the tetramethyl ester **118** (2.6 g, 3.91 mmol, 1 eq.) in tetrahydrofuran (125 mL) was added water (125 mL) and a solution of potassium hydroxide (KOH, 2 $\frac{mol}{L}$, 13.7 mL, 27.4 mmol, 7 eq.). The reaction was heated to reflux for 2-3 hours and was monitored by TLC. Upon consumption of compound **118**, the reaction mixture was allowed to cool to room temperature. The reaction mixture was concentrated in vaccuum to remove most of the THF. The residue was diluted with water (250 mL) and concentrated hydrochloric acid was added dropwise until pH $2-5$ was reached. This resulted in the precipitation of the tetracarboxylic acid. The suspension was centrifuged and the liquid phase was discarded. The precipitate was washed with water and then dried in vacuum.

Yield: 1.57 g (2.40 mmol, 85%); white powder; **M:** [$C_{34}H_{27}NO_{10}$] 609.6 $\frac{g}{mol}$; **m.p.:** 255 °C (decomposition); **opt. rot.:** $[\alpha]_D^{27} = -82.7$ (c = 0.73, MeOH); **HRMS (ESI+):** $\frac{m}{z}$ = 610.1721 (calc. for MH$^+$: 610.1708); **elem. anal.:** % = C (55.79), H (4.62), N (1.33), O (24.09) calc. for $C_{38}H_{35}NO_{10}$: C (66.99), H (4.46), N (2.30), O (26.25).

294
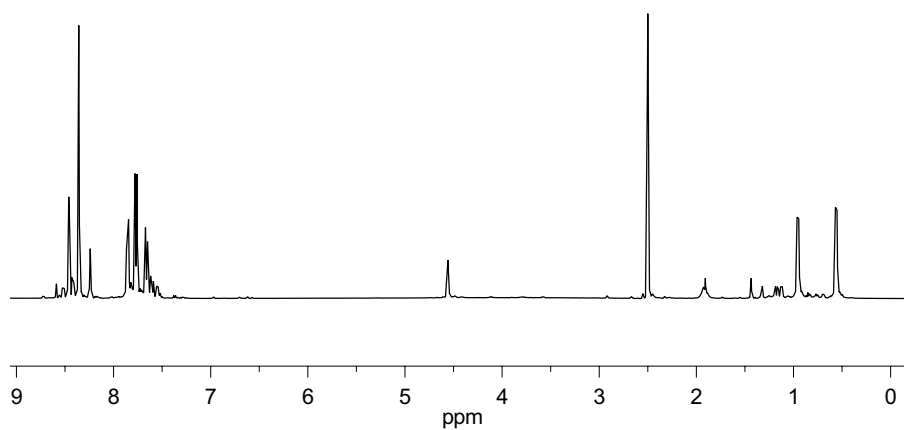
**$^1$H-NMR (300 MHz, DMSO$-$d$_6$):** $\delta$ [ppm] = 8.50-8.45 (m, 2H, H15), 8.40-8.32 (m, 4H, H13), 8.24 (s, 1H, H1), 7.89-7.82 (m, 2H, H9A), 7.80-7.73 (m, 4H; H8A, H9B), 7.70-7.63 (m, 2, H8B), 4.59-4.53 (m, 1H, H5), 1.99-1.85 (m, 1H, H6), 0.96 (d, 3H, $^3J_{\text{H-H}}$ = 6.5 Hz, H6A), 0.56 (d, 3H, $^3J_{\text{H-H}}$ = 6.5 Hz, H6B).
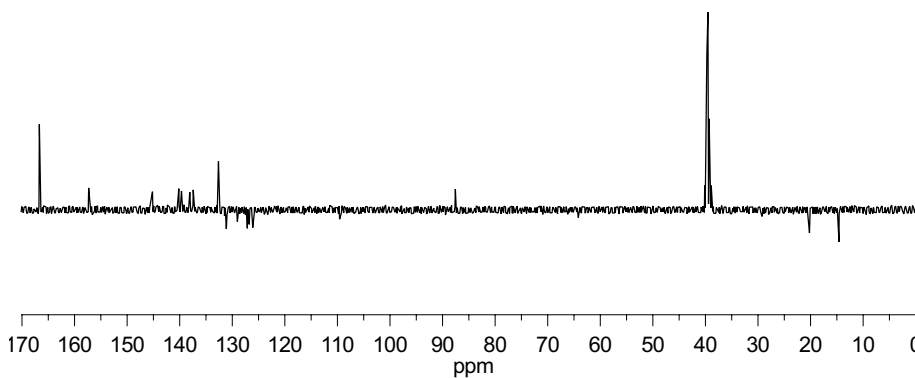


**$^{13}$C-NMR (75 MHz, DMSO$-$d$_6$):** $\delta$ [ppm] = 166.8 (4C, C16) 157.3 (1C, C2), 145.2 (2C, C14), 139.7 (2C, C10), 138.1, 137.5 (2C, C8), 132.8, 131.1 (2C, C12), 129.1 (2C, C12), 128.9, 128.7 (2C, C14), 127.2, 126.8, 126.5, 126.1 (8C, C9, C10), 87.6 (1C, C4), 64.2 (1C, C5), 29.2 (1C, C6), 20.2, 14.6 (2C, C7).
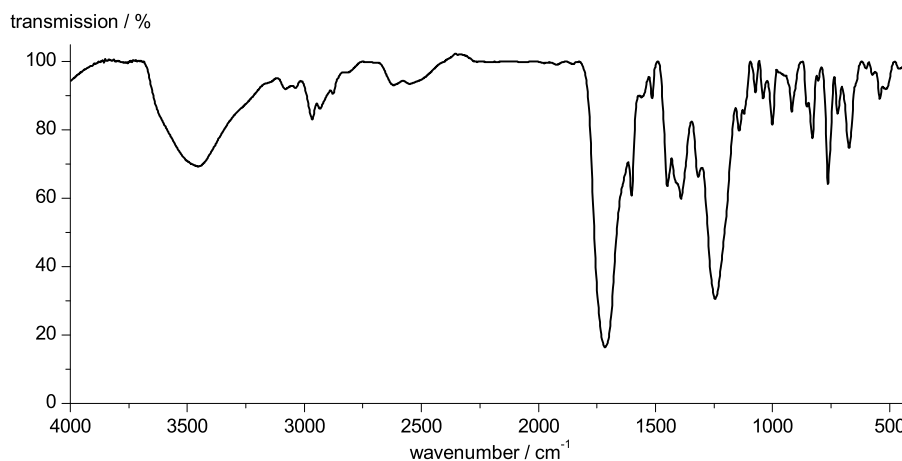
**IR (KBr):** $\widetilde{\nu}$ [cm$^{-1}$] = 3454 (m), 2966 (w), 2934 (w), 1717 (s), 1603 (m), 1514 (w), 1450 (m), 1391 (m), 1317 (m), 1246 (s), 1142 (m), 1123 (w), 1040 (w), 1001 (w), 918 (w), 853 (w), 829 (m), 764 (m), 721 (w), 673 (m), 542 (w).

## 4.31 4,4-Di-(3′,5′-dicarboxybiphenyl)-5-benzyl-oxazo-lidin-2-one (126)
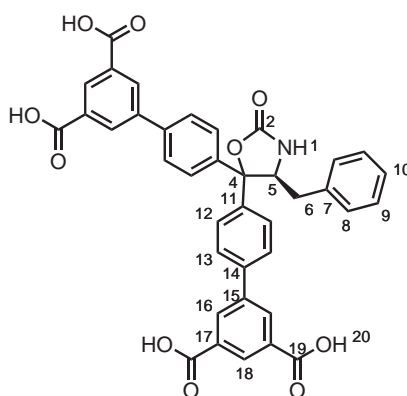


To a solution of the tetramethyl ester **119** (1.0 g, 1.40 mmol, 1 eq.) in tetrahydro-furan (75 mL) was added water (75 mL) and a solution of potassium hydroxide

(KOH, 2 $\frac{mol}{L}$, 4.9 mL, 9.8 mmol, 7 eq.). The reaction was heated to reflux for 2-3 hours and was monitored by TLC. Upon consumption of compound **119**, the reaction mixture was allowed to cool to room temperature. The reaction mixture was concentrated in vaccuum to remove most of the THF. The residue was diluted with water (200 mL) and concentrated hydrochloric acid was added dropwise until pH $2-5$ was reached. This resulted in the precipitation of the tetracarboxylic acid. The suspension was centrifuged and the liquid phase was discarded. The precipitate was washed with water and then dried in vacuum.

Yield: 0.92 g (1.40 mmol, quant.); white powder; **M:** [$C_{38}H_{27}NO_{10}$] 657.6 $\frac{g}{mol}$; **m.p.:** 253.5 °C (decomposition); **opt. rot.:** $[\alpha]_D^{27} = -45.0$ (c = 0.20, MeOH); **HRMS (ESI+):** $\frac{m}{z}$ = 658.1708 (calc. for MH$^+$: 658.1708); **elem. anal.:** % = C (59.34), H (3.99), N (1.87), O (2.02) calc. for $C_{38}H_{27}NO_{10}$: C (69.40), H (4.14), N (2.13), O (24.33).
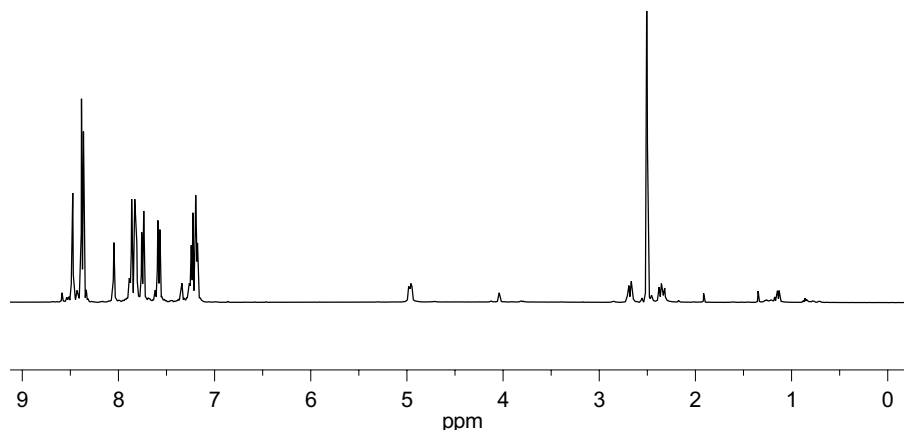


**$^1$H-NMR (300 MHz, DMSO$-$d$_6$):** $\delta$ [ppm] = 8-50-8.47 (m, 2H, H18), 8.38 (d, 2H, $^4J_{H-H}$ = 1.6 Hz, H16B), 8.37 (d, 2H, $^4J_{H-H}$ = 1.6 Hz, H16B), 8.04 (s, 1H, H1), 7.91-7.79 (m, 4H, H12A, H13A), 7.78-7.70 (m, 2H, H13B), 7.62-7.53 (m, 2H, H12B), 7.31–7.13 (m, 5H, H8, H0, H10), 4.96 (dd, 1H, $^3J_{H-H}$ = 9.2, 4.1 Hz, H4), 2.68 (dd, 1H, $^2J_{H-H}$ = 13.7, 4.1 Hz, H6A), 2.35 (dd, 1H, $^3J_{H-H}$ = 13.7, 9.4 Hz, H6B).
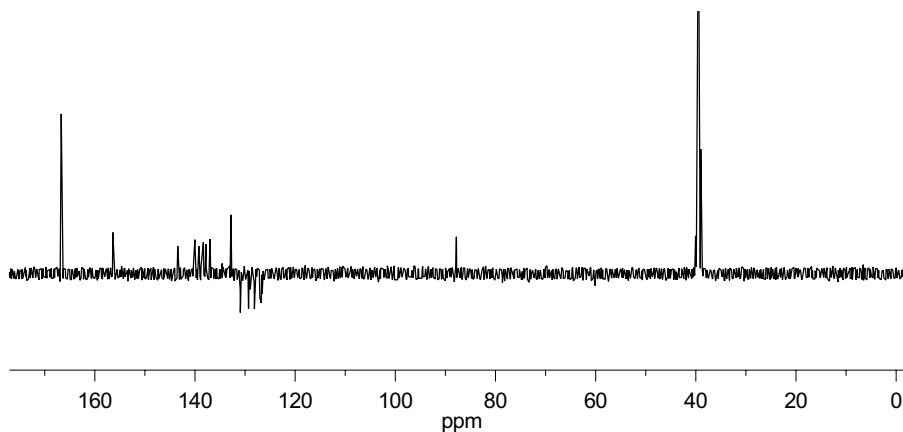
**$^{13}$C-NMR (75 MHz, DMSO$-$d$_6$):** $\delta$ [ppm] = 166.9 (4C, C19), 156.5 (1C, C2), 143.5, 139.3 (2C, C14), 138.5 (1C, C11A), 138.0 (1C, C6), 137.1 (1C, C11B), 133.0 (6C, C16A, C17), 131.0 (2C, C16B), 129.4 (2C, C8), 128.5, 128.4 (2C, C18), 128.2 (4C, C15, C9), 127.2 (2C, C13A), 126.8 (4C, C11A, C13B), 126.7 (2C, C12A), 126.3 (1C, C10), 87.9 (1C, C4), 60.3 (1C, C5), 38.6 (1C, C6).



**IR (KBr):** $\widetilde{\nu}$ [cm$^{-1}$] = 3443 (s), 3084 (w), 3063 (w), 3032 (w), 2922 (w), 1715 (s), 1603 (m), 1555 (w), 1514 (w), 1497 (w), 1452 (m), 1394 (m), 1244 (s), 1144 (w), 1074 (w), 1032 (w), 1001 (w), 916 (w), 833 (m), 764 (m), 741 (w), 719 (w), 702 (w), 675 (m), 511 (w).

## 4.32 Di-(3′,5′-dicarboxybiphenyl)-prolinol (128)
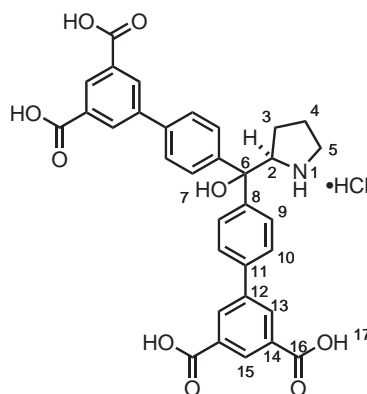


To a suspension of tetramethyl ester **120** (3.35 g, 4.60 mmol, 1 eq.) in MeOH (125 mL) concentrated sulfuric acid ($H_2SO_4$) was added dropwise until a clear, light yellow solution was obtained. This solution was transferred to a glass-lined steel autoclave, where it was stirred under nitrogen atmosphere (8 bar) for one hour. To this solution was added palladium on carbon (Pd/C, 10 wt %, 400 mg). The autoclave was flushed with nitrogen, then with hydrogen. The reaction was heated to 50 °C and stirred under a hydrogen atmosphere (50 bar) for at least three days. The reaction was monitored by TLC. Upon consumption of compound **120**, the reaction mixture was allowed to cool to room temperature and was filtered over celite to remove the catalyst. The filter cake was washed with MeOH (50 mL). The filtrate was concentrated in vacuum and used without further purification in the next step.

The residue was dissolved in THF (150 mL). Water (150 mL) and a solution of potassium hydroxide (KOH, $2\,\frac{mol}{L}$, 16.1 mL, 32.5 mmol, 7 eq.) were added. The reaction was heated to reflux for 2.5 hours. The reaction mixture was allowed to cool to room temperature and was concentrated in vaccum to remove most of the THF. The residue was diluted with water (300 mL) and concentrated hydrochloric acid was added dropwise until pH $2-5$ was reached. This resulted in the precipitation of the tetracarboxylic acid. The suspension was centrifuged and the liquid phase was discarded. The precipitate was washed with water and then dried in vacuum.

Yield: 2.02 g (3.29 mmol, 71% over two steps); white powder;
**M:** [$C_{33}H_{28}ClNO_9$] 618.0 $\frac{g}{mol}$; **opt. rot.:** $[\alpha]_D^{26} = +41.3$ (c = 0.30, MeOH); **HRMS (ESI+):** $\frac{m}{z}$ = 582.1773 (calc. for $C_{33}H_{28}NO_9$: 582.1759); **elem. anal.:** % = C

(55.91), H (4.87), N (1.71), O (25.11), calc. for $C_{33}H_{28}ClNO_9$: C (61.13), H (4.57), Cl (2.27), O (23.30) .
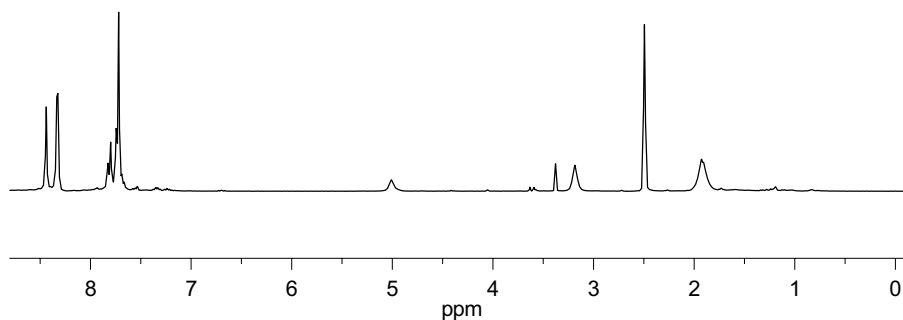


**$^1$H-NMR (300 MHz, DMSO$-$d$_6$):** $\delta$ [ppm] = 8.47-8.40 (m, 2H, H15), 8.37-8.29 (m, 4H, H13), 7.86-7.65 (m, 8H, H9, H10), 5.13-4.93 (m, 1H, H2), 3.28-3.09 (m, 2H, H5), 2.05-1.79 (m, 4H, H3, H4).
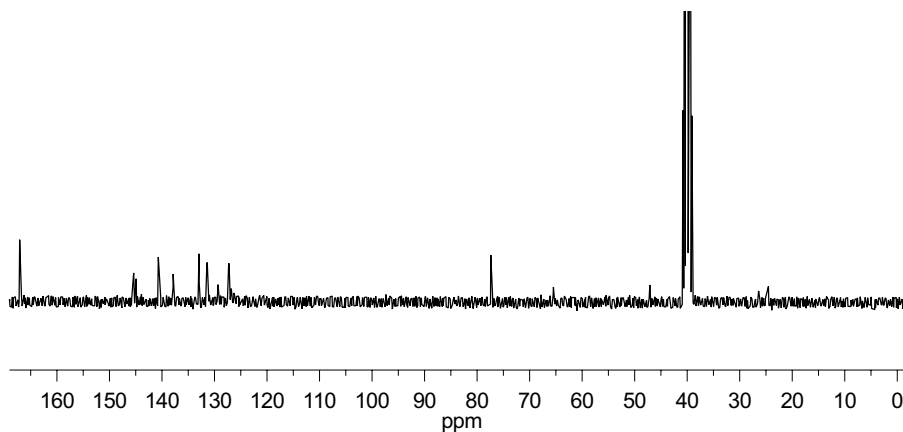


**$^{13}$C-NMR (75 MHz, DMSO$-$d$_6$):** $\delta$ [ppm] = 166.72, 166.67 (4C, C16), 144.96, 144.49 (2C, C8 or C11), 140.28 (br, 2C, C8 or C11), 137.45,137.22 (2C, C12), 132.64, 132.52 (4C, C14), 131.03, 130.95 (4C, C13), 128.90 (br, 2C, C15), 126.97, 126.88,

126.79, 126.46 (8C, C9, C10), 76.97 (1C, C6), 65.04 (1C, C2), 46.69 (1C, C5), 25.97 (1C, C3), 24.11 (1C, C2).
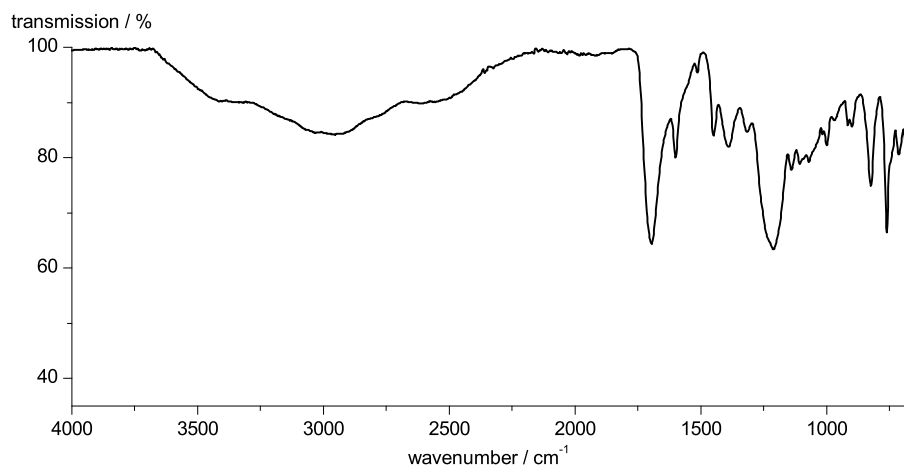


**IR (KBr):** $\widetilde{\nu}$ [cm$^{-1}$] = 3400 (br), 2966 (br), 1697 (s), 1600 (m), 1452 (m), 1388 (m), 1207 (s), 997 (m), 916 (m), 898 (m), 823 (m), 759 (s), 665 (s).

## 4.33   1,1-Di-(3',5'-dicarboxybiphenyl)-alaninol (129)
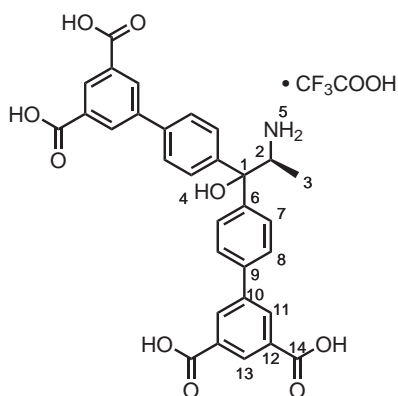
A suspension of tetracarboxylic acid **121** (600 mg, 0.92 mmol, 1 eq.) in $CH_2Cl_2$ (100 mL) was cooled to 0 °C. Trifluoro acetic acid (25 mL) was added. The reaction was stirred for two hours while the mixture was allowed to warm to room temperature. Upon the addition of diethyl ether (150 mL) a white precipitate of the ammonium salt of the tetracarboxylic acid was obtained. The suspension was cooled to 4 °C and the precipitate was collected by filtration. After washing with diethyl ether (50 mL), the ammonium salt of the tetracarboxylic acid was dried in vacuum.

Yield: 458 mg (0.68 mmol, 75%); white powder; **M:** $[C_{33}H_{26}F_3NO_{11}]$ 669.9 $\frac{g}{mol}$; **opt. rot.:** $[\alpha]_D^{27} = -17.5$ (c = 0.40, MeOH); **HRMS (ESI+):** $\frac{m}{z}$ = 556.1611 (calc. for $C_{31}H_{26}NO_{11}^+$: 556.1602) **elem. anal.:** % = C (54.52), H (5.06), F (n.d.), N (1.40), O (24.51) calc. for $C_{23}H_{29}Br_2NO_3$: C (60.76), H (4.53), F (8.01), N (1.97), O (24.73). .
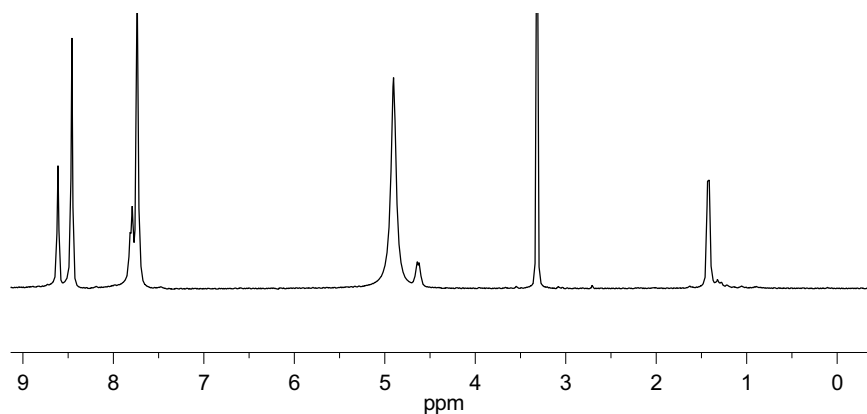


**$^1$H-NMR (300 MHz, CD$_3$OD):** $\delta$ [ppm] = 8.63-8.56 (m, 2H, H13), 8.44-8.40 (m, 2H, H11), 7.81-7.65 (m, 8H, H7, H8), 4.60 (q, 1H, $^3J_{H-H}$ = 6.5 Hz H2), 1.41 (d, 3H, $^3J_{H-H}$ = 6.5 Hz, H3).
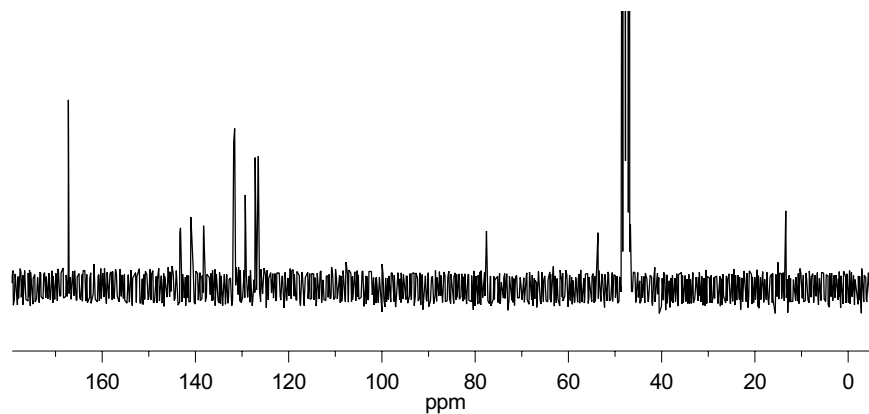
**¹³C-NMR (75 MHz, CD₃OD):** $\delta$ [ppm] = 168.7(br) (4C, C14), 144.73, 144.58 (4C, C6 or C9), 142.34, 142.28 (4C, C6 or C9), 139.82, 139.61 (2C, C10), 133.23, 133.20 (4C, C14), 132.99, 132.96 (4C, C11), 130.7(br) (2C, C13), 128.56, 128.18, 128.07, 127.87 (8C, C7, C8), 78.95 (1C, C1), 55.02 (1C, C2), 14.75 (1C, C3).
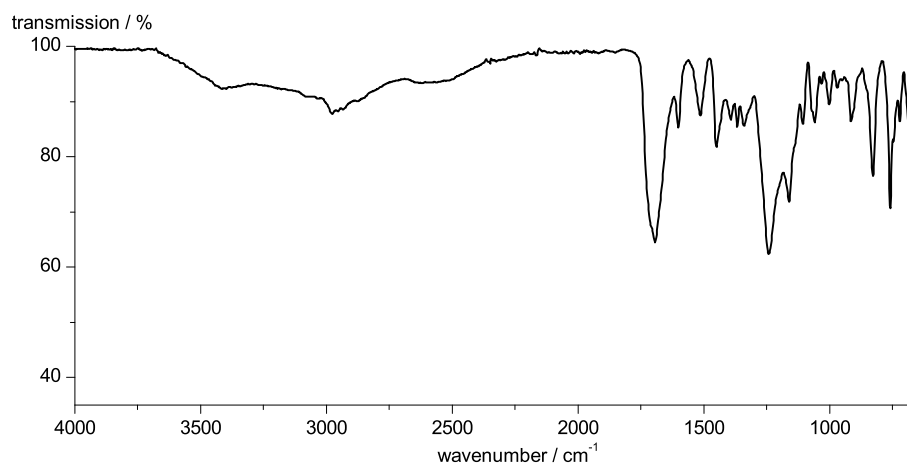


**IR (ATR):** $\widetilde{\nu}$ = 3415 (br), 2977 (w), 2952 (w), 2931 (w), 2557 (br), 1963 (s), 1600 (m), 1515 (m), 1446 (m), 1394 (m), 1367 (m), 1338 (m), 1240 (s), 1159 (s), 1107 (m), 1058 (m), 999 (w), 916 (m), 827 (m), 757 (m), 673 (m).

## 4.34 1,1-Di-(3′,5′-dicarboxybiphenyl)-valinol (130)
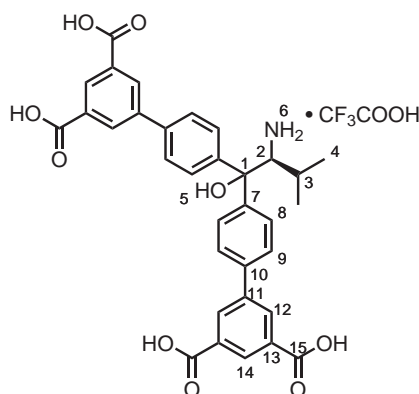


A suspension of tetracarboxylic acid **122** (500 mg, 0.73 mmol, 1 eq.) in $CH_2Cl_2$ (100 mL) was cooled to 0 °C. Trifluoro acetic acid (25 mL) was added. The reaction was stirred for two hours while the mixture was allowed to warm to room temperature. Upon the addition of diethyl ether (150 mL) a white precipitate of the ammonium salt of the tetracarboxylic acid was obtained. The suspension was cooled to 4 °C and the precipitate was collected by filtration. After washing with diethyl ether (50 mL), the ammonium salt of the tetracarboxylic acid was dried in vacuum.

Yield: 370 mg (0.53 mmol, 75%); white powder; **M:** $[C_{35}H_{30}F_3NO_{11}]$ 697.6 $\frac{g}{mol}$; **opt. rot.:** $[\alpha]_D^{27} = -19.2$ (c = 0.26, MeOH); **HRMS (ESI+):** $\frac{m}{z}$ = 584.1911 (calc. for $C_{33}H_{30}NO_9^+$: 584.1921).
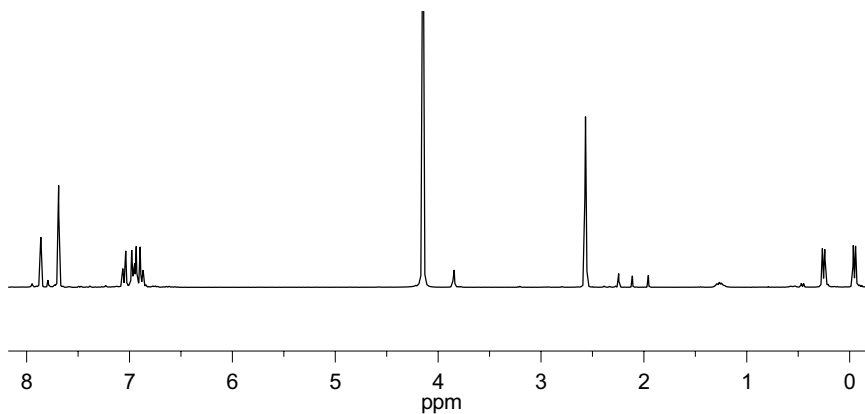
**¹H-NMR (300 MHz, DMSO−d₆):** $\delta$ [ppm] = 8.60-8.58 (m, 2H, H14) 8.44-8.42 (m, 4Hm H12), 7.81-7.69 (m, 8H, H8, H9), 4.58 (d, $^3J_{H\text{-}H}$ = 2.8 Hz, H2), 2.32-2.17 (m, 1H, H3), 1.18 (d, 3H, $^3J_{H\text{-}H}$ = 7.1 Hz, H4A), 1.11 (d, 3H, $^3J_{H\text{-}H}$ = 6.9 Hz, H4B).
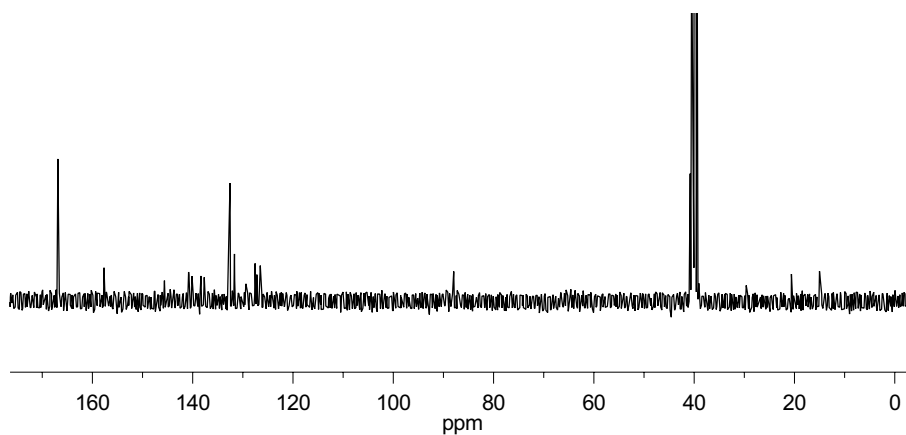


**¹³C-NMR (75 MHz, CD₃OD):** $\delta$ [ppm] = 167.2 (br) (4C, C15), 144.7, 144.6 (4C, C7 or C10), 141.0, 140.9 (4C, C7 or C10), 138.5, 138.3 (2C, C11), 131.9, 131.8 (4C, C15), 131.6, 131.5 (4C, C12), 129.3 (br) (2C, C14), 127.2, 126.8, 126.6 (br) (8C, C8, C9), 79.4 (1C, C1), 62.1 (1C, C2), 27.1 (1C, C3), 21.3, 16.0 (2C, C4).

**IR (ATR):** $\tilde{\nu}$ [cm$^{-1}$] = 2960(w), 2929 (w), 2873 (m), 1655 (s), 1594 (s), 1570 (m), 1545 (m), 1518 (m), 1395 (s), 1366 (m), 1312 (m), 1247 (m), 1159 (m), 1090 (m), 1004 (w), 868 (m), 781 (s).

## 4.35 1,1-Di-(3′,5′-dicarboxybiphenyl)-leucinol (131)
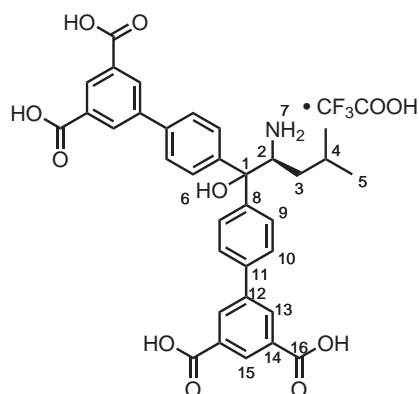


A suspension of tetracarboxylic acid **123** (500 mg, 0.72 mmol, 1 eq.) in $CH_2Cl_2$ (80 mL) was cooled to 0 °C. Trifluoro acetic acid (20 mL) was added. The reaction was stirred for two hours while the mixture was allowed to warm to room temperature. Upon the addition of diethyl ether (150 mL) a white precipitate of the ammonium salt of the tetracarboxylic acid was obtained. The suspension was cooled to 4 °C and the precipitate was collected by filtration. After washing with diethyl ether (50 mL), the ammonium salt of the tetracarboxylic acid was dried in vacuum.

Yield: 408 mg (0.57 mmol, 75%); white powder; **M:** $[C_{36}H_{32}F_3NO_{11}]$ 711.6 $\frac{g}{mol}$; **opt. rot.:** $[\alpha]_D^{26} = +15.0$ (c = 0.60, MeOH); **HRMS (ESI+):** $\frac{m}{z}$ = 598.2074 (calc. for $C_{34}H_{32}NO_9^+$: 598.2072) .
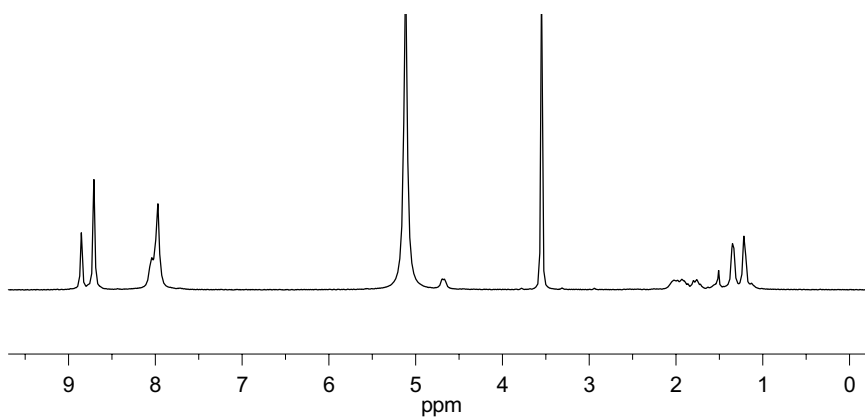
**$^1$H-NMR (300 MHz, CD$_3$OD):** $\delta$ [ppm] = 8.62 (q, 2H, $^2J_{\text{H-H}}$ = 1.5 Hz, H15), 8.50-8.46 (m, 4H, H13), 7.83-7.69 (m, 8H, H9, H10), 4.43 (d, 1H, $^3J_{\text{H-H}}$ = 10.3 Hz, H2), 1.86-1.64 (m, 2H, H3A, H4), 1.61-1.45 (m, 1H, H3B), 1.11 (d, 3H, $^3J_{\text{H-H}}$ = 6.4 Hz, H5A), 0.98 (d, 3H, $^3J_{\text{H-H}}$ = 6.4 Hz, H5B).
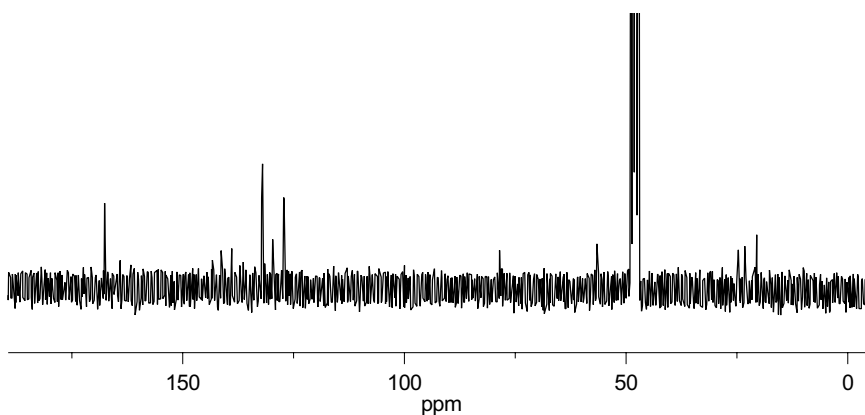


**$^{13}$C-NMR (75 MHz, CD$_3$OD):** $\delta$ [ppm] = 167.2 (4C, C16), 143.1, 142.9 (2C, C8 or C11), 141.0, 140.9 (2C, C8 or C11), 138.63(2C, C12), 131.8 (4C, C14), 131.63, 131.60 (4C, C13), 129.36 (2C, C15), 127.19, 126.89, 126.82, 126.75 (8C, C12, C13) 78.1 (1C, C1), 56.3 (1C, C2), 24.3 (1C, C3), 22.8 (1C, C4), 20.0 (br, 2C, C5).

**IR (ATR):** $\widetilde{\nu}$ = 3083 (br), 2962 (w), 2900 (w), 2871 (w), 1455 (s), 1598 (m), 1450 (m), 1411 (m), 1388 (m), 1319 (m), 1186 (s), 1141 (s), 1065 (m), 916 (w), 831 (m), 761 (m), 717 (m), 665 (m).

## 4.36   1,1-Di-(3′,5′-dicarboxybiphenyl)-alaninol (132)
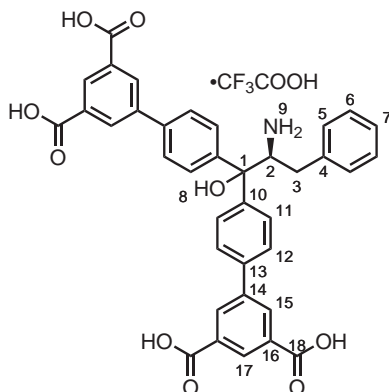


A suspension of tetracarboxylic acid **124** (500 mg, 0.73 mmol, 1 eq.) in $CH_2Cl_2$ (100 mL) was cooled to 0 °C. Trifluoro acetic acid (25 mL) was added. The reaction was stirred for two hours while the mixture was allowed to warm to room

temperature. Upon the addition of diethyl ether (150 mL) a white precipitate of the ammonium salt of the tetracarboxylic acid was obtained. The suspension was cooled to 4 °C and the precipitate was collected by filtration. After washing with diethyl ether (50 mL), the ammonium salt of the tetracarboxylic acid was dried in vacuum.

Yield: 384 mg (0.51 mmol, 75%); white powder; **M:** $[C_{39}H_{30}F_3NO_{11}]$ 745.1 $\frac{g}{mol}$; **opt. rot.:** $[\alpha]_D^{25} = +21.2$ (c = 0.52, MeOH); **HRMS (ESI+):** $\frac{m}{z}$ = 632.1922 (calc. for $C_{37}H_{30}NO_9^+$: 632.1915), **elem. anal.:** % = C (52.26), H (4.02), N (1.31), O (n.d.), calc. for $C_{39}H_{30}F_3NO_{11}$: C (62.82), H (4.06), N (1.88), O (23.60) .
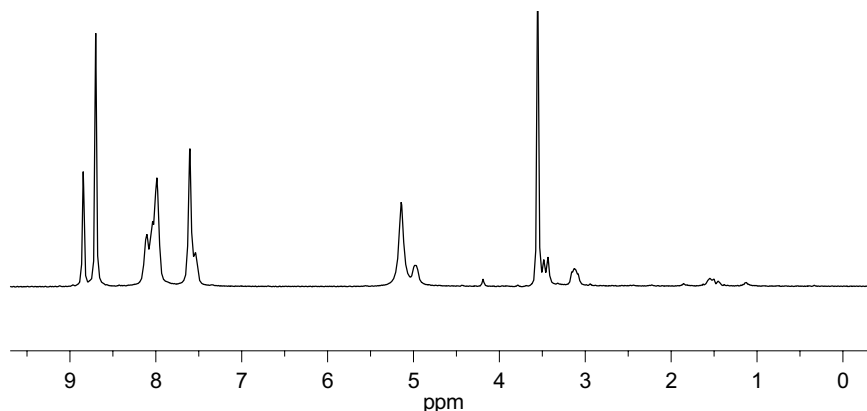


**$^1$H-NMR (300 MHz, CD$_3$OD):** $\delta$ [ppm] = 8.96-8.78 (m, 2H, H17), 8.77-8.60 (m, 4H, H15), 8.18-7.91 (m, 8H, H11, H12), 7.67-7.48 (m, 5H, H5, H6, H7), 4.97 (d, 1H, $^3J_{H-H}$ = 9.5 Hz, H2), 3.46 (d, $^2J_{H-H}$ = 14.9 Hz, H3A), 3.19-3.04 (m, 1H, H3B).
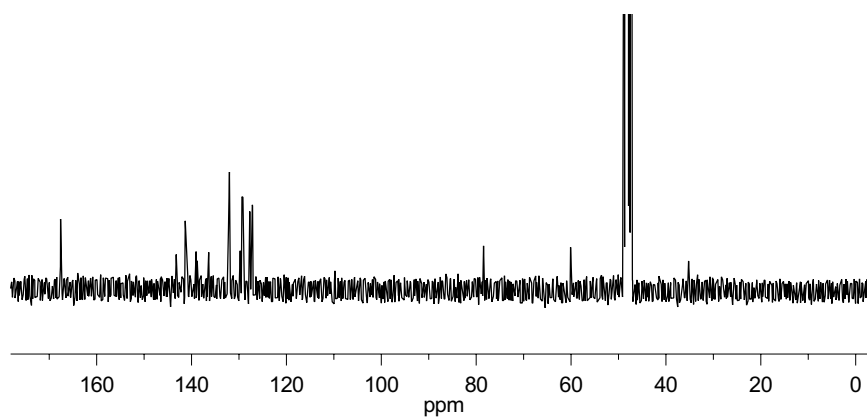
**¹³C-NMR (75 MHz, CD₃OD):** $\delta$ [ppm] = 167.7 (4C, C18), 143.3, 143.2 (4C, C16), 141.3 (br), 139.0. 138.8 (4C, C10, C13), 136.4 (1C, C4), 132.2, 132.0 (4C, C15) 129.7 (2C, C17) 129.4 (2C, C5), 129.2 (2C, C14), 128.4 (2C, C6), 127.7, 127.3, 127.2, 127.1 (8C, C11, C12), 127.5 (1C, C7), 78.4 (1C, C1), 60.1 (1C, C2), 35.2 (1C, C3).
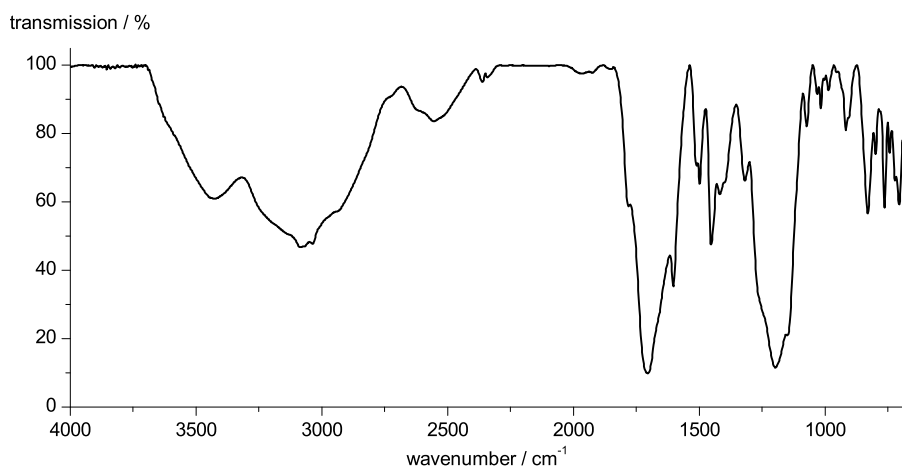


**IR (KBr):** $\widetilde{\nu}$ = 34440 (br), 3191. (br), 3083 (w), 3031 (w), 2621 (br), 2551 (br), 1971 (w), 1782 (m), 1708 (s), 1600 (s), 1498 (m), 1450 (s), 1417 (m), 1319 (m), 1195 (m), 1147 (m), 1076 (m), 918 (m), 829 (m), 763 (m), 703 (m), 667 (m).

## 4.37 Di-(3,5-dimethylphenyl)methanol (135)
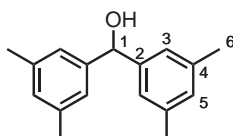


The reaction was performed oven-dried glassware under argon. Magnesium (1.96 g, 80.6 mmol, 4 eq.) was suspended in 30 mL THF and a small amount of iodine (ca. 30 mg) was added to the mixture. To this suspension 1-bromo-3,5-dimethylbenzene (5.80 ml, 41.6 mmol, 2 eq.) was added dropwise. After the addition of the bromide which resulted in an exothermic reaction, the solution was stirred for two hours and Ethylformiate (1.72 ml, 21.3 mmol, 1 eq.) was added. The reaction was heated to reflux for two hours. The reaction was cooled and excess magnesium was removed by filtration. The filtrate was treated with a saturated, aqueous solution of $NH_4Cl$ (75 mL). The resulting mixture was extracted with EtOAc (4× 30 mL). The combined organic phases were washed with the organic phase was washed with an aqueous solution of NaCl (sat.), dried over $Na_2SO_4$ and the solvent was evaporated in vacuum. The crude reaction product was recrystallized from $Et_2O$.

Yield: 8.80 g (36.6 mmol, 88%); colorless crystals; **M:** $[C_{17}H_{20}O]$ 240.3 $\frac{g}{mol}$; **TLC:** $R_f = 0.49$ (heptane/EtOAc, 4:1); **MS (EI-):** $\frac{m}{z} = 240$ (calc. for $M^+$: 240).
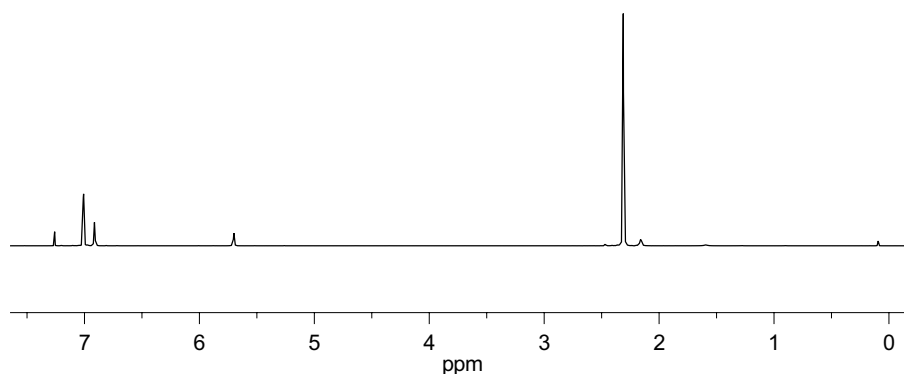
**$^1$H-NMR (300 MHz, CDCl$_3$):** $\delta$ [ppm] = 8.71 (t, 2H, $^4J_{\text{H-H}}$ = 1.63 Hz, H5), 8.44 (d, 4H, $^4J_{\text{H-H}}$ = 1.63 Hz, H3), 5.72 (s, 1H, H1), 2.33 (s, 12H, H6).
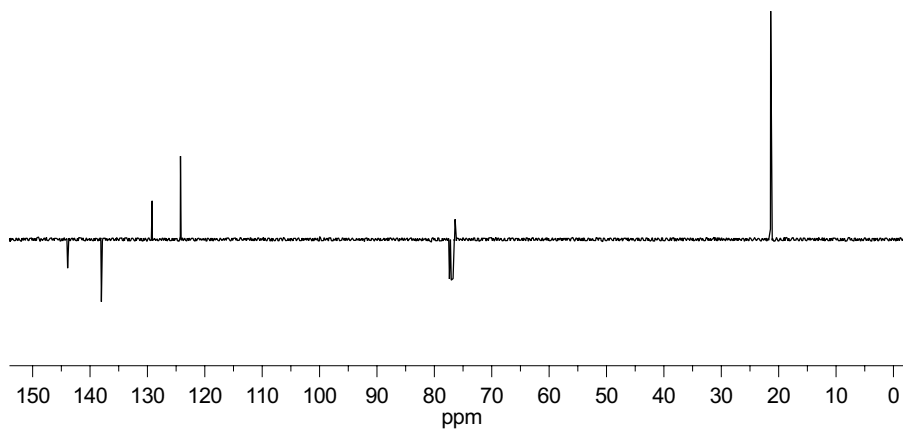


**$^{13}$C-NMR (75 MHz, CDCl$_3$):** $\delta$ [ppm] = 143.9 (2C, C2), 138.0 (4C, C4), 129.2 (2C, C5), 124.2 (4C, C3), 76.4 (1C, C1), 21.4 (4C, C6).
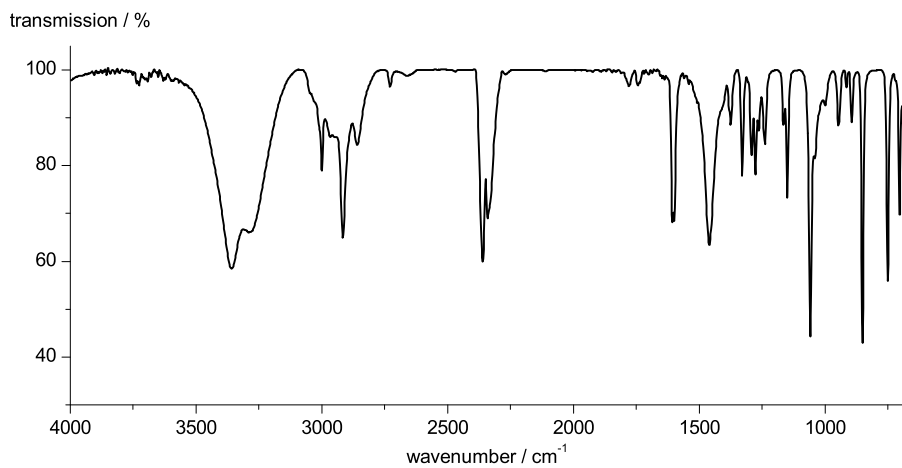


**IR (ATR):** $\widetilde{\nu}$ [cm$^{-1}$] = 3353 (br), 3280 (br), 3037 (w), 2999 (w), 2916 (m), 2858 (m), 1598 (s), 1460 (s), 1328 (m), 1238 (m), 1149 (m), 1056 (s), 947 (w), 850 (s), 750 (s).

## 4.38 3,3′,5,5′-Tetracarboxy benzophenone (136)
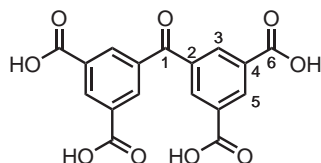


A suspension of di-(3,5-dimethylphenyl)methanol (**135**) (1.50 g, 3.35 mmol) in 30 mL of $HNO_3$ (20 %) was sealed in a teflon-lined, stainless steel autoclave. The reaction was heated in a oven at 140 °C for 14 hours. After the mixture was cooled to room temperature the reaction mixture was removed from the autoclave and filtrated. This afforded a colorless crystalline material that was washed with nitric acid (20 %) and water. The product was dried in vacuum.

Yield: 12.0 g (3.35 mmol, 53%); colorless crystals; **M:** $[C_{17}H_{10}O_9]$ 358.0 $\frac{g}{mol}$; **TLC:** $R_f = 0.0$ (EtOAc); **MS (EI-):** $\frac{m}{z} = 358$ (calc. for M$^+$: 358).
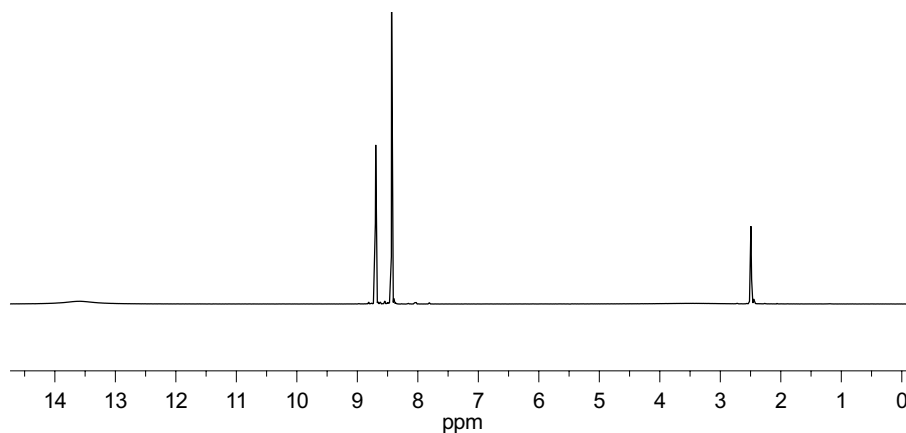


**$^1$H-NMR (300 MHz, DMSO−d$_6$):** $\delta$ [ppm] = 13.59 (s, 4H, H6), 8.70 (t, 2H, $^4J_{H\text{-}H}$ = 1.6 Hz, H5), 8.43 (d, 4H, $^4J_{H\text{-}H}$ = 1.6 Hz, H3).
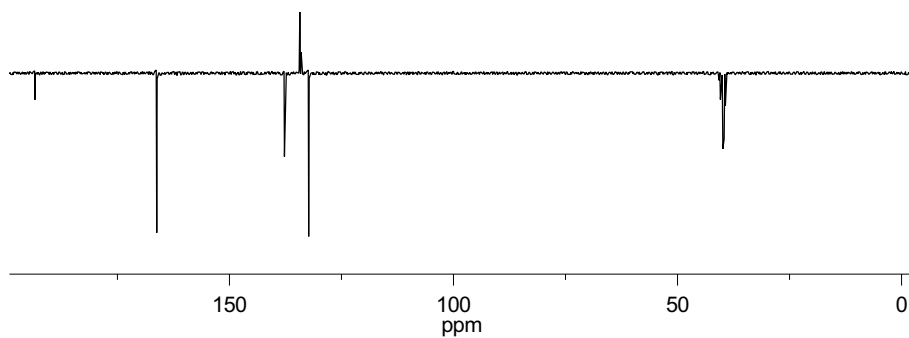
**$^{13}$C-NMR (75 MHz, DMSO$-$d$_6$):** $\delta$ [ppm] = 193.4 (1C, C1), 166.2 (4C, C6), 137.7 (2C, C2), 134.3 (4C, C3), 134.0 (2C, C5), 132.3 (4C, C4).
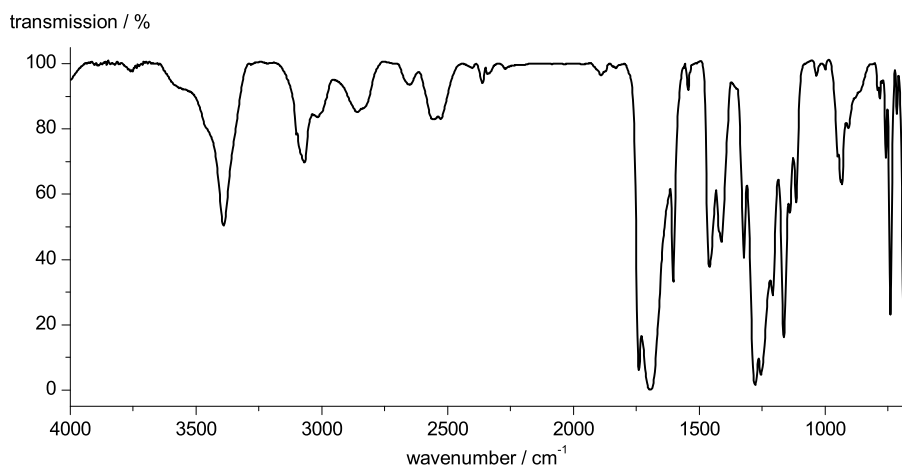


**IR (ATR):** $\widetilde{\nu}$ [cm$^{-1}$] = 3390 (br), 3068 (m), 3024 (w), 2864 (w), 1739 (s), 1685 (s), 1602 (s), 1458 (s), 1409 (m), 1323 (s), 1276 (s), 1253 (s), 1163 (s), 931 (m), 738 (s), 686 (s).

## 4.39   UHM-24-Ala-Boc (137)
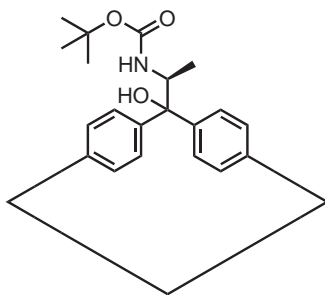


Dicarboxylic acid **99** (28.3 mg, 0.05 mmol, 1 eq.) was dissolved in DMA (4.7 mL). To this solution was a solution of zinc nitrate hexahydrate in DMA (c = 100 g/L, 0.3 mL, 30 mg $Zn(NO_3)_2 \cdot 6 H_2O$, 0.1 mmol, 2.0 eq.) The reaction mixture was placed in a screw-capped vial in an oven at 80 °C for one day. The reaction mixture was filtrated and colorless crystals were collected. These crystals were washed with DMA and dried in air.
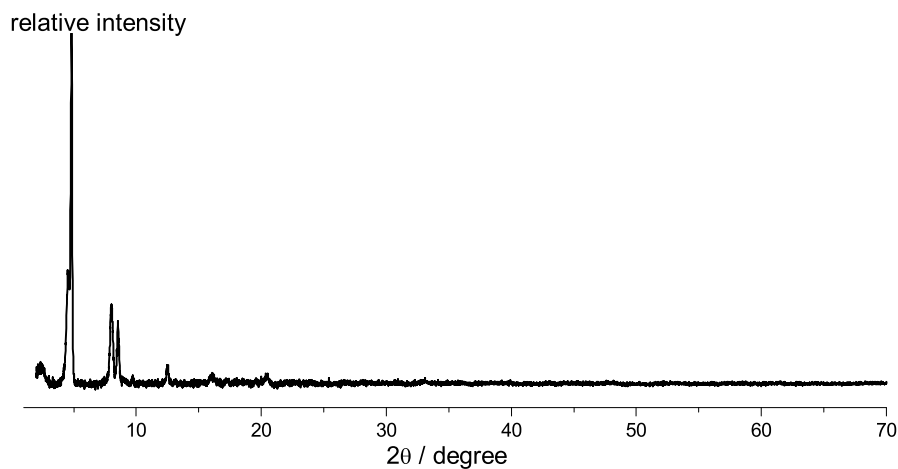


**Figure 4.1** – Powder X-ray diffractogram of UHM-24-Ala-Boc (**137**).
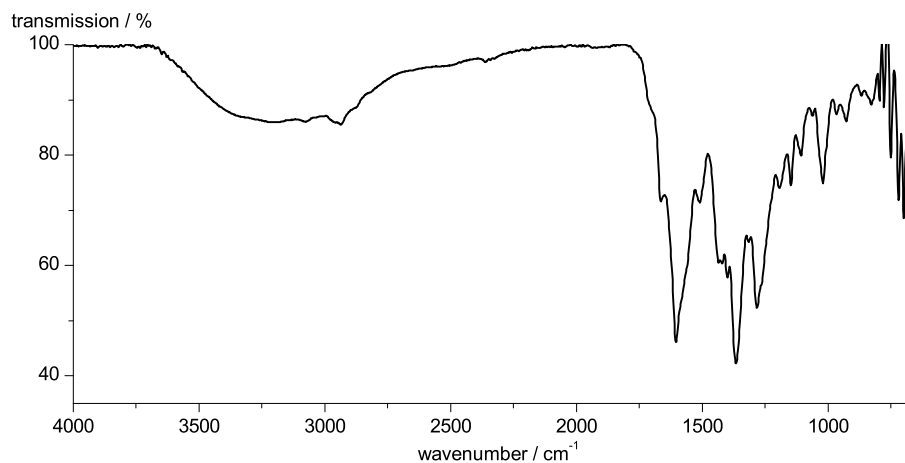
**IR (ATR):** $\widetilde{\nu}$ = 3378 (m), 2973 (w), 2934 (w), 1632 (s), 1574 (m), 1442 (m), 1367 (s), 1281 (m), 1281 (m), 1145 (m), 1112 (m), 1061 (w), 923 (w), 823 (w), 771 (m), 700 (m).

## 4.40   UHM-24-Val-Boc (138)
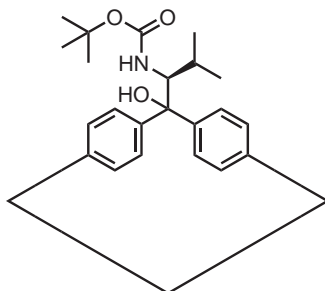


Dicarboxylic acid **100** (29.8 mg, 0.05 mmol, 1 eq.) was dissolved in DMA (4.7 mL). To this solution was a solution of zinc nitrate hexahydrate in DMA (c = 100 g/L, 0.3 mL, 30 mg $Zn(NO_3)_2 \cdot 6 H_2O$, 0.1 mmol, 2.0 eq.) The reaction mixture was placed in a screw-capped vial in an oven at 80 °C for one day. The reaction mixture was filtrated and colorless crystals were collected. These crystals were washed with DMA and dried in air.
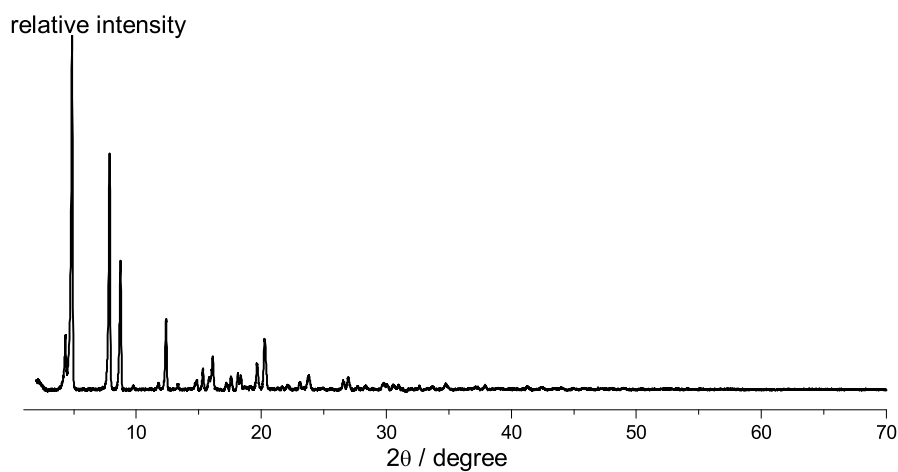
**Figure 4.2** – Powder X-ray diffractogram of UHM-24-Val-Boc (**138**).
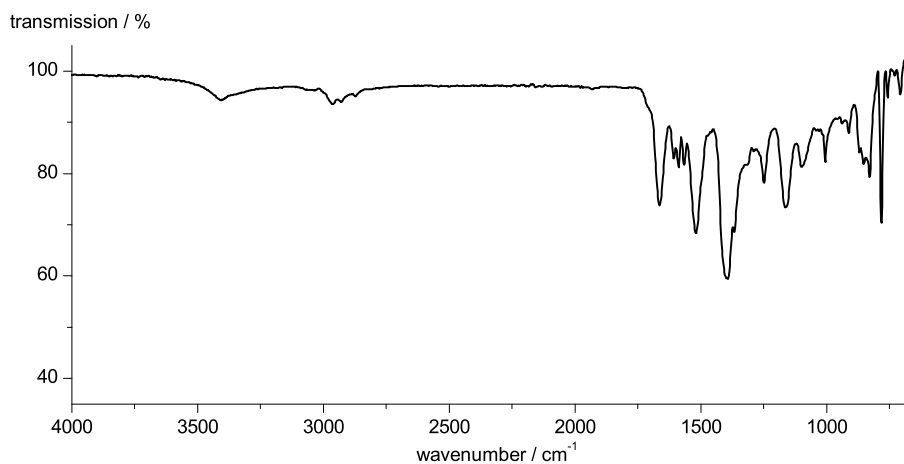


**IR (ATR):** $\widetilde{\nu}$ = 3408 (m), 2963 (w), 2929 (w), 2872 (w), 1663 (m) 1607 (m), 1587 (m), 1519 (m), 1392 (m), 1366 (m), 1288 (m), 1248 (m). 1164 (m), 1099 (w), 1005 (m), 911 (w), 781 (m).

## 4.41   UHM-24-Phe-Boc (139)
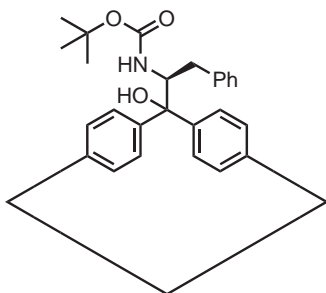


Dicarboxylic acid **101** (32.1 mg, 0.05 mmol, 1 eq.) was dissolved in DMA (4.7 mL). To this solution was a solution of zinc nitrate hexahydrate in DMA (c = 100 g/L, 0.3 mL, 30 mg Zn(NO$_3$)$_2 \cdot$ 6 H$_2$O, 0.1 mmol, 2.0 eq.) The reaction mixture was placed in a screw-capped vial in an oven at 80 °C for one day. The reaction mixture was filtrated and colorless crystals were collected. These crystals were washed with DMA and dried in air.
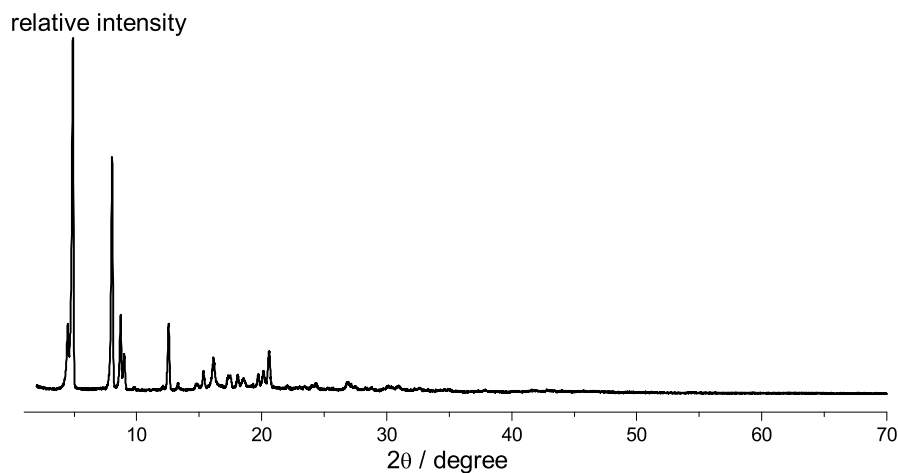


**Figure 4.3** – Powder X-ray diffractogram of UHM-24-Phe-Boc (**143**).
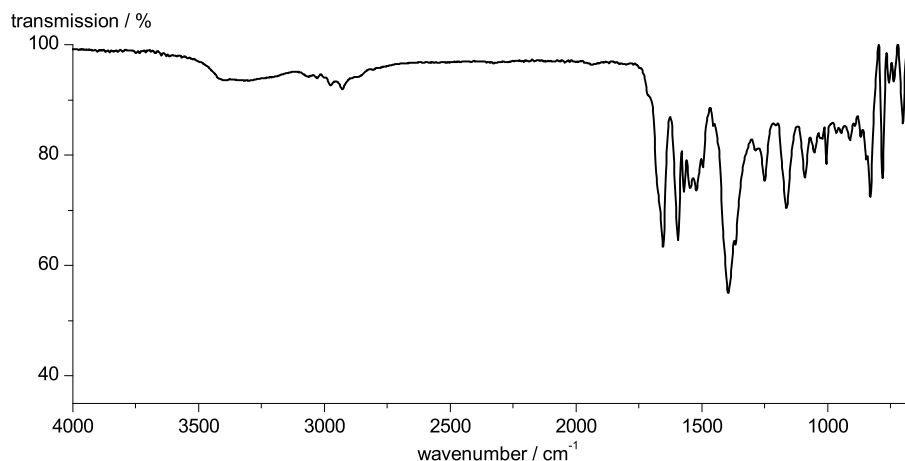
**IR (ATR):** $\widetilde{\nu}$ = 3396 (m), 3068 (m), 3026 (m), 2977 (m), 2927 (m), 1654 (s), 1596 (s), 1569 (m), 1544 (m), 1521 (m), 1494 (m), 1394 (s), 1363 (s), 1249 (m), 1159 (s), 1089 (m), 1002 (m), 827 (m), 781 (m), 700 (m).

## 4.42   UHM-25-Ala-Boc (140)
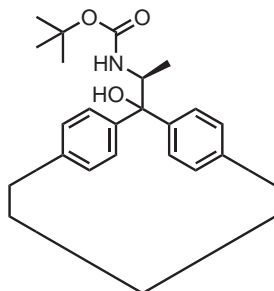


For the synthesis of bulk material, tetracarboxylic acid **121** (377 mg, 0.58 mmol, 1 eq.) was dissolved in DMF (24 mL). To this solution was added nitric acid (20 %, 1.9 mL), and then an aqueous solution of copper nitrate trihydrate (c = 100 g/L, 8.8 mL, 88 mg $Cu(NO_3)_2 \cdot 3\,H_2O$, 0.4 mmol, 0.6 eq.) The reaction mixture was placed in an oven at 50 °C for three days. The mother liquor was decanted and the crystals suspended in fresh DMF. This procedure was repeated

319

twice after 24 hours each. DMF was then replaced with THF in the same manner. The solvent-exchanged MOF was kept under THF and stored in a closed container.

A fraction of the MOF was digested in diluted hydrochloric acid to reisolate the linker for spectroscopic measurements: **HRMS (ESI+):** $\frac{m}{z}$ = 678.1918 (calc. for MNa$^+$: 678.1951); **opt. rot.:** $[\alpha]_D^{25} = -18.7$ (c = 0.33 g/100 mL, MeOH).
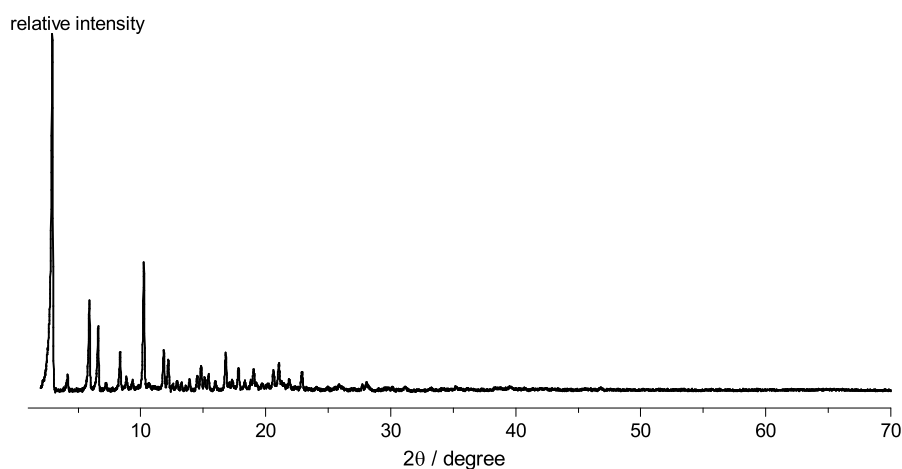


**Figure 4.4** – Powder X-ray diffractogram of UHM-25-Ala-Boc (**140**).
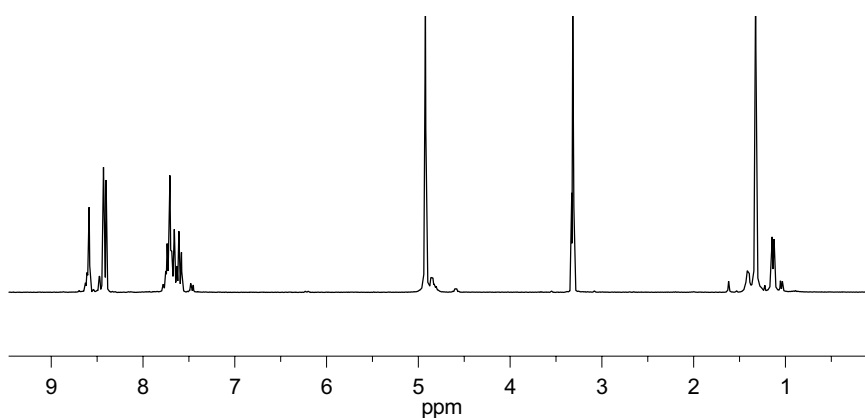


**Figure 4.5** – $^1$H-NMR of the digested MOF UHM-25-Ala-Boc

**$^1$H-NMR (300 MHz, CD$_3$OD):** $\delta$ [ppm] = 8.60-8.58 (m, 2H, H16), 8.42 (d, 2H $^4J_{\text{H-H}}$ = 1.7 Hz, H14A), 8.49 (d, 2H, $^4J_{\text{H-H}}$ = 1.6 Hz, H14B), 7.76-7.56 (m, 8H, H10, H11), 4.85 (q, 1H $^3J_{\text{H-H}}$ = 6.5 Hz, H2), 1.32 (s, 9H, H8), 1.13 (d, 3H, $^3J_{\text{H-H}}$ = 6.5 Hz, H3).
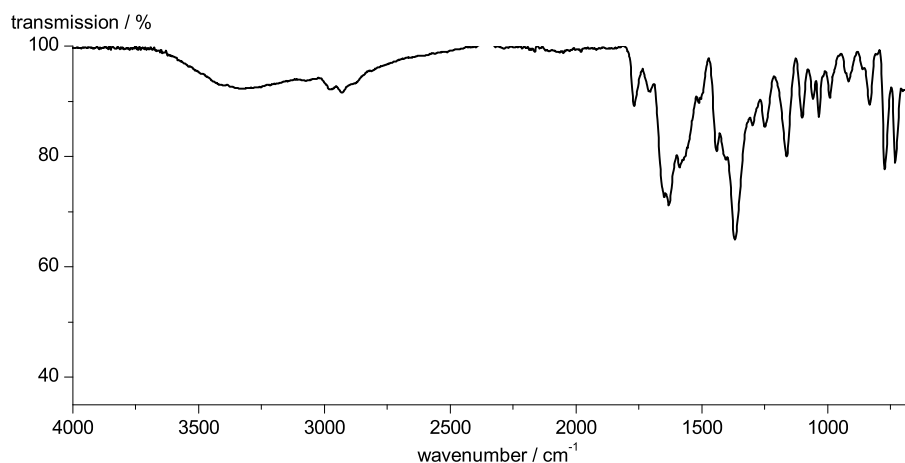


**IR (ATR):** $\tilde{\nu}$ = 2979 (w), 2929 (w), 2873 (w), 1768 (m), 1704 (w), 1650 (s), 1631 (s), 1591 (m), 1512 (m), 1442 (m), 1407 (m), 1369 (s), 1297 (m), 1247 (m), 1159 (m), 1101 (m), 1058 (m), 1031 (m), 989 (m), 916 (m), 931 (m), 771 (m), 729 (m), 663 (m).
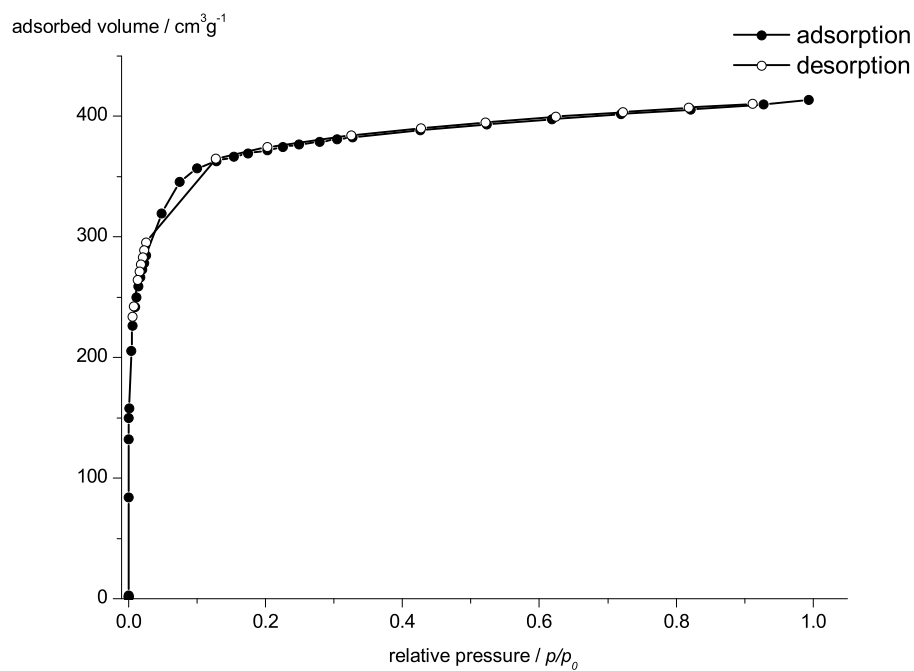
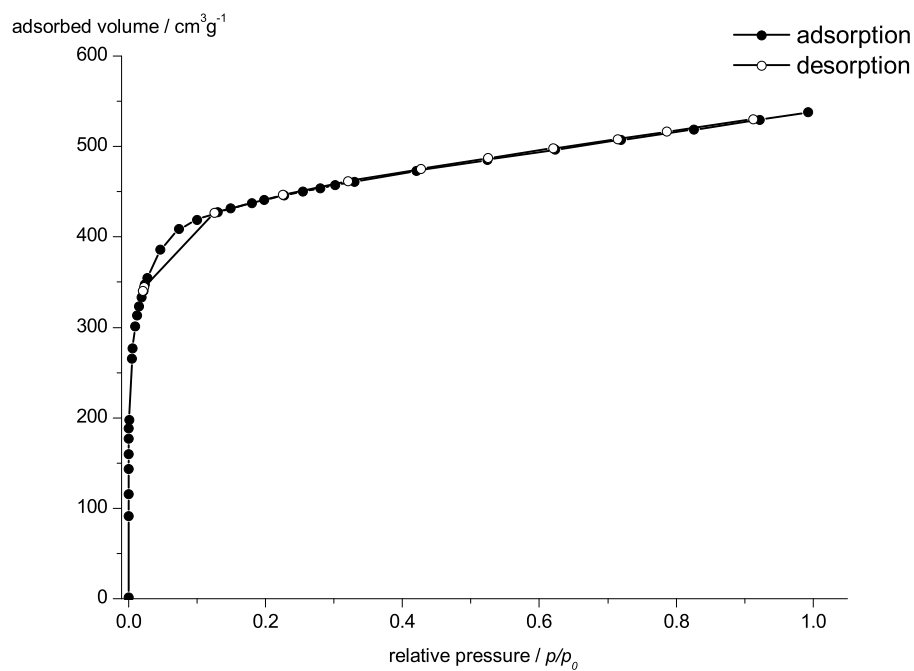**Figure 4.6** – $N_2$ physisorption of UHM-25-Ala-Boc (**140**) after activation with supercritical $CO_2$.

$S_{BET} = 1474 \, m^2 \, g^{-1}$ (determined for $p/p_0 = 0.016$–$0.100$)
$V_{micropore} = 0.58 \, cm^3 \, g^{-1}$ (determined at $p/p_0 = 0.20$)

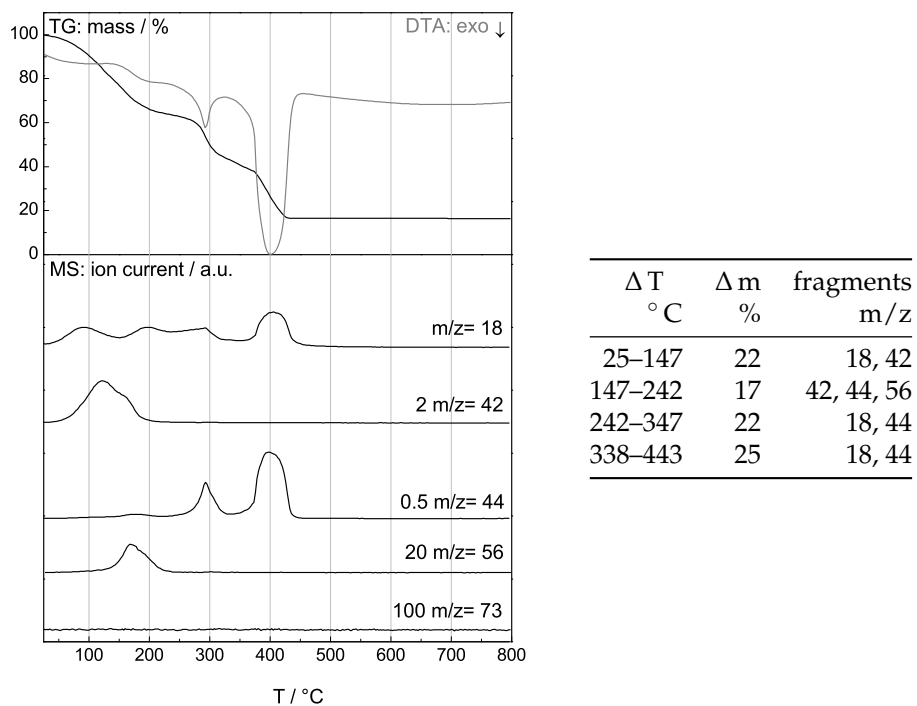| $\Delta T$ | $\Delta m$ | fragments |
|:---:|:---:|---:|
| °C | % | m/z |
| 25–145 | 11 | 18, 42 |
| 145–240 | 28 | 44, 56 |
| 240–330 | 21 | 18, 42, 44 |
| 338–432 | 25 | 18, 44 |
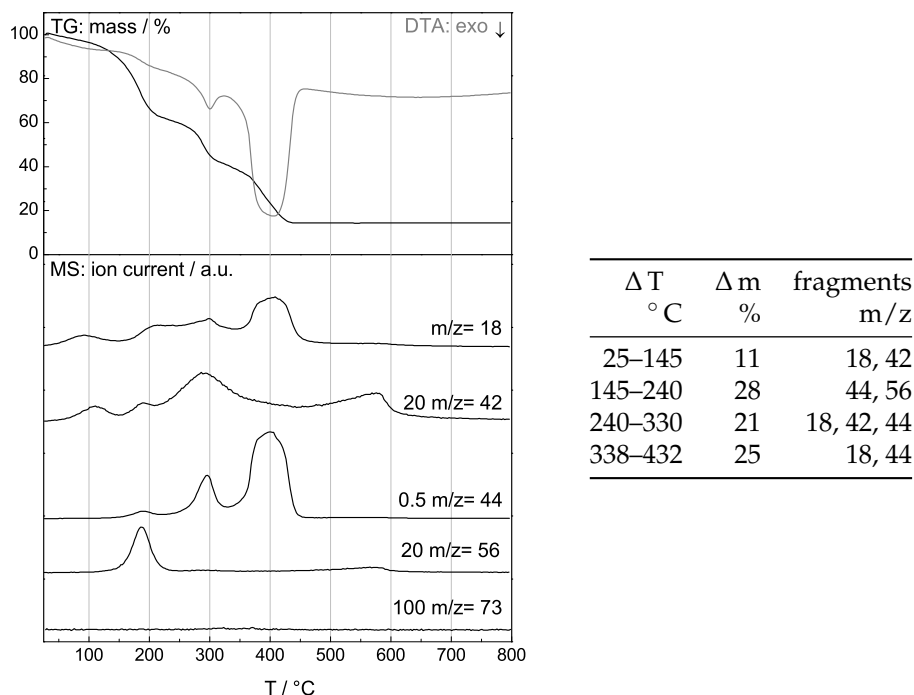
**Figure 4.7** – TG/MS analysis of UHM-25-Ala-Boc (**140**), weight loss (black) and DTA (grey) are plotted in the upper part and in the lower part of the diagram the characteristic single ion currents are shown for $\frac{m}{z}$ = 18 ($H_2O$), 42 (THF), 44 ($CO_2$), 56 (isobutene), and 73 (DMF).

## 4.42.1  Crystal Structure Determination and Refinement

Single crystals were obtained from a small-scale reaction of a solution of te-tracarboxylic acid **121** (21 mg, 0.03 mmol, 1 eq.) in DMF (0.8 mL) to which was added nitric acid (20 %, 66 µL),with an aqueous solution of copper nitrate tri-hydrate (c = 100 g/L, 0.5 mL, 5.0 mg $Cu(NO_3)_2 \cdot 3\,H_2O$, 22 µmol, 0.6 eq.) The reaction mixture was placed in a 6 mL test tube which was placed in a 100 mL screw-capped flask and was heated at 50 °C in an oven for three days. This resulted in light blue, block-shaped crystals that were kept in the mother liquor.
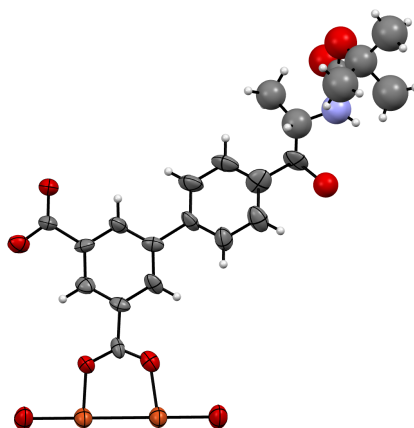
**Figure 4.8** – ORTEP-like plot of the asymmetric unit of UHM-25-Ala-Boc (orange: copper, red: oxygen, light blue: nitrogen, grey: carbon, white: hydrogen; probability level 15%).

X-ray single crystal diffraction for UHM-25-Ala-Boc (**140**) was collected on an Oxford Diffraction (Agilent Technologies) SuperNova diffractometer at 100(2) K with Cu $K\alpha$ radiation (154.178 pm) by $\omega$ scanning mode. The program CrysAlisPro was used for integration of the diffraction profiles and absorption corrections. The structure was solved by direct methods using the SHELXS program of the SHELXTL package and refined by full-matrix least-squares methods with SHELXL against $|F|^2$. All non-hydrogen atoms –except for the chiral moiety on the linker molecule– were refined with anisotropic displacement parameters. A high degree of disorder has been found for the chiral moiety on the organic SBU, which can be ascribed to statistical disorder of the linker within the framework and the conformational flexibility of the substituent. Therefore, the chiral moiety in UHM-25-Ala-Boc has been modeled as a substituent with chemically reasonable bond lengths and angles but without any conformational disorder. The atomic positions of this group were held fixed during the refinement. Only one possible site of the severely disordered substituent was taken into account with small s.o.f. values. Note, without the chiral substitutent the framework posseses almost the symmetry of the space group $Pm\bar{3}m$.

SQUEEZE/PLATON[320] was used to account for the electron density from disordered copper atoms and DMF solvent molecules, which could not be resolved. The contributions of 2766.3 electrons were removed from the unit cell contents. In the space group $P432$ 2766.3/24 = 115.3 electrons were removed from the asymmetric unit. With $Z$ being 12, 1383.6 electrons would be associ-

ated with one formula unit, consistent with 0.5 copper atoms and 57 DMF solvent molecules per unit cell.

| identification code | UHM-25-Ala-Boc |
|---|---|
| empirical formula | C36 H32 Cu2 N1 O13 |
| formular weight | 870.70 g/mol |
| temperature | 100(2) K |
| wavelength | 154.178 pm, Cu $K\alpha$ |
| crystal system | cubic |
| space group | $P432$ |
| unit cell dimensions | $a = 2894.16(4)$ pm $\alpha = 90°$ |
|  | $b = 2894.16(4)$ pm $\beta = 90°$ |
|  | $c = 2894.16(4)$ pm $\gamma = 90°$ |
| volume | $24\,242.0(5)$ Å$^3$ |
| Z | 12 |
| calculated density | 0.928 g/cm$^3$ |
| absorption coefficient | $\mu = 0.91$ mm$^{-1}$ |
| $F(000)$ | 5004 |
| crystal size | $0.12 \times 0.12 \times 0.08$ mm$^3$ |
| $\theta$ range for data collection | 3.4 to 37.0 |
| index ranges | $h = -22 \to 22, k = -22 \to 22, l = -22 \to 22$ |
| reflections collected | 73768 |
| independent reflections | 2046 |
| observed reflections ($I > 2\sigma(I)$) | 1668 ($R_{int} = 0.068$) |
| completeness to $\theta = 37.0$ | 99.67 % |
| absorption correction | multi-scan |
| refinement method | Full-matrix least squares on $F^2$ |
| data / restraints / parameters | 2046 / 67 / 198 |
| goodness-of-fit on $F^2$ | $S = 1.10$ |
| final $R$ indices $[I > \sigma(I)]$ | $R1 = 0.077\ wR2 = 0.241$ |
| $R$ indices (all data) | $R1 = 0.086, wR2 = 0.242$ |
| largest diff. peak and hole | $\Delta\rho_{max}0.27$ e/Å$^3$, $\Delta\rho_{min}-0.24$ e/Å$^3$ |

## 4.43   UHM-25-Val-Boc (141)
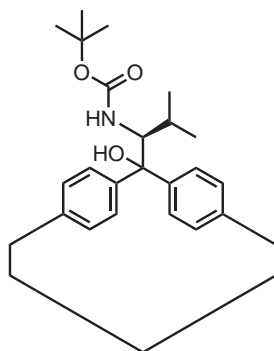


Tetracarboxylic acid **122** (392 mg, 0.58 mmol, 1 eq.) was dissolved in DMF (24 mL). To this solution was added nitric acid (20 %, 1.9 mL), then an aqueous solution of copper nitrate trihydrate (c = 100 g/L, 8.8 mL, 88 mg $Cu(NO_3)_2 \cdot 3 H_2O$, 0.4 mmol, 0.6 eq.) The reaction mixture was placed in an oven at 50 °C for three days. The mother liquor was decanted and the crystals suspended in fresh DMF. This procedure was repeated twice after 24 hours each. DMF was then replaced with THF in the same manner. The solvent-exchanged MOF was kept under THF and stored in a closed container.

A fraction of the MOF was digested in diluted hydrochloric acid to reisolate the linker for spectroscopic measurements: **HRMS (ESI+):** $\frac{m}{z}$ = 706.2238 (calc. for MNa$^+$: 706.2264); **opt. rot.:** $[\alpha]_D^{25} = -12.3$ (c = 0.29 g/100 mL, MeOH).
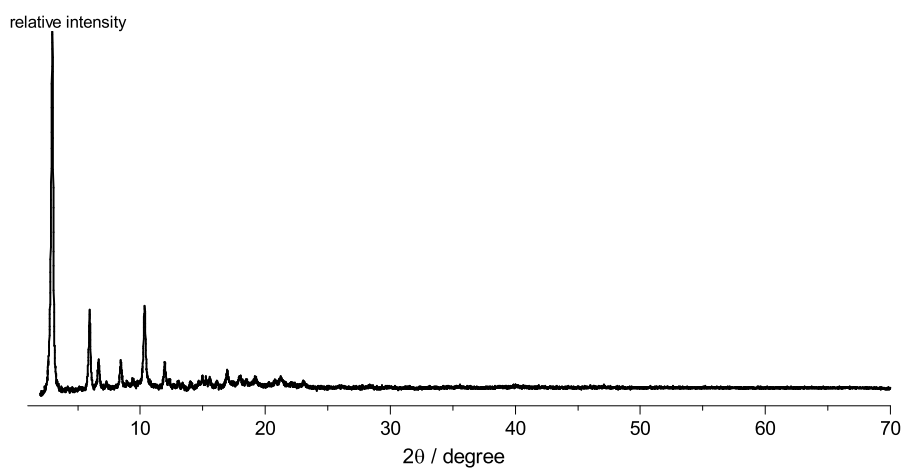
**Figure 4.9** – Powder X-ray diffractogram of UHM-25-Val-Boc (**141**).
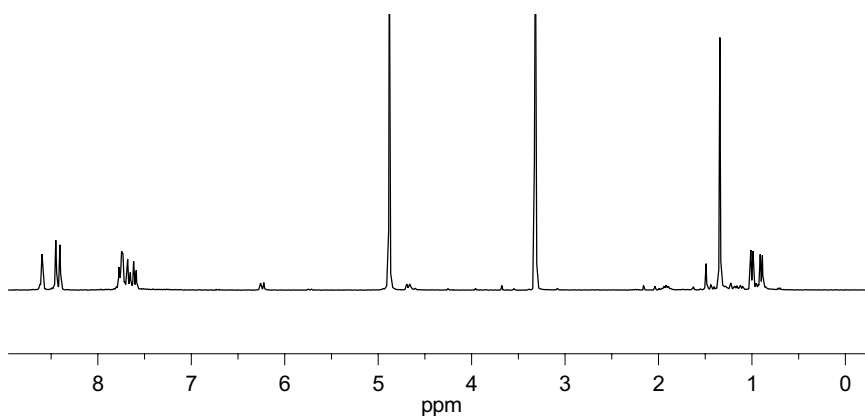


**Figure 4.10** – $^1$H-NMR of digested UHM-25-Val-Boc

**$^1$H-NMR (300 MHz, DMSO$-$d$_6$):** $\delta$ [ppm] = 8.62-8.58 (m, 2H, H17), 8.45 (d, 2H, $^3J_{H-H}$ = 1.7 Hz, H15A), 8.40 (d, 2H, $^3J_{H-H}$ = 1.7 Hz, H15B), 7.91-7.56 (m, 8H, H11, H12), 6.24 (d, 1H, $^3J_{H-H}$ = 10.3 Hz, H6), 4.68 (dd, 1H, $^3J_{H-H}$ = 10.3, 2.0 Hz, H2), 2.03-1.84 (m, 1H, H3), 1.34 (s, 9H, H9), 1.00 (d, 3H, $^3J_{H-H}$ = 6.8 Hz, H4A), 0.90 (d, 3H, $^3J_{H-H}$ = 6.9 Hz, H4B).
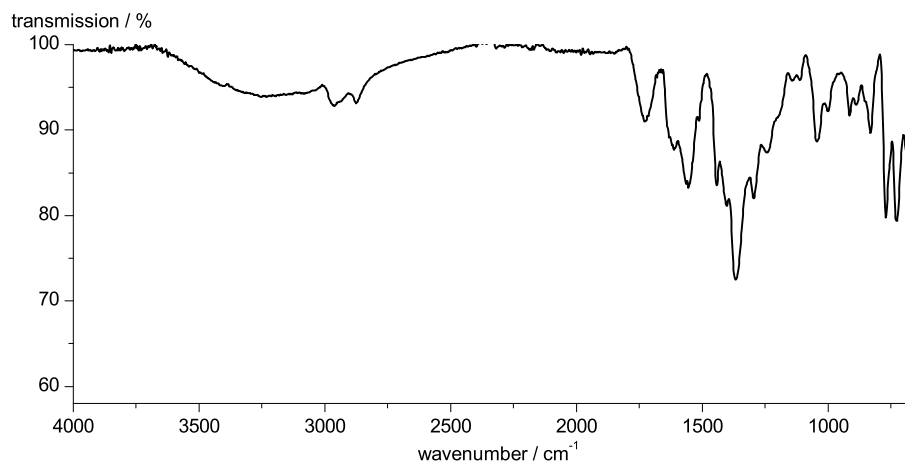
**IR (ATR):** $\tilde{\nu}$ = 2964 (w), 2875 (w), 1729 (m), 1612 (m), 1554 (m), 1442 (m), 1400 (m), 1365 (s), 1294 (m), 1236 (m), 1108 (m), 1043 (m), 997 (m), 916 (m), 885 (m), 829 (m), 767 (m), 730 (m), 686 (m).
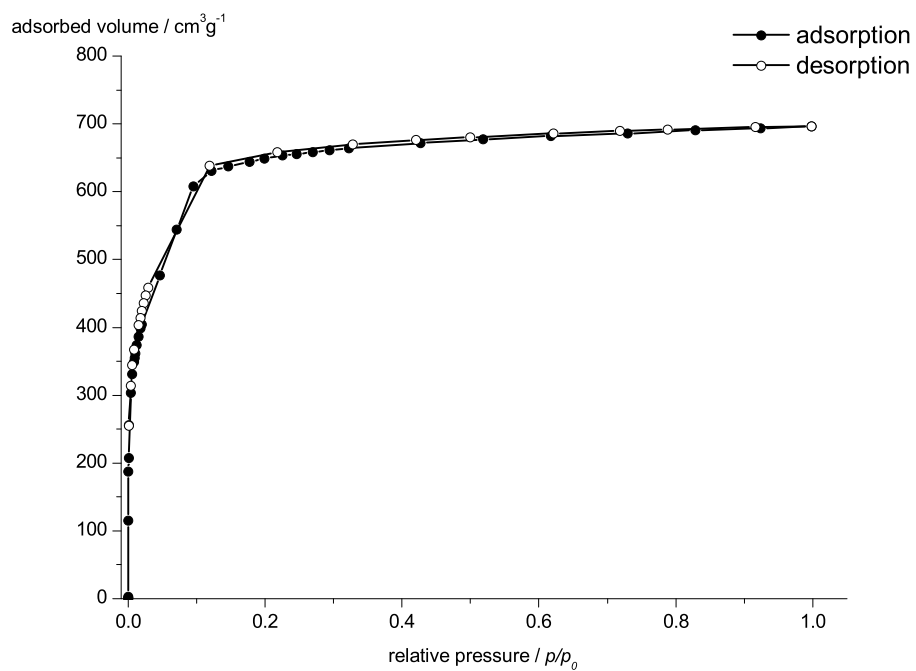
**Figure 4.11** – $N_2$ physisorption of UHM-25-Val-Boc (**141**) after activation with supercritical $CO_2$.

$S_{BET} = 1922\,\mathrm{m^2\,g^{-1}}$ (determined for $p/p_0 = 0.009$–$0.020$)
$V_{micropore} = 1.00\,\mathrm{cm^3\,g^{-1}}$ (determined at $p/p_0 = 0.20$)
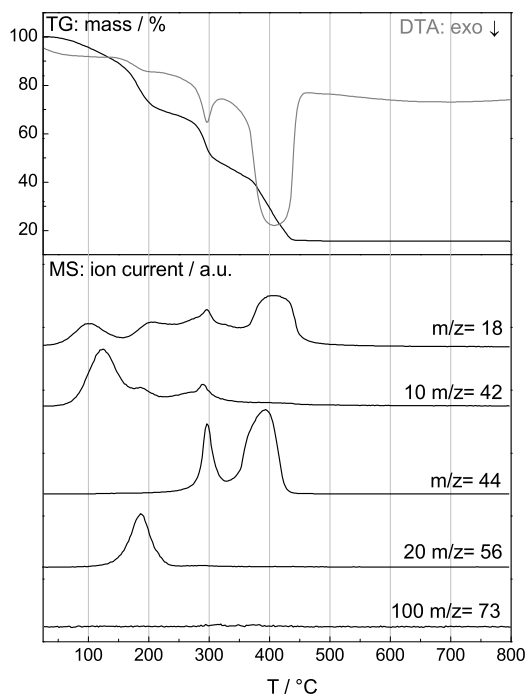
| $\Delta T$<br>$^\circ$C | $\Delta m$<br>% | fragments<br>m/z |
|---|---|---|
| 25–150 | 11 | 18, 42 |
| 150–240 | 19 | 44, 56 |
| 240–338 | 23 | 18, 42, 44 |
| 338–443 | 29 | 18, 44 |

**Figure 4.12** – TG/MS analysis of UHM-25-Val-Boc (**141**), weight loss (black) and DTA (grey) are plotted in the upper part and in the lower part of the diagram the characteristic single ion currents are shown for $\frac{m}{z}$ = 18 ($H_2O$), 42 (THF), 44 ($CO_2$), 56 (isobutene), and 73 (DMF).

## 4.44   UHM-25-Leu-Boc (142)
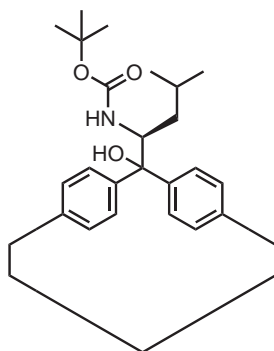


Tetracarboxylic acid **123** (401 mg, 0.58 mmol, 1 eq.) was dissolved in DMF (24 mL). To this solution was added nitric acid (20 %, 1.9 mL), then an aqueous solution of copper nitrate trihydrate (c = 100 g/L, 8.8 mL, 88 mg $Cu(NO_3)_2 \cdot 3 H_2O$, 0.4 mmol, 0.6 eq.) The reaction mixture was placed in an oven at 50 °C for three days. The mother liquor was decanted and the crystals suspended in fresh DMF. This procedure was repeated twice after 24 hours each. DMF was then replaced with THF in the same manner. The solvent-exchanged MOF was kept under THF and stored in a closed container.

A fraction of the MOF was digested in diluted hydrochloric acid to reisolate the linker for spectroscopic measurements: **HRMS (ESI+):** $\frac{m}{z}$ = 720.2406 (calc. for MNa$^+$: 720.2421); **opt. rot.:** $[\alpha]_D^{25}$ = +12.4 (c = 0.56 g/100 mL, MeOH).
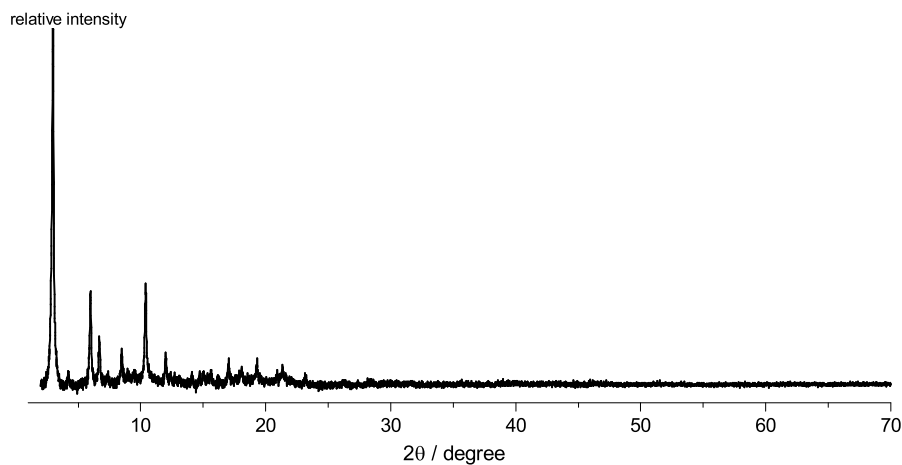
**Figure 4.13** – Powder X-ray diffractogram of UHM-25-Leu-Boc (**142**).
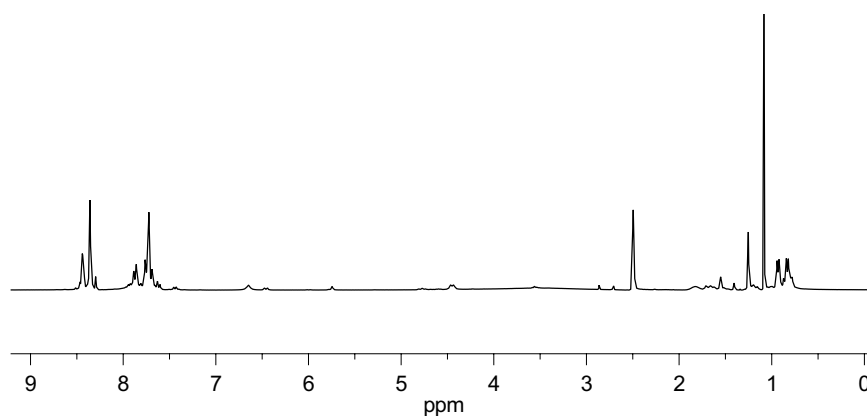


**Figure 4.14** – $^1$H-NMR of digested UHM-25-Leu-Boc

**$^1$H-NMR (300 MHz, DMSO$-$d$_6$):** $\delta$ [ppm] = 8.49-8.40 (m, 2H, H18), 8.39-8.33 (m, 4H, H16), 7.93-7.67 (m, 8H, H12, H13), 6.65 (s, 1H, H7), 4.45 (d, 1H, $^3J_{\text{H-H}}$ = 9.7 Hz, H2), 1.91-1.77 (m, 1H, H4), 1.74-1.59 (m, 1H, H3A), 1.22-1.14 (m, 1Hm H3B), 1.08 (s, 9H, H10), 0.93 (d, 3H, $^3J_{\text{H-H}}$ = 6.3 Hz, H5A), 0.83 (d, 3H, $^3J_{\text{H-H}}$ = 6.3 Hz, H5B).
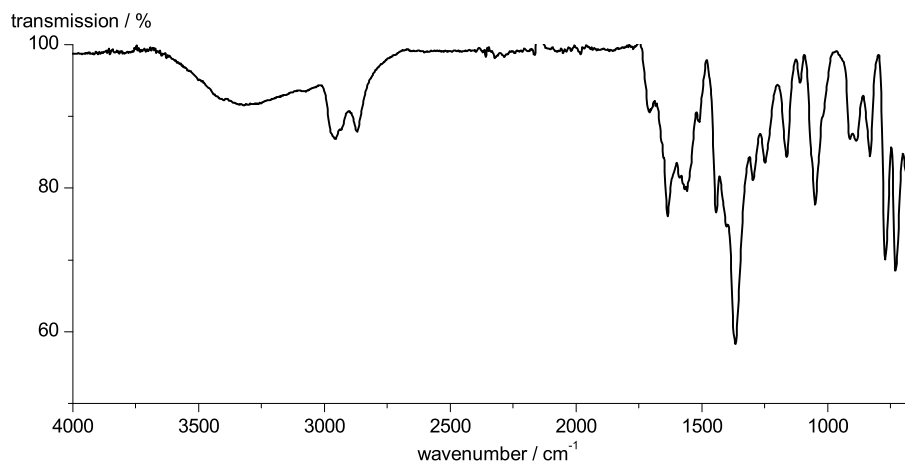
**IR (ATR):** $\widetilde{\nu}$ = 2959 (w), 2931 (w), 2869 (w), 1708 (w), 1635 (m), 1558 (m), 1508 (w), 1444 (m), 1402 (m), 1365 (s), 1296 (m), 1247 (m), 1162 (m), 1049 (m), 912 (m), 887 (m), 831 (m), 771 (m), 729 (s), 684 (m).

**Figure 4.15** – $N_2$ physisorption of UHM-25-Leu-Boc (**142**) after activation with supercritical $CO_2$.

$S_{BET} = 1474\,m^2\,g^{-1}$ (determined for $p/p_0 = 0.016$–$0.074$)
$V_{micropore} = 0.68\,cm^3\,g^{-1}$ (determined at $p/p_0 = 0.20$)

| $\Delta T$ | $\Delta m$ | fragments |
|:---:|:---:|---:|
| °C | % | m/z |
| 25–147 | 22 | 18, 42 |
| 147–242 | 17 | 42, 44, 56 |
| 242–347 | 22 | 18, 44 |
| 338–443 | 25 | 18, 44 |

**Figure 4.16** – TG/MS analysis of UHM-25-Leu-Boc (**142**), weight loss (black) and DTA (grey) are plotted in the upper part and in the lower part of the diagram the characteristic single ion currents are shown for $\frac{m}{z}$ = 18 ($H_2O$), 42 (THF), 44 ($CO_2$), 56 (isobutene), and 73 (DMF).

## 4.45   UHM-25-Phe-Boc (143)
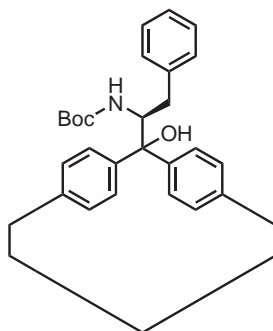


Tetracarboxylic acid **123** (423 mg, 0.58 mmol, 1 eq.) was dissolved in DMF (24 mL). To this solution was added nitric acid (20 %, 1.9 mL), then an aqueous solution of copper nitrate trihydrate (c = 100 g/L, 8.8 mL, 88 mg $Cu(NO_3)_2 \cdot 3 H_2O$, 0.4 mmol, 0.6 eq.) The reaction mixture was placed in an oven at 50 °C for three days. The mother liquor was decanted and the crystals suspended in fresh DMF. This procedure was repeated twice after 24 hours each. DMF was then replaced with THF in the same manner. The solvent-exchanged MOF was kept under THF and stored in a closed container.

A fraction of the MOF was digested in diluted hydrochloric acid to reisolate the linker for spectroscopic measurements: **HRMS (ESI+):** $\frac{m}{z}$ = 754.2284 (calc. for MNa$^+$: 754.2264); **opt. rot.:** $[\alpha]_D^{25} = +22.9$ (c = 0.28 g/100 mL, MeOH).
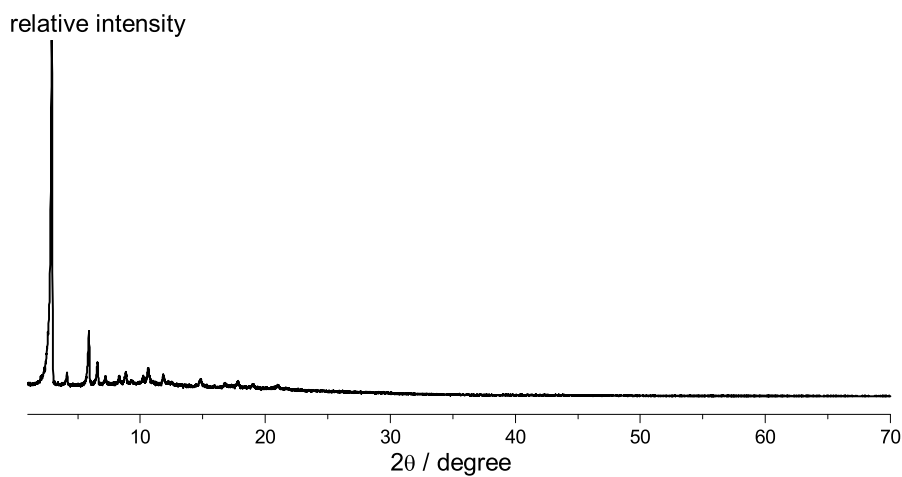
**Figure 4.17** – Powder X-ray diffractogram of UHM-25-Phe-Boc (**143**).
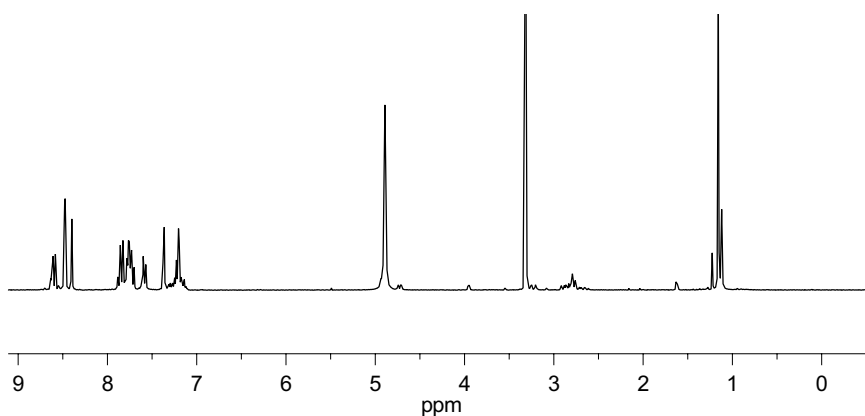


**Figure 4.18** – $^1$H-NMR of digested UHM-25-Phe-Boc

**$^1$H-NMR (300 MHz, CD$_3$OD):** $\delta$ [ppm] = 8-62-8.60 (m, 1H, H20A), 8.58 (t, 1H, $^4J_{H\text{-}H}$ = 1.5 Hz, H20B), 8.49-8.47 (m, 2H, H18A), 8.40 (d, 2H, $^4J_{H\text{-}H}$ = 1.5 Hz, H18B), 7-88-7.69 (m, 6H, H14A, H15), 7.62-7.55 (m, 2H, H14B), 7.39-7.12 (m, 5H, H5, H6, H7), 3.23 (dd, 1H, $^3J_{H\text{-}H}$ = 15.2, 2.7 Hz, H2), 2.89-2.72 (m, 2H, H3). 1.15 (s, 9H, H11).

337

transmission / %



wavenumber / cm$^{-1}$
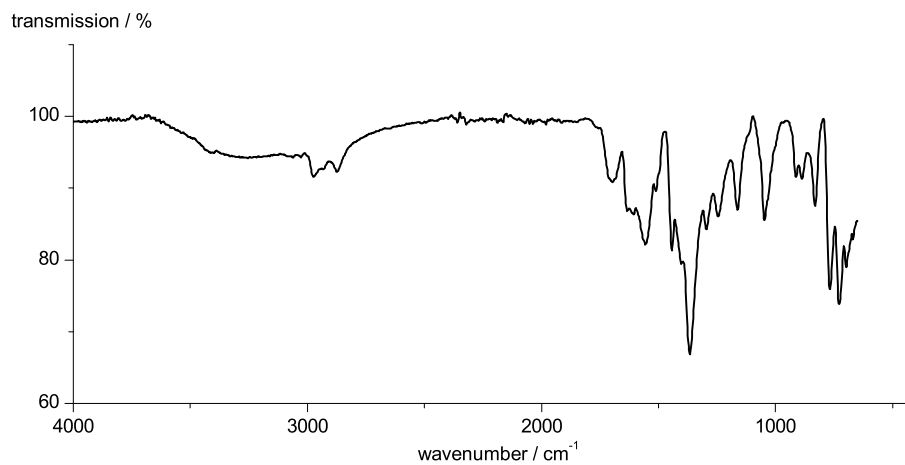
**IR (ATR):** $\widetilde{v}$ = 2973 (w), 2939 (w), 2871 (w), 1702 (w), 1631 (m), 1554 (m), 1506 (m), 1442 (m), 1402 (s), 1367 (s), 1292 (m), 1243 (m), 1161 (m), 1047 (m), 914 (m), 887 (m), 833 (m), 767 (m), 727 (s).
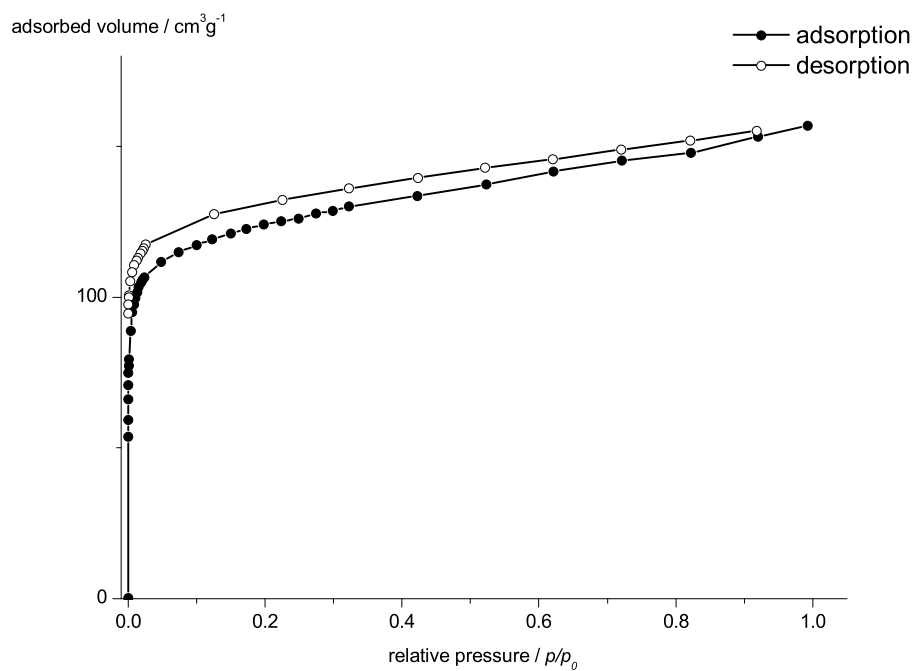
**Figure 4.19** – $N_2$ physisorption of UHM-25-Phe-Boc (**143**) after activation with supercritical $CO_2$.

$S_{\text{BET}} = 623.2 \, \text{m}^2 \, \text{g}^{-1}$ (determined for $p/p_0 = 0.007$–$0.024$)
$V_{\text{micropore}} = 0.25 \, \text{cm}^3 \, \text{g}^{-1}$ (determined at $p/p_0 = 0.20$)
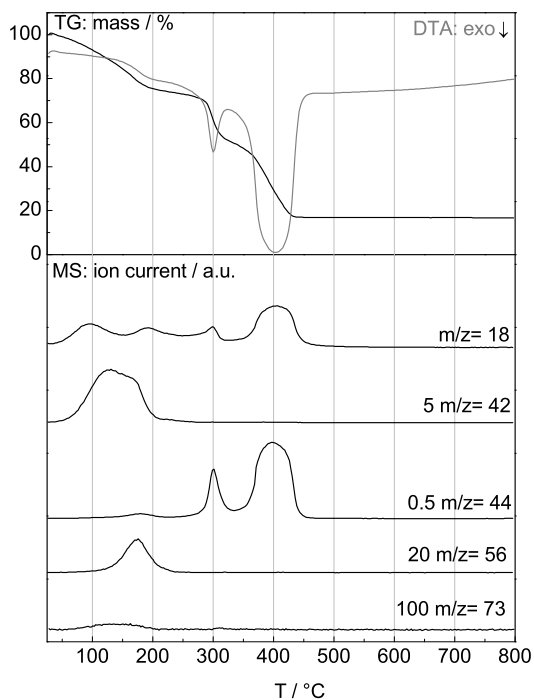
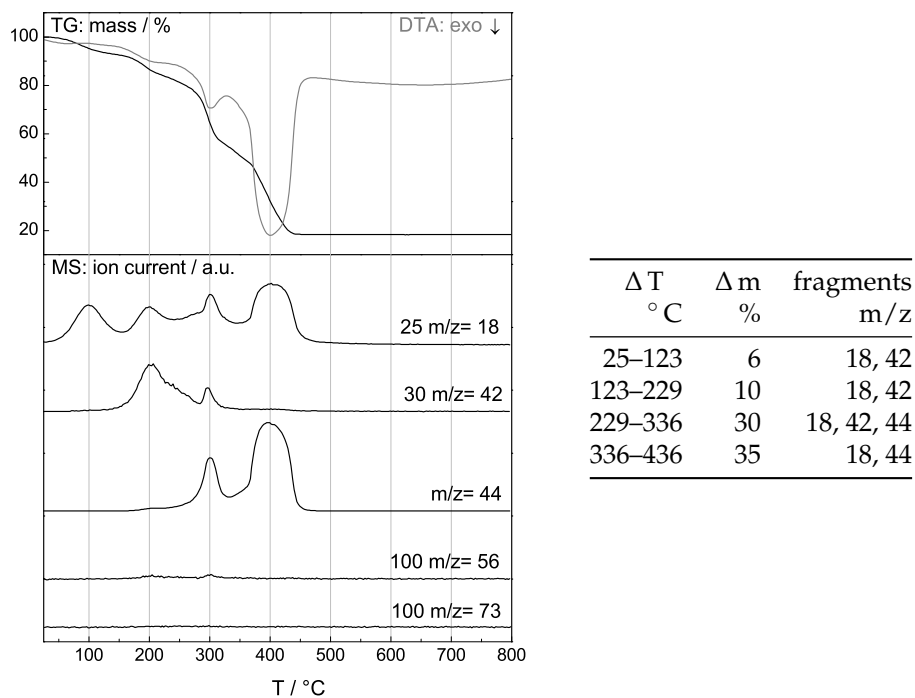| $\Delta T$ | $\Delta m$ | fragments |
|---|---|---|
| °C | % | m/z |
| 25–125 | 11 | 18, 42 |
| 125–227 | 25 | 42, 44, 56 |
| 227–337 | 24 | 18, 44 |
| 337–457 | 33 | 18, 44 |

**Figure 4.20** – TG/MS analysis of UHM-25-Phe-Boc (**143**), weight loss (black) and DTA (grey) are plotted in the upper part and in the lower part of the diagram the characteristic single ion currents are shown for $\frac{m}{z}$ = 18 ($H_2O$), 42 (THF), 44 ($CO_2$), 56 (isobutene), and 73 (DMF).

## 4.46 UHM-25-Ala (149)
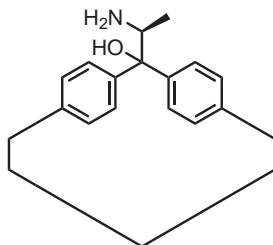
Tetracarboxylic acid **129** (388 mg, 0.58 mmol, 1 eq.) was dissolved in DMF (24 mL). To this solution was added nitric acid (20 %, 1.9 mL), then an aqueous solution of copper nitrate trihydrate (c = 100 g/L, 8.8 mL, 88 mg $Cu(NO_3)_2 \cdot 3 H_2O$, 0.4 mmol, 0.6 eq.) The reaction mixture was placed in an oven at 50 °C for three days. The mother liquor was decanted and the crystals suspended in fresh DMF. This procedure was repeated twice after 24 hours each. DMF was then replaced with THF in the same manner. The solvent-exchanged MOF was kept under THF and stored in a closed container.

A fraction of the MOF was digested in diluted hydrochloric acid to reisolate the linker for spectroscopic measurements: **HRMS (ESI+):** $\frac{m}{z}$ = 556.1599 (calc. for $MH^+$: 556.1602); **opt. rot.:** $[\alpha]_D^{25} = -17.9$ (c = 0.32), MeOH).
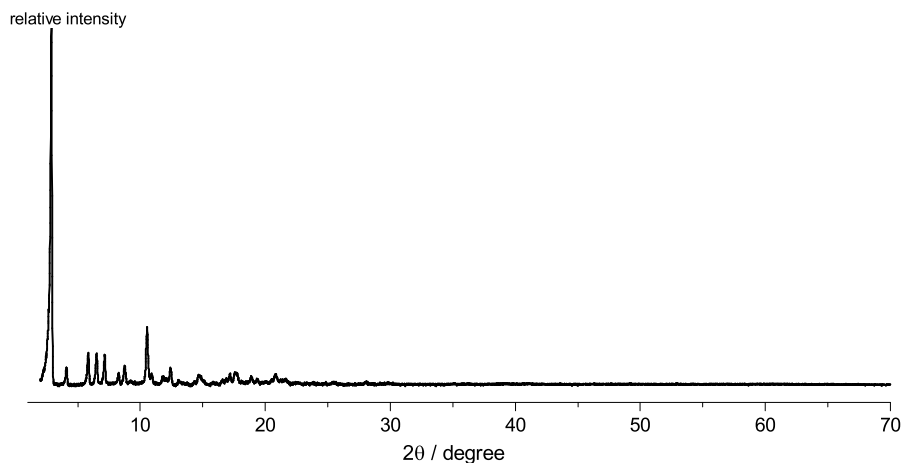


**Figure 4.21** – Powder X-ray diffractogram of UHM-25-Ala (**149**).
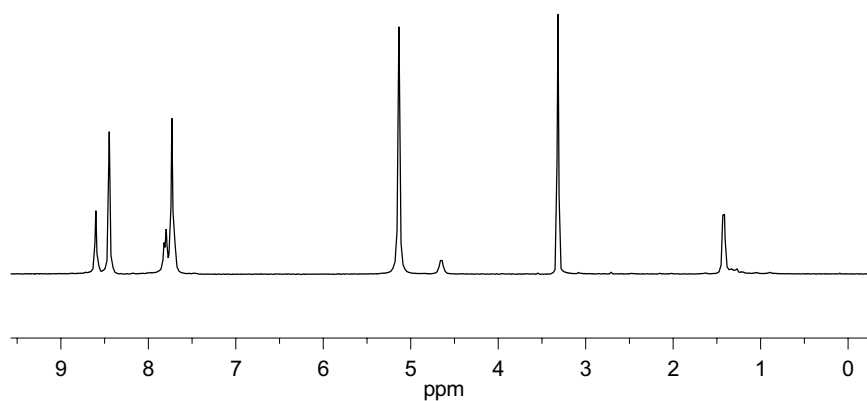
**Figure 4.22** – $^1$H-NMR of digested UHM-25-Ala-Boc

**$^1$H-NMR (300 MHz, CD$_3$OD):** $\delta$ [ppm] = 8.64-8.57 (m, 2H, H13), 8.49-8.39 (m, 4H, H11), 7.90-7.64 (m, 8H, H7, H8), 4.65 (q, 1H, $^3J_{\text{H-H}}$ = 5.9 Hz, H2), 1.42 (d, 3H, $^3J_{\text{H-H}}$ = 5.9 Hz, H3).
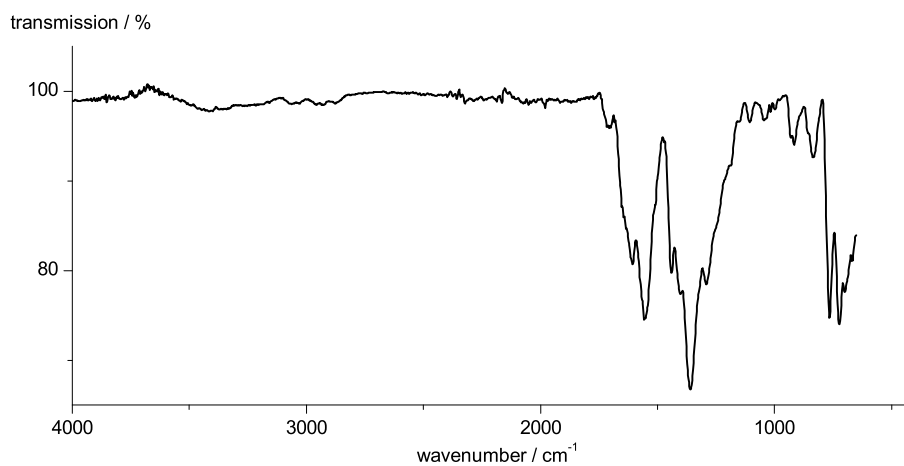


**IR (ATR):** $\widetilde{\nu}$ = 2927 (w), 2987, 1710 (w), 1602 (m), 1556 (s), 1444 (m), 1400 (m), 1359 (s), 1286 (m), 1110 (w), 1037 (w), 916 (m), 833 (m), 765 (s), 721 (s).
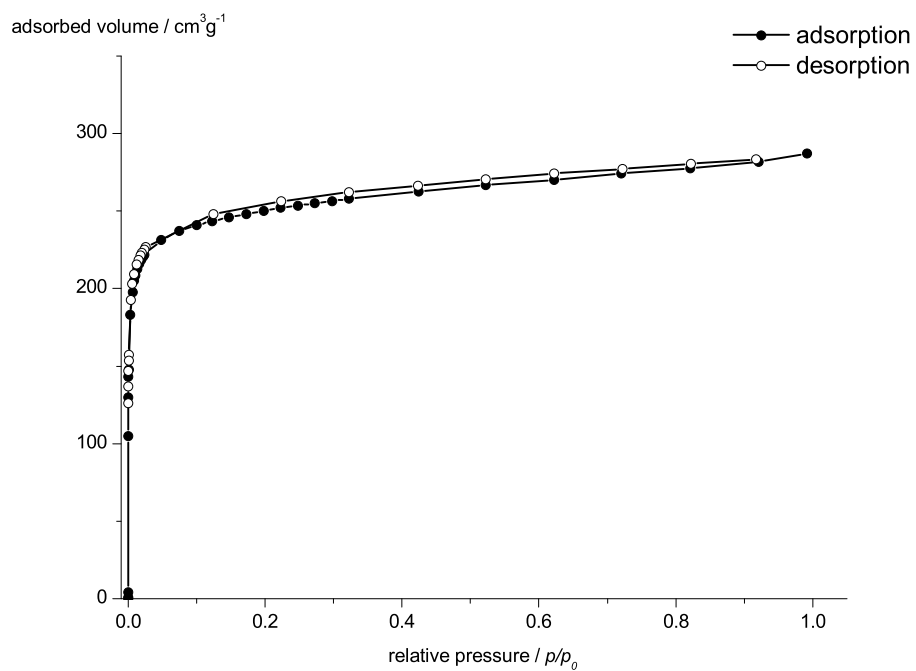
**Figure 4.23** – $N_2$ physisorption of UHM-25-Ala (**149**) after activation with supercritical $CO_2$.

$S_{BET} = 975.7\,\mathrm{m^2\,g^{-1}}$ (determined for $p/p_0 = 0.010$–$0.048$)
$V_{micropore} = 0.39\,\mathrm{cm^3\,g^{-1}}$ (determined at $p/p_0 = 0.20$)
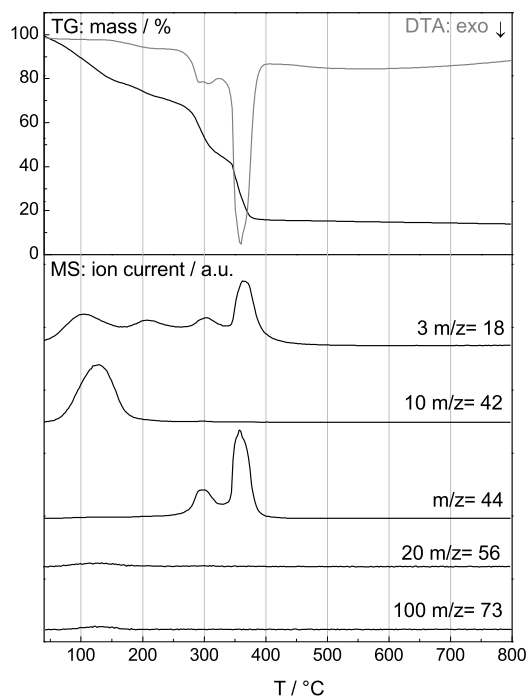
| $\Delta T$ | $\Delta m$ | fragments |
|:---:|:---:|:---:|
| $^{\circ}C$ | % | m/z |
| 25–217 | 28 | 42, 44 |
| 217–327 | 27 | 18, 44 |
| 327–380 | 30 | 18, 44 |

**Figure 4.24** – TG/MS analysis of UHM-25-Ala (**149**), weight loss (black) and DTA (grey) are plotted in the upper part and in the lower part of the diagram the characteristic single ion currents are shown for $\frac{m}{z}$ = 18 ($H_2O$), 42 (THF), 44 ($CO_2$), 56 (isobutene), and 73 (DMF).

## 4.47 UHM-25-Val (150)



344
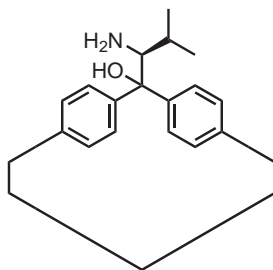
Tetracarboxylic acid **130** (405 mg, 0.58 mmol, 1 eq.) was dissolved in DMF (24 mL). To this solution was added nitric acid (20 %, 1.9 mL), then an aqueous solution of copper nitrate trihydrate (c = 100 g/L, 8.8 mL, 88 mg $Cu(NO_3)_2 \cdot 3 H_2O$, 0.4 mmol, 0.6 eq.) The reaction mixture was placed in an oven at 50 °C for three days. The mother liquor was decanted and the crystals suspended in fresh DMF. This procedure was repeated twice after 24 hours each. DMF was then replaced with THF in the same manner. The solvent-exchanged MOF was kept under THF and stored in a closed container.

A fraction of the MOF was digested in diluted hydrochloric acid to reisolate the linker for spectroscopic measurements: **HRMS (ESI+):** $\frac{m}{z}$ = 584.2027 (calc. for MH$^+$: 584.1915); **opt. rot.:** $[\alpha]_D^{25} = -18.8$ (c = 0.34), MeOH).
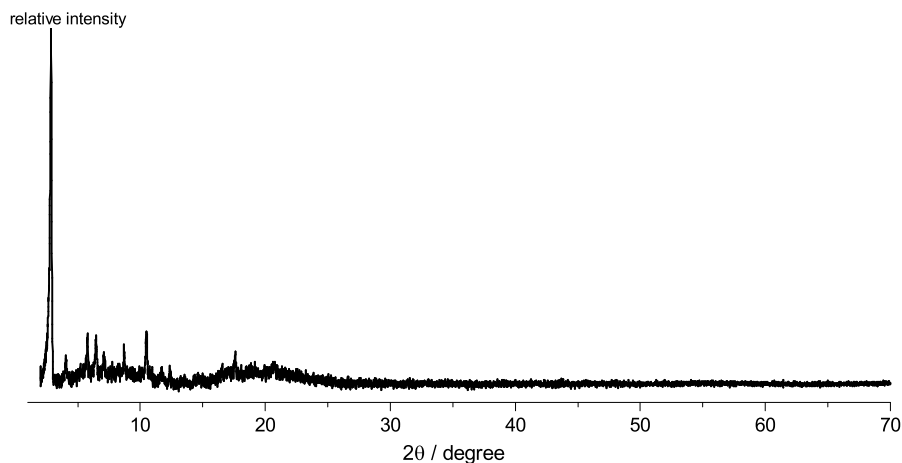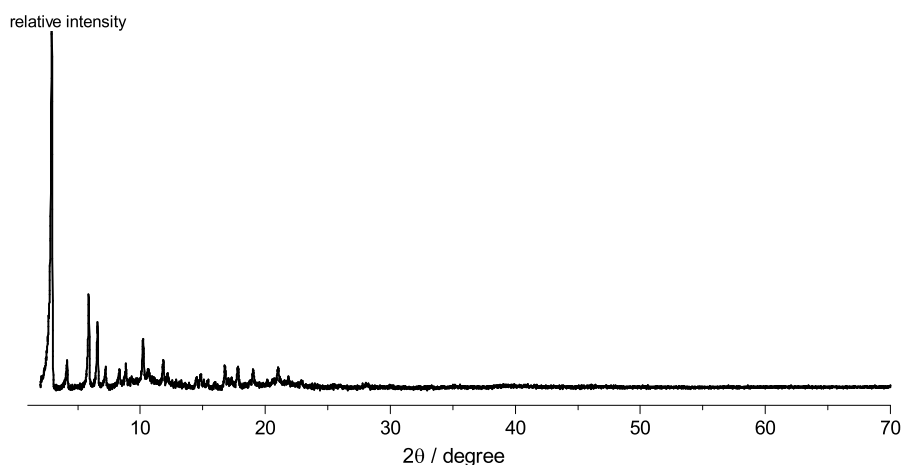


**Figure 4.25** – Powder X-ray diffractogram of UHM-25-Val (**150**).
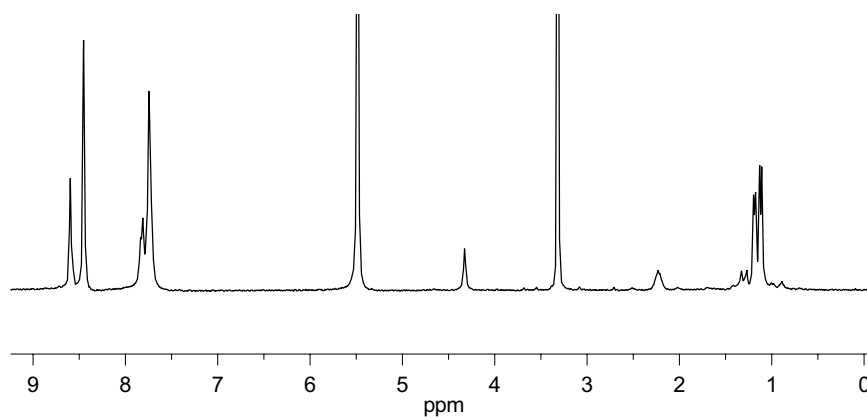
**Figure 4.26** – ¹H-NMR of digested UHM-25-Val

**¹H-NMR (300 MHz, CD₃OD):** $\delta$ [ppm] = 8.68-8.53 (m, 2H, H14), 8.50-8.39 (m, 4H, H12), 7.91-7.76 (m, 8H, H8, H9), 4.33 (s, 1H, H2), 2.31-2.15 (m, 1H, H3), 1.19 (d, 3H, $^3J_{\text{H-H}}$ = 6.6 Hz, H4A), 1.12 (d, 3H, $^3J_{\text{H-H}}$ = 6.6 Hz, H4B).
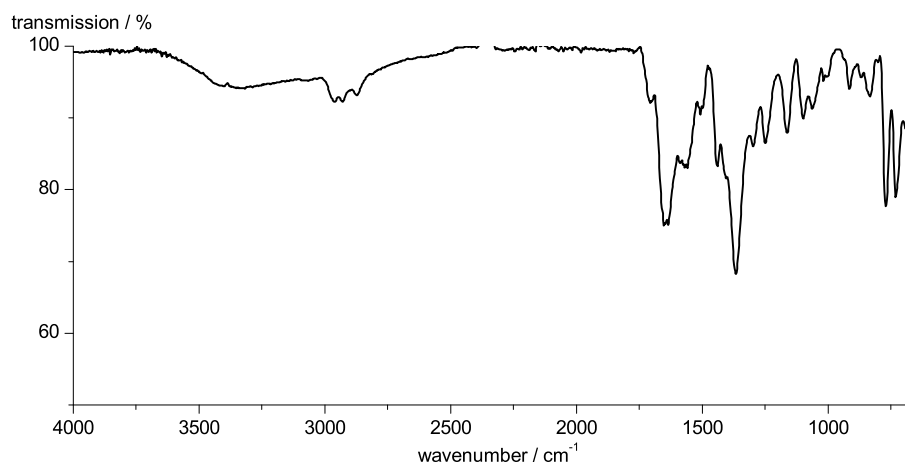


**IR (ATR):** $\widetilde{\nu}$ = 2962 (w), 2929 (w), 2873 (w), 1706 (m), 1652 (s), 1589 (m), 1506 (m), 1436 (m), 1402 (m), 1365 (s), 1294 (m), 1247 (m), 1159 (m), 1097 (m), 1062 (m), 1016 (m), 916 (m), 833 (m), 769 (s), 729 (s), 688 (m).
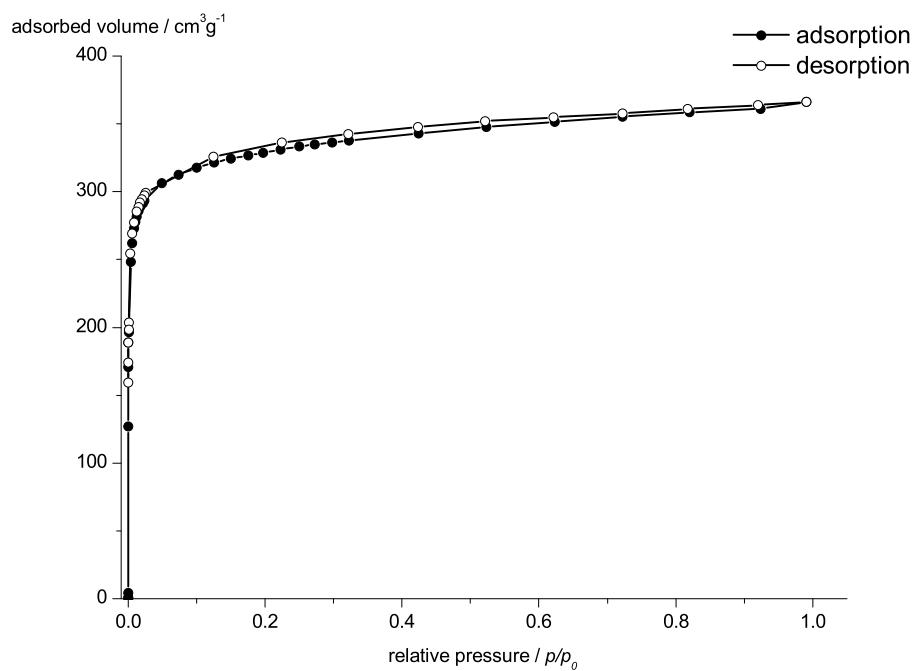
**Figure 4.27** – $N_2$ physisorption of UHM-25-Val (**150**) after activation with supercritical $CO_2$.

$S_{\mathrm{BET}} = 1286\,\mathrm{m^2\,g^{-1}}$ (determined for $p/p_0 = 0.011$–$0.049$)
$V_{\mathrm{micropore}} = 0.51\,\mathrm{cm^3\,g^{-1}}$ (determined at $p/p_0 = 0.20$)
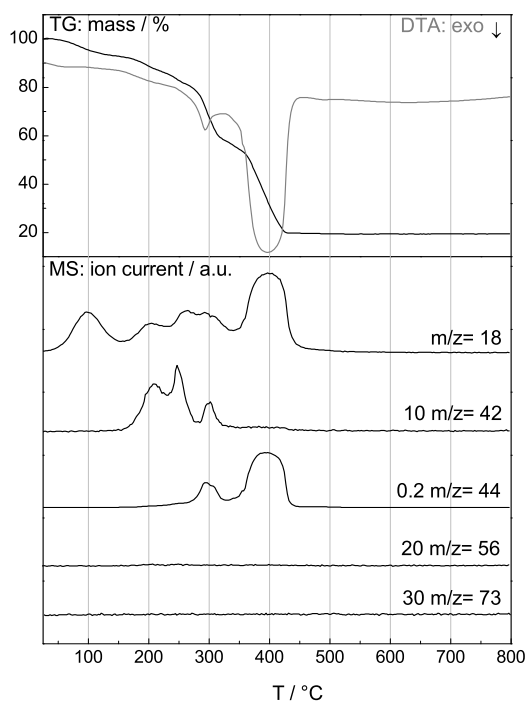
| $\Delta T$ | $\Delta m$ | fragments |
|:---:|:---:|---:|
| °C | % | m/z |
| 25–142 | 7 | 18 |
| 142–266 | 13 | 18, 42 |
| 266–336 | 24 | 18, 42, 44 |
| 336–450 | 37 | 18, 44 |

**Figure 4.28** – TG/MS analysis of UHM-25-Val (**150**), weight loss (black) and DTA (grey) are plotted in the upper part and in the lower part of the diagram the characteristic single ion currents are shown for $\frac{m}{z}$ = 18 ($H_2O$), 42 (THF), 44 ($CO_2$), 56 (isobutene), and 73 (DMF).

## 4.48   UHM-25-Leu (151)
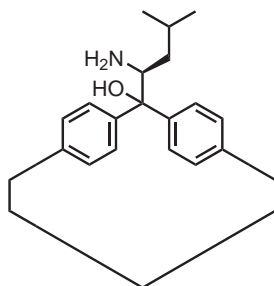


Tetracarboxylic acid **131** (412 mg, 0.58 mmol, 1 eq.) was dissolved in DMF (24 mL). To this solution was added nitric acid (20 %, 1.9 mL), then an aqueous solution of copper nitrate trihydrate (c = 100 g/L, 8.8 mL, 88 mg $Cu(NO_3)_2 \cdot 3 H_2O$, 0.4 mmol, 0.6 eq.) The reaction mixture was placed in an oven at 50 °C for three days. The mother liquor was decanted and the crystals suspended in fresh DMF. This procedure was repeated twice after 24 hours each. DMF was then replaced with THF in the same manner. The solvent-exchanged MOF was kept under THF and stored in a closed container.

A fraction of the MOF was digested in diluted hydrochloric acid to reisolate the linker for spectroscopic measurements: **HRMS (ESI+):** $\frac{m}{z}$ = 598.2105 (calc. for MH$^+$: 598.2072); **opt. rot.:** $[\alpha]_D^{26} = +15.6$ (c = 0.51), MeOH).
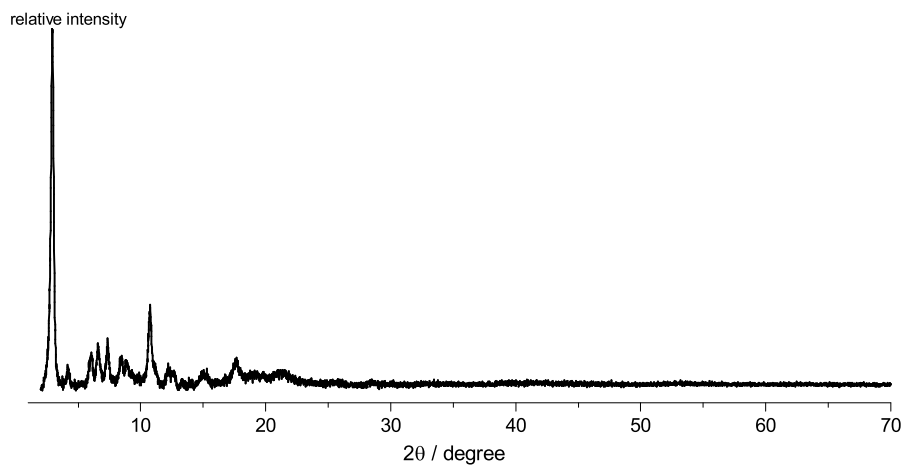
**Figure 4.29** – Powder X-ray diffractogram of UHM-25-Leu (**151**).
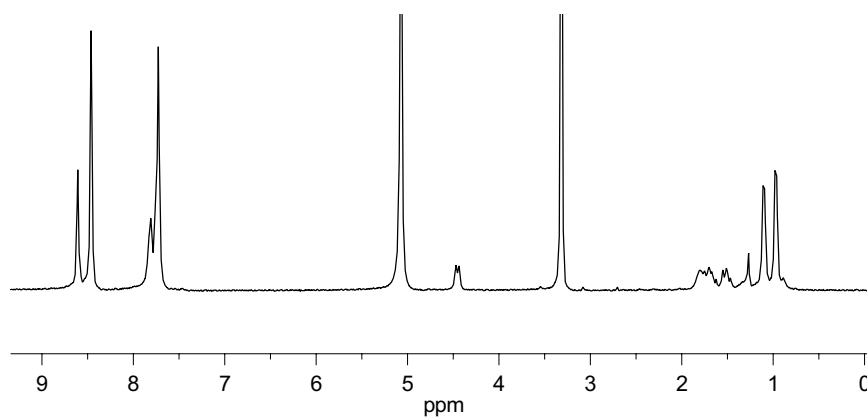


**Figure 4.30** – $^1$H-NMR of digested UHM-25-Leu

**$^1$H-NMR (300 MHz, CD$_3$OD):** $\delta$ [ppm] = 8.66-8.56 (m, 2H, H15), 7.89-7.66 (m, 4H, H13), 7.89-7.66 (m, 8H, H9, H10), 4.45 (d, 1H, $^3J_{\text{H-H}}$ = 9.6 Hz, H2), 1.84-1.60 (m, 2H, H3A, H4), 1.59-.144 (m, 1H, H3B), 1.10 (d, 3H, $^3J_{\text{H-H}}$ = 5.7 Hz, H4A), 0.97 (d, 3H, $^3J_{\text{H-H}}$ = 5.8 Hz, H4B).
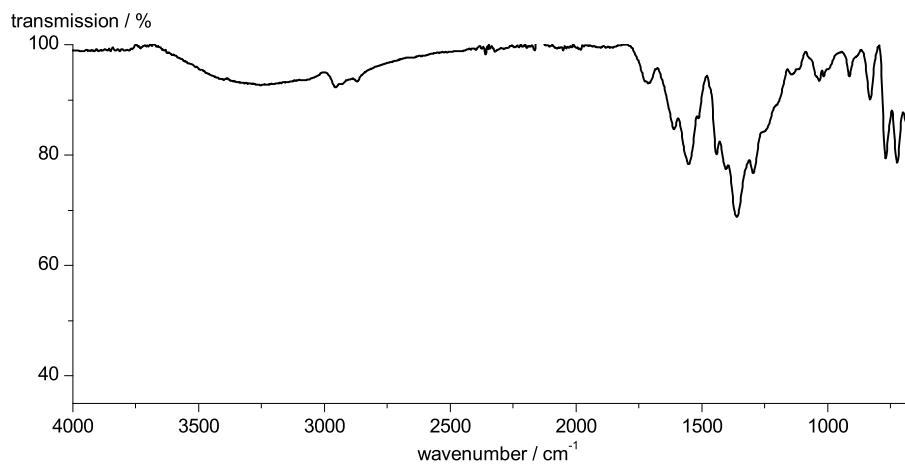
**IR (ATR):** $\widetilde{\nu}$ = 2956 (w), 2927 (w), 2869 (w), 1714 (w), 1608 (w), 1554 (m), 1512 (w), 1442 (m), 1404 (m), 1359 (s), 1294 (m), 1245 (m), 1135 (w), 1031 (w), 912 (w), 831 (m), 769 (m), 723 (m), 684 (m).
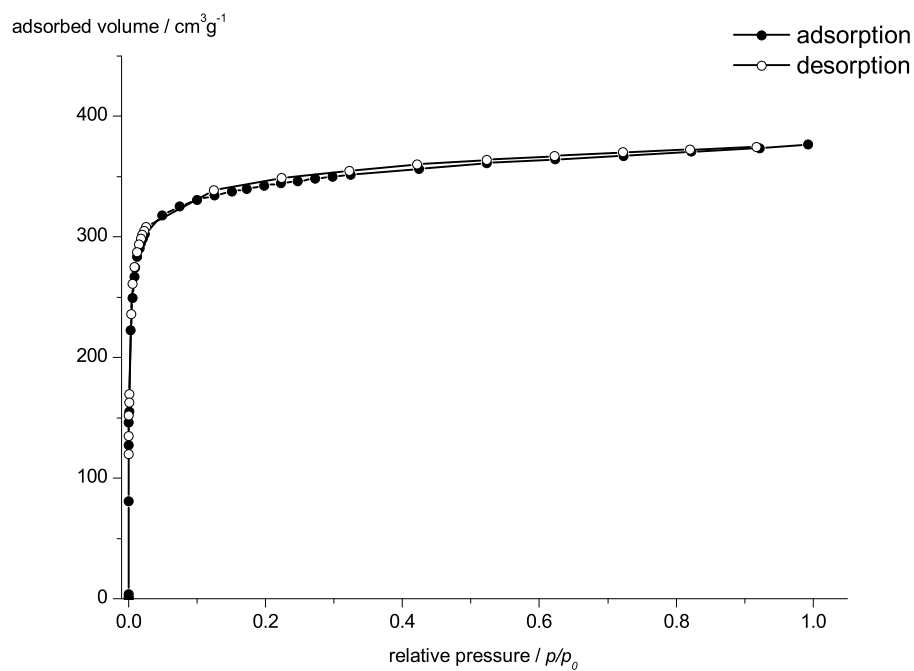
**Figure 4.31** – $N_2$ physisorption of UHM-25-Leu (**151**) after activation with supercritical $CO_2$.

$S_{BET} = 1351\,m^2\,g^{-1}$ (determined for $p/p_0 = 0.010\text{–}0.049$)
$V_{micropore} = 0.53\,cm^3\,g^{-1}$ (determined at $p/p_0 = 0.20$)

| $\Delta T$ | $\Delta m$ | fragments |
|:---:|:---:|---:|
| $^\circ$C | % | m/z |
| 25–123 | 6 | 18, 42 |
| 123–229 | 10 | 18, 42 |
| 229–336 | 30 | 18, 42, 44 |
| 336–436 | 35 | 18, 44 |

**Figure 4.32** – TG/MS analysis of UHM-25-Leu (**151**), weight loss (black) and DTA (grey) are plotted in the upper part and in the lower part of the diagram the characteristic single ion currents are shown for $\frac{m}{z}$ = 18 ($H_2O$), 42 (THF), 44 ($CO_2$), 56 (isobutene), and 73 (DMF).

## 4.49   UHM-25-Phe (152)
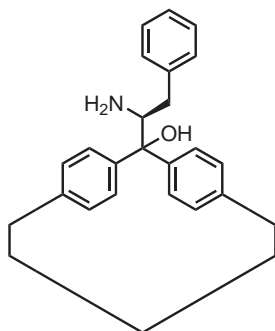


Tetracarboxylic acid **132** (432 mg, 0.58 mmol, 1 eq.) was dissolved in DMF (24 mL). To this solution was added nitric acid (20 %, 1.9 mL), then an aqueous solution of copper nitrate trihydrate (c = 100 g/L, 8.8 mL, 88 mg $Cu(NO_3)_2 \cdot 3 H_2O$, 0.4 mmol, 0.6 eq.) The reaction mixture was placed in an oven at 50 °C for three days. The mother liquor was decanted and the crystals suspended in fresh DMF. This procedure was repeated twice after 24 hours each. DMF was then replaced with THF in the same manner. The solvent-exchanged MOF was kept under THF and stored in a closed container.

A fraction of the MOF was digested in diluted hydrochloric acid to reisolate the linker for spectroscopic measurements: **HRMS (ESI+):** $\frac{m}{z}$ = 632.1975 (calc. for MH⁺: 632.1915); **opt. rot.:** $[\alpha]_D^{25}$ = +20.2 (c = 0.50), MeOH).

relative intensity
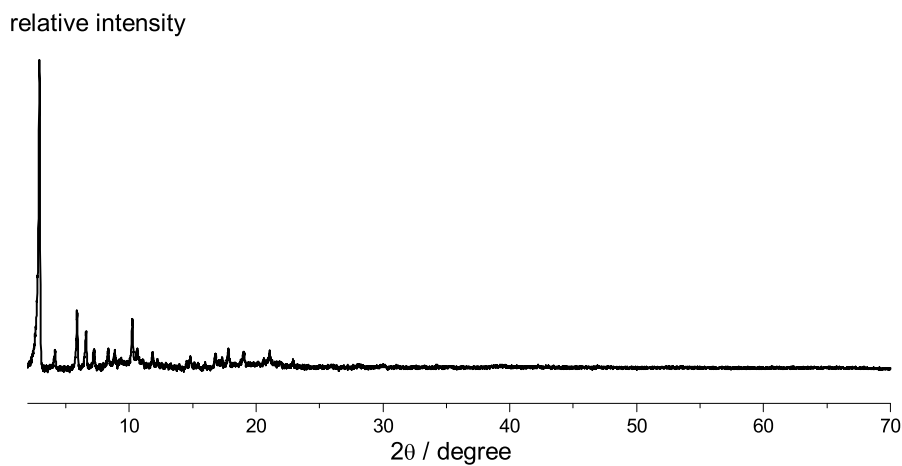


**Figure 4.33** – Powder X-ray diffractogram of UHM-25-Phe (**152**).
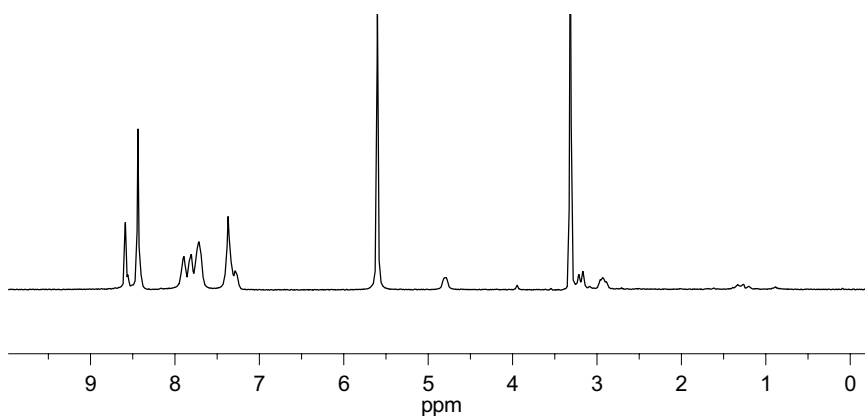


**Figure 4.34** – $^1$H-NMR of digested UHM-25-Phe

**$^1$H-NMR (300 MHz, CD$_3$OD):** $\delta$ [ppm] = 8.64-5.54 (m, 2H, H17), 8.48-8.38 (m, 4H, H15), 7.95-7.65 (m, 8H, H11, H12), 7.47-7.24 (m, 5H, H5, H6, H7), 4.80 (d, 1H, $^3J_{\text{H-H}}$ = 9.1 Hz, H2), 3.19 (d, 1H, $^2J_{\text{H-H}}$ = 14.6 Hz, H3A), 3.00-2.84 (m, 1H, H3B).
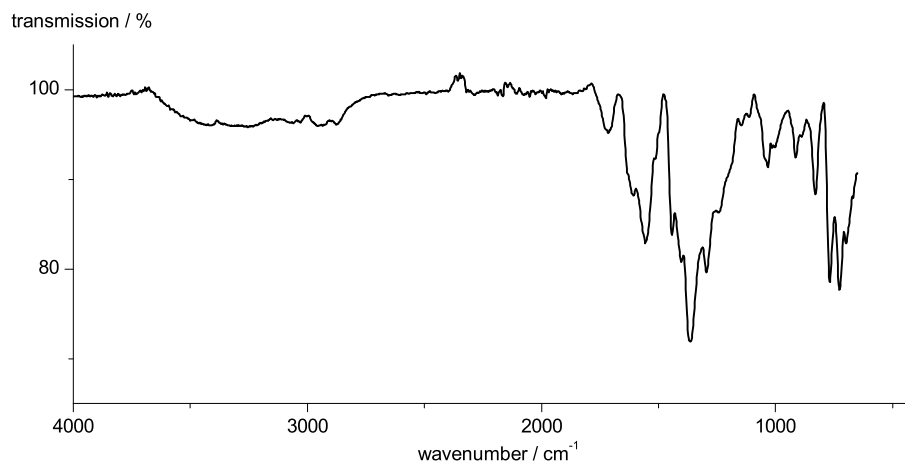
**IR (ATR):** $\widetilde{\nu}$ = 2943 (w), 2873 (w), 1714 (m), 1612 (m), 1554 (s), 1512 (m), 1442 (s), 1404 (s), 1365 (s), 1294 (m), 1035 (m), 914 (m), 831 (m), 767 (m), 727 (m).
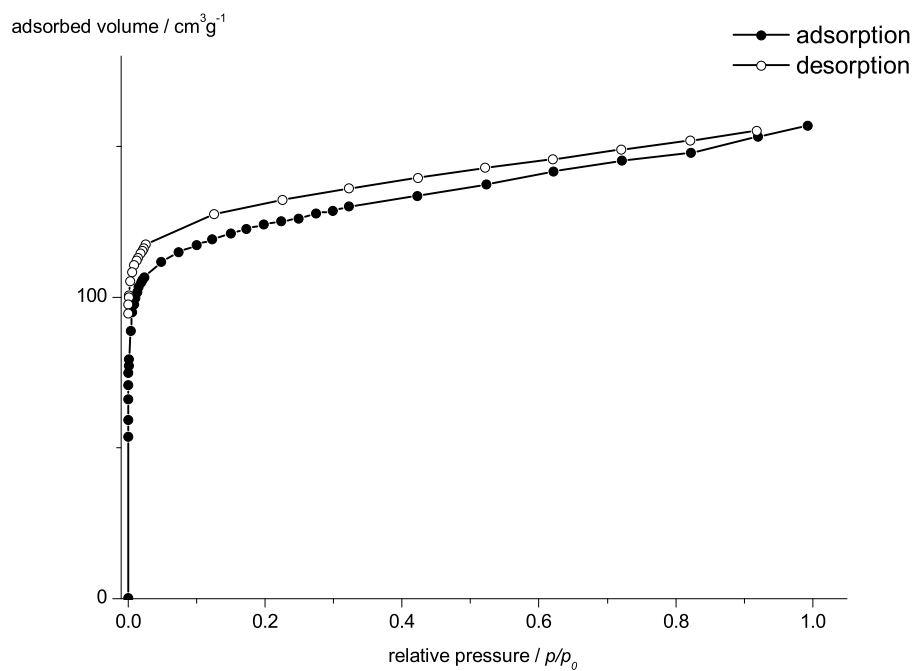
**Figure 4.35** – $N_2$ physisorption of UHM-25-Phe (**152**) after activation with supercritical $CO_2$.

$S_{\text{BET}} = 469.6 \, \text{m}^2 \, \text{g}^{-1}$ (determined for $p/p_0 = 0.010$–$0.048$)
$V_{\text{micropore}} = 0.15 \, \text{cm}^3 \, \text{g}^{-1}$ (determined at $p/p_0 = 0.20$)
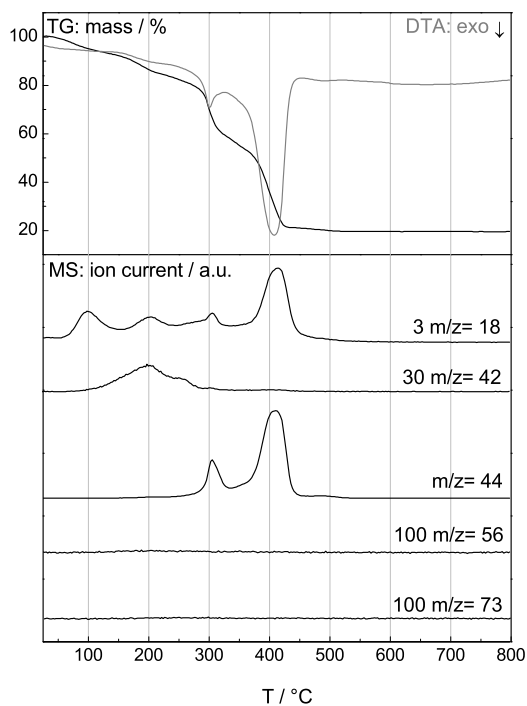
| $\Delta T$ | $\Delta m$ | fragments |
|:---:|:---:|---:|
| °C | % | m/z |
| 25–127 | 6 | 18 |
| 127–228 | 12 | 18, 42 |
| 228–340 | 24 | 18, 44 |
| 340–427 | 35 | 18, 44 |

**Figure 4.36** – TG/MS analysis of UHM-25-Phe (**152**), weight loss (black) and DTA (grey) are plotted in the upper part and in the lower part of the diagram the characteristic single ion currents are shown for $\frac{m}{z}$ = 18 ($H_2O$), 42 (THF), 44 ($CO_2$), 56 (isobutene), and 73 (DMF).

## 4.50  UHM-25-Pro (153)



358
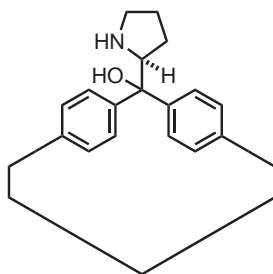
For the synthesis of bulk material, tetracarboxylic acid **128** (358 mg, 0.58 mmol, 1 eq.) was dissolved in DMF (24 mL). To this solution was added nitric acid (20 %, 1.9 mL), and then an aqueous solution of copper nitrate trihydrate (c = 100 g/L, 8.8 mL, 88 mg $Cu(NO_3)_2 \cdot 3 H_2O$, 0.4 mmol, 0.6 eq.) The reaction mixture was placed in an oven at 50 °C for three days. The mother liquor was decanted and the crystals suspended in fresh DMF. This procedure was repeated twice after 24 hours each. DMF was then replaced with THF in the same manner. The solvent-exchanged MOF was kept under THF and stored in a closed container.

A fraction of the MOF was digested in diluted hydrochloric acid to reisolate the linker for spectroscopic measurements: **HRMS (ESI+):** $\frac{m}{z}$ = 582.1773 (calc. for $MH^+$: 582.1759); **opt. rot.:** $[\alpha]_D^{25}$ = +41.0 (c = 0.34), MeOH).



**Figure 4.37** – Powder X-ray diffractogram of UHM-25-Pro (**153**).

**$^1$H-NMR (300 MHz, DMSO$-$d$_6$):** $\delta$ [ppm] = 8.44 (t, 1H, $^4J_{H\text{-}H}$ = 1.6 Hz, H15A), 8.42 (t, 1H, $^4J_{H\text{-}H}$ = 1.7 Hz, H15B), 8.32 (d, 2H, $^4J_{H\text{-}H}$ = 1.6 Hz, H13A), 8.26 (d, 2H, $^4J_{H\text{-}H}$ = 1.7 Hz, H13B), 7.86-7.78 (m, 2H, H9A), 7.75-7.62 (m, 6H, H9B, H10), 5.07-4.95 (m, 1H, H2), 3.33-3.07 (m, 2H, H5), 2.11-1.72 (m, 4H, H3, H4).
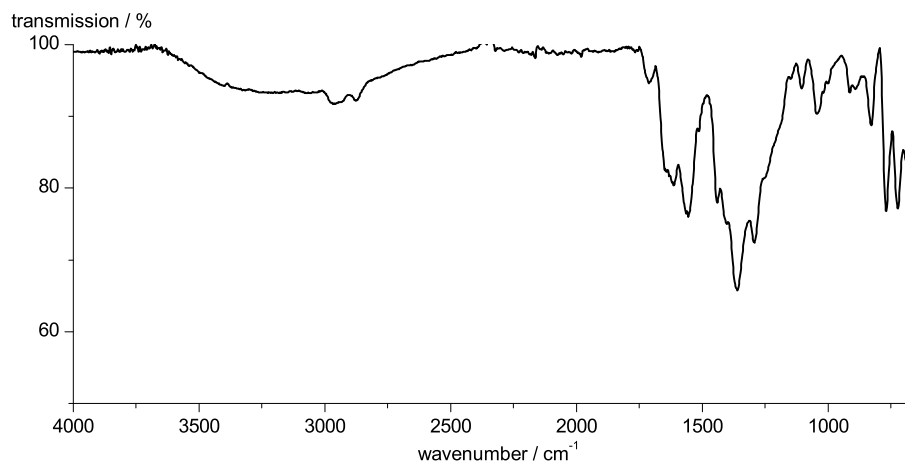
**IR (ATR):** $\widetilde{\nu}$ = 2975 (w), 2935 (w), 2875 (w), 1710 (w), 1612 (m), 1556 (m), 1510 (w), 1442 (m), 1402 (m), 1357 (s), 1296 (m), 1105 (w), 1040 (w), 910 (w), 827 (m), 767 (m), 719 (m), 686 (m), 665 (m).
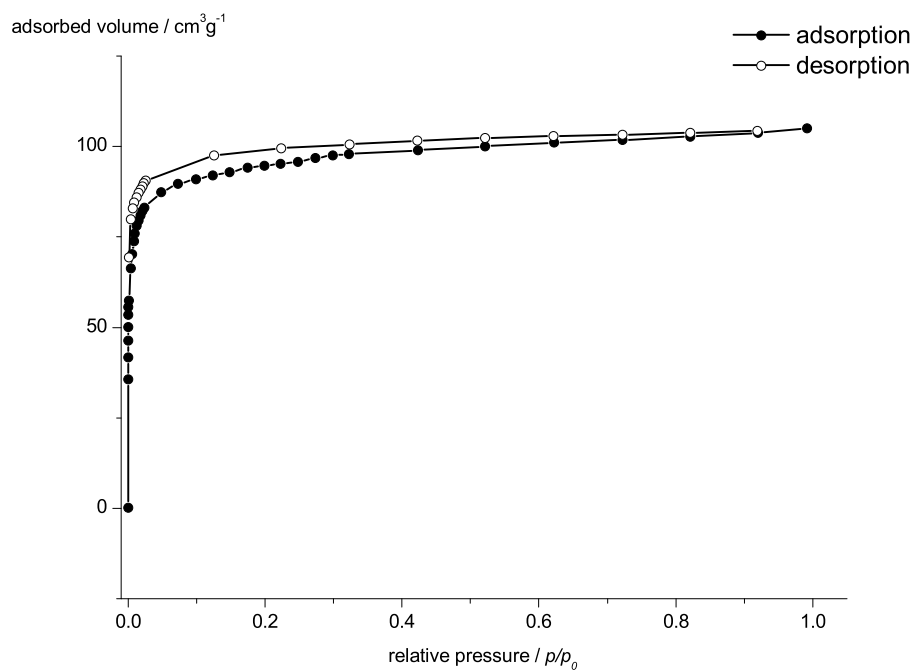
**Figure 4.38** – $N_2$ physisorption of UHM-25-Pro (**153**) after activation with supercritical $CO_2$.

$S_{\text{BET}} = 371.5\,\text{m}^2\,\text{g}^{-1}$ (determined for $p/p_0 = 0.010$–$0.048$)
$V_{\text{micropore}} = 0.15\,\text{cm}^3\,\text{g}^{-1}$ (determined at $p/p_0 = 0.20$)
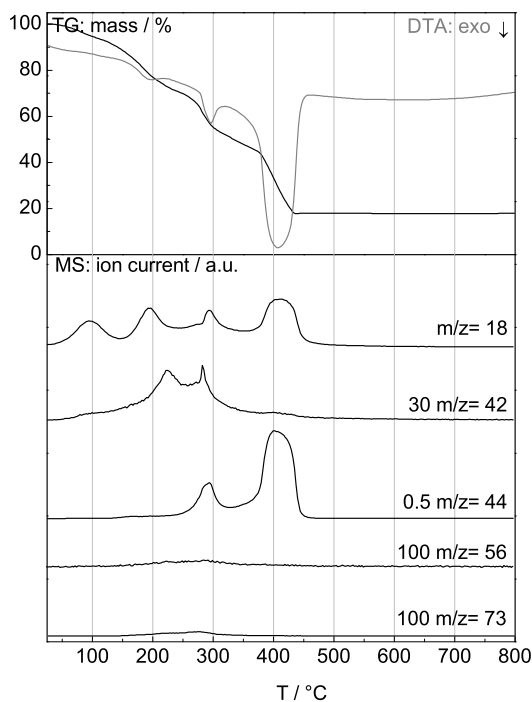
| Δ T | Δ m | fragments |
| °C | % | m/z |
| --- | --- | --- |
| 25–121 | 7 | 18 |
| 121–244 | 22 | 42, 44 |
| 244–343 | 22 | 18, 42, 44 |
| 337–457 | 31 | 18, 44 |

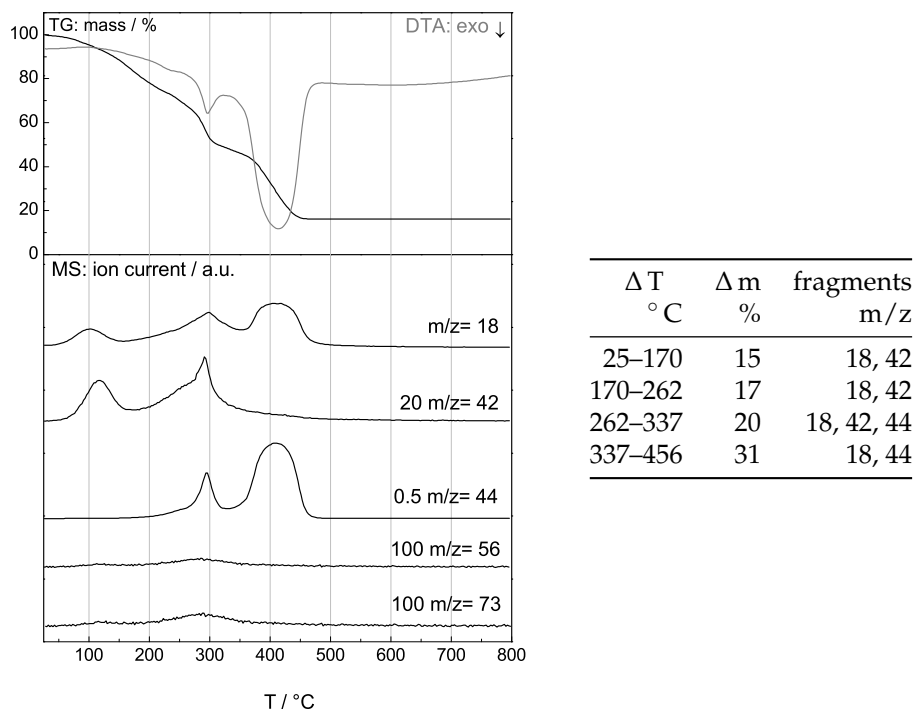**Figure 4.39** – TG/MS analysis of UHM-25-Pro (**153**), weight loss (black) and DTA (grey) are plotted in the upper part and in the lower part of the diagram the characteristic single ion currents are shown for $\frac{m}{z}$ = 18 ($H_2O$), 42 (THF), 44 ($CO_2$), 56 (isobutene), and 73 (DMF).

### 4.50.1 Crystal Structure Determination and Refinement

Single crystals were obtained from a small-scale reaction of a solution of tetracarboxylic acid **128** (19 mg, 0.03 mmol, 1 eq.) in DMF (0.8 mL) to which was added nitric acid (20 %, 66 µL),with an aqueous solution of copper nitrate trihydrate (c = 100 g/L, 0.5 mL, 5.0 mg Cu($NO_3$)$_2$ · 3 $H_2O$, 22 µmol, 0.6 eq.) The reaction mixture was placed in a 6 mL test tube which was placed in a 100 mL screw-capped flask and was heated at 50 °C in an oven for three days. This resulted in light blue, block-shaped crystals that were kept in the mother liquor.
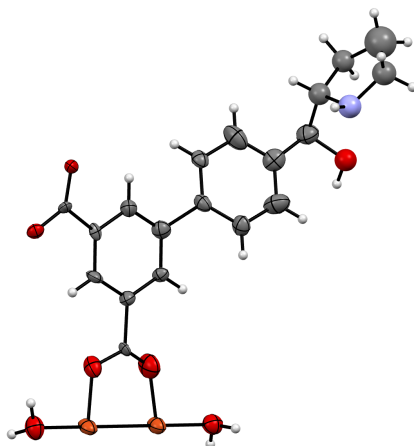
**Figure 4.40** – ORTEP-like plot of the asymmetric unit of UHM-25-Pro (orange: copper, red: oxygen, light blue: nitrogen, grey: carbon, white: hydrogen; probability level 15%).

X-ray single crystal diffraction for UHM-25-Pro (**153**) was collected on an Oxford Diffraction (Agilent Technologies) SuperNova diffractometer at 100(2) K with Cu $K\alpha$ radiation (154.178 pm) by $\omega$ scanning mode. The program CrysAlisPro was used for integration of the diffraction profiles and absorption corrections. The structure was solved by direct methods using the SHELXS program of the SHELXTL package and refined by full-matrix least-squares methods with SHELXL by successive Fourier syntheses against $|F|^2$. All non-hydrogen atoms –except for the chiral moiety on the linker molecule– were refined with anisotropic displacement parameters. The location of the hydrogen atoms of the coordinated water molecules at the copper atoms of the paddle-wheel motif could not be assigned. A high degree of disorder has been found for the chiral moiety on the organic SBU, which can be ascribed to statistical disorder of the linker within the framework and the conformational flexibility of the substituent. Hence, this group cannot be sufficiently located from the difference Fourier map. Therefore the chiral substituent in UHM-25-Pro has been modeled as a substituent with chemically reasonable bond lengths and angles but without any conformational disorder. The atomic positions of this group were held fixed during the refinement.

SQUEEZE/PLATON[320] was used to account for the electron density from disordered copper atoms and DMF solvent molecules, which could not be resolved. The contributions of 5571 electrons were removed from the unit cell contents. In the space group $P432$ $5571/24 = 232.1$ electrons were removed from the

asymmetric unit. With $Z$ being 12, 2785.5 electrons would be associated with one formula unit, consistent with 0.5 copper(II) ions and 76 DMF solvent molecules per unit cell.

| identification code | UHM-25-Pro |
|---|---|
| empirical formula | C33 H27 Cu2 N1 O11 |
| formular weight | 740.63 g/mol |
| temperature | 100(2) K |
| wavelength | 154.178 pm, Cu $K\alpha$ |
| crystal system | cubic |
| space group | $P432$ |
| unit cell dimensions | $a = 2902.61(6)$ pm $\alpha = 90°$ |
| | $b = 2902.61(6)$ pm $\beta = 90°$ |
| | $c = 2902.61(6)$ pm $\gamma = 90°$ |
| volume | 24 454.9(15) $\text{Å}^3$ |
| Z | 12 |
| calculated density | 0.603 g/cm$^3$ |
| absorption coefficient | $\mu = 0.86$ mm$^{-1}$ |
| $F(000)$ | 4536 |
| crystal size | $0.10 \times 0.10 \times 0.09$ mm$^3$ |
| $\theta$ range for data collection | 3.4 to 45.0 |
| index ranges | $h = -14 \to 15, k = 0 \to 18, l = 2 \to 26$ |
| reflections collected | 160315 |
| independent reflections | 3326 |
| independent reflections ($I > 2\sigma(I)$) | 2055 ($R_{int} = 0.075$) |
| absorption correction | multi-scan |
| refinement method | Full-matrix least squares on $F^2$ |
| data / restraints / parameters | 3326 / 38 / 189 |
| goodness-of-fit on $F^2$ | $S = 1.09$ |
| final $R$ indices $[I > \sigma(I)]$ | R1 = 0.121 wR2 = 0.311 |
| $R$ indices (all data) | $R1 = 0.149, wR2 = 0.336$ |
| largest diff. peak and hole | $\Delta\rho_{max}0.76$ e/$\text{Å}^3$, $\Delta\rho_{min}-0.60$ e/$\text{Å}^3$ |

## 4.51   UHM-25-Val-Evans (154)
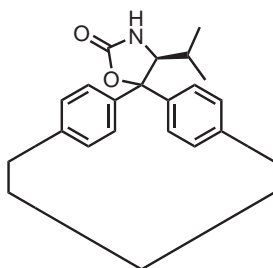


Tetracarboxylic acid **125** (353 mg, 0.58 mmol, 1 eq.) was dissolved in DMF (24 mL). To this solution was added nitric acid (20 %, 1.9 mL), then an aqueous solution of copper nitrate trihydrate (c = 100 g/L, 8.8 mL, 88 mg Cu(NO$_3$)$_2$ · 3 H$_2$O, 0.4 mmol, 0.6 eq.) The reaction mixture was placed in an oven at 50 °C for three days. The mother liquor was decanted and the crystals suspended in fresh DMF. This procedure was repeated twice after 24 hours each. DMF was then replaced with THF in the same manner. The solvent-exchanged MOF was kept under THF and stored in a closed container.

A fraction of the MOF was digested in diluted hydrochloric acid to reisolate the linker for spectroscopic measurements: **HRMS (ESI+):** $\frac{m}{z}$ = 610.1707 (calc. for MH$^+$: 610.1708); **opt. rot.:** $[\alpha]_D^{27} = -81.5$ (c = 0.38), MeOH).
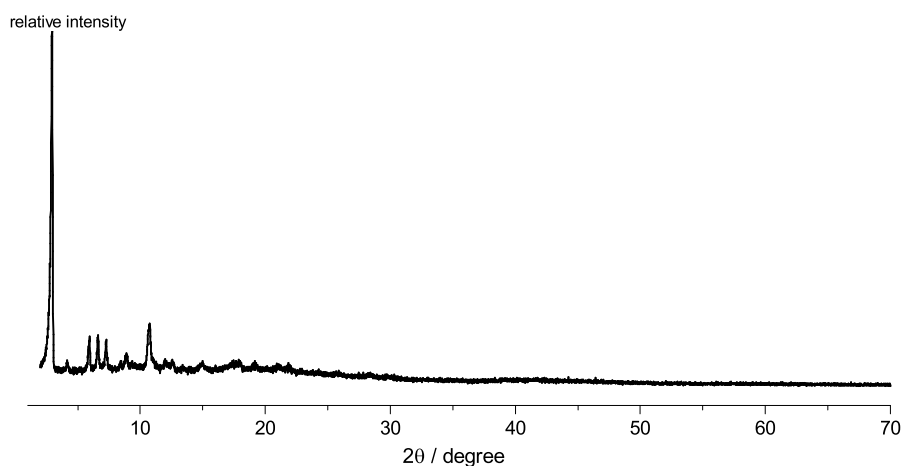


**Figure 4.41** – Powder X-ray diffractogram of UHM-25-Val-Evans (**154**).
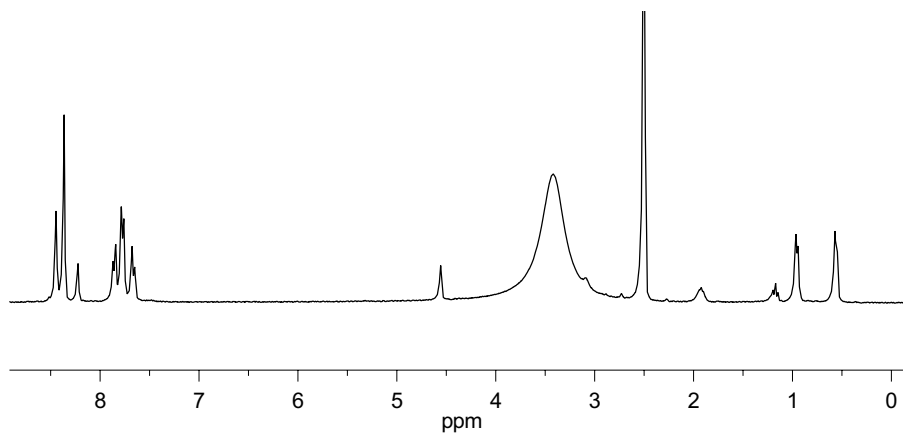
**Figure 4.42** – $^1$H-NMR of digested UHM-25-Val-Evans

**$^1$H-NMR (300 MHz, DMSO$-$d$_6$):** $\delta$ [ppm] = 8.50-8.41 (m, 2H, H15), 8.41-5.30 (m, 4H, H13), 8.23 (s, 1H, H1), 7.96-7.60 (m, 8H, H9, H10), 4.56 (s, 1H, H2), 2.08-1.83 (m, 1H, H6), 0.95 (d, 3H, $^3J_{\text{H-H}}$ = 6.8 Hz, H7A), 0.56 (d, 3H, $^3J_{\text{H-H}}$ = 6.5 Hz, H7B).
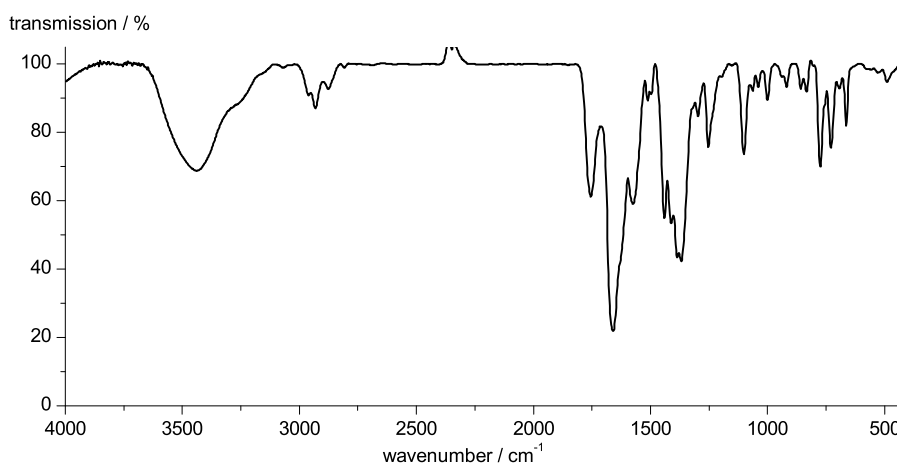


**IR (KBr):** $\widetilde{\nu}$ [cm$^{-1}$] = 3439 (w), 2961 (w), 2932 (w), 2878 (w), 1755 (m), 1661 (s), 1574 (m), 1512 (w), 1497 (w), 1441 (s), 1412 (s), 1387 (s), 1367 (s), 1298 (w), 1254

(m), 1101 (m), 1063 (w), 1040 (w), 1001 (w), 918 (w), 858 (w), 833 (w), 775 (m), 729 (m), 694 (w), 663 (w).
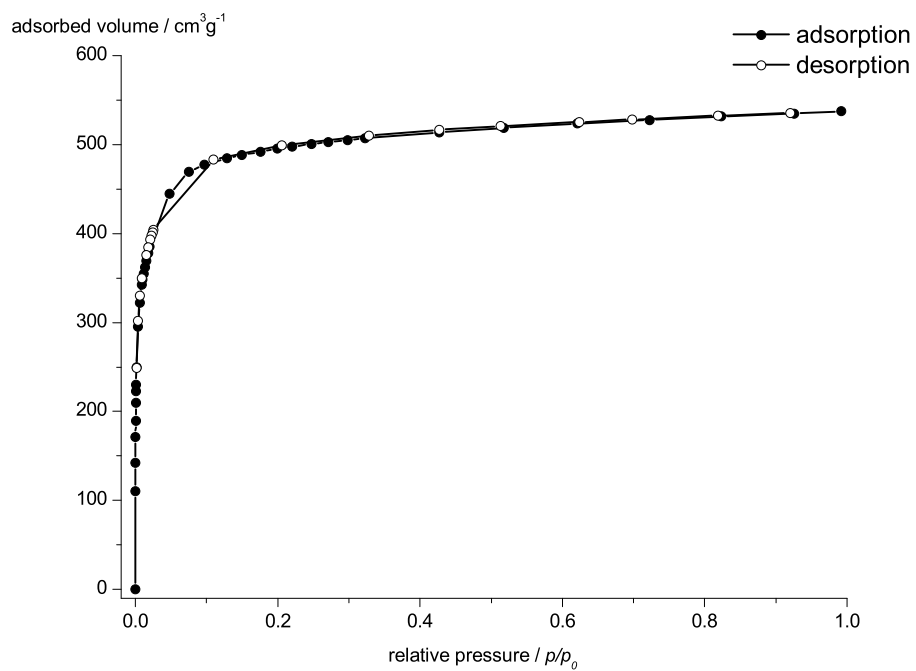


**Figure 4.43** – $N_2$ physisorption of UHM-25-Val-Evans (**154**) after thermal activation at 40 °C.

$S_{BET} = 1978 \, \text{m}^2 \, \text{g}^{-1}$ (determined for $p/p_0 = 0.012$–$0.075$)
$V_{\text{micropore}} = 0.76 \, \text{cm}^3 \, \text{g}^{-1}$ (determined at $p/p_0 = 0.20$)
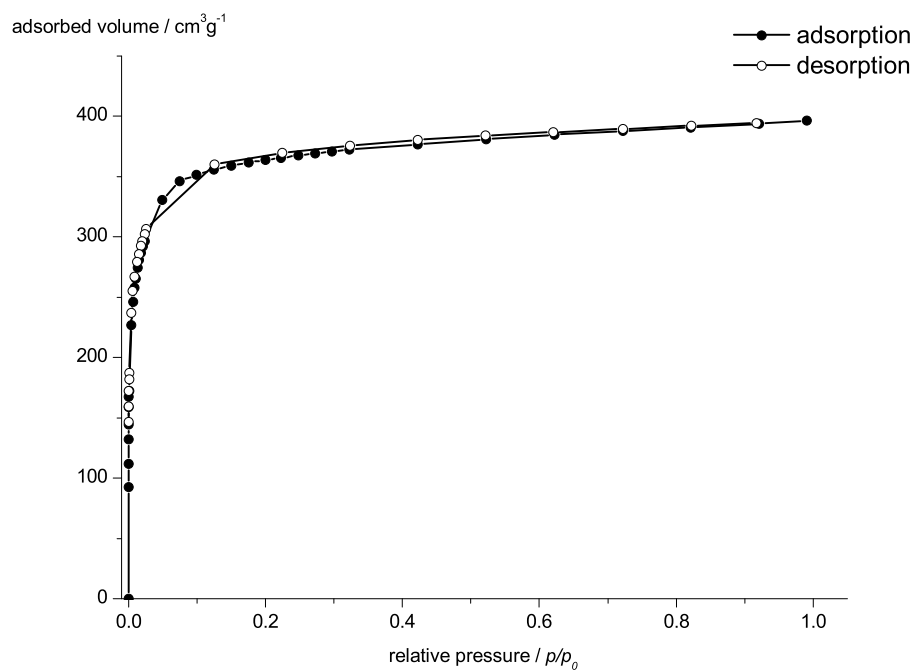
**Figure 4.44** – N$_2$ physisorption of UHM-25-Val-Evans (**154**) after activation with supercritical CO$_2$.

$S_{\text{BET}} = 1454 \, \text{m}^2 \, \text{g}^{-1}$ (determined for $p/p_0 = 0.014$–$0.075$)
$V_{\text{micropore}} = 0.56 \, \text{cm}^3 \, \text{g}^{-1}$ (determined at $p/p_0 = 0.20$)

| $\Delta T$ | $\Delta m$ | fragments |
|:---:|:---:|---:|
| °C | % | m/z |
| 25–170 | 15 | 18, 42 |
| 170–262 | 17 | 18, 42 |
| 262–337 | 20 | 18, 42, 44 |
| 337–456 | 31 | 18, 44 |

**Figure 4.45** – TG/MS analysis of UHM-25-Val-Evans (**154**), weight loss (black) and DTA (grey) are plotted in the upper part and in the lower part of the diagram the characteristic single ion currents are shown for $\frac{m}{z}$ = 18 ($H_2O$), 42 (THF), 44 ($CO_2$), 56 (isobutene), and 73 (DMF).

369

## 4.52 UHM-25-Phe-Evans (155)
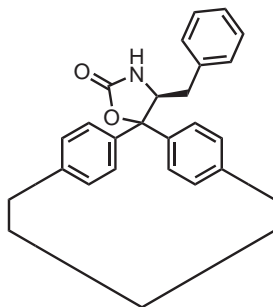


Tetracarboxylic acid **126** (381 mg, 0.58 mmol, 1 eq.) was dissolved in DMF (24 mL). To this solution was added nitric acid (20 %, 1.9 mL), then an aqueous solution of copper nitrate trihydrate (c = 100 g/L, 8.8 mL, 88 mg $Cu(NO_3)_2 \cdot 3 H_2O$, 0.4 mmol, 0.6 eq.) The reaction mixture was placed in an oven at 50 °C for three days. The mother liquor was decanted and the crystals suspended in fresh DMF. This procedure was repeated twice after 24 hours each. DMF was then replaced with THF in the same manner. The solvent-exchanged MOF was kept under THF and stored in a closed container.

A fraction of the MOF was digested in diluted hydrochloric acid to reisolate the linker for spectroscopic measurements: **HRMS (ESI+):** $\frac{m}{z}$ = 658.1697 (calc. for MH$^+$: 658.1708); **opt. rot.:** $[\alpha]_D^{27} = -43.8$ (c = 0.27, MeOH).

relative intensity
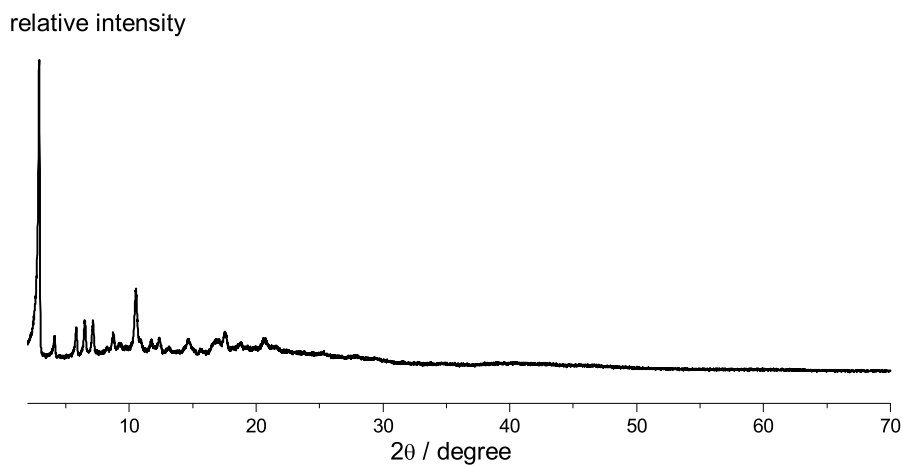


**Figure 4.46** – Powder X-ray diffractogram of UHM-25-Phe-Evans (**155**).
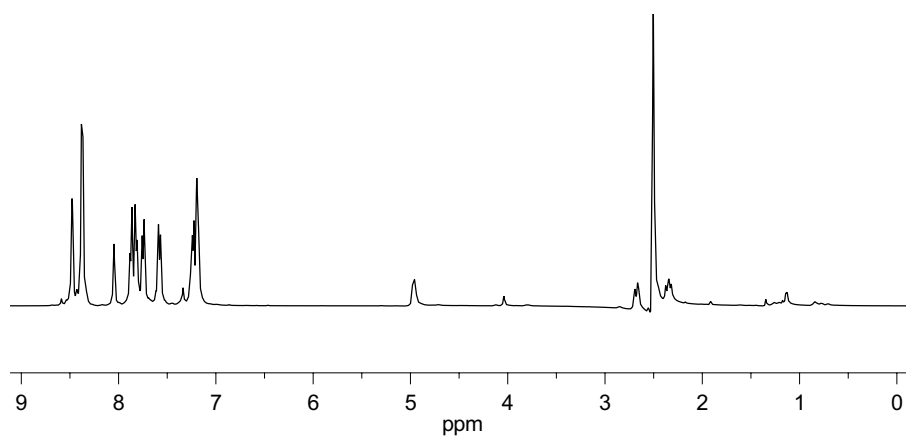


**Figure 4.47** – $^1$H-NMR of digested UHM-25-Phe-Evans

**$^1$H-NMR (300 MHz, DMSO−d$_6$):** $\delta$ [ppm] = 8.50-8.45 (m, 2H, H18), 8.48 (d, 2H, $^4J_{\text{H-H}}$ = 1.6 Hz, H16A), 8.38 (d, 2H, $^4J_{\text{H-H}}$ = 1.6 Hz, H16B), 8.05 (s, 1H, H1), 7.91-7.72 (m, 6H, H12A, H13), 7.63-7.56 (m, 2H, H12B), 7.29-7.15 (m, 5H, H8, H9, H10), 4.96 (dd, 1H, $^3J_{\text{H-H}}$ = 9.9, 4.5 Hz, H5), 2.68 (dd, 1H, $^3J_{\text{H-H}}$ = 13.6, 4.0 Hz, H6A), 2.35 (dd, 1H, $^3J_{\text{H-H}}$ = 13.8, 9.4 Hz, H6B).

371
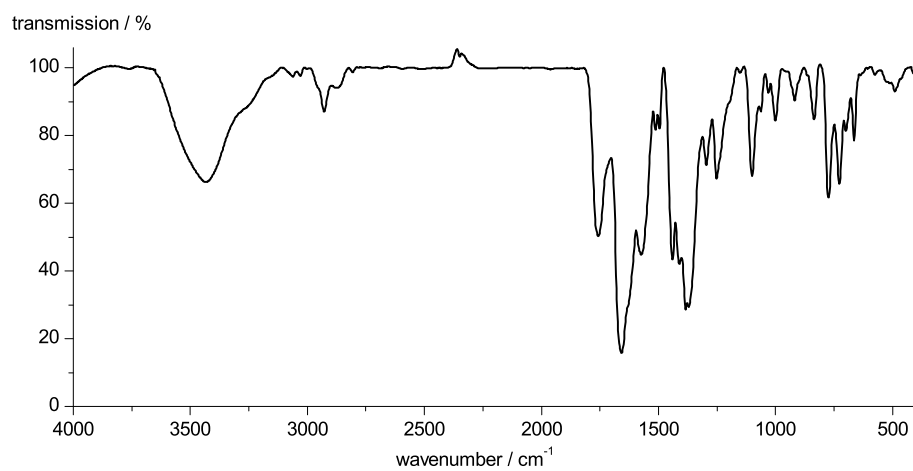
**IR (KBr):** $\widetilde{\nu}$ [cm$^{-1}$] = 3433 (m), 2928 (w), 1757 (s), 1659 (s), 1574 (s), 1512 (w), 1497 (w), 1441 (s), 1412 (s), 1385 (s), 1371 (s), 1296 (m), 1252 (m), 1099 (m), 1063 (w), 1030 (w), 1001 (w), 918 (w), 835 (w), 773 (m), 727 (m), 700 (w), 665 (w), 490 (w).
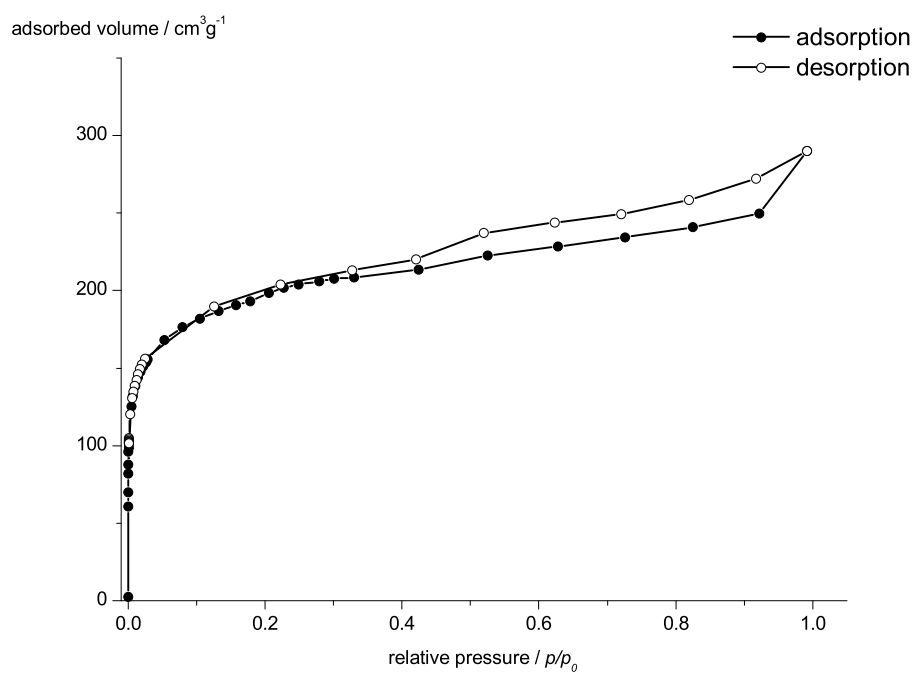
**Figure 4.48** – $N_2$ physisorption of UHM-25-Phe-Evans (**155**) after activation with supercritical $CO_2$.

$S_{BET} = 728.9\,\text{m}^2\,\text{g}^{-1}$ (determined for $p/p_0 = 0.022–0.104$)
$V_{micropore} = 0.31\,\text{cm}^3\,\text{g}^{-1}$ (determined at $p/p_0 = 0.21$)
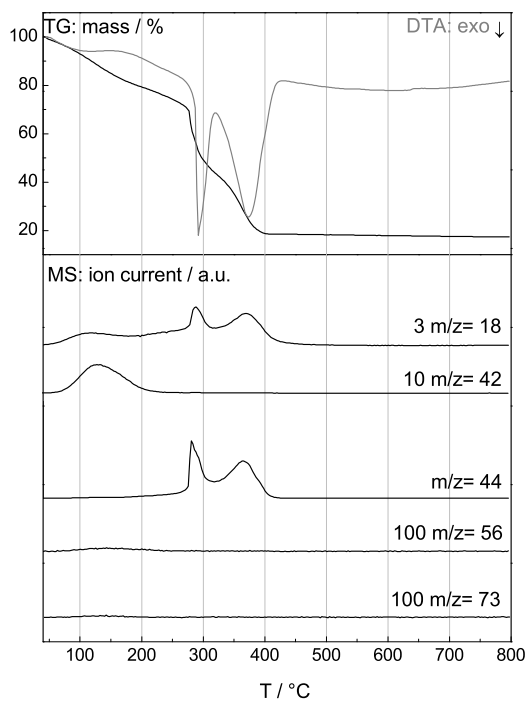
| $\Delta T$ | $\Delta m$ | fragments |
|:---:|:---:|---:|
| $^\circ C$ | % | m/z |
| 25–209 | 15 | 18, 42 |
| 209–314 | 17 | 18, 44 |
| 314–406 | 20 | 18, 44 |

**Figure 4.49** – TG/MS analysis of UHM-25-Phe-Evans (**155**), weight loss (black) and DTA (grey) are plotted in the upper part and in the lower part of the diagram the characteristic single ion currents are shown for $\frac{m}{z}$ = 18 ($H_2O$), 42 (THF), 44 ($CO_2$), 56 (isobutene), and 73 (DMF).

## 4.53 UHM-20 (156)
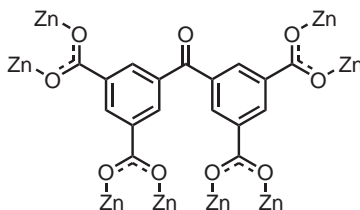


3,3′,5,5′-Tetracarboxy benzophenone (**136**, 72.1 mg, 0.20 mmol, 1 eq.) was dissolved in DMA (7.0 mL). To this solution was added *N*-Boc-Valinol (260 mg, 1.3 mmol, 64 eq.) and a solution of zinc nitrate hexahydrate in DMA (c = 100 g/L, 3.0 mL, 300 mg $Zn(NO_3)_2 \cdot 6 H_2O$, 1.0 mmol, 2.0 eq.). The reaction mixture was placed in a screw-capped vial in an oven at 80 °C for one day. The reaction mixture was filtrated and colorless crystals were collected. These crystals were washed with DMA and dried in air. This material constituted mixture of different solid phases. The structure of one of them was solved through single crystal X-Ray diffraction experiments.
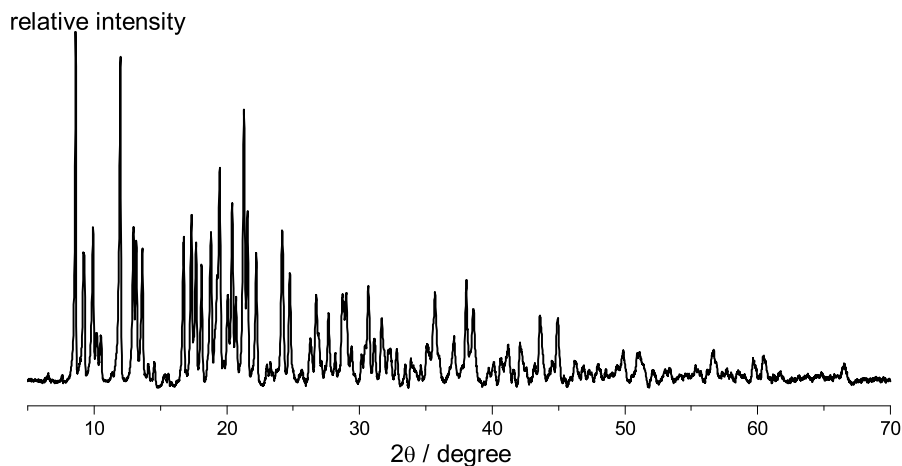


**Figure 4.50** – Powder X-ray diffractogram of UHM-20 that is contaminated with unknown solid phases.

375
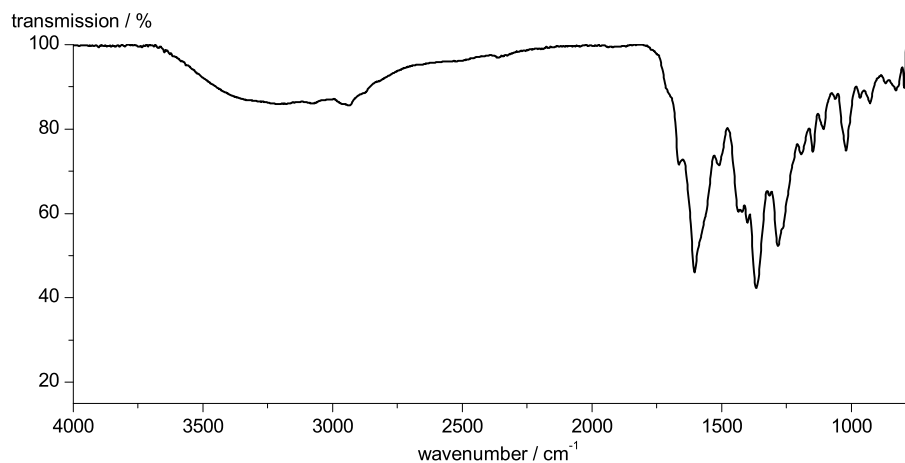
**IR (ATR):** $\widetilde{\nu}$ = 2958 (w), 2936 (w), 1664 (m), 1604 (s), 1508 (m), 1420 (m), 1399 (m), 1365 (s), 1315 (m9), 1282 (s), 1192 (m), 1106 (m) 1061 (m), 965 (m), 827 (m).

### 4.53.1 Crystal Structure Determination and Refinement
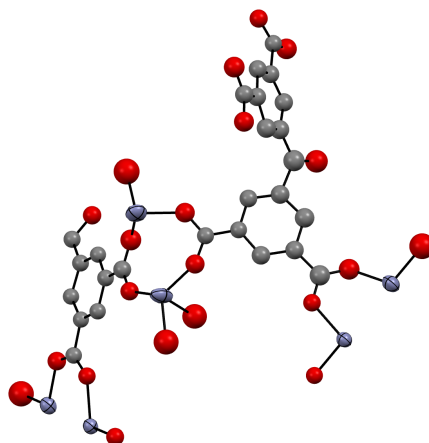


**Figure 4.51** – ORTEP-like plot of the asymmetric unit of UHM-20 (light blue: zinc, red: oxygen, grey: carbon, hydrogen atoms omitted for clarity; probability level 25%).

| identification code | UHM-20 |
| --- | --- |
| empirical formula | C16 H16 N4 O8 Zn4 |
| formular weight | 653.81 g/mol |
| temperature | 100(0) K |
| wavelength | 70.926 pm, Mo $K\alpha$ |
| crystal system | tetragonal |
| space group | $I4/m$ |
| unit cell dimensions | $a = 2675.1(41)$ pm $\alpha = 90°$ |
| | $b = 2675.1(41)$ pm $\beta = 90°$ |
| | $c = 3570.1(62)$ pm $\gamma = 90°$ |
| volume | 25 549.4(19) $\text{Å}^3$ |
| Z | 42 |
| calculated density | 1.785 g/cm$^3$ |
| absorption coefficient | $\mu = 3.94$ mm$^{-1}$ |
| $F(000)$ | 13608 |
| crystal size | $0.10 \times 0.03 \times 0.3$ mm$^3$ |
| $\theta$ range for data collection | 1.87 to 22.5 |
| index ranges | $h = -35 \rightarrow 35, k = -35 \rightarrow 35, l = -46 \rightarrow 47$ |
| reflections collected | 97260 |
| independent reflections | 8504 |
| independent reflections $(I > 2\sigma(I))$ | 5041 ($R_{int} = 0.070$) |
| absorption correction | numerical |
| refinement method | Full-matrix least squares on F$^2$ |
| data / restraints / parameters | 8504 / 0 / 255 |
| goodness-of-fit on F$^2$ | $S = 2.06$ |
| final R indices $[I > \sigma(I)]$ | R1 = 0.177 wR2 = 0.533 |
| R indices (all data) | $R1 = 0.224, wR2 = 0.494$ |
| largest diff. peak and hole | $\Delta\rho_{max}$2.31 e/$\text{Å}^3$, $\Delta\rho_{min}$−0.81 e/$\text{Å}^3$ |

## 4.54   UHM-26 (157)
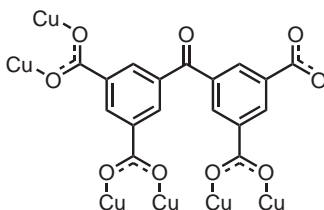


Single crystals were obtained from a small-scale reaction of a solution of 3,3′,5,5′-tetracarboxy benzophenone (**136**, 11 mg, 0.03 mmol, 1 eq.) in DMF (0.8 mL) to which was added nitric acid (20 %, 66 μL),and an aqueous solution of copper nitrate trihydrate (c = 100 g/L, 0.5 mL, 5.0 mg Cu(NO$_3$)$_2$ · 3 H$_2$O, 22 μmol, 0.6 eq.). The reaction mixture was placed in a 6 mL test tube which was placed in a 100 mL screw-capped flask and was heated at 50 °C in an oven for three days. This resulted in light blue, block-shaped crystals that were kept in the mother liquor. This material constituted mixture of different solid phases. The structure of one of them was solved through single crystal X-Ray diffraction experiments.
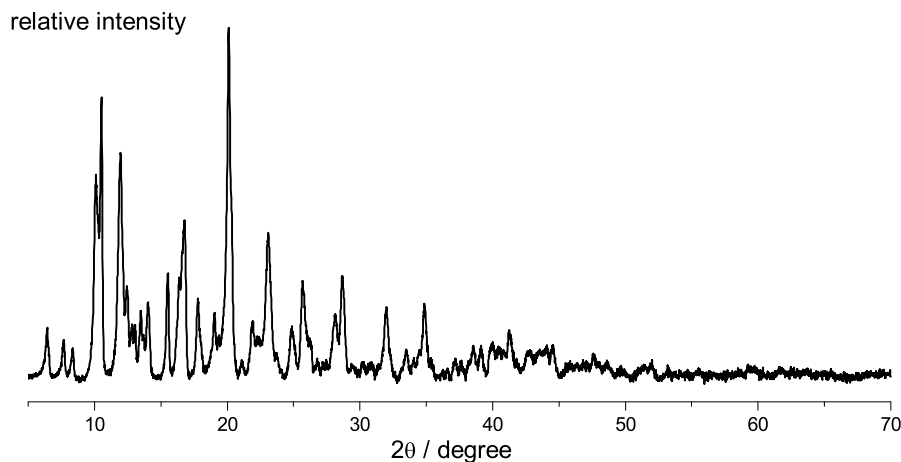


**Figure 4.52** – Powder X-ray diffractogram of UHM-26 that is contaminated with unknown solid phases.
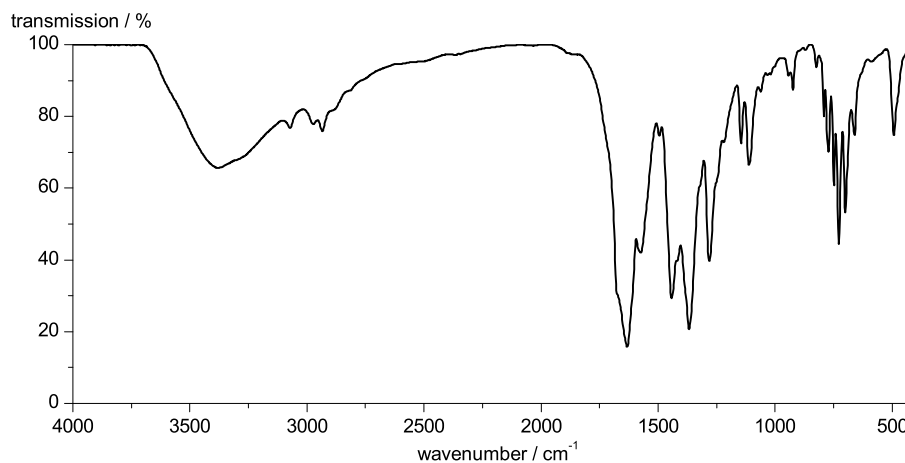
**IR (ATR):** $\widetilde{\nu}$ = 3228 (br), 2966 (w), 2935 (w), 1666 (m), 1604 (s), 1506 (m), 1436 (m), 1402 (m), 1365 (s), 1282 (s), 1147 (m), 1105 (w), 1016 (m), 923 (m), 775 (w), 750 (m).

## 4.54.1 Crystal Structure Determination and Refinement
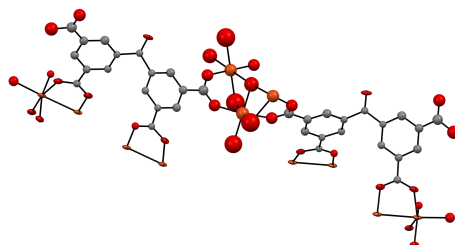


**Figure 4.53** – ORTEP-like plot of the asymmetric unit of UHM-26 (orange: copper, red: oxygen, light blue: nitrogen, grey: carbon, white: hydrogen; probability level 25%).

| identification code | UHM-26 |
| --- | --- |
| empirical formula | C17 H6 Cu O9 |

| | |
|---|---|
| formular weight | 418.84 g/mol |
| temperature | 100(0) K |
| wavelength | 154.178 pm, Cu $K\alpha$ |
| crystal system | monoclinic |
| space group | $C2/c$ |
| unit cell dimensions | $a = 3202.2(3)$ pm $\alpha = 90°$ |
| | $b = 2147.3(1)$ pm $\beta = 101.090(7)°$ |
| | $c = 9.4652(7)$ pm $\gamma = 90°$ |
| volume | 6386.8(8) $\text{Å}^3$ |
| Z | 13 |
| calculated density | 1.416 g/cm$^3$ |
| absorption coefficient | $\mu = 1.99$ mm$^{-1}$ |
| $F(000)$ | 2724 |
| crystal size | $0.10 \times 0.50 \times 0.3$ mm$^3$ |
| $\theta$ range for data collection | 4.1 to 50.4 |
| index ranges | $h = -32 \rightarrow 32, k = -21 \rightarrow 21, l = -9 \rightarrow 9$ |
| reflections collected | 30816 |
| independent reflections | 3349 |
| independent reflections $(I > 2\sigma(I))$ | 2431 $(R_{int} = 0.108)$ |
| absorption correction | numerical |
| refinement method | Full-matrix least squares on F$^2$ |
| data / restraints / parameters | 3349 / 0 / 259 |
| goodness-of-fit on F$^2$ | $S = 3.3$ |
| final R indices $[I > \sigma(I)]$ | R1 =0.181 wR2 =0.464 |
| R indices (all data) | $R1 = 0.253, wR2 = 0.527$ |
| largest diff. peak and hole | $\Delta\rho_{max}$1.93 e/$\text{Å}^3$, $\Delta\rho_{min}$−2.38 e/$\text{Å}^3$ |

## 4.55  3(*S*)-1,1-Dimethoxy-3-hydroxy-butane (165)
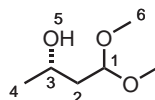


The reaction was performed oven-dried glassware under argon. The solvent was degassed by three freeze-pump-thaw cycles prior to use. UHM-25-Pro (**153** was transferred to a schlenk tube, dried in stream of Argon and then weighed in the closed reaction vessel (220 mg). The MOF was suspended in $CH_2Cl_2$ (5 mL) and freshly distilled acetaldehyde (0.50 mL, 63,5 mg, 1.44 mmol) were added.

After five days, the reaction mixture was filtered and the remaining solid was washed with $CH_2Cl_2$ (2 mL). The filtrate was collected in a flask containing MeOH (10 mL) and Amberlyst® 15 (200 mg). After 24 hours, the reaction mixture was over celite and the filtrate was concentrated in vacuum. A clear liquid with a characteristic odour was obtained.

The reaction product was analyzed by GC-MS. The measuremetn was performed on a 50 m stationary silica phase modified with heptakis-(2,3-di-*O*-methyl-6-*O*-*tert*-butyldimethylsilyl)-β-cyclodextrin with hydrogen as the carrier gas. A complete separation of the enantiomers of reaction product on the column was achieved using a temperature gradient of 1 °C/min after keeping the column heated to 70 °C for five minutes after injection of the sample. The chromatogram of the separation of the reaction product is shown in Figure 3.42. The reaction product was identified by comparison of the mass spectrum (see Figure 4.55) with reference spectra of the mass spectral database from the National Institute of Standards and Technology.[321]
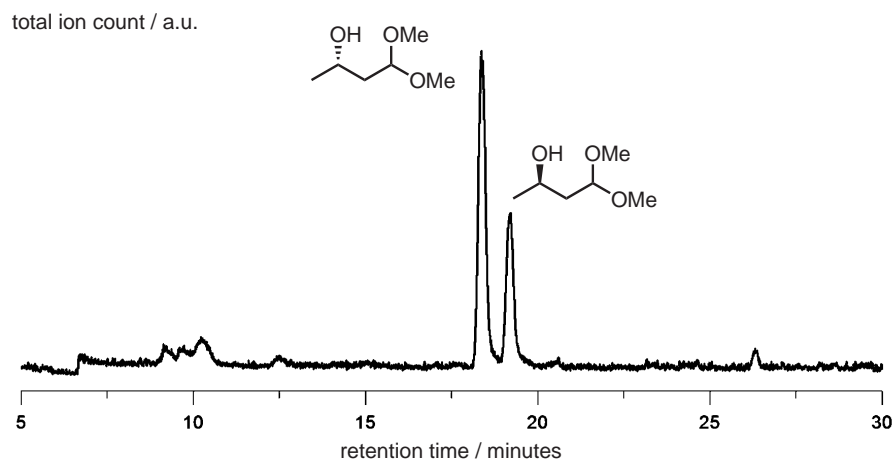


**Figure 4.54** – Total ion count of the enantioselective gas chromatographic separation of the 1,1-Dimethoxy-3-hydroxy-butane (**165**).
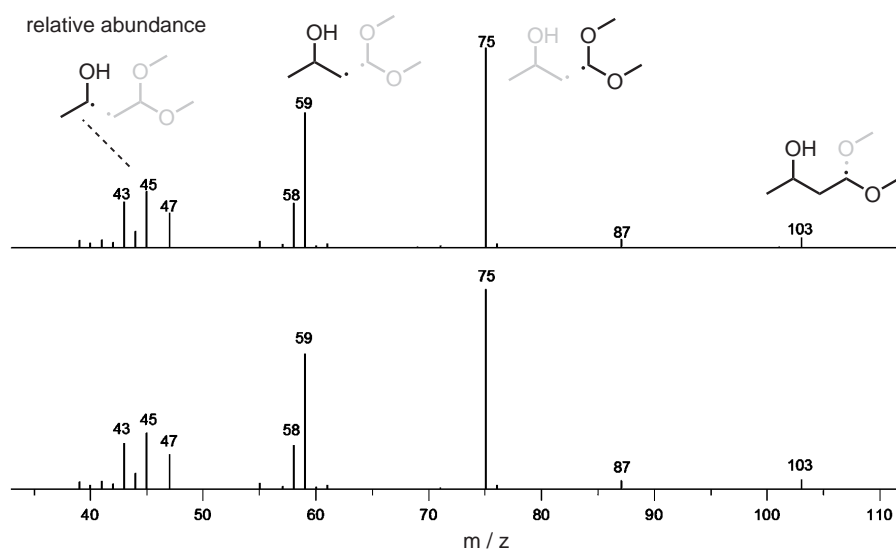
**Figure 4.55** – Mass spectra for the peaks at retention time 18.4 (top) and 19.2 minutes (bottom) that correspond to the (*R*)- and the (*S*)-enantiomer of 3*S*)-1,1-Dimethoxy-3-hydroxy-butane (**165**.

## 4.56  *N*-Propionyl-UHM-25-Val-Evans (187)
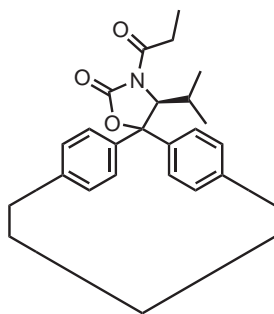


The reaction was performed oven-dried glassware under argon. UHM-25-Val-Evans (**154**) was transferred to a schlenk tube, dried in stream of Argon and then weighed in the closed reaction vessel (90 mg, 0.09 mmol). The MOF was

suspended in THF (0.9 mL, 130 eq.) and Triethylamine (0.1 mL, 13 eq.), a solution of dimethylaminopyridine in THF (183 $\frac{mmol}{L}$, 0.16 mL, 0.03 mmol, 0.25 eq.) and propionic anhydride (0.16 mL, 1.2 mmol, 13 eq.). After 72 hours, the reaction mixture was filtered and the MOF was washed with THF (10 mL) and dried in vacuum. Prior to powder diffraction measurements, DMF was restored as the pore-filling solvent by solvent exchange. For characterization purposes, the MOF was digested in hydrochloric acid (2 M) under ultrasonic irridation. This resulted in the precipitation of the linker which was washed with water and dried in vacuum. **HRMS (ESI+):** 666.1961 (calc. for $[C_{37}H_{32}NO_{10} + H]^+$: 666.1970).
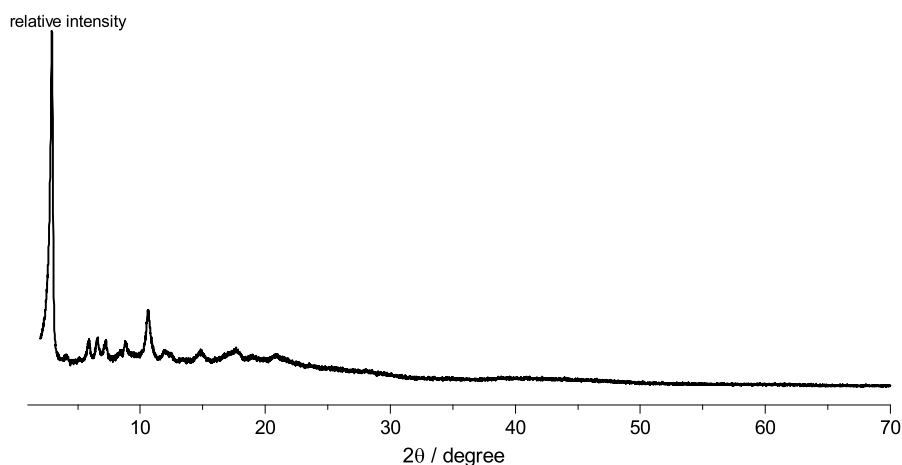


**Figure 4.56** – Powder X-ray diffractogram of UHM-25-Val-Evans-*N*-propionyl (**187**).
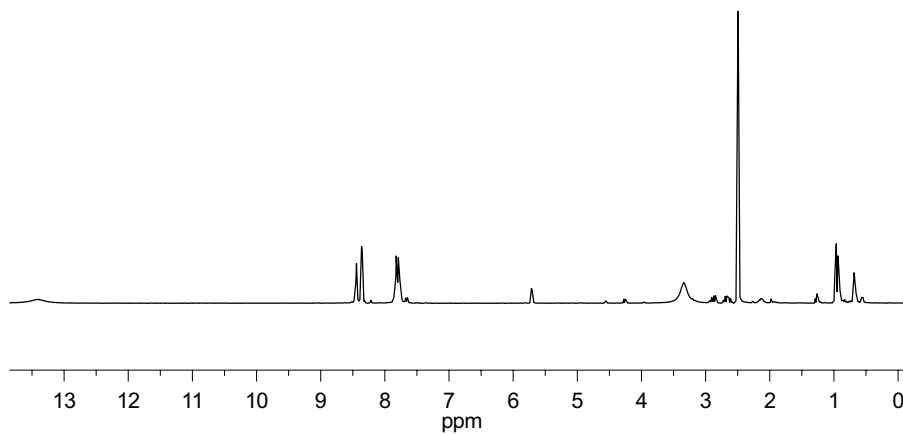
**$^1$H-NMR (300 MHz, DMSO$-$d$_6$):** $\delta$ [ppm] = 14.33-12.70 (s, 4H, H20), 8.47-8.42 (m, 2H, H18), 8.40-8.33 (m, 4H, H16), 7.80-7.73 (m, 4H, H12, H13), 5.76-5.66 (m, 1H, H5), 2.89 (dq, 1H, $^2J_{H-H}$ = 17.3 Hz, $^3J_{H-H}$ = 7.3 Hz , H7A), 2.89 (dq, 1H, $^2J_{H-H}$ = 17.5 Hz, $^3J_{H-H}$ = 7.3 Hz , H7B), 2.22-2.04 (m, 1H, H9), 1.01-0.88 (m, 6H, H6A , H8), 0.68 (d, 3H, $^3J_{H-H}$ = 6.6 Hz, H6B).



384

transmission / %
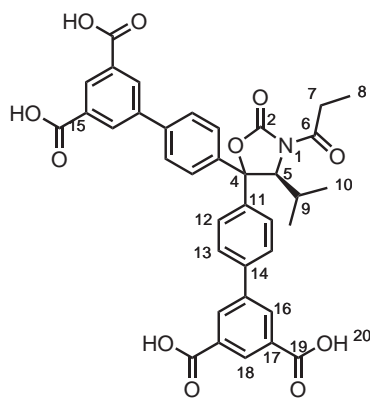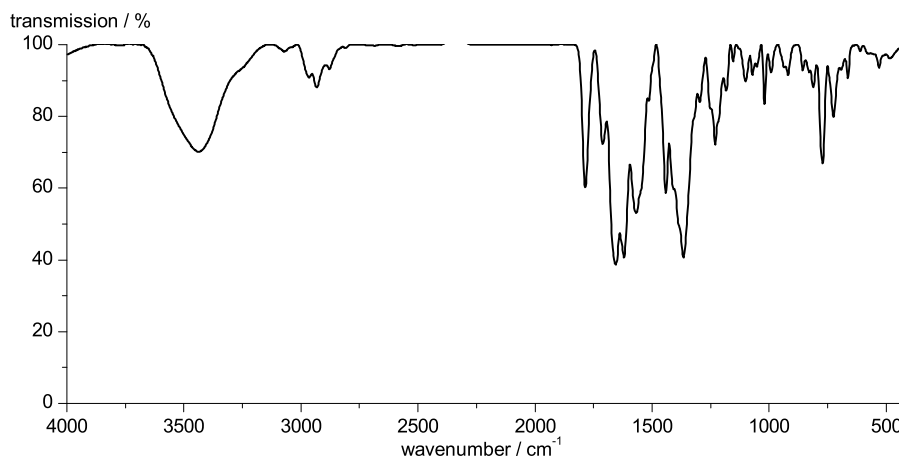
**IR (KBr):** $\widetilde{\nu}$ [cm$^{-1}$] = 3437 (m), 2964 (w), 2934 (w), 1786 (s), 1711 (m), 1655 (s), 1620 (s), 1568 (s), 1514 (m), 1441 (s), 1366 (s), 1296 (m), 1231 (m), 1182 (w), 1101 (w), 1070 (w), 1020 (m), 991 (w), 918 (w), 829 (w), 812 (w), 772 (m), 725 (m), 663 (w).

## 4.57   *N*-Propionyl-UHM-25-Phe-Evans (188)

The reaction was performed oven-dried glassware under argon. UHM-25-Phe-Evans (**155**) was transferred to a schlenk tube, dried in stream of Argon and then weighed in the closed reaction vessel (70 mg, 0.07 mmol). The MOF was suspended in THF (0.7 mL, 130 eq.) and Triethylamine (0.75 mL, 13 eq.), a solution of dimethylaminopyridine in THF (183 $\frac{mmol}{L}$, 0.12 mL, 0.02 mmol, 0.25 eq.) and propionic anhydride (0.12 mL, 0.92 mmol, 13 eq.). After 72 hours, the reaction mixture was filtered and the MOF was washed with THF (10 mL) and dried in vacuum. Prior to powder diffraction measurements, DMF was restored as the pore-filling solvent by solvent exchange. For characterization purposes,

the MOF was digested in hydrochloric acid (2 M) under ultrasonic irridation. This resulted in the precipitation of the linker which was washed with water and dried in vacuum. **HRMS (ESI+):** 714.1944 (calc. for $[C_{41}H_{31}NO_{10} + H]^+$: 714.1970).
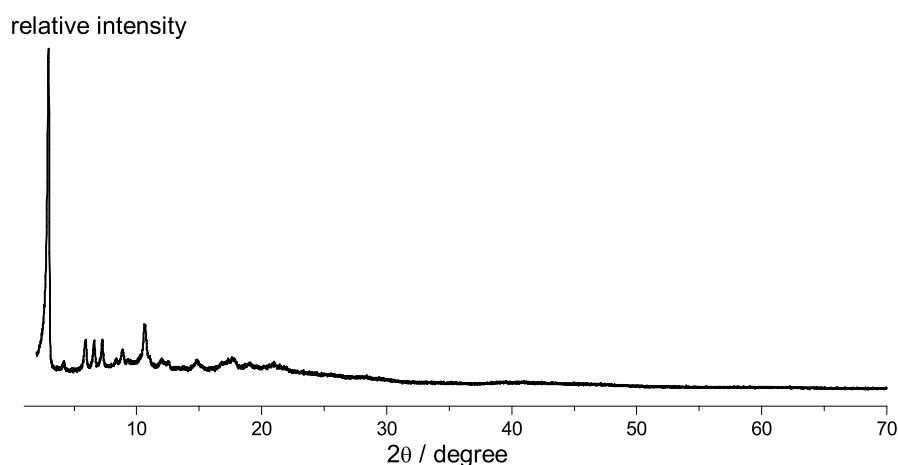


**Figure 4.57** – Powder X-ray diffractogram of UHM-25-Phe-Evans-*N*-propionyl (**188**).

**^{1}H-NMR (300 MHz, DMSO−d6):** $\delta$ [ppm] = 14.33-12.70 (s, 4H, H20), 8.51-8.42 (m, 2H, H17), 8.42-8.32 (m, 2H, H15), 7.89-7.76 (m, 4H, H11A, H12B), 7.76-7-67 (m, 2H, H12B), 7.63-7.55 (m, 2H, H11B), 7.28-7.02 (m, 3H, H7, H9), 6.94-6.81 (m, 2H, H8), 5.64 (t, 1H, $^3J_{H-H}$ = 6.3 Hz, H3), 2.96-2.53 (m, 4H, H5, H22), 0.85 (t, 3H, $^3J_{H-H}$ = 7.3 Hz, H23).
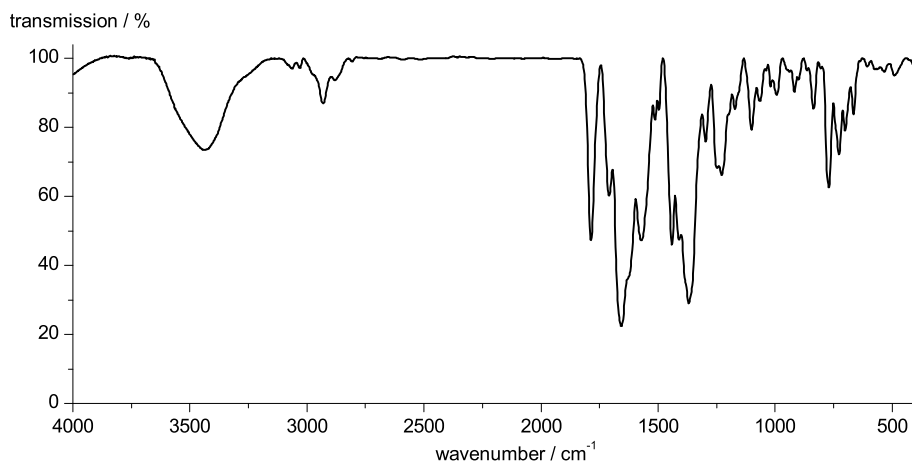
**IR (KBr):** $\widetilde{\nu}$ [cm$^{-1}$] = 3441 (m), 2932 (w), 1786 (m), 1709 (m), 1657 (s), 1572 (m), 1514 (m), 1497 (w), 1441 (m), 1410 (m), 1369 (s), 1298 (m), 1248 (m), 1229 (m), 1171 (w), 1101 (m), 1065 (w), 993 (w), 918 (w), 835 (w), 770 (m), 727 (m), 700 (m), 665 (m).

## 4.58   *N*-Crotonyl-UHM-25-Val-Evans (189)
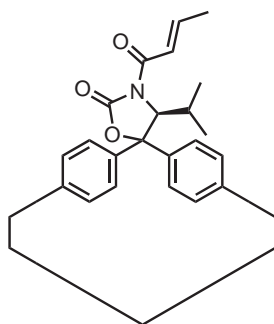


The reaction was performed oven-dried glassware under argon. UHM-25-Val-Evans (**154**) was transferred to a tube, dried in stream of Argon and then weighed in the closed reaction vessel (30 mg, 0.03 mmol). The MOF was suspended in THF (5 mL, 100 eq.) and a solution of sodium hexamethyldisilazide

(NaHMDS) in THF (1 $\frac{mol}{L}$, 0.33 mL, 0.33 mmol, 13 eq.) and crotonic anhydride (52 mg, 0.33 mmol, 13 eq.). After 24 hours, the reaction mixture was filtered and the MOF was washed with THF and dried in vacuum. For characterization purposes, the MOF was digested in hydrochloric acid (2 M) under ultrasonic irridation. This resulted in the precipitation of the linker which was washed with water and dried in vacuum. As determined from the $^1$H-NMR spectrum and the ESI-HR mass spectrum only an incomplete conversion was achieved. **HRMS (ESI+):** 678.1985 (calc. for $[C_{38}H_{32}NO_{11}]^+$: 678.1970).
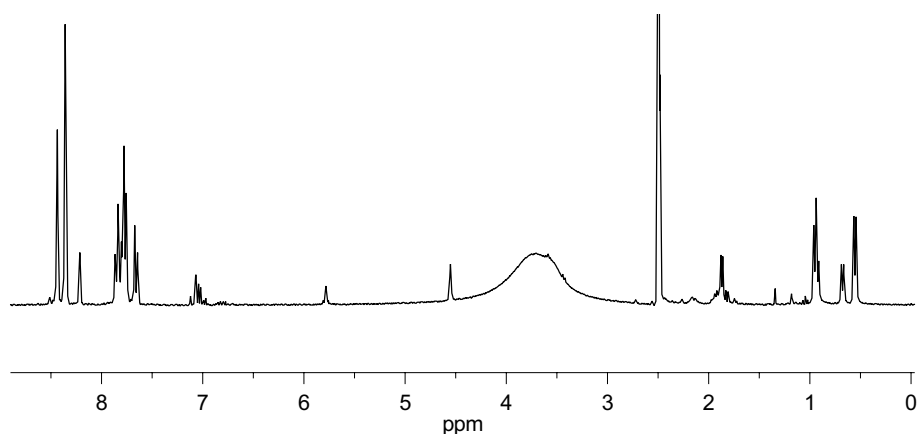


**Figure 4.58** – $^1$H-NMR spectrum of the mixture of linkers that were reisolated after the post-synthetic modification of UHM-25-Val-Evans with crotonic acid.

# Chapter 5

# Bibliography

# Bibliography

[1]  S. R. Batten, N. R. Champness, X.-M. Chen, J. Garcia-Martinez,
     S. Kitagawa, L. Öhrström, M. O'Keeffe, M. Paik Suh, J. Reedijk,
     "Terminology of metal-organic frameworks and coordination polymers
     (IUPAC Recommendations 2013)", *Pure Appl. Chem.* **2013**, *85*, 1715–1724,
     DOI `10.1351/PAC-REC-12-11-20`.

[2]  C. Janiak, J. K. Vieth, "MOFs, MILs and more: concepts, properties and
     applications for porous coordination networks (PCNs)", *New J. Chem.*
     **2010**, *34*, 2366, DOI `10.1039/c0nj00275e`.

[3]  H Li, M. Eddaoudi, M. O'Keeffe, O. M. Yaghi, "Design and synthesis of
     an exceptionally stable and highly porous metal-organic framework",
     *Nature* **1999**, *402*, 276–279, DOI `10.1038/46248`.

[4]  E. L. First, C. a. Floudas, "MOFomics: Computational pore
     characterization of metal-organic frameworks", *Microporous Mesoporous
     Mater.* **2013**, *165*, 32–39, DOI `10.1016/j.micromeso.2012.07.049`.

[5]  M. O'Keeffe, O. M. Yaghi, "Deconstructing the crystal structures of
     metal-organic frameworks and related materials into their underlying
     nets.", *Chem. Rev.* **2012**, *112*, 675–702, DOI `10.1021/cr200205j`.

[6]  W. Lu, Z. Wei, Z.-Y. Gu, T.-F. Liu, J. Park, J. Park, J. Tian, M. Zhang,
     Q. Zhang, T. Gentle Iii, M. Bosch, H.-C. Zhou, "Tuning the structure and
     function of metal-organic frameworks via linker design.", *Chem. Soc.
     Rev.* **2014**, *43*, 5561, DOI `10.1039/c4cs00003j`.

[7]  Y. He, B. Li, M. O'Keeffe, B. Chen, "Multifunctional metal-organic
     frameworks constructed from meta-benzenedicarboxylate units.",
     *Chem. Soc. Rev.* **2014**, *43*, 5618, DOI `10.1039/c4cs00041b`.

[8]  Z.-J. Lin, J. Lü, M. Hong, R. Cao, "Metal-organic frameworks based on
     flexible ligands (FL-MOFs): structures and applications.", *Chem. Soc.
     Rev.* **2014**, *43*, 5867–5895, DOI `10.1039/c3cs60483g`.

[9]   K. J. Gagnon, H. P. Perry, A. Clearfield, "Conventional and unconventional metal-organic frameworks based on phosphonate ligands: MOFs and UMOFs", *Chem. Rev.* **2012**, *112*, 1034–1054, DOI `10.1021/cr2002257`.

[10]  G. K. H. Shimizu, R. Vaidhyanathan, J. M. Taylor, "Phosphonate and sulfonate metal organic frameworks.", *Chem. Soc. Rev.* **2009**, *38*, 1430–1449, DOI `10.1039/b802423p`.

[11]  S. S. Chui, "A Chemically Functionalizable Nanoporous Material $[Cu_3(TMA)_2(H_2O)_3]_n$", *Science* **1999**, *283*, 1148–1150, DOI `10.1126/science.283.5405.1148`.

[12]  F. Hoffmann, personal communication, Universität Hamburg, **2015**.

[13]  O. Delgado-Friedrichs, M. O'Keeffe, "Crystal nets as graphs: Terminology and definitions", *J. Solid State Chem.* **2005**, *178*, 2480–2485, DOI `10.1016/j.jssc.2005.06.011`.

[14]  S. J. Ramsden, V. Robins, S. T. Hyde, "Three-dimensional Euclidean nets from two-dimensional hyperbolic tilings: Kaleidoscopic examples", *Acta Crystallogr. Sect. A: Found. Crystallogr.* **2009**, *65*, 81–108, DOI `10.1107/S0108767308040592`.

[15]  V. A. Blatov, "Topological relations between three-dimensional periodic nets. I. Uninodal nets", *Acta Crystallogr. Sect. A: Found. Crystallogr.* **2007**, *63*, 329–343, DOI `10.1107/S0108767307022088`.

[16]  V. A. Blatov, D. M. Proserpio, "Topological relations between three-periodic nets. II. Binodal nets", *Acta Crystallogr. Sect. A: Found. Crystallogr.* **2009**, *65*, 202–212, DOI `10.1107/S0108767309006096`.

[17]  M. O'Keeffe, M. A. Peskov, S. J. Ramsden, O. M. Yaghi, "The Reticular Chemistry Structure Resource (RCSR) database of, and symbols for, crystal nets", *Acc. Chem. Res.* **2008**, *41*, 1782–1789, DOI `10.1021/ar800124u`.

[18]  N. W. Ockwig, O. Delgado-Friedrichs, M. O'Keeffe, O. M. Yaghi, "Reticular chemistry: occurrence and taxonomy of nets and grammar for the design of frameworks.", *Acc. Chem. Res.* **2005**, *38*, 176–82, DOI `10.1021/ar0200221`.

[19]  O. Delgado-Friedrichs, M. O'Keeffe, O. M. Yaghi, "Taxonomy of periodic nets and the design of materials.", *Phys. Chem. Chem. Phys.* **2007**, *9*, 1035–1043, DOI `10.1039/b615006c`.

[20]  O. M. Yaghi, M. O'Keeffe, N. W. Ockwig, H. K. Chae, M. Eddaoudi, J. Kim, "Reticular synthesis and the design of new materials.", *Nature* **2003**, *423*, 705–14, DOI `10.1038/nature01650`.

[21] A. F. Wells, "The geometrical basis of crystal chemistry. Part 1", *Acta Cryst.* **1954**, *7*, 535–544, DOI `10.1107/S0365110X5400182X`.

[22] A. F. Wells, "The geometrical basis of crystal chemistry. Part 2", *Acta Cryst.* **1954**, *7*, 545–554, DOI `10.1107/S0365110X54001831`.

[23] A. F. Wells, "The geometrical basis of crystal chemistry. XII. Review of structures on three-dimensional 3-connected nets", *Acta Crystallogr. Sect. B: Struct. Sci.* **1976**, *32*, 2619–2626, DOI `10.1107/S0567740876008376`.

[24] J. H. Cavka, S. r. Jakobsen, U. Olsbye, N. Guillou, C. Lamberti, S. Bordiga, K. P. Lillerud, "A new zirconium inorganic building brick forming metal organic frameworks with exceptional stability.", *J. Amer. Chem. Soc.* **2008**, *130*, 13850–1, DOI `10.1021/ja8057953`.

[25] B. Chen, M. Eddaoudi, T. M. Reineke, J. W. Kampf, M. O'Keeffe, O. M. Yaghi, "$Cu_2$(ATC)6$H_2$O: Design of open metal sites in porous metal-organic crystals", *J. Amer. Chem. Soc.* **2000**, *122*, 11559–11560, DOI `10.1021/ja003159k`.

[26] J. Kim, B. Chen, T. M. Reineke, H. Li, M. Eddaoudi, D. B. Moler, M. O'Keeffe, O. M. Yaghi, "Assembly of metal-organic frameworks from large organic and inorganic secondary building units: New examples and simplifying principles for complex structures", *J. Amer. Chem. Soc.* **2001**, *123*, 8239–8247, DOI `10.1021/ja010825o`.

[27] B. Chen, M. Eddaoudi, S. T. Hyde, M. O'Keeffe, O. M. Yaghi, "Interwoven metal-organic framework on a periodic minimal surface with extra-large pores.", *Science* **2001**, *291*, 1021–1023, DOI `10.1126/science.1056598`.

[28] M. Eddaoudi, J. Kim, N. Rosi, D. Vodak, J. Wachter, M. O'Keeffe, O. M. Yaghi, "Systematic design of pore size and functionality in isoreticular MOFs and their application in methane storage", *Science* **2002**, *295*, 469–472, DOI `10.1126/science.1067208`.

[29] H. Furukawa, Y. B. Go, N. Ko, Y. K. Park, F. J. Uribe-Romo, J. Kim, M. O'Keeffe, O. M. Yaghi, "Isoreticular expansion of metal-organic frameworks with triangular and square building units and the lowest calculated density for porous crystals", *Inorg. Chem.* **2011**, *50*, 9147–9152, DOI `10.1021/ic201376t`.

[30] A. Schaate, P. Roy, A. Godt, J. Lippke, F. Waltz, M. Wiebcke, P. Behrens, "Modulated synthesis of Zr-based metal-organic frameworks: From nano to single crystals", *Chem.– Eur. J.* **2011**, *17*, 6643–6651, DOI `10.1002/chem.201003211`.

[31]   A. Schaate, P. Roy, T. Preuß e, S. J. Lohmeier, A. Godt, P. Behrens, "Porous interpenetrated zirconium-organic frameworks (PIZOFs): A chemically versatile family of metal-organic frameworks", *Chem.– Eur. J.* **2011**, *17*, 9320–9325, DOI `10.1002/chem.201101015`.

[32]   D. Frahm, F. Hoffmann, M. Fröba, "Linker extensions in metal-organic frameworks: a way to isoreticular networks or new topologies?", *Cryst. Eng. Comm.* **2013**, DOI `10.1039/C3CE40594J`.

[33]   J. I. Feldblyum, D. Dutta, A. G. Wong-Foy, A. Dailly, J. Imirzian, D. W. Gidley, A. J. Matzger, "Interpenetration, porosity, and high-pressure gas adsorption in $Zn_4O(2,6-naphthalenedicarboxylate)_3$", *Langmuir* **2013**, *29*, 8146–8153, DOI `10.1021/la401323t`.

[34]   R. Grünker, V. Bon, P. Müller, U. Stoeck, S. Krause, U. Mueller, I. Senkovska, S. Kaskel, "A new metal-organic framework with ultra-high surface area.", *Chem. Commun.* **2014**, *50*, 3450–2, DOI `10.1039/c4cc00113c`.

[35]   H. Furukawa, N. Ko, Y. B. Go, N. Aratani, S. B. Choi, E. Choi, A. O. Yazaydin, R. Q. Snurr, M. O'Keeffe, J. Kim, O. M. Yaghi, "Ultrahigh porosity in metal-organic frameworks.", *Science* **2010**, *329*, 424–428, DOI `10.1126/science.1192160`.

[36]   O. K. Farha, I. Eryazici, N. C. Jeong, B. G. Hauser, C. E. Wilmer, A. a. Sarjeant, R. Q. Snurr, S. T. Nguyen, O. Yazaydin, J. T. Hupp, "Metal-Organic Framework Materials with Ultrahigh Surface Areas: Is the Sky the Limit?", *J. Amer. Chem. Soc.* **2012**, DOI `10.1021/ja3055639`.

[37]   Aristotle, *Physics IV*, pp. 6–9.

[38]   J. E. Mondloch, O. Karagiaridi, O. K. Farha, J. T. Hupp, "Activation of metal-organic framework materials", *Cryst. Eng. Comm.* **2013**, *15*, 9258–9264, DOI `10.1039/c3ce41232f`.

[39]   L. Ma, A. Jin, Z. Xie, W. Lin, "Freeze drying significantly increases permanent porosity and hydrogen uptake in 4,4-connected metal-organic frameworks", *Angew. Chem. Int. Ed.* **2009**, *48*, DOI `10.1002/anie.200904983`.

[40]   Y. P. He, Y. X. Tan, J. Zhang, "Comparative study of activation methods on tuning gas sorption properties of a metal-organic framework with nanosized ligands", *Inorg. Chem.* **2012**, *51*, 11232–11234, DOI `10.1021/ic3017529`.

[41]  A. P. Nelson, O. K. Farha, K. L. Mulfort, J. T. Hupp, "Supercritical processing as a route to high internal surface areas and permanent microporosity in metal-organic framework materials", *J. Amer. Chem. Soc.* **2009**, *131*, 458–460, DOI `10.1021/ja808853q`.

[42]  A. I. Cooper, "Porous materials and supercritical fluids", *Adv. Mater.* **2003**, *15*, 1049–1059, DOI `10.1002/adma.200300380`.

[43]  Y. Peng, V. Krungleviciute, I. Eryazici, J. T. Hupp, O. K. Farha, T. Yildirim, "Methane storage in metal-organic frameworks: Current records, surprise findings, and challenges", *J. Amer. Chem. Soc.* **2013**, *135*, 11887–11894, DOI `10.1021/ja4045289`.

[44]  M. P. Suh, H. J. Park, T. K. Prasad, D. W. Lim, "Hydrogen storage in metal-organic frameworks", *Chem. Rev.* **2012**, *112*, 782–835, DOI `10.1021/cr200274s`.

[45]  Y. Yan, S. Yang, A. J. Blake, M. Schröder, "Studies on metal-organic frameworks of Cu(II) with isophthalate linkers for hydrogen storage", *Acc. Chem. Res.* **2014**, *47*, 296–307, DOI `10.1021/ar400049h`.

[46]  K. Sumida, D. L. Rogow, J. A. Mason, T. M. McDonald, E. D. Bloch, Z. R. Herm, T. H. Bae, J. R. Long, "Carbon dioxide capture in metal-organic frameworks", *Chem. Rev.* **2012**, *112*, 724–781, DOI `10.1021/cr2003272`.

[47]  W. L. Queen, M. R. Hudson, E. D. Bloch, J. A. Mason, M. I. Gonzalez, J. S. Lee, D. Gygi, J. D. Howe, K. Lee, T. A. Darwish, M. James, V. K. Peterson, S. J. Teat, B. Smit, J. B. Neaton, J. R. Long, C. M. Brown, "Comprehensive study of carbon dioxide adsorption in the metal-organic frameworks M 2 (dobdc) (M = Mg, Mn, Fe, Co, Ni, Cu, Zn)", *Chem. Sci.* **2014**, *5*, 4569–4581, DOI `10.1039/C4SC02064B`.

[48]  P. Horcajada, T. Chalati, C. Serre, B. Gillet, C. Sebrie, T. Baati, J. F. Eubank, D. Heurtaux, P. Clayette, C. Kreuz, J.-S. Chang, Y. K. Hwang, V. Marsaud, P.-N. Bories, L. Cynober, S. Gil, G. Férey, P. Couvreur, R. Gref, "Porous metal-organic-framework nanoscale carriers as a potential platform for drug delivery and imaging.", *Nature materials* **2010**, *9*, 172–178, DOI `10.1038/nmat2608`.

[49]  R. C. Huxford, J. Della Rocca, W. Lin, "Metal-organic frameworks as potential drug carriers", *Curr. Op. Chem. Biol.* **2010**, *14*, 262–268, DOI `10.1016/j.cbpa.2009.12.012`.

[50]  K. Deng, Z. Hou, X. Li, C. Li, Y. Zhang, X. Deng, Z. Cheng, J. Lin, "Aptamer-Mediated Up-conversion Core/MOF Shell Nanocomposites for Targeted Drug Delivery and Cell Imaging", *Sci. Rep.* **2015**, *5*, 7851, DOI `10.1038/srep07851`.

[51]  Q. Hu, J. Yu, M. Liu, A. Liu, Z. Dou, Y. Yang, "A low cytotoxic cationic metal-organic framework carrier for controllable drug release", *J. Med. Chem.* **2014**, *57*, 5679–5685, DOI `10.1021/jm5004107`.

[52]  C. Rösler, R. A. Fischer, "Metal-organic frameworks as hosts for nanoparticles", *Cryst. Eng. Comm.* **2015**, *17*, 199–217, DOI `10.1039/C4CE01251H`.

[53]  H. Li, Z. Zhu, F. Zhang, S. Xie, H. Li, P. Li, X. Zhou, "Palladium nanoparticles confined in the cages of MIL-101: An efficient catalyst for the one-pot indole synthesis in water", *ACS Catalysis* **2011**, *1*, 1604–1612, DOI `10.1021/cs200351p`.

[54]  Y. Huang, Z. Lin, R. Cao, "Palladium nanoparticles encapsulated in a metal-organic framework as efficient heterogeneous catalysts for direct C2 arylation of indoles", *Chem.– Eur. J.* **2011**, *17*, 12706–12712, DOI `10.1002/chem.201101705`.

[55]  H. Deng, S. Grunder, K. E. Cordova, C. Valente, H. Furukawa, M. Hmadeh, F. Gándara, A. C. Whalley, Z. Liu, S. Asahina, H. Kazumori, M. O'Keeffe, O. Terasaki, J. F. Stoddart, O. M. Yaghi, "Large-pore apertures in a series of metal-organic frameworks.", *Science* **2012**, *336*, 1018–23, DOI `10.1126/science.1220131`.

[56]  D. P. Barondeau, C. J. Kassmann, J. A. Tainer, E. D. Getzoff, "Structural chemistry of a green fluorescent protein Zn biosensor", *J. Amer. Chem. Soc.* **2002**, *124*, 3522–3524, DOI `10.1021/ja0176954`.

[57]  H.-S. Shin, "Metabolism of Selegiline in Humans Identification, Excretion, and Stereochemistry of Urine Metabolites", *Drug Metab. Dispos.* **1997**, *25*, 657–662.

[58]  E. K. Curtis, "Meth mouth: A review of methamphetamine abuse and its oral manifestations", *Gen. Dentistry* **2006**, *54*, 125–129.

[59]  B. D. Homer, T. M. Solomon, R. W. Moeller, A. Mascia, L. DeRaleau, P. N. Halkitis, "Methamphetamine abuse and impairment of social functioning: a review of the underlying neurophysiological causes and behavioral implications.", *Psych. Bull.* **2008**, *134*, 301–310, DOI `10.1037/0033-2909.134.2.301`.

[60]  J. C. Scott, S. P. Woods, G. E. Matt, R. A. Meyer, R. K. Heaton, J. H. Atkinson, I. Grant, "Neurocognitive effects of methamphetamine: A critical review and meta-analysis", *Neuropsych. Rev.* **2007**, *17*, 275–297, DOI `10.1007/s11065-007-9031-0`.

[61]  E. J. Ariens, "Stereochemistry, a Basis for sophisticated Nonsense in Pharmacokinetics and Clinical Pharmacology", *Eur. J. Clin. Pharmacol.* **1984**, *24*, 663–668.

[62] S. Branch, A. Hutt in *Drug Stereochemistry - Analytical Methods and Pharmacology*, (Eds.: K. Józwiak, W. Lough, I. Wainer), informa healthcare, London, **2012**, pp. 240–273, DOI `10.3109/9781420092394.013`.

[63] L. Zhang, L. Cui, S. Luo, J. Cheng in *Green Techniques for Organic Synthesis and Medicinal Chemistry*, (Eds.: W. Zhang, B. W. Cue), John Wiley & Sons, Ltd, Chichester, **2012**, pp. 99–135, DOI `10.1002/9780470711828`.

[64] M. Heitbaum, F. Glorius, I. Escher, "Asymmetric heterogeneous catalysis", *Angew. Chem. Int. Ed.* **2006**, *45*, 4732–4762, DOI `10.1002/anie.200504212`.

[65] H. U. Blaser, "The chiral pool as a source of enantioselective catalysts and auxiliaries", *Chem. Rev.* **1992**, *92*, 935–952, DOI `10.1021/cr00013a009`.

[66] P. I. Dalko, L. Moisan, "Enantioselective Organocatalysis", *Angew. Chem. Int. Ed.* **2001**, *40*, 3726–3748, DOI `10.1002/1521-3773(20011015)40:20<3726::aid-anie3726>3.0.co;2-d`.

[67] P. I. Dalko, L. Moisan, "In the golden age of organocatalysis", *Angew. Chem. Int. Ed.* **2004**, *43*, 5138–5175, DOI `10.1002/anie.200400650`.

[68] A. Berkessel, H. Gröger, *Asymmetric Organocatalysis*, 1st ed., Wiley-VCH, Weinheim, **2005**, pp. 1–7.

[69] B. List, "Introduction: Organocatalysis", *Chem. Rev.* **2007**, *107*, 5413–5415, DOI `10.1021/cr078412e`.

[70] C. Grondal, C. Grondal, M. R. M. Huttl, M. R. M. Huttl, "Asymmetric Organocatalytic Domino Reactions", *Angew. Chem. Int. Ed.* **2007**, *46*, 1570–1581, DOI `10.1002/anie.200603129`.

[71] S. Bertelsen, K. A. Jø rgensen, "Organocatalysis–after the gold rush.", *Chem. Soc. Rev.* **2009**, *38*, 2178–2189, DOI `10.1039/b903816g`.

[72] C.-J. Li, P. T. Anastas, "Green Chemistry: present and future", *Chem. Soc. Rev.* **2012**, *41*, 1413, DOI `10.1039/c1cs90064a`.

[73] D. W. C. MacMillan, "The advent and development of organocatalysis.", *Nature* **2008**, *455*, 304–308, DOI `10.1038/nature07367`.

[74] M. J. Gaunt, C. Johansson, A. McNally, N. T. Vo, "Enantioselective organocatalysis", *Drug Disc. Tod.* **2007**, *12*, 8–27, DOI `10.1016/j.drudis.2006.11.004`.

[75] S. Mukherjee, J. W. Yang, S. Hoffmann, B. List, "Asymmetric enamine catalysis", *Chem. Rev.* **2007**, *107*, 5471–5569, DOI `10.1021/cr0684016`.

[76] U. Eder, G. Sauer, R. Wiechert, "New Type of Asymmetric Cyclization to Optically Active Steroid CD Partial Structures", *Angew. Chem. Int. Ed.* **1971**, *10*, 496–497, DOI `10.1002/anie.197104961`.

[77] Z. G. Hajos, D. R. Parrish, "Asymmetric synthesis of bicyclic intermediates of natural product chemistry", *J. Org. Chem.* **1974**, *39*, 1615–1621, DOI `10.1021/jo00925a003`.

[78] F. R. Clemente, K. N. Houk, "Computational evidence for the enamine mechanism of intramolecular aldol reactions catalyzed by proline", *Angew. Chem. Int. Ed.* **2004**, *43*, 5766–5768, DOI `10.1002/anie.200460916`.

[79] G. Lelais, D. MacMillan, "Modern Strategies in Organic Catalysis: The Advent and Development of Iminium Activation", *Aldrichim. Acta* **2006**, *39*, 79–87.

[80] M. Marigo, T. C. Wabnitz, D. Fielenbach, K. A. Jø rgensen, "Enantioselective organocatalyzed $\alpha$ sulfenylation of aldehydes", *Angew. Chem. Int. Ed.* **2005**, *44*, 794–797, DOI `10.1002/anie.200462101`.

[81] Y. Hayashi, H. Gotoh, T. Hayashi, M. Shoji, "Diphenylprolinol silyl ethers as efficient organocatalysts for the asymmetric Michael reaction of aldehydes and nitroalkenes", *Angew. Chem. Int. Ed.* **2005**, *44*, 4212–4215, DOI `10.1002/anie.200500599`.

[82] J. Franzén, M. Marigo, D. Fielenbach, T. C. Wabnitz, A. Kjæ rsgaard, K. A. Jø rgensen, "A general organocatalyst for direct $\alpha$-functionalization of aldehydes: Stereoselective C-C, C-N, C-F, C-Br, and C-S bond-forming reactions. Scope and mechanistic insights", *J. Amer. Chem. Soc.* **2005**, *127*, 18296–18304, DOI `10.1021/ja056120u`.

[83] A. Mielgo, C. Palomo, "$\alpha$,$\alpha$-diarylprolinol ethers: New tools for functionalization of carbonyl compounds", *Chem.– Asian J.* **2008**, *3*, 922–948, DOI `10.1002/asia.200700417`.

[84] K. L. Jensen, G. Dickmeiss, H. Jiang, L. Albrecht, K. A. Jø rgensen, "The diarylprolinol silyl ether system: a general organocatalyst.", *Acc. Chem. Res.* **2012**, *45*, 248–264, DOI `10.1021/ar200149w`.

[85] M. B. Schmid, K. Zeitler, R. M. Gschwind, "Formation and stability of prolinol and prolinol ether enamines by NMR: Delicate selectivity and reactivity balances and parasitic equilibria", *J. Amer. Chem. Soc.* **2011**, *133*, 7065–7074, DOI `10.1021/ja111544b`.

[86] A. Lattanzi, "$\alpha$,$\alpha$-diarylprolinols: bifunctional organocatalysts for asymmetric synthesis.", *Chem. Commun.* **2009**, 1452–1463, DOI `10.1039/b900098d`.

[87]  S. Meninno, A. Lattanzi, "Asymmetric organocatalysis mediated by α,α-l-diaryl prolinols: recent advances.", *Chem. Commun.* **2013**, *49*, 3821–32, DOI `10.1039/c3cc36928e`.

[88]  K. Ahrendt, C. J. Borths, D. W. C. Macmillan, "New strategies for organic catalysis: the first highly enantioselective organocatalytic Diels-Alder reaction", *J. Amer. Chem. Soc.* **2000**, *122*, 4243–4244, DOI `10.1021/ja000092s`.

[89]  M. T. H. Fonseca, B. List, "Catalytic asymmetric intramolecular Michael reaction of aldehydes", *Angew. Chem. Int. Ed.* **2004**, *43*, 3958–3960, DOI `10.1002/anie.200460578`.

[90]  N. A. Para, D. W. C. MacMillan, "New strategies in organic catalysis: The first enantioselective organocatalytic Friedel-Crafts alkylation [18]", *J. Amer. Chem. Soc.* **2001**, *123*, 4370–4371, DOI `10.1021/ja015717g`.

[91]  J. M. McBride, R. L. Carter, "Spontaneous resolution by stirred crystallization", *Angew. Chem.* **1991**, *103*, 298–300, DOI `10.1002/anie.199102931`.

[92]  R. E. Morris, X. Bu, "Induction of chiral porous solids containing only achiral building blocks.", *Nature Chem.* **2010**, *2*, 353–361, DOI `10.1038/nchem.628`.

[93]  D Bradshaw, J. B. Claridge, E. J. Cussen, T. J. Prior, M. J. Rosseinsky, "Design, chirality, and flexibility in nanoporous molecule-based materials.", *Acc. Chem. Res.* **2005**, *38*, 273–82, DOI `10.1021/ar0401606`.

[94]  T. Ezuhara, K. Endo, Y. Aoyama, "Helical Coordination Polymers from Achiral Components in Crystals. Homochiral Crystallization, Homochiral Helix Winding in the Solid State, and Chirality Control by Seeding", *J. Amer. Chem. Soc.* **1999**, *121*, 3279–3283, DOI `10.1021/ja9819918`.

[95]  D. L. Murphy, M. R. Malachowski, C. F. Campana, S. M. Cohen, "A chiral, heterometallic metal-organic framework derived from a tris(chelate) coordination complex.", *Chem. Commun.* **2005**, 5506–5508, DOI `10.1039/b510915a`.

[96]  X.-L. Tong, T.-L. Hu, J.-P. Zhao, Y.-K. Wang, H. Zhang, X.-H. Bu, "Chiral magnetic metal-organic frameworks of Mn(II) with achiral tetrazolate-based ligands by spontaneous resolution.", *Chem. Commun.* **2010**, *46*, 8543–5, DOI `10.1039/c0cc03111a`.

[97]  J.-T. Yu, Y.-Y. Shi, J. Sun, J. Lin, Z.-T. Huang, Q.-Y. Zheng, "Spontaneous chiral resolution directed by symmetry restriction and $\pi$-$\pi$ interaction.", *Sci. Rep.* **2013**, *3*, 2947, DOI `10.1038/srep02947`.

[98]    I. Mihalcea, N. Zill, V. Mereacre, C. E. Anson, A. K. Powell, "Spontaneous Resolution in Homochiral Helical [Ln(nic)$_2$(Hnic)(NO$_3$)] Coordination Polymers Constructed from a Rigid Non-chiral Organic Ligand", *Cryst. Growth Des.* **2014**, *14*, 4729–4734, DOI `10.1021/cg500827u`.

[99]    H.-X. Mei, T. Zhang, D.-F. Wang, R.-B. Huang, L.-S. Zheng, "A Zn-oxalate helix linked by a water helix: spontaneous chiral resolution of a Zn helical coordination polymer", *New J. Chem.* **2015**, *39*, 2075–2080, DOI `10.1039/C4NJ02017K`.

[100]   W.-T. Liu, Y.-C. Ou, Z.-j. Lin, M.-L. Tong, "Spontaneous resolution of four-coordinate Zn(ii) complexes in the formation of three-dimensional metalâĂŞorganic frameworks", *Cryst. Eng. Comm.* **2010**, *12*, 3487, DOI `10.1039/c0ce00206b`.

[101]   S. Zang, Y. Su, Y. Li, H. Zhu, Q. Meng, "One dense and two open chiral metal-organic frameworks: crystal structures and physical properties.", *Inorg. Chem.* **2006**, *45*, 2972–8, DOI `10.1021/ic0520418`.

[102]   H. Dong, H. Hu, Y. Liu, J. Zhong, G. Zhang, F. Zhao, X. Sun, Y. Li, Z. Kang, "Obtaining chiral metal-organic frameworks via a prochirality synthetic strategy with achiral ligands step-by-step", *Inorg. Chem.* **2014**, *53*, 3434–3440, DOI `10.1021/ic402867x`.

[103]   J. K. Clegg, S. S. Iremonger, M. J. Hayter, P. D. Southon, R. A. B. Macquart, M. B. Duriska, P. Jensen, P. Turner, K. a. Jolliffe, C. J. Kepert, G. V. Meehan, L. F. Lindoy, "Hierarchical Self-Assembly of a Chiral Metal-Organic Framework Displaying Pronounced Porosity", *Angew. Chem.* **2010**, *122*, 1093–1096, DOI `10.1002/ange.200905497`.

[104]   R. Feng, F.-L. Jiang, L. Chen, C.-F. Yan, M.-Y. Wu, M.-C. Hong, "A luminescent homochiral 3D Cd(II) framework with a threefold interpenetrating uniform net 8(6).", *Chem. Commun.* **2009**, 5296–8, DOI `10.1039/b908792c`.

[105]   D. Bradshaw, T. J. Prior, E. J. Cussen, J. B. Claridge, M. J. Rosseinsky, "Permanent microporosity and enantioselective sorption in a chiral open framework.", *J. Amer. Chem. Soc.* **2004**, *126*, 6106–14, DOI `10.1021/ja0316420`.

[106]   X.-R. Hao, X.-L. Wang, C. Qin, Z.-M. Su, E.-B. Wang, Y.-Q. Lan, K.-Z. Shao, "A 3D chiral nanoporous coordination framework consisting of homochiral nanotubes assembled from octuple helices.", *Chem. Commun.* **2007**, 4620–4622, DOI `10.1039/b711405b`.

[107] K. K. Bisht, E. Suresh, "Spontaneous resolution to absolute chiral induction: Pseudo-kagomé type homochiral Zn(II)/Co(II) coordination polymers with achiral precursors", *J. Amer. Chem. Soc.* **2013**, *135*, 15690–15693, DOI `10.1021/ja4075369`.

[108] X. Zhao, H. He, F. Dai, D. Sun, Y. Ke, "Supramolecular isomerism in honeycomb metal-organic frameworks driven by CH-$\pi$ interactions: homochiral crystallization from an achiral ligand through chiral inducement.", *Inorg. Chem.* **2010**, *49*, 8650–2, DOI `10.1021/ic100603g`.

[109] X. Jing, C. He, D. Dong, L. Yang, C. Duan, "Homochiral crystallization of metal-organic silver frameworks: Asymmetric [3+2] cycloaddition of an azomethine ylide", *Angew. Chem. Int. Ed.* **2012**, *51*, 10127–10131, DOI `10.1002/anie.201204530`.

[110] D. Dang, P. Wu, C. He, Z. Xie, C. Duan, "Homochiral metal-organic frameworks for heterogeneous asymmetric catalysis.", *J. Amer. Chem. Soc.* **2010**, *132*, 14321–3, DOI `10.1021/ja101208s`.

[111] M. J. Ingleson, J. Bacsa, M. J. Rosseinsky, "Homochiral H-bonded proline based metal organic frameworks.", *Chem. Commun.* **2007**, 3036–8, DOI `10.1039/b706557d`.

[112] C. Livage, N. Guillou, P. Rabu, P. Pattison, J. Marrot, G. Férey, "Bulk homochirality of a 3-D inorganic framework: ligand control of inorganic network chirality.", *Chem. Commun.* **2009**, 4551–3, DOI `10.1039/b904622d`.

[113] M. J. Ingleson, J. P. Barrio, J. Bacsa, C. Dickinson, H. Park, M. J. Rosseinsky, "Generation of a solid Brønsted acid site in a chiral framework.", *Chem. Commun.* **2008**, 1287–9, DOI `10.1039/b718443c`.

[114] T. Kaczorowski, I. Justyniak, T. Lipinska, J. Lipkowski, J. Lewinski, "Metal complexes of cinchonine as chiral building blocks: a strategy for the construction of nanotubular architectures and helical coordination polymers.", *J. Amer. Chem. Soc.* **2009**, *131*, 5393–5, DOI `10.1021/ja8098867`.

[115] H.-Q. Hao, W.-T. Liu, W. Tan, Z. Lin, M.-L. Tong, "Enantiopure and Racemic Sandwich-like Networks with Dehydration, Readsorption, and Selective Guest-Exchange Phase Transformations", *Cryst. Growth Des.* **2009**, *9*, 457–465, DOI `10.1021/cg800710q`.

[116] J. A. Rood, B. C. Noll, K. W. Henderson, "Homochiral frameworks derived from magnesium, zinc and copper salts of L-tartaric acid", *J. Solid State Chem.* **2010**, *183*, 270–276, DOI `10.1016/j.jssc.2009.11.003`.

[117]  N. L. Strutt, H. Zhang, J. F. Stoddart, "Enantiopure pillar[5]arene active domains within a homochiral metal-organic framework.", *Chem. Commun.* **2014**, *50*, 7455–8, DOI `10.1039/c4cc02559h`.

[118]  D. N. Dybtsev, A. L. Nuzhdin, H. Chun, K. P. Bryliakov, E. P. Talsi, V. P. Fedin, K. Kim, "A homochiral metal-organic material with permanent porosity, enantioselective sorption properties, and catalytic activity.", *Angew. Chem. - Int. Ed.* **2006**, *45*, 916–20, DOI `10.1002/anie.200503023`.

[119]  D. N. Dybtsev, M. P. Yutkin, D. G. Samsonenko, V. P. Fedin, A. L. Nuzhdin, A. a. Bezrukov, K. P. Bryliakov, E. P. Talsi, R. V. Belosludov, H. Mizuseki, Y. Kawazoe, O. S. Subbotin, V. R. Belosludov, "Modular, Homochiral, Porous Coordination Polymers: Rational Design, Enantioselective Guest Exchange Sorption and ab initio Calculations of Host-Guest Interactions.", *Chemistry* **2010**, 10348 –10356, DOI `10.1002/chem.201000522`.

[120]  G. Férey, C. Mellot-Draznieks, C. Serre, F. Millange, J. Dutour, S. Surblé, I. Margiolaki, "A chromium terephthalate-based solid with unusually large pore volumes and surface area.", *Science* **2005**, *309*, 2040–2042, DOI `10.1126/science.1116275`.

[121]  M. Banerjee, S. Das, M. Yoon, H. J. Choi, M. H. Hyun, S. M. Park, G. Seo, K. Kim, J. C. Hee, H. H. Myung, M. P. Se, G. Seo, O. Kim, "Postsynthetic modification switches an achiral framework to catalytically active homochiral metal-organic porous materials.", *J. Amer. Chem. Soc.* **2009**, *131*, 7524–5, DOI `10.1021/ja901440g`.

[122]  Z. Wang, S. M. Cohen, "Postsynthetic modification of metal-organic frameworks", *Chem. Soc. Rev.* **2009**, *38*, 1315, DOI `10.1039/b802258p`.

[123]  P. Wu, C. He, J. Wang, X. Peng, X. Li, Y. An, C. Duan, "Photoactive chiral metal-organic frameworks for light-driven asymmetric $\alpha$-alkylation of aldehydes", *J. Amer. Chem. Soc.* **2012**, *134*, 14991–14999, DOI `10.1021/ja305367j`.

[124]  A. L. W. Demuynck, M. G. Goesten, E. V. Ramos-Fernandez, M. Dusselier, J. Vanderleyden, F. Kapteijn, J. Gascon, B. F. Sels, "Induced Chirality in a Metal-Organic Framework by Postsynthetic Modification for Highly Selective Asymmetric Aldol Reactions", *Chem. Cat. Chem.* **2014**, *6*, 2211–2214, DOI `10.1002/cctc.201402082`.

[125]  J. Seo, D Whang, H Lee, S. Jun, J Oh, Y. Jeon, K Kim, "A homochiral metal-organic porous material for enantioselective separation and catalysis", *Nature* **2000**, *404*, 982–6, DOI `10.1038/35010088`.

[126] C. Valente, E. Choi, M. E. Belowich, C. J. Doonan, Q. Li, T. B. Gasa, Y. Y. Botros, O. M. Yaghi, J. F. Stoddart, "Metal-organic frameworks with designed chiral recognition sites.", *Chem. Commun.* **2010**, DOI `10.1039/c0cc00997k`.

[127] D. J. Lun, G. I. N. Waterhouse, S. G. Telfer, "A general thermolabile protecting group strategy for organocatalytic metal-organic frameworks", *J. Amer. Chem. Soc.* **2011**, *133*, 5806–5809, DOI `10.1021/ja202223d`.

[128] T. M. Reineke, M. Eddaoudi, D. Moler, M. O'Keeffe, O. M. Yaghi, "Large free volume in maximally interpenetrating networks: The role of secondary building units exemplified by $Tb_2(ADB)_3[(CH_3)_2SO]_4 \cdot 16\,[(CH_3)_2SO]$", *J. Amer. Chem. Soc.* **2000**, *122*, 4843–4844, DOI `10.1021/ja000363z`.

[129] R. K. Deshpande, J. L. Minnaar, S. G. Telfer, "Thermolabile groups in metal-organic frameworks: suppression of network interpenetration, post-synthetic cavity expansion, and protection of reactive functional groups.", *Angew. Chem. - Int. Ed.* **2010**, *49*, 4598–602, DOI `10.1002/anie.200905960`.

[130] C. Kutzscher, H. C. Hoffmann, S. Krause, U. Stoeck, I. Senkovska, E. Brunner, S. Kaskel, "Proline Functionalization of the Mesoporous MetalâĹŠOrganic Framework DUT-32", *Inorg. Chem.* **2015**, *54*, 1003–1009, DOI `10.1021/ic502380q`.

[131] K. Gedrich, M. Heitbaum, A. Notzon, I. Senkovska, R. Fröhlich, J. Getzschmann, U. Mueller, F. Glorius, S. Kaskel, "A family of chiral metal-organic frameworks.", *Chemistry* **2011**, *17*, 2099–106, DOI `10.1002/chem.201002568`.

[132] O. R. Evans, H. L. Ngo, W. Lin, "Chiral Porous Solids Based on Lamellar Lanthanide Phosphonates", *J. Amer. Chem. Soc.* **2001**, *123*, 10395–10396, DOI `10.1021/ja0163772`.

[133] O. R. Evans, D. R. Manke, W. Lin, "Homochiral Metal-Organic Frameworks Based on Transition Metal Bisphosphonates", *Chem. Mater.* **2002**, *14*, 3866–3874, DOI `10.1021/cm0202714`.

[134] C. D. Wu, A. Hu, L. Zhang, W. Lin, "A homochiral porous metal-organic framework for highly enantioselective heterogeneous asymmetric catalysis", *J. Amer. Chem. Soc.* **2005**, *127*, 8940–8941, DOI `10.1021/ja052431t`.

[135]  C.-D. Wu, W. Lin, "Heterogeneous asymmetric catalysis with homochiral metal-organic frameworks: network-structure-dependent catalytic activity.", *Angew. Chem. Int. Ed.* **2007**, *46*, 1075–8, DOI `10.1002/anie.200602099`.

[136]  C.-D. Wu, L. Ma, W. Lin, "Hierarchically ordered homochiral metal-organic frameworks built from exceptionally large rectangles and squares.", *Inorg. Chem.* **2008**, *47*, 11446–8, DOI `10.1021/ic800514f`.

[137]  J. M. Falkowski, T. Sawano, T. Zhang, G. Tsun, Y. Chen, J. V. Lockard, W. Lin, "Privileged phosphine-based metal-organic frameworks for broad-scope asymmetric catalysis", *J. Amer. Chem. Soc.* **2014**, *136*, 5213–5216, DOI `10.1021/ja500090y`.

[138]  Y. Peng, T. Gong, K. Zhang, X. Lin, Y. Liu, J. Jiang, Y. Cui, "Engineering chiral porous metal-organic frameworks for enantioselective adsorption and separation.", *Nature communications* **2014**, *5*, 4406, DOI `10.1038/ncomms5406`.

[139]  K. Tanaka, S. Oda, M. Shiro, "A novel chiral porous metal-organic framework: asymmetric ring opening reaction of epoxide with amine in the chiral open space.", *Chem. Commun.* **2008**, 820–822, DOI `10.1039/b714083e`.

[140]  K. Tanaka, D. Yanamoto, K. Yoshimura, T. Anami, Z. Urbanczyk-Lipkowska, "Interpenetrated and non-interpenetrated homochiral metal-organic frameworks based on (R)-2,2'-dihydroxy-1,1'-binaphthyl-5,5'-dibenzoic acid", *Cryst. Eng. Comm.* **2015**, *17*, 1291–1295, DOI `10.1039/C4CE02210F`.

[141]  K. S. Jeong, Y. B. Go, S. M. Shin, S. J. Lee, J. Kim, O. M. Yaghi, N. Jeong, "Asymmetric catalytic reactions by NbO-type chiral metal-organic frameworks", *Chem. Sci.* **2011**, *2*, 877, DOI `10.1039/c0sc00582g`.

[142]  K. Gedrich, I. Senkovska, I. A. Baburin, U. Mueller, O. Trapp, S. Kaskel, "New Chiral and Flexible Metal-Organic Framework with a Bifunctional Spiro Linker and Zn(4)O-Nodes.", *Inorg. Chem.* **2010**, 4293–4297, DOI `10.1021/ic9022085`.

[143]  X. Ouyang, Z. Chen, X. Liu, Y. Yang, M. Deng, L. Weng, Y. Zhou, Y. Jia, "One-dimensional (1D) helical and 2D homochiral metal-organic frameworks built from a new chiral octahydrobinaphthalene-derived dicarboxylic acid", *Inorg. Chem. Commun.* **2008**, *11*, 948–950, DOI `10.1016/j.inoche.2008.04.023`.

[144] X. Xi, Y. Fang, T. Dong, Y. Cui, "Bottom-Up Assembly from a Helicate to Homochiral Micro- and Mesoporous Metal-Organic Frameworks", *Angew. Chem. Int. Ed.* **2010**, *50*, 1154–1158, DOI `10.1002/anie.201004885`.

[145] L. Ma, J. M. Falkowski, C. Abney, W. Lin, "A series of isoreticular chiral metal-organic frameworks as a tunable platform for asymmetric catalysis.", *Nature Chem.* **2010**, *2*, 838–46, DOI `10.1038/nchem.738`.

[146] J. M. Brunel, P. Ce, "Update 1 of : BINOL : A Versatile Chiral Reagent", *Chem. Rev.* **2007**, *107*, DOI `10.1021/cr078004a`.

[147] S.-H. Cho, B. Ma, S. T. Nguyen, J. T. Hupp, T. E. Albrecht-Schmitt, "A metal-organic framework material that functions as an enantioselective catalyst for olefin epoxidation.", *Chem. Commun.* **2006**, 2563–5, DOI `10.1039/b600408c`.

[148] F. Song, C. Wang, W. Lin, "A chiral metal-organic framework for sequential asymmetric catalysis.", *Chem. Commun.* **2011**, *47*, 8256–8258, DOI `10.1039/c1cc12701b`.

[149] C. Zhu, G. Yuan, X. Chen, Z. Yang, Y. Cui, "Chiral Nanoporous Metal-Metallosalen Frameworks for Hydrolytic Kinetic Resolution of Epoxides.", *J. Amer. Chem. Soc.* **2012**, DOI `10.1021/ja302340b`.

[150] Y. Cui, W. Xuan, C. Ye, M. Zhang, Z. Chen, "A Chiral Porous Metallosalan-Organic Framework Containing Titanium-Oxo Clusters for Enantioselective Catalytic Sulfoxidation", *Chem. Sci.* **2013**, *4*, 3154–3159, DOI `10.1039/c3sc50487e`.

[151] J. Zhang, Y.-G. Yao, X. Bu, "Comparative Study of Homochiral and Racemic Chiral Metal-Organic Frameworks Built from Camphoric Acid", *Chem. Mater.* **2007**, *19*, 5083–5089, DOI `10.1021/cm071689a`.

[152] X.-L. Yang, C.-D. Wu, "Recent advances on porous homochiral coordination polymers containing amino acid synthons", *Cryst. Eng. Comm.* **2014**, *16*, 4907, DOI `10.1039/c3ce42508h`.

[153] E. V. Anokhina, A. J. Jacobson, "[Ni$_2$O(L$-$Asp)(H$_2$O)$_2$)] · 4 H$_2$O: a homochiral 1D helical chain hybrid compound with extended Ni-O-Ni bonding.", *J. Amer. Chem. Soc.* **2004**, *126*, 3044–5, DOI `10.1021/ja031836f`.

[154] R. Vaidhyanathan, D. Bradshaw, J.-N. Rebilly, J. P. Barrio, J. a. Gould, N. G. Berry, M. J. Rosseinsky, "A family of nanoporous materials based on an amino acid backbone.", *Angew. Chem. - Int. Ed.* **2006**, *45*, 6495–9, DOI `10.1002/anie.200602242`.

[155]    J. Rood, B. Noll, K. Henderson, "A homochiral metal-organic
         framework with amino-functionalized pores", *Main Group Chem.* **2009**,
         *8*, 237–250, DOI `10.1080/10241220903125989`.

[156]    X.-Q. Liang, D.-P. Li, X.-H. Zhou, Y. Sui, Y.-Z. Li, J.-L. Zuo, X.-Z. You,
         "Metal-Organic Coordination Polymers Generated from Chiral
         Camphoric Acid and Flexible Ligands with Different Spacer Lengths:
         Syntheses, Structures, and Properties", *Cryst. Growth Des.* **2009**, *9*,
         4872–4883, DOI `10.1021/cg900676x`.

[157]    X. Zhao, M. Wong, C. Mao, T. X. Trieu, J. Zhang, P. Feng, X. Bu,
         "Size-Selective Crystallization of Homochiral Camphorate
         Metal-Organic Frameworks for Lanthanide Separation.", *J. Amer. Chem.
         Soc.* **2014**, DOI `10.1021/ja5067306`.

[158]    J. Perez Barrio, J.-N. Rebilly, B. Carter, D. Bradshaw, J. Bacsa,
         A. Y. Ganin, H. Park, A. Trewin, R. Vaidhyanathan, A. I. Cooper,
         J. E. Warren, M. J. Rosseinsky, "Control of porosity geometry in amino
         acid derived nanoporous materials.", *Chem. Eur. J.* **2008**, *14*, 4521–32,
         DOI `10.1002/chem.200701556`.

[159]    C. Martí-Gastaldo, J. E. Warren, K. C. Stylianou, N. L. O. Flack,
         M. J. Rosseinsky, "Enhanced Stability in Rigid Peptide-Based Porous
         Materials", *Angew. Chem. Int. Ed.* **2012**, n/a–n/a, DOI
         `10.1002/anie.201203929`.

[160]    J Rabone, Y.-F. Yue, S. Y. Chong, K. C. Stylianou, J Bacsa, D Bradshaw,
         G. R. Darling, N. G. Berry, Y. Z. Khimyak, A. Y. Ganin, P Wiper,
         J. B. Claridge, M. J. Rosseinsky, "An adaptable peptide-based porous
         material.", *Science* **2010**, *329*, 1053–7, DOI
         `10.1126/science.1190672`.

[161]    B. Sreenivasulu, J. J. Vittal, "Helix inside a helix: Encapsulation of
         hydrogen-bonded water molecules in a staircase coordination
         polymer", *Angew. Chem. Int. Ed.* **2004**, *43*, 5769–5772, DOI
         `10.1002/anie.200460516`.

[162]    X.-L. Yang, M.-H. Xie, C. Zou, F.-F. Sun, C.-D. Wu, "A series of
         metal-organic coordination polymers containing multiple chiral
         centers", *Cryst. Eng. Comm.* **2011**, *13*, 1570, DOI `10.1039/c0ce00633e`.

[163]    G. Zhang, S.-Y. Yao, D.-W. Guo, Y.-Q. Tian, "Noncentrosymmetric and
         Homochiral Metal-Organic Frameworks of (*S*)-2-(H-Imidazoleyl)
         Propionic Acid", *Cryst. Growth Des.* **2010**, *10*, 2355–2359, DOI
         `10.1021/cg1001368`.

[164]  M. Wang, M.-H. Xie, C.-D. Wu, Y.-G. Wang, "From one to three: a serine derivate manipulated homochiral metal-organic framework.", *Chem. Commun.* **2009**, *1*, 2396–8, DOI `10.1039/b823323c`.

[165]  S. Banerjee, N. N. Adarsh, P. Dastidar, "An unprecedented all helical 3D network and a rarely observed non-interpenetrated octahedral network in homochiral Cu(II) MOFs: effect of steric bulk and $\pi$-$\pi$ stacking interactions of the ligand backbone", *Cryst. Eng. Comm.* **2009**, *11*, 746, DOI `10.1039/b820087b`.

[166]  S. Banerjee, P. Dastidar, "Coordination polymers in selective separation of cations and anions: A series of rarely observed all helical three-dimensional coordination polymers derived from various chiral amino acid based bis-pyridyl-bis-amide ligands", *Cryst. Growth Des.* **2011**, *11*, 5592–5597, DOI `10.1021/cg201161q`.

[167]  L. Lin, R. Yu, X.-Y. Wu, W.-B. Yang, J. Zhang, X.-G. Guo, Z.-J. Lin, C.-Z. Lu, "Enantioselective inclusion of alcohols by solvent-controlled assembled flexible metal-organic frameworks.", *Inorg. Chem.* **2014**, *53*, 4794–6, DOI `10.1021/ic500436g`.

[168]  A. Rossin, B. Di Credico, G. Giambastiani, M. Peruzzini, G. Pescitelli, G. Reginato, E. Borfecchia, D. Gianolio, C. Lamberti, S. Bordiga, "Synthesis, characterization and $CO_2$ uptake of a chiral Co(II) metal-organic framework containing a thiazolidine-based spacer", *J. Mater. Chem.* **2012**, *22*, 10335, DOI `10.1039/c2jm16236a`.

[169]  W. Lin, "Asymmetric Catalysis with Chiral Porous MetalâĂŞOrganic Frameworks", *Top. Catal.* **2010**, *53*, 869–875, DOI `10.1007/s11244-010-9519-3`.

[170]  K. Mo, Y. Yang, Y. Cui, "A homochiral metal-organic framework as an effective asymmetric catalyst for cyanohydrin synthesis", *J. Amer. Chem. Soc.* **2014**, *136*, 1746–1749, DOI `10.1021/ja411887c`.

[171]  S. Regati, Y. He, M. Thimmaiah, P. Li, S. Xiang, B. Chen, J. C.-G. Zhao, "Enantioselective ring-opening of meso-epoxides by aromatic amines catalyzed by a homochiral metal-organic framework.", *Chem. Commun.* **2013**, *49*, 9836–9838, DOI `10.1039/c3cc45988h`.

[172]  J. M. Falkowski, S. Liu, W. Lin, "Metal-organic frameworks as single-site solid catalysts for asymmetric reactions", *Israel J. Chem.* **2012**, *52*, 591–603, DOI `10.1002/ijch.201100159`.

[173]  T. Duerinck, J. Denayer, "Metal-organic frameworks as stationary phases for chiral chromatographic and membrane separations", *Chem. Eng. Sci.* **2015**, *124*, 179–187, DOI `10.1016/j.ces.2014.10.012`.

[174]  Z.-X. Fei, M. Zhang, J.-H. Zhang, L.-M. Yuan, "Chiral metal-organic framework used as stationary phases for capillary electrochromatography.", *Anal. Chim. Acta* **2014**, *830*, 49–55, DOI `10.1016/j.aca.2014.04.054`.

[175]  X. Kuang, Y. Ma, H. Su, J. Zhang, Y.-B. Dong, B. Tang, "High-Performance Liquid Chromatographic Enantioseparation of Racemic Drugs Based on Homochiral Metal-Organic Framework.", *Anal. Chem.* **2014**, DOI `10.1021/ac403674p`.

[176]  R. Bueno-Perez, A. Martin-Calvo, P. Gómez-Álvarez, J. J. Gutiérrez-Sevillano, P. J. Merkling, T. J. H. Vlugt, T. S. van Erp, D. Dubbeldam, S. Calero, "Enantioselective adsorption of ibuprofen and lysine in metal-organic frameworks", *Chem. Commun.* **2014**, *50*, 10849, DOI `10.1039/C4CC03745F`.

[177]  M. Padmanaban, P. Müller, C. Lieder, K. Gedrich, R. Grünker, V. Bon, I. Senkovska, S. Baumgärtner, S. Opelt, S. Paasch, E. Brunner, F. Glorius, E. Klemm, S. Kaskel, "Application of a chiral metal-organic framework in enantioselective separation", *Chem. Commun.* **2011**, *47*, 12089, DOI `10.1039/c1cc14893a`.

[178]  M Zhang, X. D. Xue, J. H. Zhang, S. M. Xie, Y Zhang, L. M. Yuan, "Enantioselective chromatographic resolution using a homochiral metal-organic framework in HPLC", *Anal. Meth.* **2014**, *6*, 341–346, DOI `10.1039/c3ay41068d`.

[179]  Y. Peng, T. Gong, Y. Cui, "A homochiral porous metal-organic framework for enantioselective adsorption of mandelates and photocyclizaton of tropolone ethers.", *Chem. Commun.* **2013**, *49*, 8253–8255, DOI `10.1039/c3cc43549k`.

[180]  A. L. Nuzhdin, D. N. Dybtsev, K. P. Bryliakov, E. P. Talsi, V. P. Fedin, "Enantioselective chromatographic resolution and one-pot synthesis of enantiomerically pure sulfoxides over a homochiral Zn-organic framework.", *J. Amer. Chem. Soc.* **2007**, *129*, 12958–9, DOI `10.1021/ja076276p`.

[181]  K. Tanaka, T. Muraoka, D. Hirayama, A. Ohnish, "Highly efficient chromatographic resolution of sulfoxides using a new homochiral MOF-silica composite.", *Chem. Commun.* **2012**, *48*, 8577–9, DOI `10.1039/c2cc33939k`.

[182]  W. Wang, X. Dong, J. Nan, W. Jin, Z. Hu, Y. Chen, J. Jiang, "A homochiral metal-organic framework membrane for enantioselective separation", *Chem. Commun.* **2012**, *48*, 7022, DOI `10.1039/c2cc32595k`.

408

[183] S.-m. Xie, X.-h. Zhang, B.-j. Wang, M. Zhang, J.-h. Zhang, L.-m. Yuan, "3D Chiral Nanoporous Metal-Organic Framework for Chromatographic Separation in GC", *Chromatographia* **2014**, DOI `10.1007/s10337-014-2719-4`.

[184] M. Zhang, Z.-J. Pu, X.-L. Chen, X.-L. Gong, A.-X. Zhu, L.-M. Yuan, "Chiral recognition of a 3D chiral nanoporous metal-organic framework.", *Chem. Commun.* **2013**, *49*, 5201–3, DOI `10.1039/c3cc41966e`.

[185] K. Suh, M. P. Yutkin, D. N. Dybtsev, V. P. Fedin, K. Kim, "Enantioselective sorption of alcohols in a homochiral metal-organic framework", *Chem. Commun.* **2012**, *48*, 513, DOI `10.1039/c1cc16209h`.

[186] G. J. Kennedy, J. H. Knox, "The Performance of Packings in High Performance Liquid Chromatography (HPLC) I. Porous and Surface Layered Supports", *J. Chrom. Sci.* **1972**, *10*, 549–556, DOI `10.1093/chromsci/10.9.549`.

[187] N. Stock, S. Biswas, "Synthesis of Metal-Organic Frameworks (MOFs): Routes to Various MOF Topologies, Morphologies, and Composites.", *Chem. Rev.* **2011**, DOI `10.1021/cr200304e`.

[188] S. Furukawa, J. Reboul, S. Diring, K. Sumida, S. Kitagawa, "Structuring of metal-organic frameworks at the mesoscopic/macroscopic scale.", *Chem. Soc. Rev.* **2014**, 5700–5734, DOI `10.1039/c4cs00106k`.

[189] T. Chalati, P. Horcajada, R. Gref, P. Couvreur, C. Serre, "Optimisation of the synthesis of MOF nanoparticles made of flexible porous iron fumarate MIL-88A", *J. Mater. Chem.* **2011**, *21*, 2220, DOI `10.1039/c0jm03563g`.

[190] L.-G. Qiu, Z.-Q. Li, Y. Wu, W. Wang, T. Xu, X. Jiang, "Facile synthesis of nanocrystals of a microporous metal-organic framework by an ultrasonic method and selective sensing of organoamines.", *Chem. Commun.* **2008**, 3642–3644, DOI `10.1039/b804126a`.

[191] D. Tanaka, A. Henke, K. Albrecht, M. Moeller, K. Nakagawa, S. Kitagawa, J. Groll, "Rapid preparation of flexible porous coordination polymer nanocrystals with accelerated guest adsorption kinetics.", *Nature Chem.* **2010**, *2*, 410–416, DOI `10.1038/nchem.627`.

[192] Q.-L. Zhu, Q. Xu, "Metal-organic framework composites.", *Chem. Soc. Rev.* **2014**, *43*, 5648–5512, DOI `10.1039/c3cs60472a`.

[193] A. M. B. Furtado, J. Liu, Y. Wang, M. D. LeVan, "Mesoporous silica-metal organic composite: synthesis, characterization, and ammonia adsorption", *J. Mater. Chem.* **2011**, *21*, 6698, DOI 10.1039/c1jm10451a.

[194] Z. Yan, J. Zheng, J. Chen, P. Tong, M. Lu, Z. Lin, L. Zhang, "Preparation and evaluation of silica-UiO-66 composite as liquid chromatographic stationary phase for fast and efficient separation", *J. Chrom. A* **2014**, *1366*, 45–53, DOI 10.1016/j.chroma.2014.08.077.

[195] W. Stöber, A. Fink, "Controlled growth of monodisperse silica spheres in the micron size range", *J. Coll. Interf. Sci.* **1967**, *26*, 62–69.

[196] S.-M. Xie, X.-H. Zhang, Z.-J. Zhang, L.-M. Yuan, "Porous Chiral Metal-Organic Framework $InH(D-C_{10}H_{14}O_4)_2$ with Anionic-Type Diamond Network for High-Resolution Gas Chromatographic Enantioseparations", *Anal. Lett.* **2012**, 121031075213001, DOI 10.1080/00032719.2012.735306.

[197] S. M. Xie, X. H. Zhang, Z. J. Zhang, M. Zhang, J. Jia, L. M. Yuan, "A 3-D open-framework material with intrinsic chiral topology used as a stationary phase in gas chromatography", *Anal. Bioanal. Chem.* **2013**, *405*, 3407–3412, DOI 10.1007/s00216-013-6714-7.

[198] S. Xie, B. Wang, X. Zhang, J. Zhang, M. Zhang, L. Yuan, "Chiral 3D open-framework material $Ni(D-cam)(H_2O)_2$ used as GC stationary phase", *Chirality* **2014**, *26*, 27–32, DOI 10.1002/chir.22260.

[199] X. H. Zhang, S. M. Xie, A. H. Duan, B. J. Wang, L. M. Yuan, "Separation performance of MOFs $Zn(ISN)_2 \cdot 2H_2O$ as stationary phase for high-resolution GC", *Chromatographia* **2013**, *76*, 831–836, DOI 10.1007/s10337-013-2484-9.

[200] P. Peluso, V. Mamane, S. Cossu, "Homochiral metal-organic frameworks and their application in chromatography enantioseparations.", *J. Chrom. A* **2014**, *1363*, 11–26, DOI 10.1016/j.chroma.2014.06.064.

[201] C.-L. Chang, X.-Y. Qi, J.-W. Zhang, Y.-M. Qiu, X.-J. Li, X. Wang, Y. Bai, J.-L. Sun, H.-W. Liu, "Facile synthesis of magnetic homochiral metal-organic frameworks for "enantioselective fishing"", *Chem. Commun.* **2015**, *51*, 3566–3569, DOI 10.1039/C4CC09988E.

[202] T. Düren, Y.-S. Bae, R. Q. Snurr, "Using molecular simulation to characterise metal-organic frameworks for adsorption applications.", *Chem. Soc. Rev.* **2009**, *38*, 1237–1247, DOI 10.1039/b803498m.

[203] Y. J. Colón, R. Q. Snurr, "High-throughput computational screening of metalâĂŞorganic frameworks", *Chem. Soc. Rev.* **2014**, *43*, 5735–5749, DOI 10.1039/C4CS00070F.

[204]  X. Bao, L. J. Broadbelt, R. Q. Snurr, "A computational study of enantioselective adsorption in a homochiral metal-organic framework", *Mol. Sim.* **2009**, *35*, 50–59, DOI 10.1080/08927020802422064.

[205]  X. Bao, R. Q. Snurr, L. J. Broadbelt, "Collective effects of multiple chiral selectors on enantioselective adsorption", *Langmuir* **2009**, *25*, 10730–10736, DOI 10.1021/la901240n.

[206]  X. Bao, L. J. Broadbelt, R. Q. Snurr, "Elucidation of consistent enantioselectivity for a homologous series of chiral compounds in homochiral metal-organic frameworks.", *Phys. Chem. Chem. Phys.* **2010**, *12*, 6466–73, DOI 10.1039/c000809e.

[207]  P. Z. Moghadam, T. Düren, "Origin of enantioselectivity in a chiral metal-organic framework: A Molecular simulation study", *J. Phys. Chem. C* **2012**, *116*, 20874–20881, DOI 10.1021/jp3056637.

[208]  T. D. Booth, K Azzaoui, I. W. Wainer, "Prediction of chiral chromatographic separations using combined multivariate regression and neural networks.", *Anal. Chem.* **1997**, *69*, 3879–83, DOI 10.1021/ac9702150.

[209]  I. Fitos, J. Visy, M. Simonyi, J. Hermansson, "Separation of enantiomers of benzodiazepines on the Chiral-AGP column", *J. Chrom. A* **1995**, *709*, 265–273, DOI 10.1016/0021-9673(95)00444-R.

[210]  J. Yongzhu, K. Hirose, T. Nakamura, R. Nishioka, T. Ueshige, Y. Tobe, "Preparation and evaluation of a chiral stationary phase covalently bound with a chiral pseudo-18-crown-6 ether having a phenolic hydroxy group for enantiomer separation of amino compounds", *J. Chrom. A* **2006**, *1129*, 201–207, DOI 10.1016/j.chroma.2006.07.003.

[211]  B. Rasulev, M. Turabekova, M. Gorska, K. Kulig, A. Bielejewska, J. Lipkowski, J. Leszczynski, "Use of quantitative structure-enantioselective retention relationship for the liquid chromatography chiral separation prediction of the series of pyrrolidin-2-one compounds", *Chirality* **2012**, *24*, 72–77, DOI 10.1002/chir.21028.

[212]  X. Bao, L. J. Broadbelt, R. Q. Snurr, "Computational screening of homochiral metal-organic frameworks for enantioselective adsorption", *Microporous Mesoporous Mater.* **2012**, *157*, 118–123, DOI 10.1016/j.micromeso.2011.08.008.

[213]  K. Hiyoshizo, N. Sasakura in *Comprehensive Enantioselective Organocatalysis*, (Ed.: P. I. Dalko), Wiley-VCH, Weinheim, **2013**, Chapter 1, pp. 1–31, DOI 10.1002/9783527658862.ch1.

411

[214] B. List, R. A. Lerner, C. F. Barbas III, "Proline-Catalyzed Direct Asymmetric Aldol Reactions", *J. Am. Chem. Soc.* **2000**, *122*, 2395–2396, DOI `10.1021/ja994280y`.

[215] L. D. Barron, *Molecular Light Scattering and Optical Activity*, 2nd ed., Cambridge University Press, Cambridge, **2004**, pp. 123–169.

[216] L. M. Pasteur, "Nouvelles recherches sur les relations qui peuvent exister, entre la forme cristalline, la composition chimique, et le pouvoir rotatoire moléculaire", *Anal. Chim. Phys.* **1848**, *24*, 442–459.

[217] R. E. Lyle, G. G. Lyle, "A Brief History of Polarimetry", *J. Chem. Edu.* **1964**, *41*, 308–313, DOI `10.1021/ed041p308`.

[218] H. D. Flack, "Louis Pasteurs discovery of molecular chirality and spontaneous resolution in 1848, together with a complete review of his crystallographic and chemical work", *Acta Crystallogr. Sect. A: Found. Crystallogr.* **2009**, *65*, 371–389, DOI `10.1107/S0108767309024088`.

[219] C. M. Earnest, "Modern thermogravimetry", *Anal. Chem.* **1984**, *56*, 1471A–1486A, DOI `10.1021/ac00277a002`.

[220] W. W. Wendlandt, *Thermal analysis*, **1986**, 250R–261R, DOI `10.1021/ac8005999`.

[221] R. Bottom in *Principles and Applications of Thermal Analysis*, (Ed.: P. Gabbot), Blackwell Publishing, Oxford, **2008**, Chapter 3, pp. 87–118.

[222] M. Thommes, "Physical adsorption characterization of nanoporous materials", *Chem.-Ing.-Tech.* **2010**, *82*, 1059–1073, DOI `10.1002/cite.201000064`.

[223] K. S. W. Sing, "Reporting physisorption data for gas/solid systems with special reference to the determination of surface area and porosity (Recommendations 1984)", *Pure Appl. Chem.* **1985**, *57*, 603–619, DOI `10.1351/pac198557040603`.

[224] S. Brunauer, P. H. Emmett, E. Teller, "Adsorption of Gases in Multimolecular Layers", *J. Amer. Chem. Soc.* **1938**, *60*, 309–319, DOI `doi:10.1021/ja01269a023`.

[225] S. Lowell, J. Shields, M. Thomas, M. Thommes in *Characterization of Porous Solids and Powders; Surface area, pore size and density, particle technology Series*, Springer, London, **2004**, pp. 58–81, DOI `10.1007/978-1-4020-2303-3\_5`.

[226] J. Moellmer, E. B. Celer, R. Luebke, A. J. Cairns, R. Staudt, M. Eddaoudi, M. Thommes, "Insights on Adsorption Characterization of Metal-Organic Frameworks: A Benchmark Study on the Novel soc-MOF", *Microporous Mesoporous Mater.* **2010**, *129*, 345–353, DOI `10.1016/j.micromeso.2009.06.014`.

[227] ISO 9277:2010, Determination of the specific surface area of solids by gas adsorption - BET method. International Organization for Standardization, Geneva, **2010**.

[228] F. Rouquerol, J. Rouquerol, K. Sing in *Adsorption by Powders and Porous Solids*, (Eds.: F. Rouquerol, J. Rouquerol, K. Sing), Academic Press, London, **1999**, Chapter 4, pp. 99–135, DOI `10.1016/B978-012598920-6/50005-1`.

[229] P. van der Sluis, A. L. Spek, "BYPASS: an effective method for the refinement of crystal structures containing disordered solvent regions", *Acta Crystallographica Section A Foundations of Crystallography* **1990**, *46*, 194–201, DOI `10.1107/S0108767389011189`.

[230] A. L. Spek, "Single-crystal Structure Validation with the Program PLATON", *J. Appl. Cryst.* **2003**, *36*, 7–13, DOI `10.1107/S0021889802022112`.

[231] D. Sun, Y. Ke, T. M. Mattox, B. A. Ooro, H.-C. Zhou, "Temperature-dependent supramolecular stereoisomerism in porous copper coordination networks based on a designed carboxylate ligand.", *Chem. Commun.* **2005**, 5447–5449, DOI `10.1039/b505664k`.

[232] B. Chen, N. W. Ockwig, F. R. Fronczek, D. S. Contreras, O. M. Yaghi, "Transformation of a metal-organic framework from the NbO to PtS net", *Inorg. Chem.* **2005**, *44*, 181–183, DOI `10.1021/ic048612y`.

[233] M. Du, X.-J. Zhao, J.-H. Guo, S. R. Batten, "Direction of topological isomers of silver(I) coordination polymers induced by solvent, and selective anion-exchange of a class of PtS-type host frameworks.", *Chem. Commun.* **2005**, 4836–4838, DOI `10.1039/b508479b`.

[234] F. Gándara, V. A. De La Peña-O'Shea, F. IIIas, N. Snejko, D. M. Proserpio, E. Gutiérrez-Puebla, M. A. Monge, "Three lanthanum MOF polymorphs: Insights into kinetically and thermodynamically controlled phases", *Inorg. Chem.* **2009**, *48*, 4707–4713, DOI `10.1021/ic801779j`.

[235] G.-X. Liu, H. Xu, H. Zhou, S. Nishihara, X.-M. Ren, "Temperature-induced assembly of MOF polymorphs: Syntheses, structures and physical properties", *Cryst. Eng. Comm.* **2012**, *14*, 1856, DOI `10.1039/c1ce05369h`.

[236]  A. E. Platero-Prats, V. A. De La Peña-O'Shea, D. M. Proserpio, N. Snejko, E. Gutiérrez-Puebla, A. Monge, "Insight into the SBU condensation in Mg coordination and supramolecular frameworks: A combined experimental and theoretical study", *J. Amer. Chem. Soc.* **2012**, *134*, 4762–4771, DOI `10.1021/ja210564a`.

[237]  X. Zhao, L. Zhang, H. Ma, D. Sun, D. Wang, S. Feng, D. Sun, "Solvent-controlled Cd(II) metalâĂŞorganic frameworks constructed from a tetrapodal silicon-based linker", *RSC Advances* **2012**, *2*, 5543, DOI `10.1039/c2ra20384g`.

[238]  V. Bon, I. Senkovska, I. A. Baburin, S. Kaskel, "Zr- and Hf-based metal-organic frameworks: Tracking down the polymorphism", *Cryst. Growth Des.* **2013**, *13*, 1231–1237, DOI `10.1021/cg301691d`.

[239]  N. Zhu, M. J. Lennox, T. Düren, W. Schmitt, "Polymorphism of metal-organic frameworks: direct comparison of structures and theoretical N2-uptake of topological - and -isomers.", *Chem. Commun.* **2014**, *50*, 4207–10, DOI `10.1039/c3cc49829h`.

[240]  D. Frahm, F. Hoffmann, M. Fröba, "Two metal-organic frameworks with a tetratopic linker: Solvent-dependent polymorphism and postsynthetic bromination", *Cryst. Growth Des.* **2014**, *14*, 1719–1725, DOI `10.1021/cg4018536`.

[241]  T. Tsuruoka, S. Furukawa, Y. Takashima, K. Yoshida, S. Isoda, S. Kitagawa, "Nanoporous nanorods fabricated by coordination modulation and oriented attachment growth", *Angew. Chem. Int. Ed.* **2009**, *48*, 4739–4743, DOI `10.1002/anie.200901177`.

[242]  A. Umemura, S. Diring, S. Furukawa, H. Uehara, T. Tsuruoka, S. Kitagawa, "Morphology design of porous coordination polymer crystals by coordination modulation", *J. Amer. Chem. Soc.* **2011**, *133*, 15506–15513, DOI `10.1021/ja204233q`.

[243]  T. Willhammar, Y. Yun, X. Zou, "Structural determination of ordered porous solids by electron crystallography", *Adv. Funct. Mater.* **2014**, *24*, 182–199, DOI `10.1002/adfm.201301949`.

[244]  M. Feyand, E. Mugnaioli, F. Vermoortele, B. Bueken, J. M. Dieterich, T. Reimer, U. Kolb, D. De Vos, N. Stock, "Automated diffraction tomography for the structure elucidation of twinned, sub-micrometer crystals of a highly porous, catalytically active bismuth metal-organic framework", *Angew. Chem. Int. Ed.* **2012**, *51*, 10373–10376, DOI `10.1002/anie.201204963`.

[245]   A. Altomare, C. Cuocci, C. Giacovazzo, A. Moliterni, R. Rizzi,
        N. Corriero, A. Falcicchio, "EXPO2013: A kit of tools for phasing crystal
        structures from powder data", *J. Appl. Cryst.* **2013**, *46*, 1231–1235, DOI
        `10.1107/S0021889813013113`.

[246]   S. Brenner, L. B. McCusker, C. Baerlocher, "Using a structure envelope
        to facilitate structure solution from powder diffraction data", *J. Appl.
        Cryst.* **1997**, *30*, 1167–1172, DOI `10.1107/S0021889897011291`.

[247]   S. Brenner, L. B. McCusker, C. Baerlocher, "The application of structure
        envelopes in structure determination from powder diffraction data", *J.
        Appl. Cryst.* **2002**, *35*, 243–252, DOI `10.1107/S0021889802001759`.

[248]   A. A. Yakovenko, J. H. Reibenspies, N. Bhuvanesh, H. C. Zhou,
        "Generation and applications of structure envelopes for porous
        metal-organic frameworks", *J. Appl. Cryst.* **2013**, *46*, 346–353, DOI
        `10.1107/S0021889812050935`.

[249]   R. Černý, V. Favre-Nicolin, "Direct space methods of structure
        determination from powder diffraction: Principles, guidelines and
        perspectives", *Z. Kristallogr.* **2007**, *222*, 105–113, DOI
        `10.1524/zkri.2007.222.3-4.105`.

[250]   N. Masciocchi, S. Galli, V. Colombo, A. Maspero, G. Palmisano,
        B. Seyyedi, C. Lamberti, S. Bordiga, "Cubic octanuclear Ni(II) clusters in
        highly porous polypyrazolyl-based materials", *J. Amer. Chem. Soc.* **2010**,
        *132*, 7902–7904, DOI `10.1021/ja102862j`.

[251]   T. Loiseau, C. Mellot-Draznieks, H. Muguerra, G. Férey, M. Haouas,
        F. Taulelle, "Hydrothermal synthesis and crystal structure of a new
        three-dimensional aluminum-organic framework MIL-69 with
        2,6-naphthalenedicarboxylate (ndc), $Al(OH)(ndc) \cdot H_2O$", *Comptes
        Rendus Chimie* **2005**, *8*, 765–772, DOI `10.1016/j.crci.2004.10.011`.

[252]   S. D. Bull, S. G. Davies, S. Jones, M. E. C. Polywka, R. Shyam Prasad,
        H. J. Sanganee, "A Practical Procedure for the Multigram Synthesis of
        the SuperQuat Chiral Auxiliaries", *Synlett* **1998**, *1998*, 519–521, DOI
        `10.1055/s-1998-1700`.

[253]   M. P. Sibi, R. Zhang, S. Manyem, "A New Class of Modular Chiral
        Ligands with Fluxional Groups", *J. Amer. Chem. Soc.* **2003**, *125*,
        9306–9307, DOI `10.1021/ja035979d`.

[254]   M. Bilo, Master Thesis, Universität Hamburg, **2014**.

[255]   D. Evans, J. Nelson, "Stereoselective aldol condensations via boron
        enolates", *J. Amer. Chem. Soc.* **1981**, *103*, 3099–3111.

[256] D. A. Evans, "Studies in Asymmetric Synthesis - The Development of Practical Chiral Enolate Synthons", *Aldrichim. Acta* **1982**, *15*, 23–32.

[257] T. Hintermann, D. Seebach, "A Useful Modification of the Evans Auxiliary: 4-Isopropyl-5,5-diphenyloxazolidin-2-one", *Helv. Chim. Acta* **1998**, *81*, 2093–2126, DOI `10.1002/(SICI)1522-2675(19981111)81:11<2093::AID-HLCA2093>3.0.CO;2-X`.

[258] M. Mazik, A. König, "Recognition properties of an acyclic biphenyl-based receptor toward carbohydrates.", *J. Org. Chem.* **2006**, *71*, 7854–7, DOI `10.1021/jo0610309`.

[259] Z. Todres, *Ion-Radical Organic Chemistry: Principles and Applications*, 2nd ed., Boca Raton, Florida, USA, **2009**, pp. 262–264.

[260] H. H. Hodgson, "The Sandmeyer reaction", *Chem. Rev.* **1947**, *40*, 251–277, DOI `10.1021/cr60126a003`.

[261] R. L.-Y. Bao, R. Zhao, L. Shi, "Progress and developments in the turbo Grignard reagent i-PrMgCl*LiCl: a ten-year journey", *Chem. Commun.* **2015**, DOI `10.1039/C4CC10194D`.

[262] F. Kopp, S. Wunderlich, P. Knochel, "Halogen-magnesium exchange on unprotected aromatic and heteroaromatic carboxylic acids", *Chem. Commun.* **2007**, 2075, DOI `10.1039/b618923g`.

[263] H. Ren, A. Krasovskiy, P. Knochel, "Stereoselective preparation of functionalized acyclic alkenylmagnesium reagents using i-PrMgCl*LiCl", *Org. Lett.* **2004**, *6*, 4215–4217, DOI `10.1021/ol048363h`.

[264] T. E. Barder, S. D. Walker, J. R. Martinelli, S. L. Buchwald, "Catalysts for Suzuki-Miyaura coupling processes: Scope and studies of the effect of ligand structure", *J. Amer. Chem. Soc.* **2005**, *127*, 4685–4696, DOI `10.1021/ja042491j`.

[265] D. S. Surry, S. L. Buchwald, "Biaryl phosphane ligands in palladium-catalyzed amination", *Angew. Chem. Int. Ed.* **2008**, *47*, 6338–6361, DOI `10.1002/anie.200800497`.

[266] P. G. M. Wuts, T. W. Greene in *Greene's Protective Groups in Organic Synthesis*, John Wiley & Sons, Ltd, Hoboken, NJ, USA, **2007**, Chapter 7, pp. 727–735, DOI `10.1002/9780470053485.ch7`.

[267] S. E. Wenzel, M. Fischer, F. Hoffmann, M. Fröba, "Highly porous metal-organic framework containing a novel organosilicon linker-a promising material for hydrogen storage", *Inorg. Chem.* **2009**, *48*, 6559–6565, DOI `10.1021/ic900478z`.

[268]  K. Peikert, personal communication (dissertation in preparation), Universität Hamburg, **2015**.

[269]  N. L. Rosi, M. Eddaoudi, J. Kim, M. O'Keeffe, O. M. Yaghi, "Infinite secondary building units and forbidden catenation in metal-organic frameworks", *Angew. Chem. Int. Ed.* **2002**, *41*, 284–287, DOI `10.1002/1521-3773(20020118)41:2<284::AID-ANIE284>3.0.CO;2-M`.

[270]  N. L. Rosi, J. Kim, M. Eddaoudi, B. Chen, M. O'Keeffe, O. M. Yaghi, "Rod packings and metal-organic frameworks constructed from rod-shaped secondary building units", *J. Amer. Chem. Soc.* **2005**, *127*, 1504–1518, DOI `10.1021/ja045123o`.

[271]  F. A. Cotton, C. Lin, C. A. Murillo, "Supramolecular arrays based on dimetal building units", *Acc. Chem. Res.* **2001**, *34*, 759–771, DOI `10.1021/ar010062+`.

[272]  T. R. Cook, Y.-R. Zheng, P. J. Stang, "Metal-organic frameworks and self-assembled supramolecular coordination complexes: comparing and contrasting the design, synthesis, and functionality of metal-organic materials.", *Chem. Rev.* **2013**, *113*, 734–77, DOI `10.1021/cr3002824`.

[273]  D. J. Tranchemontagne, Z. Ni, M. O'Keeffe, O. M. Yaghi, "Reticular chemistry of metal-organic polyhedra", *Angew. Chem. Int. Ed.* **2008**, *47*, 5136–5147, DOI `10.1002/anie.200705008`.

[274]  J.-R. Li, H.-C. Zhou, "Bridging-ligand-substitution strategy for the preparation of metal-organic polyhedra.", *Nature Chem.* **2010**, *2*, 893–898, DOI `10.1038/nchem.803`.

[275]  M. H. Alkordi, J. L. Belof, E. Rivera, L. Wojtas, M. Eddaoudi, "Insight into the construction of metal-organic polyhedra: metal-organic cubes as a case study", *Chem. Sci.* **2011**, *2*, 1695, DOI `10.1039/c1sc00269d`.

[276]  J. Park, L. B. Sun, Y. P. Chen, Z. Perry, H. C. Zhou, "Azobenzene-functionalized metal-organic polyhedra for the optically responsive capture and release of guest molecules", *Angew. Chem. Int. Ed.* **2014**, *53*, 5842–5846, DOI `10.1002/anie.201310211`.

[277]  M. D. Young, Q. Zhang, H.-C. Zhou, "Metal-organic polyhedra constructed from dinuclear ruthenium", *Inorg. Chim. Acta* **2015**, *424*, 216–220, DOI `10.1016/j.ica.2014.09.010`.

[278]  Z.-J. Zhang, W. Shi, Z. Niu, H.-H. Li, B. Zhao, P. Cheng, D.-Z. Liao, S.-P. Yan, "A new type of polyhedron-based metal-organic frameworks with interpenetrating cationic and anionic nets demonstrating ion exchange, adsorption and luminescent properties.", *Chem. Commun.* **2011**, *47*, 6425–7, DOI `10.1039/c1cc00047k`.

[279]  X. Liu, M. Park, S. Hong, M. Oh, J. W. Yoon, J.-S. Chang, M. S. Lah, "A twofold interpenetrating porous metal-organic framework with high hydrothermal stability: structure and gas sorption behavior.", *Inorg. Chem.* **2009**, *48*, 11507–9, DOI `10.1021/ic901924z`.

[280]  J. J. Perry, J. A. Perman, M. J. Zaworotko, "Design and synthesis of metal-organic frameworks using metal-organic polyhedra as supermolecular building blocks.", *Chem. Soc. Rev.* **2009**, *38*, 1400–1417, DOI `10.1039/b807086p`.

[281]  B. Chen, N. W. Ockwig, A. R. Millward, D. S. Contreras, O. M. Yaghi, "High $H_2$ adsorption in a microporous metal-organic framework with open metal sites", *Angew. Chem. Int. Ed.* **2005**, *44*, 4745–4749, DOI `10.1002/anie.200462787`.

[282]  D. Sun, D. J. Collins, Y. Ke, J. L. Zuo, H. C. Zhou, "Construction of open metal-organic frameworks based on predesigned carboxylate isomers: From achiral to chiral nets", *Chem.– Eur. J.* **2006**, *12*, 3768–3776, DOI `10.1002/chem.200501340`.

[283]  Y. Liu, J. F. Eubank, A. J. Cairns, J. Eckert, V. C. Kravtsov, R. Luebke, M. Eddaoudi, "Assembly of Metal-Organic Frameworks (MOFs) based on indium-trimer building blocks: A porous MOF with soc topology and high hydrogen storage", *Angew. Chem. Int. Ed.* **2007**, *46*, 3278–3283, DOI `10.1002/anie.200604306`.

[284]  V. A. Blatov, A. P. Shevchenko, D. M. Proserpio, "Applied Topological Analysis of Crystal Structures with the Program Package ToposPro", *Cryst. Growth Des.* **2014**, *14*, 3576–3586, DOI `10.1021/cg500498k`.

[285]  O. Delgado-Friedrichs, M. O'Keeffe, "Identification of and symmetry computation for crystal nets", *Acta Crystallogr. Sect. A: Found. Crystallogr.* **2003**, *59*, 351–360, DOI `10.1107/S0108767303012017`.

[286]  J. J. Perry, V. C. Kravtsov, G. J. McManus, M. J. Zaworotko, "Bottom up synthesis that does not start at the bottom: quadruple covalent cross-linking of nanoscale faceted polyhedra.", *J. Amer. Chem. Soc.* **2007**, *129*, 10076–7, DOI `10.1021/ja0734952`.

[287]  X. S. Wang, S. Ma, P. M. Forster, D. Yuan, J. Eckert, J. J. López, B. J. Murphy, J. B. Parise, H. C. Zhou, "Enhancing $H_2$ uptake by "close-packing" alignment of open copper sites in metal-organic frameworks", *Angew. Chem. Int. Ed.* **2008**, *47*, 7263–7266, DOI `10.1002/anie.200802087`.

[288]   D. Frahm, M. Fischer, F. Hoffmann, M. Fröba, "An interpenetrated metal-organic framework and its gas storage behavior: Simulation and experiment", *Inorg. Chem.* **2011**, *50*, 11055–11063, DOI `10.1021/ic201596x`.

[289]   D. Frahm, Dissertation, University of Hamburg, **2013**, pp. 123–131.

[290]   T. Stein, Master Thesis, University of Hamburg, **2015**.

[291]   V. Blatov, D. Proserpio, "TOPOS 4.0, A Program Package for Multipurpose Crystallochemical Analysis, www.topospro.com", **2011**.

[292]   I. Accelrys, Materials Studio, V5.5, San Diego, CA, USA, **2010**.

[293]   V. A. Blatov, D. M. Proserpio, TTD Collection, www.topospro.com/collections/TTD.php, **2015**.

[294]   D. Kim, X. Liu, M. Oh, X. Song, Y. Zou, D. Singh, K. S. Kim, M. S. Lah, "Isoreticular MOFs based on a rhombic dodecahedral MOP as a tertiary building unit", *Cryst. Eng. Comm.* **2014**, *16*, 6391, DOI `10.1039/c4ce00017j`.

[295]   Y. Hayashi, S. Samanta, T. Itoh, H. Ishikawa, "Asymmetric, catalytic, and direct self-aldol reaction of acetaldehyde catalyzed by diarylprolinol.", *Org. Lett.* **2008**, *10*, 5581–3, DOI `10.1021/ol802438u`.

[296]   S. E. Denmark, T. Bui, "Lewis base catalyzed enantioselective aldol addition of acetaldehyde-derived silyl enol ether to aldehydes", *J. Org. Chem.* **2005**, *70*, 10190–10193, DOI `10.1021/jo0517500`.

[297]   M. B. Boxer, H. Yamamoto, "Tris(trimethylsilyl)silyl-governed aldehyde cross-aldol cascade reaction", *J. Amer. Chem. Soc.* **2006**, *128*, 48–49, DOI `10.1021/ja054725k`.

[298]   Y. Hayashi, T. Itoh, S. Aratake, H. Ishikawa, "A diarylprolinol in an asymmetric, catalytic, and direct crossed-aldol reaction of acetaldehyde", *Angew. Chem. Int. Ed.* **2008**, *47*, 2082–2084, DOI `10.1002/anie.200704870`.

[299]   L. Kryger, S. E. Rasmussen, F. R. Forgaard, A. Haaland, S. Svensson, "Walden Inversion. II. The Crystal Structure and Absolute Configuration of Cobalt(II) (-)-Malate Trihydrate.", *Acta Chem. Scand.* **1972**, *26*, 2349–2359, DOI `10.3891/acta.chem.scand.26-2349`.

[300]   E. Hungerbühler, D. Seebach, D. Wasmuth, "Doppelt und dreifach funktionalisierte, enantiomerenreine C4-Synthesebausteine aus beta-Hydroxybuttersäure, Apfelsäure und Weinsäure", *Helv. Chim. Acta* **1981**, *64*, 1467–1487, DOI `10.1002/hlca.19810640523`.

[301] A. V. Malkov, M. A. Kabeshov, M. Bella, O. Kysilka, D. A. Malyshev, K. Pluháčková, P. Kočovský, "Vicinal amino alcohols as organocatalysts in asymmetric cross-aldol reaction of ketones: Application in the synthesis of convolutamydine A", *Org. Lett.* **2007**, *9*, 5473–5476, DOI `10.1021/ol7023983`.

[302] J. R. Gage, D. A. Evans, "Diastereoselective aldol condensation using a chiral oxazolidinone auxiliary: 2(*S*)-3(*S*)-3-hydroxy-3-phenyl-2-methylpropanic acid", *Org. Synth.* **1990**, *68*, 83, DOI `10.15227/orgsyn.068.0083`.

[303] J. F. McGarrity, C. A. Ogle, "High-field proton NMR study of the aggregation and complexation of n-butyllithium in tetrahydrofuran", *J. Amer. Chem. Soc.* **1985**, *107*, 1805–1810, DOI `10.1021/ja00293a001`.

[304] J. A. Rood, PhD Thesis, Notre Dame, Indiana, **2009**, pp. 132–133.

[305] G.-J. Ho, D. J. Mathre, "Lithium-Initiated Imide Formation. A Simple Method for N-Acylation of 2-Oxazolidinones and Bornane-2,10-Sultam", *J. Org. Chem.* **1995**, *60*, 2271–2273, DOI `10.1021/jo00112a060`.

[306] D. J. Ager, D. R. Allen, D. R. Schaad, "Simple and Efficient N-Acylation Reactions of Chiral Oxazolidine Auxiliaries", *Synthesis* **1996**, *1996*, 1283–1285, DOI `10.1055/s-1996-4402`.

[307] S. Xu, I. Held, B. Kempf, H. Mayr, W. Steglich, H. Zipse, "The DMAP-catalyzed acetylation of alcohols - A mechanistic study (DMAP = 4-(dimethylamino)pyridine)", *Chem.– Eur. J.* **2005**, *11*, 4751–4757, DOI `10.1002/chem.200500398`.

[308] V. Guerlavais, P. J. Carroll, M. M. Joullié, "Progress towards the total synthesis of callipeltin A. Asymmetric synthesis of (2R,3R,4S)-3-hydroxy-2,4,6-trimethylheptanoic acid", *Tetrahedron: Asymmetry* **2002**, *13*, 675–680, DOI `10.1016/S0957-4166(02)00045-9`.

[309] A. S. Franklin, I. Paterson, "Recent developments in asymmetric aldol methodology", *Cont. Org. Synth.* **1994**, *1*, 317, DOI `10.1039/co9940100317`.

[310] P. Arya, H. Qin, "Advances in asymmetric enolate methodology", *Tetrahedron* **2000**, *56*, 917–947, DOI `10.1016/S0040-4020(99)00964-3`.

[311] C. J. Cowden, I. Paterson, "Asymmetric Aldol Reactions Using Boron Enolates", *Org. React.* **1997**, *51*, 1–200, DOI `10.1002/0471264180.or051.01`.

[312] S. A. Kozmin, S. He, V. H. Rawal, "Preparation of (E)-1-Dimethylamino-3-tert-Butyldimethylsiloxy-1,3-Butadiene", *Org. Synth.* **2002**, *78*, 152, DOI `10.15227/orgsyn.078.0152`.

[313] B. T. Watson in *Handbook of Reagents for Organic Synthesis: Reagents for Silicon-Mediated Organic Synthesis*, (Ed.: P. L. Fuchs), John Wiley & Sons, Ltd, Hoboken, NJ, USA, **2011**, pp. 469–478.

[314] D. A. Evans, K. T Chapman, J Bisaha, "Asymmetric Diels-Alder Cycloaddition Reactions with Chiral alpha-Unsaturated N-Acyloxazolidinones", *J. Amer. Chem. Soc.* **1988**, *110*, 1238–1256, DOI `10.1021/ja00212a037`.

[315] M. F. Mayahi, M. F. El-Bermani, "Maleic Anhydride - Triethylamine Complex", *Canadian J. Chem.* **1973**, *51*, 3539–3540, DOI `10.1139/v73-527`.

[316] K. Momma, F. Izumi, "VESTA 3 for three-dimensional visualization of crystal, volumetric and morphology data", *J. Appl. Cryst.* **2011**, *44*, 1272–1276, DOI `10.1107/S0021889811038970`.

[317] H. E. Gottlieb, V. Kotlyar, A. Nudelman, "NMR Chemical Shifts of Common Laboratory Solvent as Trace-Impurities", *J. Org. Chem.* **1997**, *62*, 7512–7515.

[318] D. S. Pedersen, C. Rosenbohm, "Dry Column Vacuum Chromatography", *Synthesis* **2001**, *2001*, 2431–2434, DOI `10.1055/s-2001-18722`.

[319] M. Mazik, A. König, "Mimicking the Binding Motifs Found in the Crystal Structures of Protein-Carbohydrate Complexes: An Aromatic Analogue of Serine or Threonine Side Chain Hydroxyl/Main Chain Amide", *Eur. J. Org. Chem.* **2007**, *2007*, 3271–3276, DOI `10.1002/ejoc.200700295`.

[320] A. L. Spek, "Structure Validation in Chemical Crystallography", *Acta Crystallogr. Sect. D: Biol. Crystallogr.* **2009**, *65*, 148–155, DOI `10.1107/S090744490804362X`.

[321] Wiley 9th Edition/NIST 2008 MS Library.

# Chapter 6

# Appendix

## 6.1 Publications

- M. Sartor, F. Hoffmann, M. Fröba, "A new set of isoreticular, homochiral metal-organic frameworks based on tetratopic linkers derived from amino acids" (manuscript in preparation).

- F. Hoffmann, M. Sartor, M. Fröba, "Couch statt Hörsaal", *Nach. a. d. Chem.* **2010**, *62*, 48-49.

- M. Fischer, M. Sartor, M. Fröba, "Kleine Poren – große Wirkung", *Nach. a. d. Chem.* **2010**, *58*, 1003-1007.

- F. Giraud, P. Marchand, D. Carbonnelle, M. Sartor, F. Lang, M. Duflos, "Synthesis of *N*-aryl-3-(indol-3-yl)propanamides and their immunosuppressive activities" *Bioorg. Med. Chem. Lett.* **2010**, *20*, 5203-5206.

## 6.2  Safety

dimethylsulfoxide (DMSO), NaCl, NaHCO$_3$, Na$_2$SO$_4$, Na$_2$S$_2$O$_3$, L-alanine, L-valine, L-phenylalanine, L-proline and SPhos are not classified as harmful substances according to EU regulation No 1272/2008. All substances that are not listed in the following table are not completely audited.

**Table 6.1** – Substances used in this work together with the respective safety informations.

| substance | pictograms | hazard statements | precautionary statements |
|---|---|---|---|
| acetyl chloride | | 225, 302, 314 | 210, 280, 305+351+338, 310 |
| acetone | | 225, 319, 336 | 210, 261, 305+351+338 |
| acetic acid | | 226, 314 | 280, 305+351+338, 310 |
| $n$-amyl acetate | | 226 | 210 |
| crotonic anhydride | | H314 | 280, 305+351+335, 310 |
| ammonium chloride | | 302, 319, 411 | 273, 305+351+338 |
| 1,4-dibromobenzene | | 315, 319, 335 | 261, 305+351+338 |
| B(OMe)$_3$ | | 226, 312, 319 | 280, 305+351+338 |
| CaCl$_2$ | | 319 | 305+351+338 |
| CaH$_2$ | | 260 | 223, 231+232, 370+378, 422 |
| CHCl$_3$ | | 302, 315, 351, 373 | 281 |

| substance | pictograms | hazard statements | precautionary statements |
|---|---|---|---|
| $CH_2Cl_2$ | | 351 | 281 |
| $Cu(NO_3)_2 \cdot 3\,H_2O$ | | 272, 302, 315, 318, 400 | 220 273 280 305 351+338 |
| cyclohexane | | 225, 304, 315, 336, 410 | 210, 261, 273, 301+310, 331, 501 |
| 1,4-dioxan | | 225, 319, 335, 351 | 210, 261, 281, 305+351+338 |
| di-tert-butyl dicarbonate | | 226, 315, 317, 319, 330, 335 | 260, 280, 284, 305+351+338 310 |
| DMA | | 312+332, 319, 360D | 201, 280, 305+351+338, 308+313 |
| DMF | | 226, 312, 319, 332, 360D | 201, 280, 305+351+338, 308+313 |
| EtOAc | | 225, 319, 336 | 210, 261, 305+351+338 |
| diethyl ether | | 224, 302, 336 | 210,261 |
| ethanol | | 225 | 210 |
| HCl (37 %) | | 290, 314, 335 | 261, 280, 305+351+338, 310 |
| $HNO_3$ (65 %) | | 272, 314 | 220, 251, 280, 305+351+338, 310 |
| $H_2O_2$ (30 %) | | 302, 318 | 280, 305+351+338 |

428

| substance | pictograms | hazard statements | precautionary statements |
|---|---|---|---|
| H$_2$SO$_4$ (98 %) | | 314 | 280, 305+351+338, 310 |
| diisopropyl-amine | | 225, 302, 314, 332 | 210, 280, 305+351+338, 310 |
| K$_2$CO$_3$ | | 302, 315, 319, 335 | 261, 305+351+338 |
| KI | | 302, 315, 319 | 305+351+338 |
| KOH | | 290, 302, 314 | 280, 305+351+338, 310 |
| K$_2$CO$_3$ | | 302, 315, 319, 335 | 261, 305+351+338 |
| K$_3$PO$_4$ | | 315, 318 | 280, 305+351+338 |
| methanol | | 225, 301, 311, 331, 370 | 210, 260, 280, 301+310, 311 |
| KO$t$Bu | | 228, 318 | 210, 280, 303+361+353, 304+340310 305+351+338 |
| $n$-BuLi (2.5 M in hexanes | | 225, 250, 261, 304, 314, 336, 361f, 373, 411 | 210, 222, 231+232, 261, 273, 422 |
| $n$-hexane | | 225, 304, 315, 336, 361f, 373, 411 | 210, 261, 273, 301+310, 331 |
| N$_2$ | | 280 | 410+403 |

| substance | pictograms | hazard statements | precautionary statements |
|---|---|---|---|
| NaNO$_2$ | | 272, 301, 319, 400 | 220, 273, 301+310, 305+351+338 |
| NaOH | | 314 | 280, 305+351+338, 310 |
| Na$_2$CO$_3$ | | 319 | 305+351+338 |
| NH$_3$ (aq. 25 %) | | 302, 314, 335, 400 | 261, 273, 280, 305+351+338, 310 |
| $n$-heptane | | 225, 304, 315, 336, 410 | 210, 261, 273, 301+310, 331, 501 |
| I$_2$ | | 312, 332, 400 | 273, 280 |
| LiCl | | 302, 315, 319, 335 | 261, 305+351+338 |
| PdCl$_2$ | | 301, 317 | 280, 301+310 |
| PPh$_3$ | | 301, 317, 373 | 280 |
| $i$PrMgCl·LiCl (1.3 M in THF) | | 225, 314, 335, 351 | 210, 261, 280, 305+351+338, 310 |
| toluene | | 225, 304, 315, 336, 361d, 373 | 210, 261, 281, 301+310, 331 |
| SiO$_2$ | | 373 | |
| SOCl$_2$ | | 302, 314, 331 | 261, 280, 305+351+338, 310 |
| THF | | 225, 319, 335, 351 | 210, 261, 281, 305+351+338 |

| substance | pictograms | hazard statements | precautionary statements |
| --- | --- | --- | --- |
| triethylamine | | 225, 302, 311+331, 314, 335 | 210, 261, 280, 303+361+353, 305+351+338, 370+378 |
| $Zn(NO_3)_2 \cdot 6\,H_2O$ | | 272, 302, 319, 335 | 220 261 305+351-338 |

## 6.3 KMR-Stoffe

Table 6.2 – Verwendete KMR-Stoffe der Kategorien 1A/1B (GHS)

| CAS-Nummer | Stoffname (IUPAC) | Verfahren und eingesetzte Menge | Kategorie (GHS) |
|---|---|---|---|
| 106-93-4 | 1,2-Dibromethan | chemische Synthese, 25 mL | K: 1B |
| 10141-05-6 | Cobalt(II)nitrat | chemische Synthese, 10 g | K: 1B, $R_F$: 1B |
| 7718-54-9 | Nickel(II)chlorid | chemische Synthese, 10 g | K: 1A, $R_E$: 1B |
| 872-50-4 | *N*-Methylpyrrolidin | Solvens, 5 mL | $R_E$: 1B |
| 68-12-2 | *N,N*-Dimethylformamid | Solvens, 10 L | $R_E$: 1B |
| 67-66-3 | Trichlormethan | Solvens, 10 L | K: 1B |
| 865-49-6 | Trichlormethan-d | Solvens, 800 mL | K: 1B |